MICROBIAL INTERACTIONS WITH POLYMER NANOCOMPOSITES THAT INCORPORATE CARBON NANOTUBES

by
David G. Goodwin Jr.

A dissertation submitted to Johns Hopkins University in conformity with the requirements for the degree of Doctor of Philosophy

Baltimore, MD
June 2016

ABSTRACT.

The incorporation of carbon nanotube (CNT) fillers into polymeric materials can improve properties such as tensile strength, conductivity, and thermal resistivity. This has led to the manufacture of CNT/polymer nanocomposites (CNT/PNCs) for use in commercial products. After consumer use, CNT/PNCs will be disposed of and encounter microorganisms in landfills, surface waters, and wastewater treatment plants where material transformation and CNT release are possible. In these environments, the ultimate fate of CNT/PNCs will be determined, in part, by polymer biodegradation processes.

A three tiered approach was taken to investigate the role of microorganisms on CNT/PNC transformation in the environment. First, the initial interaction of microorganisms (*Pseudomonas aeruginosa*) with CNT/PNC surfaces was assessed using CNT mass loadings relevant to those used in products (0.1-10% w/w). The CNT surface concentration was well controlled and characterized using a modified X-ray photoelectron spectroscopy (XPS) technique as well as scanning electron microscopy (SEM). The microorganisms on the CNT/PNC surfaces were LIVE/DEAD stained and imaged using confocal laser scanning microscopy (CLSM) to assay the antimicrobial properties as a function of CNT loading. The results indicated that CNTs had an increasingly cytotoxic effect on the microorganisms when the CNT surface concentration was systematically increased. Next, the impact of CNT cytotoxicity on biofilm development (cell proliferation), the precursor to biodegradation, at the CNT/PNC surface was investigated. Viable biofilm development (*P. aeruginosa)* was observed on top of dead cells that coated CNT/PNCs with high CNT surface concentrations. Since viable biofilms were able to form in close proximity to the polymer substrate, the overall

transformation of the CNT/PNCs as a result of biodegradation was further investigated. CNT/PNCs containing varied CNT loadings were biodegraded and analyzed using gravimetric measurements and SEM imaging before and after transformation. Supernatants were also analyzed for CNT release using a single particle ICP-MS technique. CNTs were found to have an inhibitory effect on biodegradation which was strongly dependent on the use of single (*P. aeruginosa)* versus mixed cultures, aerobic versus anaerobic biodegradation processes, and polymer type. The generalizability of the results as well as the implications for CNT/PNC use in consumer products will be discussed.

Advisor: Dr. D. Howard Fairbrother

Co-Advisor: Dr. Ed J. Bouwer

Reader: Dr. Christopher J. Falzone

ACKNOWLEDGEMENTS.

I have had the privilege of interacting with and learning from a great number of individuals during my graduate career at Hopkins. The lasting impact these individuals have had on both my professional and personal life will forever be a part of my approach to new endeavors.

First, I have to thank my current Fairbrother group labmates: Michael Barclay for teaching me the intricacies of our instrumentation and how to troubleshoot problems; Miranda Gallagher for her helpful critiques and attention to detail in designing experiments; Ronald Lankone for his constant patience and his role as partner in crime at conferences; Julie Spencer for her intriguing stories, perseverant attitude, and supportive nature; Dave Durkin for his continued excitement about science and his can-do attitude, which is contagious; Rachel Thorman for replacing rigidity with fun whenever possible; and Ben Frank, for his patience, positive attitude, and willingness to take on the remaining challenges associated with the project. Most importantly, I would like to thank all of my labmates for the team atmosphere we were able to create and the support that was always shown whenever someone required assistance or feedback. I would also to thank my former labmates: Dr. Kevin Wepasnick, Dr. Julie Bitter, Dr. Justin Gorham, Dr. Billy Smith, and Dr. Samantha Rosenberg for training, constructive criticism, and the many collaborative efforts we took part in after they moved on to other positions. Next I have to thank my advisor, Dr. D. Howard Fairbrother who kept me on my toes, challenged me intellectually, introduced me to an international network of colleagues, sent me to many conferences, and helped me improve my writing. Howard was always accessible, dedicated to the research, had my back, and let me have my say while also

having his. Our working relationship was very productive and I can't thank him enough for teaching me to become an independent scientist.

My experience was unique in that I had the opportunity to become a part of second research group in another department, Geography and Environmental Engineering (DoGEE). I thank Dr. Ed Bouwer for incorporating me into his group, providing me a lab space to independently work, and being accessible despite his massive number of responsibilities as Department Chair. I thank his group members: Marielle Remillard for helping me start the project; Dr. Jessica Lawson for her clear and thorough explanations of concepts that enabled me to get started in the lab; Dr. Pavlo Bohutskyi for collaborating with me on the biogas project, teaching me by example where to focus my efforts when deadlines are looming, and being a beast; Duc Phan and Zehui Xia for their kindness, dedication, and teamwork; and Steven Chow for his intellectual feedback and being my favorite lab neighbor in DoGEE. I would also like to thank Huan Long, Dr. Bill Ball, Chris Kelley, Dr. Yaqi Yu, Dr. Eric Sakowski, and Dr. Sarah Preheim for including me as part of the DoGEE family and sharing their lab space. It was a highly valuable experience learning both the chemist's and the engineer's perspective in approaching research problems.

I am also grateful to have worked with an incredible research technologist (Kris Marsh, 1 yr.) and some incredibly talented international students: Dr. Iruhany Boyer Sosa (Venezuela, 6 mo.), Thomas Devahif (Belgium, 3 mo.), and Cong Gao (China, 1 yr.). I am so happy to have met them and I could not have effectively developed the project without their input. I had a great time learning about their culture and showing them 'Murica- I cannot wait to take a world tour and pay them all a visit! I also cannot begin to

thank the undergraduates, REU students, and Master's students that I worked with over the years (Christie Checketts, Alex Dang, Jenny Chiang, Gaurav Ajmani, Pat Geronimo, Julianne Payne, Putarut Sunthranand, Roderick Go, Tucker Gordon, Leo Kuwama, and Xier Lu) – their patience, dedication, hard work, and wide range of talents was truly impressive and taught me how to effectively manage a complex project. There are also too many collaborators to name, but I'd like to express my gratitude for having the opportunity to partake in such a diverse set of projects and perspectives.

I would like to thank Dr. Chris Falzone, a member of my thesis committee and the professor who took me on as an organic chemistry TA for two years. As a physical/analytical chemist, this was a challenge that allowed me to improve my organic chemistry and teaching skills and I sincerely thank Dr. Falzone for his mentorship throughout this experience. I would like to thank my former committee members: Dr. Haiou Huang, Dr. Rebekkah Klausen, and Dr. Jerry Meyer for their time and efforts. A big shout-out also goes to the chemistry department staff: Boris Steinberg, Jean Goodwin, John Kidwell, Dave Brewster, Joe Russell, and Rosalie Elder. Rosalie, in particular, looked out for me from the day I started and I cannot thank her enough for being a part of my Hopkins' career. I would also like to thank the National Science Foundation and the Owens Fellowship from the JHU Department of Chemistry for funding my research.

With intense expectations, the 99% failure rate of challenging experiments, and the insatiable call to throw everything in the book at a problem, enormous levels of pressure and stress can begin to wear you down during the Ph.D. Luckily, I had the privilege of going through this entire ride with a close group of people experiencing the same hurdles at the same time. In the process, I have forged some of the greatest

friendships of my life: Drs. Ryan O'Donnell, Heather Neu, Jesse Neu, Steven! Bloom, John Sheckleton, and Allison McQuilken. They have been my lifeblood throughout this experience and have been there at the end of every long week to unwind and rip down curtains. From the Blue Jay shuttle rides, dabbling in gardening and music production, trips to local eating establishments where the freshest of foods are served, and nights listening to the fireworks, I can't thank them enough for keeping me grounded and always making me laugh. I look forward to climbing some more blue mountains with these amazing people.

My Mom used to say that I always asked "why, why, why?" from the moment I could speak and it was no surprise to her that I took this road after college. I would like to thank my parents and little brother for their unwavering support and encouragement as I went through this process. Lastly, I'd like to thank Katherine Holmes (not the actress, I'm talking about the girlfriend) for her patience, love, and support throughout this experience. Katie has taught me how to be balanced, stay positive, have fun, and to always find a path forward. We built a fantastic life over the past six years and I look forward to taking many new adventures with her in the years to come.

TABLE OF CONTENTS.

LIST OF TABLES.

LIST OF FIGURES.

LIST OF SCHEMES.

Chapter 1. Introduction to Carbon Nanotube/Polymer Nanocomposites

1. 1. Nanomaterials

Materials are classified as nanomaterials when they have at least one dimension on the nanoscale, typically between 1 - 100 nm. The atomic structure of nanomaterials, which are also called nanoparticles, falls somewhere between that of discrete molecules existing in exact stoichiometric ratios and bulk materials with less well-defined regions.[1] A nanoparticle is typically considered a colloid, or a microscopically dispersed substance (with dimensions up to 1 μm) when it is mixed into another medium such as water, organic solvents, or air.[2] When nanomaterials are the solid dispersed phase within a liquid dispersion medium, they are considered sols. Other sols can include microorganisms, natural organic matter, and oils dispersed in water.[3] Nanomaterials can also disperse into the air; in this case they are called aerosols.[4]

Natural nanomaterials have long been present in soils, sediments, natural waters, and volcanic dust in the form of carbonaceous clays, soot, and metal oxides while engineered nanomaterials are synthesized in the laboratory using a variety of precursors.[1, 5] Engineered nanomaterials are often tailored for specific applications and have controlled purity, shape, size, and coatings. With recent advances in microscopy that enable characterization and the manipulation of matter at the nanoscale, the production of engineered nanomaterials has increased substantially in many applications, which is broadly described as nanotechnology.[1] In fact, it is estimated that 260,000- 309,000 metric tons of engineered nanomaterials were produced globally in 2010.[6]

Owing to quantum confinement effects and a large surface area to volume ratio at dimensions below 100 nm, unique chemical, mechanical, physical, and optical properties have been observed for nanomaterials. This has spurred interest in the many potential applications of nanomaterials, as evidenced by the exponentially increasing number of publications on the topic each year, the exponential increase in government funding to academic researchers working in the field of nanotechnology, and the large number of government agencies working in this research area.[7] Interestingly, properties such as fluorescence, chemical reactivity, electrical conductivity, and magnetic permeability can be tuned by varying nanomaterial size. The large surface area to volume ratio also allows for enhanced reactivity.[1] Engineered nanomaterials can be broadly classified as metal/metal oxide, nonmetallic, and carbonaceous.[8] Metal/metal oxide nanomaterials can include titanium dioxide (TiO_2), silver (Ag), zinc oxide (ZnO), quantum dots (QDs), and cerium oxide (CeO_2) while non-metallic nanomaterials can include hydrogels and dendrimers.[9-12] In terms of applications, TiO_2 and ZnO are photoactive in the UVB and UVA range, respectively, and are used in solar cells, catalysis, cosmetics, and sunscreens. Quantum dots are used in a wide array electronics due to their high intensity luminescence.[13] Nano-Ag is often used in fabrics, dietary supplements, food packaging, and coatings, to make use of its antimicrobial properties.[14] Non-metallic nanomaterials such as hydrogels and dendrimers are used in catalysis, drug delivery, and other in vivo applications.[9, 12] Carbonaceous nanomaterials can include fullerenes (C_{60}), graphene, nanodiamond, nanocellulose, carbon nanofibers, and carbon nanotubes.[15, 16] Carbonaceous nanomaterials are employed in a wide range of applications that can include electronics, plastic reinforcement, catalysts, and membranes.[15]

1. 2. Carbon Nanotubes

Carbon nanotubes (CNTs) are novel engineered nanoparticles that consist of sp^2-hybridized sheets of graphene rolled into cylindrical tubes with diameters on the nanometer scale and lengths typically on the micron scale. They are considered allotropes of carbon. CNTs can be either single-wall (SWCNTs) or multi-wall (MWCNTs) with a single cylinder or multiple concentric cylinders of graphene held together by van der Waals forces, respectively (Figure 1.1).[17]

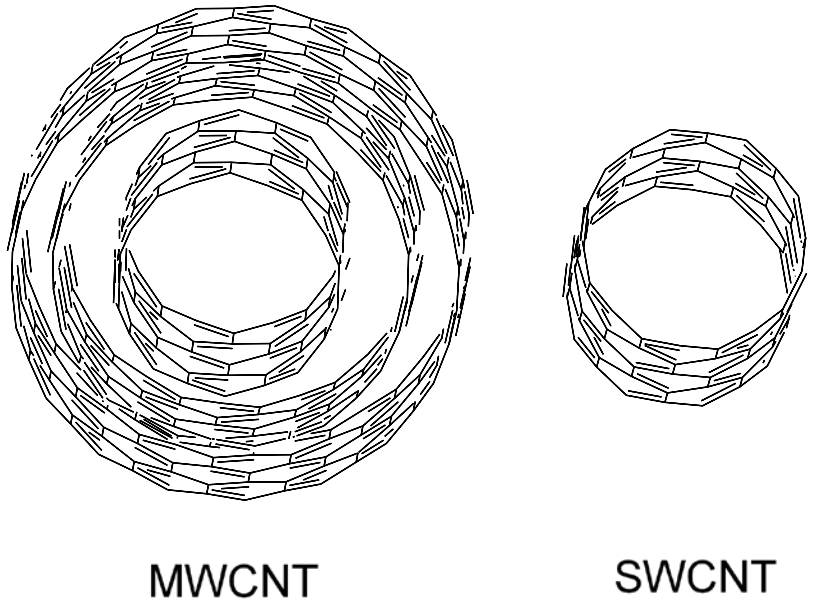

Figure 1.1. A comparison of the structure of a) MWCNTs and b) SWCNTs.

The high aspect ratio (150 to > 2000) of CNTs along with their mechanical, colloidal, and electronic properties have generated much interest in the scientific community with respect to their applications and behavior when released into the environment.[18, 19] CNTs can be more than 1000 times stronger than steel with tensile strengths up to 150 GPa and Young's moduli up to 1.8 TPa. [20, 21] Another extraordinary property of CNTs is their thermal conductivity, which has been reported to be as high as 6600 W/mK for some

CNT types.[21] Through reflection loss and absorbance loss, CNTs can be used for electromagnetic interference (EMI) shielding applications.[22] CNTs are also electrically conductive, with metallic CNTs having conductivity as high as 104 S/cm.[21] The conductivity of CNTs depends on the different possible angles of graphene wall wrapping, or the chirality of the tubes. CNTs can wrap in a zigzag, armchair, and chiral configuration. Armchair configurations are always metallic, or fully conductive, while zigzag and chiral CNTs can be metallic or semi-conducting.[23] For electronic applications, metallic CNTs are sought after since their electrical resistance is low and ballistic transport through the CNT structure allows for excellent conductivity with scattering mostly coming from defect sites.[24] CNTs are typically produced in batches containing both metallic and semi-conducting CNTs and production and purification of metallic CNTs is still prohibitively expensive, but progress on more cost-efficient means of synthesis are underway.[25] The electrical properties of MWCNTs are more complex than for SWCNTs since each of the concentric tubes that make up a MWCNT can have a different chirality. However, MWCNTs are oftentimes superior to SWCNTs in electrical applications since MWCNTs are cheaper. Furthermore, MWCNT conductivity is not as significantly impacted by defect sites on the outer CNT wall as is the case with SWCNTs since MWCNTs have inner CNT walls available to "re-route" electrical current past the disrupted aromatic network.[26]

Four of the major approaches to synthesizing CNTs are chemical vapor deposition (CVD), arc discharge, laser ablation, and plasma torch deposition.[27-29] CVD is by far the most widely used approach; it involves CNT growth on a metal catalyst using a flowing hydrocarbon gas as the carbon feedstock such as methane, carbon monoxide, ethylene,

and acetylene. The catalytic species are typically spherical transition-metal nanoparticles supported by underlying materials such as alumina or silica. In fact, the size of the metal nanoparticle can dictate whether or not the CNTs are grown as SWCNTs or MWCNTs and can control the number of walls in a MWCNT. This type of approach is typically carried out in a tube furnace at temperatures between 500 – 1000 °C. Although the high temperatures and the metal catalysts increase cost, this method is easily scaled-up for mass production. In this process, residual metals catalysts such iron, nickel, cobalt, and yttrium, can become embedded within the CNTs.[27, 30, 31] While it is not ideal that the CNTs contain metal impurities, the presence of these metal catalysts can allow for tracking CNT release and concentration in complex media using single-particle ICP-MS.[30] This technique is described in Section 1.47. A modified version of CVD called the HiPco® process, reacts an iron tricarbonyl precursor and high pressure carbon monoxide in a continuous flow system to scale up CNT production.[32] The second CNT synthesis method, arc discharge, involves the use of two high purity graphite rods as an anode and cathode within a vessel under a Helium atmosphere. The rods are brought together at a close distance (1-2 mm) and a voltage is applied (~25 V) until a stable arc is achieved. At this point, carbon atoms ionize at the anode and move towards the cathode, where they deposit as CNTs and carbon impurities. As the anode is consumed, the rods are kept at a constant distance from one another.[31] The third method, laser ablation, also uses a graphite target in a controlled atmosphere at temperatures near 1200 °C. In this case, the graphite target is vaporized using a laser and the CNTs and carbonaceous material condense on a water-cooled target.[28] A similar method makes use of a plasma torch and a hydrocarbon gas that is flowed through the plasma to deposit carbonaceous material on a

water-cooled target.[29] Arc discharge, laser ablation, and plasma torch methods tend to produce more carbonaceous impurities, such as amorphous carbon and non-tubular fullerenes, than CVD.[28] However, CVD produces CNTs containing residual metal nanoparticles while the other methods do not, except in the case of SWCNT synthesis, where metal nanoparticles are required as a seed in all production methods.[28, 31] For SWCNTs, the metal catalyst seed usually needs to be extremely small (>1-2 nm) and in only some cases, is not required for SWCNT growth under very well-controlled laser ablation conditions.[28, 31] The much tighter processing controls required for SWCNT production relative to MWCNT production has led to higher SWCNT prices.[33] Overall, the four most commonly used CNT production methods are energy-intensive and lacking to different degrees in purity.[27-29] However, the scale-up, use of low cost feedstocks, energy and waste reduction, as well as increasing demand have led to decreasing costs of CNTs.[33]

CNTs can be purified using a combination of acid and base washing. Hydrochloric acid is commonly used to reduce the metal nanoparticle content generated by CVD.[34] Strong acids such as nitric and sulfuric acid can be used to oxidize the carbon impurities on defect sites for suspension and removal, however, these oxidizing conditions can also introduce oxygen functional groups onto carbon nanotube defect sites.[35, 36] This can have a negative impact on the properties of pure CNTs.[37] Base washing is used to deprotonate and suspend oxidized amorphous carbon species for removal by washing or centrifugation.[38, 39] Other types of cleaning and purification methods involve thermal annealing to oxidize and etch away amorphous carbon, which has a different thermal oxidation rate than CNTs, and surfactant separation techniques,

which are typically only used for SWCNTs.[25, 40] Surfactants have been shown to bind selectively to SWCNTs of different species, most notably in terms of CNT chirality (graphene wrapping pattern), a property that affects the electronic properties of CNTs. The different surfactants can then impart density differences between different CNT structures when placed in a density gradient and ultracentrifuged. The CNT species are then isolated using established fractionation methods.[25] Different variations of this technique have also been investigated.[41-44] Although complex, this is one of the most common methods for separating CNTs by diameter, bandgap, and electronic type for purification.[25]

CNTs have been widely studied in aqueous media that mimics environmentally relevant conditions. Many studies involving aggregation, deposition, and facilitated transport have been conducted.[45] CNTs have also been oxidized to make them more readily dispersible in water, other polar solvents, and polymer matrices using strong oxidants and acids such as $KMnO_4$, HNO_3, and HNO_3/H_2SO_4.[46-49] Oxidation can occur readily in the environment through many different mechanisms such as photo-oxidation and weathering, increasing the transport properties of the CNTs.[50-52] Oxidation commonly takes place at defect sites in the sp^2-hybridized network, since it is more energetically favorable to oxidize these sites rather than break the aromaticity of the pi-conjugated structure. Defect sites occur regularly at the ends of CNTs but are also common along the CNT structure.[53] The level of surface oxidation can be measured using X-ray photoelectron spectroscopy (XPS), a technique outlined in the next chapter. The surface concentration of specific oxygen functional groups can also be tagged with fluorine-containing reagents and quantified using XPS. Specifically, chemical

derivatization-XPS (CD-XPS) selectively tags hydroxyl, carbonyl, and carboxyl groups with 2,2,2-trifluoroacetic anhydride, 2,2,2-trifluoroethylhydrazine, and 2,2,2-trifluoroethanol with N,N'-di-tert-butylcarbodiimide and pyridine (Scheme 1.1). Reactions are carried out separately, in the vapor phase, using the freeze-pump-thaw method.[53] Other methods available to quantify oxygen functional group concentrations include fluorescent tagging, potentiometric titrations, and X-ray absorption near edge spectroscopy (XANES).[54-59] CD-XPS is one of the more robust methods since the reactions are highly selective for each functional group, the technique is fairly straightforward to perform, and the results are precise and semi-quantitative.[53]

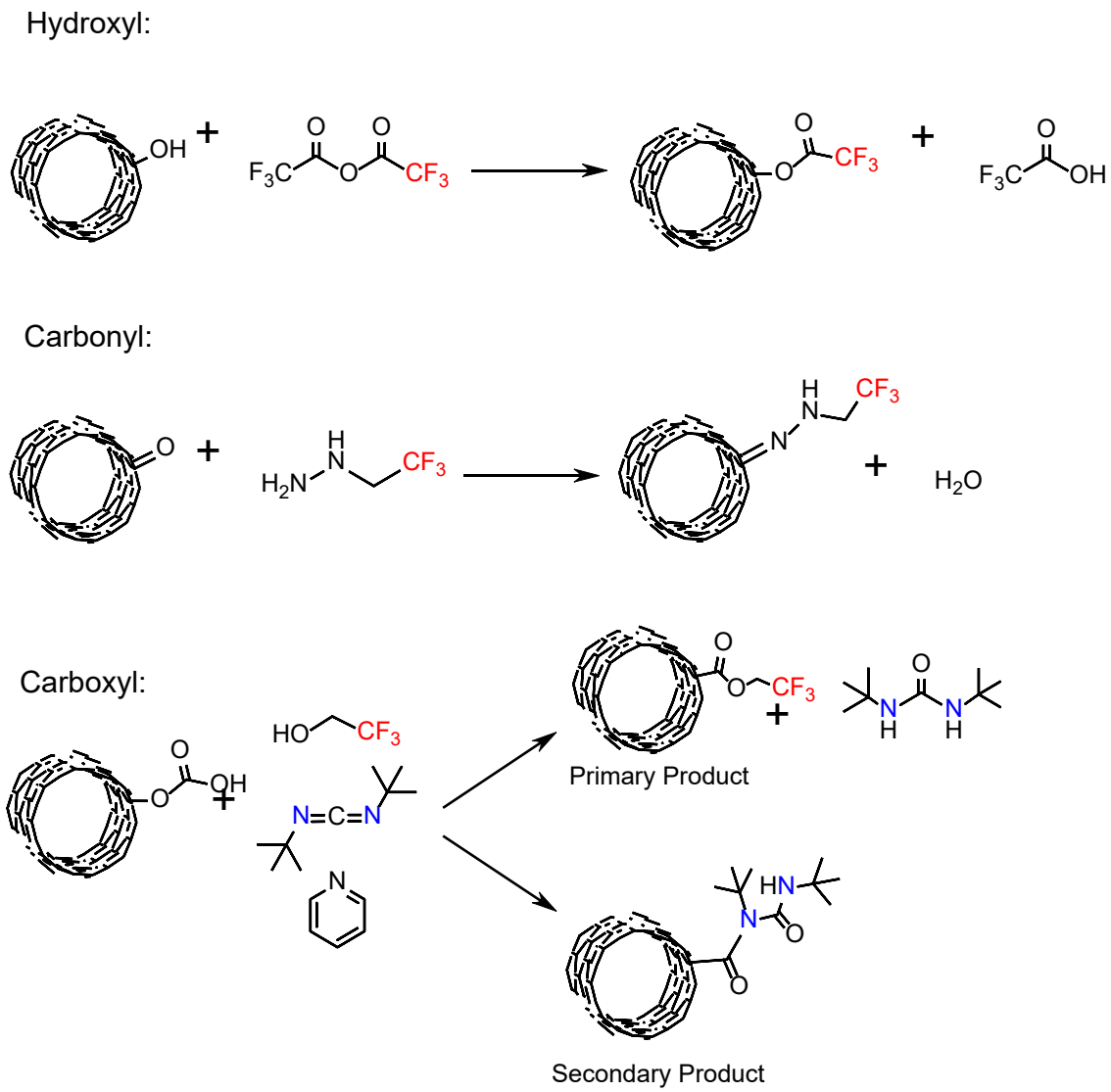

Scheme 1.1. Quantification of common oxygen functional group concentrations at the CNT surface using CD-XPS.

1. 3. The Impact of Carbon Nanotubes on the Environment and Human Health

The use of CNTs in many applications has prompted concerns over their environmental impacts and risks to human health.[60, 61] In particular, the carcinogenic nature of CNTs, the inherent toxicity of CNTs to a range of organisms in the environment, CNT persistence, CNT transport through porous media, the ability of CNTs

to adsorb toxic co-contaminants are all issues that have been investigated to varying degrees.[15, 62-65] Research in these areas has been challenging since CNTs are produced in batches of varying lengths, diameters, surface functionalities, and with residual trace metal catalysts. The role of each of these variables on CNT transport, transformation, fate, and toxicity can be challenging to isolate.[61] Nevertheless, a large number of studies have helped to provide some generalizations with regards to the impacts of CNTs on human health and the environment.[33, 62, 64, 66]

In terms of human health, CNTs pose a risk from bioaccumulation throughout the food chain, dermal contact from CNT-containing products, and their inherent carcinogenicity.[62-64] The similarities between CNTs and asbestos, most notably in terms of their high aspect ratios, has led to major concern and a multitude of preventative measures.[63, 67] Asbestos, or hydrated silicates with fibrous morphology, were found to be highly carcinogenic in the 1970s after widespread exposure of construction workers and consumers to over 3000 asbesto-containing products, the most common type being insulation.[63] In fact, mesothelioma diagnoses as a result of asbestos inhalation from products are expected to continue until 2020.[63] Asbestos consist of several forms which are broadly classified as serpentines and amphiboles, and have lengths of 0.1 – 200 μm and diameters that can reach below the sub-micron level.[63] The high aspect ratio (length/diameter) of asbestos is markedly similar to that of CNTs. Furthermore, other important properties that contribute to the pathogenicity and carcinogenicity of asbestos, might also be inherent to CNTs.[63, 67, 68] These properties can include biopersistence, reactive oxygen species generation, and pulmonary penetration potential which can lead to inflammation and the formation of lesions known as granulomas.[63, 68] Although CNT

carcinogenicity has not been explicitly observed in humans, CNTs have induced mesothelioma in mice, most notably when the CNTs were rigid and long.[68] This is similar to asbestos, which were found to be most problematic when rigid and long due to pulmonary penetration and difficulty in lung clearance, respectively. CNTs have been found to be less toxic when curved, bundled, and tangled due to minimal pulmonary penetration and easier lung clearance.[67] These concerns are especially important for longer CNTs (up to the mm scale), which are already being produced as sheets, cables, and armor.[67, 69, 70] So far, specialized steps have been voluntarily taken by companies to mitigate the inhalation of CNTs by workers during CNT synthesis, weighing of CNT powders, and mechanical abrasion of CNT nanocomposites. Some approaches to preventing CNT aerosol inhalation have included modified ventilation, personal protection equipment, and nano-hoods.[71, 72] Furthermore, as of 2008, CNTs have been designated a distinct carbonaceous substance by the Environmental Protection Agency (EPA) under the Toxic Substances Control Act (TSCA). This has provided the EPA more control over required labeling, the use of PPE by manufacturers, toxicity testing, new product reviews, and record keeping.[73]

In terms of inherent toxicity in the environment, CNT exposure to aquatic and terrestrial multicellular organisms has been primarily shown to have a toxic effect as a result of interactions with epithelial cell surfaces. Absorption of CNTs across epithelial cell membranes, or uptake by tissues surrounding organs, has not been readily observed. For both soil and aquatic organisms, intake of CNTs led to minimal tissue adsorption and many cases, CNT clearance from the gut. When toxicity was observed from CNTs in the gut, CNT aggregation tended to be more prevalent and the toxicity was attributed to gut

clogging. In terrestrial environments, such as soils and sediments, CNTs tend to have a minimal ecotoxicological effect at artificially high concentrations (g/kg). The same was true of organisms in aquatic environments, however, the inherent toxicity of dispersed CNTs in this environment required much lower concentrations (mg/L) to take effect.[62] For microorganisms in controlled laboratory settings, CNT toxicity has also been observed both in suspension and at surfaces.[62, 74-80] The toxicity observed has been hypothesized to be a result of membrane penetration, reactive oxygen species generation, and cellular membrane disruption.[75, 76, 81-85] CNT toxicity to microorganisms has also been shown in many cases, with only a few studies claiming that CNTs were benign.[86-88] This could most likely be a result of varying conditions such as length, diameter, CNT purity, aggregation state, and metal content.[89] Furthermore, only at artificially high CNT mass loadings, was cellular growth affected by the presence of CNTs in suspension.[79, 80] Overall, CNTs have been shown to exhibit cytotoxic effects, but the severity of these effects have been localized and minimal uptake of CNTs by epithelial cells has been observed.[62, 74-80]

CNTs cannot be easily transformed in the environment to more benign products. Instead, CNTs tend to persist and have the potential to bioaccumulate in organisms, especially when not readily excreted from the gut in an aggregated form.[62] Furthermore, when CNTs are embedded as a filler in CNT/polymer nanocomposites, they may enhance the persistence of the polymer and worsen plastic waste accumulation issues in the environment.[33, 62, 66] CNT transformations occur by photo-oxidation, usually at defect sites in the sp^2-hybridized network, directly by the UV component of solar radiation or indirectly by reactive oxygen species generation in the presence of Fenton reagents or

H_2O_2. However, photo-oxidation does not lead to complete mineralization of CNTs, even with oxidized SWCNTs.[51, 52, 90, 91] Biodegradation of CNTs has only been shown to occur partially (6.8% mass loss maximum) for oxidized CNTs under harsh enzymatic conditions.[92-95] Thus, the majority of CNT transformations will not significantly alter the CNT structure or remove CNTs from the environment.

The transformation of CNTs to a more oxidized form or the disposal of already oxidized CNTs will have an important effect on CNT transport in the environment. Oxidation stabilizes CNTs in aqueous systems through hydrogen bonding, dipole-dipole, and electrostatic interactions. Oxygen functional groups also decrease CNT aggregation by disrupting pi-pi stacking between individual CNTs. Thus, oxidation can enhance CNT dispersion in aqueous environments and as a result, promote the spread of CNTs from one site to other locales.[35, 53, 96] The sorption of natural organic matter (NOM) to CNTs can also lead to transport through the environment as NOM tends to stabilize CNTs in aqueous suspension through steric repulsion and electrostatic interactions.[97] NOM coatings have been shown to increase uptake of MWCNTs in *Daphnia magna*, a model organism. This led to gut clogging and increased toxicity relative to MWCNTs without an NOM coating, which were more poorly dispersed in the media and not as easily uptaken.[98] NOM coatings may potentially mitigate CNT toxicity by preventing direct contact with cells, but this has not yet been validated by experimental data due to differences in transport effects between CNTs with and without NOM stabilization. Deposition of CNTs onto porous media such as sand and soils has also been shown to play a role in CNT transport. The critical deposition coefficient, or the minimal salt concentration required for favorable deposition of a colloid onto a surface, is commonly

used to measure the degree to which a particle favorably attaches to a surface. The particles and the surfaces they attach to both have an inherent charge that can be screened by ions of opposite charge. The higher the charge of the ions, the greater the compression of this charged double layer. When a particle and a surface are each screened by a critical concentration of counterions that allow for a close particle approach to the surface, the van der Waals forces between the particle and surface can overcome the electrostatic repulsion, leading to deposition.[65, 99, 100] A similar interaction can also be observed between two colloidal particles that coagulate; the salt concentration at which this process becomes favorable is called the critical coagulation coefficient (CCC).[3] For both deposition and coagulation, a higher CCC and critical deposition coefficient (CDC) have been observed with increasing CNT oxidation as a result of the greater number of carboxylic acid groups and dipole-dipole moments present on oxidized CNTs as compared to pristine CNTs. This indicates that oxidized CNTs are more prone to transport than pristine CNTs.[99, 100] However, the CCC and CDC concentrations have been shown to be more affected by NOM than by oxidation as a result of steric repulsion. Lowering the pH also tends to enhance coagulation and deposition more than the level of CNT oxidation since a low pH can decrease the negative charge of the carboxylic acid groups on CNTs or NOM coatings and requires less charge screening for coagulation or deposition to occur. Overall, NOM can transport both oxidized and pristine CNTs, leading to their distribution throughout the environment.[97, 99]

Not only is there concern about inherently cytotoxic CNTs transporting through the environment, but there is also the issue of CNTs facilitating the transport of co-contaminants.[15] Specifically, CNTs can adsorb organic contaminants such as polycyclic

aromatic hydrocarbons (PAHs) from synthesis or the environment, petroleum byproducts, and disinfection byproducts from wastewater treatment plants.[15, 62, 101, 102] In fact, CNTs are considered super sorbents, with higher sorption capacity relative to black carbon as a result of their high surface area.[15] Oxidized CNTs can also adsorb toxic heavy metals such as arsenic, lead, and cadmium at the carboxylic acid sites, as has been shown with Zn (II) and Cd(II).[103] Once co-contaminants are adsorbed, the CNTs can then transport them to other locales, leading to biological uptake, cytotoxicity and persistence of both CNTs and their co-contaminant.[15, 62]

1. 4. Carbon Nanotube Detection and Quantification in Environmental Media

1.4.1. Introduction

Carbon nanotubes are challenging to detect in complex environmental matrices. The biggest issue in detecting CNTs is distinguishing the carbonaceous nanomaterial from the predominantly carbonaceous background which can consist of natural organic matter (NOM), cellular material, and black carbon. Allotropes of black carbon such as soot and charcoal are at much higher concentrations than CNTs in the environment, yet are indistinguishable with most methods. CNTs can potentially be found in aqueous environments, soils, sediments, and wastewater treatment plants. Furthermore, CNTs have a broad distribution of diameters, lengths, metal catalyst impurities, functional group distributions, and aggregation states which hinders the use of traditional organic contaminant analysis such as mass spectrometry and also limits development of a universal analytical technique. Nevertheless, several analytical techniques have been developed to detect and quantify CNTs in simple and complex media.[104] Each of these techniques have certain drawbacks, and further research is ongoing as to how to

overcome these issues. This list is not exhaustive, but covers some of the most commonly used techniques.

1.4.2. Ultraviolet/Visible Spectroscopy

Ultraviolet/visible spectroscopy (UV/Vis) is a common analytical method used to measure the concentration of a molecular or colloidal species, monitor changes in a molecules UV/Vis profile as reactants transform to products, and sometimes to aid in structural determination of a compound under investigation, oftentimes in tandem with nuclear magnetic resonance spectroscopy (NMR), infrared spectroscopy (IR), and/or mass spectrometry (MS). UV/Vis works by transmitting light through a solution, with the intensity of the transmitted light reduced by molecular adsorption. The reduced intensity of light ($\boldsymbol{I}$) reaching the detector relative to the initial intensity of light ($\boldsymbol{I_0}$) is proportional to the concentration ($\boldsymbol{c}$) of the species in solution. The Beer-Lambert law (Equation 1) relates the ratio of the incident and detected light intensity to the absorption ($\boldsymbol{A}$) of light by the molecule. It also shows that the concentration of a compound is directly proportional to the light absorption; this relationship remains linear up to an absorption of 1. In this equation, the path length through the solution is ($\boldsymbol{b}$), and the molar absorptivity, ($\boldsymbol{\varepsilon}$), is a measure of how well a substance absorbs light.[105]

$$\boldsymbol{A = \log\left(\frac{I}{I_0}\right) = \varepsilon bc} \qquad \text{(Equation 1)}$$

In simple aqueous systems, CNTs can absorb across the entire UV/Vis spectrum. Similar to other colloids, CNTs can also scatter light. A combination of absorption and light scattering by CNTs reduces the transmission intensity of light to the detector in proportion to the concentration of CNTs, thus following the Beer-Lambert law

relationship. Wavelengths of 270 nm and 350 nm have typically been used in CNT analysis via UV/Vis, since there is minimal interference from salts, acids, bases, and many surfactants.[91, 99] The molar absorptivity of CNTs can be estimated by preparing several CNT suspensions of varying concentration, measuring the absorbance of each suspension, and generating a calibration curve. Since CNTs suspended in a solvent represent a distribution of diameters, lengths, and impurities, the molar absorptivity varies with the CNT batch used. This makes comparing the concentrations of different CNT batches challenging. It also prevents concentration determination when the CNT type is unknown. One approach has been to use absorbance as a means to compare CNT density of different types of CNTs.[91] This can be useful in terms of comparing different CNT types by a common metric, but is not useful for comparing CNTs on a mass basis, or determining the mass concentration of an unknown type of CNT. CNT detection and quantification with UV-Vis is limited to very simple systems, as complex media will have absorption profiles that interfere with CNT adsorption bands. UV/Vis also has a low sensitivity for CNTs (10^{-1} mg/L or mg/kg).[104]

1.4.3. Raman Spectroscopy

Raman spectroscopy measures the energy of inelastic photon scattering from the absorption of high intensity, monochromatic light, usually generated with a laser. This light can be ultraviolet, visible, or near infrared. Vibrational energies as well as rotational energies can be measured with this method. Photons are absorbed, exciting the molecules to a higher virtual energy state followed by relaxation and detection of photon emission at a higher (Stokes) or lower (Anti-Stokes) energy state then it had originated from. In order for this technique to work, molecules must be polarizable and the laser light must be

highly intense to generate detectable emission. Raman spectroscopy can identify and quantify the presence of CNTs using the defect ($\boldsymbol{I_D}$) and graphitic ($\boldsymbol{I_G}$) bands. The vibrational defect and graphitic modes measured for CNTs come from disorder and order in the sp^2-hybridized sidewall structure of CNTs. The ratio ($\boldsymbol{I_D/I_G}$) is often used to measure the defect level of CNTs, or the level of oxidation.[106, 107] For SWCNTs, the diameter can be determined from a vibrational mode called the radial breathing mode (RBM).[108] Unfortunately, sp^2 hybridized carbon from CNTs and from other sources cannot be distinguished from one another with Raman. This makes identification and quantification in mixtures limited. Furthermore, the detection limits are relatively high, on the order of 10^{-1} mg/L or mg/kg.[104]

1.4.4. Near Infrared Fluorescence Spectroscopy

Near infrared fluorescence spectroscopy (NIRF) measures photon emission from vibrational excited states at wavelengths ranging from 800 – 2500 nm. CNT samples are excited with a broadband near-IR source, or a laser source of one particular wavelength, and a complex spectrum of near-IR fluorescence bands is produced. For SWCNTs, near-IR bands are produced for different chiralities with the peak area proportional to the CNT concentration. This makes the method very powerful in terms of quantifying CNT concentration and chirality distribution.[109] However, aggregation can significantly quench the fluorescence of SWCNTs, and MWCNTs cannot be detected at all with this technique since the side-walls cause quenching. Thus, this technique is useful for analyzing SWCNTs, particularly when surfactants are used to prevent their aggregation or after extraction from complex matrices. NIRF has been shown to work in tandem with

extraction of SWCNTs from sediments.[62] The detection limits are between 10^{-3} and 10^{-2} mg/L or mg/kg, lower than those of UV/Vis and Raman spectroscopy.[104]

1.4.5. Thermal Methods

Thermogravimetric analysis (TGA) is the most commonly used method to study the decomposition of CNTs under controlled thermal conditions. It typically measures the change in mass of CNTs as a function of temperature; the TGA profile can then be used to estimate mass concentration of CNT and CNT purity. CNTs can usually be distinguished from natural water and media whose components degrade at lower temperatures. However, there may be some overlaps in the degradation events of CNTs and other contaminants (i.e. amorphous carbon, adsorbed solvent) that can make TGA data interpretation difficult. This can be improved by combining TGA with enhanced gas analyzers such as FTIR or MS. Furthermore, the effect of the matrix on CNT profiles is not always known.[104]

Other thermal methods such as total organic carbon (oxidizing all carbon in a sample to CO_2), TGA-MS (measuring byproducts of thermal degradation with MS), and thermal optical transmittance (using optical transmittance or reflectance to determine when the volatile organic carbon is removed, and converting remaining carbon to CH_4 for flame ionization detection) are all different variations of thermally detecting carbon. The ability to distinguish between different CNT types has not yet been systematically investigated. Extraction can also be used to lower detection limits and eliminate interference. TGA has the lowest detection limit of 10^1 mg/L or mg/kg with decreasing detection limits for more sophisticated techniques such as TGA-MS and TOT. So far, this

technique has shown substantial variation between different CNTs and requires further method development for complex environmental samples.[104]

Another thermal method is the microwave technique, which involves heating the CNT samples and measuring the increase in sample temperature as a function of heating. This increase in temperature is proportional to the concentration of CNTs. This method has a detection limit of 10^{-1} mg/L or mg/kg but has not been tested extensively for interference issues.[104]

1.4.6. Electron Microscopy

Electron microscopy can be used to image CNTs at the nanoscale and unambiguously identify the presence of CNTs in a given matrix. Transmission electron microscopy is the most common electron microscopy technique used to identify CNTs, as a result of the high resolution that can be used to distinguish CNT walls and image defect sites. Transmission electron microscopy makes use of a focused, high energy electron beam (~300 keV) aimed at a thin sample, with the transmitted electrons detected below the sample. Electrons that are scattered by the sample do not make it to the detector, and heavier elements allow less electron transmission to the detector than lighter elements due to a greater electron density. Thus, heavier elements show up darker in TEM images. Although TEM can be used to image individual atoms, this is not typically done for CNTs since the high energy required for the electron beam at this resolution can damage the CNT walls. CNTs are usually imaged for length measurements, structural integrity, and structural changes after functionalization. TEM is also used to count the number of CNT walls and measure the inner and outer CNT diameters.[110, 111]

TEM is not typically used for concentration determination in an environmental matrix. Known volumes of CNT samples have been ultracentrifuged onto filters, and counted in several areas from multiple TEM images. However, it becomes impractical to count a statistically relevant number of CNTs per area at the ng level expected to exist in environmental samples.[104]

1.4.7. Single-Particle ICP-MS

Single-particle ICP-MS (sp-ICP-MS) can be used to quantify CNT mass concentration and sometimes particle number in both simple and complex matrices. sp-ICP-MS makes use of residual metal catalysts from the CVD synthesis process to detect CNTs. A particular isotope of a metal particle can be counted as pulses of ions once a particle within an individual CNT makes its way through the plasma. In single-particle mode, each peak represents a pulse of metal ions that come from metal particles embedded within a CNT structure. This requires dilute samples of CNTs (200-800 ng/L) to prevent multiple CNTs from showing up in a single pulse. The correlation between particle number and CNT mass concentration can be determined using a calibration curve (Figure 1.2).[30] This is in contrast to traditional ICP-MS where CNTs would first be digested in concentrated acid to provide a constant stream of ions to the plasma. This method can be more challenging since CNTs take a lot of energy input and time to fully digest.[104]

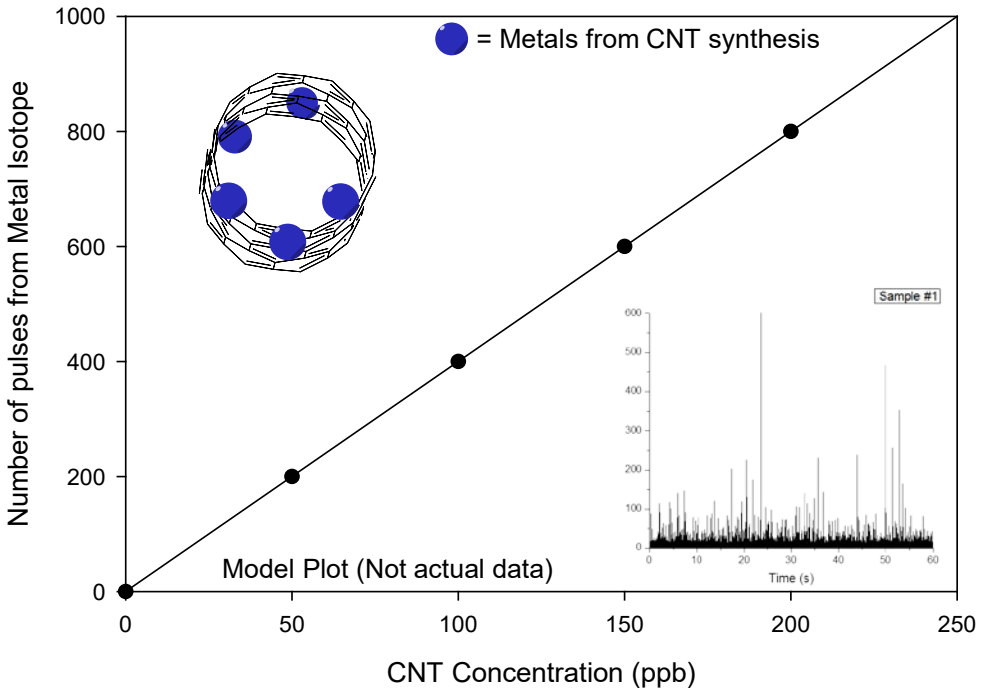

Figure 1.2. CNT detection using sp-ICP-MS. The trace metal catalysts from CNT synthesis (blue spheres within CNT) are used as a proxy for CNTs in this method. Known mass concentrations of CNTs are analyzed for residual metal counts to generate a calibration curve, which is then used to assay the concentration of CNTs in a matrix. An example of sp-ICP-MS data output is shown on the bottom right inset.

sp-ICP-MS is by far the most sensitive method for detection of CNTs, with detection limits at the low parts-per-trillion level. However, the CNT type has to be known, the metal nanoparticle has to be uncommon in the environment to prevent interference from the matrix, and it is challenging to ensure that CNT particles are individually dispersed and to ensure a pulse is the equivalent of only one CNT. Additionally, since the metal catalysts embedded in the CNTs vary in size and number, pulse height/intensity (counts) may vary from tube to tube. Metals such as Ni, Y, Co, and Mo have been successfully used to detect and quantify CNT concentration. Residual iron, however, has proven challenging to use as a proxy for CNT detection since an oxidized

argon isotope interferes with the major isotope of iron (^{56}Fe). This is problematic since many CNT types contain iron, and can be challenging to work around by detecting other, less abundant isotopes of iron.[30] One other disadvantage of sp-ICP-MS is that many types of CNTs made using arc-discharge and laser ablation do not typically contain metal nanoparticles. Nevertheless, this technique has significant advantages in terms of detection limits when the CNT type is known and contains an exotic trace metal catalyst. In this research, CNT release was measured from polymer nanocomposites using this method, which will be discussed in later sections.[30, 104]

1. 5. Polymers

Polymers are large molecules made up of smaller, repeating units called monomers.[112] Polymer chains composed of two or more different types of monomers are called copolymers and can be arranged in a random, alternating, or block configuration. The number of monomer units in a polymer is called the degree of polymerization. Polymers can be linear or branched, have covalent cross-linking between chains, and be packed in varying degrees of ordered to disordered configurations. These areas are called crystalline and amorphous regions, and both types of regions can exist in a polymeric material.[113, 114] Polymers can be broadly grouped into two categories: synthetic polymers and biopolymers which have feedstocks that originate from petroleum or by biological organisms, respectively. Both synthetic polymers and biopolymers are ubiquitous in society since they are used in construction, transportation, packaging, and consumer products. Biopolymers are found in the environment, organisms, and the human body in the form of polysaccharides, polypeptides, and polynucleotides.[112]

Four of the most common types of polymers are thermosets, elastomers, oriented polymers, and thermoplastics. Thermosetting polymers are cross-linked and cannot melt upon heating while elastomers are thermosets with rubber-like properties. This means that elastomers have all of the general properties of thermosets but can also be stretched and reverted back to their original shape. Elastomers tend to have a smaller degree of cross-linking, which allows them to crystallize upon stretching. However, the van der Waals forces in the crystalline form are not strong enough to hold the polymer together after the stretching force is removed. Some common thermosets include epoxy resins, polyurethanes, and polyester resins while some common elastomers include silicone and rubber (cis-polyisoprene). Oriented polymers are another class of polymers that can be stretched and packed together in a new, more ordered configuration.[113] One of the most commonly used classes of commercial polymers are thermoplastics, which can be repeatedly molded and shaped above their melting temperature. The word "plastics" is often used synonymously with "polymers," but plastics are synthetically derived thermoplastics, which are only one class of polymers. The low cost and ease of production has led to an increase in the use of thermoplastics in everyday life.

Since thermoplastics are one of the most commonly used polymers in consumer products, both synthetically and biologically derived thermoplastics was used in this research. Synthetically derived thermoplastics such as polyurethane, polyethylene, and polystyrene, are made from petroleum resources and make up the largest fraction of polymers used in consumer products.[112] Biologically derived polymers, or biopolymers used in products, are typically synthesized from pre-cursors produced by plants, fungi, and algae. These pre-cursors are more sustainable than petroleum resources and

sometimes more cost-effective which has led to their increasing use in consumer products.[115, 116] Some common biopolymers include cellulose, starch, and polyhydroxyalkanoates.[116-119] In many cases, bio-derived and synthetic polymers can have poor properties which sometimes makes them impractical for use in applications.

Thermoplastics are often hard at room temperature but can be molded when heated since the polymer chains can slip past one another; the temperature as which the chains can start slipping past each other is called the glass transition temperature. There are both crystalline and amorphous regions within a thermoplastic, and as the fraction of crystallinity (X_c) increases, thermoplastics tend to become denser, harder, and more resistant to thermal, chemical, and biological degradation.[114] Similar to impurities, the molecular weight of a polymer can affect the fraction of crystallinity since an increase in chain ends are considered an increase in the number of impurities that can disrupt the packed, ordered crystalline regions of the polymer. The fraction crystallinity is usually measured using the heat of fusion determined by differential scanning calorimetry, which is described in Chapter 2.[112]

Polymers are often modified for cost or to tailor their properties for a given application. Polymers and copolymers are sometimes combined to generate polymer blends, which is typically an approach to lower cost. Diluting one polymer with a cheaper polymer type can save money without affecting performance. In contrast to blends, composites contain two or more material components within a polymer matrix. Polymer composites are most commonly used to replace metals with materials of lighter weight but similar mechanical strength.[112] For example, the 787 Dreamliner has replaced 50% of the primary airplane structure with unidirectional carbon fiber/epoxy composites, which

has increased the fuel efficiency by 20% and extended the airplane's range. The use of carbon fiber/epoxy composites has also improved the tensile strength to 1,724 MPa compared to 600 MPa for aluminum alloys.[120] A substance that is added to a polymer matrix is called an additive which can be broadly divided into several categories: platicizers, stabilizers, colorants, flame retardants, and fillers.[112, 121] Plasticizers are often used to improve the flexibility of polymers by disrupting ordered regions across the polymer. These types of additives are sometimes controversial since they commonly consist of phthalates, which are known endocrine-disruptors. Bisphenol A (BPA) is one phthalate that is an excellent plasticizer but has been banned to improve product safety since BPA can leach from plastics and epoxy resins over time.[122] Stabilizers, such as amines, carbon black, and lead oxides, are used to slow degradation of polymers by sunlight and oxygen. Colorants and flame retardants are chemical additives that provide pigment and flame resistance, respectively, to products. Fillers, the focus in this thesis, are a second material component added to a polymer matrix to improve its properties.[112, 121] Fillers can take a variety of forms (e.g. fibers, spherical particles, and chemicals) with sizes as large as millimeters and as small as nanometers. The type of filler under investigation in this research are nanofillers, which have at least one dimension on the nanoscale from 1 - 100 nm. When nanofillers are incorporated into polymer matrices, the material is called a polymer nanocomposite (Scheme 1.2).[121, 123]

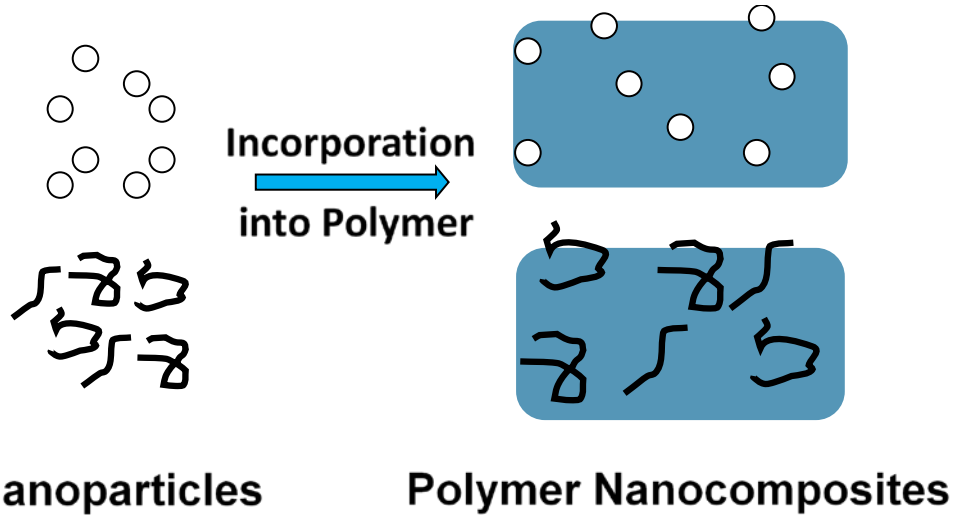

Scheme 1.2. Incorporation of nanofillers into polymer matrices to produce polymer nanocomposites.

1. 6. CNT/Polymer Nanocomposites

CNT/polymer nanocomposites (CNT/PNCs) are prepared to modify or improve the structural and functional properties of a polymer.[124-133] Structural properties such as tensile strength, toughness, and elastic (Young's) modulus can be improved using fibrous nanomaterials, such as nanocellulose, carbon nanofibers, and carbon nanotubes.[33, 125, 128-131, 134] These properties are defined by stress and strain: stress is the force applied per area while strain is the change in polymer length with respect to the original length during an applied stress. Stress and strain are measured with a universal tensile strength machine which measures the force per area (stress) as a material is stretched to specified distances (i.e. strained). Tensile strength is defined as the maximum stress applied to a material prior to fracture. Toughness is the amount of energy absorbed during fracture, or the area under the stress/strain curve. Young's modulus is the slope of the stress-strain curve during elastic deformation measured at a given length. The higher the Young's modulus,

the more stress needed to be applied to deform the polymer.[114] The tensile strength, toughness, and Young's modulus have all been shown to improve for various polymers after CNT incorporation into the polymer matrix.[33, 125, 128-131, 134] Other functional properties, such as electrical conductivity, light adsorption, flame retardancy, thermal stability, magnetic permeability, have also been improved or provided through the incorporation of carbon nanotubes.[135-138] Since carbon nanotubes can improve both the structural and functional properties of a polymer, they have become one of the most widely used nanoparticle fillers in consumer products. In fact, CNT production is estimated to be 380 ton/year (scaled to EU GDP) with the largest fraction of manufactured CNTs used for nanocomposite production. In general, CNTs are considered the third most produced nanomaterial (TiO_2 > ZnO > CNT > Ag > C_{60}) when materials that consist of both nano and larger particles are not included (e.g. iron, silicon, cerium and aluminum oxides).[6, 139]

Carbon nanotubes can improve the structural properties of a polymer without significantly increasing polymer weight. Thus, CNTs are used in sporting equipment such as tennis rackets, golf clubs, and baseball bats. This has also led to the use of CNTs in boat hulls, helicopter blades, and airplane hulls and wings.[33, 124, 140-144] In aerospace applications, incorporation of CNTs can enhance electrical conductivity, allowing for dissipation of electricity during lightning strikes, and EMI shielding for cables. Aligned CNTs have been used by Lockheed Martin for aerospace applications in defense but have not yet been prominently used in commercial aircraft.[120, 145] The use of CNTs in polymer composites has not yet reached that of carbon fibers, especially in aerospace applications and construction.[20] Carbon fibers (CF) are fibrallar sheets of graphenic carbon, stacked

either along the fiber axis or perpendicular to the axis, the latter CF type generally produced using CVD. 95% of commercially available carbon fibers are stacked parallel to the fiber axis and are derived from polyacrylonitrile (PAN) using electrospinning techniques followed by heat treatment to carbonize the fibers (>1000 °C, at least 92% C), and sometimes graphitization at even higher temperatures (2500 °C). Carbon fibers typically have aspect ratios greater than 1:100 (diameter/length) and diameters on the micron scale. Carbon fibers can also be prepared with diameters of 50-200 nm, and in this case, are called carbon nanofibers.[146, 147] Commercially available CFs can have a Young's modulus as high as 900 GPa, a tensile strength up to 6.4 GPa, and an elongation at break of 2.2%. In contrast, CNTs can have a Young's modulus as high as 1800 GPa, a tensile strength up to 150 GPa, and an elongation at break of 15%. However, when embedded into a polymer matrix, the higher mechanical strength of CNTs relative to CFs has not always translated to better improvement of the polymer properties by CNTs. This has been attributed to the difficulty in dispersing CNTs into polymers (especially longer CNTs which provide the best mechanical properties), debundling CNTs, aligning CNTs, generating strong interfacial interactions between the CNTs and the matrix, and purifying CNTs. As a result of these issues, CNTs often impart sub-optimal properties on a polymer matrix. Furthermore, the higher production costs of CNTs ($0.5 - $136/g for MWCNTs) relative to carbon fibers ($0.037- $1.8/g) combined with the challenges of CNT incorporation into polymer matrices has led to a lag in CNT/PNC production (2011 production costs).[20, 129] Nevertheless, the enhanced properties of CNTs relative to carbon fibers and the continuously improving technology for production of pure and long CNTs at a low cost indicates that their use in products will continue to increase.[129, 148]

CNTs are already incorporated into “Kevlar-like” backpacks, lightweight armor, headphone speaker diaphragms and spools of wire that are strong, durable, and electrically conductive.[33, 70] Functionally, CNT/PNCs are used as linings in fuel tanks and filters to dissipate charge such as in the Audi A4 and A5 models.[33, 149] They are also used for charge dissipation in electronic packaging materials and battery linings. Furthermore, CNTs have been commercially used in paints and coatings to reduce marine organism growth on boat hulls. In this configuration, CNTs provide a nanostructure underlayer to a silicone or fluoropolymer surface containing a low free energy of cell attachment, further limiting the anchoring of marine organisms such as barnacles to the nano-structured surface.[143, 150, 151]

In many commonly used plastics, such as polyethylene, polyethylene terephthalate, and polystyrene, the addition of CNTs can enhance polymer properties.[112] The majority of these types of polymers are synthetically derived from petroleum sources and are commonly used without added CNTs. However, addition of CNTs can enhance the already desirable properties of a polymer or make the polymer multifunctional.[33, 140, 152] CNTs have also been useful as additives in polymers that have some but not all of the properties required to make the polymer useable in a particular application. For example, synthetically derived poly-ε-caprolactone is ideal for use in the body but requires the inclusion of CNTs for improved mechanical strength and temporal stability in tissue scaffolding applications.[153-155] At the other end of the spectrum, the incorporation of CNTs can transform the properties of polymers whose nascent properties preclude their use in many products and applications.[116] Bio-derived polymers, in particular, often have physico-chemical properties such as low melting points, poor tensile strength, and

minimal conductivity, which prevents or limits their use in a range of applications.[115, 116] However, there is considerable interest in the manufacture and use of bio-polymers because of their low production costs that result from the minimal number of synthetic steps required and the use of renewable precursors that are derived from microorganisms, plants, and fungus.[115, 116] Even at low mass fractions, CNTs can dramatically improve the properties of these more cost-effective, bio-derived polymers.[116] For example, it has been shown that < 1% w/w MWCNTs can increase the stiffness of starch by 70%.[156] Furthermore, addition of only 0.8% w/w oxidized MWCNTs (O-MWCNTs) to chitosan, a bio-derived polymer used in food packaging and filtration, has been shown to improve the tensile modulus and strength by 93% and 99%, respectively.[157-160]

1. 7. Life Cycle of CNT/PNCs

The use of CNT/PNCs in consumer products has many advantages, but concern has arisen over the environmental impacts and human health and safety along the life cycle of these products. The life cycle includes manufacture, consumer use, disposal, and sometimes reuse.[161] During manufacture, worker exposure from aerosol generation during abrading, sanding, and cutting of CNT/PNCs has been considered. In general, when CNT/PNCs were exposed to a Taber abrader, minimal CNT release was observed from several different polymer matrices (e.g. epoxy, polyurethane, polyamides) while released particles containing embedded and exposed CNTs were prevalent.[4, 162-165] During manufacture, respiratory health is considered most at risk during compounding of CNT powders and polymers to generate dusts, treating CNT/PNCs during recycling processes, and uncontrolled incineration of the polymer matrix to release CNTs which require a much higher temperature to burn.[161, 162]

During consumer use, products are expected to be coated or in many cases carbon nanotubes will be buried within the polymer matrix. The main concern during consumer use is wear, which could lead to CNT exposure and potential release.[166] Design of CNT/PNCs to minimize CNT exposure is the main approach to protecting human health and safety at the use stage of the CNT/PNC life cycle.[73] Following consumer use, CNT/PNCs will be properly disposed of in landfills and incinerators or improperly disposed of in the environment. CNT/PNCs can end up in soils, surface waters, and sediments and CNT/PNC fragments may even make their way to waste water treatment plants (WWTP).[33, 62, 66] Many studies have provided a basic understanding of CNT behavior in the environment but most studies have not yet focused on the behavior of CNTs in a solid phase matrix.[167] Since one of the most important CNT applications involves their incorporation into polymers for commercial applications, the behavior of this nanocomposite material in the environment requires substantial investigation as well.[152, 168-170] However, limited information on the types of CNT/PNCs available in commerce has previously limited full investigation of CNT release scenarios. Since CNTs are now listed under the TCSA (as of 2013), better tracking of CNT/PNC products and research on CNT release from actual products on the market can be undertaken.[72, 73]

Once disposed of in the environment, CNT/PNCs can be subjected to aging (further wear), thermal degradation, weathering, photolysis, and biodegradation (Scheme 1.3).

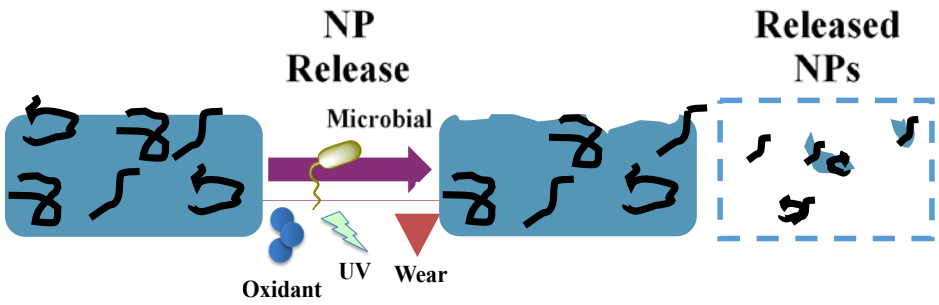

Scheme 1.3. Potential release pathways of CNTs from CNT/PNCs.

CNT/PNCs can undergo wear under any type of mechanical strain experienced in transport, compacting, and agitation.[161, 162] Thermal degradation can occur in incinerators and fires. CNTs require temperatures in excess of 800 °C to degrade, and in the case of incinerators and fires, this can be accomplished.[62, 171] As far as weathering, conditions such as acid rain, alkaline soil, and humidity can have an effect on the CNT/PNC transformation. Most importantly, UV-weathering in the presence of oxygen can break down polymer matrices to oxidized, smaller molecular weight polymer chains that can dissolve or be subjected to biodegradation.[62, 162] Photolysis of CNT/PNCs that include polystyrene, epoxy, polyurethane, and polyamides have been investigated using MWCNTs. In these studies, the polymer matrix was transformed by oxidation and chain scission. In all cases, CNT accumulation was observed at the CNT/PNC surface. Furthermore, mass loss inhibition was sometimes observed and CNT release tended to be minimal during photolysis.[162, 163, 172, 173]

1. 8. Microbial Interactions and Biodegradation of CNT/PNCs

CNT/PNCs are likely to encounter a wide variety of microorganisms in the environment**.** Microorganisms are present in landfills, surface waters, soils, sediments,

and wastewater treatment plants where plastic waste is commonly discarded following consumer use. Since disposal of CNT/PNCs at these sites is also inevitable, the interactions of microorganisms with CNT/PNCs as well as the transformation of CNT/PNCs by biodegradation warrants investigation. Polymer biodegradation is typically initiated by attachment of microbes to the surface, the proliferation of microbes at the surface to form communities called biofilms, and the release of extracellular enzymes from the biofilms to degrade the polymer substrate for use in microbial metabolism (Scheme 1.4).[117, 174-176] Most polymers are initially fragmented into shorter polymer chains by enzymes prior to being taken up and broken down further within the microorganism. Full biodegradation ultimately leads to the transformation of polymers to small molecular weight species such as carbon dioxide, methane, and water.[177]

Scheme 1.4. Three steps of microbial interactions with CNT/PNCs.

The effect of CNT fillers on the microbial transformation of polymers has not yet been studied. However, the cytotoxic effects of CNTs on microorganisms has been generally observed, except in a few cases.[28, 42-48, 86-88] Therefore, it is unclear if CNTs will be cytotoxic to microorganisms at the surface of CNT/PNCs and if CNTs will have an effect on the ability of microorganisms to biodegrade the polymer matrix. This has implications for the fate and exposure of the CNTs in the polymer matrix and the persistence of CNT/PNCs in the environment. The approach used in this study was to assess the initial interactions of microorganisms with CNT/PNC surfaces, biofilm formation on CNT/PNCs with different surface characteristics, and the effect of CNT incorporation on polymer biodegradation to evaluate the long term fate of these novel materials.

In order to first understand the effect of CNT/PNCs on a simple, model system, the gram-negative bacterium *Pseudomonas aeruginosa* was chosen. Single culture conditions are not necessarily representative of all types of microorganisms in the

environment or the synergistic ability of a microbial community to degrade a contaminant, but *P. aeruginosa* is ubiquitous in the environment and can provide a straightforward assessment of microorganism interactions with CNT/PNCs, growth on CNT/PNCs, and biodegradation of the CNT/PNC polymer matrix during this process.[178] The first stage of this study involved the preparation of CNT/PNCs with controlled CNT concentrations (0 – 10% w/w) at the polymer surface, characterization of these CNT/PNCs using SEM and a newly developed X-ray photoelectron spectroscopy technique (highlighted in Chapter 2), and exposing the CNT/PNCs for one hour to *Pseudomonas aeruginosa*, to determine the fraction of living and dead cells that attached to the surfaces using LIVE/DEAD viability staining coupled to confocal laser scanning microscopy (CLSM), which is further described in Chapter 3. The second stage of this study investigated biofilm development, or the proliferation of microbial communities on CNT/PNCs that accumulated CNTs at the surface, initially contained CNTs at the surface, and had a low and a high CNT loading. Lastly, the overall fate of the CNT/PNCs with regards to biodegradation, or the enzymatic degradation of the polymer matrix by microorganisms, was investigated in the presence of *P. aeruginosa* as well as mixed cultures.

Many synthetically and biologically derived polymers are biodegradable, or able to break down to smaller molecules and eventually CO_2 and water in the presence of microorganisms. These polymers tend to have poor properties that can be improved by adding a small mass fraction of CNTs. This is particularly true for both synthetic and bio-derived polymers that exhibit poor physico-chemical properties such as PCL, poly(vinyl alcohol) (PVOH), poly(butylene succinate) (PBS), poly(ethylene succinate) (PES),

starch, cellulose, and polyhydroxyalkanoates (PHA) which are known to biodegrade on the order of days to months.[116-119] Furthermore, polymers such as chitosan and polylactides (PLA) can biodegrade on a slower time scale or more rapidly when blended with more highly degradable polymers.[117, 179, 180] The chemical structures of a few biodegradable synthetic and bio-derived polymers are shown in Figure 1.3. Other polymers, are typically persistent with respect to biodegradation, but abiotic degradation by UV-weathering can facilitate polymer biodegradation over time by oxidation and chain scission to lower molecular weight species that are more metabolically accessible to microorganisms than the original polymer.[51, 52 181] Consequently, there is the potential for CNT exposure and release into the environment as a result of microbial degradation when many types of polymer nanocomposites are discarded at the end of consumer use.[112, 116, 118, 182] For this reason, two model polymers, one synthetic and one bio-derived, were chosen to investigate the transformation of CNT/PNCs in the environment. These polymer types were also chosen since they could biodegrade at different rates under all of the conditions studied, but were both able to biodegrade on an experimentally relevant time scale (days – months). This approach provided insight into the effect of CNTs on a polymer that was more persistent relative to a polymer that was more rapidly biodegradable, enabling some generalization to biodegradation of more persistent polymers in commercial use. The polymers chosen are described in Chapter 2.

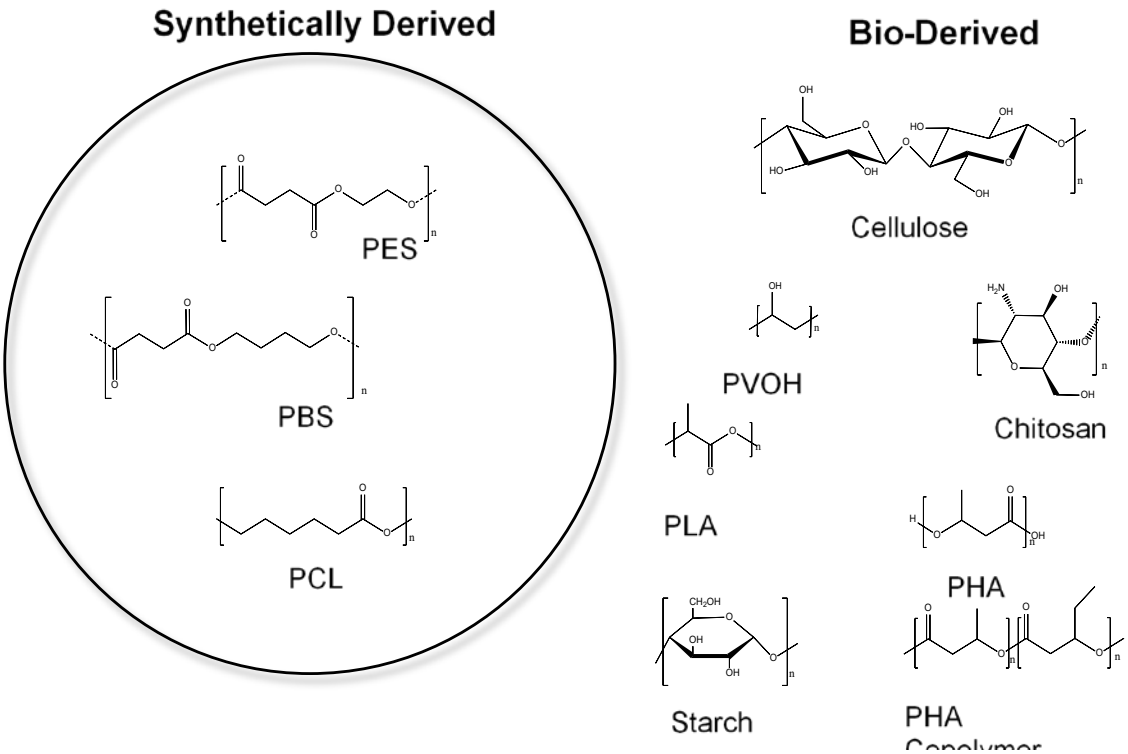

Figure 1.3. Chemical structures of biodegradable synthetic polymers and bio-derived polymers.

First, detailed understanding of CNT/PNC transformation was obtained under single culture conditions in the presence of *P. aeruginosa*. The initial microbial interactions and biofilm studies provided mechanistic insight into the biodegradation behavior of CNT/PNCs under these conditions. For greater environmental relevance, albeit with less control over the system, further investigation of CNT/PNC biodegradation was assessed under both aerobic and anaerobic mixed culture conditions. Primary effluent and digestor sludge from the Back River Wastewater treatment plant in Baltimore, MD were used as the aerobic and anaerobic mixed cultures, respectively. Since mixed culture conditions accelerated polymer degradation relative to single culture conditions, mixed cultures were used to evaluate the effect of polymer type on CNT/PNC

transformation. Overall, the effect of CNT additives on polymer biodegradation was studied for several reasons: to assess the risk of CNT exposure and release, determine whether CNT incorporation will change the persistence of polymers in the environment, and thereby provide guidelines for selection of an appropriate CNT/PNC type in a particular application. The overarching goal was to determine when, if ever, the benefits of using CNT additives in polymers during consumer use may be compromised by the ultimate fate of the CNT/PNC when it biodegrades in landfills, surface waters, and/or wastewater treatment plants.[33, 62, 66, 116, 183]

1. 9. References

1. Nano.gov, National Nanotechnology Initiative.
2. Berti, D.; Palazzo, G.; Editors, *Colloidal Foundations Of Nanoscience*. Elsevier B.V.: 2014; p 273 pp.
3. Hotze, E. M.; Phenrat, T.; Lowry, G. V., Nanoparticle aggregation: challenges to understanding transport and reactivity in the environment. *Journal of environmental quality* **2010,** *39*, (6), 1909-1924.
4. Golanski, L.; Guiot, A.; Pras, M.; Malarde, M.; Tardif, F., Release-ability of nano fillers from different nanomaterials (toward the acceptability of nanoproduct). *J. Nanopart. Res.* **2012,** *14*, (7), 962/1-962/9.
5. Handy, R. D.; Owen, R.; Valsami-Jones, E., The ecotoxicology of nanoparticles and nanomaterials: current status, knowledge gaps, challenges, and future needs. *Ecotoxicology* **2008,** *17*, (5), 315-325.
6. Keller, A. A.; McFerran, S.; Lazareva, A.; Suh, S., Global life cycle releases of engineered nanomaterials. *J. Nanopart. Res.* **2013,** *15*, (6), 1-17.
7. Roco, M. C., The long view of nanotechnology development: the National Nanotechnology Initiative at 10 years. *J. Nanopart. Res.* **2011,** *13*, (2), 427-445.
8. Dowling, A.; Clift, R.; Grobert, N.; Hutton, D.; Oliver, R.; O'neill, O.; Pethica, J.; Pidgeon, N.; Porritt, J.; Ryan, J., Nanoscience and nanotechnologies: opportunities and uncertainties. *London: The Royal Society & The Royal Academy of Engineering Report* **2004,** *61*, e64.
9. Bosman, A. W.; Janssen, H. M.; Meijer, E. W., About Dendrimers: Structure, Physical Properties, and Applications. *Chem. Rev. (Washington, D. C.)* **1999,** *99*, (7), 1665-1688.

10. Smijs, T. G.; Pavel, S., Titanium dioxide and zinc oxide nanoparticles in sunscreens: focus on their safety and effectiveness. *Nanotechnology, Science and Applications* **2011,** *4*, 95-112.
11. Pillai, K. V.; Gray, P. J.; Tien, C.-C.; Bleher, R.; Sung, L.-P.; Duncan, T. V., Environmental release of core–shell semiconductor nanocrystals from free-standing polymer nanocomposite films. *Environmental Science: Nano* **2016**.
12. Hamidi, M.; Azadi, A.; Rafiei, P., Hydrogel nanoparticles in drug delivery. *Adv. Drug Del. Rev.* **2008,** *60*, (15), 1638-1649.
13. Bourzac, K., Quantum dots go on display. *Nature* **2013,** *493*, (7432), 283.
14. Mitrano, D. M.; Barber, A.; Bednar, A.; Westerhoff, P.; Higgins, C. P.; Ranville, J. F., Silver nanoparticle characterization using single particle ICP-MS (SP-ICP-MS) and asymmetrical flow field flow fractionation ICP-MS (AF4-ICP-MS). *J. Anal. At. Spectrom.* **2012,** *27*, (7), 1131-1142.
15. Mauter, M. S.; Elimelech, M., Environmental Applications of Carbon-Based Nanomaterials. *Environ. Sci. Technol.* **2008,** *42*, (16), 5843-5859.
16. Sobkowicz, M. J.; Dorgan, J. R.; Gneshin, K. W.; Herring, A. M.; McKinnon, J. T., Renewable Cellulose Derived Carbon Nanospheres as Nucleating Agents for Polylactide and Polypropylene. *J. Polym. Environ.* **2008,** *16*, (2), 131-140.
17. Iijima, S., Helical microtubules of graphitic carbon. *Nature* **1991,** *354*.
18. Mauter, M. S.; Elimelech, M., Environmental applications of carbon-based nanomaterials. *Environ. Sci. Technol.* **2008,** *42*, (16), 5843-5859.
19. Abu Al-Rub, R. K.; Ashour, A. I.; Tyson, B. M., On the aspect ratio effect of multi-walled carbon nanotube reinforcements on the mechanical properties of cementitious nanocomposites. *Construction and Building Materials* **2012,** *35*, 647-655.
20. Loos, M. R.; Schulte, K., Is It Worth the Effort to Reinforce Polymers With Carbon Nanotubes? *Macromol. Theory Simul.* **2011,** *20*, (5), 350-362.
21. Wong, C.; Moon, K.-S.; Li, Y., *Nano-bio-electronic, photonic and MEMS packaging*. Springer: 2010.
22. Phan, C. H.; Jaafar, M.; Koh, Y. H., Mild functionalization of carbon nanotubes filled epoxy composites: Effect on electromagnetic interferences shielding effectiveness. *J. Appl. Polym. Sci.* **2015,** *132*, (38), n/a.
23. Saito, R.; Fujita, M.; Dresselhaus, G.; Dresselhaus, u. M., Electronic structure of chiral graphene tubules. *Appl. Phys. Lett.* **1992,** *60*, (18), 2204-2206.
24. White, C. T.; Todorov, T. N., Carbon nanotubes as long ballistic conductors. *Nature* **1998,** *393*, (6682), 240-242.
25. Arnold, M. S.; Green, A. A.; Hulvat, J. F.; Stupp, S. I.; Hersam, M. C., Sorting carbon nanotubes by electronic structure using density differentiation. *Nature nanotechnology* **2006,** *1*, (1), 60-65.
26. Green, A. A.; Hersam, M. C., Properties and Application of Double-Walled Carbon Nanotubes Sorted by Outer-Wall Electronic Type. *ACS Nano* **2011,** *5*, (2), 1459-1467.
27. Dai, H., Carbon nanotubes: opportunities and challenges. *Surf. Sci.* **2002,** *500*, (1–3), 218-241.

28. Thostenson, E. T.; Ren, Z.; Chou, T. W., Advances in the science and technology of carbon nanotubes and their composites: a review. *Compos. Sci. Technol.* **2001,** *61*, (13), 1899-1912.
29. Chen, C.-K.; Perry, W. L.; Xu, H.; Jiang, Y.; Phillips, J., Plasma torch production of macroscopic carbon nanotube structures. *Carbon* **2003,** *41*, (13), 2555-2560.
30. Reed, R. B.; Goodwin, D. G.; Marsh, K. L.; Capracotta, S. S.; Higgins, C. P.; Fairbrother, D. H.; Ranville, J. F., Detection of single walled carbon nanotubes by monitoring embedded metals. *Environ. Sci.: Processes Impacts* **2013,** *15*, (1), 204-213.
31. Saito, Y.; Nishikubo, K.; Kawabata, K.; Matsumoto, T., Carbon nanocapsules and single-layered nanotubes produced with platinum-group metals (Ru, Rh, Pd, Os, Ir, Pt) by arc discharge. *J. Appl. Phys.* **1996,** *80*, (5), 3062-3067.
32. Nikolaev, P.; Bronikowski, M. J.; Bradley, R. K.; Rohmund, F.; Colbert, D. T.; Smith, K.; Smalley, R. E., Gas-phase catalytic growth of single-walled carbon nanotubes from carbon monoxide. *Chem. Phys. Lett.* **1999,** *313*, (1), 91-97.
33. De, V. M. F. L.; Tawfick, S. H.; Baughman, R. H.; Hart, A. J., Carbon Nanotubes: Present and Future Commercial Applications. *Science* **2013,** *339*, (6119), 535-539.
34. Hiura, H.; Ebbesen, T. W.; Tanigaki, K., Opening and purification of carbon nanotubes in high yields. *Adv. Mater.* **1995,** *7*, (3), 275-276.
35. Smith, B.; Wepasnick, K.; Schrote, K. E.; Bertele, A. R.; Ball, W. P.; O'Melia, C.; Fairbrother, D. H., Colloidal Properties of Aqueous Suspensions of Acid-Treated, Multi-Walled Carbon Nanotubes. *Environ. Sci. Technol.* **2009,** *43*, (3), 819-825.
36. Smith, B.; Wepasnick, K.; Schrote, K. E.; Cho, H.-H.; Ball, W. P.; Fairbrother, D. H., Influence of Surface Oxides on the Colloidal Stability of Multi-Walled Carbon Nanotubes: A Structure-Property Relationship. *Langmuir* **2009,** *25*, (17), 9767-9776.
37. Wepasnick, K. A.; Smith, B. A.; Schrote, K. E.; Wilson, H. K.; Diegelmann, S. R.; Fairbrother, D. H., Surface and structural characterization of multi-walled carbon nanotubes following different oxidative treatments. *Carbon* **2010,** *49*, (1), 24-36.
38. Shao, L.; Tobias, G.; Salzmann, C. G.; Ballesteros, B.; Hong, S. Y.; Crossley, A.; Davis, B. G.; Green, M. L., Removal of amorphous carbon for the efficient sidewall functionalisation of single-walled carbon nanotubes. *Chemical Communications* **2007**, (47), 5090-5092.
39. Fogden, S.; Verdejo, R.; Cottam, B.; Shaffer, M., Purification of single walled carbon nanotubes: The problem with oxidation debris. *Chem. Phys. Lett.* **2008,** *460*, (1-3), 162-167.
40. Park, Y. S.; Choi, Y. C.; Kim, K. S.; Chung, D. C.; Bae, D. J.; An, K. H.; Lim, S. C.; Zhu, X. Y.; Lee, Y. H., High yield purification of multiwalled carbon nanotubes by selective oxidation during thermal annealing. *Carbon* **2001,** *39*, (5), 655-661.
41. Chen, Z.; Du, X.; Du, M.-H.; Rancken, C. D.; Cheng, H.-P.; Rinzler, A. G., Bulk Separative Enrichment in Metallic or Semiconducting Single-Walled Carbon Nanotubes. *Nano Lett.* **2003,** *3*, (9), 1245-1249.

42. Maeda, Y.; Kimura, S.; Kanda, M.; Hirashima, Y.; Hasegawa, T.; Wakahara, T.; Lian, Y.; Nakahodo, T.; Tsuchiya, T.; Akasaka, T.; Lu, J.; Zhang, X.; Gao, Z.; Yu, Y.; Nagase, S.; Kazaoui, S.; Minami, N.; Shimizu, T.; Tokumoto, H.; Saito, R., Large-Scale Separation of Metallic and Semiconducting Single-Walled Carbon Nanotubes. *J. Am. Chem. Soc.* **2005,** *127*, (29), 10287-10290.
43. Strano, M. S.; Dyke, C. A.; Usrey, M. L.; Barone, P. W.; Allen, M. J.; Shan, H.; Kittrell, C.; Hauge, R. H.; Tour, J. M.; Smalley, R. E., Electronic structure control of single-walled carbon nanotube functionalization. *Science (Washington, DC, U. S.)* **2003,** *301*, (5639), 1519-1522.
44. Zheng, M.; Jagota, A.; Strano, M. S.; Santos, A. P.; Barone, P.; Chou, S. G.; Diner, B. A.; Dresselhaus, M. S.; McLean, R. S.; Onoa, G. B.; Samsonidze, G. G.; Semke, E. D.; Usrey, M.; Walls, D. J., Structure-Based Carbon Nanotube Sorting by Sequence-Dependent DNA Assembly. *Science (Washington, DC, U. S.)* **2003,** *302*, (5650), 1545-1548.
45. Chen, K. L.; Smith, B. A.; Ball, W. P.; Fairbrother, D. H., Assessing the colloidal properties of engineered nanoparticles in water: case studies from fullerene C60 nanoparticles and carbon nanotubes. *Environmental Chemistry* **2010,** *7*, (1), 10-27.
46. Banerjee, S.; Wong, S. S., Rational sidewall functionalization and purification of single-walled carbon nanotubes by solution phase ozonolysis. *J. Phys. Chem. B* **2002,** *106*, 12144-12151.
47. Datsyuk, V.; Kalyva, M.; Papagelis, L.; Parthenios, J.; Tasis, D.; Siokou, A., Chemical oxidation of multiwalled carbon nanotubes. *Carbon* **2008,** *46*, 833-840.
48. Li, M.; Boggs, M.; Beebe, T. P.; Huang, C. P., Oxidation of single-walled carbon nanotubes in dilute aqueous solutions by ozone as affected by ultrasound. *Carbon* **2008,** *46*, 466-475.
49. Rosca, I. D.; Watari, F.; Uo, M.; Akasak, T., Oxidation of multiwalled carbon nanotubes by nitric acid. *Carbon* **2005,** *43*, 3124-3131.
50. Savage, T.; Bhattacharya, S.; Sadanadan, B.; Gaillard, J.; Tritt, T. M.; Sun, Y. P.; Wu, Y.; Naya, S.; Marzari, N.; Ajayan, P. M.; Rao, A. M., Photoinduced oxidation of carbon nanotubes. *J. Phys.: Condens. Matter* **2003,** *15*, 5915-5921.
51. Hou, W.-C.; BeigzadehMilani, S.; Jafvert, C. T.; Zepp, R. G., Photoreactivity of Unfunctionalized Single-Wall Carbon Nanotubes Involving Hydroxyl Radical: Chiral Dependency and Surface Coating Effect. *Environ. Sci. Technol.* **2014,** *48*, (7), 3875-3882.
52. Qu, X.; Alvarez, P. J.; Li, Q., Photochemical Transformation of Carboxylated Multiwalled Carbon Nanotubes: Role of Reactive Oxygen Species. *Environ. Sci. Technol.* **2013,** *47*, (24), 14080-14088.
53. Wepasnick, K. A.; Smith, B. A.; Schrote, K. E.; Wilson, H. K.; Diegelmann, S. R.; Fairbrother, D. H., Surface and structural characterization of multi-walled carbon nanotubes following different oxidative treatments. *Carbon* **2011,** *49*, (1), 24-36.
54. Dementev, N.; Feng, X.; Borguet, E., Fluorescence Labeling and Quantification of Oxygen-Containing Functionalities on the Surface of Single-Walled Carbon Nanotubes. *Langmuir* **2009,** *25*, (13), 7573-7577.

55. Dementev, N.; Ronca, R.; Borguet, E., Oxygen-containing functionalities on the surface of multi-walled carbon nanotubes quantitatively determined by fluorescent labeling. *Appl. Surf. Sci.* **2012,** *258*, (24), 10185-10190.
56. Gong, H.; Kim, S.-T.; Lee, J. D.; Yim, S., Simple quantification of surface carboxylic acids on chemically oxidized multi-walled carbon nanotubes. *Applied Surface Science* **2013,** *266*, 219-224.
57. González-Guerrero, A. B.; Mendoza, E.; Pellicer, E.; Alsina, F.; Fernández-Sánchez, C.; Lechuga, L. M., Discriminating the carboxylic groups from the total acidic sites in oxidized multi-wall carbon nanotubes by means of acid–base titration. *Chemical Physics Letters* **2008,** *462*, (4–6), 256-259.
58. Hu, H.; Bhowmik, P.; Zhao, B.; Hamon, M. A.; Itkis, M. E.; Haddon, R. C., Determination of the acidic sites of purified single-walled carbon nanotubes by acid–base titration. *Chemical Physics Letters* **2001,** *345*, (1–2), 25-28.
59. Kim, K.; Zhu, P.; Li, N.; Ma, X.; Chen, Y., Characterization of oxygen containing functional groups on carbon materials with oxygen K-edge X-ray absorption near edge structure spectroscopy. *Carbon* **2011,** *49*, (5), 1745-1751.
60. NNI 2011 National Nanotechnology Innitiative: http://www.nano.gov/sites/default/files/pub_resource/nni_2011_ehs_research_strategy.pdf.
61. Maynard, A. D.; Aitken, R. J.; Butz, T.; Colvin, V.; Donaldson, K.; Oberdorster, G.; Philbert, M. A.; Ryan, J.; Seaton, A.; Stone, V.; Tinkle, S. S.; Tran, L.; Walker, N. J.; Warheit, D. B., Safe handling of nanotechnology. *Nature* **2006,** *444*, (7117), 267-269.
62. Petersen, E. J.; Zhang, L. W.; Mattison, N. T.; O'Carroll, D. M.; Whelton, A. J.; Uddin, N.; Nguyen, T.; Huang, Q. G.; Henry, T. B.; Holbrook, R. D.; Chen, K. L., Potential release pathways, environmental fate, and ecological risks of carbon nanotubes. *Environ. Sci. Technol.* **2011,** *45*, (23), 9837-9856.
63. Pacurari, M.; Castranova, V.; Vallyathan, V., Single-and multi-wall carbon nanotubes versus asbestos: are the carbon nanotubes a new health risk to humans? *J. Toxicol. Environ. Health, A* **2010,** *73*, (5-6), 378-395.
64. Som, C.; Wick, P.; Krug, H.; Nowack, B., Environmental and health effects of nanomaterials in nanotextiles and fac¸ade coatings. *Environ. Int.* **2011,** *37*, (6), 1131-1142.
65. Jaisi, D. P.; Saleh, N. B.; Blake, R. E.; Elimelech, M., Transport of single-walled carbon nanotubes in porous media: filtration mechanisms and reversibility. *Environ. Sci. Technol.* **2008,** *42*, (22), 8317-8323.
66. Gottschalk, F.; Nowack, B., The release of engineered nanomaterials to the environment. *J. Environ. Monit.* **2011,** *13*, (5), 1145-1155.
67. Luanpitpong, S.; Wang, L.; Davidson, D. C.; Riedel, H.; Rojanasakul, Y., Carcinogenic potential of high aspect ratio carbon nanomaterials. *Environmental Science: Nano* **2016**.
68. Poland, C. A.; Duffin, R.; Kinloch, I.; Maynard, A.; Wallace, W. A.; Seaton, A.; Stone, V.; Brown, S.; MacNee, W.; Donaldson, K., Carbon nanotubes introduced into the abdominal cavity of mice show asbestos-like pathogenicity in a pilot study. *Nature nanotechnology* **2008,** *3*, (7), 423-428.

69. Huang, S.; Cai, X.; Liu, J., Growth of Millimeter-Long and Horizontally Aligned Single-Walled Carbon Nanotubes on Flat Substrates. *J. Am. Chem. Soc.* **2003,** *125*, (19), 5636-5637.
70. Nanocomp. Technologies, I. Products. http://www.nanocomptech.com/nanocomp-technologies-products
71. SAFENANO, Safe Handling.
72. Inc., N., Engineering Controls. **2008-2013**.
73. Godwin, H.; Nameth, C.; Avery, D.; Bergeson, L. L.; Bernard, D.; Beryt, E.; Boyes, W.; Brown, S.; Clippinger, A. J.; Cohen, Y.; Doa, M.; Hendren, C. O.; Holden, P.; Houck, K.; Kane, A. B.; Klaessig, F.; Kodas, T.; Landsiedel, R.; Lynch, I.; Malloy, T.; Miller, M. B.; Muller, J.; Oberdorster, G.; Petersen, E. J.; Pleus, R. C.; Sayre, P.; Stone, V.; Sullivan, K. M.; Tentschert, J.; Wallis, P.; Nel, A. E., Nanomaterial Categorization for Assessing Risk Potential To Facilitate Regulatory Decision-Making. *ACS Nano* **2015,** *9*, (4), 3409-3417.
74. Rodrigues, D. F.; Elimelech, M., Toxic effects of single-walled carbon nanotubes in the development of *E. coli* biofilm. *Environ. Sci. Technol.* **2010,** *44*, (12), 4583-4589.
75. Kang, S.; Herzberg, M.; Rodrigues, D. F.; Elimelech, M., Antibacterial effects of carbon nanotubes: Size does matter. *Langmuir* **2008,** *24*, (13), 6409-6413.
76. Kang, S.; Pinault, M.; Pfefferle, L. D.; Elimelech, M., Single-walled carbon nanotubes exhibit strong antimicrobial activity. *Langmuir* **2007,** *23*, (17), 8670-8673.
77. Liu, S.; Wei, L.; Hao, L.; Fang, N.; Chang, M. W.; Xu, R.; Yang, Y.; Chen, Y., Sharper and faster "nano darts" kill more bacteria: a study of antibacterial activity of individually dispersed pristine single-walled carbon nanotube. *Acs Nano* **2009,** *3*, (12), 3891-3902.
78. Alpatova, A. L.; Shan, W. Q.; Babica, P.; Upham, B. L.; Rogensues, A. R.; Masten, S. J.; Drown, E.; Mohanty, A. K.; Alocilja, E. C.; Tarabara, V. V., Single-walled carbon nanotubes dispersed in aqueous media via non-covalent functionalization: Effect of dispersant on the stability, cytotoxicity, and epigenetic toxicity of nanotube suspensions. *Water Res.* **2010,** *44*, (2), 505-520.
79. Ahmed, F.; Santos, C. M.; Vergara, R. A. M. V.; Tria, M. C. R.; Advincula, R.; Rodrigues, D. F., Antimicrobial applications of electroactive PVK-SWNT nanocomposites. *Environ. Sci. Technol.* **2012,** *46*, (3), 1804-1810.
80. Arias, L. R.; Yang, L., Inactivation of Bacterial Pathogens by Carbon Nanotubes in Suspensions. *Langmuir* **2009,** *25*, (5), 3003-3012.
81. Aslan, S.; Loebick, C. Z.; Kang, S.; Elimelech, M.; Pfefferle, L. D.; Van, T. P. R., Antimicrobial biomaterials based on carbon nanotubes dispersed in poly(lactic-co-glycolic acid). *Nanoscale* **2010,** *2*, (9), 1789-1794.
82. Vecitis, C. D.; Zodrow, K. R.; Kang, S.; Elimelech, M., Electronic-Structure-Dependent Bacterial Cytotoxicity of Single-Walled Carbon Nanotubes. *ACS Nano* **2010,** *4*, (9), 5471-5479.
83. Pasquini, L. M.; Hashmi, S. M.; Sommer, T. J.; Elimelech, M.; Zimmerman, J. B., Impact of surface functionalization on bacterial cytotoxicity of single-walled carbon nanotubes. *Environ. Sci. Technol.* **2012,** *46*, (11), 6297-6305.

84. Pasquini, L. M.; Sekol, R. C.; Taylor, A. D.; Pfefferle, L. D.; Zimmerman, J. B., Realizing Comparable Oxidative and Cytotoxic Potential of Single- and Multiwalled Carbon Nanotubes through Annealing. *Environ. Sci. Technol.* **2013,** *47*, (15), 8775-8783.
85. Yang, C.; Mamouni, J.; Tang, Y.; Yang, L., Antimicrobial Activity of Single-Walled Carbon Nanotubes: Length Effect. *Langmuir* **2010,** *26*, (20), 16013-16019.
86. Qi, X.; Poernomo, G.; Wang, K.; Chen, Y.; Chan-Park, M. B.; Xu, R.; Chang, M. W., Covalent immobilization of nisin on multi-walled carbon nanotubes: superior antimicrobial and anti-biofilm properties. *Nanoscale 3*, (4), 1874-1880.
87. Woerle-Knirsch, J. M.; Pulskamp, K.; Krug, H. F., Oops They Did It Again! Carbon Nanotubes Hoax Scientists in Viability Assays. *Nano Lett.* **2006,** *6*, (6), 1261-1268.
88. Pantanella, F.; Berlutti, F.; Passeri, D.; Sordi, D.; Frioni, A.; Natalizi, T.; Terranova, M. L.; Rossi, M.; Valenti, P., Quantitative evaluation of bacteria adherent and in biofilm on single-wall carbon nanotube-coated surfaces. *Interdiscipl. Perspect. Infect. Dis.* **2011,** *2011*, 1-9.
89. Hussain, M.; Kabir, M.; Sood, A., On the cytotoxicity of carbon nanotubes. *Curr. Sci.* **2009,** *96*, (5), 664-673.
90. Chen, C.-Y.; Jafvert, C. T., Photoreactivity of carboxylated single-walled carbon nanotubes in sunlight: reactive oxygen species production in water. *Environ. Sci. Technol.* **2010,** *44*, (17), 6674-6679.
91. Bitter, J. L.; Yang, J.; Milani, S. B.; Jafvert, C. T.; Fairbrother, D. H., Transformations of oxidized multiwalled carbon nanotubes exposed to UVC (254 nm) irradiation. *Environmental Science: Nano* **2014,** *1*, (4), 324-337.
92. Zhang, L.; Petersen, E. J.; Habteselassie, M. Y.; Mao, L.; Huang, Q., Degradation of multiwall carbon nanotubes by bacteria. *Environ. Pollut. (Oxford, U. K.)* **2013,** *181*, 335-339.
93. Bianco, A.; Kostarelos, K.; Prato, M., Making carbon nanotubes biocompatible and biodegradable. *Chem. Commun.* **2011,** *47*, (37), 10182-10188.
94. Allen, B. L.; Kotchey, G. P.; Chen, Y. N.; Yanamala, N. V. K.; Klein-Seetharaman, J.; Kahan, V. E.; Star, A., Mechanistic Investigations of horseradish peroxidase-catalyzed degradation of single-walled carbon nanotubes. *J. Am. Chem. Soc.* **2009,** *131*, 17194-17205.
95. Russier, J.; Ménard-Moyon, C.; Venturelli, E.; Gravel, E.; Marcolongo, G.; Meneghetti, M.; Doris, E.; Bianco, A., Oxidative biodegradation of single-and multi-walled carbon nanotubes. *Nanoscale* **2011,** *3*, (3), 893-896.
96. Smith, B.; Wepasnick, K.; Schrote, K. E.; Cho, H.-H.; Ball, W. P.; Fairbrother, D. H., Influence of Surface Oxides on the Colloidal Stability of Multi-walled Carbon Nanotubes: A Structure-Property Relationship *Langmuir* **2009,** *25*, (17), 9767-9776.
97. Smith, B.; Yang, J.; Bitter, J. L.; Ball, W. P.; Fairbrother, D. H., Influence of Surface Oxygen on the Interactions of Carbon Nanotubes with Natural Organic Matter. *Environmental Science & Technology* **2012,** *46*, (23), 12839-12847.

98. Edgington, A. J.; Roberts, A. P.; Taylor, L. M.; Alloy, M. M.; Reppert, J.; Rao, A. M.; Mao, J.; Klaine, S. J., The influence of natural organic matter on the toxicity of multiwalled carbon nanotubes. *Environ. Toxicol. Chem.* **2010,** *29*, (11), 2511-2518.
99. Yang, J.; Bitter, J. L.; Smith, B. A.; Fairbrother, D. H.; Ball, W. P., Transport of oxidized multi-walled carbon nanotubes through silica based porous media: Influences of aquatic chemistry, surface chemistry, and natural organic matter. *Environ. Sci. Technol.* **2013,** *47*, (24), 14034-14043.
100. Yi, P.; Chen, K. L., Influence of surface oxidation on the aggregation and deposition kinetics of multiwalled carbon nanotubes in monovalent and divalent electrolytes. *Langmuir* **2011,** *27*, (7), 3588-3599.
101. Cho, H.-H.; Smith, B. A.; Wnuk, J. D.; Fairbrother, D. H.; Ball, W. P., Influence of surface oxides on the adsorption of naphthalene onto multiwalled carbon nanotubes. *Environ. Sci. Technol.* **2008,** *42*, (8), 2899-2905.
102. Plata, D. L.; Hart, A. J.; Reddy, C. M.; Gschwend, P. M., Early evaluation of potential environmental impacts of carbon nanotube synthesis by chemical vapor deposition. *Environ. Sci. Technol.* **2009,** *43*, (21), 8367-8373.
103. Cho, H.-H.; Wepasnick, K.; Smith, B. A.; Bangash, F. K.; Fairbrother, D. H.; Ball, W. P., Sorption of Aqueous Zn[II] and Cd[II] by Multiwall Carbon Nanotubes: The Relative Roles of Oxygen-Containing Functional Groups and Graphenic Carbon. *Langmuir* **2010,** *26*, (2), 967-981.
104. Petersen, E. J.; Flores-Cervantes, D. X.; Bucheli, T. D.; Elliott, L. C. C.; Fagan, J. A.; Gogos, A.; Hanna, S.; Kägi, R.; Mansfield, E.; Bustos, A. R. M.; Plata, D. L.; Reipa, V.; Westerhoff, P.; Winchester, M. R., Quantification of Carbon Nanotubes in Environmental Matrices: Current Capabilities, Case Studies, and Future Prospects. *Environ. Sci. Technol.* **2016,** *50*, (9), 4587-4605.
105. Skoog, D. A. H., F. J.; Nieman, T. A., *Principles of Instrumental Analysis*. Philadelphia, 1998; Vol. 5th ed.
106. Schönfelder, R.; Avilés, F.; Bachmatiuk, A.; Cauich-Rodriguez, J.; Knupfer, M.; Büchner, B.; Rümmeli, M., On the merits of Raman spectroscopy and thermogravimetric analysis to asses carbon nanotube structural modifications. *Appl. Phys. A* **2012,** *106*, (4), 843-852.
107. Kim, U. J.; Furtado, C. A.; Liu, X. M.; Chen, G. G.; Eklund, P. C., Raman and IR spectroscopy of chemically processed single-walled carbon nanotubes. *J. Am. Chem. Soc.* **2005,** *127*, (44), 15437-15445.
108. Rao, A. M.; Chen, J.; Richter, E.; Schlecht, U.; Eklund, P.; Haddon, R.; Venkateswaran, U.; Kwon, Y.-K.; Tomanek, D., Effect of van der Waals interactions on the Raman modes in single walled carbon nanotubes. *Phys. Rev. Lett.* **2001,** *86*, (17), 3895.
109. Schierz, A.; Parks, A. N.; Washburn, K. M.; Chandler, G. T.; Ferguson, P. L., Characterization and quantitative analysis of single-walled carbon nanotubes in the aquatic environment using near-infrared fluorescence spectroscopy. *Environ. Sci. Technol.* **2012,** *46*, (22), 12262-12271.
110. Čech, J.; Kalbáč, M.; Curran, S.; Zhang, D.; Dettlaff-Weglikowska, U.; Dunsch, L.; Yang, S.; Roth, S., HRTEM and EELS investigation of functionalized carbon

nanotubes. *Physica E: Low-dimensional Systems and Nanostructures* **2007,** *37*, (1), 109-114.
111. Wepasnick, K. A.; Smith, B. A.; Bitter, J. L.; Fairbrother, D. H., Chemical and structural characterization of carbon nanotube surfaces. *Anal. Bioanal. Chem.* **2010,** *396*, (3), 1003-1014.
112. Stuart, B. H., *Polymer analysis*. John Wiley & Sons: 2008; Vol. 30.
113. Bruice, P. Y., *Organic chemistry*. Pearson: 2016.
114. Hiemenz, P. C.; Lodge, T. P., *Polymer chemistry*. CRC press: 2007.
115. Posen, I. D.; Jaramillo, P.; Griffin, W. M., Uncertainty in the Life Cycle Greenhouse Gas Emissions from U.S. Production of Three Biobased Polymer Families. *Environ. Sci. Technol.* **2016,** *50*, (6), 2846-2858.
116. Mittal, V., *Nanocomposites with Biodegradable Polymers: Synthesis, Properties, and Future Perspectives*. Oxford University Press: 2011.
117. Tokiwa, Y.; Calabia, B. P.; Ugwu, C. U.; Alba, S., Biodegradability of Plastics. *International Journal of Molecular Sciences* **2009,** *10*, (9), 3722-3742.
118. Luckachan, G. E.; Pillai, C. K. S., Biodegradable Polymers-A Review on Recent Trends and Emerging Perspectives. *J. Polym. Environ.* **2011,** *19*, (3), 637-676.
119. R, P.; Doble, M., Biodegradation of polymers. *Indian J. Biotechnol.* **2005,** *4*, 186-193.
120. Lu, B., The Boeing 787 Dreamliner Designing an Aircraft for the Future. *Journal of Young Investigators, ISSN: 1539* **2010,** *4026*, 34.
121. Zaman, I.; Manshoor, B.; Khalid, A.; Araby, S., From clay to graphene for polymer nanocomposites-a survey. *J. Polym. Res.* **2014,** *21*, (5), 1-11.
122. Erler, C.; Novak, J., Bisphenol a exposure: human risk and health policy. *Journal of pediatric nursing* **2010,** *25*, (5), 400-407.
123. Kumar, A. P.; Depan, D.; Tomer, N. S.; Singh, R. P., Nanoscale particles for polymer degradation and stabilization-Trends and future perspectives. *Prog. Polym. Sci.* **2009,** *34*, (6), 479-515.
124. Du, J.-H.; Bai, J.; Cheng, H. M., The present status and key problems of carbon nanotube based polymer composites. *Express Polymer Letters* **2007,** *5*, 253-272.
125. Ajayan, P. M.; Schadler, L. S.; Giannaris, C.; Rubio, A., Single-walled carbon nanotube-polymer composites: Strength and weakness. *Adv. Mater.* **2000,** *12*, (10), 750-753.
126. Allaoui, A.; Bai, S.; Cheng, H. M.; Bai, J. B., Mechanical and electrical properties of a MWNT/epoxy composite. *Compos. Sci. Technol.* **2002,** *62*, 1993-1998.
127. Andrews, R.; Jacques, D.; Minot, M.; Rantell, T., Fabrication of carbon multiwall nanotube/polymer composites by shear mixing. *Macromol. Mater. Eng.* **2002,** *287*, (6), 395-403.
128. Baughman, R. H.; Zakhidov, A. A.; de Heer, W. A., Carbon nanotubes - the route toward applications. *Science* **2002,** *297*, (5582), 787-792.
129. Coleman, J. N.; Khan, U.; Blau, W. J.; Gun'ko, Y. K., Small but strong: A review of the mechanical properties of carbon nanotube-polymer composites. *Carbon* **2006,** *44*, (9), 1624-1652.
130. Lau, K. T., Interfacial bonding characteristics of nanotube/polymer composites. *Chem. Phys. Lett.* **2003,** *370*, (3-4), 399-405.

131. Lau, K. T.; Hui, D., Effectiveness of using carbon nanotubes as nano-reinforcements for advanced composite structures. *Carbon* **2002,** *40*, (9), 1605-1606.
132. Martin, C. A.; Sandler, J. K. W.; Shaffer, M. S. P.; Schwarz, M. K.; Bauhofer, W.; Schulte, K.; Windle, A. H., Formation of percolating networks in multi-wall carbon-nanotube-epoxy composites. *Compos. Sci. Technol.* **2004,** *64*, (15), 2309-2316.
133. Sandler, J. K. W.; Kirk, J. E.; Kinloch, I. A.; Shaffer, M. S. P.; Windle, A. H., Ultra-low electrical percolation threshold in carbon-nanotube-epoxy composites. *Polymer* **2003,** *44*, (19), 5893-5899.
134. Rahmat, M.; Das, K.; Hubert, P., Interaction stresses in carbon nanotube-polymer nanocomposites. *ACS Appl. Mater. Interfaces* **2011,** *3*, (9), 3425-3431.
135. Lu, D. D.; Li, Y. G.; Wong, C. P., Recent advances in nano-conductive adhesives. *J. Adhes. Sci. Technol.* **2008,** *22*, (8-9), 815-834.
136. Li, J.; Lumpp, J. K.; Andrews, R.; Jacques, D., Aspect ratio and loading effects of multiwall carbon nanotubes in epoxy for electrically conductive adhesives. *J. Adhes. Sci. Technol.* **2008,** *22*, (14), 1659-1671.
137. Paik, K. W.; Han, S. H., A study on B-stage CNT/epoxy composite films for electronic packaging applications. *Pricm 7, Pts 1-3* **2010,** *654-656*, 2755-2758.
138. Makarova, T. L.; Zakharchuk, I.; Geydt, P.; Lahderanta, E.; Komlev, A. A.; Zyrianova, A. A.; Lyubchyk, A.; Kanygin, M. A.; Sedelnikova, O. V.; Kurenya, A. G.; Bulusheva, L. G.; Okotrub, A. V., Assessing carbon nanotube arrangement in polystyrene matrix by magnetic susceptibility measurements. *Carbon* **2016,** *96*, 1077-1083.
139. Nowack, B.; Bornhöft, N.; Ding, Y.; Riediker, M.; Jiménez, A. S.; Sun, T.; van Tongeren, M.; Wohlleben, W., The Flows of Engineered Nanomaterials from Production, Use, and Disposal to the Environment. **2015**.
140. Moniruzzaman, M.; Winey, K. I., Polymer nanocomposites containing carbon nanotubes. *Macromolecules* **2006,** *39*, (16), 5194-5205.
141. Sahoo, N. G.; Rana, S.; Cho, J. W.; Li, L.; Chan, S. H., Polymer nanocomposites based on functionalized carbon nanotubes. *Prog. Polym. Sci.* **2010,** *35*, (7), 837-867.
142. Harrison, B. S.; Atala, A., Carbon nanotube applications for tissue engineering. *Biomaterials* **2007,** *28*, (2), 344-353.
143. Nanocyl Biocyl. http://www.nanocyl.com/kr/Products-Solutions/Products/BIOCYL.
144. Nanocyl Carbon nanotube applications: fuel system components: http://www.nanocyl.com/Products-Solutions/Sectors/Automotive/Fuel-System-Components.
145. Corporation, L. M., Infused Carbon Nanostructures, Manufacturing Solutions for Next-Generation Products. In Bethesda, MD, 2013.
146. Feng, L.; Xie, N.; Zhong, J., Carbon nanofibers and their composites: a review of synthesizing, properties and applications. *Materials* **2014,** *7*, (5), 3919-3945, 27.
147. Endo, M.; Iijima, S.; Dresselhaus, M. S., *Carbon nanotubes*. Elsevier: 2013.

148. Wang, X.; Yong, Z.; Li, Q.; Bradford, P. D.; Liu, W.; Tucker, D. S.; Cai, W.; Wang, H.; Yuan, F.-G.; Zhu, Y., Ultrastrong, stiff and multifunctional carbon nanotube composites. *Materials Research Letters* **2013,** *1*, (1), 19-25.
149. BASF Electrically conductive BASF plastic Ultraform with nanotubes being used by Bosch. http://worldaccount.basf.com/wa/plasticsAP~ja_JP/portal/show/common/plasticsportal_news/2009/09_176?doc_lang=en_GB
150. Cao, S.; Wang, J.; Chen, H.; Chen, D., Progress of marine biofouling and antifouling technologies. *Chin. Sci. Bull.* **2011,** *56*, (7), 598-612.
151. Krishnan, S.; Weinman, C. J.; Ober, C. K., Advances in polymers for anti-biofouling surfaces. *J. Mater. Chem.* **2008,** *18*, (29), 3405-3413.
152. McClory, C.; Chin, S. J.; McNally, T., Polymer/Carbon Nanotube Composites. *Aust. J. Chem.* **2009,** *62*, (8), 762-785.
153. Gupta, A.; Woods, M. D.; Illingworth, K. D.; Niemeier, R.; Schafer, I.; Cady, C.; Filip, P.; El-Amin, S. F., Single walled carbon nanotube composites for bone tissue engineering. *J. Orth. Res.* **2013,** *31*, (9), 1374-1381.
154. Pan, L.; Pei, X.; He, R.; Wan, Q.; Wang, J., Multiwall carbon nanotubes/polycaprolactone composites for bone tissue engineering application. *Colloids Surf., B* **2012,** *93*, 226-234.
155. Mattioli-Belmonte, M.; Vozzi, G.; Whulanza, Y.; Seggiani, M.; Fantauzzi, V.; Orsini, G.; Ahluwalia, A., Tuning polycaprolactone-carbon nanotube composites for bone tissue engineering scaffolds. *Mater. Sci. Eng., C* **2012,** *32*, (2), 152-159.
156. Fama, L. M.; Pettarin, V.; Goyanes, S. N.; Bernal, C. R., Starch/multi-walled carbon nanotubes composites with improved mechanical properties. *Carbohydr. Polym.* **2011,** *83*, (3), 1226-1231.
157. Aider, M., Chitosan application for active bio-based films production and potential in the food industry: Review. *LWT - Food Science and Technology* **2010,** *43*, 837-842.
158. Wan Ngah, W. S.; Teong, L. C.; Hanafiah, M. A. K. M., Adsorption of dyes and heavy metal ions by chitosan composites: A review. *Carbohydr. Polym.* **2011,** *83*, 1446-1456.
159. Miretzky, P.; Cirelli, A. F., Fluoride removal from water by chitosan derivatives and composites: A review. *J. Fluorine Chem.* **2011,** *132*, 231-240.
160. Wang, S.-F.; Shen, L.; Zhang, W.-D.; Tong, Y.-J., Preparation and mechanical properties of chitosan/carbon nanotubes composites. *Biomacromolecules* **2005,** *6*, 3067-3072.
161. Nowack, B.; David, R. M.; Fissan, H.; Morris, H.; Shatkin, J. A.; Stintz, M.; Zepp, R.; Brouwer, D., Potential release scenarios for carbon nanotubes used in composites. *Environ. Int.* **2013,** *59*, 1-11.
162. Kingston, C.; Zepp, R.; Andrady, A.; Boverhof, D.; Fehir, R.; Hawkins, D.; Roberts, J.; Sayre, P.; Shelton, B.; Sultan, Y.; Vejins, V.; Wohlleben, W., Release characteristics of selected carbon nanotube polymer composites. *Carbon* **2014,** *68*, (0), 33-57.

163. Hirth, S.; Cena, L.; Cox, G.; Tomović, Ž.; Peters, T.; Wohlleben, W., Scenarios and methods that induce protruding or released CNTs after degradation of nanocomposite materials. *J. Nanopart. Res.* **2013,** *15*, (4), 1-15.
164. Schlagenhauf, L.; Nüesch, F.; Wang, J., Release of Carbon Nanotubes from Polymer Nanocomposites. *Fibers* **2014,** *2*, (2), 108-127.
165. Huang, G.; Park, J. H.; Cena, L. G.; Shelton, B. L.; Peters, T. M., Evaluation of airborne particle emissions from commercial products containing carbon nanotubes. *J. Nanopart. Res.* **2012,** *14*, (11), 1231/1-1231/13.
166. Wohlleben, W.; Meier, M. W.; Vogel, S.; Landsiedel, R.; Cox, G.; Hirth, S.; Tomovic, Z., Elastic CNT-polyurethane nanocomposite: synthesis, performance and assessment of fragments released during use. *Nanoscale* **2013,** *5*, (1), 369-380.
167. Ging, J.; Tejerina-Anton, R.; Ramakrishnan, G.; Nielsen, M.; Murphy, K.; Gorham, J. M.; Nguyen, T.; Orlov, A., Development of a conceptual framework for evaluation of nanomaterials release from nanocomposites: Environmental and toxicological implications. *Sci. Total Environ.* **2014,** *473*, 9-19.
168. Esawi, A. M. K.; Farag, M. M., Carbon nanotube reinforced composites: Potential and current challenges. *Mater. Des.* **2007,** *28*, 2394-2401.
169. Jones, J., W. E.; Chiguma, J.; Johnson, E.; Pachamuthu, A.; Santos, D., Electrically and thermally conducting nanocomposites for electronic applications. *Materials* **2010,** *3*, (2), 1478-1496.
170. Rahmat, M. H., P., Carbon nanotube-polymer interactions in nanocomposites: A review. *Compos. Sci. Technol.* **2011,** *72*, (1), 72-84.
171. Roes, L.; Patel, M. K.; Worrell, E.; Ludwig, C., Preliminary evaluation of risks related to waste incineration of polymer nanocomposites. *Sci. Total Environ.* **2012,** *417*, 76-86.
172. Petersen, E. J.; Lam, T.; Gorham, J. M.; Scott, K. C.; Long, C. J.; Stanley, D.; Sharma, R.; Alexander Liddle, J.; Pellegrin, B.; Nguyen, T., Methods to assess the impact of UV irradiation on the surface chemistry and structure of multiwall carbon nanotube epoxy nanocomposites. *Carbon* **2014,** *69*, (0), 194-205.
173. Nguyen, T.; Pellegrin, B.; Mermet, L.; Shapiro, A.; Gu, X.; Chin, J., Network aggregation of CNTs at the surface of epoxy/MWCNT composite exposed to UV radiation. *Nanotechnology* **2009**, 90-3.
174. Leja, K.; Lewandowicz, G., Polymer Biodegradation and Biodegradable Polymers--A Review. *Pol. J. Environ. Stud.* **2010,** *13*, (2), 255-266.
175. Shah, A. A.; Hasan, F.; Hameed, A.; Ahmed, S., Biological Degradation of Plastics: A Comprehensive Review. *Biotechnology Advances* **2008,** *26*, (3), 246-265.
176. Sivan, A., New Perspectives in Plastic Biodegradation. *Curr. Opin. Biotechnol.* **2011,** *22*, (3), 422-426.
177. Shah, A. A.; Hasan, F.; Hameed, A.; Ahmed, S., Biological degradation of plastics: A comprehensive review. *Biotechnol. Adv.* **2008,** *26*, (3), 246-265.
178. Madigan, M. T.; Martinko, J. M.; Dunlap, P. V.; Clark, D. P., *Brock Biology of Microorganisms*. 12th ed.; Pearson: San Francisco, 2009.

179. Wu, C.-S., A comparison of the structure, thermal properties, and biodegradability of polycaprolactone/chitosan and acrylic acid grafted polycaprolactone/chitosan. *Polymer* **2005,** *46*, (1), 147-155.
180. Wu, C.-S.; Liao, H.-T., Study on the preparation and characterization of biodegradable polylactide/multi-walled carbon nanotubes nanocomposites. *Polymer* **2007,** *48*, (15), 4449-4458.
181. Gewert, B.; Plassmann, M. M.; MacLeod, M., Pathways for degradation of plastic polymers floating in the marine environment. *Environ. Sci.: Processes Impacts* **2015,** *17*, (9), 1513-1521.
182. Deshmukh, S.; Mhadeshwar, N., Biodegradable polymers. *Popular Plastics & Packaging* **2011,** *56*, (9), 48-52.
183. Goodwin, D. G.; Marsh, K. M.; Sosa, I. B.; Payne, J. B.; Gorham, J. M.; Bouwer, E. J.; Fairbrother, D. H., Interactions of Microorganisms with Polymer Nanocomposite Surfaces Containing Oxidized Carbon Nanotubes. *Environ. Sci. Technol.* **2015,** *49*, (9), 5484-5492.

Chapter 2. Carbon Nanotube/Polymer Nanocomposite Preparation and Characterization

2.1. Polymer Grafting, Solution Blending, and Melt-Mixing/Extrusion

There are three methods available for the production of carbon nanotube (CNT)/polymer nanocomposites (CNT/PNCs) in research laboratories and industrial settings. These methods include polymer grafting, solution blending, and melt-mixing/extrusion, which generally produce excellent to poorer CNT dispersion qualities, respectively.[1-4] A homogeneous CNT dispersion quality is necessary for CNTs to impart their beneficial properties to a polymer matrix, and dispersion quality is generally optimized in consumer products according to cost and application.[5-9] In all three production methods, the best approach to achieve homogeneous dispersion quality is to match the polymer matrix polarity with that of the CNT polarity and provide a high shear energy during mixing of the two materials. This minimizes the formation of heterogeneous phases of CNT aggregates and polymer chains throughout the matrix.[3, 4, 10] The CNT polarity can be varied by mild to strong acid oxidation, which can be controlled by refluxing CNTs in acid for short to long periods of time, respectively.[11, 12] The downside of oxidation is that it can cause sidewall damage to CNTs which can negatively affect some of their beneficial properties. However, the more homogeneous dispersion quality achieved with oxidized CNTs has been shown to lead to improved CNT/PNC properties, sometimes balancing out the CNT functionality loss caused by CNT oxidation.[13] CNTs can also be modified with surfactants to match their polarity with that

of the polymer matrix. In this case, the surfactant must be carefully selected so that it does not affect the performance of the CNT/PNC.[14-19]

The first method of CNT/PNC production, polymer grafting, involves anchoring a polymer chain "to" or "from" a CNT surface (Figure 2.1). This approach typically requires the CNTs to first be oxidized to contain oxygen functional groups that can serve as a grafting point for polymer chain attachment or growth. Grafting a polymer "to" a CNT involves covalent attachment of a pre-formed polymer chain to a CNT while grafting a polymer "from" a CNT involves growing a polymer chain "from" a CNT surface using monomer units. Both methods have disadvantages: the grafting "to" approach requires the attachment of macromolecular polymer chains to the CNT, and only a few of these attached polymer chains can sterically hinder diffusion of more polymer chains to the CNT surface for reaction. For the grafting "from" approach, strict conditions are necessary for control over the polymerization, which is often challenging with CNTs in suspension. However, this technique does not face the same steric hindrance issues that the grafting "to" technique faces. Since the same polymer used as the polymer matrix in the CNT/PNC can be grafted onto the CNT, the polarity of the CNT can be matched exactly with the polymer matrix and lead to excellent CNT dispersion quality.[4] CNTs with polymer grafts can be incorporated into polymer matrices using solution blending or melt-mixing techniques, as described below. However, control of the oxygen functional group grafting sites between different batches of CNTs can be challenging. Furthermore, this is the most expensive and time-consuming method to incorporate CNTs into polymers due to the many required synthetic and purification steps and is impractical for large scale production.[3, 4] Thus, this method has only been used in

academic research or for production of CNT/PNCs in electronic devices that require fine control of the CNT percolation network.[20-22]

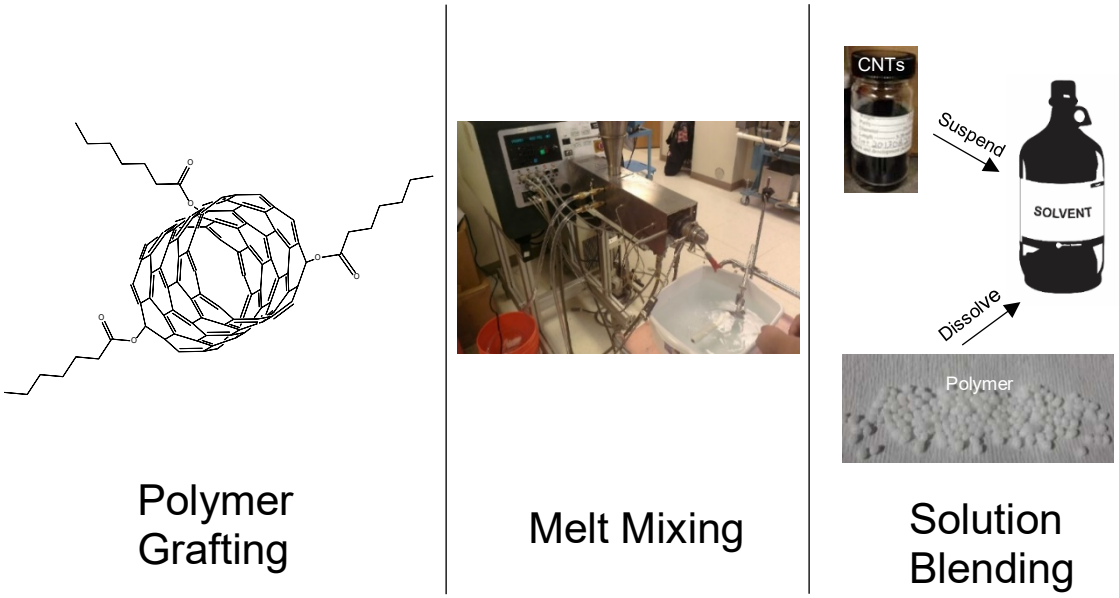

Figure 2.1. A comparison of polymer grafting, melt-mixing/extrusion, and solution blending approaches for preparation of CNT/PNCs.

The second method of CNT incorporation is solution blending, in which CNTs are first suspended in a solvent that can also dissolve the polymer of interest. The solution containing dissolved polymer and suspended CNTs is called the CNT/PNC casting solution. The solvent can be removed through a variety of means such as evaporation (with or without heating), spin-coating, and spray-coating/nebulizing (Figure 2.1).[1, 2] In this case, the polarity of the solvent, polymer, and CNT all have to be well matched to generate a well-dispersed CNT/PNC. Oftentimes, trial and error are required to optimize conditions for homogeneous CNT/PNCs.[3, 4, 10] Small concentrations of surfactants are also needed in some cases to match the polarity of the CNTs with that of the solvent.[14-19] The CNT suspension is typically sonicated using an ultrasonic bath and either sonicated

for a longer period of time once the polymer is added or stirred until the polymer has fully dissolved in the solvent.[1, 2] If the polymer is further sonicated with the CNT suspension, care must be taken to sonicate the polymer for the same amount of time in all samples and with sonicators of consistent power since polymer chain scission can occur during this process. Chain scission can lower the molecular weight of the polymer and as a result, enhance biodegradability.[23] Therefore, consistency is vital for CNT/PNC preparation using solution blending coupled with polymer sonication. Solution blending is the most cost-effective CNT/PNC preparation method on the research lab scale since it does not require sophisticated equipment for CNT/PNC processing.[3] However, this method requires a significant amount of trial and error, is not environmentally friendly in terms of organic solvent evaporation, and cannot be easily scaled up. However, CNT/PNCs made using solution blending can have a homogeneous dispersion quality once optimized and reproducible CNT/PNC batches can be prepared for controlled research studies.[1, 2] For this reason, solution blended CNT/PNCs were the most common type of CNT/PNC used in this research.

Melt-mixing coupled to extrusion is the third technique used to generate CNT/PNCs. This method involves heating a polymer past its melting point, adding a CNT powder or CNTs dispersed in a solvent, and mechanically shearing the melted polymer with the CNT down the length of a single or double extrusion screw (Figure 2.1). At the end of the extrusion screw, the mixture is discharged and simultaneously cooled to form a CNT/PNC fiber, ribbon, or sheet. The CNT/PNC can then be run through the melt mixer/extruder for several cycles to generate a well dispersed CNT/PNC. Furthermore, the CNT/PNC can be shaped using heated molds and presses.[3,

[24, 25] Melt mixer/extruders range in size and capacity, with some used at the gram scale and others used at the kilogram scale.[26, 27] Therefore, this method can be easily scaled up and is the most widely used method of CNT/PNC production in industry for manufacturing. However, at the academic research scale, melt-mixer/extruders can be cost-prohibitive. Furthermore, CNT/PNCs produced using melt-mixing tend to have the poorest dispersion quality since the shear forces produced are not usually as strong as those provided by ultrasonication.[1, 2, 28] Nonetheless, this method is often sufficient for CNT/PNCs with enhanced mechanical strength or functional properties that do not require fine control of electronic properties.[28]

2.2. Polymers and Carbon Nanotubes Used

Throughout this thesis research, three types of polymer matrices were modified with CNT fillers using solution blending techniques modified from other protocols: polyvinyl alcohol (PVOH), poly-ε-caprolactone (PCL), and polyhydroxyalkanoates (PHA).[29-37] Other CNT/PNCs made of chitosan, polycarbonate (PC), polylactides (PLA), polyvinyl acetate (PVA) and lignin polymer matrices were also prepared and tested, but had issues ranging from inherent antimicrobial properties, slow biodegradation rates, poor dispersion quality and brittleness.[38, 39] PVOH, PCL and PHA were found to be ideal for use in this research for a variety of reasons (Figure 2.2).

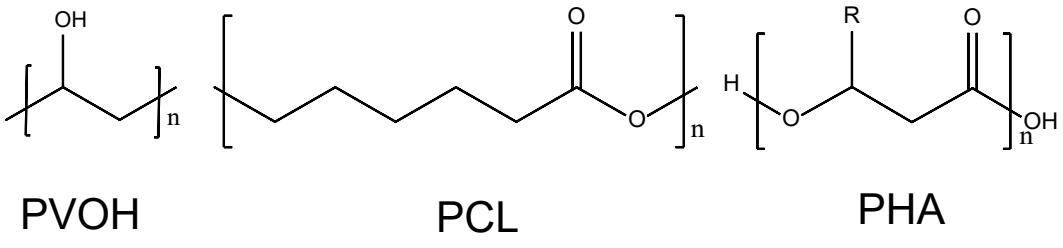

Figure 2.2. Chemical structures of PVOH, PCL, and PHA.

Specifically, as outlined in Chapter 3, oxidized multi-wall CNTs (O-MWCNTs) could be homogeneously incorporated into PVOH using a spray-coating technique with O-MWCNT and oxidized single-wall CNT (O-SWCNT) concentrations at the CNT/PVOH surface representative of the mass concentration prepared in the casting solution. This allowed for control over the CNT surface concentration in contact with microorganisms in the initial interactions study. Furthermore, CNT/PVOH nanocomposites easily adhered to glass slides, allowing for microscopy of microorganisms at their surface. PCL and PHA were ideal for biofilm studies and biodegradation studies since they did not dissolve in water over time, were biodegradable on a feasible laboratory time scale (weeks – months), were able to be prepared without an underlying substrate, and were able to achieve a highly homogeneous CNT dispersion in their matrices using a small quantity (4 % w/w ethyl cellulose) of ethyl cellulose (EC), a natural and biocompatible surfactant. Similar to a few other studies, this surfactant was found to stabilize the CNTs during preparation of the casting solution in all solvents used (tetrahydrofuran, chloroform, and dichloromethane).[10, 40-42] PCL and PHA were also used since both pristine and slightly oxidized MWCNTs (LO-MWCNTs, ~4% surface atomic oxygen) were dispersible in these polymer matrices.

In all studies, oxidized (O-MWCNTs and LO-MWCNTs) and/or pristine multi-wall CNTs (MWCNTs) were used since they are more commonly incorporated into products than single-wall CNTs (SWCNTs).[1, 5, 43] O-SWCNTs were used in the initial microbial interactions study (Chapter 3) as a point of comparison to the O-MWCNTs. O-MWCNTs (~9%) were also selected for this study since they are highly dispersible in PVOH and pristine MWCNTs have already been investigated for cytotoxicity alone and

in a few studies when embedded in polymer nanocomposites.[44] In contrast, O-MWCNTs have not systematically been investigated for cytotoxicity either alone or embedded in a CNT/PNC. LO-MWCNTs from Nanocyl (~4% atomic oxygen) and pristine MWCNTs from two different manufacturers (NanoLab Inc. and Southwest Nanotechnologies) were embedded in PCL. The same pristine MWCNTs from NanoLab Inc. were embedded in PHA. High purity pristine and oxidized CNTs were used "as is" from the manufacturer to represent the form in which CNTs will be embedded in products. LO-MWCNTs were generated in house using 70% w/v HNO_3. By virtue of the oxidation procedure used for the "as-received" O-MWCNTs and O-SWCNTs as well as the "in-house" LO-MWCNTs, CNTs were purified as part of the oxidation process. Lastly, the MWCNTs from Southwest Nanotechnologies were chosen since they contain residual cobalt and molybdenum particles from the chemical vapor deposition (CVD) synthesis process, which could be used as a proxy for CNT release studies.[45] Table 2.1 outlines the CNTs used in each study, the purity, the length distribution, and diameters.

Table 2.1. The type of carbon nanotubes used in the various studies throughout this thesis. Properties such as atomic surface oxidation level (%), purity, outer diameter, length, and residual metal catalyst type are listed.

CNTs Used	Manufacturer	Type	% O (at.)	Outer Diameter (nm)	Length (μm)	Purity (%)	Residual Metal Catalyst	Studies
O-MWCNT	NanoLab Inc.	PD15L5-20-COOH	8.6	15 ± 5	5-20	>95	Fe	Initial interactions with microorganisms
O-SWCNT	Carbon Solutions	P3-SWNT	9.2	1-5	1 ± 0.5	>90	Y	Initial interactions with microorganisms
MWCNT	NanoLab Inc.	PD15L520		15 ± 5	5-20	>95	Fe	Biodegradation- Single, aerobic mixed, and anaerobic mixed cultures
LO-MWCNT	Nanocyl	Nanocyl NC7000	4.1	9.5	1.5	>90	Fe, Co	Biofilm development, Biodegradation- Single, anaerobic mixed cultures
MWCNT	Southwest Nanotechnol. Inc.	SMW200		10 ± 1	3-6	≥ 98	Co, Mo	Biodegradation- Single culture (release)

2.3. Solution Blending and Melt-Mixing Procedures for CNT/PNCs Used in this Study

2.3.1. Solution Blending

CNTs were first sonicated in solvent at a desired mass loading for a specific period of time. Oxidized CNTs were sonicated without surfactant while pristine and LO-MWCNTs were sonicated with EC. Polymer (typically 10 mg/mL) was then added to the CNT suspension and sonicated for a specific period of time. The polymer sonication time was kept consistent from batch to batch in a particular study since sonication can shorten polymer chain length.[23] In some cases, the sonicator bath water was changed hourly with ice water since it was found to improve the CNT dispersion quality. Table 2.2 highlights the various preparation procedures.

Table 2.2. The preparation procedures used for CNT/PNCs in this research.

CNT type	Polymer	M_n	Solvent	Concentration of polymer (mg/mL)	% w/w EC	CNT/EC sonication time (h)	Polymer sonication time (h)	Casting
LO-MWCNTs	PCL	45,000	THF	10	4	2	3	Al Dish
LO-MWCNTs	PCL	45,000	$CHCl_3$	10	20	3	3	Al Dish
LO-MWCNTs	PCL	45,000	$CHCl_3$	10	20	3	2	Spray-Coating
LO-MWCNTs	PCL	45,000	DCM	10	4	1	3	Al Dish
MWCNTs	PCL	45,000	DCM	10	4	3	3	Al Dish
MWCNTs	PHA		$CHCl_3$	10	5	3	2	Al Dish
O-MWCNTs	PVOH	31,000-50,000	H_2O	2	0	~20	0.08	Spray-Coating
O-SWCNTs	PVOH	31,000-50,000	H_2O	2	0	~20	0.08	Spray-Coating

CNT/PNC casting solutions were added in 5 mL aliquots to aluminum dishes (44 mm diameter, 12.5 mm height, Fisher Scientific brand) and dried slowly overnight to remove solvent. CNT/PNCs were peeled from their dishes, sometimes after soaking in water for easier removal, and trimmed to a consistent diameter of ~30 mm. When an underlying substrate was required for microscopy, CNT/PNC casting solutions were spray-coated onto heated glass slides with manual spray bottles or a Badger 200 Single Action, Internal Mix Series Air-brush (Badger Air-Brush Co. Franklin Park, IL) operating at 30 PSI. Further details are provided in Chapters 3 and 4. PVOH was spray-coated onto sterilized glass slides at 150 °C while PCL was spray-coated onto octadecyltrichlorosilane modified glass slides at 80 °C for better adhesion of the hydrophobic polymer to a hydrophobic surface.[46-50]

2.3.2. Melt-Mixing/Extrusion

Pristine MWCNTs were incorporated into PCL using melt mixing/extrusion. PCL was first granulated to a 1-3 mm size using a chopper system. Granulated PCL and pristine MWCNTs (NanoLab Inc.) were then dried overnight in an oven at 65 °C and 100 °C, respectively. PCL and MWCNTs were mixed in different weight percentages with a twin rotor mixing bowl. Then, the MWCNT/PCL nanocomposite mixture was put through a single-screw melt mixer/extruder several times and pelletized. The pellets were dried overnight, heated, and pressed (using a heated Carver press) into 13 x 13 cm squares with a thickness slightly less than 1 mm. Melt-mixed MWCNT/PCL nanocomposites were substantially thicker than CNT/PNCs prepared via solution blending, so they were thinned out in some cases. A casting knife (3580 Casting Knife

Application, 0 - 6000 microns thickness, 150 mm wide) was used to decrease the thickness of melt-mixed MWCNT/PCL nanocomposites to 3-5 μm.

2.4. CNT/PNC Characterization Techniques

CNT/PNCs were characterized using both qualitative and quantitative techniques. Qualitatively, CNT/PNCs were characterized by visual observation and scanning electron microscopy (SEM) for CNT dispersion quality, attenuated total reflectance infrared spectroscopy for polymer functional group characterization, and energy-dispersive X-ray analysis (EDS) and thermal gravimetric analysis (TGA) for residual solvent detection. Quantitatively, CNT/PNCs were analyzed with X-ray photoelectron spectroscopy (XPS) and differential scanning calorimetry (DSC) for CNT surface concentration and fraction of crystallinity, respectively. After transformation, CNT/PNCs were analyzed using SEM for CNT accumulation.

2.4.1. Visual observation and SEM

Visually, CNT/PNCs were uniformly dark, with minimal signs of CNT aggregation when held up to light. CNT/PNCs also increased in darkness/decreased in translucence as a function of CNT loading. A comparison of CNT/PCL nanocomposites prepared using solution blending and melt-mixing are shown in Figure 2.3.

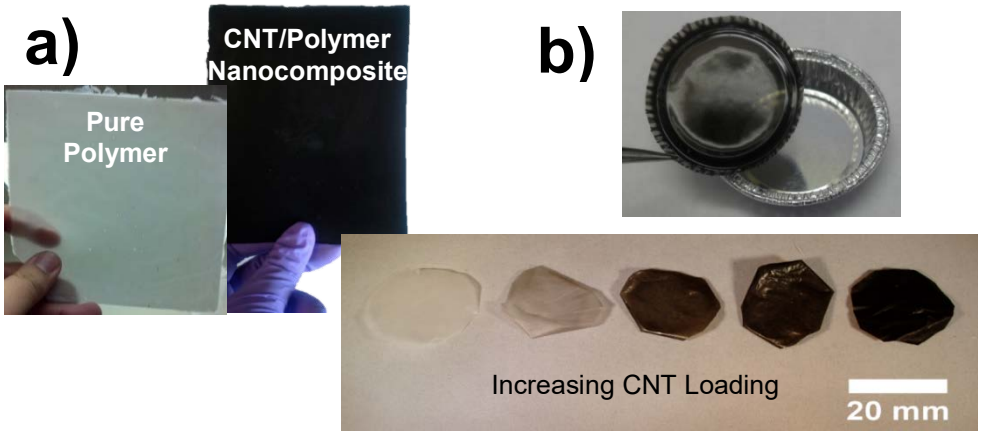

Figure 2.3. A comparison of CNT/PCL nanocomposites prepared using a) solution blending and b) melt-mixing/extrusion techniques for biodegradation studies.

In many cases, CNT/PNCs had poorly dispersed CNTs within the polymer matrix (Figure 2.4), and only under optimized conditions could well-dispersed CNT/PNCs be prepared (Figure 2.3).

Figure 2.4. CNT/PNCs prepared with a poor CNT dispersion quality.

In order to qualitatively determine the uniformity and morphology of the CNTs at the CNT/PNC surface, SEM was employed. SEM utilizes a high energy, focused electron beam that strikes a sample surface to generate different types of signals that reach several types of detectors. Secondary electrons, or low energy electrons, are inelastically emitted from atoms in the sample upon interaction with the incident electron beam. Secondary electrons generate an image of the CNT/PNC surface, with the heavier elements emitting more secondary electrons and the lighter elements emitting less. This creates contrast between different elements, with heavy elements showing up brighter and lighter elements showing up darker. The topography also affects the contrast.[51] Similarly, backscattering electrons can be used to obtain images with more emphasis on the contrast between atomic composition (heavy versus light atoms), and less on the topography. Backscattered electrons are electrons that originate from the incident beam and are elastically scattered back in the direction of the electron beam with high energy. For this reason the backscattering electron detector is typically placed parallel to the beam. In contrast, secondary electrons are lower in energy and are biased towards detectors at a greater angle from the samples.[52] SEM resolution depends on the working distance, material type, and accelerating voltage but is typically 1-2 nm at 15-20 keV. Owing to the high accelerating voltage, insulating samples such as polymers can charge and become damaged under the incident electron beam.[51] This issue becomes less apparent as a function of CNT loading, since CNTs can dissipate charge, but still remains an issue for the matrix at all CNT loadings studied. To counteract electron beam charging, a thin layer of platinum was sputter coated onto nanocomposite surfaces prior to SEM imaging. This platinum coating successfully prevents charge build-up, but can artificially broaden the

diameter of CNTs at the CNT/PNC surface. However, the CNTs are consistently broadened when this is the case.

In all CNT/PNCs investigated, CNTs were visually well distributed throughout the polymer matrices. But as evidenced by SEM, not all CNT/PNCs have CNTs present at the polymer surface. As discussed previously, the CNT/polymer polarities and the method of CNT/PNC casting can influence the CNT content at the surface.[3, 4, 10] A comparison of spray-coated PVOH, and casted PVOH, each containing 5% w/w O-MWCNTs, are shown in (Figure 2.5a,b) to highlight the difference between casting methods. Furthermore, a comparison of PCL and PHA containing the same pristine MWCNTs at 5% w/w are shown to highlight the differences between polymer types (Figure 2.5c,d). For CNT/PNCs that had CNTs initially present at the surface, the distribution of CNTs could be determined as a function of CNT loading. For CNT/PNCs that did not have CNTs at the surface, CNT distribution often became more obvious after polymer degradation accumulated CNTs at the surface.

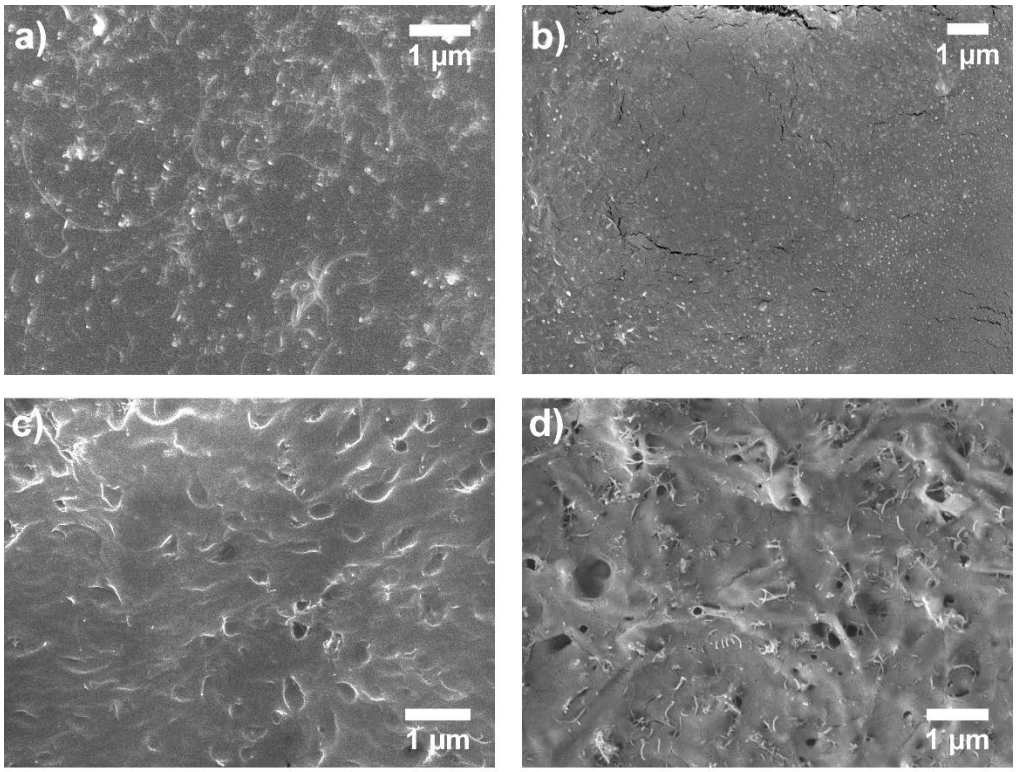

Figure 2.5. A comparison of a) spray-coated PVOH and b) casted PVOH, each containing 5% w/w O-MWCNTs and a comparison of c) PCL and d) PHA, each containing 5% w/w MWCNTs.

2.4.2. Bulk Characterization of CNT/PNCs

Energy dispersive X-ray analysis (EDS) is obtained using the electron beam in an SEM or transmission electron microscope (TEM). Instead of detecting secondary or backscattered electrons, EDS detects X-rays generated from the different elements within a sample. X-rays are produced when the incident electron beam ionizes an atom by emission of a core level electron. Electrons in a higher energy level within the atom then relax and in this process, emit an X-ray with an energy characteristic of this transition which is unique to the atom it came from. Peaks for each element allow for quantification of the atomic composition in a given area of the sample. Since X-rays have a large mean free path, their interaction volume is large (µm), and the atomic composition information

that is obtained is representative of the bulk.[53] EDS cannot be used for CNT concentration within the CNT/PNC since the polymer matrix is also made up of carbon. However, EDS can be used to ensure that residual solvent is not trapped within the CNT/PNC. This control measure was considered important since CNTs are shown to be strong sorbents.[54] As described in the next chapter, CNT/PNCs were originally prepared with a tetrahydrofuran casting solution but as indicated by the literature, THF can be readily adsorbed by other carbonaceous nanomaterials and generate false positive results in toxicity studies; this prompted us to switch to casting solvents that could be easily identified within the bulk CNT/PNC if adsorption was an issue.[55, 56] For this reason, chlorinated solvents such as chloroform and dichloromethane were always used to prepare solution blended CNT/PNCs. The presence of chlorine was tracked using EDS in samples with low and high CNT loading. CNT/PNCs did not contain chlorine for both the PCL and PHA matrices.

Thermogravimetric analysis (TGA), which is described in Chapter 1, was also used as a secondary measure to ensure that residual solvent did not remain in the CNT/PNCs from the casting process. In the TGA profile, solvents would provide a characteristic mass loss profile at low temperature. In this case they did not, further supporting the EDS data.

2.4.3. Attenuated Total Reflectance Infrared Spectroscopy (ATR-IR)

ATR-IR makes use of an incident infrared beam that enters a crystal, typically made of diamond or germanium.[57] The solid sample of interest is pressed against the crystal and the infrared beam totally reflects at the crystal/sample interface. However, the light is not directly reflected by the boundary surface, but it is reflected by a virtual plane within the sample, which is typically less optically dense then the crystal. The component

of the light that penetrates slightly into the sample prior to reflectance is called the evanescent wave. As in transmission IR, IR radiation is absorbed by excited vibrational states, and the transmitted IR radiation makes it to the detector. The IR spectrum typically provides functional group information and can have a spectrum unique to the material being analyzed, especially in the fingerprint region (< 1450 cm^{-1}).[58] ATR-IR was useful in characterizing the PCL and PHA surfaces within the top few micrometers. The addition of CNTs to the polymer matrices was not apparent, as CNTs do not absorb readily at any particular band. Furthermore, oxygen functional groups are difficult to detect using an ATR-IR, especially at low CNT loadings in CNT/PNCs, because diamond and CNTs have a very similar refractive index.[59] However, CNT incorporation and oxygen functional group identifications are possible with a germanium crystal, which has an index of refraction that is different from the sample. This is not the case for diamond and ZnSe crystals.[60] ATR-IR spectra were acquired using a Thermo Scientific Nicolet iS5 ATR-IR with a diamond crystal and a dTGS room-temperature detector (< 0.8 cm^{-1} resolution). 500 scans were taken for each IR spectrum obtained.

2.4.4. X-ray Photoelectron Spectroscopy (XPS)

XPS is a surface analytical technique that determines the atomic composition of a material within the top 10 nm of the surface. Under ultra-high vacuum conditions, a sample is bombarded with X-rays, which eject core level electrons that have kinetic energies characteristic of the energy levels from which they originate. Electrons are then passed through a hemispherical energy analyzer, where only electrons of specific kinetic energies are allowed through while all others are deflected. Different kinetic energies are

allowed through the analyzer to the detector to obtain a spectrum which is reported as binding energy using the (Equation 1):

$$\boldsymbol{h\upsilon = KE + BE + \phi} \qquad \text{(Equation 1)}$$

where $\boldsymbol{h\upsilon}$ is the X-ray energy (Planck's constant * wavenumbers), KE is the electron's kinetic energy, BE is the binding energy from which the electron was ejected, and $\boldsymbol{\phi}$ is the work function, or the correction factor for the energy lost to ejection from a solid and from interaction with the energy analyzer. The peaks at different binding energies are indicative of the atoms they come from and are used to identify and quantify the atomic composition using peak integration.[61] Furthermore, higher resolution scans can provide information on the oxidation state of an atom. For example, C-OR, C=O, O=C-OR, and C-F_x components can show up within the carbon envelope, and depending on the level of surface oxygen or fluorine on the material surface, can be de-convoluted using peak fitting. However, peak-fitting can become subjective at low levels of oxygen, with overlapping peaks, and with broad $\pi - \pi^*$ features in the C(1s) region.[62] An XPS C(1s) spectrum of LO-MWCNTs is shown in Appendix 4.

In this study, XPS was used to quantify the surface oxygen of carbon nanotubes and to determine the fraction of CNTs at the CNT/PNC surface using a specialized setup. In order to determine the fraction of CNTs at the CNT/PNC surface in Chapter 3, XPS experiments were run using a monochromatic X-ray source at NIST (Gaithersburg, MD). This provided a localized area of highly intense irradiation that caused the polymer to charge. Typically, under monochromatic conditions or with insulating samples, positive charge builds up from the ejection of electrons, or photoelectrons.[61] This can be counteracted using a charge neutralizer, which usually utilizes a low energy electron

flood gun to replace the photoelectrons. Since the polymer used is insulating while the CNTs are more conductive, it was found that turning off the charge neutralizer led to differential charging of the polymer component and the CNT component in the C(1s) envelope. The integrated area of the CNT component relative to that of the polymer component allowed for quantification of the surface CNT content. It was then compared to the concentration of CNTs used in the casting solution and found to be proportional. This technique has been used with epoxy in other studies as well.[63] The disadvantage is that the technique is not sensitive at CNT mass loadings below 5% w/w and only works with some types of CNTs. However, this method is the most quantitative method available for CNT content at a material surface considering the challenge of differentiating carbonaceous nanomaterials from a carbonaceous matrix.

2.4.5. Differential Scanning Calorimetry (DSC)

Differential scanning calorimetry (DSC) is used to measure the endothermic and exothermic transitions of a material as a function of temperature. This technique is particularly useful for characterizing polymer blends, polymers containing additives, pharmaceuticals, inorganics, curing reactions, and decomposition reactions. A DSC apparatus is made up of a temperature controlled chamber that contains a sample and a reference, each of which is simultaneously heated or cooled at a particular heating rate under an inert atmosphere. The difference in the amount of energy or heat it takes to increase the sample temperature to the same temperature as that of the reference is plotted to obtain transition information. This is useful for transition temperatures, such as melting point, where more energy is required to increase the temperature as the polymer melts.

DSC transitions are mass dependent, and a small sample sized is used, typically around 3-5 mg.[51]

DSC is widely employed in polymer analysis to determine the glass transition temperature (T_g), the melting temperature (T_m), and the crystallization temperature (T_c) which are all important transitions for semicrystalline thermoplastics. T_g is the temperature at which the polymer transitions from a glassy state to a rubbery state. This is the point at which the polymer chains are able to shift past one another or "move." The T_m is the temperature at which the solid becomes a liquid. For semicrystalline thermoplastics, such as PCL and PHA used in this research, the fraction of crystallinity within the polymer can be measured using the peak area of the endothermic melting peak (ΔH_M) when ratioed to a theoretical, 100% crystalline reference. This is because the crystalline regions require the most energy to break apart into the disordered state present in liquid form.[51] The T_c is the temperature at which the polymer nucleates into crystalline form as the temperature is decreased and is an exothermic process. The area under the T_c peak is highly dependent on the cooling rate, since the polymer chains have a shorter time to arrange themselves into crystals at faster cooling rates. Because the T_m is less dependent on the heating rate than the T_c is on the cooling rate in semicrystalline polymers, the heat of fusion is more commonly used to calculate crystallinity. Another important factor when analyzing semicrystalline polymers with DSC is thermal history. The degree of crystallinity in a polymer is largely dependent on the rate at which it was previously cooled or casted.[51] Solution blended polymers tend to have higher crystallinity after slow solvent evaporation while thermally processed polymers tended to have lower crystallinity. In order to bring polymers to the same origin of crystallinity and permit

comparison among polymer samples prepared in different ways, polymers are often annealed above their melting point or heated one time with DSC to remove their thermal history. In this research, the first DSC scan was used for the solution blended CNT/PNCs since these were already at maximum, consistent crystallinity from slow solvent evaporation.[51] For the melt-mixed CNT/PNCs used in biodegradation studies, the thermal history was removed by annealing to bring all samples to the same origin of crystallinity prior to DSC analysis.

Since the fraction of crystallinity can have a large impact on the biodegradability of a polymer, these data were obtained for the CNT/PNCs used in this research.[51] In particular, since additives have been shown to alter the crystallinity of a polymer in some cases, the effect of CNTs on the polymer crystallinity was investigated.[64] As shown in Chapters 6-8, the degree of crystallinity did not change significantly with CNT loading for both melt-mixed and solution blended CNT/PNCs as well as pristine and LO-MWCNTs. However, similar to a study by Sobkowicz et al., LO-MWCNTs did have an effect on the rate of crystallization as a function of CNT loading, but all CNT/PNCs eventually reached the same level of crystallinity (Figure 2.6).[65]

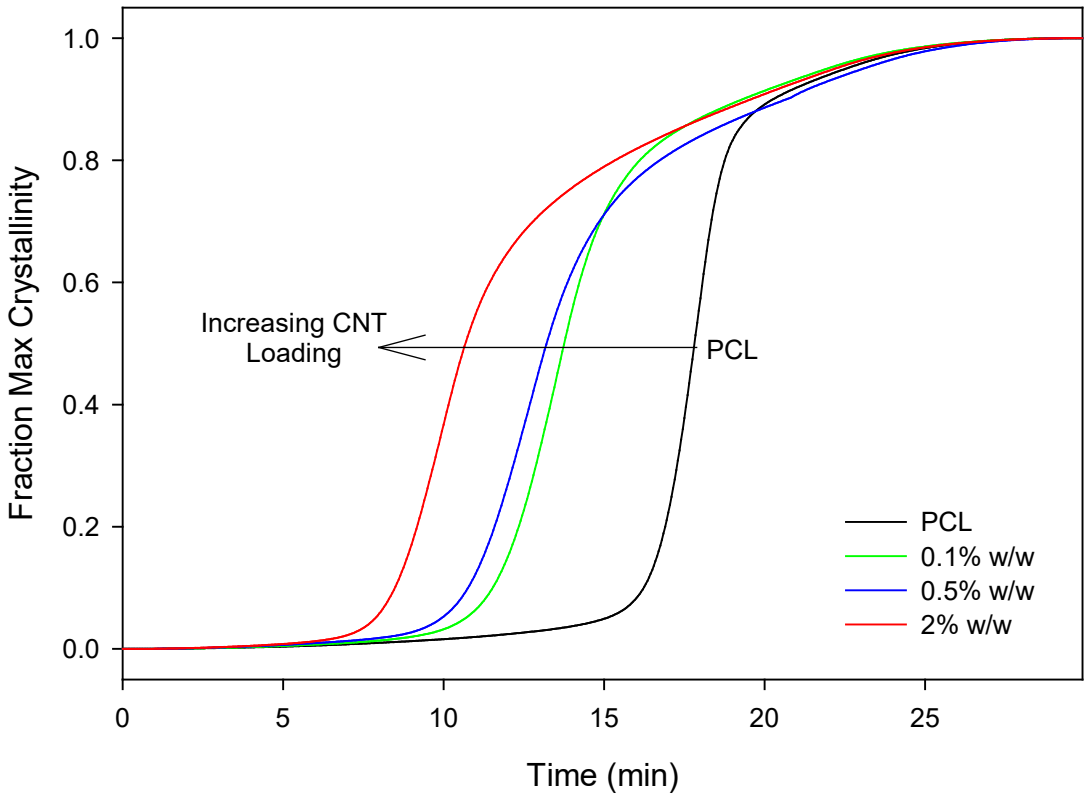

Figure 2.6. The rate of crystallization of LO-MWCNT/PCL nanocomposites as a function of LO-MWCNT mass loading.

2.5. References

1. Moniruzzaman, M.; Winey, K. I., Polymer nanocomposites containing carbon nanotubes. *Macromolecules* **2006,** *39*, (16), 5194-5205.
2. Sahoo, N. G.; Rana, S.; Cho, J. W.; Li, L.; Chan, S. H., Polymer nanocomposites based on functionalized carbon nanotubes. *Prog. Polym. Sci.* **2010,** *35*, (7), 837-867.
3. Hollertz, R.; Chatterjee, S.; Gutmann, H.; Geiger, T.; Nuesch, F. A.; Chu, B. T. T., Improvement of toughness and electrical properties of epoxy composites with carbon nanotubes prepared by industrially relevant processes. *Nanotechnology* **2011,** *22*, (12), 125702/1-125702/9.
4. Spitalsky, Z.; Tasis, D.; Papagelis, K.; Galiotis, C., Carbon nanotube–polymer composites: chemistry, processing, mechanical and electrical properties. *Prog. Polym. Sci.* **2010,** *35*, (3), 357-401.
5. McClory, C.; Chin, S. J.; McNally, T., Polymer/Carbon Nanotube Composites. *Aust. J. Chem.* **2009,** *62*, (8), 762-785.

6. Jones Jr., W. E.; Chiguma, J.; Johnson, E.; Pachamuthu, A.; Santos, D., Electrically and thermally conducting nanocomposites for electronic applications. *Materials* **2010,** *3*, (2), 1478-1496.
7. Esawi, A. M. K.; Farag, M. M., Carbon nanotube reinforced composites: Potential and current challenges. *Materials and Design* **2007,** *28*, 2394-2401.
8. Rahmat, M.; Hubert, P., Carbon nanotube-polymer interactions in nanocomposites: A review. *Compos. Sci. Technol.* **2011,** *72*, (1), 72-84.
9. Mittal, V., *Polymer Nanotube Nanocomposites:Synthesis, Properties, and Applications* John Wiley and Sons: New York, 2010
10. Kim, S. W.; Kim, T.; Kim, Y. S.; Choi, H. S.; Lim, H. J.; Yang, S. J.; Park, C. R., Surface modifications for the effective dispersion of carbon nanotubes in solvents and polymers. *Carbon* **2012,** *50*, (1), 3-33.
11. Smith, B.; Wepasnick, K.; Schrote, K. E.; Cho, H.-H.; Ball, W. P.; Fairbrother, D. H., Influence of Surface Oxides on the Colloidal Stability of Multi-walled Carbon Nanotubes: A Structure-Property Relationship *Langmuir* **2009,** *25*, (17), 9767-9776.
12. Smith, B.; Wepasnick, K.; Schrote, K. E.; Bertele, A. R.; Ball, W. P.; O'Melia, C.; Fairbrother, D. H., Colloidal Properties of Aqueous Suspensions of Acid-Treated, Multi-Walled Carbon Nanotubes. *Environ. Sci. Technol.* **2009,** *43*, (3), 819-825.
13. Kim, J. A.; Seong, D. G.; Kang, T. J.; Youn, J. R., Effects of surface modification on rheological and mechanical properties of CNT/epoxy composites. *Carbon* **2006,** *44*, (10), 1898-1905.
14. Yesil, S.; Winkelmann, C.; Bayram, G.; La Saponara, V., Surfactant-modified multiscale composites for improved tensile fatigue and impact damage sensing. *Materials Science & Engineering, A: Structural Materials: Properties, Microstructure and Processing* **2010,** *A527*, 7340-7352.
15. Park, I.; Park, M.; Kim, J.; Lee, H.; Lee, M. S., Multiwalled carbon nanotubes functionalized with PS via emulsion polymerization. *Macromolecular Research* **2007,** *15*, 498-505.
16. Zhang, X.; Zhang, J.; Liu, Z., Conducting polymer/carbon nanotube composite films made by in situ electropolymerization using an ionic surfactant as the supporting electrolyte. *Carbon* **2005,** *43 (2005)* 2186-2191.
17. Geng, Y.; Liu, M. Y.; Li, J.; Shi, X. M.; Kim, J. K., Effects of surfactant treatment on mechanical and electrical properties of CNT/epoxy nanocomposites. *Compos. Part A-Appl. S.* **2008,** *39*, (12), 1876-1883.
18. Tzong-Ming, W.; Shih-Hsinag, L., Synthesis, Characterization, and Electrical Properties of Polypyrrole/Multiwalled Carbon Nanotube Composites. *Journal of Polymer Science: Part A: Polymer Chemistry* **2006,** *44*, 6449-6457.
19. Micusik, M.; Omastova, M.; Pionteck, J.; Pandis, C.; Logakis, E.; Pissis, P., Influence of surface treatment of multiwall carbon nanotubes on the properties of polypropylene/carbon nanotubes nanocomposites. *Polym. Adv. Technol.* **2011,** *22*, 38-47.
20. Sobkowicz, M. J.; Dorgan, J. R.; Gneshin, K. W.; Herring, A. M.; McKinnon, J. T., Supramolecular BioNanocomposites: Grafting of Biobased Polylactide to Carbon Nanoparticle Surfaces. *Aust. J. Chem.* **2009,** *62*, (8), 865-870.

21. Sobkowicz, M. J.; Braun, B.; Dorgan, J. R., Decorating in green: surface esterification of carbon and cellulosic nanoparticles. *Green Chem.* **2009,** *11*, (5), 680-682.
22. Kumar, S. K.; Jouault, N.; Benicewicz, B.; Neely, T., Nanocomposites with Polymer Grafted Nanoparticles. *Macromolecules* **2013,** *46*, (9), 3199-3214.
23. Suslick, K. S.; Price, G. J., Applications of ultrasound to materials chemistry. *Annu. Rev. Mater. Sci.* **1999,** *29*, (1), 295-326.
24. Haggenmueller, R.; Gommans, H. H.; Rinzler, A. G.; Fischer, J. E.; Winey, K. I., Aligned single-wall carbon nanotubes in composites by melt processing methods. *Chem. Phys. Lett.* **2000,** *330*, (3–4), 219-225.
25. Andrews, R.; Jacques, D.; Minot, M.; Rantell, T., Fabrication of carbon multi-wall nanotube/polymer composites by shear mixing. *Macromol. Mater. Eng.* **2002,** *287*, (6), 395-403.
26. Dynisco Laboratory Mixing Extruder (LME).
27. Scientific, T. Extrusion and Compounding Equipment. https://www.thermofisher.com/us/en/home/industrial/manufacturing-processing/extrusion-compounding-equipment.html
28. Ma, P.-C.; Siddiqui, N. A.; Marom, G.; Kim, J.-K., Dispersion and functionalization of carbon nanotubes for polymer-based nanocomposites: a review. *Composites, Part A* **2010,** *41A*, (10), 1345-1367.
29. Ryan, K. P.; Cadek, M.; Nicolosi, V.; Blond, D.; Ruether, M.; Armstrong, G.; Swan, H.; Fonseca, A.; Nagy, J. B.; Maser, W. K.; Blau, W. J.; Coleman, J. N., Carbon nanotubes for reinforcement of plastics? A case study with poly(vinyl alcohol). *Compos. Sci. Technol.* **2007,** *67*, (7-8), 1640-1649.
30. Lou, J.; Schimmel, K.; Kuzviwanza, P.; Warren, D.; Yan, J., Characterization of biodegradable polymers: (I) Biodegradation of poly(vinyl alcohol) under aerobic and aqueous conditions. **2007**.
31. Shaffer, M. S. P.; Windle, A. H., Fabrication and characterization of carbon nanotubes/poly(vinyl alcohol) composites. *Adv. Mater.* **1999,** *11*, 937-941.
32. Taghizadeh, A.; Favis, B. D., Carbon nanotubes in blends of polycaprolactone/thermoplastic starch. *Carbohydr. Polym.* **2013,** *98*, (1), 189-198.
33. Chakoli, A. N.; Wan, J.; Feng, J. T.; Amirian, M.; Sui, J. H.; Cai, W., Functionalization of multiwalled carbon nanotubes for reinforcing of poly(-lactide-co-ϵ-caprolactone) biodegradable copolymers. *Appl. Surf. Sci.* **2009,** *256*, (1), 170-177.
34. Pan, L.; Pei, X.; He, R.; Wan, Q.; Wang, J., Multiwall carbon nanotubes/polycaprolactone composites for bone tissue engineering application. *Colloids Surf., B* **2012,** *93*, 226-234.
35. Chan, K. H. K.; Wong, S. Y.; Tiju, W. C.; Li, X.; Kotaki, M.; He, C. B., Morphologies and electrical properties of electrospun poly [(R)-3-hydroxybutyrate-co-(R)-3-hydroxyvalerate]/multiwalled carbon nanotubes fibers. *J. Appl. Polym. Sci.* **2010,** *116*, (2), 1030-1035.
36. Ma, Y.; Zheng, Y.; Wei, G.; Song, W.; Hu, T.; Yang, H.; Xue, R., Processing, structure, and properties of multiwalled carbon nanotube/poly (hydroxybutyrate-co-valerate) biopolymer nanocomposites. *J. Appl. Polym. Sci.* **2012,** *125*, (S1), E620-E629.

37. Lai, M.; Li, J.; Yang, J.; Liu, J.; Tong, X.; Cheng, H., The morphology and thermal properties of multi-walled carbon nanotube and poly (hydroxybutyrate-co-hydroxyvalerate) composite. *Polym. Int.* **2004,** *53*, (10), 1479-1484.
38. Wang, S.-F.; Shen, L.; Zhang, W.-D.; Tong, Y.-J., Preparation and mechanical properties of chitosan/carbon nanotubes composites. *Biomacromolecules* **2005,** *6*, 3067-3072.
39. Aslan, S.; Loebick, C. Z.; Kang, S.; Elimelech, M.; Pfefferle, L. D.; Van, T. P. R., Antimicrobial biomaterials based on carbon nanotubes dispersed in poly(lactic-co-glycolic acid). *Nanoscale* **2010,** *2*, (9), 1789-1794.
40. Neo, C. Y.; Ouyang, J., Ethyl cellulose and functionalized carbon nanotubes as a co-gelator for high-performance quasi-solid state dye-sensitized solar cells. *Journal of Materials Chemistry A* **2013,** *1*, (45), 14392-14401.
41. Boccaccini, A. R.; Cho, J.; Roether, J. A.; Thomas, B. J.; Minay, E. J.; Shaffer, M. S., Electrophoretic deposition of carbon nanotubes. *Carbon* **2006,** *44*, (15), 3149-3160.
42. Zhao, H.; Song, H.; Li, Z.; Yuan, G.; Jin, Y., Electrophoretic deposition and field emission properties of patterned carbon nanotubes. *Appl. Surf. Sci.* **2005,** *251*, (1), 242-244.
43. De, V. M. F. L.; Tawfick, S. H.; Baughman, R. H.; Hart, A. J., Carbon Nanotubes: Present and Future Commercial Applications. *Science* **2013,** *339*, (6119), 535-539.
44. Akhavan, O.; Ghaderi, E., Toxicity of graphene and graphene oxide nanowalls against bacteria. *ACS nano* **2010,** *4*, (10), 5731-5736.
45. Reed, R. B.; Goodwin, D. G.; Marsh, K. L.; Capracotta, S. S.; Higgins, C. P.; Fairbrother, D. H.; Ranville, J. F., Detection of single walled carbon nanotubes by monitoring embedded metals. *Environ. Sci.: Processes Impacts* **2013,** *15*, (1), 204-213.
46. McGovern, M. E.; Kallury, K. M. R.; Thompson, M., Role of Solvent on the Silanization of Glass with Octadecyltrichlorosilane. *Langmuir* **1994,** *10*, (10), 3607-3614.
47. Mutin, P. H.; Guerrero, G.; Vioux, A., Hybrid materials from organophosphorus coupling molecules. *J. Mater. Chem.* **2005,** *15*, (35-36), 3761-3768.
48. Song, J. E.; Phenrat, T.; Marinakos, S.; Xiao, Y.; Liu, J.; Wiesner, M. R.; Tilton, R. D.; Lowry, G. V., Hydrophobic Interactions Increase Attachment of Gum Arabic- and PVP-Coated Ag Nanoparticles to Hydrophobic Surfaces. *Environ. Sci. Technol.* **2011,** *45*, (14), 5988-5995.
49. Sodagari, M.; Wang, H.; Newby, B.-m. Z.; Ju, L.-K., Effect of rhamnolipids on initial attachment of bacteria on glass and octadecyltrichlorosilane-modified glass. *Colloids Surf. B. Biointerfaces* **2013,** *103*, 121-128.
50. Wang, H.; Sodagari, M.; Chen, Y.; He, X.; Newby, B.-m. Z.; Ju, L.-K., Initial bacterial attachment in slow flowing systems: effects of cell and substrate surface properties. *Colloids Surf. B. Biointerfaces* **2011,** *87*, (2), 415-422.
51. Zhang, S.; Li, L.; Kumar, A., *Materials characterization techniques*. CRC press: 2008.
52. Services, C. T., Scanning Electron Microscopy (SEM) Imaging Modes. In.

53. Hafner, B., Energy Dispersive Spectroscopy on the SEM: a primer. *Characterization Facility, University of Minnesota* **2006**, 1-26.
54. Mauter, M. S.; Elimelech, M., Environmental Applications of Carbon-Based Nanomaterials. *Environ. Sci. Technol.* **2008,** *42*, (16), 5843-5859.
55. Firme, C. P., III; Bandaru, P. R., Toxicity issues in the application of carbon nanotubes to biological systems. *Nanomedicine (Philadelphia, PA, U. S.)* **2010,** *6*, (2), 245-256.
56. Henry, T. B.; Menn, F.-M.; Fleming, J. T.; Wilgus, J.; Compton, R. N.; Sayler, G. S., Attributing effects of aqueous C60 nano-aggregates to tetrahydrofuran decomposition products in larval zebrafish by assessment of gene expression. *Environ. Health Perspect.* **2007,** *115*, (7), 1059-1065.
57. Chaberska, H., Attenuated total reflectance infrared spectroscopy. *Przem. Chem.* **2008,** *87*, (3), 274-276.
58. Schmitt, J.; Flemming, H.-C., FTIR-spectroscopy in microbial and material analysis. *Int. Biodeterior. Biodegrad.* **1998,** *41*, (1), 1-11.
59. Wepasnick, K. A.; Smith, B. A.; Bitter, J. L.; Fairbrother, D. H., Chemical and structural characterization of carbon nanotube surfaces. *Anal. Bioanal. Chem.* **2010,** *396*, (3), 1003-1014.
60. Zenkel, C.; Albuerne, J.; Emmler, T.; Boschetti-de-Fierro, A.; Helbig, J.; Abetz, V., New strategies for the chemical characterization of multi-walled carbon nanotubes and their derivatives. *Microchimica Acta* **2012,** *179*, (1-2), 41-48.
61. Moulder, J. F.; Chastain, J.; King, R. C., *Handbook of X-ray photoelectron spectroscopy: a reference book of standard spectra for identification and interpretation of XPS data*. Physical Electronics Eden Prairie, MN: 1995.
62. Wepasnick, K. A.; Smith, B. A.; Schrote, K. E.; Wilson, H. K.; Diegelmann, S. R.; Fairbrother, D. H., Surface and structural characterization of multi-walled carbon nanotubes following different oxidative treatments. *Carbon* **2011,** *49*, (1), 24-36.
63. Petersen, E. J.; Lam, T.; Gorham, J. M.; Scott, K. C.; Long, C. J.; Stanley, D.; Sharma, R.; Alexander Liddle, J.; Pellegrin, B.; Nguyen, T., Methods to assess the impact of UV irradiation on the surface chemistry and structure of multiwall carbon nanotube epoxy nanocomposites. *Carbon* **2014,** *69*, (0), 194-205.
64. Stuart, B. H., *Polymer analysis*. John Wiley & Sons: 2008; Vol. 30.
65. Sobkowicz, M. J.; Sosa, R.; Dorgan, J. R., Supramolecular bionanocomposites, part 2: Effects of carbon nanoparticle surface functionality on polylactide crystallization. *J. Appl. Polym. Sci.* **2011,** *121*, (4), 2029-2038.

Chapter 3. Initial Interactions of Microorganisms with Carbon Nanotube/Polymer Nanocomposites

This work was co-written with the following authors and is adapted from the following published work:

Goodwin Jr, D. G., Marsh, K. M., Sosa, I. B., Payne, J. B., Gorham, J. M., Bouwer, E. J., & Fairbrother, D. H. (2015). Interactions of Microorganisms with Polymer Nanocomposite Surfaces Containing Oxidized Carbon Nanotubes. *Environmental Science & Technology*, *49* (9), 5484-5492.

Note: Certain commercial entities, equipment or materials may be identified in this document in order to describe an experimental procedure or concept adequately. Such identification is not intended to imply recommendation or endorsement by the National Institute of Standards and Technology, nor is it intended to imply that the entities, materials, or equipment are necessarily the best available for the purpose.

3.1. Introduction

One of the most important projected commercial applications of engineered nanomaterials (ENMs) such as carbon nanotubes (CNTs), nano-silver, and nano-scale metal oxides involves their use as fillers in polymer matrices at low concentrations, typically at a mass fraction of less than 5% w/w, to produce polymer nanocomposites.[1-6] The advantage of incorporating ENMs into polymers derives from their ability to greatly expand the material's value and utility by enhancing numerous polymer properties.[6-8]

Carbon nanotubes are becoming one of the most widely studied fillers in view of their large aspect ratio and excellent thermal, chemical, and mechanical properties. This collection of desirable attributes makes them ideal candidates to improve tensile strength, elastic modulus, thermal conductivity, and current carrying capacities of polymers.[9-22] For example, multi-wall CNT (MWCNT) - polystyrene nanocomposites containing only 1% w/w MWCNTs exhibit a 36–42% increase in elastic modulus and a 25% increase in break stress relative to pure polystyrene.[16] Consequently, CNT-containing nanocomposites are already present in a diverse array of products that include bicycles, tennis racquets, sail boats, anti-static parts for fuel filter lines, and packaging materials used in the electronics industries.[23-27]

As the use of CNTs embedded in polymer matrices increases, it is inevitable that a significant fraction of commercially produced CNTs will first enter the environment embedded in plastic materials.[28-30] Thus, it is important to understand the behavior of CNT/PNCs in the environment.[28, 31-33] One of the situations that will determine the fate of CNT/PNCs occurs at the end of their life cycle where disposal follows consumer use. Under these conditions, the impact and persistence of a CNT/PNC will depend on its interactions with microbial populations present in landfills. Other CNT/PNCs will be improperly disposed of on land (i.e. litter) and in surface waters where they can also encounter and interact with a wide variety of microorganisms.

The first step in the interaction of microbes with solid substrates is the attachment of planktonic cells to the surface followed by growth and colonization. If the microorganisms survive upon surface attachment, they colonize through proliferation and produce extracellular polymeric substances (EPS) to form biofilms.[34, 35] In contrast, if the

surface exhibits antimicrobial properties, cell proliferation can be retarded or even inhibited.[36, 37] If biofilm formation occurs, the metabolic activity of the attached microorganisms can initiate biodegradation through the release of extracellular enzymes.[38-41] Thus, the initial interactions of microorganisms with CNT/PNCs will play an important role in determining the nanomaterial's long term fate and persistence.

In the majority of studies involving CNTs and microorganisms, antimicrobial properties have been observed regardless of whether the CNTs were dispersed or aggregated in the aqueous phase or collected on a membrane or surface.[28, 42-48] For example, surfaces coated with pristine SWCNTs markedly reduced the amount of *Escherichia coli* that could form a biofilm due to the antimicrobial nature of the surface.[42] Three of the main mechanistic hypotheses for CNT cytotoxicity include puncturing of the cell membrane, membrane disruption, and oxidative stress.[43, 44, 49-53]A smaller number of studies, however, have claimed that CNTs exhibit weak or no observable cytotoxic response towards microbes.[54-56] Thus, Pantanella *et al.* found that SWCNT-coated surfaces do not affect adhesion or biofilm formation and attributed this to a lack of antimicrobial properties for selected bacterial species.[56] Therefore, the cytotoxicity of CNTs remains controversial.[57, 58]

In the case of CNT/PNCs, a few studies have evaluated the influence of pristine CNTs exposed at the surface of PNCs on cell death. For example, polyvinyl-N-carbazole (PVK) nanocomposites containing only 3% w/w SWCNTs caused significant cell death (> 80%) of *Escherichia coli* and *Bacillus subtilis* relative to pure PVK. MWCNTs embedded in the same polymer also led to significant cytotoxicity.[47, 59] Similarly, Schiffman *et al.* found that the inclusion of pristine SWNTs in electrospun polysulfone

fibers caused an increase in cell death as the SWNT concentration increased from 0 - 1% w/w.[60] Consequently, it has been suggested that CNT-modified materials can serve as antimicrobial coatings to resist biofouling or biofilm formation in applications ranging from medical devices to membranes, piping, and boat hulls.[27, 49, 61, 62]

In nanocomposite products, cycles of weathering and biodegradation can eventually cause CNTs to reach the surface and to potentially even accumulate, regardless of whether or not the CNTs are initially exposed at the PNC surface or buried under a thin polymer layer or surface coating.[30, 63-65] Under these conditions, the interactions of microorganisms with CNT/PNC surfaces will be important during the life cycle of the material. To date, studies on the interactions of microbes with CNTs embedded in polymeric matrices or in membranes have focused on pristine CNTs. In contrast, we have focused on the antimicrobial properties of oxidized single- and multi-wall CNTs embedded in CNT/PNCs. This decision was motivated by the likelihood that many pristine CNTs initially introduced into PNCs will have their surfaces oxidized by weathering in landfills and other environments prior to their interactions with microorganisms.[66, 67]

To explore the initial interactions of microorganisms with CNT/PNCs, oxidized CNTs (O-CNTs) were well-dispersed in polyvinyl alcohol (PVOH), which was chosen as the polymer matrix due to its lack of antimicrobial properties, allowing the effect of CNT inclusion to be clearly delineated.[68, 69] CNT/PVOH nanocomposites were exposed to the gram-negative microorganism *Pseudomonas aeruginosa*, a model aquatic and soil bacterium that can readily proliferate to form biofilms. Indeed, *Pseudomonas* species are ubiquitous in the environment where they are likely to encounter plastic waste and are

frequently responsible for biodegradation of organic matter and organic contaminants.[70] The interaction of *P. aeruginosa* with CNT/PNCs containing O-CNTs of different type (O-MWCNT vs. O-SWCNT) and CNT loading (0-10% w/w) was assessed using SYTO 9 and propidium iodide fluorescent stains to differentiate living and dead bacteria, as measured by the integrity of the cell membrane. This study was motivated by the desire to provide insights into the initial interaction of microorganisms with CNT/PNC surfaces having different CNT concentrations, representative of nanocomposite surfaces that may be present following weathering and/or other environmental degradation processes.

3.2. Experimental

3.2.1. O-CNT/PVOH Nanocomposite Preparation

A 2 mg/mL stock solution of polyvinyl alcohol (PVOH) was prepared by dissolving PVOH (Sigma Aldrich, M_w=31,000-50,000, 98%-99% hydrolyzed) into deionized water while stirring at 105 ˚C for four hours. The solution was filter-sterilized using a 0.2 μm acetate filter. A 0.05 mg/mL O-MWCNT stock suspension (NanoLab Inc., PD15L5-20-COOH, Lot. # 06-16-10, outer diameter 15 ± 5 nm, length 5-20 μm from the manufacturer) was prepared by sonicating 10 mg of O-MWCNTs into 200 mL of deionized water for ~20 hours using a Branson 1510 ultrasonic bath operating at 70 watts. The stock suspension was then centrifuged (5 min, 3000 rpm, Powerspin LX, Unico) to remove glass etched during sonication and some larger CNT bundles for a final concentration of slightly less than or equal to 0.05 mg/mL; the same stock solution was used throughout this study. The same procedure was followed for O-SWCNTs (Carbon

Solutions, P3-SWNT, Lot # 03-A014, outer diameter of individual or bundles 1-5 nm, length 1 ± 0.5 μm).

Immediately prior to spray-coating, the stock PVOH solution and stock O-CNT suspensions (O-MWCNTs and O-SWCNTs) were combined aseptically in different volume ratios to prepare casting solutions containing 0, 0.1, 1, 5, and 10% w/w O-CNT/PVOH. Each casting solution was shaken vigorously, sonicated for 5 min, and added to a spray bottle capable of nebulizing the solution. Autoclaved glass slides (1 x 25 x 75 mm) were placed onto a hot plate at 150 ˚C and sprayed from a consistent distance (approximately 25 cm) in 10 second intervals to flash dry the casting solution upon contact (Figure A3.1). This helped to minimize CNT aggregation during the drying process. Casting solutions were sprayed 30 times (1.07 mL/spray ± 0.05 mL/spray) to fully cover the glass slides with CNT/PNC. The uniformity and average thickness of the coating was determined by measuring the decrease in the Si(2p) signal from the underlying glass substrate using X-ray photoelectron spectroscopy (XPS) on different, randomly selected regions of a PVOH and 10% w/w O-MWCNT/PVOH nanocomposite.[71, 72] This analysis revealed that regardless of CNT/PNC type, the average thickness of the overlayer was ≈8 nm; further information on how film thicknesses were determined can be found in the appendix. All spray-coating was carried out inside a sterile biosafety cabinet (Labconco Purifier Class II Biosafety Cabinet). To verify consistency in the preparation and properties of the nanocomposites, replicate samples (at

least in duplicate) of each nanocomposite type (0 - 10% w/w) were prepared separately and studied in terms of their initial interactions with microorganisms.

3.2.2. CNT/PVOH Nanocomposite Characterization

Scanning electron microscopy (SEM) and X-ray photoelectron spectroscopy (XPS): Procedures for XPS and SEM imaging of PVOH and O-CNT/PVOH samples are outlined in the appendix. Replicate SEM images of different nanocomposite areas and separately sprayed slides are shown for each nanocomposite type in Figure A3.2. Spectra of O-SWCNT/PVOH nanocomposites are shown in Figure A3.3.

3.2.3. Dissolution Controls

To ensure PVOH dissolution did not have an effect on this study, high M_w PVOH (M_w=31,000-50,000) was used since it is less susceptible to dissolution compared to lower M_w analogues. Nevertheless, qualitative SEM control experiments were run to verify that CNT/PNCs did not change in surface composition, specifically in terms of the relative concentration of CNTs, over the short time course of our immersion experiments (1-6 h, Figures A3.4 and A3.5). Further information can be found in the appendix.

The upper limits of metal ion (from residual metal catalyst impurities in CNTs) and CNT release that could occur during one hour of nanocomposite immersion were assessed in separate experiments using ICP-MS. In both cases, the experiments involved exposing the highest loading of O-SWCNTs in PVOH (10% w/w) to sterile Milli-Q water for one hour. To determine the concentration of metal ions released, the supernatant that was generated after one hour was filtered through a 0.02 μm glass fiber membrane to remove all particulate matter and the metal ion concentration in the filtrate was measured with ICP-MS. This analysis revealed that the yttrium ion concentration in the supernatant was at or below the detection limit of the ICP-MS (<1 ppt). In contrast, the concentration

of released CNTs was determined by analyzing the supernatant (no filtration) for the presence of yttrium nanoparticles as a proxy for CNTs, as described in our previous publication, using ICP-MS in single particle mode (sp-ICP-MS).[73] Using this method we determined that the upper limit of the released CNT concentration from the nanocomposites was approximately 90 ppb after one hour immersion time in sterile Milli-Q water. Further information can be found in the appendix.

3.2.4. Microbial Growth and O-CNT/PVOH Nanocomposite Inoculation (1 h and 6 h)

To assess the effect of CNT loading on the antimicrobial properties of O-CNT/PVOH nanocomposites, the initial cytotoxicity of *P. aeruginosa* (ATC 27853) on CNT/PNC surfaces was determined. Each O-CNT/PVOH slide was submerged in a petri dish containing 15 mL of exponential phase *P. aeruginosa* in BMM under ambient conditions. The nanocomposite slides were then removed from the inoculum after one or six hours, washed with depleted media, and immediately transferred into fresh sterile petri dishes for subsequent LIVE/DEAD staining. Each CNT/PNC sample of a particular CNT loading was exposed to three separately grown *P. aeruginosa* cultures to ensure consistency in the number of attached cells between cultures. Examples of the reproducibility of the data acquired from these replicates are shown for PVOH, 10% w/w O-MWCNT/PVOH and 10% w/w O-SWCNT/PVOH in Figure A3.6. Similarly, we verified that for each nanocomposite type (0 – 10% w/w), the number of attached cells was statistically the same for samples that were spray-coated on different occasions. Media composition, growth conditions, and six hour LIVE/DEAD images are described in the appendix (Figures A3.7-A3.9).

To assess the possibility that released CNTs could affect the microorganisms in solution, two separate growth curves were conducted in the presence of 90 ppb O-

MWCNTs and 90 ppb O-SWCNTs. These CNT concentrations were selected because they represent the upper limit of released CNTs observed during the course of our release control experiments using sp-ICP-MS. Results from these growth curves revealed that there was no effect at these low (ppb) CNT concentrations relative to a growth curve without CNTs. Indeed, previous studies have shown that CNT concentrations in the ppm range are typically needed to inhibit cell growth.[48] Results of this analysis can be found in the appendix (Figure A3.8 and related text).

3.2.5. LIVE/DEAD Staining

A FilmTracer LIVE/DEAD Biofilm Viability Kit (Molecular Probes, Invitrogen) containing SYTO 9 and propidium iodide (PI) stains was used.[74] At least 15 images per CNT loading prepared at different times (at least two different occasions) and exposed to three different cultures, were analyzed to determine the average percentage and standard deviation of living *P. aeruginosa* cells on a given CNT/PNC slide. Positive and negative controls for cytotoxicity were run: these included staining microbes attached to PVOH (0% w/w O-CNTs) and microbes purposely lysed with ethanol on PVOH (Fig. S10), respectively. Further details, as well as a significant number of experimental controls, can be found in the appendix (Figures A3.11-A3.15). A FilmTracer SYPRO Ruby Red Biofilm Viability Kit (Invitrogen, Life Technologies) was used to stain the EPS on PVOH, 10% w/w O-MWCNT/PVOH and 10% w/w O-SWCNT/PVOH samples after one hour of microbial exposure (Figure A3.16). Background fluorescent controls were run for this stain as well (Figure A3.17).[75]

3.2.6. Confocal Laser Scanning Microscopy

Microbes on CNT/PNC surfaces stained with SYTO® 9 and PI were imaged using a Zeiss LSM 510 Multiphoton Confocor 3 CLSM with a 40x water immersion objective

(N.A. 1.2) to generate dual channel 3D images for each sample. Confocal laser scanning microscopy (CLSM), which is commonly referred to as laser confocal fluorescence spectroscopy, is a type of fluorescent microscopy that involves excitation of a molecule to a higher energy state using a monochromatic laser source and emission of a lower energy photon. This emission process is called fluorescence and certain chromophores are able to absorb at one wavelength and fluorescence at a higher (lower energy) wavelength. In this study, bacteria are stained with SYTO 9 (482 nm excitation, 500 nm emission) and propidium iodide (490 nm, 635 nm) and the fluorescent signal is detected to generate an image.[74] In contrast to traditional fluorescent microscopy, CLSM is able to focus at one point on individual planes of a sample and operate using dual channels (both dyes can be seen at once). A pinhole is used to eliminate any fluorescence coming from outside of the focal point and images can be raster in the x and y direction with a very small depth. Then the focal plane in increased and further sectioning in the z direction can take place. This allows the user to build a 3D image as a series of confocal stacks.[71] This is most useful in Chapter 4, when biofilms are imaged, since they have significant thicknesses that cannot be captured with tradition fluorescence microscopy. Details of the CLSM used in this study are described below. Further information can be found in the appendix.

3.3. Results and Discussion

3.3.1. CNT/PNC Characterization

While the SEM images of pure PVOH exhibited surfaces devoid of any cylindrical, CNT-like structures (Figure 3.1), the presence of CNTs at the surface of O-

CNT/PVOH nanocomposites became increasingly apparent as a function of increasing CNT loading.

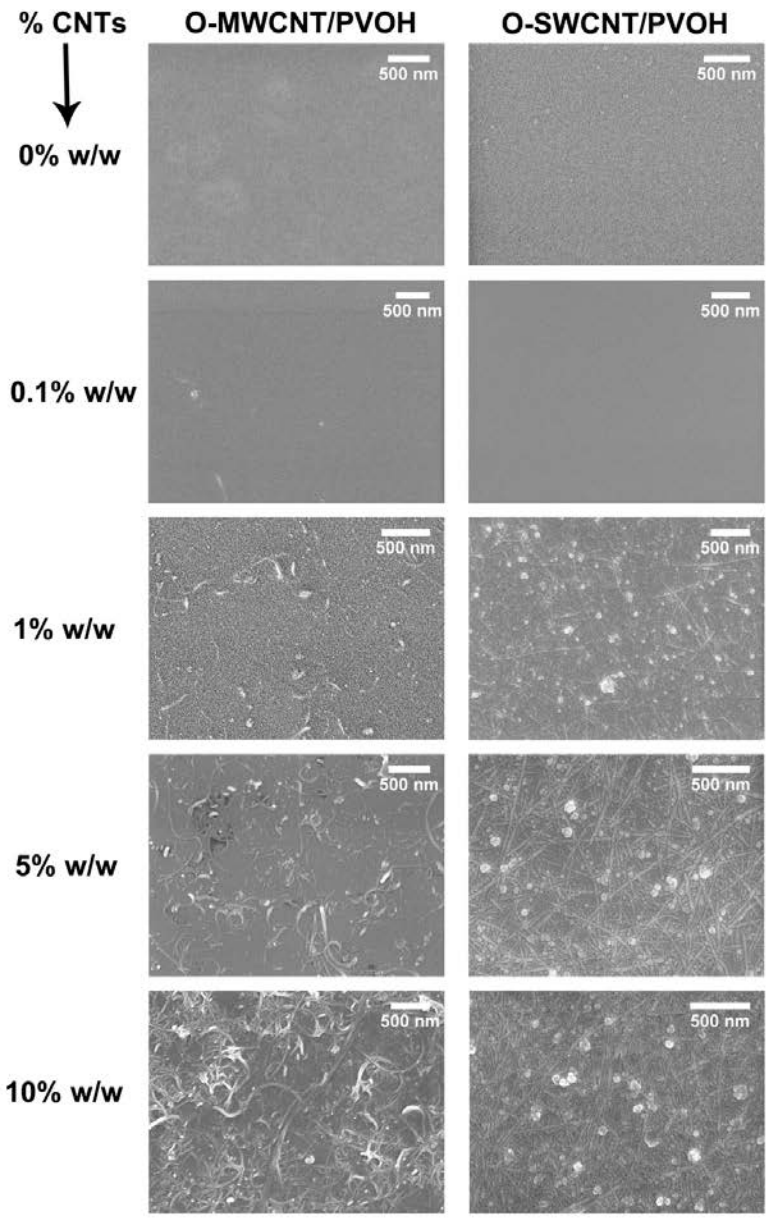

Figure 3.1 SEM images of well-dispersed, spray-dried O-MWCNT/PVOH and O-SWCNT/PVOH nanocomposites as a fraction of CNT loading ranging from 0-10% w/w.

SEM images also show O-SWCNTs and O-MWCNTs randomly distributed across the surface with minimal signs of aggregation across the range of CNT loadings

studied (0 – 10% w/w). The uniformity of the surface is demonstrated by the consistency of SEM images acquired in different, randomly selected regions (Figure A3.2a-i).

To complement SEM data, XPS analysis was performed for PVOH nanocomposites with varied O-MWCNT loadings (≥ 5% w/w), with the goal of evaluating the CNT concentration at the O-CNT/PVOH surfaces (Figure 3.2). For O-MWCNT/PVOH nanocomposites, the C(1s) spectral envelope could be well fit by contributions from the PVOH and the CNT components, along with a small (≤ 7.5%) contribution from amorphous carbon contamination. The ability to determine the O-MWCNT surface concentration from the C(1s) fitting protocol can be attributed to the differential charging behavior of PVOH and the O-MWCNTs, which effectively separates their spectral envelopes.[32, 76] In contrast to the behavior of O-MWCNT/PVOH nanocomposites, O-SWCNT/PVOH nanocomposites did not differentially charge to an extent that permitted spectral deconvolution of the individual components (Figure A3.3).

XPS analysis of the C(1s) region indicates that the O-MWCNT concentration at the surface in the % w/w region under investigation (< 10% w/w) should be directly proportional to the composition of the casting solution (R^2=0.92) (Figure 3.2). We attribute this proportionality in large part to a consequence of the flash drying method used to prepare the CNT/PNCs, which greatly restricts CNT aggregation, and essentially

"locks" their structure and composition within the polymer into a close representation of the O-CNT/PVOH distribution in the casting solution.

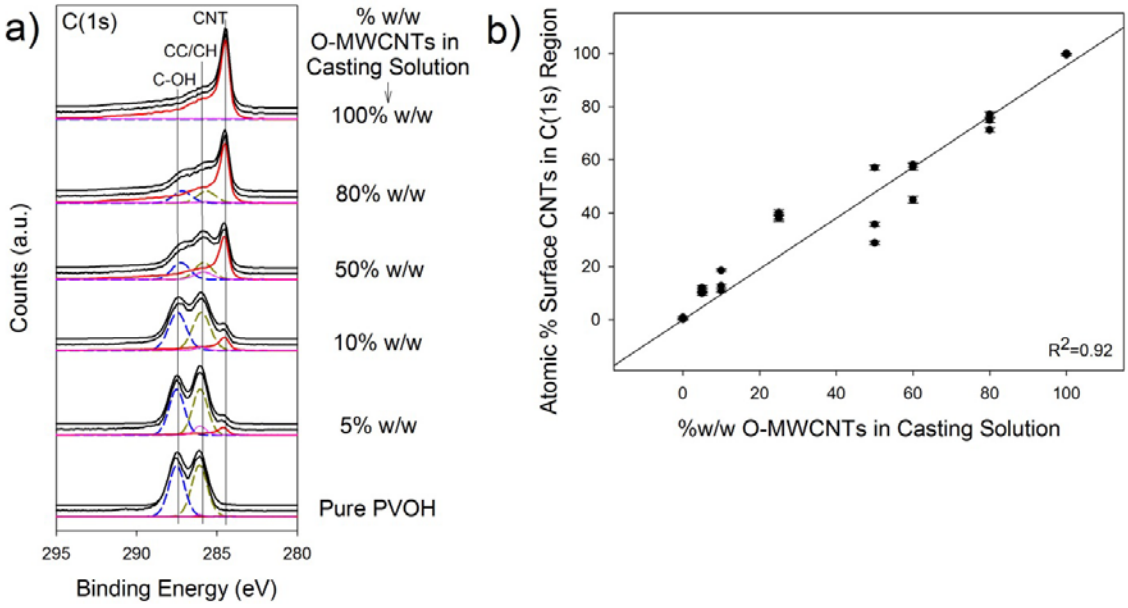

Figure 3.2. X-ray photoelectron spectroscopy (XPS) characterization of O-CNT/PVOH nanocomposites. a) C(1s) region of O-MWCNT/PVOH nanocomposites with increasing O-MWCNT loading. The fitted PVOH components (dashed lines) and the O-MWCNT component (solid line) are shown within the carbon envelope. b) % w/w O-MWCNTs in casting solution vs. atomic % surface CNTs determined using XPS fitting of the C(1s) envelope. Error bars are reflective of the error in the fitting protocol for a given sample.

3.3.2. Antimicrobial Properties of CNT/PNCs

Figure 3.3 and Figure 3.4 show representative results of LIVE/DEAD staining used in conjunction with CLSM to assess the cytotoxicity of *P. aeruginosa* attached to O-MWCNT and O-SWCNT/PVOH surfaces after one hour of inoculation. This time period was selected because it was sufficient for > 1500 microbes to attach directly onto the CNT/PNC surfaces and therefore provide a statistically significant measure of the surface's initial antimicrobial properties.

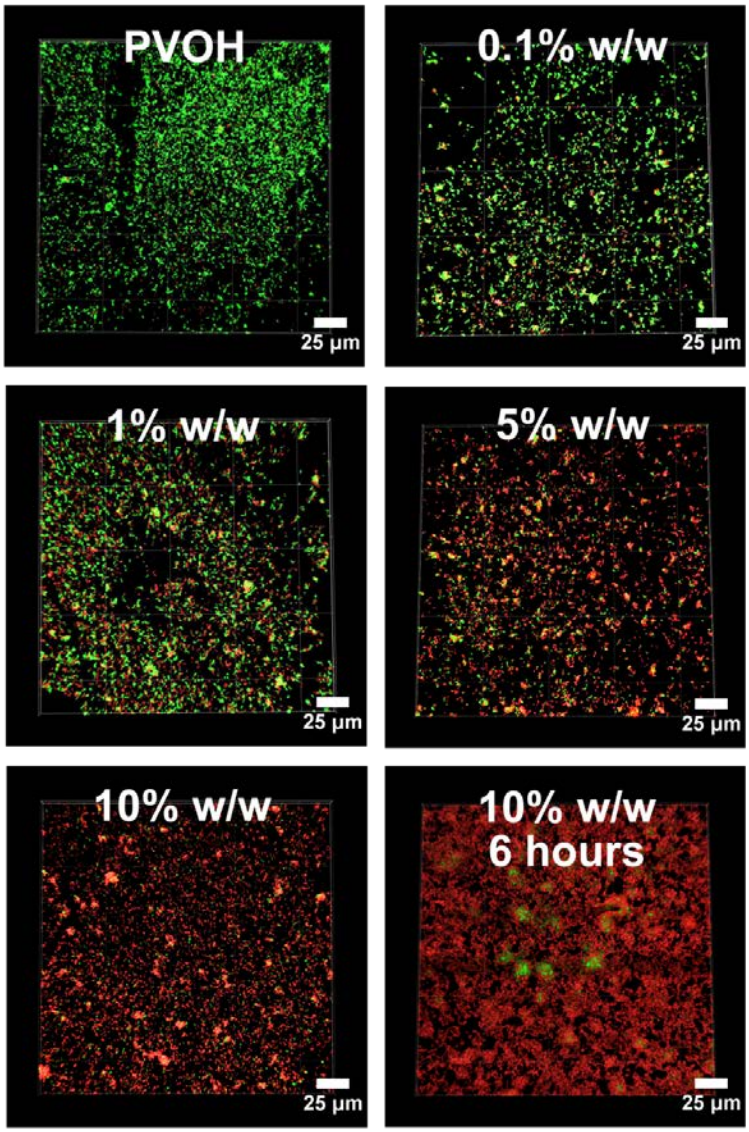

Figure 3.3. CLSM images of LIVE/DEAD stained *P. aeruginosa* grown statically for 1 hour on O-MWCNT/PVOH slides with increasing O-MWCNT loading from 0 - 10% w/w and at 6 hours on a 10% w/w nanocomposite.

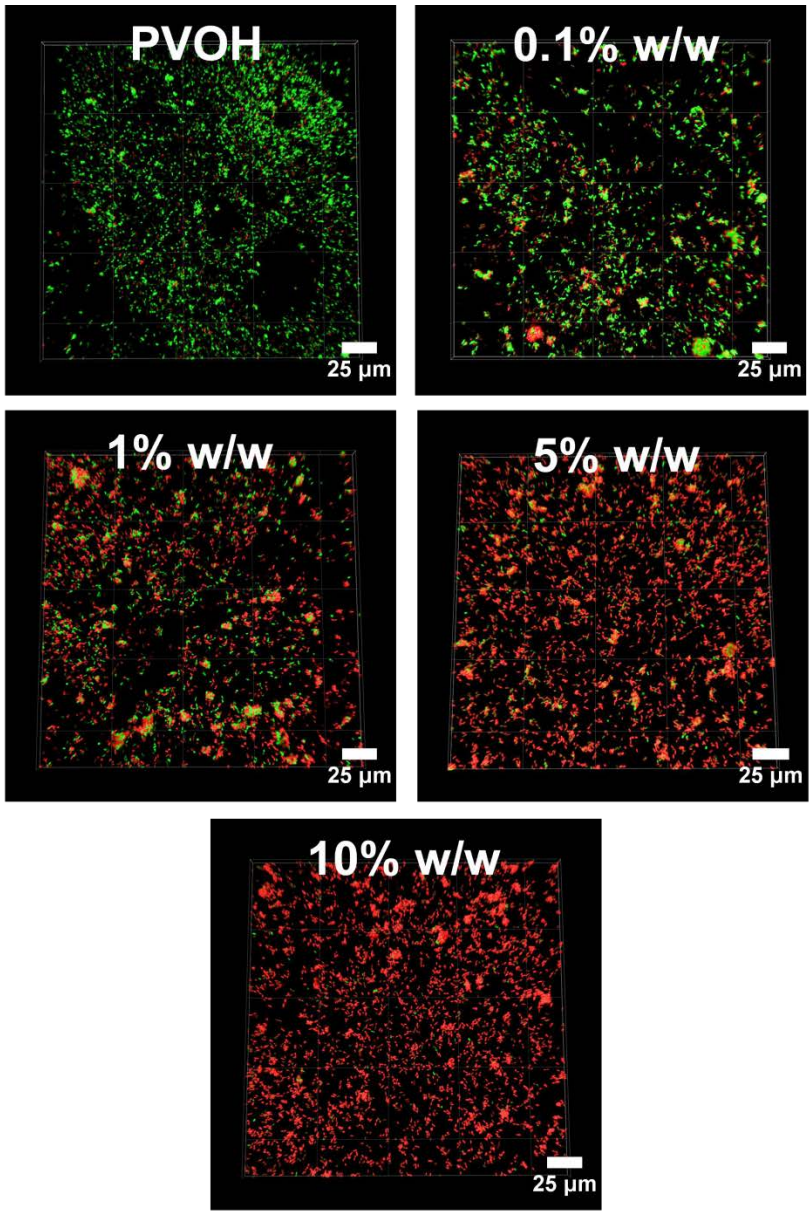

Figure 3.4. CLSM images of LIVE/DEAD stained *P. aeruginosa* grown statically for 1 hour on O-SWCNT/PVOH slides with increasing O-SWCNT loading from 0-10% w/w.

Cells that were considered attached were those that remained on the nanocomposite surfaces during the staining procedure. Living and dead cells were counted using image analysis software and results are shown in Figure 3.5.

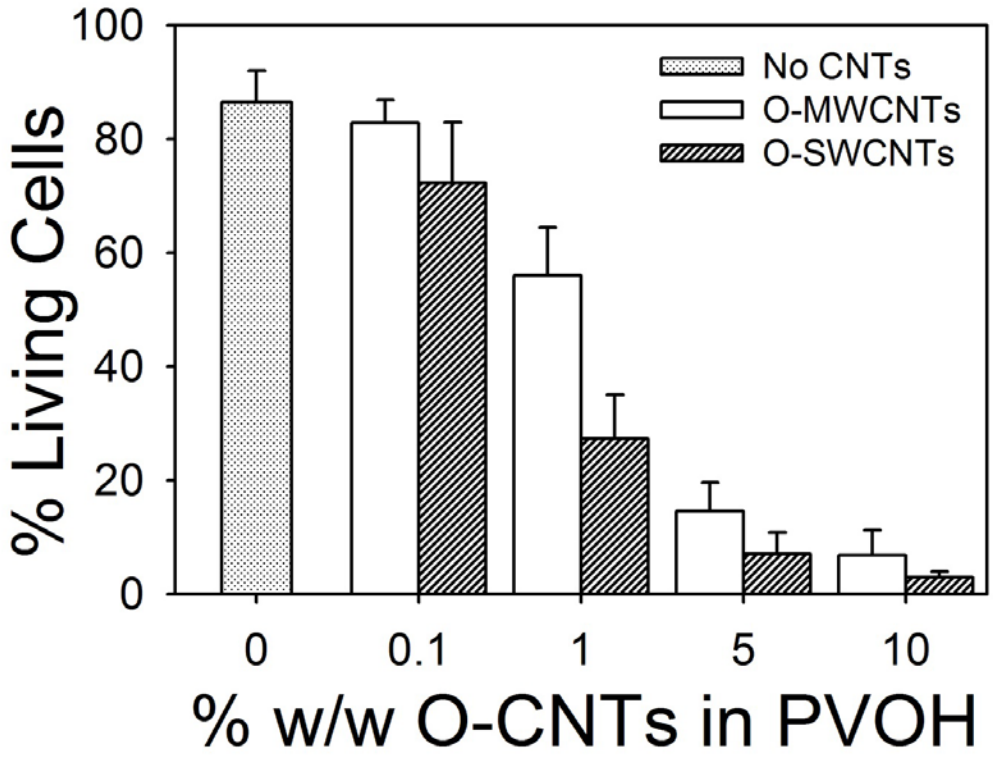

Figure 3.5. Live and dead cell counting of *P. aeruginosa* confocal images using image analysis software. The average percentage ± one standard deviation of attached living cells from ≥15 images of each O-MWCNT and O-SWCNT/PVOH nanocomposite loading (0 – 10% w/w) is shown.

For PVOH, the CLSM image is dominated by green fluorescent cells, indicating that PVOH is benign to *P. aeruginosa*. In contrast, the antimicrobial properties of the CNT/PNC surfaces increased systematically with both O-MWCNT and O-SWCNT loading as evidenced by the increasing number of red fluorescent cells (Figure 3.3 &

Figure 3.4). Consequently, the antimicrobial properties exhibited by the O-CNT/PVOH nanocomposite surfaces are due to the inclusion of O-CNTs (Figure 3.3 & Figure 3.4).

At the highest O-MWCNT and O-SWCNT loadings of 10% w/w, virtually all (> 90%) of the *P. aeruginosa* fluoresced red, indicating that the majority of cells had died. However, longer term (6 h) experiments conducted on 10% w/w O-MWCNTs (Figure 3.3) showed evidence of healthy (green) biofilm formation for microorganisms located on top of dead cells (red). Similarly, careful analysis of the CLSM images acquired after one hour of contact time between the *P. aeruginosa* and the CNT/PNC surfaces revealed that some of the living microorganisms are actually deposited on top of dead microorganisms. CLSM analysis of these "live on top of dead" structures exhibited heights in the range of ~4 - 7 μm. In contrast, individual microorganisms attached to the surfaces had apparent heights of ~4 - 5 μm. It should be noted that in CLSM, the height of the microbes appears stretched and taller than their actual height (0.5-1 μm) due to the limited vertical resolution of the CLSM (>1 μm) compounded by fluorescence scattering between optical slices (Figure A3.18 & A3.19).[70] Thus, "live on top of dead" structures were consistent with about two microbial layers, with living cells located on top of dead cells, the latter in direct contact with the CNT/PNC surfaces. Examples of this phenomenon are circled in white for 1% w/w O-CNT/PVOH samples (Figures A3.18 & A3.19). The nature of these structures supports the idea that CNT contact is necessary to cause cell death.

Additional insights into the antimicrobial properties of CNTs observed during the initial stages of microbial attachment can be attained by considering the distribution and concentration of CNTs at the interface in relationship to the two-dimensional footprint of an attached *P. aeruginosa* microorganism, which is rod-shaped and approximately 1 μm

in length by > 0.5 μm wide, as revealed by SEM (Figure A3.20).[70] By superimposing this two-dimensional microbe footprint onto an SEM image of a PNC surface, we can gauge the degree of direct interaction/contact between attached *P. aeruginosa* microorganisms and CNTs at a particular CNT loading (Figures A3.18 and A3.19). As shown in Figure A3.19, this analysis reveals that the 1% w/w O-SWCNT/PVOH nanocomposite surface consists of a relatively dense O-SWCNT mesh, which is a reflection of the extremely high aspect ratio of CNTs (micro-sized lengths and nanometer-scaled widths). Consequently, most microorganisms that attach to the CNT/PNC surface must make contact with multiple CNTs (> 5 CNTs). However, the corresponding CLSM image for 1% w/w O-SWCNTs shown in Figure 3.4 reveals that more than 20% of the attached microorganisms are still alive despite many appearing to be in direct contact with the underlying surface. Moreover, the distribution of living and dead microorganisms on the surface is entirely random with no evidence of any patchiness that would indicate a lack of CNT dispersion in localized areas. Thus, our experimental observations indicate that a single contact event or interaction between a CNT and an attached microorganism does not guarantee that the microorganism will die; otherwise, all of the attached *P. aeruginosa* on the 1% w/w O-SWCNT/PVOH nanocomposites surface would be dead, which is not the case.

We note that it is possible that not every CNT contact event with an adsorbed microorganism is disposed to cause membrane disruption. This would be the case, for example, if a specific interaction were required, such as the puncturing of the membrane by the exposed ends of a CNT. The amount of EPS excretion, a common defense used in biofilms to protect cells from environmental stressors,[42] was tested as it could serve to

diminish the antimicrobial nature of the CNT/PNCs by effectively shielding attached bacteria from the CNTs. The level of EPS was shown to be minimal on the CNT/PNC surfaces after one hour using a biofilm matrix stain (SYPRO Ruby Biofilm Matrix Stain), indicating that EPS excretion is not an important factor in the present study (Figure A3.16). Regardless of the detailed explanation of this phenomenon, once the O-SWCNT loading was increased to 10% w/w, almost all *P. aeruginosa* (97%) attached to the PNC surface experienced >5 CNT contact events. Under these circumstances, the number of CNT contact events and greater contact area between adsorbed microorganisms and surface-bound CNTs was apparently sufficient to cause almost all of the attached microorganisms to die (Figure 3.4 and Figure 3.5). An analogous argument can be made for O-MWCNTs on the basis of the data shown in Figure 3.3 and Figure 3.5. The present study is uniquely well-positioned to assess the role that contact area plays in determining the antimicrobial properties of CNTs because the distribution and concentration of CNTs at the surface has been well-defined through the use of SEM and XPS across a range of CNT loadings.

Our experimental data also clearly demonstrates that the antimicrobial properties of CNTs are not eliminated when they are oxidized, regardless of type (SWCNT or MWCNT) or manufacturer (Carbon Solutions and NanoLab Inc., respectively). Figure A3.21 demonstrates that as a function of increasing CNT loading, the fraction of living cells deposited on both O-SWCNT and O-MWCNT/PVOH surfaces can be reasonably well fit with a first order exponential decay profile. On the basis of this analysis, the O-SWCNTs are approximately three times more cytotoxic than O-MWCNTs on a % w/w basis. We ascribe this enhancement of O-SWCNT/PVOH antimicrobial properties in part

to a number density effect, since at the same CNT loading there is a greater number of O-SWCNTs than O-MWCNTs at the PNC surface. As a result, the number of contact events and total contact area between attached microbes and CNTs will always be greater for O-SWCNTs as compared to O-MWCNTs (Figure A3.22). Regardless, the antimicrobial properties of O-SWCNTs and O-MWCNTs do not differ markedly from one another as a function of CNT loading. We ascribe this similarity to be a consequence, at least in part, of the high oxygen levels on the CNTs used (8.6% O for O-MWCNTs, 9.2% O for O-SWCNTs as measured by XPS). This level of surface oxidation is expected to significantly disrupt the graphenic sidewall structure and cause the surfaces of O-SWNCNTs and O-MWCNTs to appear somewhat structurally and chemically similar, containing graphenic sidewalls, interspersed with defect regions (and ends) where oxygen-functional groups are localized.

Results from the present investigation can be compared with other related studies. For example, Schiffman *et al.* evaluated the cytotoxicity of pristine SWCNTs towards *E. coli*, another gram-negative bacterium, as a function of SWCNT loading in electrospun polymer mats. As the loading of pristine SWCNTs increased from 0.1 to 1% w/w, cell death increased from 18% to 76%, respectively.[60] In the present study, the cytotoxicity we observed for *P. aeruginosa* increased from 27% to 73% cell death as the O-SWCNT loading increased from 0.1% to 1%, respectively. In another study, Rodrigues *et al.* saw 90% cell death of *E. coli* on MWCNT/poly(N-vinylcarbazole) nanocomposites with 6% w/w MWCNT, while in our studies on O-CNT/PVOH nanocomposites, we observed 86% cell death of *P. aeruginosa* for 5% w/w O-MWCNT.[59] Although the microorganisms and type of CNTs differed amongst these CNT/PNC studies, the

similarities in the results are striking and suggest that the antimicrobial properties of CNT/PNCs toward gram-negative bacteria may be broadly similar across a range of CNT types. Interestingly, in studies where pristine SWCNTs and MWCNTs were simply deposited onto surfaces, only 85% and 30% cell death occurred for *E. coli*, respectively.[43, 44, 77] Similar or even greater levels of cytotoxicity were observed in the present study for surfaces that contained ≤ 10% w/w CNTs. This suggests that the CNT dispersion state may also be important in determining antimicrobial properties.[43, 44, 47, 59, 77]

Although our experimental data does not provide a means to definitively prove which mechanism(s) are responsible for the cytotoxicity of oxidized CNTs, a mechanism that we can rule out in this study is one being caused by the release of metal ions from metal nanoparticles that are often present in CNTs (Figure A3.23). This was evaluated explicitly in the present study by using ICP-MS to measure the yttrium ion concentration released from O-SWCNT/PVOH nanocomposites (~0.2 ppt) after an hour of immersion in sterilized Milli-Q water. Results showed that the metal ion concentration was at or below the detection limit of the ICP-MS (~0.1-1 ppt) (Figure A3.23), much lower than the typical concentrations within the parts per billion to parts per million range that can lead to an inhibitory effect on microbial growth.[78, 79] Moreover, a cytotoxicity mechanism governed by the release of metal ions would be unlikely to require direct contact to exist between CNTs and the microorganisms. Cell death simply caused by an increase in hydrophobicity from an increase in CNT content was also ruled out by showing that a hydrophobic surface (poly-ε-caprolactone) does not exhibit antimicrobial properties towards *P. aeruginosa* after one hour of bacterial deposition (Figure A3.24). We note that

most of the commonly proposed mechanisms that are used to explain CNT cytotoxicity could reasonably be expected to scale with the total contact area between attached microorganisms and polymer-surface bound CNTs. For example, the probability that the end of a CNT would align correctly so as to puncture the cell membrane of an attached microorganism should increase with the CNT-microorganism contact area.[43, 44, 49] A cytotoxicity mechanism that scaled with the number of contact events and/or the CNT-microorganism contact area would also be anticipated should membrane lipid disruption or protein binding contribute to cell death.[50, 80] Similarly, the magnitude of oxidative stress generated by CNTs would also increase with CNT loading.[43, 50-52]

In terms of broader environmental implications, this investigation reveals that the cytotoxicity of CNTs will be preserved for both SWNCTs and MWCNTs embedded in commercial products after oxidation. Consistent with previous studies, our results demonstrate the necessity for direct contact to exist between surface-bound CNTs and attached microorganisms for antimicrobial effects to occur, with the caveat that not every CNT-microorganism interaction leads to cell death. [43, 44, 47, 59, 60, 77] In most commercial products where CNTs are not directly exposed to the surrounding environment, antimicrobial properties will not manifest themselves until CNTs are exposed at the surface of the material (e.g. after a coating has been degraded). However, even under these conditions, CNT-containing surfaces cannot be considered truly antimicrobial since the onset of biofilm growth will only be slowed by the presence of surface-bound CNTs, but not inhibited.

3.4. Acknowledgements

The authors would like to thank Marielle Remillard, Julie Bitter, and Miranda Gallagher for their contributions as well as Dr. Michael McCaffery, Alice Sanchez, and

Erin Pryce of the Integrated Imaging Center for their guidance in image acquisition, processing, and development of image analysis software. Additionally, we would like to acknowledge Mark Koontz for his help in acquiring the SEM images and Jingjing Wang and Jim Ranville from the Colorado School of Mines for their analysis of metal ion release. The authors would also like to thank the JHU INBT Pilot Project, the NSF (CBET #1236493), and the Owens Graduate Fellowship for their financial support.

3.5. Appendix 3 Summary

Additional information on spray-coating (Figure A3.1); SEM analysis; CNT broadening in SEM; replicate images at each nanocomposite loading (Figure A3.2); details of XPS analysis and spectra of O-SWCNT/PVOH nanocomposites (Figure A3.3); qualitative SEM dissolution controls (Figures A3.4 & A3.5); replicate CLSM images of LIVE/DEAD stained *P. aeruginosa* on PVOH, 10% w/w O-MWCNT/PVOH, and 10% w/w O-SWCNT/PVOH nanocomposites from three separately grown cultures to showcase cell attachment consistency in the CLSM data (Figure A3.6); microbial frozen stock preparation; growth curves in LB broth with kinetic analysis (Figure A3.7); BMM media composition, microbial growth procedures; growth curves in BMM with and without 90 ppb O-SWCNTs and O-MWCNTs with kinetic analysis (Figure A3.8); details of the LIVE/DEAD staining procedure, a CLSM image of LIVE/DEAD stained *P. aeruginosa* grown on PVOH for 6 hours (Figure A3.9); a CLSM image of a dead control where *P. aeruginosa* was intentionally lysed with ethanol and LIVE/DEAD stained (Figure A3.10); details of CLSM; details of the LIVE/DEAD cell counting software analysis; LIVE/DEAD stained background fluorescence controls (Figure A3.11); cell attachment controls (Figure A3.12); fluorescence photobleaching and quenching controls (Figures A3.13-A3.14); EPS staining and EPS stain background fluorescence controls

(Figures A3.16 & A3.17); spatial comparison of *P. aeruginosa* on 1% w/w O-MWCNT and O-SWCNT/PVOH nanocomposites using SEM with "live-on-dead" structures shown in CLSM (Figures A3.18 & A3.19), SEM microbial fixation procedure details and images of *P. aeruginosa* on PVOH and 10% w/w O-MWCNT/PVOH (Figure A3.20); antimicrobial trends on O-MWCNT/PVOH and O-SWCNT/PVOH nanocomposites as a function of surface CNT loading (Figure A3.21); an illustration of the number density effect of O-MWCNTs versus O-SWCNTs in PVOH at 1% w/w with respect to microorganism attachment (Figure A3.22); ICP-MS analysis of metal ion release (Figure A3.23); sp-ICP-MS analysis of CNT release using ^{89}Y as a proxy for CNTs released from nanocomposites in this study; a CLSM image of LIVE/DEAD stained *P. aeruginosa* on hydrophobic PCL (Figure A3.24); and a table of CNT metal content as determined by energy dispersive X-ray analysis (EDS).

3.6. References

1. McClory, C.; Chin, S. J.; McNally, T., Polymer/Carbon Nanotube Composites. *Aust. J. Chem.* **2009,** *62*, (8), 762-785.
2. Jones, J., W. E.; Chiguma, J.; Johnson, E.; Pachamuthu, A.; Santos, D., Electrically and thermally conducting nanocomposites for electronic applications. *Materials* **2010,** *3*, (2), 1478-1496.
3. Esawi, A. M. K.; Farag, M. M., Carbon nanotube reinforced composites: Potential and current challenges. *Mater. Des.* **2007,** *28*, 2394-2401.
4. Rahmat, M. H., P., Carbon nanotube-polymer interactions in nanocomposites: A review. *Compos. Sci. Technol.* **2011,** *72*, (1), 72-84.
5. Gangopadhyay, R.; De, A., Conducting Polymer Nanocomposites: A Brief Overview. *Chem. Mater.* **2000,** *12*, (3), 608-622.
6. Moniruzzaman, M.; Winey, K. I., Polymer nanocomposites containing carbon nanotubes. *Macromolecules* **2006,** *39*, (16), 5194-5205.
7. Sahoo, N. G.; Rana, S.; Cho, J. W.; Li, L.; Chan, S. H., Polymer nanocomposites based on functionalized carbon nanotubes. *Prog. Polym. Sci.* **2010,** *35*, (7), 837-867.
8. Du, J.; Bai, J.; Cheng, H., The present status and key problems of carbon nanotube based polymer composites. *Express Polymer Letters* **2007,** *1*, (5), 253-273.

9. Allaoui, A.; Bai, S.; Cheng, H. M.; Bai, J. B., Mechanical and electrical properties of a MWNT/epoxy composite. *Compos. Sci. Technol.* **2002,** *62*, (15), 1993-1998.
10. Ajayan, P. M.; Schadler, L. S.; Giannaris, C.; Rubio, A., Single-walled carbon nanotube-polymer composites: strength and weakness. *Adv. Mater. (Weinheim, Ger.)* **2000,** *12*, (10), 750-753.
11. Baughman, R. H.; Zakhidov, A. A.; de Heer, W. A., Carbon nanotubes - the route toward applications. *Science* **2002,** *297*, (5582), 787-792.
12. Coleman, J. N.; Khan, U.; Blau, W. J.; Gun'ko, Y. K., Small but strong: A review of the mechanical properties of carbon nanotube-polymer composites. *Carbon* **2006,** *44*, (9), 1624-1652.
13. Lau, K. T., Interfacial bonding characteristics of nanotube/polymer composites. *Chem. Phys. Lett.* **2003,** *370*, (3-4), 399-405.
14. Lau, K. T.; Hui, D., Effectiveness of using carbon nanotubes as nano-reinforcements for advanced composite structures. *Carbon* **2002,** *40*, (9), 1605-1606.
15. Rahmat, M.; Das, K.; Hubert, P., Interaction stresses in carbon nanotube-polymer nanocomposites. *ACS Appl. Mater. Interfaces* **2011,** *3*, (9), 3425-3431.
16. Qian, D.; Dickey, E. C.; Andrews, R.; Rantell, T., Load transfer and deformation mechanisms in carbon nanotube-polystyrene composites. *Appl. Phys. Lett.* **2000,** *76*, (20), 2868-2870.
17. Mylvaganam, K.; Zhang, L. C., Fabrication and application of polymer composites comprising carbon nanotubes. *Recent Pat. Nanotechnol.* **2007,** *1*, (1), 59-65.
18. Martin, C. A.; Sandler, J. K. W.; Shaffer, M. S. P.; Schwarz, M. K.; Bauhofer, W.; Schulte, K.; Windle, A. H., Formation of percolating networks in multi-wall carbon-nanotube-epoxy composites. *Compos. Sci. Technol.* **2004,** *64*, (15), 2309-2316.
19. Sandler, J. K. W.; Kirk, J. E.; Kinloch, I. A.; Shaffer, M. S. P.; Windle, A. H., Ultra-low electrical percolation threshold in carbon-nanotube-epoxy composites. *Polymer* **2003,** *44*, (19), 5893-5899.
20. Lu, D. D.; Li, Y. G.; Wong, C. P., Recent advances in nano-conductive adhesives. *J. Adhes. Sci. Technol.* **2008,** *22*, (8-9), 815-834.
21. Li, J.; Lumpp, J. K.; Andrews, R.; Jacques, D., Aspect ratio and loading effects of Multiwall carbon nanotubes in epoxy for electrically conductive adhesives. *J. Adhes. Sci. Technol.* **2008,** *22*, (14), 1659-1671.
22. Paik, K. W.; Han, S. H., A study on B-stage CNT/epoxy composite films for electronic packaging applications. *Pricm 7, Pts 1-3* **2010,** *654-656*, 2755-2758.
23. (WWICS) Woodrow Wilson International Center for Scholars "The Project on Emerging Nanotechnologies" Nanotechnology Consumer Products Inventory http://www.nanotechproject.org/inventories/consumer/.
24. Duncan, T. V., Applications of nanotechnology in food packaging and food safety: Barrier materials, antimicrobials and sensors. *J. Coll. Interface Sci.* **2011,** *363*, (1), 1-24.
25. Nanocyl Carbon nanotube applications: fuel system components: http://www.nanocyl.com/Products-Solutions/Sectors/Automotive/Fuel-System-Components.

26. Soulestin, J.; Prashantha, K.; Lacrampe, M. F.; Krawczak, P., *Bioplastics based nanocomposites for packaging applications*. 2011.
27. De, V. M. F. L.; Tawfick, S. H.; Baughman, R. H.; Hart, A. J., Carbon Nanotubes: Present and Future Commercial Applications. *Science* **2013,** *339*, (6119), 535-539.
28. Petersen, E. J.; Zhang, L. W.; Mattison, N. T.; O'Carroll, D. M.; Whelton, A. J.; Uddin, N.; Nguyen, T.; Huang, Q. G.; Henry, T. B.; Holbrook, R. D.; Chen, K. L., Potential release pathways, environmental fate, and ecological risks of carbon nanotubes. *Environ. Sci. Technol.* **2011,** *45*, (23), 9837-9856.
29. Hirth, S.; Cena, L.; Cox, G.; Tomović, Ž.; Peters, T.; Wohlleben, W., Scenarios and methods that induce protruding or released CNTs after degradation of nanocomposite materials. *J. Nanopart. Res.* **2013,** *15*, (4), 1-15.
30. Kingston, C.; Zepp, R.; Andrady, A.; Boverhof, D.; Fehir, R.; Hawkins, D.; Roberts, J.; Sayre, P.; Shelton, B.; Sultan, Y.; Vejins, V.; Wohlleben, W., Release characteristics of selected carbon nanotube polymer composites. *Carbon* **2014,** *68*, (0), 33-57.
31. Gottschalk, F.; Nowack, B., The release of engineered nanomaterials to the environment. *J. Environ. Monit.* **2011,** *13*, (5), 1145-1155.
32. Ging, J.; Tejerina-Anton, R.; Ramakrishnan, G.; Nielsen, M.; Murphy, K.; Gorham, J. M.; Nguyen, T.; Orlov, A., Development of a conceptual framework for evaluation of nanomaterials release from nanocomposites: Environmental and toxicological implications. *Sci. Total Environ.* **2014,** *473*, 9-19.
33. Nguyen, T.; Pelligrin, B.; Bernard, C.; Gu, X.; Gorham, J. M.; Stutzman, P.; Stanley, D.; Shapiro, D.; Bryrd, E.; Hettenhouse, R.; Chin, J., Fate of nanoparticles during life cycle of polymer nanocomposites. *J. Phys.: Conf. Ser.* **2011,** *34*, 012060.
34. Costerton, J. W.; Cheng, K. J.; Geesey, G. G.; Ladd, T. I.; Nickel, J. C.; Dasgupta, M.; Marrie, T. J., Bacterial biofilms in Nature and disease. *Annu. Rev. Microbiol.* **1987,** *41*, 435-64.
35. Andersson, S.; Rajarao, G. K.; Land, C. J.; Dalhammar, G., Biofilm formation and interactions of bacterial strains found in wastewater treatment systems. *FEMS Microbiol. Lett.* **2008,** *283*, (1), 83-90.
36. Francolini, I.; Norris, P.; Piozzi, A.; Donelli, G.; Stoodley, P., Usnic acid, a natural antimicrobial agent able to inhibit bacterial biofilm formation on polymer surfaces. *Antimicrob. Agents Chemother.* **2004,** *48*, (11), 4360-4365.
37. Carlson, R. P.; Taffs, R.; Davison, W. M.; Stewart, P. S., Anti-biofilm properties of chitosan-coated surfaces. *J. Biomater. Sci., Polym. Ed.* **2008,** *19*, (8), 1035-1046.
38. Leja, K.; Lewandowicz, G., Polymer Biodegradation and Biodegradable Polymers--A Review. *Pol. J. Environ. Stud.* **2010,** *13*, (2), 255-266.
39. Shah, A. A.; Hasan, F.; Hameed, A.; Ahmed, S., Biological degradation of plastics: A comprehensive review. *Biotechnol. Adv.* **2008,** *26*, (3), 246-265.
40. Sivan, A., New Perspectives in Plastic Biodegradation. *Curr. Opin. Biotechnol.* **2011,** *22*, (3), 422-426.
41. Tokiwa, Y.; Calabia, B. P.; Ugwu, C. U.; Alba, S., Biodegradability of Plastics. *International Journal of Molecular Sciences* **2009,** *10*, (9), 3722-3742.

42. Rodrigues, D. F.; Elimelech, M., Toxic effects of single-walled carbon nanotubes in the development of *E. coli* biofilm. *Environ. Sci. Technol.* **2010,** *44*, (12), 4583-4589.
43. Kang, S.; Herzberg, M.; Rodrigues, D. F.; Elimelech, M., Antibacterial effects of carbon nanotubes: Size does matter. *Langmuir* **2008,** *24*, (13), 6409-6413.
44. Kang, S.; Pinault, M.; Pfefferle, L. D.; Elimelech, M., Single-walled carbon nanotubes exhibit strong antimicrobial activity. *Langmuir* **2007,** *23*, (17), 8670-8673.
45. Liu, S.; Wei, L.; Hao, L.; Fang, N.; Chang, M. W.; Xu, R.; Yang, Y.; Chen, Y., Sharper and faster "nano darts" kill more bacteria: a study of antibacterial activity of individually dispersed pristine single-walled carbon nanotube. *Acs Nano* **2009,** *3*, (12), 3891-3902.
46. Alpatova, A. L.; Shan, W. Q.; Babica, P.; Upham, B. L.; Rogensues, A. R.; Masten, S. J.; Drown, E.; Mohanty, A. K.; Alocilja, E. C.; Tarabara, V. V., Single-walled carbon nanotubes dispersed in aqueous media via non-covalent functionalization: Effect of dispersant on the stability, cytotoxicity, and epigenetic toxicity of nanotube suspensions. *Water Res.* **2010,** *44*, (2), 505-520.
47. Ahmed, F.; Santos, C. M.; Vergara, R. A. M. V.; Tria, M. C. R.; Advincula, R.; Rodrigues, D. F., Antimicrobial applications of electroactive PVK-SWNT nanocomposites. *Environ. Sci. Technol.* **2012,** *46*, (3), 1804-1810.
48. Arias, L. R.; Yang, L., Inactivation of Bacterial Pathogens by Carbon Nanotubes in Suspensions. *Langmuir* **2009,** *25*, (5), 3003-3012.
49. Aslan, S.; Loebick, C. Z.; Kang, S.; Elimelech, M.; Pfefferle, L. D.; Van, T. P. R., Antimicrobial biomaterials based on carbon nanotubes dispersed in poly(lactic-co-glycolic acid). *Nanoscale* **2010,** *2*, (9), 1789-1794.
50. Vecitis, C. D.; Zodrow, K. R.; Kang, S.; Elimelech, M., Electronic-Structure-Dependent Bacterial Cytotoxicity of Single-Walled Carbon Nanotubes. *ACS Nano* **2010,** *4*, (9), 5471-5479.
51. Pasquini, L. M.; Hashmi, S. M.; Sommer, T. J.; Elimelech, M.; Zimmerman, J. B., Impact of surface functionalization on bacterial cytotoxicity of single-walled carbon nanotubes. *Environ. Sci. Technol.* **2012,** *46*, (11), 6297-6305.
52. Pasquini, L. M.; Sekol, R. C.; Taylor, A. D.; Pfefferle, L. D.; Zimmerman, J. B., Realizing Comparable Oxidative and Cytotoxic Potential of Single- and Multiwalled Carbon Nanotubes through Annealing. *Environ. Sci. Technol.* **2013,** *47*, (15), 8775-8783.
53. Yang, C.; Mamouni, J.; Tang, Y.; Yang, L., Antimicrobial Activity of Single-Walled Carbon Nanotubes: Length Effect. *Langmuir* **2010,** *26*, (20), 16013-16019.
54. Qi, X.; Poernomo, G.; Wang, K.; Chen, Y.; Chan-Park, M. B.; Xu, R.; Chang, M. W., Covalent immobilization of nisin on multi-walled carbon nanotubes: superior antimicrobial and anti-biofilm properties. *Nanoscale 3*, (4), 1874-1880.
55. Woerle-Knirsch, J. M.; Pulskamp, K.; Krug, H. F., Oops They Did It Again! Carbon Nanotubes Hoax Scientists in Viability Assays. *Nano Lett.* **2006,** *6*, (6), 1261-1268.
56. Pantanella, F.; Berlutti, F.; Passeri, D.; Sordi, D.; Frioni, A.; Natalizi, T.; Terranova, M. L.; Rossi, M.; Valenti, P., Quantitative evaluation of bacteria

adherent and in biofilm on single-wall carbon nanotube-coated surfaces. *Interdiscipl. Perspect. Infect. Dis.* **2011,** *2011*, 1-9.
57. Hussain, M.; Kabir, M.; Sood, A., On the cytotoxicity of carbon nanotubes. *Curr. Sci.* **2009,** *96*, (5), 664-673.
58. Du, J.; Wang, S.; You, H.; Zhao, X., Understanding the toxicity of carbon nanotubes in the environment is crucial to the control of nanomaterials in producing and processing and the assessment of health risk for human: A review. *Environ. Toxicol. Pharmacol.* **2013,** *36*, (2), 451-462.
59. Santos, C. M.; Milagros Cui, K.; Ahmed, F.; Tria, M. C. R.; Vergara, R. A. M. V.; de Leon, A. C.; Advincula, R. C.; Rodrigues, D. F., Bactericidal and anticorrosion properties in PVK/MWNT nanocomposite coatings on stainless steel. *Macromol. Mater. Eng.* **2012,** *297*, (8), 807-813.
60. Schiffman, J. D.; Elimelech, M., Antibacterial activity of electrospun polymer mats with incorporated narrow diameter single-walled carbon nanotubes. *ACS Appl. Mater. Interfaces* **2011,** *3*, (2), 462-468.
61. Mauter, M. S.; Elimelech, M., Environmental applications of carbon-based nanomaterials. *Environ. Sci. Technol.* **2008,** *42*, (16), 5843-5859.
62. Upadhyayula, V. K. K.; Gadhamshetty, V., Appreciating the role of carbon nanotube composites in preventing biofouling and promoting biofilms on material surfaces in environmental engineering: a review. *Biotechnol. Adv.* **2010,** *28*, (6), 802-816.
63. Jones, P. H.; Prasad, D.; Heskins, M.; Morgan, M. H.; Guillet, J. E., Biodegradability of photodegraded polymers. I. Development of experimental procedures. *Environ. Sci. Technol.* **1974,** *8*, (10), 919-923.
64. Guillet, J. E.; Regulski, T. W.; McAneney, T. B., Biodegradability of photodegraded polymers. II. Tracer studies of biooxidation of Ecolyte PS polystyrene. *Environ. Sci. Technol.* **1974,** *8*, (10), 923-925.
65. Nguyen, T.; Pellegrin, B.; Mermet, L.; Shapiro, A.; Gu, X.; Chin, J., Network aggregation of CNTs at the surface of epoxy/MWCNT composite exposed to UV radiation. *Nanotechnology* **2009**, 90-3.
66. Hou, W.-C.; BeigzadehMilani, S.; Jafvert, C. T.; Zepp, R. G., Photoreactivity of Unfunctionalized Single-Wall Carbon Nanotubes Involving Hydroxyl Radical: Chiral Dependency and Surface Coating Effect. *Environ. Sci. Technol.* **2014,** *48*, (7), 3875-3882.
67. Qu, X.; Alvarez, P. J.; Li, Q., Photochemical Transformation of Carboxylated Multiwalled Carbon Nanotubes: Role of Reactive Oxygen Species. *Environ. Sci. Technol.* **2013,** *47*, (24), 14080-14088.
68. Chiellini, E.; Corti, A.; Solaro, R., Biodegradation of poly(vinyl alcohol) based blown films under different environmental conditions. *Polym. Degrad. Stab.* **1999,** *64*, (2), 305-312.
69. Tang, X.; Alavi, S., Recent advances in starch, polyvinyl alcohol based polymer blends, nanocomposites and their biodegradability. *Carbohydr. Polym.* **2011,** *85*, 7-18.
70. Madigan, M. T.; Martinko, J. M.; Dunlap, P. V.; Clark, D. P., *Brock Biology of Microorganisms*. 12th ed.; Pearson: San Francisco, 2009.

71. Vickerman, J. C.; Gilmore, I. S., *Surface analysis: the principal techniques*. Wiley Online Library: 2009; Vol. 2.
72. Tanuma, S.; Powell, C. J.; Penn, D. R., Calculations of electorn inelastic mean free paths. II. Data for 27 elements over the 50–2000 eV range. *Surf. Interface Anal.* **1991,** *17*, (13), 911-926.
73. Reed, R. B.; Goodwin, D. G.; Marsh, K. L.; Capracotta, S. S.; Higgins, C. P.; Fairbrother, D. H.; Ranville, J. F., Detection of single walled carbon nanotubes by monitoring embedded metals. *Environ. Sci.: Processes Impacts* **2013,** *15*, (1), 204-213.
74. Invitrogen, FilmTracer LIVE/DEAD Biofilm Viability Kit. In Probes, M., Ed. 2009.
75. Invitrogen, FilmTracer SYPRO Ruby Biofilm Matrix Stain. In Probes, M., Ed. 2009.
76. Petersen, E. J.; Lam, T.; Gorham, J. M.; Scott, K. C.; Long, C. J.; Stanley, D.; Sharma, R.; Alexander Liddle, J.; Pellegrin, B.; Nguyen, T., Methods to assess the impact of UV irradiation on the surface chemistry and structure of multiwall carbon nanotube epoxy nanocomposites. *Carbon* **2014,** *69*, 194-205.
77. Kang, S.; Mauter, M. S.; Elimelech, M., Microbial Cytotoxicity of Carbon-Based Nanomaterials: Implications for River Water and Wastewater Effluent. *Environ. Sci. Technol.* **2009,** *43*, (7), 2648-2653.
78. Teitzel, G. M.; Parsek, M. R., Heavy metal resistance of biofilm and planktonic Pseudomonas aeruginosa. *Appl. Environ. Microbiol.* **2003,** *69*, (4), 2313-2320.
79. Vicente, A. d.; Avilés, M.; Codina, J. C.; Borrego, J. J.; Romero, P., Resistance to antibiotics and heavy metals of Pseudontonas aeruginosa isolated from natural waters. *J. Appl. Bacteriol.* **1990,** *68*, (6), 625-632.
80. Corredor, C.; Hou, W.-C.; Klein, S. A.; Moghadam, B. Y.; Goryll, M.; Doudrick, K.; Westerhoff, P.; Posner, J. D., Disruption of model cell membranes by carbon nanotubes. *Carbon* **2013,** *60*, 67-75.

Chapter 4. Biofilm Development on Carbon Nanotube/Polymer Nanocomposites

This work was co-written with the following authors and is adapted from following the published work:

Goodwin, D. G., Xia, Z., Gordon, T. B., Gao, C., Bouwer, E. J., & Fairbrother, D. H. (2016). Biofilm Development on Carbon Nanotube/Polymer Nanocomposites. *Environmental Science: Nano*.

4.1. Nanoimpacts

Following consumer use, microorganisms will associate with and potentially form biofilms on carbon nanotube/polymer nanocomposite (CNT/PNC) surfaces in the environment. These CNT/PNC surfaces can have a range of different characteristics as a result of polymer matrix type, manufacturing method, wear during consumer use, or environmental transformations. This study shows that CNTs at the surface of a CNT/PNC are cytotoxic to microorganisms, and their presence causes a layer of dead cells to form, regardless of whether the CNTs are initially at the CNT/PNC surface or reach the surface as a result of polymer degradation during biofilm growth. CNT/PNCs used in consumer products therefore have the potential to be cytotoxic to microorganisms as the polymer matrix degrades. However, once CNTs at the surface are coated with a layer of dead cells, live-on-dead biofilm formation occurs under both static and low shear conditions, indicating that healthy biofilm growth on CNT/PCL nanocomposites will be delayed, but not prevented. The need for direct contact to be present between CNTs and

microorganisms for cytotoxicity to occur will likely limit the use of CNT/PNCs in antimicrobial applications as biofouling will ultimately still occur. The existence of a dead layer of cells at the interface between the CNT/PNC and the active biofilm may, however, have implications for the physical stability of the biofilm (e.g. to sheer forces) and to the long term fate of the polymer itself (e.g. biodegradability).

4.2. Introduction

Polymers, by virtue of their wide range of desirable properties and ease of production, are prevalent in every aspect of life ranging from familiar daily plastics such as rubber bands, garbage bags, and packaging materials to coatings used in the automobile and aerospace industries.[1-3] Incorporation of carbon nanotubes (CNTs) into polymers to prepare CNT/polymer nanocomposites (CNT/PNCs) has received increasing attention due to the beneficial material properties that CNTs can impart to polymers, greatly enhancing their range of potential applications. These improved properties can include high tensile strength, extraordinary hardness, and excellent thermal and electrical conductivity.[4-8] For this reason, industrial manufacturing of nanoproducts for consumer use, typically within the range of 1 - 5% w/w CNTs, is already underway for applications that include electronic devices, charge-dissipating packaging, fuel tanks, and anti-biofouling surfaces.[9-12]

Since plastic products that include CNT/PNCs will eventually enter the environment at the end of their consumer use, their ultimate fate will be strongly influenced by their interactions with microbial communities.[13-17] During the earliest stages of microbial exposure to CNTs that are present at a CNT/PNC surface, cell death has been observed with a number of different microorganisms such as *Escherichia coli* (*E. coli*), *Bacillus subtilus*, *Staphylococcus epidermidis (S. epidermidis)* and

Pseudomonas aeruginosa (*P. aeruginosa*).[18-22] For *E. coli* and *P. aeruginosa*, it has been shown that this antimicrobial effect increases with mass fraction of CNTs (% w/w) at the surface, regardless of whether the CNTs are pristine, oxidized (O-CNT), multi-wall (MWCNT), or single-wall (SWCNT).[22, 23] Mechanistic explanations of CNT cytotoxicity have been proposed that include cell membrane penetration by CNTs due to their high aspect ratio, cell membrane disruption, and oxidative stress.[21, 24-29] While it has not been proved definitively which one or combination of these mechanisms is responsible for CNT cytotoxicity, it has been shown that cell death tends to occur only when CNTs are in direct contact with microorganisms, although not every single contact event necessarily leads to cell death.[22]

The initial interactions of microbes with CNT/PNCs can also potentially influence biofilm development, or the growth of microbial communities, at the CNT/PNC surface.[18, 19, 22, 23] Biofilm formation begins with: (1) reversible cell attachment followed by, (2) cell division, (3) irreversible attachment using secreted extracellular polymeric substances (EPS), (4) maturation, and (5) cell dispersion to promote biofilm formation at other locales.[17, 30, 31] Biofilm formation occurs ubiquitously on most surfaces exposed to microbial populations and improves the tolerance of microorganisms to dry and/or nutrient deficient conditions, promotes nutrient accumulation from the environment, and keeps extracellular enzymes in close proximity to cells to aid in the metabolism of substrates.[32] Biofilms also play an important role in a wide range of environmental processes including the sieving, attachment to, or removal of contaminants from water; the stabilization of sediments; flocculation, settling, and dewatering in wastewater treatment; and biodegradation processes involving dissolved, colloidal, and solid organic

materials such as oil droplets and polymeric materials.[32-34] For polymer surfaces that can be degraded by microorganisms, biofilm formation is also the prerequisite to biodegradation and the presence of CNTs could therefore influence the rate of this process.[35-37] In addition to their role in the natural environment, biofilms can decrease the efficiency of processes in industrial settings such as water flow in pipes and biofilms can lead to infections in the human body, oftentimes through formation on medical devices, where they have been shown to be 10-1000 times more resistant to antibiotics than planktonic cells.[16, 30, 38-45] Consequently, biofilm reduction and/or removal are commonly targeted by toxic release agents, low energy surfaces, and/or antimicrobial surfaces.[40, 44-50]

CNTs are thought to have a physicochemical-dependent antimicrobial effect that derives from their ability to disrupt the formation of biofilms that develop on the surface of CNT/PNCs.[18-20, 22, 51] As a result, efforts have been made to exploit the cytotoxicity of CNTs to create new anti-biofouling surfaces or improve existing anti-biofouling technologies.[18-21, 43, 52, 53] For example, the use of CNT/PNCs as an antimicrobial surface coating has been proposed for SWCNTs dispersed into the biomedical polymer, poly(lactic-co-glycolic) acid (PLGA), which demonstrated a significant diminishment in the viability and metabolic activities of *E. coli* and *S. epidermidis* at the CNT/PNC surface.[21] CNT antimicrobial properties have also been exploited in water disinfection applications by modifying membranes with CNTs, although the long term biofilm growth on these surfaces has not been investigated.[43, 54-56] To our knowledge, no studies have shown that CNT-containing surfaces can be used to detach microorganisms due solely to their antimicrobial properties. Instead, they have been used commercially in existing

paints and coatings to further reduce marine organism growth on boat hulls by providing a nanostructured underlayer to a silicone or fluoropolymer surface with a low free energy of cell attachment.[44, 45, 52, 53]

Since CNT/PNCs are expected to be one of the biggest projected commercial uses of CNTs, it is important to study the growth and development of biofilms on different types of CNT/PNC surfaces that will be present in the environment following consumer use.[4-8] In many cases, CNT/PNC products would be expected to have a buried CNT-structure or surface coating on which a biofilm would first grow. On the other hand, some CNT/PNCs might initially have CNTs exposed at the surface or CNTs that become exposed as a result of environmental degradation processes.[15, 57-60] The effect of CNTs on mature biofilm growth has only been investigated or partially considered in a few studies.[43, 51] In one study, Rodrigues and Elimelech determined that the antimicrobial properties of CNTs reduced biofilm growth on a CNT-coated surface over a 48 h time period but led to the release of nutrients from attached dead cells.[51] This release of nutrients was hypothesized to promote biofilm colonization on top of the dead microbial layer which could serve as a protective barrier for living cells from the underlying, cytotoxic CNTs.[41, 51] These "live-on-dead" biofilm structures have been observed in a biofilm development study on a silver-palladium antimicrobial surface, where cell death of a silver-resistant strain of *E. coli* occurred at the surface due to an electrochemical redox processes while silver-resistant microorganisms readily formed colonies atop this dead layer of cells.[61] "Live-on-dead" structures have also been observed in *Geobacter anodireducens* biofilms, grown on an electrode surface to form an active component in a bioelectrical system, under electrochemical conditions that were not conducive to

maintaining a homogenous, metabolically active biofilm.[62] In contrast, a systematic study to analyze how biofilms develop on CNT/PNCs has not yet been investigated.

To address this question, the focus of the present study has been to compare and contrast biofilm growth on a range of different surfaces, including; (a) a polymer without CNTs, (b) PNC surfaces with different CNT loadings, where the CNTs were initially buried below the surface but became exposed as a result of polymer degradation during biofilm growth, and (c) a PNC surface where CNTs were initially exposed at the surface. To facilitate a comparison of these different scenarios, we used poly-ε-caprolactone (PCL) as a common polymer matrix. PCL was selected because it is benign to microorganisms and is commonly found in polymer blends used in trash bags, incontinence products, and bandage wrappers.[63] As a result, biofilm growth on PCL could be directly compared to biofilm growth on CNT/PNCs to clearly delineate any observed CNT effects from normal biofilm development processes.[38, 39, 64-68] PCL is also biodegradable, which allowed us to study how biofilm growth was impacted by the accumulation of CNTs at a polymer surface as a result of PCL biodegradation.[64-66, 69] Oxidized multi-wall carbon nanotubes (O-MWCNTs) were chosen as the CNT filler since they were able to uniformly disperse within the PCL matrix and have previously been shown to exhibit cytotoxicity.[22] It should be noted that biodegradation of CNTs was not a factor in this study since this process has only been observed for oxidized CNTs exposed to harsh, acellular conditions involving enzymes such as horseradish peroxidase and even then, only partial biodegradation of O-MWCNTs was observed.[70, 71]

Pseudomonas aeruginosa (*P. aeruginosa*) wild type was chosen as a model microorganism since *Pseudomonas* species readily form biofilms, are commonly found in

the environment, and are able to biodegrade PCL.[64-66, 69] For comparison of different aqueous environments, biofilms were grown under drip flow reactor (DFR) and static conditions, with and without low shear and constant replenishment of a food source, respectively.[72, 73] Biofilm development on surfaces prepared with 0.5% and 2% w/w O-MWCNT/PCL with the CNT loadings chosen for their commercial relevance, were monitored and compared at various growth stages to PCL (0% w/w O-MWCNTs) under the same conditions using LIVE/DEAD staining coupled to confocal laser scanning microscopy (CLSM).[9-12] This allowed us to differentiate green-fluorescent living cells from red-fluorescent dead cells based on membrane integrity.[74] Biomass and thickness analysis measurements were also made using COMSTAT 2 software to compare biofilm development on PCL versus CNT/PCL nanocomposites.[75, 76]

4.3. Experimental

The experimental section is organized as follows: section I describes the preparation of CNT/PCL nanocomposites, section II describes the characterization of the prepared CNT/PCL nanocomposites, section III describes the methods and conditions used to grow biofilms on the CNT/PCL nanocomposite surfaces, and section IV describes how biofilm development was analyzed.

4.3.1. Section I: CNT/PCL Nanocomposite Preparation

4.3.1.1. Preparation of PCL and CNT/PCL Casting Solutions

Pristine MWCNTs (Nanocyl NC7000, outer diameter 9.5 nm, 1.5 μm length, 90% purity) were oxidized “in-house” to obtain O-MWCNTs with a total oxygen content of 4.1%, measured using X-ray photoelectron spectroscopy (XPS). Further information is provided in the appendix. O-MWCNTs were also dispersed in 70:30 ethanol/water, sonicated for 30 s, and dried on a holey carbon

grid for TEM characterization (JEOL JEM 1220, 120 kV accelerating voltage). From the TEM images, the O-MWCNT diameter distribution was measured in 15-20 areas using DigitalMicrograph software (Gatan Inc., Pleasanton, CA). The average O-MWCNT diameter was 9.4 ± 1.2 nm, consistent with the 9.5 nm diameter measured by the manufacturer. TEM data is shown in Figure A4.1 along with XPS data on the atomic surface composition of the O-MWCNTs. O-MWCNTs were dispersed in chloroform (99.8% GR ACS, Cat #CX1055-6, EMD) to prepare two suspensions having concentrations of 50 mg/L (for 0.5% w/w O-MWCNT/PCL) and 200 mg/L (for 2% w/w O-MWCNT/PCL) O-MWCNTs. 1 g/L of ethyl cellulose (Sigma-Aldrich, Cat #433837), a natural and biocompatible surfactant, was added to each suspension to enhance the O-MWCNT colloidal stability in chloroform.[77, 78] The O-MWCNT/ethyl cellulose suspensions were ultra-sonicated in a cold ice-water bath for 3 h (Branson 1510 bath sonicator, 70 watts) with the water changed every 20 min to avoid heating the suspension; these low temperatures optimized the CNT dispersion quality. 10 g/L poly-ε-caprolactone (PCL, Sigma-Aldrich, Cat #440752) was then added to each O-MWCNT/ethyl cellulose suspension to produce 0.5 or 2% w/w O-MWCNT/PCL casting solutions that were then ultra-sonicated for another 2 h following the same ice-water bath procedure. At this stage the suspensions were centrifuged (PowerSpin LX Centrifuge, Unico, USA) at 3000 rpm for 5 min to remove any glass or remaining bundled CNTs for a final concentration of slightly less than or equal to 50 or 200 mg/mL O-MWCNTs in the casting solution.

Unmodified polymer without O-MWCNTs was prepared by sonicating 10 g/L PCL in chloroform for 2 h with 1 g/L ethyl cellulose.

4.3.1.2. Preparation of PCL and CNT/PCL Films Suitable for CLSM Imaging

Thin films of PCL and CNT/PCL nanocomposites were spray-coated onto modified glass microscope slides, since an underlying support is required for CLSM imaging. Due to the hydrophobicity of PCL, it was found that the glass slides required octadecyltrichlorosilane (OTS) modification to increase CNT/PCL nanocomposite adhesion (Figure A4.2).[79-83] Further information on OTS modification and characterization can be found in the appendix. The spray-coating process, which is detailed in the appendix and shown in Figure A4.3, yielded uniformly dark O-MWCNT/PCL coatings (0.5 and 2% w/w) as demonstrated in Figure A4.2.

4.3.1.3. Preparation of Photolyzed CNT/PCL Nanocomposites

Photodegraded samples were prepared by exposing CNT/PCL nanocomposites to hydroxyl radicals to mimic the effects of indirect photolysis in aqueous environments.[84-86] This represents a form of accelerated weathering. To generate these photodegraded CNT/PNC samples, thicker 2% w/w O-MWCNT/PCL nanocomposites, without an underlying OTS-modified slide, were prepared as described in the appendix. CNT/PCL nanocomposites spray-coated onto OTS-modified glass slides were not used because initial studies revealed that photolysis caused some of the CNT/PCL coatings to detach into solution. As illustrated in Figure A4.4, photolysis was effected by tightly wrapping thick CNT/PCL samples around glass slides (4.0 cm x 1.2 cm x 0.1 cm) using Teflon

tape and immersing these prepared samples individually into quartz test tubes (12.5 cm length, 1.3 cm diameter, Southern New England Ultraviolet Company, Branford, Connecticut) containing 0.5 M hydrogen peroxide solution.[86] The surfaces of these CNT/PCL samples were then exposed to both hydroxyl radicals and UV light by irradiating the hydrogen peroxide and immersed samples at 254 nm for 24 h at 35 °C in a Rayonet Photochemical Chamber Reactor (Model: RPR-100, Southern New England Ultraviolet Company, Branford, Connecticut, $1.62*10^{17}$ Photons/sec/cm^3, 16 bulbs).

4.3.2. Section II: CNT/PNC Characterization

4.3.2.1. Surface Morphology and Composition

Replicate SEM images of PCL, 2% w/w O-MWCNT/PCL, and 2% w/w O-MWCNT/polyvinyl alcohol (PVOH) nanocomposites are shown in Figures A4.5-A4.7 and triplicate SEM images are shown for 0.5% w/w O-MWCNT/PCL nanocomposites in Figure A4.8. The preparation and analysis of replicate areas and separately prepared CNT/PNCs is further outlined in the appendix. The 2% w/w O-MWCNT/PVOH nanocomposites were prepared by spray-coating and imaged using SEM to serve as a comparison to 2% w/w O-MWCNT/PCL nanocomposites as described in more detail in the appendix. An SEM image of pure PVOH is provided for reference (Figure A4.7). In addition to the SEM image shown in Figure 4.5, replicate SEM images (Figure A4.9) were also taken for 2% w/w O-MWCNT/PCL nanocomposites before and after photodegradation. Attempts were also made to image the surfaces of biodegraded CNT/PCL nanocomposites by removing the biofilm coating using 1% w/w sodium

polyphosphate immersion for 5 days followed by rinsing with Milli-Q water, an example of which is shown in Figure A4.10.

4.3.2.2. PCL and CNT/PCL Film Thickness

Side-views of PCL and 2% w/w O-MWCNT/PCL coatings on OTS-modified slides were imaged in replicate areas (>5) using SEM. For each image, replicate thickness measurements (>5) of the PCL or 2% w/w O-MWCNT/PCL coating were made using ImageJ software (Bethesda, MD). Both PCL and 2% w/w O-MWCNT/PCL had a consistent thickness of approximately 1 μm across the OTS-modified slide.

4.3.3. Section III: Methods and Conditions of Biofilm Growth on CNT/PCL Surfaces

4.3.3.1. Inoculation of PCL and CNT/PCL Surfaces

To begin a biofilm experiment, a 0.5 mL frozen culture of *P. aeruginosa* wild type (ATCC 27853) was added to 75 mL LB broth (25 g L-1) and grown overnight to the stationary phase on an incubator shaker at 225 rpm and 37 °C. The overnight cultures were grown in LB broth for rapid microbial growth which enabled practical timing in terms of transfer and growth in basal mineral media (BMM) followed by flow cell setup the next day. BMM was used for further growth and to match that of the sterile feed used in the DFR since it is well defined and more environmentally relevant.[87] Next, 0.20 mL of the overnight culture was transferred to 100 mL of BMM containing 3.270 g/L acetate and grown to the exponential phase (O.D. 0.040 to 0.060 at 540 nm) on the incubator shaker at 300 rpm. This corresponded to $3.0 \pm 0.1 \times 10^8$ CFU/mL, the average CFU/mL and standard deviation of two separately grown *P. aeruginosa* cultures.

Further information on the *P. aeruginosa* frozen stocks and the BMM composition are provided in the appendix.

In order to initiate biofilm growth under both static and drip flow conditions, PCL and CNT/PCL samples were first inoculated with 20 mL of the exponential phase *P. aeruginosa* culture for 1 h at room temperature. This allowed the *P. aeruginosa* to initially attach to the samples prior to biofilm development. Following initial *P. aeruginosa* attachment, a sterile BMM feed was flowed over the samples for the remainder of the experiments.

4.3.3.2. Drip Flow Reactor (DFR)

The DFR used in this study was capable of housing six slides at one time for biofilm studies.[88] Immediately prior to an experiment, the DFR (Model DFR 110-6, BioSurface Inc., Bozeman, MT) was aseptically assembled and prepared according to the manufacturer's specifications. Modifications were made to meet our experimental needs (see Figure A4.11). Specifically, this involved setting the apparatus at a negative angle of -2.3° with the port side higher than the drip side, opposite to the ordinary DFR setting.[40, 88, 89] This allowed media to drip down the samples at a downward (positive) angle, facilitating complete sample immersion and a uniform media flow over the hydrophobic PCL and CNT/PCL samples. This prevented inconsistent growth patterns and bacteria dry-out in different sample areas that would occur in the typical DFR configuration.

Biofilm experiments in the DFR were initiated by rinsing samples that had been inoculated for 1 h in depleted media (BMM with no acetate) to remove loosely adhered cells. Samples were then gently transferred into the DFR chambers, which were pre-filled with media to prevent drying. The media was

then allowed to flow through 1.30 mm inner diameter tubing into each reactor chamber at a flow rate of 0.35 mL/min, corresponding to a flow residence time of 40 min, using an Ismatec BVK peristaltic pump (IDEX, Germany). This flow was sustained throughout the course of each experiment, which ranged in time from 6 to 96 h. Low carbon source (0.2 g/L acetate) BMM (low C BMM) was used since higher carbon source concentrations were found to cause additional biofilm formation at the air-liquid interface that hampered biofilm development on the samples, presumably as a result of oxygen depletion. The flow rate was checked before and after the experiment to ensure an approximate value of 0.35 mL/min was maintained; the flow rate was kept constant by using large inner diameter (8 mm) exit tubing to minimize fouling due to biofilm formation at the exit port. For every O-MWCNT/PCL nanocomposite placed in the DFR there was a corresponding PCL control. Four biofilm thickness regimes were identified based on the biofilm thicknesses measured on the PCL control.

4.3.3.3. Static Experiments

After 1 h of initial microbial attachment, PCL and O-MWCNT/PCL nanocomposites were rinsed in depleted media to removed loosely attached microorganisms, and then transferred to sterile dishes containing 20 mL of low C BMM (0.2 g/L acetate) and sat for approximately 2 weeks under static conditions.

Photodegraded CNT/PCL nanocomposites were rinsed gently with sterile Milli-Q water five times and left tied to the glass slide for the inoculation procedure. Photodegraded CNT/PCL nanocomposites were inoculated under static conditions for 1 h and 2 weeks. The 2 week samples had 1 mL of BMM containing 3.270 g/L acetate added twice at regularly spaced intervals. This

provided an additional food source sufficient to maintain microbial growth for the duration of the experiment.

4.3.4. Section IV: Analysis of Biofilm Development on CNT/PCL Nanocomposites

4.3.4.1. LIVE/DEAD Staining and Confocal Laser Scanning Microscopy (CLSM) Imaging

At the end of an experiment, each sample was gently removed from the DFR chamber or dish used for static inoculation. Samples were then rinsed in depleted media (DM) to wash away any loosely adhered bacteria.[88] As outlined in the SI, a FilmTracer LIVE/DEAD Biofilm Viability Kit (Molecular Probes, Invitrogen) was used to differentiate the living and dead cells within the biofilms. Samples were then rinsed with depleted media to remove excess stain. LIVE/DEAD stained biofilms on the PCL and CNT/PCL surfaces were imaged using CLSM. Further information on image acquisition is detailed in the appendix. Because the depth of field was too high to image biofilms within the DFR, biofilms were directly imaged using an inverted 40x water immersion objective, a method used previously to image LIVE/DEAD stained biofilms.[90, 91] In this configuration, samples were coated with Vectashield Mounting Media (Vector Laboratories Inc., Burlingame, CA) to maintain fluorescence and prevent dryout that could interfere with the imaging results. Fluorescence intensity remained constant throughout the scanning of all biofilms, indicating that there were no photobleaching or quenching effects as a result of the CNTs, polymer, or the imaging conditions. Numerous staining procedural details were also followed to ensure the accuracy and validity of the results; these are outlined in our previous study and listed in the appendix.[22] Additional background staining

controls performed for the PCL and CNT/PCL samples used in this study are described in the appendix and shown in Figures A4.12 and A4.13.

4.3.4.2. Biofilm Controls on Glass Slides and OTS-Modified Glass Slides

Biofilms were grown on glass slides under both static (Figure A4.14) and drip flow conditions (Figure A4.15) for the longest exposures studied; 2 weeks and 72-96 h, respectively. They were then stained and imaged according to the protocol outlined in the previous section. Bacteria grown on OTS-modified slides for 6 h were also LIVE/DEAD stained and imaged to show that OTS was not cytotoxic (Figure A4.16).

4.3.4.3. Analysis of Biofilm Images

Three dimensional biofilm images (XYZ projections) were reconstructed by the microscope software Slidebook (Intelligent Imaging Innovations, Denver, CO). At least 6 replicate biofilm images were taken in different sample areas for every sample imaged. Replicate CLSM images are shown in Figures A4.17-A4.21 for Figures 4.2, 4.3, 4.4, and 4.5, respectively. Separately grown biofilms were also imaged (Figure A4.17) under DFR conditions to show consistency in biofilm development.

COMSTAT 2 biofilm analysis software was used to measure the biomass volume ($\mu m^3/\mu m^2$) and biomass thickness (μm) under both drip flow and static conditions for PCL and 2% w/w O-MWCNT/PCL nanocomposites (Figure 4.2 & 4.4, Table A1). These measurements were also made for 0.5% w/w O-MWCNT/PCL under DFR conditions.[75, 76, 92] As described in the appendix,

manual thickness measurements were also made to validate the COMSTAT 2 measurements and yielded similar results, as shown in Table A1.

4.4. Results and Discussion

The SEM images in Figure 4.1 show the structure and morphology of: (a) PCL, (b) a 2% w/w O-MWCNT/PCL nanocomposite, and (c) a 2% w/w O-MWCNT/PVOH nanocomposite after spray-coating.

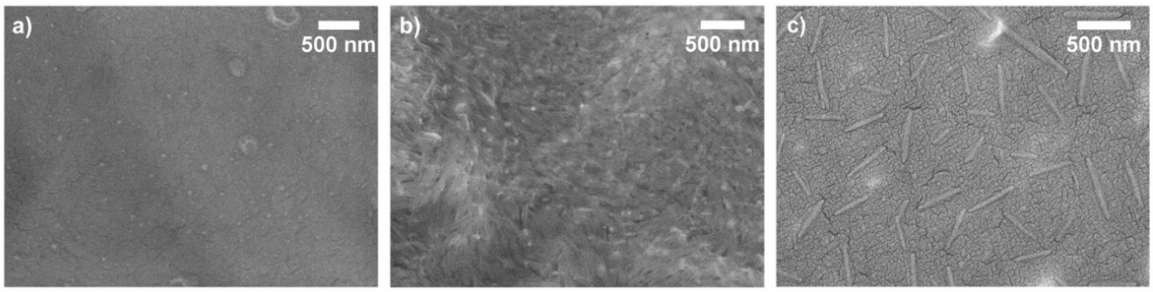

Figure 4.1. SEM comparison of the surface morphology and CNT content of: a) PCL, b) 2% w/w O-MWCNT/PCL, and c) 2% w/w O-MWCNT/PVOH.

A comparison of Figure 4.1a,b reveals that the addition of CNTs to the PCL matrix leads to a rougher surface. Faint, but discernible CNT like structures are also observed in the 2% w/w O-MWCNT/PCL nanocomposite images. In contrast, SEM data for the 2% w/w O-MWCNT/PVOH nanocomposite (Figure 4.1c) shows clearly distinguishable CNT structures. It should be noted that the CNTs are somewhat broadened in diameter due to the presence of a platinum coating that was used to prevent charging during SEM.[22] Previous XPS studies have shown that CNTs present at the surface of PVOH are at a concentration representative of the CNT concentration (2% w/w) in the casting solution.[22] Although CNTs were not clearly distinguishable at the 2% w/w O-MWCNT/PCL nanocomposite surface, a uniformly dark PNC was produced, indicating the presence of well-distributed CNTs throughout the PCL matrix.[22] We interpret the difference in the

SEM images between the CNT/PVOH and CNT/PCL nanocomposites to be an indication that the CNTs in the CNT/PCL nanocomposite are not present at the very topmost surface layer, but are slightly buried below the surface. This is also supported by the initially benign interaction of the microorganisms with the 2% w/w O-MWCNT/PCL nanocomposite, indicated by the green-fluorescent living cells in the bottom left panel of Figure 4.2a, which is in sharp contrast to the cytotoxicity of the CNT/PVOH nanocomposites at similar CNT mass fractions in our previous study.[22] Buried-CNT structures have been observed previously with CNT/PNCs such as MWCNT/epoxy while in other cases, CNTs have been shown to reside at the surface or accumulate gradually during environmental degradation processes.[15, 22, 23, 57, 93]

Figure 4.2a shows the progression of *P. aeruginosa* biofilm growth on PCL (top panels) and 2% w/w O-MWCNT/PCL (bottom panels) surfaces.

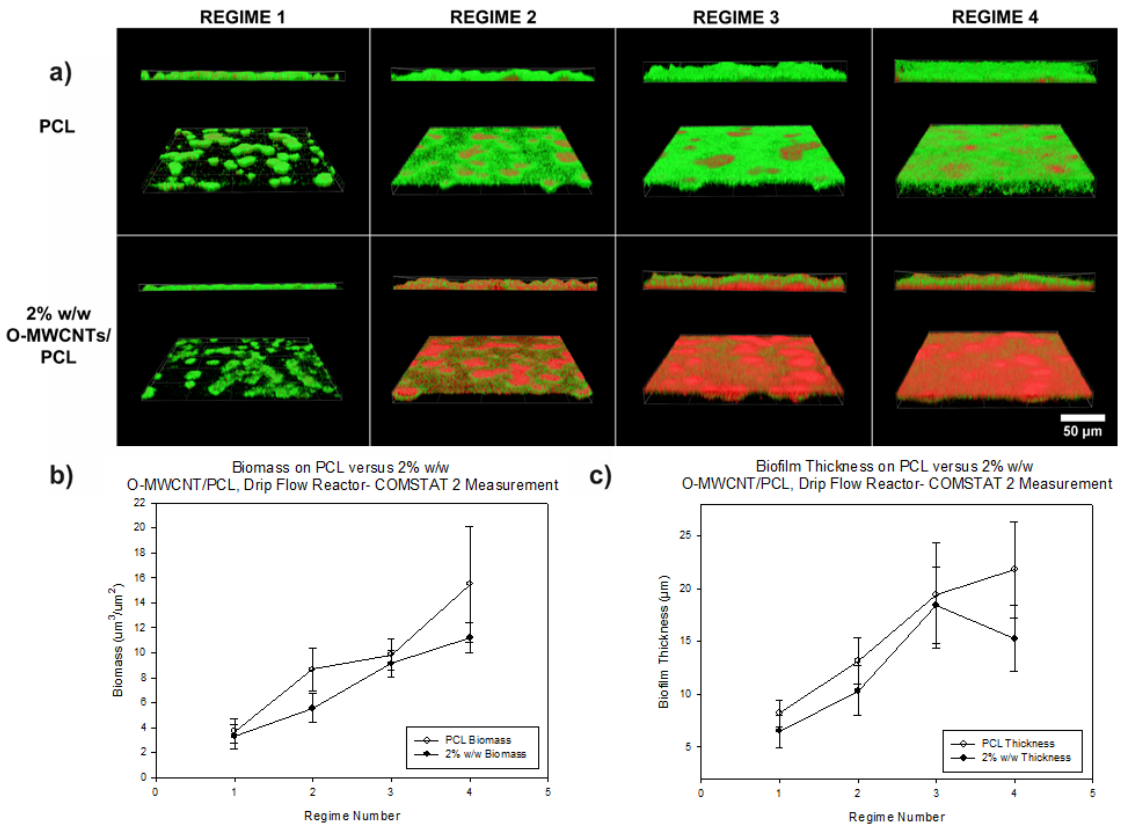

Figure 4.2. a) CLSM images of LIVE/DEAD stained P. aeruginosa grown in a DFR on PCL (top row) and 2% w/w O-MWCNT/PCL (bottom row). Regimes 1-4 (6 – 96 h) represent increasing levels of biofilm growth based on the biofilm thicknesses observed on PCL. For each panel, the top image is a side view of the biofilm and the bottom image is the inverted biofilm to show where the biofilm makes contact with the sample surface. Quantitative comparison of biofilms on PCL and 2% w/w O-MWCNT/PCL under DFR conditions is also made using COMSTAT 2 b) biomass volume and c) thickness analysis. Each data point represents duplicate samples with at least five replicate areas per sample.

Since *P. aeruginosa* can biodegrade PCL but not CNTs, our hypothesis was that the CNT/PCL surface characteristics would transform, and that these changes would influence biofilm development. The top CLSM image within each panel (e.g. PCL Regime 1) is a side view of the biofilm while the bottom image is inverted to show the part of the biofilm in direct contact with the surface. In these experiments *P. aeruginosa* biofilms were grown on PCL and 2% w/w O-MWCNT/PCL surfaces in a DFR. The DFR was used to simulate slow-flowing water in the environment (~200 mL/h) such as

freshwater rivers and thermal hot springs.[72] In these experiments, the biofilm thicknesses on PCL samples were used as a point of reference to track the maturity of the biofilms on the CNT/PCL nanocomposites. The use of the PCL samples as an internal reference was found to be necessary as precise time-course evolution between different *P. aeruginosa* cultures was too variable. Based on this approach, the maturity levels of the biofilms were classed into four regimes based on the biofilm thickness observed on the PCL surface (measured as an average of ≥ 6 images with COMSTAT 2): the primary (regime 1), secondary (regime 2), tertiary (regime 3) and final (regime 4) stage with biofilm thicknesses of 8 ± 1 μm, 13 ± 2 μm, 19 ± 5 μm, and 22 ± 5 μm, respectively (Figure 4.2c). Biomass volume measurements also increased on PCL between each regime as shown in Figure 4.2b and Table A1.

During the initial period of biofilm growth (regime 1) the CLSM images show discrete colonies formed on both PCL and 2% w/w O-MWCNT/PCL surfaces, dominated almost exclusively by living cells. Indeed, the structure of the biofilms that initially form on the two surfaces are similar in terms of a high number of green-fluorescent, living cells with a slight difference in terms of thickness (8 ± 1 μm for PCL versus 7 ± 1 μm for 2% w/w O-MWCNTs). The initially benign interaction of microorganisms with the nanocomposite surface is further supported by Figure A4.22 which shows green-fluorescent, living cells on the 2% w/w O-MWCNT/PCL surface from 1 h of initial attachment to 6 h of static microbial growth. In our previous study O-MWCNTs were shown to be cytotoxic towards *P. aeruginosa.* Consequently, the initially benign nature of the 2% w/w O-MWCNT/PCL surface is consistent with the lack of CNTs at the PNC surface as suggested by the SEM data in Figure 4.1b. The absence of initial cytotoxicity

for the CNT/PCL nanocomposite surface is also a reflection of the need for direct contact to occur between CNTs and microorganisms for the antimicrobial effect of CNTs to become operative.[22]

In regime 2, however, differences begin to appear in the nature of the biofilms on the two surfaces. For PCL, the thickness of the biofilm increases (8 ± 1 μm to 13 ± 2 μm) as the surface becomes uniformly covered with *P. aeruginosa*. Although the vast majority of the attached cells are green-fluorescent, living cells, a small number of dead cells (red-fluorescent) are now observed at the interface between the PCL surface and the biofilm. These red-fluorescent dead cells are localized inside the mushroom-like colonies, consistent with the natural biofilm development process in which dead cells appear deep within the biofilm because they are used as an additional food source or aid in biofilm sloughing.[38, 39, 67, 68] On the 2% w/w O-MWCNT/PCL nanocomposite, the biofilm thickness also increases between regimes 1 and 2 (7 ± 1 μm to 10 ± 2 μm) although it remains thinner than the biofilm formed on the PCL. However, the most striking difference in the biofilms on the PCL and O-MWCNT/PCL surfaces is the distribution of living and dead cells. Specifically, the biofilm on the 2% w/w O-MWCNT/PCL surface in regime 2 is now dominated by red (dead) cells in direct contact with the surface, although some green (living) cells are still observed. We attribute this marked change in the properties of the 2% w/w O-MWCNT/PCL nanocomposite between regime 1 and 2 to biodegradation of the PCL polymer, leading to exposure of CNTs at the surface and the onset of cytotoxicity. The delayed onset of cytotoxicity at the 2% w/w O-MWCNT/PCL

surface is consistent with the idea that the CNTs were initially present below the nascent PNC surface prior to biodegradation (see Figure 4.1b).

PCL biodegradation has been observed before by biofilms used in denitrification applications and with *P. aeruginosa* in mass loss studies conducted in our laboratory.[94] In this study, only a thin (nanometer scale) thickness of the PCL coating is required to expose CNTs at the surface by PCL biodegradation. Although we could not directly measure PCL biodegradation on the 1 μm thick CNT/PNC film used in this study, we have performed related studies where mg quantities of pure PCL are degraded by *P. aeruginosa* cultures over the course of a few months. In contrast, we have seen no evidence that *P. aeruginosa* can biodegrade CNTs or the ethyl cellulose surfactant over a similar timescale. Thus, all of the experimental evidence points to the accumulation of CNTs at the surface being a result of PCL biodegradation.

It should be noted that the cytotoxicity of the CNTs in the present study is observed despite the fact that the CNT surfaces are oxidized and presumably at least partially coated with the surfactant ethyl cellulose. In our previous study, we have confirmed that oxidized MWCNTs and SWCNTs can exhibit antimicrobial properties at the surface of CNT/PNCs.[22] In this case, the addition of ethyl cellulose clearly does not mitigate the cytotoxicity of the O-MWCNTs as well. Ethyl cellulose itself does not contribute to the cytotoxicity since it is known to be biocompatible and is also present in the unmodified polymer references on which active biofilm growth occured.[76, 77] Collectively, these observations suggest that different CNTs embedded in PNC materials

will display cytotoxicity regardless of CNT type, surface oxidation, or the presence of a surfactant.[22, 23]

By the tertiary stage of growth, differences between the biofilms on the PCL and 2% w/w O-MWCNT/PCL surfaces are even more dramatic. While the bacteria at the PCL/biofilm interface are still composed almost exclusively of living cells with the exception of some dead cells in the thicker biofilm regions, the 2% w/w O-MWCNT/PCL surface is now best described as a carpet of dead cells at the PNC/biofilm interface. Relative to regime 2, the increase in cytotoxicity of the 2% w/w O-MWCNT/PCL surface for regime 3 can be explained by the continued biodegradation of the PCL polymer, leading to a continuously increasing concentration of CNTs at the PNC/biofilm interface and a correspondingly more cytotoxic surface. In general, the appearance of the PNC/biofilm interface for regime 4 was similar to regime 3 with slightly more dead cells carpeting the surface of the CNT/PNC. One possible explanation for the cell death observed in the lower layers of the biofilm is that the CNTs are simply blocking access of the microorganisms to the underlying PCL substrate, which is serving as a food source. This possibility was ruled out by conducting separate control studies where biofilms were grown on glass slides to similar thicknesses (>20 μm) as those observed in regime 4. These studies revealed that the acetate and oxygen concentrations in the media were sufficient to keep the majority of the biofilm cells alive on an inert, glass surface (Figure A4.15). Consequently, the cell death observed on 2% w/w O-MWCNT/PCL nanocomposites can be reasonably attributed to antimicrobial contact between *P. aeruginosa* and CNTs.

In addition to the carpet of dead cells at the PNC/biofilm interface, the CLSM images in Figure 4.2a (regime 3) reveal the presence of a layer of living (green) cells on top of the dead layer. This observation is indicative of the ability of a metabolically active biofilm to form on top of a dead layer, the latter acting to effectively shield the living cells from the cytotoxicity of the CNTs.[41, 51] Upon moving from regime 2 to regime 3, the biofilm thickness increases on both the PCL (13 ± 2 μm to 19 ± 5 μm) and the 2% w/w O-MWCNT/PCL nanocomposite (10 ± 1 μm to 18 ± 4 μm), despite the differences in cytotoxicity between the two surfaces.

Transitioning from regime 3 to 4, the biofilm thickness increases on the PCL surface (19 ± 5 μm to 22 ± 5 μm) while the biofilm thickness on the 2% w/w O-MWCNT/PCL nanocomposite decreases slightly (18 ± 4 μm to 15 ± 3 μm). However, on the 2% w/w O-MWCNT/PCL nanocomposite, biomass volume (>20%) increases from regime 3 to 4. This indicates further microbial growth despite a compression in biofilm thickness, possibly a result of living microorganisms consuming cellular material from the underlying dead layer of microorganisms.[51] Overall, the same type of "live-on-dead" biofilm structure observed in regime 3 is also present in regime 4 on the 2% w/w O-MWCNT/PCL nanocomposite.

A schematic representation of biofilm development on PCL and 2% w/w O-MWCNT/PCL nanocomposites from regimes 1 to 4 is shown in Figure 4.6a,b, respectively, highlighting the increase in cytotoxicity of the CNT/PCL surface due to the accumulation of CNTs as a result of PCL biodegradation and the subsequent formation of a "live-on-dead layer." This "live on dead" phenomenon is consistent with our previous study, where even at very short time points (1 h) on initially CNT-covered surfaces, some

living bacteria were shielded by a layer of dead bacteria in direct contact with the underlying CNTs. It should be noted that biofilm formation will also be accompanied by the secretion of EPS which contributes to the increase in biomass volume. Although we did not stain specifically for EPS, the EPS produced during biofilm growth did not prevent the onset of CNT cytotoxicity as indicated by the formation of a dead cell layer in Figure 4.2a. Accounting for the vertical resolution and fluorescence scattering between optical slices discussed in our previous publication, we estimate that this dead layer corresponds to a layer of one to three microorganisms (2-7 μm thick), consistent with the need for direct contact to occur in order for CNTs to exert their cytotoxicity.[22]

DFR experiments and biofilm analysis were also performed after initial attachment and at the final growth stage (regime 4) on an O-MWCNT/PCL nanocomposite with a lower (0.5% w/w) CNT concentration. CLSM images of LIVE/DEAD stained *P. aeruginosa* after 1 h of attachment to 0.5% w/w O-MWCNT/PCL nanocomposites (Figure A4.23) show that the CNT/PCL surface is initially benign. This is consistent with the absence of CNTs or a low CNT loading at the surface, the latter suggested by the SEM images (Figure A4.8). At regime 4 of biofilm development, or the final growth stage (Figure 4.3b), the 0.5% w/w O-MWCNT/PCL nanocomposite surface contains a mixture of living and dead cells, somewhere intermediate between the fraction of dead cells on the PCL control shown in Figure 4.3a and the 2% w/w O-MWCNT/PCL nanocomposite shown in Figure 4.3c. Thus, for the 0.5% w/w O-MWCNT/PCL nanocomposite it appears that the accumulation of CNTs from polymer biodegradation has not yet reached a point where the concentration of CNTs exposed at the surface is sufficient to have a cytotoxic effect on all of the attached

P. aeruginosa. This implies that the rate at which a biofilm forms a dead layer of cells would vary with CNT loading as the surface degrades.

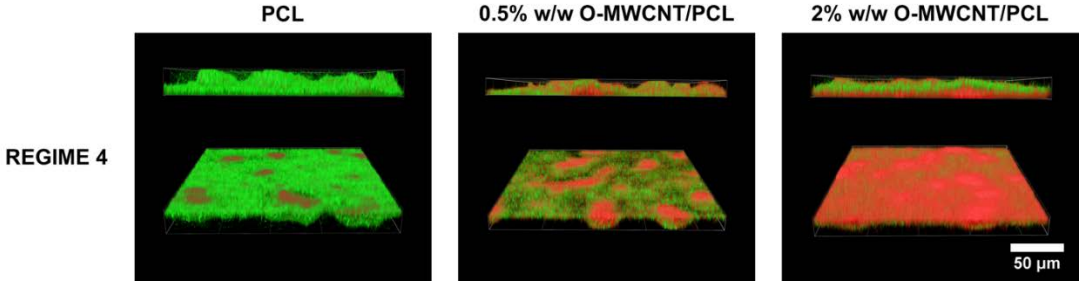

Figure 4.3. A CLSM comparison of LIVE/DEAD stained *P. aeruginosa* biofilms grown in a drip flow reactor on PCL, 0.5% w/w, and 2% w/w O-MWCNT/PCL at regime 4.

COMSTAT analysis also reveals that the biofilm thickness (and biomass volume) on the 0.5% O-MWCNT/PCL nanocomposite is less than on the PCL (15 ± 1 µm versus 22 ± 3 µm). In contrast, the biofilm thickness on the 0.5% w/w is similar to the biofilm thickness on the 2% w/w O-MWCNT/PCL nanocomposite (15 ± 1 µm versus 15 ± 3 µm) despite the significantly larger fraction of dead cells on the 2% w/w O-MWCNT/PCL nanocomposite.

To compare the effect of growth conditions, biofilms were grown on PCL and 2% w/w O-MWCNT/PCL nanocomposites under static conditions without shear or food source replenishment. In contrast to the DFR, static conditions simulate another type of environmentally relevant setting involving microbial growth in stagnant water such as puddles, swamps, slow moving groundwater, or small ponds.[73] In these experiments, biofilm development was monitored on O-MWCNT/PCL nanocomposites at three stages, each corresponding to an increasing biofilm thickness on PCL reference samples. A comparison of drip flow (Figure 4.2a) and static conditions (Figure 4.4a) reveals that the biofilms grown under static conditions differ in terms of morphology. Specifically, the biofilm structure is much more uniform under static conditions because growth is not

influenced by flow currents. This is most evident by the mushroom-like colonies and heterogeneous biofilms formed in the DFR.[72, 88] However, both drip flow and static conditions produce similar biofilm growth patterns on PCL and 2% w/w O-MWCNT/PCL surfaces (compare Figure 4.2 and 4.4). Under both growth conditions, the initial biofilms on PCL and 2% w/w O-MWCNT/PCL surfaces consist of mostly living cells, the green-fluorescent biofilm becomes thicker on the PCL control, and a red-fluorescent dead layer of cells eventually forms at the 2% w/w O-MWCNT/PCL nanocomposite/biofilm interface (Figure 4.2a and Figure 4.4a). Additionally, for the 2% w/w O-MWCNT/PCL nanocomposites, green-fluorescent living cells are observed on top of dead cells in the later stages of biofilm development (Figure 4.2a & Figure 4.4a, Regime 3). For the same samples, similar biofilm development trends were observed in terms of changes in biofilm thickness and biomass volumes under both static and DFR conditions (summarized in Figure 4.2b-c, Figure 4.4b-c, and Table A1). The absolute values of biofilm thickness and biomass volume were generally lower on CNT/PCL nanocomposites than on the pure polymer, presumably because CNT accumulation from polymer degradation led to cell death. However, biofilm thickness and biomass volume still increased at each stage of biofilm development as a result of active biofilm growth that continued on top of a dead layer of cells.

It is also worth noting that although both DFR and static conditions produce a "live-on-dead" biofilm structure, a much thicker layer of green-fluorescent living cells atop a carpet of dead cells is observed for the DFR biofilm than for the static biofilm. We ascribe this difference to carbon source depletion that limits cell growth under static

conditions (Figure 4.4) and carbon source replenishment under DFR conditions that promotes cell division at the surface.

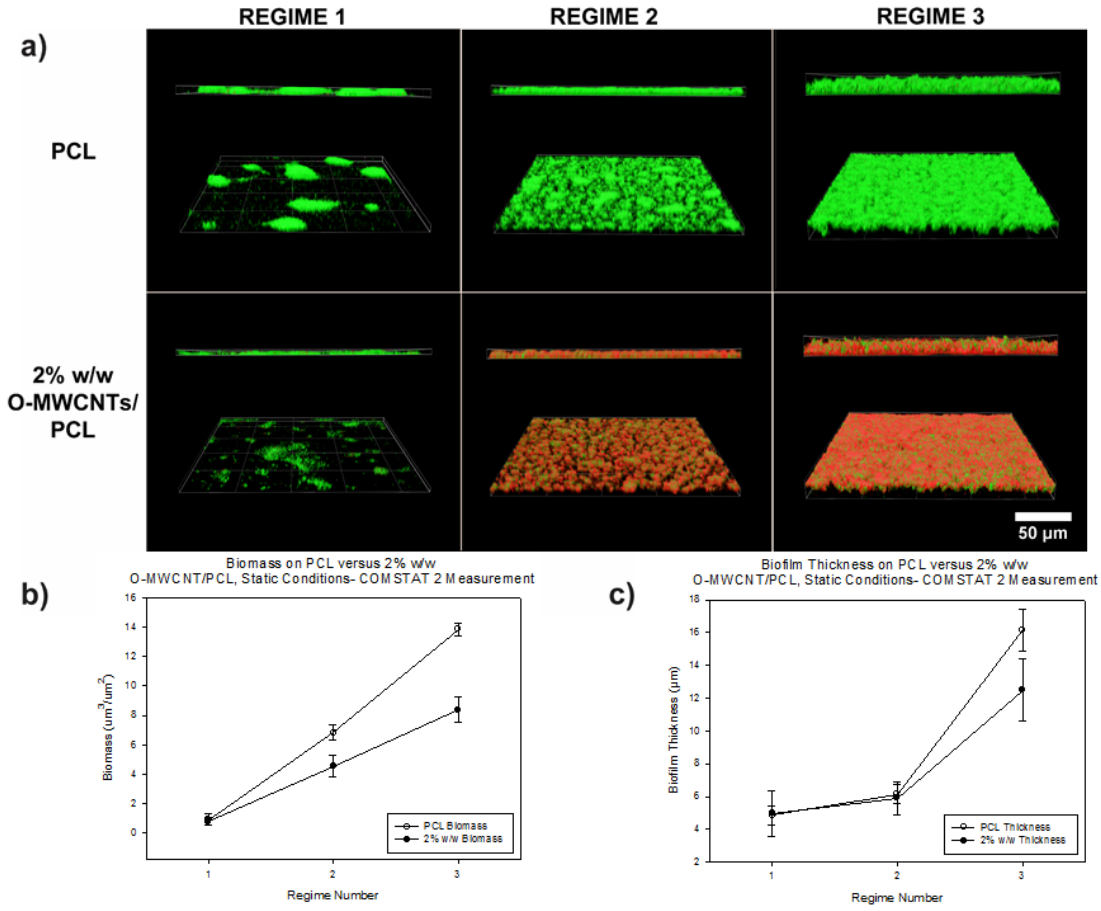

Figure 4.4. a) CLSM images of LIVE/DEAD stained P. aeruginosa grown under static conditions on PCL (top row) and 2% w/w O-MWCNT/PCL (bottom row). Regimes 1-3 (1 h – 2 weeks) represent increasing levels of biofilm growth based on the biofilm thicknesses observed on PCL. Quantitative comparison of biofilms on PCL and 2% w/w O-MWCNT/PCL under static conditions is also made using COMSTAT 2 b) biomass volume and c) thickness analysis. Each data point represents duplicate samples with at least five replicate areas per sample.

Rapid cell division as a result of the continuous carbon source feed can also account for the similarities in the biofilm thickness and volume on both 0.5 and 2% w/w O-MWCNT/PCL under DFR conditions (Figure 4.3). Regardless, under both growth conditions a dead cell layer was required to allow living cells to grow on top of the CNT

surfaces, as illustrated in Figure 4.6b (DFR conditions) and Figure A4.24 (static conditions). Under both flow and static conditions, the antimicrobial effect of CNTs on biofilm formation could be clearly observed over time as the CNTs accumulated at the PNC/biofilm interface due to biodegradation of the surrounding polymer matrix.[64-66] However, attempts were made to remove the biofilm without success by immersing samples in a 2% w/w sodium polyphosphate solution for 48 h with and without shaking followed by several washes with the same solution; this prevented us from directly observing CNTs at the CNT/PNC surface following polymer biodegradation (with SEM).[95, 96]

To study the biofilm formation characteristics of a CNT/PNC where CNTs were initially present at the surface, static biofilms were grown on 2% w/w O-MWCNT/PCL nanocomposites that were first degraded under aggressive oxidizing conditions (Figure 4.5).

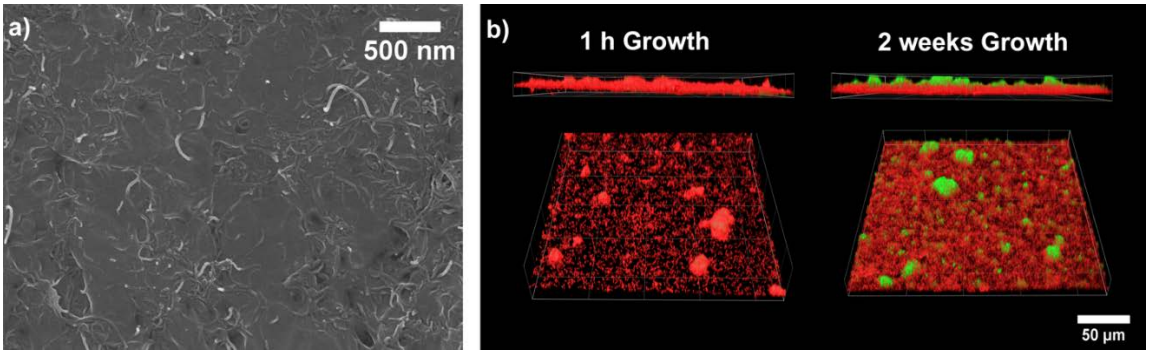

Figure 4.5. a) An SEM image showing CNT accumulation at the surface of a 2% w/w O-MWCNT/PCL nanocomposite following exposure to H_2O_2 in the presence of UV irradiation for 24 h and b) CLSM images of LIVE/DEAD stained *P. aeruginosa* grown on this type of photolyzed surface under static conditions for 1 h and 2 weeks with acetate food source replenishment.

This was carried out by exposing O-MWCNT/PCL nanocomposites to H_2O_2 in the presence of UV irradiation for 24 h. SEM analysis shown in Figure 4.5 reveals that this

treatment causes the removal of a thin layer of PNC and the accumulation of a large concentration of CNTs at the surface (2.1% average mass loss). Studying biofilm growth on this type of surface was also motivated by the expectation that many PNC surfaces will accumulate CNTs at the PNC/air interface over time as a result of naturally occurring environmental degradation processes such as photolysis and weathering.[15, 57, 59, 60] As shown in Figure 4.5, after 1 h of *P. aeruginosa* inoculation, almost all of the cells that attached to this type of CNT/PNC surface experienced cell death. This is in marked contrast to the initially benign surfaces observed for the 2% w/w O-MWCNT/PCL nanocomposites that had not been photolyzed (compare Figure 4.4a, Regime 1 and Figure 4.5b). However, after 2 weeks of growth under static conditions with the acetate food source replenished twice, "live-on-dead" structures were observed. Results from these studies further support the idea that a CNT-covered surface leads to cell death for bacteria that come into direct contact with the CNTs but not for those protected by a conditioning layer of dead cells.

Overall, "live-on-dead" biofilm structures formed on all CNT/PCL surfaces once coated by a full dead layer of cells under both static and DFR conditions. This was in stark contrast to the green-fluorescent biofilms formed on PCL. To highlight biofilm development on CNT/PNCs with different surface characteristics, a side-by-side comparison of biofilm progression is illustrated for: (a) pure PCL, (b) 2% w/w O-MWCNT/PCL nanocomposites that accumulate CNTs at the surface during polymer biodegradation, and (c) and 2% w/w O-MWCNT/PCL nanocomposites that have CNTs initially present at the surface (Figure 4.6).

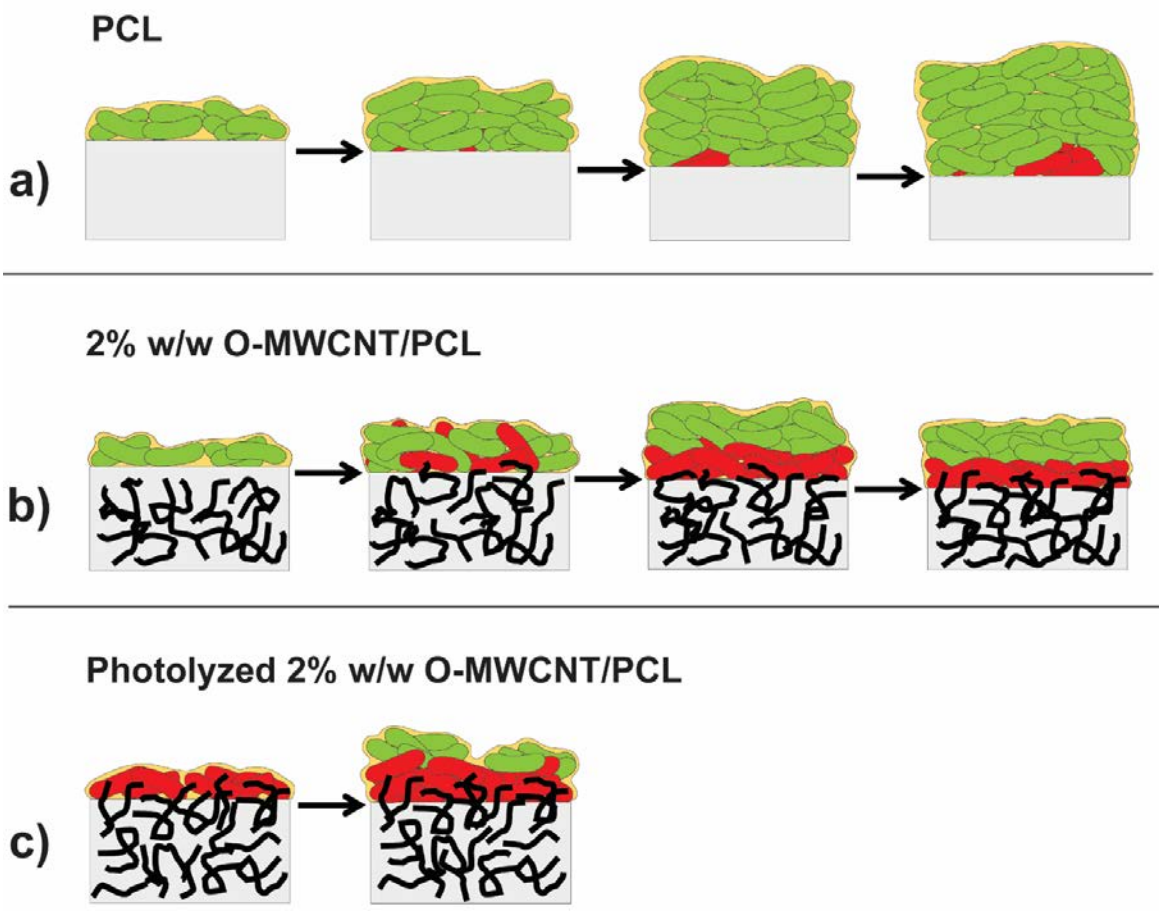

Figure 4.6. Illustrations that compare biofilm development on a) PCL and b) 2% w/w O-MWCNT/PCL, transformed as a result of polymer biodegradation under DFR conditions, and on c) photolyzed 2% w/w O-MWCNT/PCL with CNTs initially present at the CNT/PNC surface.

We assert that the biofilm development process observed on CNT/PCL nanocomposites in this study can be generalized to other types of polymer matrices. Figure 4.6c represents how biofilms would develop on CNT/PNCs where CNTs are initially present at the surface, or CNT/PNCs where CNTs have accumulated as result of weathering (e.g. photolysis, wear) prior to microbial interaction, while Figure 4.6b would be appropriate for CNT/PNCs in contact with microorganisms as CNTs accumulate at the PNC surface over time during environmental transformation processes (e.g. biodegradation, dissolution, etc.).[15, 57-60]

Our results demonstrate that CNT/PNC surfaces are only cytotoxic until they become coated with dead bacteria, limiting their use as antimicrobial materials. This conditioning layer of dead cells has been observed on other surfaces such as Ag-Pd and can be considered an inherent weakness of many anti-biofouling technologies that use solely cytotoxic effects to combat biofilm growth.[61] However, further studies on the stability of this "live-on-dead" biofilm structure will be useful to assess if there are conditions under which this type of biofilm sloughs away, allowing biofilms to form and subsequently be released in cycles on CNT/PNC surfaces. If biofilms are able to detach from CNT/PNCs, this would improve the potential for CNT/PNC surfaces to be used as antimicrobial coatings, at least in certain situations.

The dead layer of bacteria observed on CNT/PNCs also has the potential to affect the biodegradation of the underlying polymer matrix, a process in which extracellular enzymes produced by the attached microbial community can use the polymer substrate as a food source and break down polymeric chains to lower molecular weight units and eventually to small molecules such as CO_2 and water.[15, 35-37, 57, 59, 60, 97-103] Since CNT accumulation can lead to a full layer of dead cells across the CNT/PNC surface but living cells can form on top of the dead cells, the living cells may still be able to metabolize the PCL substrate using the EPS of the biofilm matrix. However, the dead cell layer may instead serve as a barrier that prevents living cells from accessing and biodegrading the underlying PCL. Therefore it is unclear whether the full dead layer of cells formed as a

result of CNT accumulation will render the CNT/PNC persistent or allow for continued biodegradation of the polymer matrix.

4.5. Conclusions

This study provides insights into how the development of biofilms on CNT/PNCs will be influenced by the surface characteristics of the CNT/PNC. The CNT/PCL nanocomposites studied had an initially benign interaction with microorganisms due to the lack of CNTs present at the surface. However, as the PCL matrix biodegraded, enrichment of CNTs at the surface increased the surface cytotoxicity. In terms of CNT loading, a dead cell layer was formed on the 2% w/w O-MWCNT/PCL nanocomposite but not on the 0.5% w/w O-MWCNT/PCL nanocomposite, indicating that CNT loading will have an effect on the rate at which the CNT/PNC surface becomes antimicrobial. On CNT/PCL samples where CNTs were initially exposed at the surface to simulate a weathered CNT/PCL nanocomposite, a full dead layer of cells was observed. At each growth stage, biofilm thickness and biofilm volume were always lower on CNT/PCL surfaces as compared to PCL. Since direct contact between the microorganisms and the CNTs was required for cell death, active biofilm growth occurred on all CNT-containing surfaces once a full layer of dead cells had formed at the PNC/biofilm interface. This demonstrates that once CNT/PNCs with a buried CNT network accumulate CNTs as a result of environmental transformation, the formation of a “live-on-dead” biofilm structure will be similar to that observed on CNT/PNCs with CNTs already present at the surface. The pattern of biofilm development was found to be similar under both DFR and static conditions although the rate of biofilm formation and structure of the biofilm differed. Collectively, the results of this study have implications for the fate and

persistence of CNT/PNC products in the environment and the likely limitations of CNT/PNCs in anti-biofouling applications.

4.6. Appendix 4 Summary

XPS and TEM data, a schematic of OTS modification of glass slides and the spray-coating process, an illustration of the CNT/PNC photodegradation procedure, replicate SEM images, a picture of the drip flow reactor setup, replicate confocal laser scanning microscopy images of LIVE/DEAD stained *P. aeruginosa* on CNT/PCL nanocomposite samples and controls, biomass volume and biofilm thickness measurements made with COMSTAT 2, and an illustration of biofilm growth on 2% w/w O-MWCNT/PCL nanocomposites under static conditions.

4.7. Acknowledgments

The authors would like to thank the NSF (CBET #1236493). DGG also acknowledges the Johns Hopkins University Chemistry Department for the award of an Owens Graduate Fellowship. The authors would like to thank Kris Marsh and Julianne Payne for their contributions as well as Dr. Michael McCaffery and Erin Pryce of the Integrated Imaging Center for their guidance in image acquisition and processing. Cong Gao acknowledges the Chinese Scholarship Council (No. 201406170083) for support to take part in this project.

4.8. References

1. N. G. McCrum, C.P. Buckley, and C.B. Bucknall, *Principles of polymer engineering*, Oxford University Press, New York, 1997.
2. P. C. a. M. M. C. Painter, *Fundamentals of polymer science: an introductory text*, Technomic Pub. Co., Lancaster, PA, 1997.
3. G. Williams, R. Trask, and I. Bond, *Composites Part A*, 2007, **38**, 1525-1532.
4. C. McClory, S. J. Chin and T. McNally, *Aust. J. Chem.*, 2009, **62**, 762-785.
5. A. M. K. Esawi and M. M. Farag, *Mater. Des.*, 2007, **28**, 2394-2401.

6. M. H. Rahmat, P., *Compos. Sci. Technol.*, 2011, **72**, 72-84.
7. R. Gangopadhyay and A. De, *Chem. Mater.*, 2000, **12**, 608-622.
8. M. Moniruzzaman and K. I. Winey, *Macromolecules*, 2006, **39**, 5194-5205.
9. (WWICS), Woodrow Wilson International Center for Scholars "The Project on Emerging Nanotechnologies" Nanotechnology Consumer Products Inventory http://www.nanotechproject.org/inventories/consumer/).
10. T. V. Duncan, *J. Coll. Interface Sci.*, 2011, **363**, 1-24.
11. Nanocyl, Carbon nanotube applications: fuel system components: http://www.nanocyl.com/Products-Solutions/Sectors/Automotive/Fuel-System-Components).
12. V. M. F. L. De, S. H. Tawfick, R. H. Baughman and A. J. Hart, *Science*, 2013, **339**, 535-539.
13. E. J. Petersen, L. W. Zhang, N. T. Mattison, D. M. O'Carroll, A. J. Whelton, N. Uddin, T. Nguyen, Q. G. Huang, T. B. Henry, R. D. Holbrook and K. L. Chen, *Environ. Sci. Technol.*, 2011, **45**, 9837-9856.
14. S. Hirth, L. Cena, G. Cox, Ž. Tomović, T. Peters and W. Wohlleben, *J. Nanopart. Res.*, 2013, **15**, 1-15.
15. C. Kingston, R. Zepp, A. Andrady, D. Boverhof, R. Fehir, D. Hawkins, J. Roberts, P. Sayre, B. Shelton, Y. Sultan, V. Vejins and W. Wohlleben, *Carbon*, 2014, **68**, 33-57.
16. P. R. Jones, M. T. Cottrell, D. L. Kirchman and S. C. Dexter, *Microb. Ecol.*, 2007, **53**, 153-162.
17. J. W. Costerton, K. J. Cheng, G. G. Geesey, T. I. Ladd, J. C. Nickel, M. Dasgupta and T. J. Marrie, *Annu. Rev. Microbiol.*, 1987, **41**, 435-464.
18. F. Ahmed, C. M. Santos, R. A. M. V. Vergara, M. C. R. Tria, R. Advincula and D. F. Rodrigues, *Environ. Sci. Technol.*, 2012, **46**, 1804-1810.
19. C. M. Santos, K. Milagros Cui, F. Ahmed, M. C. R. Tria, R. A. M. V. Vergara, A. C. de Leon, R. C. Advincula and D. F. Rodrigues, *Macromol. Mater. Eng.*, 2012, **297**, 807-813.
20. M. S. Mauter and M. Elimelech, *Environ. Sci. Technol.*, 2008, **42**, 5843-5859.
21. S. Aslan, C. Z. Loebick, S. Kang, M. Elimelech, L. D. Pfefferle and T. P. R. Van, *Nanoscale*, **2**, 1789-1794.
22. D. G. Goodwin, K. M. Marsh, I. B. Sosa, J. B. Payne, J. M. Gorham, E. J. Bouwer and D. H. Fairbrother, *Environ. Sci. Technol.*, 2015, **49**, 5484-5492.
23. J. D. Schiffman and M. Elimelech, *ACS Appl. Mater. Interfaces*, 2011, **3**, 462-468.
24. S. Kang, M. Herzberg, D. F. Rodrigues and M. Elimelech, *Langmuir*, 2008, **24**, 6409-6413.
25. S. Kang, M. Pinault, L. D. Pfefferle and M. Elimelech, *Langmuir*, 2007, **23**, 8670-8673.
26. C. D. Vecitis, K. R. Zodrow, S. Kang and M. Elimelech, *ACS Nano*, 2010, **4**, 5471-5479.
27. L. M. Pasquini, R. C. Sekol, A. D. Taylor, L. D. Pfefferle and J. B. Zimmerman, *Environ. Sci. Technol.*, 2013, **47**, 8775-8783.
28. L. M. Pasquini, S. M. Hashmi, T. J. Sommer, M. Elimelech and J. B. Zimmerman, *Environ. Sci. Technol.*, 2012, **46**, 6297-6305.
29. C. Yang, J. Mamouni, Y. Tang and L. Yang, *Langmuir*, 2010, **26**, 16013-16019.

30. D. Monroe, *PLoS Biol.*, 2007, **5**, e307.
31. S. Andersson, G. K. Rajarao, C. J. Land and G. Dalhammar, *FEMS Microbiol. Lett.*, 2008, **283**, 83-90.
32. H.-C. Flemming and J. Wingender, *Nat. Rev. Microbiol.*, 2010, **8**, 623-633.
33. S. U. Gerbersdorf, T. Jancke, B. Westrich and D. M. Paterson, *Geobiology*, 2008, **6**, 57-69.
34. M. M. Klausen, T. R. Thomsen, J. L. Nielsen, L. H. Mikkelsen and P. H. Nielsen, *FEMS Microbiol. Ecol.*, 2004, **50**, 123-132.
35. A. Sivan, *Curr. Opin. Biotechnol.*, 2011, **22**, 422-426.
36. L. V. Evans, *Biofilms: recent advances in their study and control*, CRC press, 2003.
37. J. D. Bryers, *Biofilms II: process analysis and applications*, Wiley-Liss, 2000.
38. L. Ma, M. Conover, H. Lu, M. R. Parsek, K. Bayles and D. J. Wozniak, *PLoS Pathog.*, 2009, **5**.
39. J. S. Webb, L. S. Thompson, S. James, T. Charlton, T. Tolker-Nielsen, B. Koch, M. Givskov and S. Kjelleberg, *J. Bacteriol.*, 2003, **185**, 4585-4592.
40. R. P. Carlson, R. Taffs, W. M. Davison and P. S. Stewart, *J. Biomater. Sci., Polym. Ed.*, 2008, **19**, 1035-1046.
41. H.-C. Flemming, T. Griebe and G. Schaule, *Water Sci. Technol.*, 1996, **34**, 517-524.
42. N. Billings, M. M. Ramirez, M. Caldara, R. Rusconi, Y. Tarasova, R. Stocker and K. Ribbeck, *PLoS Pathog.*, 2013, **9**, e1003526.
43. V. K. K. Upadhyayula and V. Gadhamshetty, *Biotechnol. Adv.*, 2010, **28**, 802-816.
44. S. Cao, J. Wang, H. Chen and D. Chen, *Chin. Sci. Bull.*, 2011, **56**, 598-612.
45. S. Krishnan, C. J. Weinman and C. K. Ober, *J. Mater. Chem.*, 2008, **18**, 3405-3413.
46. A. K. Epstein, T.-S. Wong, R. A. Belisle, E. M. Boggs and J. Aizenberg, *Proc. Natl. Acad. Sci. USA*, 2012, **109**, 13182-13187.
47. I. Francolini, P. Norris, A. Piozzi, G. Donelli and P. Stoodley, *Antimicrob. Agents Chemother.*, 2004, **48**, 4360-4365.
48. M. Ratova and A. Mills, *J. Photochem. Photobiol. A: Chem.*, 2015, **299**, 159-165.
49. X. Khoo, G. A. O'Toole, S. A. Nair, B. D. Snyder, D. J. Kenan and M. W. Grinstaff, *Biomaterials*, 2010, **31**, 9285-9292.
50. C. Liu, D. Zhang, Y. He, X. Zhao and R. Bai, *J. Membr. Sci.*, 2010, **346**, 121-130.
51. D. F. Rodrigues and M. Elimelech, *Environ. Sci. Technol.*, 2010, **44**, 4583-4589.
52. Nanocyl, Biocyl. http://www.nanocyl.com/kr/Products-Solutions/Products/BIOCYL).
53. A. Beigbeder, P. Degee, S. L. Conlan, R. J. Mutton, A. S. Clare, M. E. Pettitt, M. E. Callow, J. A. Callow and P. Dubois, *Biofouling*, 2008, **24**, 291-302.
54. R. J. Narayan, C. Berry and R. Brigmon, *Mater. Sci. Eng., B*, 2005, **123**, 123-129.
55. V. Vatanpour, S. S. Madaeni, R. Moradian, S. Zinadini and B. Astinchap, *J. Membr. Sci.*, 2011, **375**, 284-294.
56. A. Tiraferri, C. D. Vecitis and M. Elimelech, *ACS Appl. Mater. Interfaces*, 2011, **3**, 2869-2877.
57. T. Nguyen, B. Pellegrin, L. Mermet, A. Shapiro, X. Gu and J. Chin, *Nanotechnology*, 2009, 90-93.
58. T. Nguyen, B. Pelligrin, C. Bernard, X. Gu, J. M. Gorham, P. Stutzman, D. Stanley, D. Shapiro, E. Bryrd, R. Hettenhouse and J. Chin, *J. Phys.: Conf. Ser.*, 2011, **34**, 012060.

59. J. E. Guillet, T. W. Regulski and T. B. McAneney, *Environ. Sci. Technol.*, 1974, **8**, 923-925.
60. P. H. Jones, D. Prasad, M. Heskins, M. H. Morgan and J. E. Guillet, *Environ. Sci. Technol.*, 1974, **8**, 919-923.
61. W.-C. Chiang, C. Schroll, L. R. Hilbert, P. Moeller and T. Tolker-Nielsen, *Appl. Environ. Microbiol.*, 2009, **75**, 1674-1678.
62. D. Sun, S. Cheng, A. Wang, F. Li, B. E. Logan and K. Cen, *Environ. Sci. Technol.*, 2015, **49**, 5227-5235.
63. R. A. Gross and B. Kalra, *Science*, 2002, **297**, 803-807.
64. V. Massardier-Nageotte, C. Pestre, T. Cruard-Pradet and R. Bayard, *Polym. Degrad. Stab.*, 2006, **91**, 620-627.
65. C. Lefevre, A. Tidjani, W. C. Vander and C. David, *J. Appl. Polym. Sci.*, 2002, **83**, 1334-1340.
66. V. K. Khatiwala, N. Shekhar, S. Aggarwal and U. K. Mandal, *J. Polym. Environ.*, 2008, **16**, 61-67.
67. E. Werner, F. Roe, A. Bugnicourt, M. J. Franklin, A. Heydorn, S. Molin, B. Pitts and P. S. Stewart, *Appl. Environ. Microbiol.*, 2004, **70**, 6188-6196.
68. K. D. Xu, P. S. Stewart, F. Xia, C.-T. Huang and G. A. McFeters, *Appl. Environ. Microbiol.*, 1998, **64**, 4035-4039.
69. M. T. Madigan, J. M. Martinko, P. V. Dunlap and D. P. Clark, *Brock Biology of Microorganisms*, Pearson, San Francisco, 12th edn., 2009.
70. B. L. Allen, G. P. Kotchey, Y. N. Chen, N. V. K. Yanamala, J. Klein-Seetharaman, V. E. Kahan and A. Star, *J. Am. Chem. Soc.*, 2009, **131**, 17194-17205.
71. J. Russier, C. Ménard-Moyon, E. Venturelli, E. Gravel, G. Marcolongo, M. Meneghetti, E. Doris and A. Bianco, *Nanoscale*, 2011, **3**, 893-896.
72. L. Hall-Stoodley, J. W. Costerton and P. Stoodley, *Nat. Rev. Microbiol.*, 2004, **2**, 95-108.
73. A. R. Horswill, P. Stoodley, P. S. Stewart and M. R. Parsek, *Anal. Bioanal. Chem.*, 2007, **387**, 371-380.
74. Invitrogen, *Journal*, 2009.
75. M. Vorregaard, Technical University of Denmark, DTU, DK-2800 Kgs. Lyngby, Denmark, 2008.
76. A. Heydorn, A. T. Nielsen, M. Hentzer, C. Sternberg, M. Givskov, B. K. Ersbøll and S. Molin, *Microbiology*, 2000, **146**, 2395-2407.
77. A. R. Boccaccini, J. Cho, J. A. Roether, B. J. Thomas, E. J. Minay and M. S. Shaffer, *Carbon*, 2006, **44**, 3149-3160.
78. H. Liu, L. Zhang, P. Shi, Q. Zou, Y. Zuo and Y. Li, *J. Biomed. Mater. Res. B Appl. Biomater.*, 2010, **95B**, 36-46.
79. M. E. McGovern, K. M. R. Kallury and M. Thompson, *Langmuir*, 1994, **10**, 3607-3614.
80. P. H. Mutin, G. Guerrero and A. Vioux, *J. Mater. Chem.*, 2005, **15**, 3761-3768.
81. J. E. Song, T. Phenrat, S. Marinakos, Y. Xiao, J. Liu, M. R. Wiesner, R. D. Tilton and G. V. Lowry, *Environ. Sci. Technol.*, 2011, **45**, 5988-5995.
82. M. Sodagari, H. Wang, B.-m. Z. Newby and L.-K. Ju, *Colloids Surf. B. Biointerfaces*, 2013, **103**, 121-128.
83. H. Wang, M. Sodagari, Y. Chen, X. He, B.-m. Z. Newby and L.-K. Ju, *Colloids*

Surf. B. Biointerfaces, 2011, **87**, 415-422.
84. S. E. Page, J. R. Logan, R. M. Cory and K. McNeill, *Environ. Sci.: Processes Impacts*, 2014, **16**, 807-822.
85. W. R. Haag and J. Hoigné, *Chemosphere*, 1985, **14**, 1659-1671.
86. W.-C. Hou, S. BeigzadehMilani, C. T. Jafvert and R. G. Zepp, *Environ. Sci. Technol.*, 2014, **48**, 3875-3882.
87. R. M. Atlas, *Handbook of media for environmental microbiology*, CRC press, 2005.
88. D. M. Goeres, M. A. Hamilton, N. A. Beck, K. Buckingham-Meyer, J. D. Hilyard, L. R. Loetterle, L. A. Lorenz, D. K. Walker and P. S. Stewart, *Nat. Protoc.*, 2009, **4**, 783-788.
89. K. Schwartz, R. Stephenson, M. Hernandez, N. Jambang and B. R. Boles, *J Vis Exp*, 2010.
90. T. R. Neu and J. R. Lawrence, *FEMS Microbiol. Ecol.*, 1997, **24**, 11-25.
91. J. Lawrence, D. Korber, T. Neu, C. Hurst, R. Crawford, J. Garland, D. Lipson, A. Mills and L. Stetzenbach, *Man. Environ. Microbiol.*, 2007, 40-68.
92. Comstat 2 Homepage, www.comstat.dk.
93. E. J. Petersen, T. Lam, J. M. Gorham, K. C. Scott, C. J. Long, D. Stanley, R. Sharma, J. Alexander Liddle, B. Pellegrin and T. Nguyen, *Carbon*, 2014, **69**, 194-205.
94. L. Chu and J. Wang, *Chemosphere*, 2013, **91**, 1310-1316.
95. M. Kubota, M. Matsui, H. Chiku, N. Kasashima, M. Shimojoh and K. Sakaguchi, *Appl. Environ. Microbiol.*, 2005, **71**, 8895-8902.
96. V. R. Hill, A. L. Polaczyk, D. Hahn, J. Narayanan, T. L. Cromeans, J. M. Roberts and J. E. Amburgey, *Appl. Environ. Microbiol.*, 2005, **71**, 6878-6884.
97. Y. Zheng, E. K. Yanful and A. S. Bassi, *Crit. Rev. Biotechnol.*, 2005, **25**, 243-250.
98. M. Kolybaba, L. Tabil, S. Panigrahi, W. Crerar, T. Powell and B. Wang, 2003.
99. A. A. Shah, F. Hasan, A. Hameed and S. Ahmed, *Biotechnol. Adv.*, 2008, **26**, 246-265.
100. P. R and M. Doble, *Indian J. Biotechnol.*, 2005, **4**, 186-193.
101. K. Leja and G. Lewandowicz, *Pol. J. Environ. Stud.*, 2010, **13**, 255-266.
102. T. Ishigaki, W. Sugano, A. Nakanishi, M. Tateda, M. Ike and M. Fujita, *Chemosphere*, 2004, **54**, 225-233.
103. M. Shimao, *Curr. Opin. Biotechnol.*, 2001, **12**, 242-247.

Chapter 5. Relevant Controls and Considerations for Aerobic Single Culture Biodegradation of Carbon Nanotube/Polymer Nanocomposites

5.1. Introduction

Polymers can be tailored for different applications by blending additives such as fillers, colorants, plasticizers, stabilizers, and flame retardants into polymer matrices.[1, 2] Carbon nanotubes (CNTs), in particular, have emerged as a useful filler since their incorporation into a polymer matrix at a low mass fraction, typically 1-5% w/w, can produce CNT/polymer nanocomposites (CNT/PNCs) with two broad types of enhancement in polymer properties: structural or functional.[3-12] Structurally, CNTs can enhance the tensile strength, elastic modulus, and hardness of a polymer without a significant increase in product weight as would be the case with metal additives.[4, 7-10, 13, 14] Enhancement of thermal or flame resistance, electrical conductivity, and thermomagnetic interference are a few of the functional properties that can be obtained from the addition of CNTs to a polymer.[15-18] Thus CNTs have already been incorporated into a wide range of commercially available products that include anti-static packaging, wind turbines, fuel tank linings, sporting equipment, headphone speaker diaphragms, and even biomedical implants and devices.[3, 13, 19-23]

With the expanding use of CNTs in products, the environmental impact of CNT-containing polymer waste warrants investigation. Similar to everyday plastics, CNT/PNCs are likely to end up in landfills, surface waters, and wastewater treatment plants following consumer use.[13, 24, 25] At this point in the life cycle of a polymeric material, its ultimate fate can be strongly influenced by interactions with microorganisms. Biodegradation of polymeric materials, or transformation by microorganisms, involves

enzymatic break-down of polymer chains to lower molecular weight products and eventually small molecules such as carbon dioxide, methane, and water.[26] The kinetics of biodegradation for different polymers can range from a few days to several hundred years.[27] Material class, crystallinity, tacticity, molecular weight, and the presence of additives can also have a large impact on polymer biodegradation rates.[27] Polymer biodegradation can proceed under aerobic or anaerobic conditions by using oxygen or an alternative electron acceptor, respectively, to drive respiration.[28, 29] Under aerobic conditions, polymers are considered biodegradable if they can be > 60% mineralized to CO_2 within 180 days by microorganisms.[30, 31]

Many petroleum based polymers, such as polyethylene, do not contain functional groups that can be easily transformed by enzymes and as a result, are recalcitrant to biodegradation. Nevertheless, even these biologically inert plastics can eventually be degraded by microorganisms, oftentimes in tandem with other environmental conditions such as weathering, hydrolysis, and photodegradation which can oxidize and shorten polymer chains to a more metabolically accessible form for microganisms.[26, 32-34] Biodegradable additives such as starch or cellulose can also be added to biologically inert polymers to promote polymer fragmentation, by introducing a biodegradable component into the polymer composite.[35, 36] A sub-class of petroleum based polymers, such as polybutylene succinate (PBS) and poly-ε-caprolactone (PCL), are considered biodegradable on a rapid time scale (days- months).[37-39] Many bio-derived polymers, such as polyhydroxyalkanoates (PHA), cellulose, and starch, are also biodegradable, and are being produced in increasing quantities due to their sustainable and economical precursors.[26, 32, 36, 40] Derived from plants, microorganisms, and fungi, these polymers

oftentimes require fillers such as CNTs to improve their mechanical properties to the have desirable materials properties and functionality.[40, 41]

In order to assess the biodegradability of CNT/PNCs, exposure of different polymer types to a single culture of microorganisms was first undertaken and the percent mass loss over time was used as a means of discriminating rapidly biodegrading polymers from those that biodegraded too slowly on an experimentally relevant timescale. This was also done prior to starting the biofilm work in Chapter 4 to ensure polymer type was consistent in both the biofilm development study and the biodegradation study. Only biodegradable polymers were used since an accelerated time scale was required to complete CNT/PNC biodegradation studies, with the prospect of generalizing observed trends to a variety of CNT/PNC types when possible. To biodegrade the polymers, *Pseudomonas aeruginosa* was used as the single culture of microorganisms since *Pseudomonas* species contain lipases, a subclass of esterase enzymes that can hydrolyze ester bonds, which were present in some of the polymer structures that were screened for rapid biodegradability.[42, 43] Furthermore, the use of a single culture provided more control relative to mixed culture conditions, which can be highly variable batch to batch.

An additional polymer screening method was the ability of a polymer to yield CNT/PNCs with a good CNT dispersion quality using solution blending methods. A polymer was only considered if the uniformity of CNTs in its matrix were, at minimum, visually homogenous. PCL was a good choice since a variety of CNT types dispersed uniformly throughout its matrix using ethyl cellulose (EC), a natural and biocompatible surfactant that has been used as a surfactant in other matrices.[44-47] Next, the polymer

chosen was not permitted for use if any mass loss could occur in an abiotic control as a result of polymer dissolution over the course of several weeks. This was to ensure that all mass loss observed from CNT/PNCs was a result of polymer biodegradation.[48] The polymers that best fit all of these criteria were PCL and PHA. Since the structure of PCL is well known while commercially available PHA exists as a copolymer consisting of unknown fractions of two or three different types of monomers, PCL was used for the majority of studies in order to have finer control over biodegradation conditions. Further advantages of using PCL for CNT/PNC biodegradation studies as well as some applications of PCL are described in the next chapter. Pristine multi-wall (MWCNT) and slightly oxidized multi-wall CNTs (LO-MWCNTs) were used for the reasons outlined in Chapter 2.

In order to design a study to assess CNT/PNC biodegradation using PCL as the polymer matrix, several considerations had to be made to ensure rapid and consistent biodegradation results. First, to produce PCL films, hereafter referred to as *coupons*, the casting solvent used had to generate a homogenous CNT dispersion quality and not substantially inhibit the rate of PCL biodegradability. Solvent boiling point and solvent/polymer interactions can alter polymer biodegradability by changing the degree of polymer crystallinity.[49] The degree of crystallinity is an important factor in biodegradation processes since crystalline regions of a polymer are more unfavorable to biodegrade due to steric hindrance during enzymatic approach and the energy input required to disrupt a stable conformation of polymer chains.[49] Solvents that include tetrahydrofuran, (THF), chloroform ($CHCl_3$), and dichloromethane (DCM) were all tested for their effect on PCL biodegradability and their ability to disperse CNTs. The molecular

weight of a polymer is also an important factor in polymer biodegradability, and was therefore kept constant throughout this study using consistent polymer sonication times.[49-52] EC content (% w/w) and EC biodegradability were also investigated since additives can have an effect on the biodegradation rate of a polymer.[1]

Lastly, the effect of carbon source on PCL biodegradation was evaluated, as the presence of an external food source can have an accelerating or decelerating effect on PCL metabolism by a microorganism.[39, 53, 54] In initial studies, sodium acetate trihydrate (ReagentPlus, ≥99.0%, Sigma-Aldrich) was used as the carbon source in basal mineral media (BMM) at high (577 mg/L C) and low (35 mg/L C) concentrations.[55] The advantage of using high carbon source BMM (high C BMM) was to first grow a large population of microorganisms using the acetate to maximize the number of bacteria available to degrade PCL. However, the bacteria could preferentially metabolize acetate in place of PCL under these conditions and as a result, degrade PCL slowly. The other approach was to use low carbon source BMM (low C BMM) to supplement the microorganisms with less carbon, and as a result, provide the microorganisms with more opportunity to acclimate to and degrade PCL.[53, 54] Lastly, the effect of using a small molecule version of PCL, or PCL triol, was attempted to accelerate acclimation of *P. aeruginosa* to PCL coupons for biodegradation. Once conditions had been optimized for PCL biodegradation and CNT/PCL preparation, biodegradation studies could be systematically conducted with CNT/PCL nanocomposites as outlined in later chapters.

5.2. Experimental

5.2.1. PCL Coupon Preparation in THF

Pure PCL coupons were prepared by adding 400 mg of PCL to 40 mL of tetrahydrofuran (THF, Omnisolv, TX0279-1) followed by 3 h sonication (Branson 1510

Ultrasonic Bath, 70 W) in ice water. The ice water bath was replenished every 1 h to minimize solvent volatilization. A 10 mL ± 0.02 mL graduated cylinder was used to distribute the polymer casting solution in 5 mL aliquots to (44 mm diameter, 12.5 mm height, Fisher Scientific) aluminum dishes. Samples were covered overnight to allow for slow, consistent solvent evaporation. The next day, PCL coupons were soaked in a DI water bath since this was found to help separate the PCL coupons from their aluminum dishes. PCL coupons were then trimmed around their outer edges to a consistent shape and size, resulting in coupons between 16-21 mg.

5.2.2. Ethyl cellulose (EC) Coupon Preparation

Pure EC coupons were prepared by adding 1600 mg EC (48.0 - 49.5% (w/w) ethoxyl basis, Lot # BCBG4792V, Sigma-Aldrich) into 160 mL of chloroform ($CHCl_3$, HPLC grade, C607-4) followed by 3 h sonication in ice water. The ice water bath was replenished every 1 h to minimize solvent volatilization. A 50 mL ± 0.25 mL graduated cylinder was used to distribute the polymer casting solution in 20 mL aliquots to aluminum dishes. Due to the brittle nature of the EC coupons, 20 mL was found to be the minimal casting volume that could be used to remove the EC coupons from the aluminum dishes. Samples were covered overnight to allow for slow, consistent solvent evaporation. EC samples were then trimmed around their outer edges to a consistent shape and size, resulting in coupons weighing between 40-50 mg.

5.2.3. PCL (4% w/w EC) and 2% w/w LO-MWCNT/PCL (4% w/w EC) Preparation in THF

2% w/w LO-MWCNT/PCL nanocomposites were prepared by adding 16 mg of EC (48.0 - 49.5% (w/w) ethoxyl basis, Lot # BCBG4792V, Sigma-Aldrich) and 8 mg of LO-MWCNTs (described in Chapter 2) to a 50 mL Erlenmeyer flask containing 40 mL of

THF. The EC macromolecules were used for CNT stabilization in THF. LO-MWCNTs in EC were sonicated in an ice water bath for 2 h. 400 mg of PCL was then added to the CNT suspension and sonicated for an additional 3 h. During all steps of sonication, the ice water bath was replenished every 1 h to minimize solvent volatilization and improve dispersion quality. In a separate flask, 400 mg of PCL and 16 mg of EC were added to 40 mL of THF and sonicated for 3 h with 1 h ice replenishment to generate PCL references. The PCL (4% w/w EC) casting solution was sonicated for 3 h for consistency with the polymer sonication time used for the CNT/PCL nanocomposites casting solution. A 10 mL ± 0.02 mL graduated cylinder was used to distribute the two casting solutions into 5 mL aliquots to aluminum dishes. Samples were covered overnight to allow for slow, consistent solvent evaporation. The next day, PCL and CNT/PCL nanocomposites were soaked in a DI water bath since this was found to help separate the coupons from their aluminum dishes. PCL and CNT/PCL nanocomposites were then trimmed around their outer edges to a consistent shape and size, resulting in coupons between 16-21 mg.

5.2.4. PCL Coupon Preparation in Chloroform and Dichloromethane

Pure PCL coupons were prepared in chloroform and dichloromethane according to the same procedure outlined for pure PCL coupon preparation in THF.

5.2.5. PCL of Varied EC Loadings and 2% w/w LO-MWCNT/PCL (20% w/w EC) Preparation in $CHCl_3$

2% w/w LO-MWCNT/PCL nanocomposites were prepared by adding 80 mg of EC (48.0 - 49.5% (w/w) ethoxyl basis, Lot # BCBG4792V, Sigma-Aldrich) and 8 mg of LO-MWCNTs (described in Chapter 2) to a 50 mL Erlenmeyer flask containing 40 mL of $CHCl_3$. LO-MWCNTs in EC were sonicated in an ice water bath for 3 h. 400 mg of PCL was then added to the CNT suspension and sonicated for an additional 3 h. During all

steps of sonication, the ice water bath was replenished every 1 h to minimize solvent volatilization and improve dispersion quality. In a separate flask, 400 mg of PCL and 80 mg of EC were added to 40 mL of $CHCl_3$ and sonicated for 3 h with 1 h ice replenishment to prepare PCL references. The PCL (20% w/w EC) casting solution was sonicated for 3 h for consistency with the polymer sonication time used for the CNT/PCL nanocomposites casting solution. A 10 mL ± 0.02 graduated cylinder was used to distribute the two casting solutions into 5 mL aliquots to aluminum dishes. Samples were covered overnight to allow for slow, consistent solvent evaporation. The next day, PCL and CNT/PCL nanocomposites were soaked in a DI water bath since this was found to help separate the coupons from their aluminum dishes. PCL and CNT/PCL nanocomposites were then trimmed around their outer edges to a consistent shape and size, resulting in coupons between 16-21 mg.

5.2.6. PCL (4% w/w EC) and 0.5% w/w LO-MWCNT/PCL (4% w/w EC) Preparation in DCM

0.5% w/w LO-MWCNT/PCL nanocomposites were prepared by adding 16 mg of EC (described in 5.2.2.) and 2 mg of LO-MWCNTs (described in Chapter 2) to a 50 mL Erlenmeyer flask containing 40 mL of DCM (DCM, >99.8%, Sigma-Aldrich). LO-MWCNTs in EC were sonicated in an ice water bath for 1 h. 400 mg of PCL was then added to the CNT suspension and sonicated for an additional 3 h. During all steps of sonication, the ice water bath was replenished every 1 h to minimize solvent volatilization and improve dispersion quality. In a separate flask, 400 mg of PCL and 16 mg of EC were added to 40 mL of DCM and sonicated for 3 h with 1 h ice replenishment to generate PCL references. The PCL (4% w/w EC) casting solution was sonicated for 3 h for consistency with the polymer sonication time used for the CNT/PCL nanocomposite

casting solution. A 10 mL ± 0.02 graduated cylinder was used to distribute the two casting solutions into 5 mL aliquots to aluminum dishes. Samples were covered overnight to allow for slow, consistent solvent evaporation. The next day, PCL and CNT/PCL nanocomposites were soaked in a DI water bath since this was found to help separate the coupons from their aluminum dishes. PCL and CNT/PCL nanocomposites were then trimmed around their outer edges to a consistent shape and size, resulting in coupons between 16-21 mg.

5.2.7. Crystallinity Measurements

Differential scanning calorimetry (DSC) measurements were made on pure PCL and PCL (4% w/w EC) prepared in $CHCl_3$, DCM, and THF to characterize the degree of polymer crystallinity, a property of polymeric materials that can have an effect on biodegradation rates.[56] DSC curves were generated using a TA instrument (New Castle, Delaware) with a temperature range of room temperature (~25 °C) to 65 °C to capture the PCL melting transition at 60 °C.[57] A heating rate of 5 °C/min and a cooling rate of 1 °C/min were used with the temperature maintained at 65 °C for 2 min before cooling began. Analysis of the DSC curves was performed using TA Universal Analysis software 2000 (TA instruments, New Castle, Delaware). The enthalpy of fusion was calculated by integrating the endothermic peak (42 to 62 °C) with a linear background. The fraction of crystallinity (Xc) was then calculated by dividing the experimental enthalpy of fusion by the theoretical enthalpy of fusion (ΔH_0 = 139.5 J/g).[58, 59]

5.2.8. Basal Mineral Media (BMM) Preparation

BMM was prepared according to standard protocols from the *Handbook of Media for Environmental Microbiology*.[55] BMM was chosen for exposure of CNT/PCL nanocomposites to *P. aeruginosa* since this type of media is optimized for *P. aeruginosa*

growth. BMM was prepared by first sterilizing sterilizing Milli-Q water (in house system) using a 45 min liquid autoclave cycle. Next, a salt stock solution (containing 7.18 mM K_2HPO_4, 2.79 mM KH_2PO_4, 0.757 mM $(NH_4)_2SO_4$, 0.0406 mM $MgSO_4*7H_2O$ and trace elements) was added to the sterilized water to prepare a 1:10 dilution of the salt stock concentration. A sodium acetate trihydrate carbon source stock was then aseptically added to the BMM solution in either a low (low C BMM) or high (high C BMM) concentration.[55] The final concentrations of sodium acetate trihydrate in low and high C BMM were 0.200 g/L (35 mg/L C) and 3.270 g/L (577 mg/L C), respectively.

5.2.9. Inoculation of PCL and CNT/PCL Nanocomposites with P. aeruginosa

0.5 mL of *P. aeruginosa* frozen stock was added to 75 mL LB broth and grown overnight at 37˚C and 225 rpm. 0.1 mL of the overnight culture was then added to 75 mL of LB broth and grown to the exponential phase (Optical Density of 0.6 - 0.8 at 540 nm). 0.1 mL of exponential phase *P. aeruginosa* was then added to 1 L of BMM and shaken vigorously. All PCL and CNT/PCL samples were sterilized with ethanol for > 5 min, washed with autoclaved Milli-Q water to remove ethanol, and aseptically placed into sterile sample flasks. The *P. aeruginosa*/BMM solutions were distributed in 100 mL aliquots to each PCL and CNT/PCL sample flask. For CNT/PCL samples, each CNT/PCL flask also contained an internal PCL reference to track the extent of biodegradation within a given culture and account for inconsistencies in biodegradation rates flask to flask. At least three or four replicates of each coupon type or CNT loading used were run. Abiotic controls were prepared by distributing 100 mL aliquots of sterile BMM solution to flasks containing separate PCL and CNT/PCL nanocomposite samples.

5.2.10. Mass Loss Experiments

P. aeruginosa cultures containing PCL and/or CNT/PCL nanocomposites were shaken at 125 rpm and 28 °C for 2 weeks prior to collection. These conditions were used since they were found to yield the most rapid rate of PCL biodegradation. PCL and CNT/PCL nanocomposite samples were collected on 9 cm high porosity filter (Fisher Scientific, Course, P8, Cat. #: 09-795C) paper by gently pouring the inoculum through the high porosity filter using a vacuum filtration system (Stericup and Steritop, Disposable Filtration System, Millipore Express Plus PES membrane, 0.22 μm). The filter paper was replaced for each sample collected. Next, the samples were removed from the filter paper and washed gently with autoclaved Milli-Q water. The samples were then placed on top of a 7.5 cm filter paper within a Petri dish for drying in the desiccator; the filter paper was used to prevent PCL and CNT/PCL nanocomposites from sticking to the Petri dishes. Abiotic controls were separately removed from their flasks following the same procedure. After the PCL and CNT/PCL nanocomposites had dried for 2 d, they were massed and photographed. Then, they were sterilized with ethanol for > 1 min, washed with autoclaved Milli-Q water to remove ethanol, placed into sterile sample flasks, and submerged in 100 mL of freshly prepared *P. aeruginosa*/BMM solutions for another two weeks of biodegradation. Samples were exposed to biodegradation conditions in two week increments until they had been fully biodegraded (> 100% mass loss) or provided enough biodegradation information to pursue further modifications to the procedure.

5.2.11. PCL Triol Priming

The preparation of PCL triol solutions and their use to prime *P. aeruginosa* for PCL biodegradation are described in Chapter 6. Triplicate PCL (4% w/w EC, DCM) coupons were prepared for mass loss experiments in *P. aeruginosa*/PCL triol cultures.

5.3. Results and Discussion

PCL was first dissolved in THF and casted into coupons using solution blending. PCL prepared in THF was exposed to *P. aeruginosa* in high C BMM for two weeks, removed, washed, sterilized, and exposed to a fresh culture of *P. aeruginosa* for the next time point. This procedure was repeated bi-weekly throughout the study. As shown in Figure 5.1, rapid biodegradation of PCL occurred over the course of 14 weeks, with 100% mass loss observed after only 10 weeks. Therefore, the use of THF as a casting solvent for PCL coupons yielded a rapidly biodegradable form of PCL.

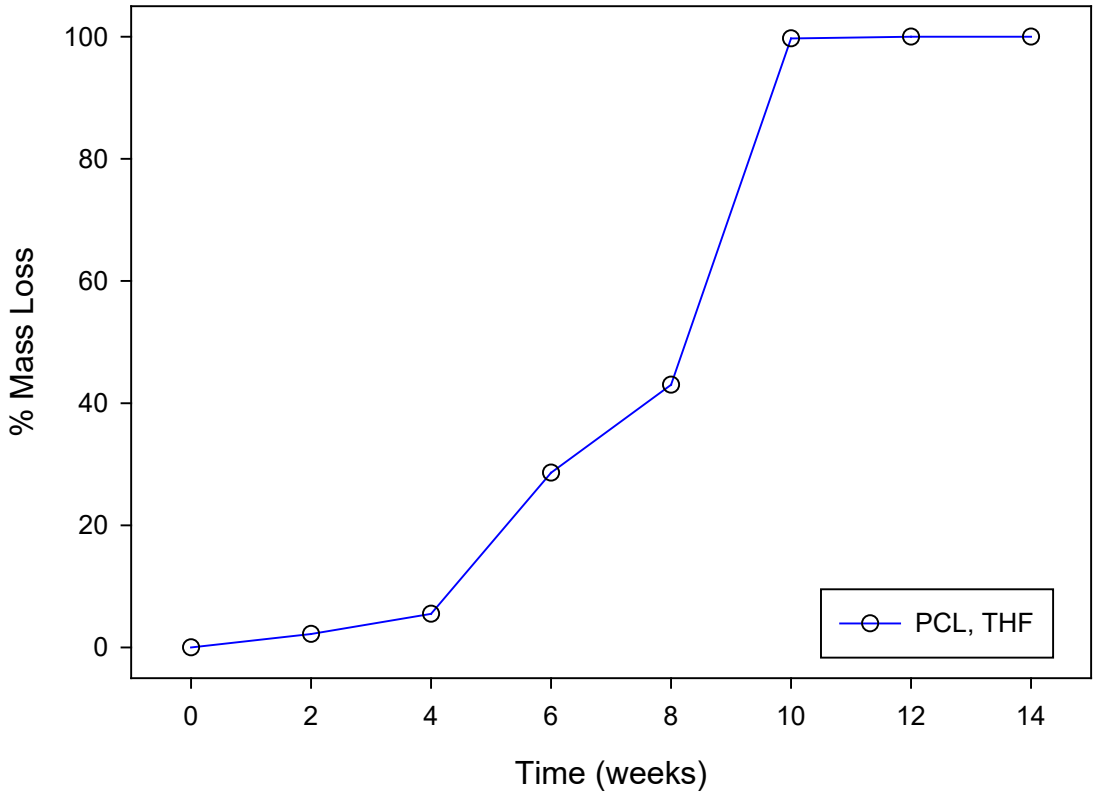

Figure 5.1. Mass loss plot of pure PCL prepared in THF, biodegraded by *P. aeruginosa* in high C BMM.

For this reason, LO-MWCNT/PCL nanocomposite coupons were prepared for biodegradation studies using THF and were found to be visually uniform in terms of CNT distribution throughout the polymer matrix (Figure 5.2).

Figure 5.2. A picture of 2% w/w LO-MWCNT/PCL and PCL prepared using THF and 4% w/w EC.

The LO-MWNCTs were dispersed at 2% w/w in the LO-MWCNT/PCL nanocomposites using 4% w/w EC. A CNT mass fraction of 2% w/w was chosen since it yielded non-translucent, black nanocomposites, that provided a good contrast to PCL and was a relatively high loading within the range of those used in products (0 – 5% w/w).[3, 13, 19-21]

For consistency with the LO-MWCNT/PCL nanocomposites, all PCL references were prepared with the same 4% w/w mass concentration of EC. This was found to be important after replicate EC samples were run to determine the biodegradability of pure EC in the presence of *P. aeruginosa*/high C BMM (Figure 5.3). Although EC is not cytotoxic and biocompatible (Chapter 4), the additive did not biodegrade under the same conditions that led to PCL biodegradation. EC was also shown to not dissolve under abiotic conditions.

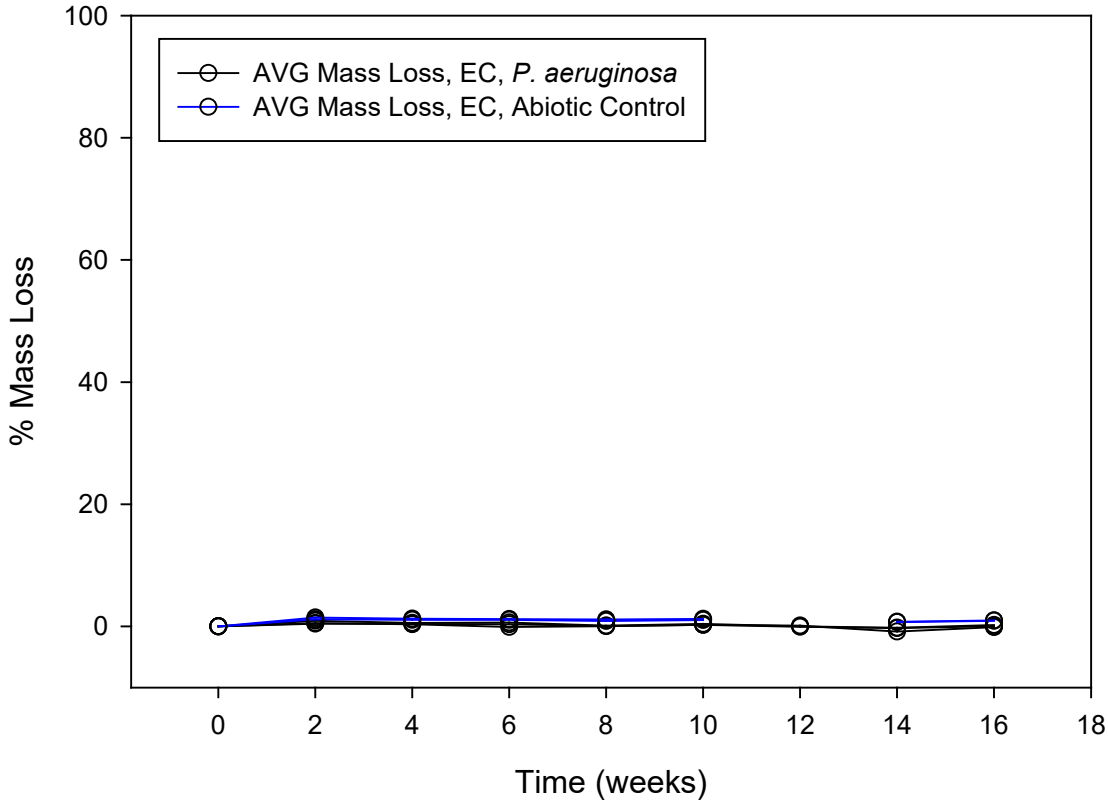

Figure 5.3. Mass loss plot of pure EC in the presence and absence of *P. aeruginosa* in high C BMM.

As an internal reference, PCL (4% w/w EC) was paired with 2% w/w LO-MWCNT/PCL nanocomposites (4% w/w EC) for initial biodegradation studies (Figure 5.4). Hereafter, whenever a set of PCL and CNT/PCL nanocomposite pairs are discussed, each contains the same level of EC. Mass loss of PCL and 2% w/w LO-MWCNT/PCL nanocomposites was conducted in high C BMM since pure PCL prepared in THF was found to rapidly degrade in this media type (Figure 5.1). PCL and 2% w/w LO-MWCNT/PCL nanocomposites were also submerged in sterile high C BMM and sampled under the same conditions to ensure that dissolution was not a factor in any mass loss observed. These abiotic controls showed that PCL and LO-MWCNT/PCL

nanocomposites do not lose mass in the absence of *P. aeruginosa* throughout the duration of the experiment, indicating that dissolution is not an issue. In the presence of *P. aeruginosa*, the internal PCL reference containing EC fully biodegraded after 20 weeks, which required roughly double the time for pure PCL to degrade (Figure 5.1). Therefore, in addition to being recalcitrant to biodegradation, the use of EC as an additive can also slow the biodegradation rate of PCL. Since EC was necessary for a good CNT dispersion quality, it was used at as low of a mass fraction as possible and kept consistent throughout a given set of PCL and CNT/PCL nanocomposites.

In contrast to the internal PCL reference, the paired 2% w/w LO-MWNCT/PCL nanocomposites lost less than 5% mass in the same amount of time, indicating that 2% w/w LO-MWCNT/PCL nanocomposites are persistent (Figure 5.4). Therefore, the results suggest that CNTs have an inhibitory effect on biodegradation, which is a topic to be discussed in more detail in the next chapter.

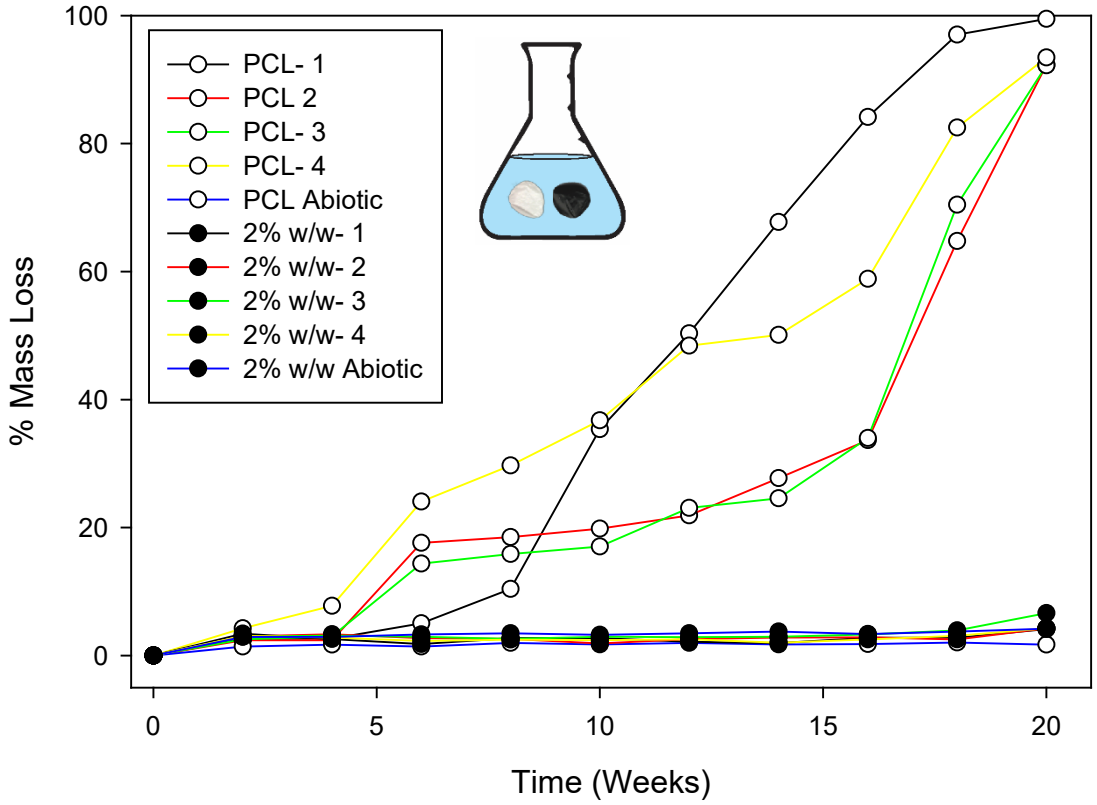

Figure 5.4. Mass loss plots of four replicates of PCL and 2% w/w LO-MWCNT/PCL nanocomposites, prepared with THF with each containing 4% w/w EC, as a result of *P. aeruginosa* biodegradation in high C BMM. The PCL and 2% w/w LO-MWCNT/PCL nanocomposite samples that were paired in a particular flask (see cartoon) are shown with the same line color. Abiotic controls for PCL and 2% w/w O-MWNCT/PCL nanocomposites are shown in blue.

The use of THF with CNTs was found to be problematic since Atlas et al. recently discovered that fullerenes, which have a similar carbonaceous structure to CNTs (spherical versus cylindrical sp^2-hybridized network of carbon, respectively), can adsorb THF to their structures and enhance fullerene toxicity.[55] This led to false positive results for fullerene cytotoxicity and could present the same issues with CNTs. Thus, the use of THF might have contributed to the CNT cytotoxicity and inhibition of LO-MWCNT/PCL nanocomposite biodegradation observed in Figure 5.4. For that reason, the preliminary

CNT/PCL nanocomposite biodegradation results collected here were deemed inconclusive and the use of alternative solvents was pursued.

In Figure 5.5, the effect of casting solvent on PCL biodegradability was explored in high C BMM. From this mass loss plot, it is clear that PCL biodegrades most rapidly when prepared with THF (PCL-THF), but the potential interference of THF with biodegradation results and the lack of analytical methods available to distinguish adsorbed THF from the CNTs and polymer matrix precluded its use in our investigation. Figure 5.5 also shows that PCL prepared with $CHCl_3$ (PCL-$CHCl_3$) degrades slightly faster than PCL prepared with DCM (PCL-DCM).

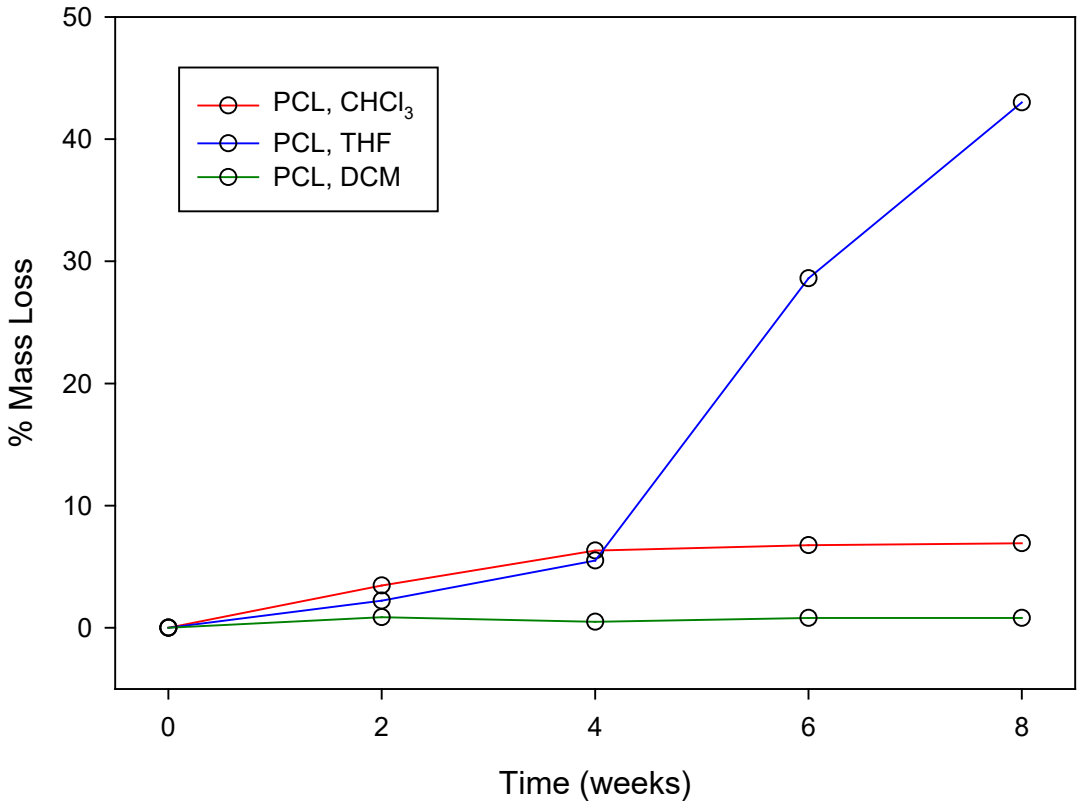

Figure 5.5. Mass loss plots of pure PCL prepared using three different solvents ($CHCl_3$, THF, and DCM) after *P. aeruginosa* biodegradation in high C BMM. All polymers were sonicated for the same amount of time.

In order to identify the difference in PCL degradation as a function of solvent casting conditions, the crystallinity fractions of PCL-$CHCl_3$, PCL-THF, and PCL-DCM were measured using differential scanning calorimetry. The fraction of crystallinity was considered an important parameter since it has been shown to have an effect on the biodegradability of polymers. Since it is more energetically unfavorable to disrupt crystalline regions, a higher fraction of crystallinity is typically associated with less biodegradability.[55] Rows 1-3 of Table 1 shows the fraction of crystallinity for PCL casted with all three solvent types. The % crystallinity (Xc) of PCL-$CHCl_3$ is much higher than for PCL-THF, which can explain the reduced biodegradation of PCL-$CHCl_3$ relative to PCL-THF. However, the Xc of PCL-DCM is similar to PCL-THF, and PCL-DCM degrades at a much slower rate than PCL-THF, opposite to what is expected. Since the crystallinities for PCL-THF and PCL-DCM are so similar, there appears to be more than one parameter affecting PCL biodegradation as a result of the casting solvent used. Although not explicitly proven, the other parameter may involve the difference in boiling points between PCL-DCM and PCL-THF: since the boiling point of DCM (39.6 °C) is one-third lower than the boiling point of THF (66 °C), the porosity of the PCL-DCM coupon formed during casting might be much lower due to rapid DCM evaporation, which would lower the available surface area for biodegradation. In contrast, PCL-THF may have the greatest biodegradability due to the highest porosity formed as a result of the highest boiling point or slowest evaporation during casting coupled to a relatively low fraction of crystallinity. Previous studies have shown that polymer morphology in terms of porosity and polymer topography can alter the properties of the polymer and interactions of cells with their surfaces after casting with different solvents.[60, 61] Although

the effect of porosity on polymer biodegradability has not been proven in this investigation, it is clear that the fraction of crystallinity is not the only factor affecting the biodegradability of PCL when using different solvents.

Table 5.1. The fraction of crystallinity (X_C) for PCL, with and without EC, prepared in three different solvents ($CHCl_3$, THF, and DCM). X_C was calculated from the heat of fusion measured using DSC.

Sample	X_C (%)	Std. Dev.	Solvent Boiling Point (°C)
PCL $CHCl_3$	67.7		61.2
PCL THF	56.0		66.0
PCL DCM	53.0		39.6
PCL/EC $CHCl_3$	52.5	4.6	61.2
PCL/EC THF	55.6	0.0	66.0
PCL/EC DCM	46.9	1.8	39.6

When the same EC fraction (4% w/w) was incorporated into a PCL coupon prepared from each of these three solvents, the fraction of crystallinity became similar (Table 1). This is not surprising as additives are commonly used to alter the crystallinity of a polymer by disrupting polymer chain stacking.[55] However, as observed with pure PCL, PCL (4% w/w EC) prepared with different solvents still had different biodegradation rates in high C BMM. A comparison of PCL-EC-THF and PCL-EC-DCM coupons are shown in Figure 5.6. As was the case for pure PCL-DCM and PCL-THF, PCL-EC-DCM biodegraded at a slower rate than PCL-EC-THF, presumably due to the difference in boiling points that could affect pore size/polymer surface area. Since PCL-EC-DCM barely biodegraded (< 5% mass loss) in 16 weeks relative to PCL-EC-THF (> 35% mass loss), PCL-EC $CHCl_3$ was used instead to attempt CNT/PNC biodegradation studies.

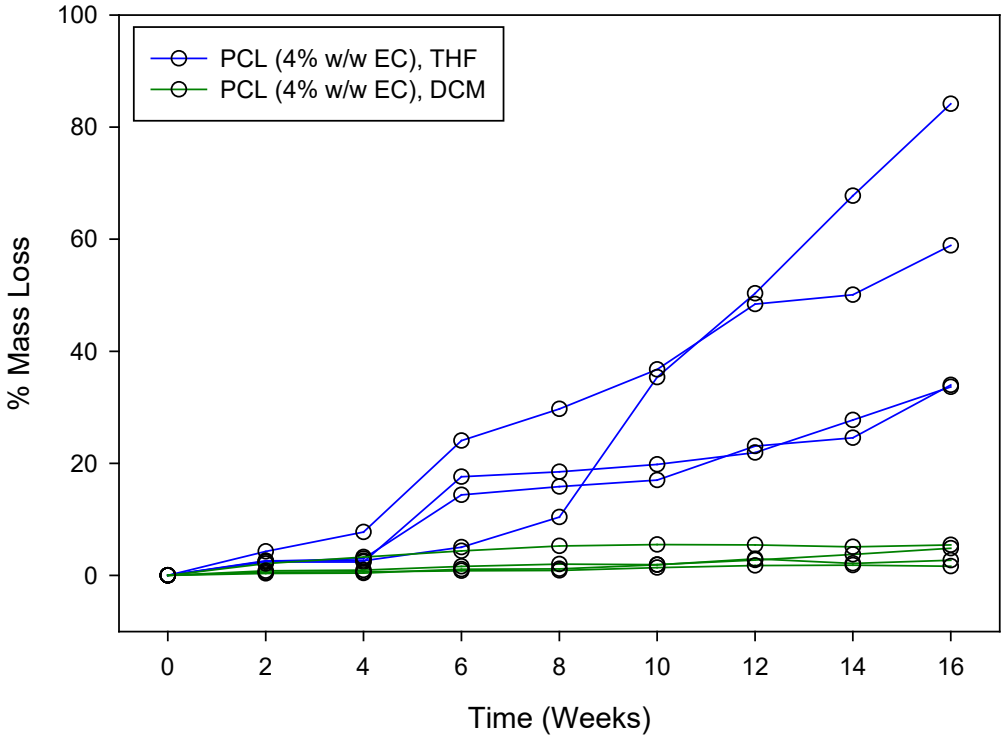

Figure 5.6. Mass loss plots of PCL (4% w/w EC) prepared using THF and DCM after *P. aeruginosa* biodegradation in high C BMM.

In Figure 5.7, biodegradation of paired PCL and 2% w/w LO-MWCNT/PCL nanocomposites, each prepared in $CHCl_3$ with the same level of EC (20% w/w EC), is shown in high C BMM. In comparison to 2% w/w LO-MWCNT/PCL nanocomposites prepared in THF, the 2% w/w LO-MWCNT/PCL nanocomposites prepared in $CHCl_3$ required a higher EC loading (4 versus 20% w/w EC for THF and $CHCl_3$, respectively) to achieve a homogenous distribution of LO-MWCNTs in the PCL matrix. Similar to Figure 5.3, PCL biodegradation is faster than 2% w/w LO-MWCNT/PCL nanocomposite biodegradation. The internal PCL reference prepared in $CHCl_3$, however, lost only 20% mass after 20 weeks in contrast to the 100% mass loss achieved by the internal PCL

reference prepared with THF shown in Figure 5.3. This can be attributed to both differences in crystallinity and the higher EC content required for $CHCl_3$ casting.

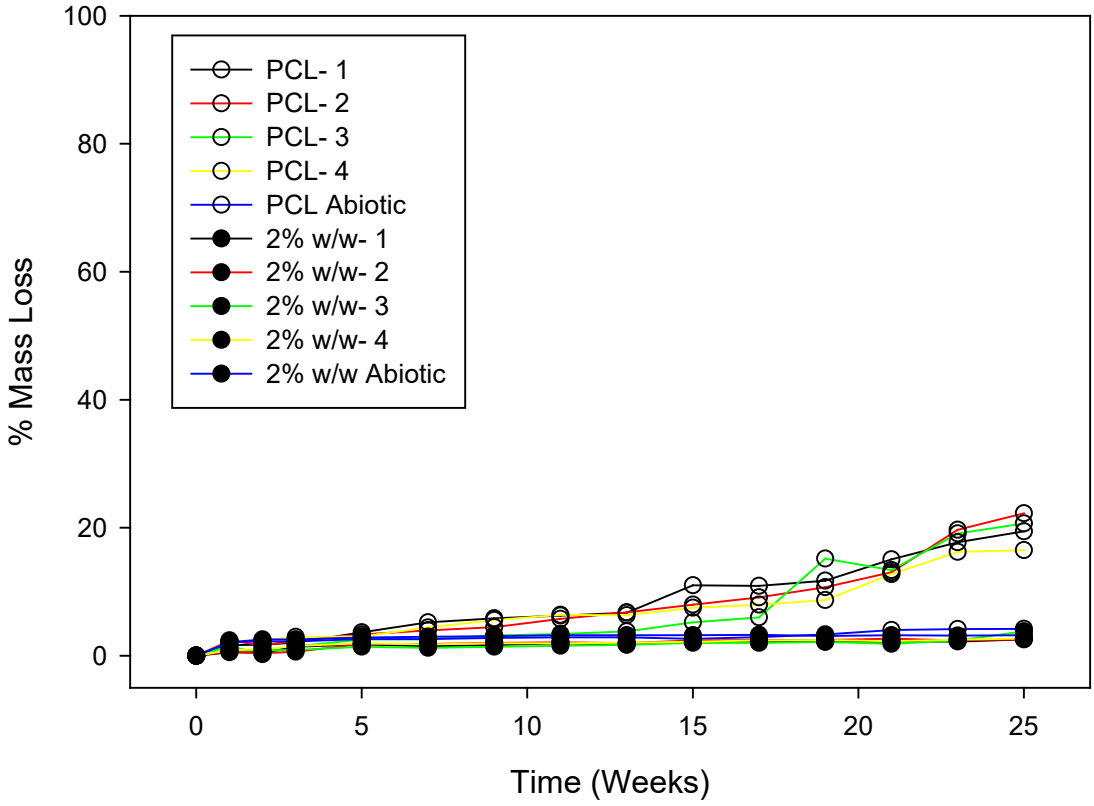

Figure 5.7. Mass loss of four replicates of PCL and 2% w/w LO-MWCNT/PCL nanocomposites, prepared in DCM with each containing 20% w/w EC, as a result of *P. aeruginosa* biodegradation in high C BMM. The PCL and 2% w/w LO-MWCNT/PCL nanocomposite samples that were paired in a particular flask are shown with the same line color. Abiotic controls for PCL and 2% w/w LO-MWNCT/PCL nanocomposites are also shown in blue.

Similar to Figure 5.3, the 2% w/w LO-MWCNT/PCL nanocomposite prepared in $CHCl_3$ also appears to be persistent (< 5% mass loss) and preliminary scanning electron microscopy (SEM) results indicate that some CNT accumulation at the surface of a 2% w/w LO-MWCNT/PCL ($CHCl_3$) occurs after 20 weeks (Figure 5.8), consistent with the effects observed due to CNT build-up at the surface in the biofilm chapter (Chapter 4).

Further investigation and discussion of CNT inhibitory effects on biodegradation can be found in Chapter 6.

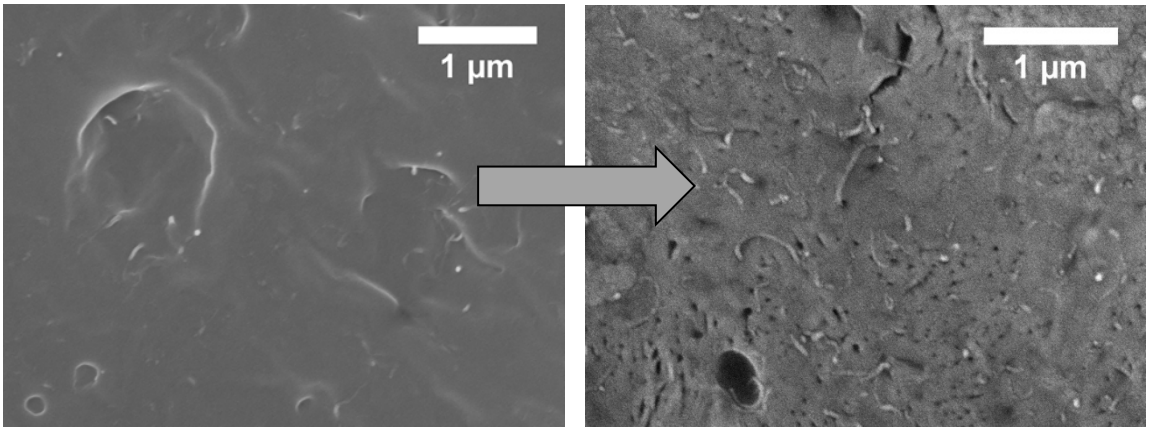

Figure 5.8. SEM images of 2% w/w LO-MWCNT/PCL nanocomposites (prepared in $CHCl_3$, 20% w/w EC) before (left) and after (right) >20 weeks of *P. aeruginosa* biodegradation.

For a good CNT dispersion quality in $CHCl_3$, the EC content required was high and only LO-MWCNT/PCL nanocomposites could be prepared. Furthermore, the rate of biodegradation was prohibitively slow for CNT/PCL nanocomposite biodegradability data collection. Another approach was taken by preparing PCL and CNT/PCL nanocomposites with DCM. Although pure PCL-DCM had the slowest rate of biodegradation in high C BMM, modifications to the culture conditions were attempted to accelerate biodegradation. The choice to use DCM instead of $CHCl_3$, when both solvents led to slow biodegradation of pure PCL, was motivated by the fact that DCM could be used to prepare LO-MWCNT/PCL nanocomposites as well as pristine MWCNT/PCL nanocomposites with a highly uniform CNT distribution at a low EC content (4% w/w). To this end, an attempt was made to biodegrade PCL and LO-MWCNT/PCL nanocomposites prepared in DCM with other types of media. The goal

was to accelerate the biodegradation rate to make CNT/PCL nanocomposite biodegradation studies more practical. First, biodegradation of PCL prepared in DCM was compared in low C BMM and high C BMM (Figure 5.9a). Consistent with previous results, there was minimal mass loss under high C BMM conditions. In contrast, biodegradation of PCL in low C BMM proceeded at a faster rate, however inconsistently. Concurrent experiments that compared PCL and LO-MWCNT/PCL nanocomposites (with 4% w/w EC) biodegradation in low C media, showed under 5% mass loss for PCL after 16 weeks of biodegradation; an example of paired PCL and 0.5% w/w LO-MWCNT/PCL nanocomposite biodegradation plots are shown in Figure 5.9b. This indicates that a reduced population of microorganisms can acclimate faster to PCL prepared with DCM for metabolism, but not consistently or on a significantly faster time scale.

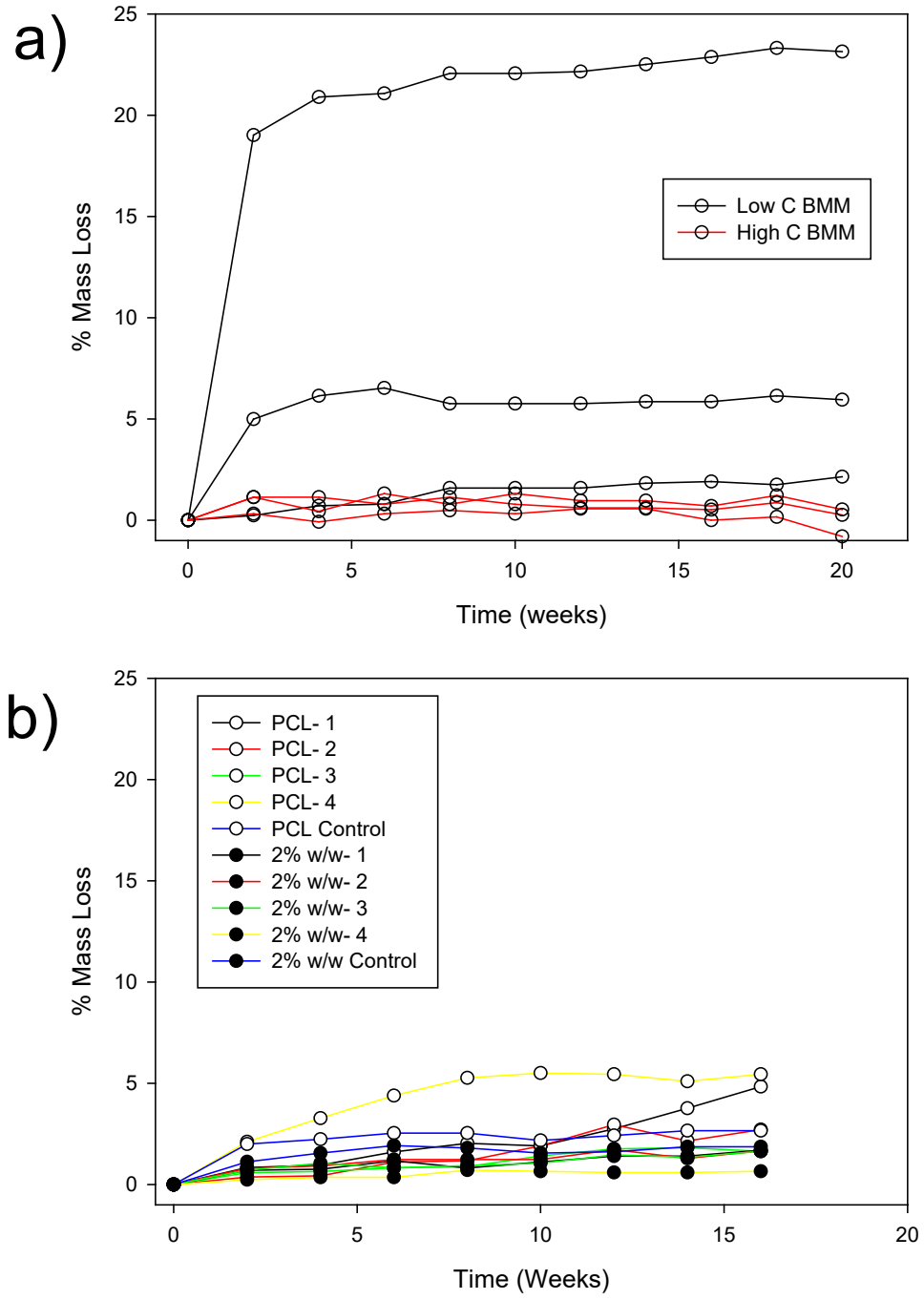

Figure 5.9. Mass loss plots of a) pure PCL replicates (DCM) in low and high C BMM as well as mass loss plots of PCL and 0.5% w/w LO-MWCNT/PCL nanocomposites (4% w/w EC in each) prepared in DCM, as a result of *P. aeruginosa* biodegradation in low C BMM.

The limitations of using an acetate food source to biodegrade PCL and LO-MWCNT/PCL nanocomposites prepared in DCM on a consistent and rapid time scale were overcome by replacing acetate with a small molecule version of PCL as the carbon source. Acclimation of *P. aeruginosa* to PCL containing EC was achieved using PCL triol (3 g/L) as the sole carbon source for microbial growth prior to PCL and CNT/PCL immersion in the inoculum. The optimized version of this process involved growing *P. aeruginosa* in PCL triol/BMM solutions for 31 hours ($8.0 \pm 0.4 \times 10^7$ CFU/mL *P. aeruginosa*, average of triplicate cultures, each sampled in duplicate) and distributing the cultures to PCL and LO-MWCNT/PCL nanocomposite coupons for two week intervals, following the bi-weekly sampling procedure used under acetate conditions (low and high C BMM). As shown in Figure 5.10, mass loss of PCL prepared with DCM (with 4% w/w EC) was rapid in the presence of *P. aeruginosa*/PCL triol, with close to 100% mass loss by 20 weeks.

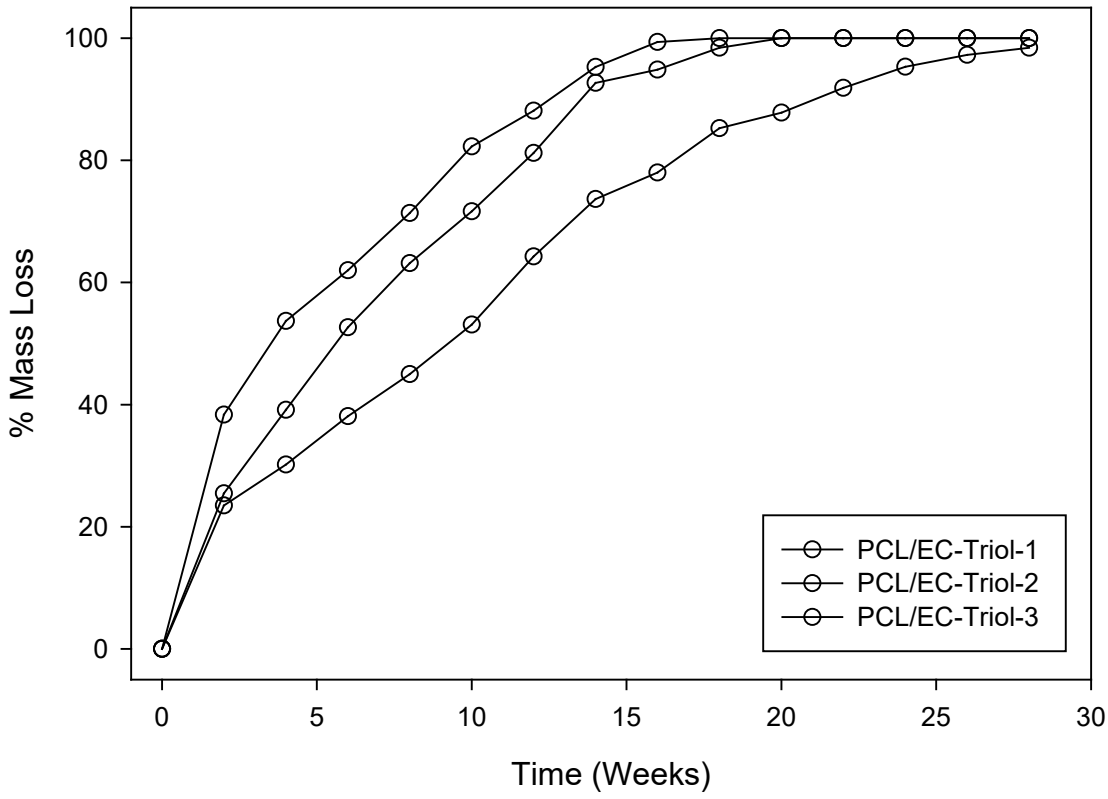

Figure 5.10. Mass loss plot of PCL (4% w/w EC, prepared in DCM), biodegraded by *P. aeruginosa* in 3 g/L PCL triol/BMM solution.

Owing to PCL triol droplets that did not fully disperse/dissolve in BMM, this method can be slightly inconsistent in rate from flask to flask. However, the biodegradation rate for PCL coupons prepared with DCM and EC are more rapid than the rates observed under all other conditions and the replicates track reasonably well (R^2=0.99) with each other to adequately distinguish different trends should they exist. Internal PCL references were paired with LO-MWCNT/PCL nanocomposites to account for any microbial consistency issues that might occur from culture to culture, and CNT/PCL nanocomposite biodegradability studies carried on with this approach as described in Chapter 6.

5.4. References

1. Stuart, B. H., *Polymer analysis*. John Wiley & Sons: 2008; Vol. 30.
2. Zaman, I.; Manshoor, B.; Khalid, A.; Araby, S., From clay to graphene for polymer nanocomposites-a survey. *J. Polym. Res.* **2014,** *21*, (5), 1-11.
3. Du, J.-H.; Bai, J.; Cheng, H. M., The present status and key problems of carbon nanotube based polymer composites. *Express Polymer Letters* **2007,** *5*, 253-272.
4. Ajayan, P. M.; Schadler, L. S.; Giannaris, C.; Rubio, A., Single-walled carbon nanotube-polymer composites: Strength and weakness. *Adv. Mater.* **2000,** *12*, (10), 750-753.
5. Allaoui, A.; Bai, S.; Cheng, H. M.; Bai, J. B., Mechanical and electrical properties of a MWNT/epoxy composite. *Compos. Sci. Technol.* **2002,** *62*, 1993-1998.
6. Andrews, R.; Jacques, D.; Minot, M.; Rantell, T., Fabrication of carbon multiwall nanotube/polymer composites by shear mixing. *Macromol. Mater. Eng.* **2002,** *287*, (6), 395-403.
7. Baughman, R. H.; Zakhidov, A. A.; de Heer, W. A., Carbon nanotubes - the route toward applications. *Science* **2002,** *297*, (5582), 787-792.
8. Coleman, J. N.; Khan, U.; Blau, W. J.; Gun'ko, Y. K., Small but strong: A review of the mechanical properties of carbon nanotube-polymer composites. *Carbon* **2006,** *44*, (9), 1624-1652.
9. Lau, K. T., Interfacial bonding characteristics of nanotube/polymer composites. *Chem. Phys. Lett.* **2003,** *370*, (3-4), 399-405.
10. Lau, K. T.; Hui, D., Effectiveness of using carbon nanotubes as nano-reinforcements for advanced composite structures. *Carbon* **2002,** *40*, (9), 1605-1606.
11. Martin, C. A.; Sandler, J. K. W.; Shaffer, M. S. P.; Schwarz, M. K.; Bauhofer, W.; Schulte, K.; Windle, A. H., Formation of percolating networks in multi-wall carbon-nanotube-epoxy composites. *Compos. Sci. Technol.* **2004,** *64*, (15), 2309-2316.
12. Sandler, J. K. W.; Kirk, J. E.; Kinloch, I. A.; Shaffer, M. S. P.; Windle, A. H., Ultra-low electrical percolation threshold in carbon-nanotube-epoxy composites. *Polymer* **2003,** *44*, (19), 5893-5899.
13. De, V. M. F. L.; Tawfick, S. H.; Baughman, R. H.; Hart, A. J., Carbon Nanotubes: Present and Future Commercial Applications. *Science* **2013,** *339*, (6119), 535-539.
14. Rahmat, M.; Das, K.; Hubert, P., Interaction stresses in carbon nanotube-polymer nanocomposites. *ACS Appl. Mater. Interfaces* **2011,** *3*, (9), 3425-3431.
15. Lu, D. D.; Li, Y. G.; Wong, C. P., Recent advances in nano-conductive adhesives. *J. Adhes. Sci. Technol.* **2008,** *22*, (8-9), 815-834.
16. Li, J.; Lumpp, J. K.; Andrews, R.; Jacques, D., Aspect ratio and loading effects of multiwall carbon nanotubes in epoxy for electrically conductive adhesives. *J. Adhes. Sci. Technol.* **2008,** *22*, (14), 1659-1671.
17. Paik, K. W.; Han, S. H., A study on B-stage CNT/epoxy composite films for electronic packaging applications. *Pricm 7, Pts 1-3* **2010,** *654-656*, 2755-2758.
18. Makarova, T. L.; Zakharchuk, I.; Geydt, P.; Lahderanta, E.; Komlev, A. A.; Zyrianova, A. A.; Lyubchyk, A.; Kanygin, M. A.; Sedelnikova, O. V.; Kurenya, A. G.; Bulusheva, L. G.; Okotrub, A. V., Assessing carbon nanotube arrangement

in polystyrene matrix by magnetic susceptibility measurements. *Carbon* **2016,** *96*, 1077-1083.
19. Moniruzzaman, M.; Winey, K. I., Polymer nanocomposites containing carbon nanotubes. *Macromolecules* **2006,** *39*, (16), 5194-5205.
20. Sahoo, N. G.; Rana, S.; Cho, J. W.; Li, L.; Chan, S. H., Polymer nanocomposites based on functionalized carbon nanotubes. *Prog. Polym. Sci.* **2010,** *35*, (7), 837-867.
21. Harrison, B. S.; Atala, A., Carbon nanotube applications for tissue engineering. *Biomaterials* **2007,** *28*, (2), 344-353.
22. Nanocyl Biocyl. http://www.nanocyl.com/kr/Products-Solutions/Products/BIOCYL.
23. Nanocyl Carbon nanotube applications: fuel system components: http://www.nanocyl.com/Products-Solutions/Sectors/Automotive/Fuel-System-Components.
24. Gottschalk, F.; Nowack, B., The release of engineered nanomaterials to the environment. *J. Environ. Monit.* **2011,** *13*, (5), 1145-1155.
25. Petersen, E. J.; Zhang, L. W.; Mattison, N. T.; O'Carroll, D. M.; Whelton, A. J.; Uddin, N.; Nguyen, T.; Huang, Q. G.; Henry, T. B.; Holbrook, R. D.; Chen, K. L., Potential release pathways, environmental fate, and ecological risks of carbon nanotubes. *Environ. Sci. Technol.* **2011,** *45*, (23), 9837-9856.
26. Luckachan, G. E.; Pillai, C. K. S., Biodegradable Polymers-A Review on Recent Trends and Emerging Perspectives. *J. Polym. Environ.* **2011,** *19*, (3), 637-676.
27. Shah, A. A.; Hasan, F.; Hameed, A.; Ahmed, S., Biological degradation of plastics: A comprehensive review. *Biotechnol. Adv.* **2008,** *26*, (3), 246-265.
28. Massardier-Nageotte, V.; Pestre, C.; Cruard-Pradet, T.; Bayard, R., Aerobic and anaerobic biodegradability of polymer films and physico-chemical characterization. *Polym. Degrad. Stab.* **2006,** *91*, (3), 620-627.
29. Madigan, M. T.; Martinko, J. M.; Dunlap, P. V.; Clark, D. P., *Brock Biology of Microorganisms*. 12th ed.; Pearson: San Francisco, 2009.
30. International, A., ASTM Standard D6954-04. In *Standard Guide for Exposing and Testing Plastics that Degrade in the Environment by a Combination of Oxidation and Biodegradation*, 2013.
31. International, A., ASTM Standard D7473 − 12. In *Standard Test Method for Weight Attrition of Plastic Materials in the Marine Environment by Open System Aquarium Incubations*, 2012.
32. Tokiwa, Y.; Calabia, B. P.; Ugwu, C. U.; Alba, S., Biodegradability of Plastics. *International Journal of Molecular Sciences* **2009,** *10*, (9), 3722-3742.
33. Jones, P. H.; Prasad, D.; Heskins, M.; Morgan, M. H.; Guillet, J. E., Biodegradability of photodegraded polymers. I. Development of experimental procedures. *Environ. Sci. Technol.* **1974,** *8*, (10), 919-923.
34. Gross, R. A.; Kalra, B., Biodegradable Polymers for the Environment. *Science* **2002,** *297*, 803-807.
35. Zheng, Y.; Yanful, E. K.; Bassi, A. S., A review of plastic waste biodegradation. *Crit. Rev. Biotechnol.* **2005,** *25*, (4), 243-250.
36. R, P.; Doble, M., Biodegradation of polymers. *Indian J. Biotechnol.* **2005,** *4*, 186-193.

37. Shih, Y. F.; Chen, L. S.; Jeng, R. J., Preparation and properties of biodegradable PBS/multi-walled carbon nanotube nanocomposites. *Polymer* **2008,** *49*, (21), 4602-4611.
38. Jayasekara, R.; Sheridan, S.; Lourbakos, E.; Beh, H.; Christie, G. B. Y.; Jenkins, M.; Halley, P. B.; McGlashan, S.; Lonergan, G. T., Biodegradation and ecotoxicity evaluation of a bionolle and starch blend and its degradation products in compost. *Int. Biodeterior. Biodegrad.* **2003,** *51*, (1), 77-81.
39. Benedict, C. V.; Cameron, J. A.; Huang, S. J., Polycaprolactone degradation by mixed and pure cultures of bacteria and a yeast. *J. Appl. Polym. Sci.* **1983,** *28*, (1), 335-342.
40. Mittal, V., *Nanocomposites with Biodegradable Polymers: Synthesis, Properties, and Future Perspectives*. Oxford University Press: 2011.
41. Posen, I. D.; Jaramillo, P.; Griffin, W. M., Uncertainty in the Life Cycle Greenhouse Gas Emissions from U.S. Production of Three Biobased Polymer Families. *Environ. Sci. Technol.* **2016,** *50*, (6), 2846-2858.
42. Liu, L.; Li, S.; Garreau, H.; Vert, M., Selective Enzymatic Degradations of Poly(L-lactide) and Poly(ε-caprolactone) Blend Films. *Biomacromolecules* **2000,** *1*, (3), 350-359.
43. Li, S.; Liu, L.; Garreau, H.; Vert, M., Lipase-Catalyzed Biodegradation of Poly(ε-caprolactone) Blended with Various Polylactide-Based Polymers. *Biomacromolecules* **2003,** *4*, (2), 372-377.
44. Kim, S. W.; Kim, T.; Kim, Y. S.; Choi, H. S.; Lim, H. J.; Yang, S. J.; Park, C. R., Surface modifications for the effective dispersion of carbon nanotubes in solvents and polymers. *Carbon* **2012,** *50*, (1), 3-33.
45. Neo, C. Y.; Ouyang, J., Ethyl cellulose and functionalized carbon nanotubes as a co-gelator for high-performance quasi-solid state dye-sensitized solar cells. *Journal of Materials Chemistry A* **2013,** *1*, (45), 14392-14401.
46. Boccaccini, A. R.; Cho, J.; Roether, J. A.; Thomas, B. J.; Minay, E. J.; Shaffer, M. S., Electrophoretic deposition of carbon nanotubes. *Carbon* **2006,** *44*, (15), 3149-3160.
47. Zhao, H.; Song, H.; Li, Z.; Yuan, G.; Jin, Y., Electrophoretic deposition and field emission properties of patterned carbon nanotubes. *Appl. Surf. Sci.* **2005,** *251*, (1), 242-244.
48. (ISO), I. O. f. S., ISO 14851:1999 In *Determination of the ultimate aerobic biodegradability of plastic materials in an aqueous medium -- Method by measuring the oxygen demand in a closed respirometer*, 1999.
49. Banker, G. S., Film coating theory and practice. *J. Pharm. Sci.* **1966,** *55*, (1), 81-89.
50. Matsumura, S.; Shimura, Y.; Terayama, K.; Kiyohara, T., Effects of molecular-weight and stereoregularity on biodegradation of poly(vinyl alcohol) by *Alcaligenes-faecalis*. *Biotechnol. Lett.* **1994,** *16*, (11), 1205-1210.
51. Jenkins, M.; Harrison, K., The effect of molecular weight on the crystallization kinetics of polycaprolactone. *Polym. Adv. Technol.* **2006,** *17*, (6), 474-478.
52. Suslick, K. S.; Price, G. J., Applications of ultrasound to materials chemistry. *Annu. Rev. Mater. Sci.* **1999,** *29*, (1), 295-326.

53. Providenti, M. A.; Lee, H.; Trevors, J. T., Selected factors limiting the microbial degradation of recalcitrant compounds. *J. Ind. Microbiol.* **1993,** *12*, (6), 379-395.
54. Wiggins, B. A.; Alexander, M., Role of chemical concentration and second carbon sources in acclimation of microbial communities for biodegradation. *Appl. Environ. Microbiol.* **1988,** *54*, (11), 2803-2807.
55. Atlas, R. M., *Handbook of media for environmental microbiology*. 2005.
56. Qiu, Z.; Wang, H.; Xu, C., Crystallization, mechanical properties, and controlled enzymatic degradation of biodegradable poly(ε-caprolactone)/multi-walled carbon nanotubes nanocomposites. *Nanosci. Nanotechnol.* **2011,** *11*, 7884-7893.
57. Speranza, V.; De, S. F.; Pantani, R.; Sorrentino, A., Characterization of the polycaprolactone melt crystallization: complementary optical microscopy, DSC, and AFM studies. *ScientificWorldJournal* **2014,** *2014*, 720157.
58. Wang, Y.; Rodriguez-Perez, M. A.; Reis, R. L.; Mano, J. F., Thermal and thermomechanical behaviour of polycaprolactone and starch/polycaprolactone blends for biomedical applications. *Macromol. Mater. Eng.* **2005,** *290*, (8), 792-801.
59. Patricio, T.; Bartolo, P., Thermal Stability of PCL/PLA Blends Produced by Physical Blending Process. *Procedia Eng.* **2013,** *59*, 292-297.
60. Tang, Z. G.; Black, R. A.; Curran, J. M.; Hunt, J. A.; Rhodes, N. P.; Williams, D. F., Surface properties and biocompatibility of solvent-cast poly[ε-caprolactone] films. *Biomaterials* **2004,** *25*, (19), 4741-4748.
61. Megelski, S.; Stephens, J. S.; Chase, D. B.; Rabolt, J. F., Micro-and nanostructured surface morphology on electrospun polymer fibers. *Macromolecules* **2002,** *35*, (22), 8456-8466.

Chapter 6. Aerobic Single Culture Biodegradation of Carbon Nanotube/Polymer Nanocomposites

Parts of this chapter were co-written with the following authors and will be published under the following citations:

David G. Goodwin Jr., Iruhany Boyer Sosa, Thomas Devahif, Tucker B. Gordon, Xier Lu, Leo Kuwama, Cong Gao, Jingjing Wang, James F. Ranville, Edward J. Bouwer, D. Howard Fairbrother.

Environ. Sci. Technol. In preparation.

6.1. Introduction

The effect of adding carbon nanotubes (CNTs) to polymers that would otherwise biodegrade is still unclear. In many cases, polymer additives have been shown to enhance biodegradation by generating reactive oxygen species (e.g. divalent transition metal salts of aliphatic acids and transition metal complexes such dithiocarbonates) and creating poor interfacial interactions (e.g. starch). In contrast, other additives have been shown to inhibit biodegradation by preventing oxidation of polymeric material (e.g. hindered phenols), reducing the biodegradable polymer surface area (e.g. clay), or having antimicrobial properties (e.g. TiO_2).[1-4] CNT additives are not expected to biodegrade readily in the presence of microorganisms, since they have only been shown to partially biodegrade under aggressive, abiotic conditions involving horseradish peroxidase and neutrophil myeloperoxidase enzymes.[5-7] Currently, there is only one report on the biodegradation of CNTs by microorganisms which found that 2 to 6.8% of the CNT mass

was transformed to $^{14}CO_2$ by a select few microorganisms within a mixed culture, presumably due to the defect sites on the CNT walls from oxidation as well as the presence of oxygen functional groups.[8] Furthermore, CNTs at the surface of CNT/polymer nanocomposites (CNT/PNCs) have been shown to be cytotoxic to *Pseudomonas aeruginosa* (*P. aeruginosa*), *Escherichia coli*, and *Bacillus subtilis* within the range of CNT loadings typically used in commercial products (< 0.1 - 5% w/w) when direct contact occurs between the CNT and the microorganism.[9-12] As described for specific cases in this chapter and the next two chapters, there are very few studies that have systematically assessed the effect of CNT additives on polymer biodegradability. Since CNTs are being increasingly incorporated into products, it is important to understand how CNT additives affect polymer biodegradation. This will help to assess the risk of CNT exposure and release, determine whether CNT incorporation will change the persistence of polymers in the environment, and thereby provide guidelines for selection of an appropriate CNT/PNC type in a particular application.

Biofilm formation, or the attachment and proliferation of microbial communities on a material's surface, is typically the prerequisite to biodegradation. Biofilms are over 1000x more resistant to antimicrobial materials and antibiotics than planktonic cells and can thrive on a surface that provides an underlying carbon source such as a biodegradable polymer. In the case of a biodegradable polymer, we have previously compared biofilm development on poly-ε-caprolactone (PCL), with and without a CNT filler (Chapter 4).[13] On PCL, active biofilm growth was observed over time as shown using LIVE/DEAD staining and confocal imaging. However, for a 2% w/w slightly oxidized multi-wall (O-MWCNT)/PCL nanocomposite, cell death occurred in the bottom layer of the biofilm as

the PCL matrix biodegraded to expose CNTs. Nonetheless, active biofilm formation continued above the dead layer of cells on the 2% w/w LO-MWCNT/PCL nanocomposite once dead cells had completely coated the sample surface. Since active biofilm formation occurs when microorganisms are "shielded" from the CNTs by a dead layer of cells, the ability of the active top layer of *P. aeruginosa* to biodegrade the underlying PCL matrix is still unknown. To answer these questions, the approach used in this study was to biodegrade CNT/PCL nanocomposites of varied CNT loadings to assess the transformation and persistence of these materials. More specifically, we investigated whether or not CNT/PNCs at high CNT loadings (> 2% w/w) would inhibit biodegradation of the bulk material, or if extracellular enzymes were able to break-down the polymer matrix despite the cytotoxic CNTs at the surface.

PCL was chosen as the polymer matrix for this study since it is often used in products for chlorine, water, oil and solvent resistance; is easily processable with a low melting point and viscosity; is commonly blended with starch and cellulose to reduce cost; and has been used in garbage bags, incontinence products, and bandage holders.[14] Incorporation of CNTs into PCL has been also shown to improve its mechanical, electrical, and interfacial properties when blended with other polymers such as PLA.[15-20] PCL was also chosen for this study and the biofilm development study in Chapter 4 after the extensive method development outlined in the previous chapter. Preliminary results indicated that PCL is readily biodegradable by *P. aeruginosa* under aerobic conditions, having been shown to biodegrade on the time scale of weeks to months. Specifically, a single culture of *P. aeruginosa* primed with PCL triol, a small molecule version of PCL, was used to accelerate the overall biodegradation rate to an experimentally relevant time

scale (Chapter 5). A further advantage of using PCL in this biodegradation study was that biofilm development on its surface, with and without CNT additives, has already been analyzed in our previous work described in Chapter 4. Since the cytotoxic effect of CNT/PCL nanocomposite surfaces on *P. aeruginosa* is well studied, this information can provide a better understanding of the relationship between microbe-CNT/PNC interactions and biodegradation trends. In terms of the microorganism chosen, *Pseudomonas* species are commonly found in soils and are representative of many types of gram negative bacteria in the environment.[21] Although mixed culture conditions are more relevant to the environment, the single culture used in this study allows for better control of the culture conditions and can provide more mechanistic insight. For this reason, single culture (e.g. *Alcaligenes faecalis, Paecilomyces lilacinus*, *Acinetobactercalcoaceticus* var. *lwojji*, and an isolated, unidentified strain from industrial composting) and selective enzyme degradation studies have previously been run for PCL and PCL blended with other polymers.[22-24]

A few studies have also looked at controlled biodegradation of PCL with CNTs acting as a filler or as a polymer graft.[25, 26] In the first study involving CNTs, PCL was fully biodegraded in the presence of *Pseudomonas* lipase, an isolated enzyme, when grafted onto the oxygen functional groups of multi-wall CNTs (MWCNTs).[25] In the other relevant CNT study, *Pseudomonas* lipase biodegradation of pure PCL and functionalized MWCNT/PCL nanocomposites at a low MWCNT loading indicated that functionalized MWCNTs reduced the rate of biodegradation. The authors hypothesized that degraded material and enzymes were potentially trapped by the CNTs. Although biofouling was not as large of a factor in this enzymatic study as it would be in the presence of a single

culture of microorganisms, the researchers had more control in terms of determining surface erosion mechanisms, consistent mass loss trends, and surface morphology changes when using a single enzyme versus a single culture.[26] To our knowledge, there has been no systematic investigation of CNT/PNC biodegradation as a function of CNT type and loading in the presence of selective enzymes or under single culture conditions.

In the present study, both pristine MWCNTs and LO-MWCNTs (4.1% surface at. oxygen) were prepared in PCL using a solution blending method at varied CNT loadings (0 – 10% w/w) and exposed to *Pseudomonas aeruginosa* for week-long studies. The effect of CNT oxidation on polymer biodegradation was also determined since both oxidized and pristine MWCNTs have been found to be cytotoxic when at the surface of CNT/PNCs.[9, 11] Moreover, CNTs may also become oxidized during processing or as a result of environmental transformations before or after they are incorporated into polymers.[27, 28] MWCNTs were chosen since they are most commonly used in commercial products due to their low cost and ease of handling relative to SWCNTs.[29-31]

CNT/PCL biodegradation was assessed bi-weekly using mass loss and compared to the degradation rates of PCL references (0% w/w CNTs) under identical conditions. This type of measurement is consistent with several international standards and many other mass loss studies under aerobic conditions.[32-35] Specifically, PCL biodegradation in blends, with different fillers, and a range of different microorganisms has been assessed using mass loss.[22, 23, 32, 36-38] CNT release as a result of biodegradation is also underway using single-particle inductively coupled mass spectrometry (sp-ICP-MS) with the residual metal catalyst (Co or Mo) from CNT synthesis used as a proxy for CNT concentration.[39] CNT/PCL nanocomposites were characterized with differential scanning

calorimetry (DSC) for degree of crystallinity since crystallinity can have an effect on biodegradation rates.[40] CNT/PCL nanocomposites were also characterized with scanning electron microscopy before biodegradation for surface morphology and CNT content. SEM characterization after biodegradation will be performed at the last time point of the experiments outlined.

6.2. Experimental

6.2.1. Nanocomposite Preparation

MWCNTs were oxidized "in-house" using Nanocyl MWCNTs (Nanocyl NC7000, outer diameter 9.5 nm, 1.5 μm length, 90% purity) and a total oxygen content of 4.1% was obtained (LO-MWCNTs), which was measured using X-ray photoelectron spectroscopy (XPS). Pristine MWCNTs were obtained from NanoLab Inc. (PD15L520, Batch 2013-08-20, outer diameter 15 ± 5 nm, 5-20 μm length, > 95% purity) and Southwest Nanotechnologies Inc. (7773840 Aldrich, outer diameter 10 ± 1 nm, 3-6 μm length, ≥ 98% carbon basis). All MWCNTs used were of similar diameter and purity on a carbon basis. MWCNTs from NanoLab Inc. were used to compare mass loss of MWCNT/PCL nanocomposites to LO-MWCNT/PCL nanocomposites. MWCNTs from Southwest Nanotechnologies Inc. were used to assess CNT release since they contained trace cobalt and molybdenum catalysts from the chemical vapor deposition process used during CNT synthesis. The residual metal particles served as a proxy for MWCNTs, allowing for detection of released MWCNTs from biodegraded CNT/PCL nanocomposites.

CNT/PCL nanocomposites were prepared by adding 16 mg of ethyl cellulose (EC) (48.0 - 49.5% (w/w) ethoxyl basis, Lot # BCBG4792V, Sigma-Aldrich) and a particular mass of CNTs to a 50 mL Erlenmeyer flask containing 40 mL of

dichloromethane (DCM, >99.8%, Sigma-Aldrich). The EC macromolecules were used for CNT stabilization in DCM. LO-MWCNTs and pristine MWCNTs in EC were sonicated in an ice water bath for 1 and 3 h, respectively; these conditions were found to optimize dispersion quality. For both LO-MWCNTs and pristine MWCNTs, 400 mg of poly-ε-caprolactone (PCL) was then added to each CNT suspension and sonicated for an additional 3 h. During all steps of sonication, the ice water bath was replenished every 1 h to minimize solvent volatilization and improve dispersion quality. A solvent resistant, disposable syringe was then used to distribute the PCL and CNT/PCL nanocomposite casting solution in 5 mL aliquots to aluminum dishes. Samples were covered overnight to allow for slow, consistent solvent evaporation. The next day, PCL and CNT/PCL nanocomposites, which are also called coupons, were soaked in a DI water bath since this was found to help separate the coupons from their aluminum dishes. PCL and CNT/PCL nanocomposites were then trimmed around their outer edges to a consistent shape and size.

6.2.2. Scanning Electron Microscopy (SEM)

SEM (JEOL 6700F, 10 keV, 7.0 nm working distance, LEI & SEI detectors) was used to qualitatively characterize the surface morphology and CNT dispersion quality at the surface of CNT/PCL nanocomposites. Prior to analysis, samples were first cut into 1 cm^2 pieces and sputter-coated with platinum to prevent polymer charging under the electron beam (Quorum Technologies Polaron SC7640 Auto/Manual High Resolution Sputter Coater, 12 mA/800V plasma current, and 5 min at 0.5 nm/min) SEM images of CNT/PCL nanocomposites with a low (0.5% w/w), mid-level (2% w/w) and high (5% w/w) CNT loading were imaged for the LO-MWCNT and MWCNT/PCL nanocomposites used in this study. 10% w/w LO-MWCNT/PCL nanocomposites and 5%

w/w MWCNT/PCL nanocomposites for CNT release studies were also imaged before biodegradation. SEM images of replicate areas for each CNT type and loading used are shown in Appendix 6. After later stages of biodegradation, SEM images of the CNT/PCL nanocomposites will also be taken.

6.2.3. Differential Scanning Calorimetry (DSC)

DSC measurements were taken for PCL and LO-MWCNT/PCL nanocomposites to measure their degree of crystallinity, a property that can affect biodegradation rates.[40] PCL and 0.1, 0.5, 1, and 2% w/w LO-MWCNT/PCL nanocomposites each were analyzed in duplicate. 1 and 5% w/w pristine MWCNT/PCL (NanoLab Inc. MWCNTs) nanocomposites will also be measured in duplicate for comparison. Since the melting point of PCL is 60 °C, a temperature range of room temperature (~25 °C) to 65 °C was selected. A heating rate of 5 °C/min and cooling rate of 1 °C/min were used with the temperature maintained at 65 °C for 2 min before cooling began. Analysis of the heating and cooling DSC curves was performed using TA Universal Analysis software 2000 (TA instruments, New Castle, Delaware). The enthalpy of fusion was calculated by integrating the endothermic peak (42 to 62 °C) with a linear background. The fraction of crystallinity (Xc) was then calculated by dividing the experimental enthalpy of fusion by the theoretical enthalpy of fusion (ΔH_0 = 139.3 J/g).[41, 42]

6.2.4. PCL Triol Solution Preparation

Solutions containing approximately 3 g/L PCL triol were prepared by adding three aliquots of 0.5 mL PCL triol (Sigma-Aldrich, M_n ~300, 1.07 g/mL density @ 25 °C, Lot #: MKBT5188V) into 450 mL Milli-Q water while stirring at 700 rpm. Solutions were prepared at a low volume (500 mL) in a 1 L Erlenmeyer flask with a foam stopper to improve solution aeration during microbial growth (Section 6.25). After addition of

PCL triol, the solution was stirred for an additional 5 min at 700 rpm followed by 2 min of sonication (Branson 1510 ultrasonic bath, 50W) to ensure an even dispersion of the PCL triol in water. Solutions were then sterilized using a 45 min liquid autoclave cycle. After cooling, 50 mL of salt stock (containing 7.18 mM K_2HPO_4, 2.79 mM KH_2PO_4, 0.757 mM $(NH_4)_2SO_4$, 0.0406 mM $MgSO_4*7H_2O$) was aseptically added to the PCL triol solution to optimize ionic strength and buffering capacity. The number of PCL triol solutions prepared depended on the number of PCL and CNT/PCL nanocomposite samples to be biodegraded: one 500 mL PCL triol solution was prepared for every four PCL and CNT/PCL sample flasks. PCL triol solutions were never prepared more than 2-3 days in advance of inoculation for consistency in PCL triol dispersion quality.

6.2.5. Inoculation & CNT/PCL Nanocomposite Biodegradation Setup

0.5 mL of *P. aeruginosa* frozen stock was added to 75 mL LB broth and grown overnight to the stationary phase at 37˚C and 225 rpm. 1 mL of stationary phase *P. aeruginosa* was aseptically added to each 500 mL PCL triol solution to prime the microorganisms for PCL biodegradation by using PCL triol as the sole carbon source. The PCL triol/*P. aeruginosa* solutions were then shaken at 125 rpm, 28 °C for approximately 31 h, which corresponded to $8.0 \pm 0.4 \times 10^7$ CFU/mL, measured from three separately grown PCL triol/*P. aeruginosa* solutions, each in duplicate. All PCL and CNT/PCL samples were sterilized with ethanol for > 1 min, washed with autoclaved Milli-Q water to remove ethanol, and aseptically placed into sterile sample flasks. At 31 h, the *P. aeruginosa*/PCL triol solutions were distributed in 100 mL aliquots to each CNT/PCL sample flask. The CNT/PCL sample flasks each contained an internal PCL reference to track the extent of biodegradation in a given culture. Four replicates of each CNT loading used were run. A schematic of PCL triol preparation, inoculation, and

distribution to samples is shown in Appendix 6. Three unpaired PCL replicates were also run concurrently as an external reference for biodegradation time and to determine if biodegradation of the internal PCL references, paired with CNT/PCL nanocomposites, were affected by the presence of CNT/PCL nanocomposites. Abiotic controls were prepared by distributing 100 mL aliquots of sterile PCL triol solution to PCL and CNT/PCL sample flasks containing CNT/PCL nanocomposites of each CNT loading.

6.2.6. Sampling

PCL triol/*P. aeruginosa* solutions containing PCL and CNT/PCL nanocomposites were shaken at 125 rpm and 28 °C for 2 weeks prior to collection. These conditions were used since they were found to yield the most rapid rate of PCL biodegradation. PCL and CNT/PCL samples were collected on 9 cm high porosity filter paper (Fisher Scientific, Course, P8, Cat. #: 09-795C) by gently pouring the inoculum through the high porosity filter using a vacuum filtration system (Stericup and Steritop, Disposable Filtration System, Millipore Express Plus PES membrane, 0.22 μm). The 9 cm high porosity filter paper was replaced for each sample collected. Next, the coupons were removed from the high porosity filter paper and washed gently with autoclaved Milli-Q water. The PCL and CNT/PCL nanocomposites were then placed on top of a 7.5 cm filter paper within a Petri dish for drying in the desiccator; the filter paper was used to prevent CNT/PCL nanocomposites from sticking to the Petri dishes. Abiotic controls were separately removed from their flasks following the same procedure. After the PCL and CNT/PCL nanocomposites had dried for 2 d, they were weighed and photographed. Then, they were sterilized with ethanol for > 1 min, washed with autoclaved Milli-Q water to remove ethanol, placed into sterile sample flasks, and submerged in 100 mL of freshly prepared PCL triol/*P. aeruginosa* solutions for another two weeks of biodegradation. PCL and

CNT/PCL samples were exposed to biodegradation conditions in two week increments until the internal PCL reference had been fully biodegraded (> 100% mass loss) and some of the CNT/PCL nanocomposites had either fully degraded or plateaued in mass loss for at least two time points.

6.2.7. CNT Release Measurements

CNT release was measured using MWCNT/PCL nanocomposites containing MWCNTs from Southwest Nanotechnologies Inc. This type of MWCNT contained residual Co and Mo (2% w/w metal content) which could be used to track the release of MWCNTs during biodegradation. Two sets of 0.1 and 5% w/w MWCNT/PCL nanocomposites were submerged in PCL triol/*P. aeruginosa* with internal PCL references and biodegraded for 4 weeks and 8 weeks, with four replicates of each CNT loading per time point. 10 mL of supplemental PCL triol was added once for the 4 week samples and twice for the 8 week samples to accelerate biodegradation. External PCL references were also used to assess the extent of biodegradation and served as a negative control for CNT release. After 4 and 8 weeks, PCL and CNT/PCL samples were removed from the flasks using sterile forceps and rinsed with 5 mL of autoclaved Milli-Q water into the inoculum. The inoculum was autoclaved, sonicated for 45 s, vortexed, and distributed in 10 mL aliquots to two polypropylene conical tubes, rinsed with 5 mL of sterile Milli-Q water, and sonicated in sodium deoxycholate (SDC, 2% w/w, Sigma-Aldrich, ≥97% by titration, D6750) for 5 min prior to sp-ICP-MS analysis. Samples were diluted as necessary prior to analysis.

Co and Mo particles were measured with a Perkin Elmer NexION 300q with S10 autosampler in single particle mode; data has yet to be collected. Cobalt/molybdenum concentrations were calculated from a calibration curve of cobalt/molybdenum particle

numbers as a function of MWCNT mass concentration prepared with controlled loadings of MWCNTs in the same media using 2% w/w SDC.

6.3. Results and Discussion

Prior to long term microbial exposure, both pristine MWCNT and LO-MWCNT/PCL nanocomposites were characterized using SEM and DSC to assess the uniformity of the CNT distribution within the polymer matrix and determine the fraction of crystallinity as a function of CNT loading, respectively. Furthermore, CNT/PCL nanocomposites of varied CNT loading were compared visually to check for homogeneity in the CNT distribution. In Figure 6.1, the LO-MWCNT and MWCNT/PCL nanocomposites used in the biodegradation studies are shown. These CNT/PNCs are uniformly black and increase in darkness with CNT loading, with LO-MWCNTs showing slightly more uniformity than the MWCNTs in the PCL matrix. In both cases, however, there are minimal signs of CNT aggregation in the majority of the CNT/PCL nanocomposites.

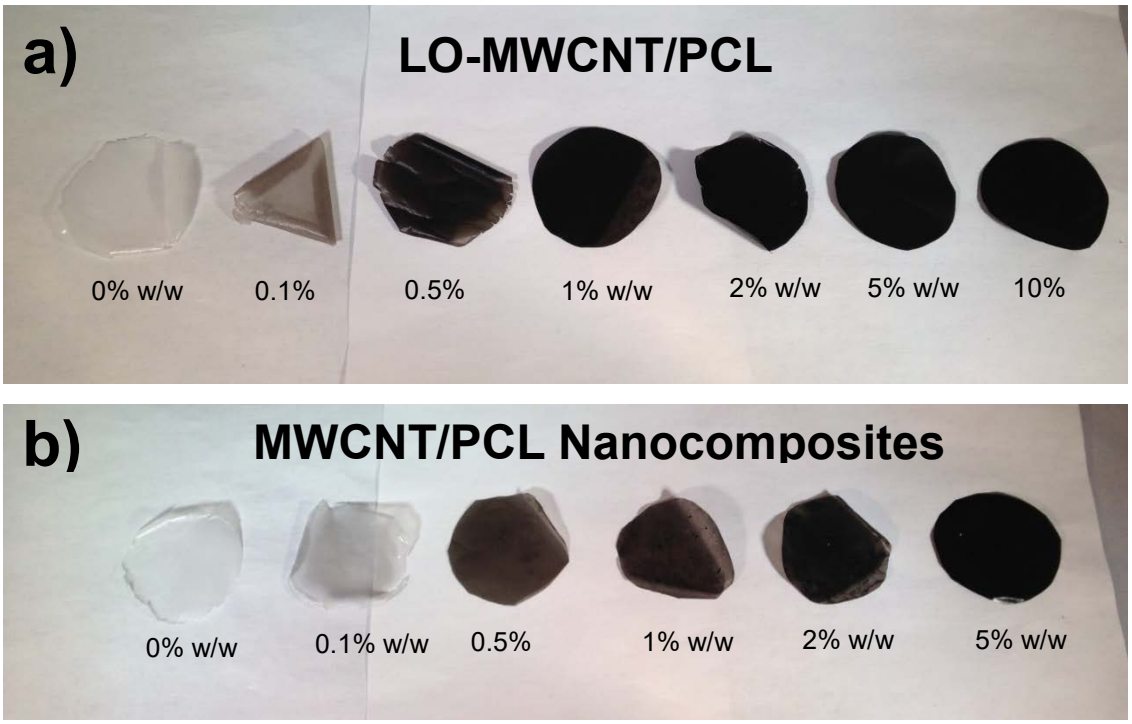

Figure 6.1. a) LO-MWCNT and b) MWCNT/PCL nanocomposites as a function of CNT loading.

SEM images in Figure 6.2 and 6.3 show the surface morphology and CNT content at the surface of LO-MWCNT/PCL and MWCNT/PCL nanocomposites, respectively. For both types of CNT/PCL nanocomposites, the majority of CNTs are initially below the PCL nanocomposite surface, even at a relatively high CNT loading of 5% w/w. However, the distribution of the few CNTs that are present at the surface as well as the CNTs that are apparent in some areas just below the nanocomposite surface appear to be fairly homogeneous. Replicate SEM figures for each CNT loading shown can be found in Appendix 6.

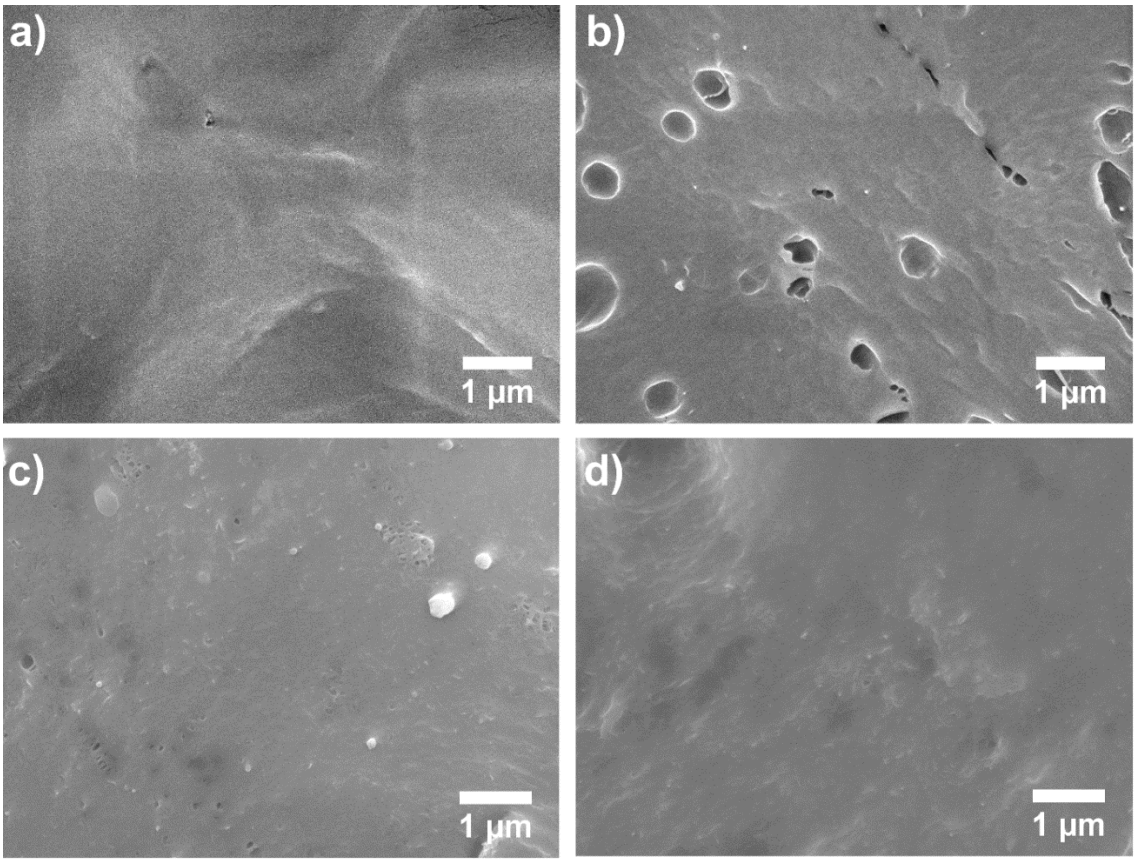

Figure 6.2. SEM images of a) PCL, b) 0.5% w/w, c) 2% w/w, and d) 5% w/w LO-MWCNT/PCL nanocomposites (all 4% w/w EC) before biodegradation.

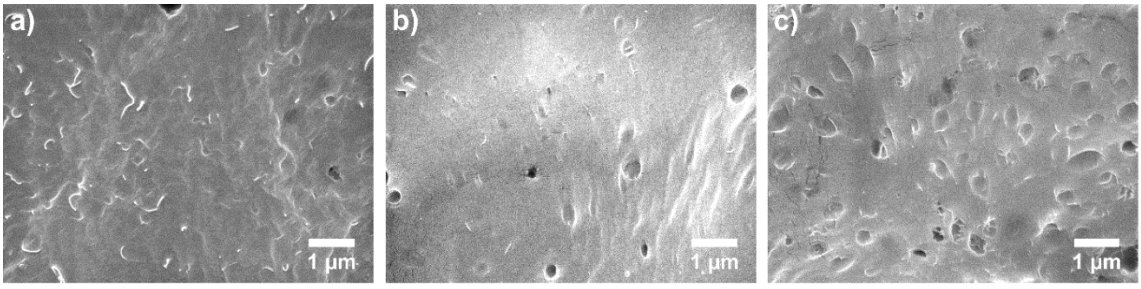

Figure 6.3. SEM images of a) 0.5% w/w, b) 2% w/w, and c) 5% w/w MWCNT/PCL nanocomposites (all 4% w/w EC) before biodegradation.

CNT/PCL nanocomposites were also characterized with DSC to measure the fraction crystallinity (X_c) as a function of CNT loading. This measurement was made since the biodegradability of a polymer generally decreases with increasing crystallinity.

In crystalline regions of a polymer, polymer chains stack together in the most tightly packed and thermodynamically stable conformation, which makes enzymatic degradation of these polymer chains less energetically favorable than those in amorphous regions.[40] In many cases, fillers have been shown to effect the crystallinity of a polymer, however, this has not been the case with CNTs from 1-13% w/w loading.[43] Nevertheless, to ensure that crystallinity did not change for the CNTs used in this study, DSC measurements of PCL were compared to those of LO-MWCNT/PCL nanocomposites at low (0.1 and 0.5% w/w), middle (1% w/w), and high (2% w/w) CNT loadings. As shown in Table 1, the fraction of crystallinity did not vary by more than 5% between all of the CNT/PCL nanocomposites. Since the polymer crystallinity did not vary with increasing mass concentrations of CNT filler, the effect of crystallinity on CNT/PCL nanocomposite biodegradability can be considered minimal. It is also important to note that all CNT/PCL nanocomposites, including pure PCL, contained the same mass concentration of EC surfactant, which enabled dispersion of the CNTs in the casting solution. As shown in Chapter 5, EC can lower the polymer crystallinity but is also not biodegradable on a timescale similar to PCL. Thus, a consistent concentration of EC (4% w/w) in all PCL and CNT/PCL nanocomposites was used to hold this variable constant.

Table 6.1. The fraction of crystallinity (X_C) of PCL and LO-MWCNT/PCL nanocomposites as a function of CNT loading. X_C was calculated from the heat of fusion measured using DSC.

Sample	X_C (%)	Std. Dev. (%)
PCL	57.0	0.5
0.1% w/w	54.3	0.3
0.5% w/w	56.7	3.9
1% w/w	59.4	3.1
2% w/w	54.0	1.3

As described above, PCL and CNT/PCL nanocomposites were biodegraded under accelerated conditions to collect results on an experimentally relevant time scale. The acceleration of biodegradation was achieved by growing *P. aeruginosa* in a solution containing PCL triol, a small molecule version of the polymer. PCL triol was used to prime the microorganisms to produce enzymes capable of PCL biodegradation. In all experiments, the CNT/PCL nanocomposites were exposed to *P. aeruginosa* for two weeks, removed, dried, weighed, sterilized, and then exposed to a fresh culture of *P. aeruginosa* grown in PCL triol for another two weeks.

The rate of PCL biodegradation in the absence of a CNT filler was first assessed in the presence of *P. aeruginosa* using mass loss. With the sampling method used, 100% mass loss of the PCL samples took approximately 20 weeks to achieve. Although complete biodegradation, which is defined as the conversion of > 60% polymer to CO_2 and H_2O, was not measured, the extent of biodegradation was significant in that a macroscopic sample was converted to a point where there was no visibly remaining material to collect.[34, 35] Therefore, the level of PCL biodegradation reached using the mass loss method was useful to assess the effect of CNT loading on the polymer biodegradation process. Mass loss was not observed for PCL under abiotic conditions in which PCL was exposed to the same media and sampling conditions over the same

course of time. In fact, the mass variably increased for abiotic controls due to PCL triol coating their surfaces. Overall, the loss of PCL material in Figure 6.4 can be reasonably attributed to biodegradation by *P. aeruginosa*.

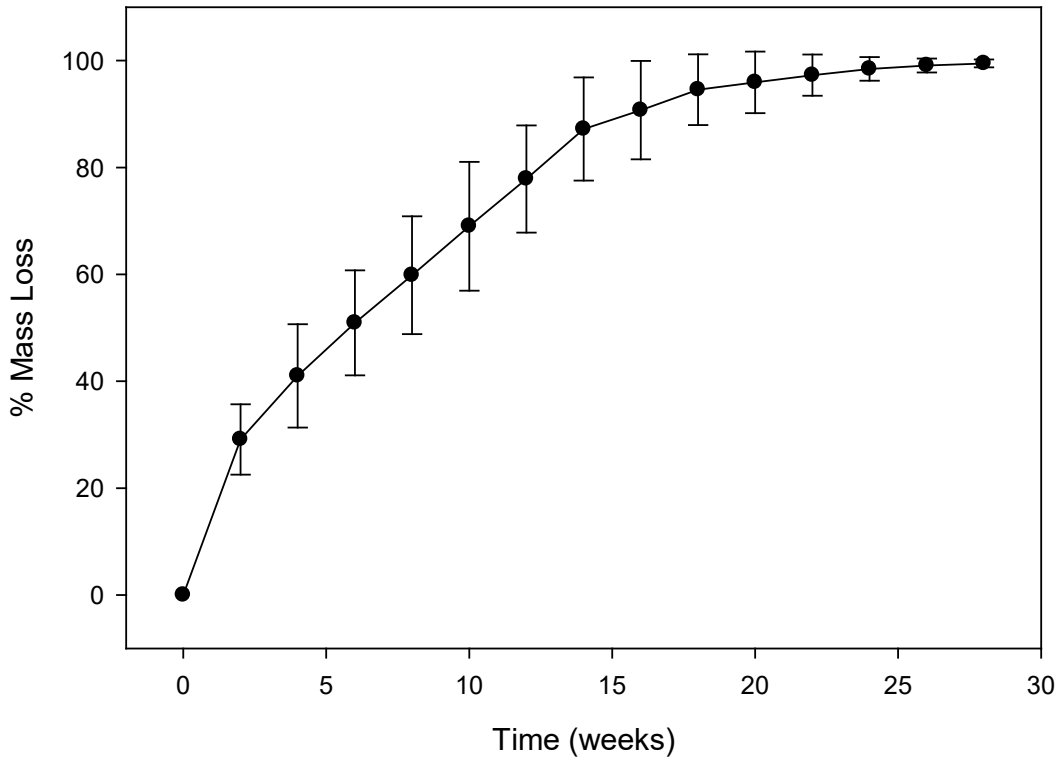

Figure 6.4. Mass loss plot of PCL (4% w/w EC) biodegraded by *P. aeruginosa* in 3 mg/L PCL triol/BMM solution.

For CNT/PCL nanocomposite biodegradation, each CNT/PCL nanocomposite was paired with a PCL sample in the same flask to serve as an internal reference. This approach was taken in case there was variation in the biodegradation rate from flask to flask as a result of an inconsistent distribution of PCL triol droplets that did not fully dissolve in the inoculum. This, however, was not the case as the initial microbial population was found to be highly consistent between replicate cultures grown in PCL triol solutions for 31 h ($8.0 \pm 0.4 \times 10^7$ CFU/mL, average of triplicates). Figure 6.5 shows mass

loss plots of PCL and LO-MWCNT/PCL nanocomposites containing 1 – 10% w/w LO-MWNCTs relative to an external PCL reference. Mass loss plots of 0.1 and 0.5% w/w are also shown in Appendix 6 relative to the same external PCL reference.

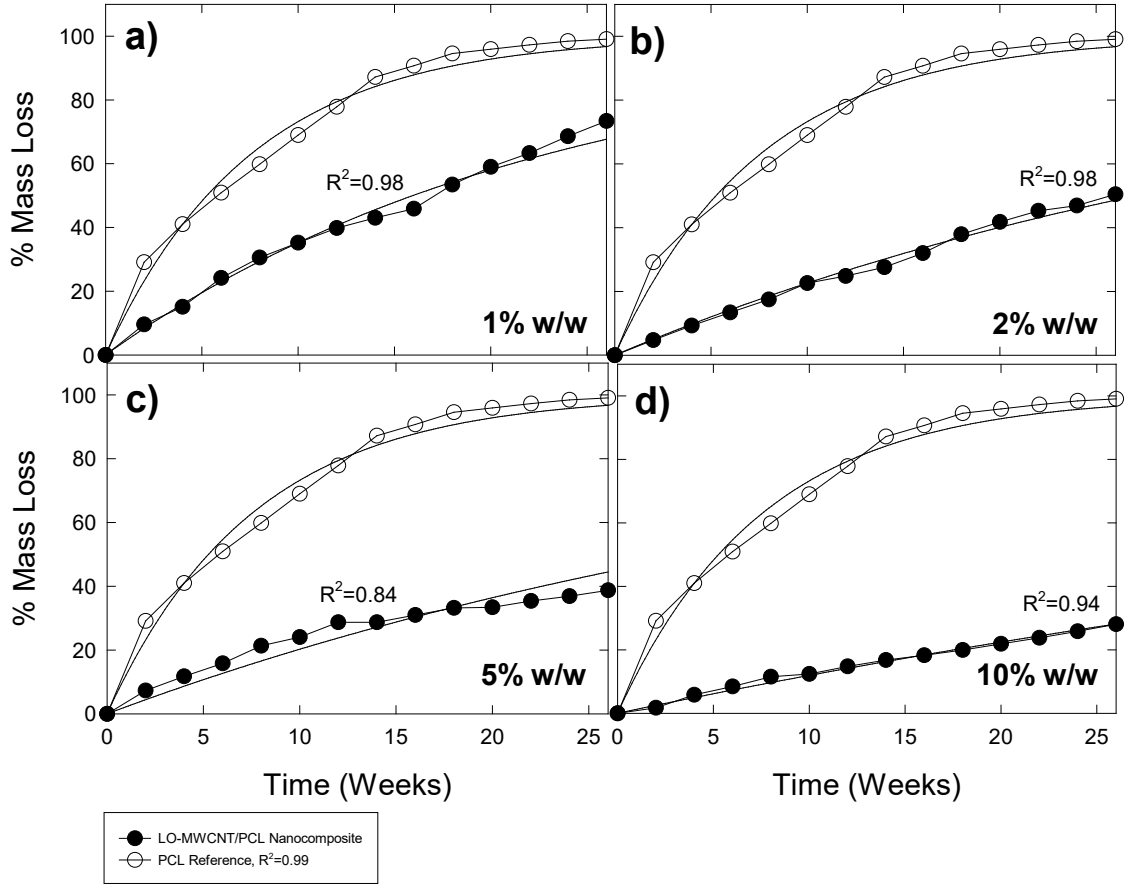

Figure 6.5. Mass loss of LO-MWCNT/PCL nanocomposites relative to mass loss of an external PCL reference as a result of *P. aeruginosa* biodegradation in 3 g/L PCL triol/BMM solution. The R^2 for each CNT loading is an average of fits (one fit shown) for at least three replicates (see Appendix 6).

Figure 6.5 shows that *P. aeruginosa* was able to degrade LO-MWCNT/PCL nanocomposites at all CNT loadings used. However, the rate of polymer degradation for LO-MWCNT/PCL nanocomposites was much lower than that of PCL, even with a small mass fractions of CNTs (0.1-1% w/w). A comparison of each CNT loading in Figure 6.5

indicates that biodegradation of the PCL matrix decreased with increasing CNT loading. For 0.1, 0.5, and 1% w/w LO-MWNCT/PCL nanocomposites, mass loss is rapidly approaching full biodegradation while 2, 5, and 10% w/w have only lost approximately 50, 38, and 26% of their mass after 26 weeks, respectively. This indicates that LO-MWCNTs could fully degrade and potentially release CNTs at lower CNT loadings (0.1-1% w/w) while LO-MWCNT/PCL nanocomposites of higher CNT loadings are more persistent, and will take much longer to reach the same level of biodegradation. In order to assess the difference in mass loss rates, PCL and CNT/PCL nanocomposites were fit to an exponential rise function (Figure 6.5).

$$\boldsymbol{y = a * (1 - e^{-kx})} \qquad \text{(Equation 1)}$$

where (y) is the % mass loss, (a) is the maximum rise of 100% biodegradation, (k) is the first order rate constant, and (x) is the time in weeks. On average, the R^2 of the fits was greater than 0.84, allowing for a relative rate constant to be extracted from the data. In all cases, the function was assumed to reach 100% mass loss, the best case scenario for the CNT/PCL nanocomposites of high CNT loading. Thus, the rate constants might be slightly overestimated with the higher CNT loadings if they don't reach 100% mass loss at longer time points. A plot of the rate constants for the external PCL reference and LO-MWCNT/PCL nanocomposites of increasing CNT loading is shown in Figure 6.6.

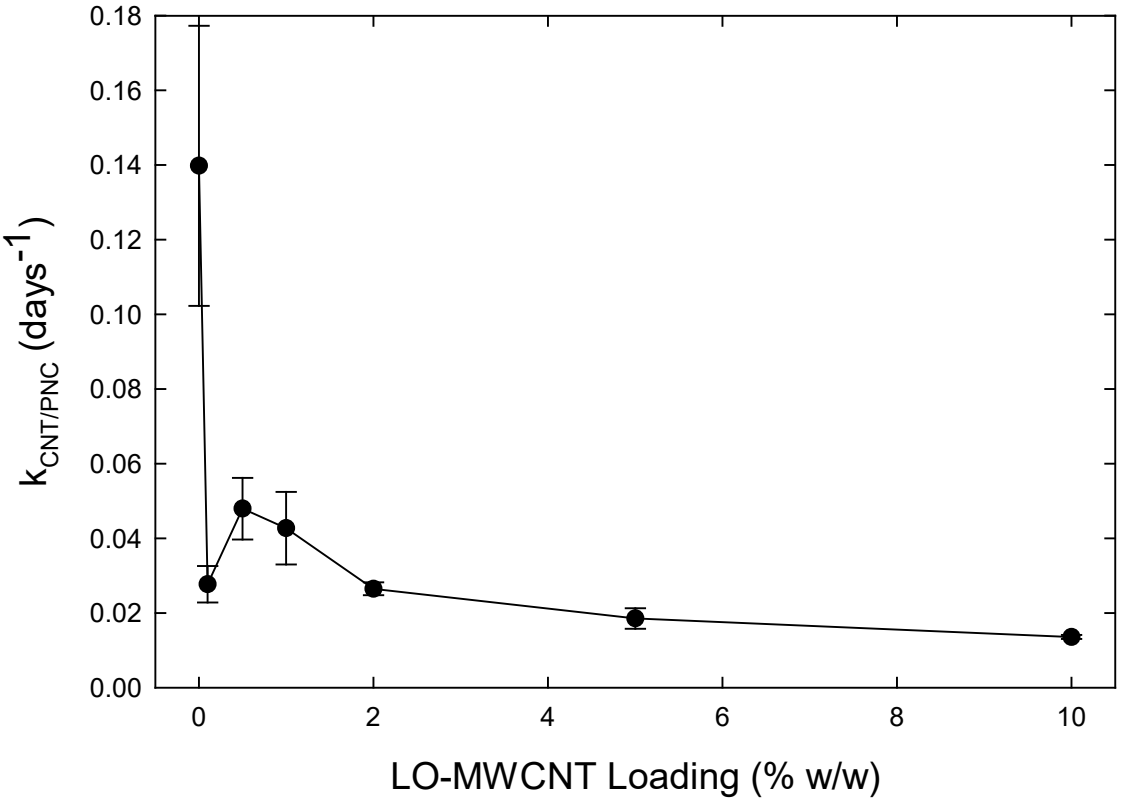

Figure 6.6. The effect of CNT loading on the rate of LO-MWCNT/PCL nanocomposite mass loss during *P. aeruginosa* biodegradation. Rate constants were extracted from exponential rise fits of the CNT/PCL nanocomposite mass loss profiles.

Similar to the mass loss trends observed in Figure 6.5, the rate constants decreased from 0.0480 to 0.0136 for CNT loadings ranging between 0.5 to 10% w/w (Figure 6.6). In contrast, the external PCL reference had a rate constant 3-3.5x times larger than that of any LO-MWCNT/PCL nanocomposite. This indicates that LO-MWCNTs, even at the lowest CNT loading of 0.1% w/w, retard biodegradation of PCL. The rate constant of 0.1% w/w LO-MWCNT/PCL appeared to be an outlier, since the rate fell below that of 0.5 and 1% w/w, but the consistency within the replicates and similar results in preliminary studies indicate that 0.1% w/w might have some unique properties that affect biodegradation such as a better CNT dispersion state than the other CNT loadings since it

has the smallest mass fraction of CNTs. Rate constants for each CNT loading and replicates are shown in Appendix 6.

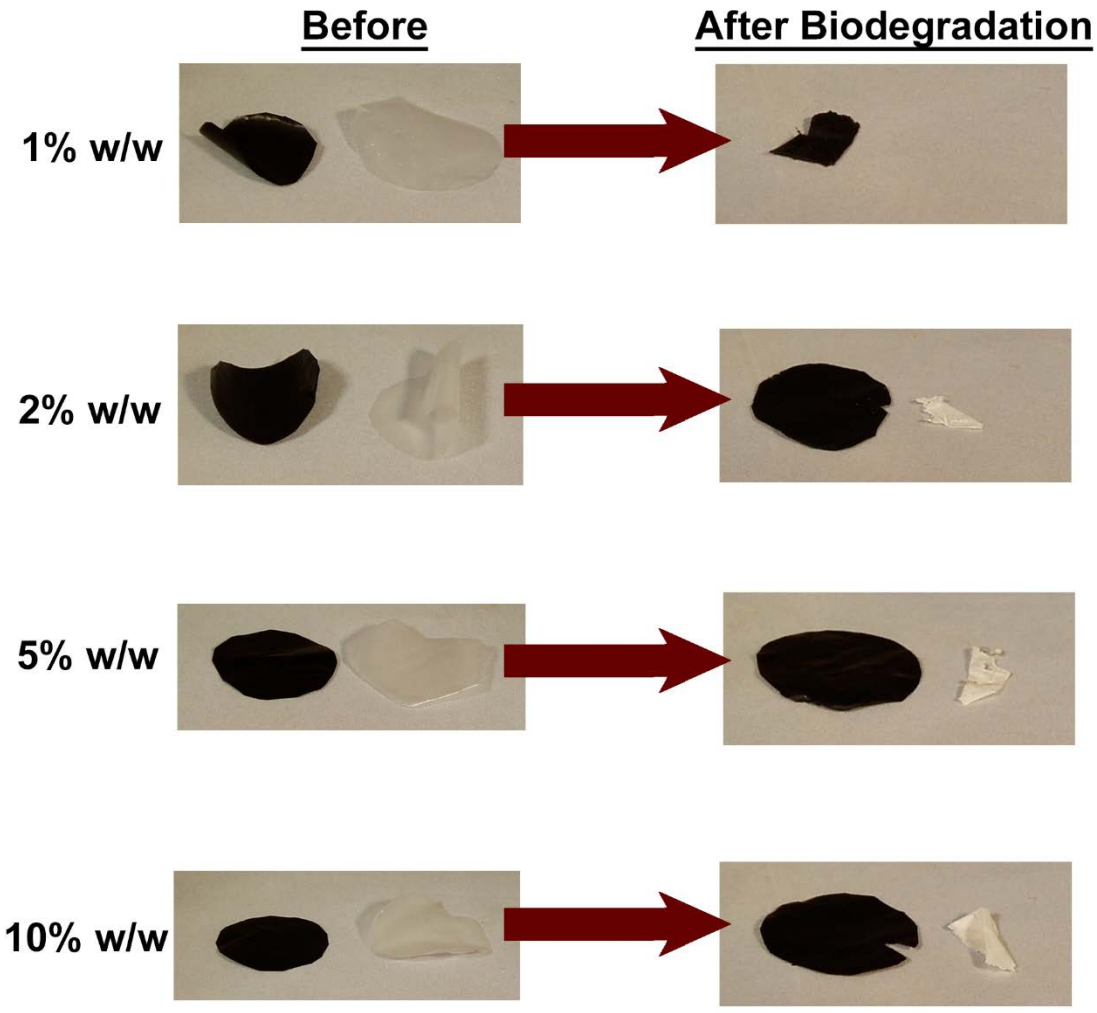

Figure 6.7. LO-MWCNT/PCL nanocomposites and their paired, internal PCL reference before and after 26 weeks of *P. aeruginosa* biodegradation.

Figure 6.7 shows the internal PCL and LO-MWCNT/PCL nanocomposite pairs before and after 26 weeks of biodegradation. For the LO-MWCNT/PCL nanocomposites, the presence of CNTs maintained the nanocomposite structure above a CNT threshold of 2% w/w after ~50% mass loss and mechanical agitation (125 rpm shaking). In contrast, 1% w/w shows a deteriorating structure after 75% mass loss and the same level of

mechanical agitation. Structural deterioration was also observed for the other CNT loadings below 1% w/w (Appendix 6). Although more time points are needed to confirm that the shapes of LO-MWCNT/PCL nanocomposites with high CNT loadings remain intact after biodegradation, LO-MWCNTs of higher CNT loading are clearly maintaining their shape while LO-MWCNT/PCL nanocomposites are losing their shape at 26 weeks. Another observation from the pictures in Figure 6.7 is that the internal PCL references lost more mass when paired to CNT/PCL nanocomposites with lower CNT loadings. Mass loss plots of internal PCL references paired with CNT/PCL nanocomposites of increasing CNT loading are shown in Figure 6.8. Inhibition of PCL mass loss became more apparent with CNT/PCL nanocomposites of increasing CNT loading with 95% mass loss for 1% w/w versus 65% mass loss for 10% w/w after 26 weeks of biodegradation. These mass loss profiles were fit to the same exponential rise function used in Figure 6.5 to extract rate constants. The rate constants for internal PCL references paired to each CNT loading used are plotted in Figure 6.9. Further rate constant information can be found in Appendix 6. Interestingly, the rate constants for the internal PCL reference (Figure 6.9) mass loss tracked well with the rate constants for the CNT/PCL nanocomposites they were paired with (Figure 6.6). However, the internal PCL references were always more degraded than the CNT/PCL nanocomposites they were paired with. The internal PCL references paired with CNT/PCL nanocomposites of higher CNT loadings (> 2% w/w) potentially had lower rate constants due to the limited ability of microbes to degrade the CNT/PCL nanocomposite and as a result, divide and proliferate to increase the microbial population available to degrade the internal PCL reference. This possibility will be further investigated by measuring the CFU in each

culture at the end of a time point to see if the microbial population within flasks containing CNT/PCL nanocomposites of low CNT loading have a relatively higher microbial population than those containing a high CNT loading.

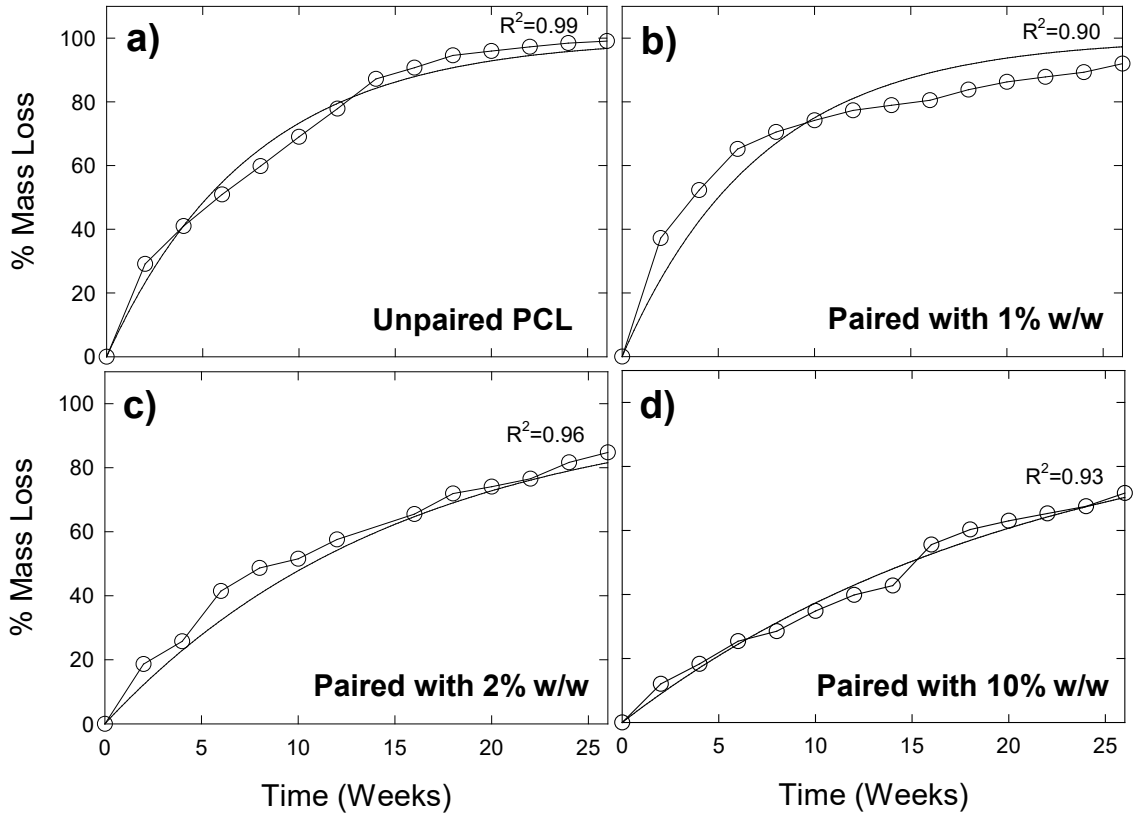

Figure 6.8. Mass loss of internal PCL references paired to LO-MWCNT/PCL nanocomposites as a result of *P. aeruginosa* biodegradation in 3 g/L PCL triol/BMM solution. The R^2 for each CNT loading is an average of fits (one fit shown) for at least three internal PCL replicates (see Appendix 6).

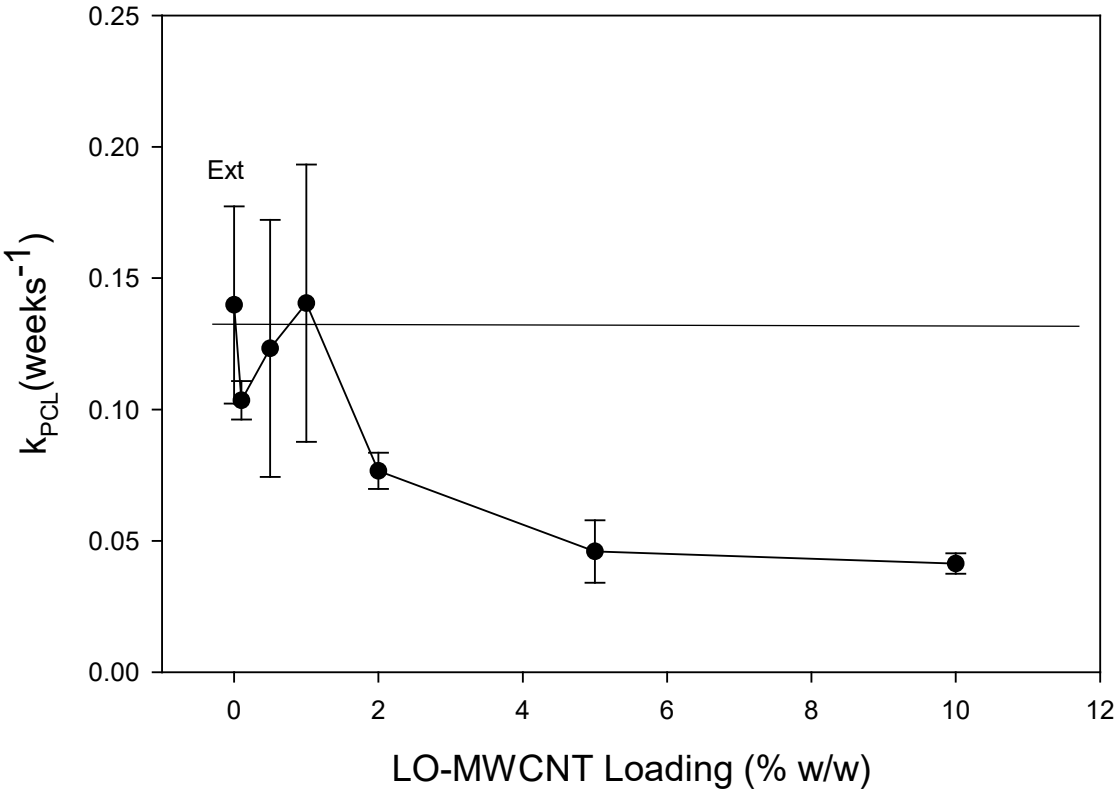

Figure 6.9. The effect of CNT loading on the rate of internal PCL reference (paired with LO-MWCNT/PCL nanocomposites) mass loss during *P. aeruginosa* biodegradation. Rate constants were extracted from exponential rise fits of the PCL mass loss profiles.

In Figure 6.10, pristine MWCNT/PCL nanocomposites from 0.1 – 5% w/w MWCNTs were also degraded under the same conditions as LO-MWCNT/PCL nanocomposites. Similar mass loss trends were observed: the rate of mass loss decreased with increasing MWCNT loading and 2 and 5% w/w degraded at a slower rate than 0.1 and 1% w/w MWCNT/PCL nanocomposites. A mass loss plot of 0.5% w/w MWCNT/PCL nanocomposites is shown in Appendix 6. A plot of the rate constants for MWCNT/PCL nanocomposite biodegradation is shown in Figure 6.11 and the rate constants of replicates are shown in Appendix 6. The R^2 values of the fits for MWCNT/PCL nanocomposites ($R^2 > 0.77$) were generally lower than for the LO-

MWCNT/PCL nanocomposite fits ($R^2 > 0.84$), but this is most likely a result of the lesser number of time points for the MWCNTs (18 weeks). Further data collection will most likely improve the accuracy of these fits.

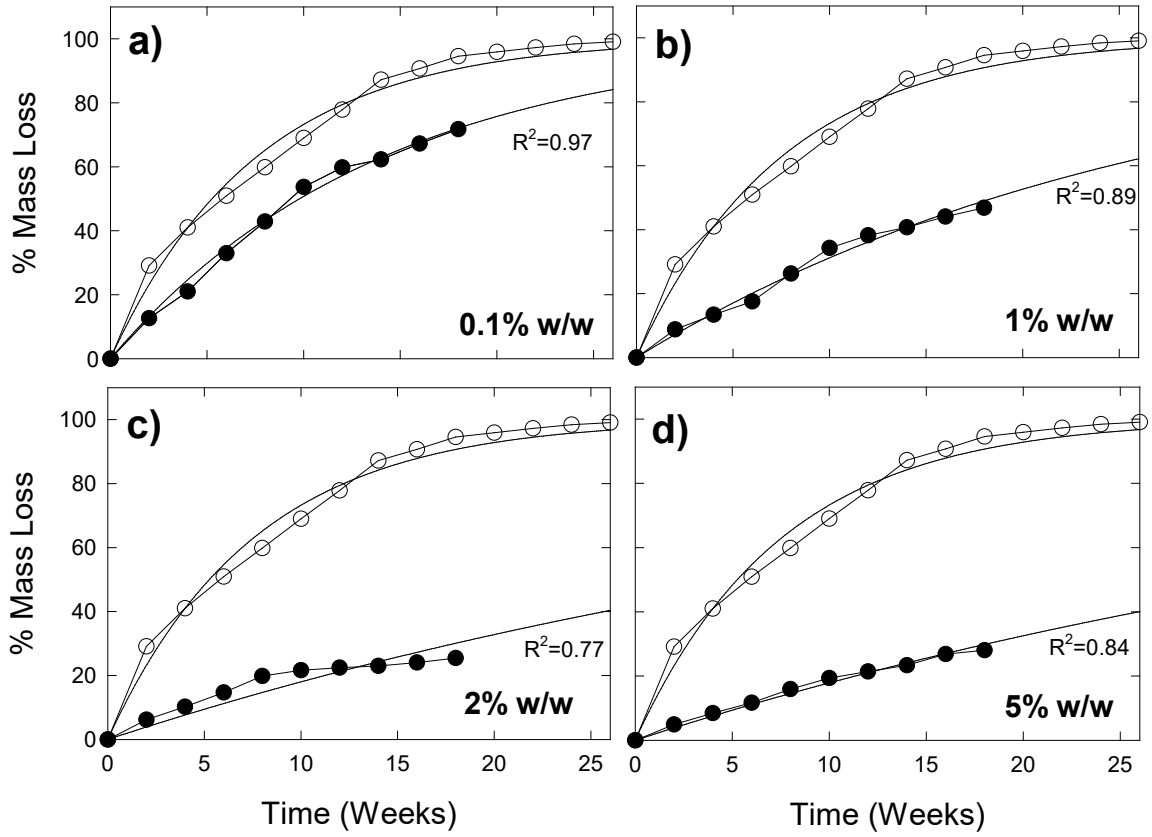

Figure 6.10. Mass loss of MWCNT/PCL nanocomposites relative to mass loss of an external PCL reference as a result of *P. aeruginosa* biodegradation in 3 g/L PCL triol/BMM solution. The R^2 for each CNT loading is an average of fits (one fit shown) for at least three replicates (see Appendix 6).

For MWCNT/PCL nanocomposites, 0.1% w/w MWNCT/PCL nanocomposites degraded rapidly while 0.5% w/w MWCNT/PCL nanocomposites degraded more slowly, the opposite to which was observed for LO-MWCNT/PCL nanocomposites. This can potentially be the result of the lower dispersion quality of the pristine MWCNTs relative to the LO-MWCNTs, leading to the optimal dispersion quality occurring at 0.5% w/w

rather than 0.1% w/w. Another possibility is that the 0.5% w/w MWCNT/PCL nanocomposite had a slightly enhanced CNT surface concentration than the other loadings which could have delayed biodegradation due to the cytotoxicity of CNTs at the PNC surface (Figure 6.3).[9, 44] This very specific low CNT loading effect that generates enhanced inhibition relative to other low CNT loadings should be explored further for other CNT types to see if it is a generalizable occurrence. For the rest of the CNT loadings studied, the rate constants decreased with CNT loading and were fairly similar for both MWCNTs and LO-MWCNTs, indicating that the presence of ~4% oxygen on the LO-MWCNTs, the difference in lengths (5-20 μm vs. 1.5 μm for MWCNT and LO-MWCNTs, respectively), as well as slight differences in CNT structure (purity and diameter) have a minimal effect on CNT/PCL nanocomposite biodegradation trends.

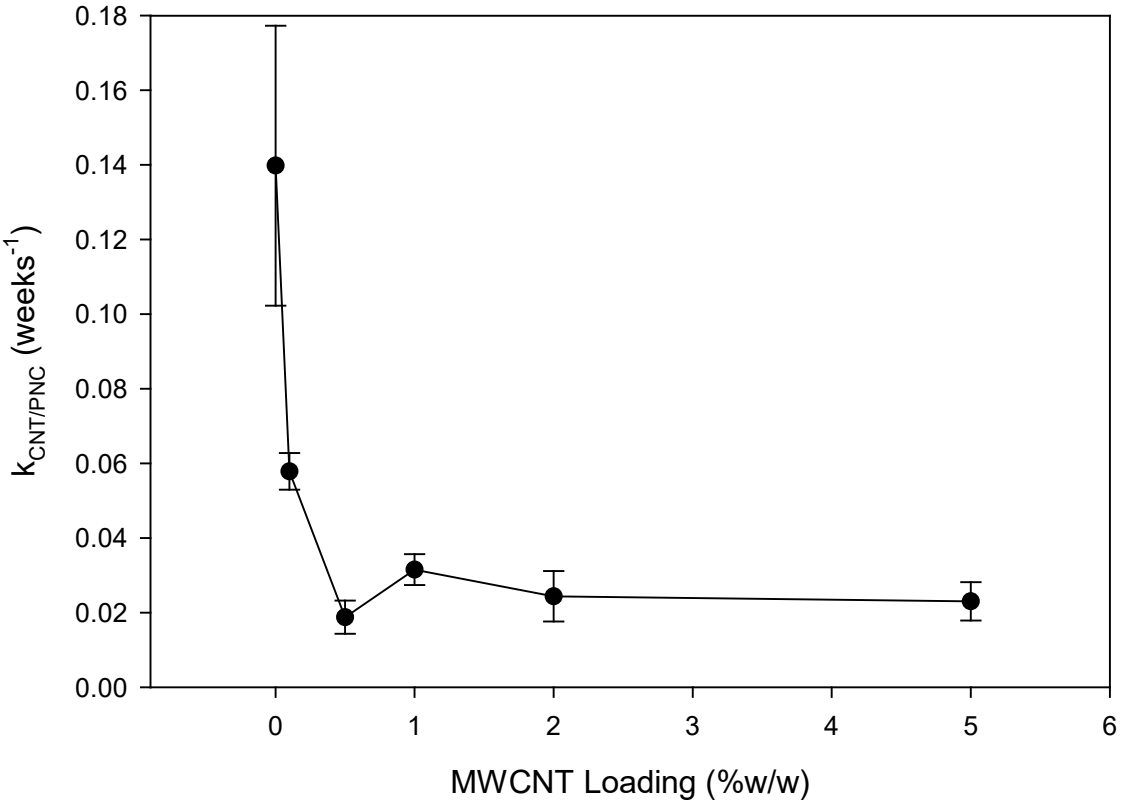

Figure 6.11. The effect of CNT loading on the rate of MWCNT/PCL nanocomposite mass loss during *P. aeruginosa* biodegradation. Rate constants were extracted from exponential rise fits of the CNT/PCL nanocomposite mass loss profiles.

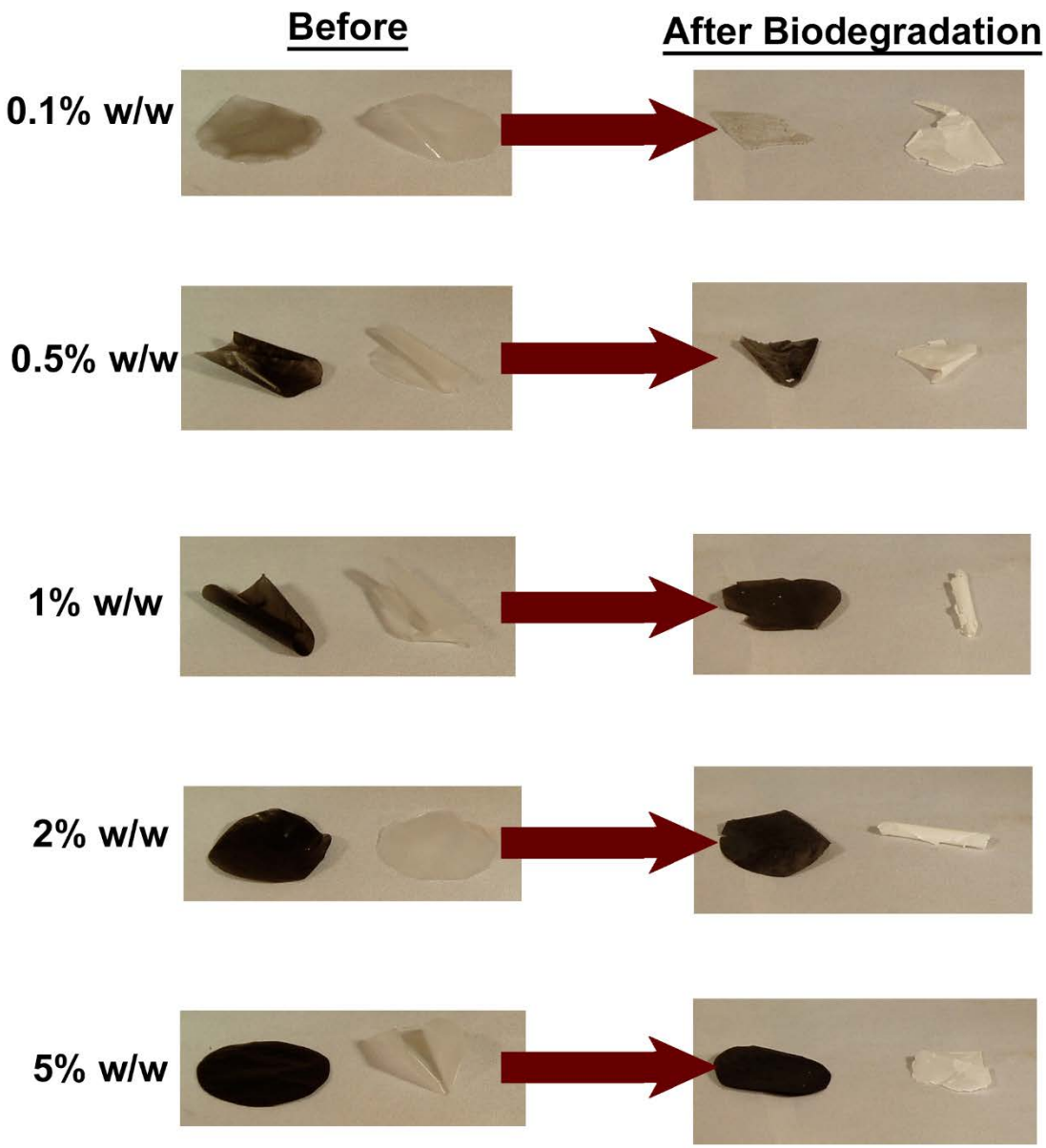

Figure 6.12. MWCNT/PCL nanocomposites and their paired, internal PCL reference before and after 26 weeks of *P. aeruginosa* biodegradation.

Figure 6.12 shows the paired internal PCL references and MWCNT/PCL nanocomposites at each CNT loading before and after biodegradation. Similar to the LO-MWCNT/PCL nanocomposites, the CNT/PCL nanocomposites of lower CNT loading have lost some of their shape and structure while the CNT/PCL nanocomposites of higher CNT loading did

not change form. The visual changes are a lot more subtle for the MWCNT/PCL nanocomposites since they have not yet degraded as long as the LO-MWCNT/PCL nanocomposites. For the paired internal PCL references, the effect of the paired MWCNT/PCL nanocomposite on the mass loss of the internal PCL reference is not as apparent visually or from the rate constants (Figure 6.13 and 6.14). This could be due to a greater spread in the data as a result of the poorer MWCNT dispersion quality relative to LO-MWCNTs or it could be due to a lack of time points. Further investigation as to whether MWCNT/PCL nanocomposites affect the rate of mass loss for internal PCL references is underway.

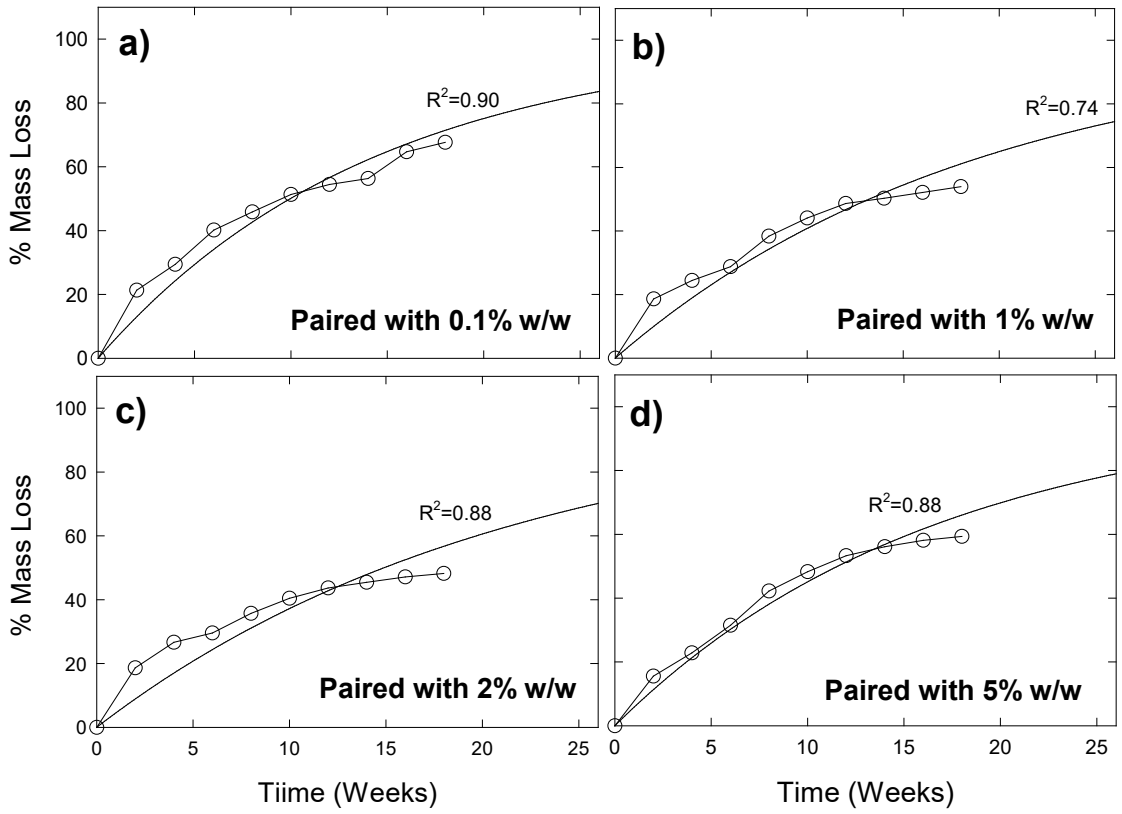

Figure 6.13. Mass loss of internal PCL references paired to MWCNT/PCL nanocomposites as a result of *P. aeruginosa* biodegradation in 3 g/L PCL triol/BMM solution. The R^2 for each CNT loading is an average of fits (one fit shown) for at least three internal PCL replicates (see Appendix 6).

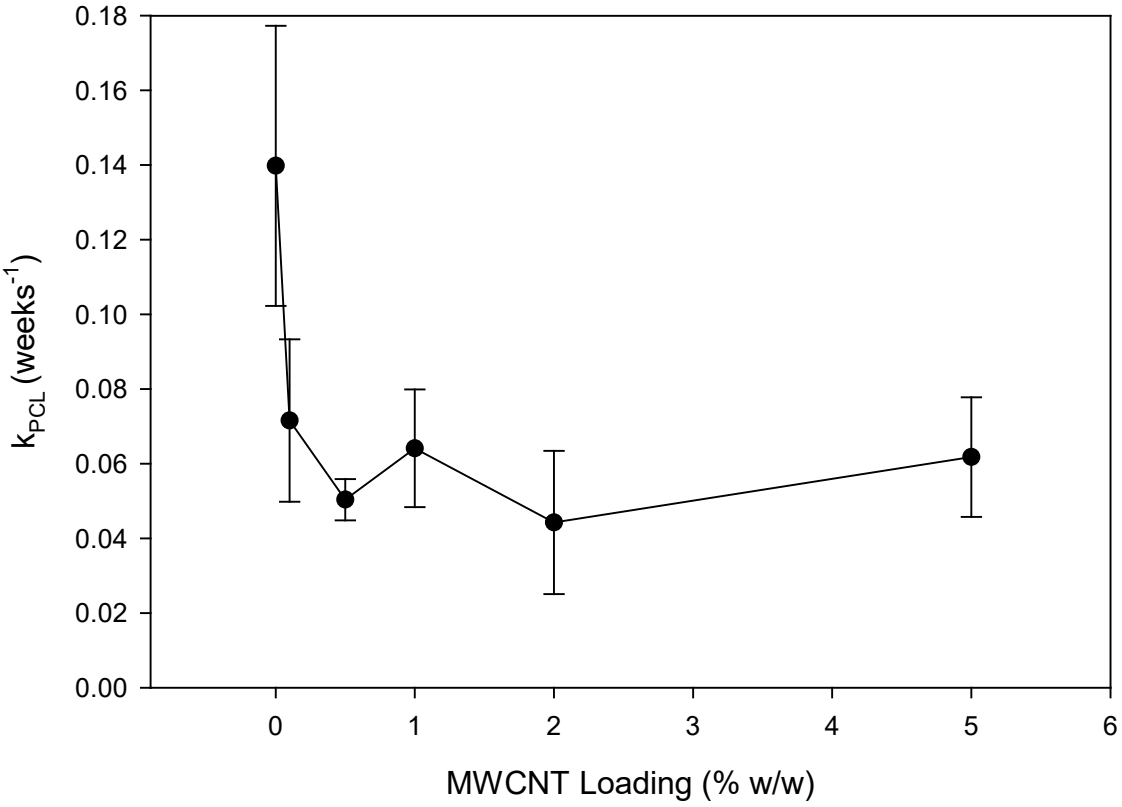

Figure 6.14. The effect of CNT loading on the rate of internal PCL reference (paired with MWCNT/PCL nanocomposites) mass loss during *P. aeruginosa* biodegradation. Rate constants were extracted from exponential rise fits of the PCL mass loss profiles.

Overall, PCL biodegraded more rapidly than all CNT/PCL nanocomposites of varied CNT loading. The rate of CNT/PCL nanocomposite biodegradation generally decreased as a function of CNT loading. As described in Chapter 4, this could be a result of the cytotoxicity of CNTs as they accumulate at the CNT/PCL nanocomposite surface during biodegradation. Although a viable biofilm can form on top of a dead layer of cells, material below the dead layer appears to take a much longer time to degrade. However, the results indicate that the PCL matrix can still be degraded eventually when it contains a high CNT loading but requires a much longer amount of time and potentially a greater amount of energy to fully degrade. CNTs might also block enzymatic access to the PCL

carbon source upon CNT accumulation at the CNT/PCL nanocomposite surface, leading to lower biodegradation rate constants. In general, CNT accumulation can lead to cytotoxicity and potentially blocked access to the PCL substrate by enzymes, decreasing the biodegradability of PCL as a function of CNT filler loading.

The effect of CNT loading on polymer biodegradability was found to be similar for two types of CNTs, one pristine and one slightly oxidized from different manufacturers. The results indicate that the biodegradation trends observed for CNT/PCL nanocomposites are fairly generalizable to CNT types that have similar purities and diameters. Although MWCNTs had longer lengths than LO-MWCNTs (5-20 μm vs. 1.5 μm) CNTs of much longer lengths (50 μm- mm scale) should also be embedded in PCL and investigated for biodegradability. Biodegradation of PCL composites containing carbon fibers with similar aspect ratios, carbon black as a filler control, and graphene oxide as a cytotoxicity control (without a high aspect ratio) should also be investigated to determine whether the inhibition effects on biodegradation are more impacted by CNT cytotoxicity or the aspect ratio of the CNTs.

Since products generally use CNT loadings within the range of 0.1 - 5% w/w, products made with greater than 2% w/w will be more persistent than those at lower CNT loadings when disposed of in the environment. This indicates that lower CNT loadings may pose more of an environmental risk since they have the most potential to fully degrade and release CNTs based on the deteriorated shape and structure of CNT/PCL nanocomposites containing CNT loadings below 1% w/w. However, CNT/PCL nanocomposites with the highest CNT loading (10% w/w) still degraded to >25% mass

loss (with minimal visual signs of initial release) and could potentially release just as many CNTs as a lower CNT loading after a longer period of time.

In order to analyze the effect of CNT release from MWCNT/PCL nanocomposites, low (0.1% w/w) and high MWCNT (5% w/w) loadings were separately prepared in PCL using a similar type of MWCNT that contains residual cobalt and molybdenum catalyst. These types of MWCNTs were utilized since their presence in solution following a biodegradation experiment could be ascertained by measuring the residual metal catalyst as a proxy for CNTs using sp-ICP-MS. Biodegradation of these MWCNT/PCL nanocomposites in PCL triol/*P. aeruginosa* solutions is ongoing and will determine whether CNT release occurs initially and/or partway through the biodegradation process. For all other CNT/PCL nanocomposites used in this study, longer mass loss time points will also determine whether CNTs release for low and high CNT-loaded PCL nanocomposites depending on whether CNT/PCL nanocomposites retain their shape as a CNT mat or release into the solution. Further investigation of CNT/PNCs under more environmentally relevant mixed culture conditions will be described in the next chapter.

6.4. Appendix 6 Summary

A schematic of the PCL triol preparation, inoculation, and growth procedure (Scheme A6.1); replicate SEM images of the surfaces of PCL and CNT/PCL nanocomposites (Figures A6.1-A6.9); mass loss plots (Figure A6.10) and pictures (Figure A6.11) of 0.1 and 0.5% w/w LO-MWCNT/PCL nanocomposites; a table of rate constants for replicate internal PCL references paired to LO-MWCNT/PCL nanocomposites (Table A6.1) and MWCNT/PCL nanocomposites (Table A6.3); a table of rate constants for replicate LO-MWCNT/PCL nanocomposites (Table A6.2) and MWCNT/PCL

nanocomposites (Table A6.4); and a mass loss plot for one 0.5% w/w MWCNT/PCL nanocomposite replicate.

6.5. References

1. Zheng, Y.; Yanful, E. K.; Bassi, A. S., A review of plastic waste biodegradation. *Crit. Rev. Biotechnol.* **2005,** *25*, (4), 243-250.
2. Luckachan, G. E.; Pillai, C. K. S., Biodegradable Polymers-A Review on Recent Trends and Emerging Perspectives. *J. Polym. Environ.* **2011,** *19*, (3), 637-676.
3. Kumar, A. P.; Depan, D.; Tomer, N. S.; Singh, R. P., Nanoscale particles for polymer degradation and stabilization-Trends and future perspectives. *Prog. Polym. Sci.* **2009,** *34*, (6), 479-515.
4. Chandra, R.; Rustgi, R., Biodegradable polymers. *Prog. Polym. Sci.* **1998,** *23*, (7), 1273-1335.
5. Bianco, A.; Kostarelos, K.; Prato, M., Making carbon nanotubes biocompatible and biodegradable. *Chem. Commun.* **2011,** *47*, (37), 10182-10188.
6. Allen, B. L.; Kotchey, G. P.; Chen, Y. N.; Yanamala, N. V. K.; Klein-Seetharaman, J.; Kahan, V. E.; Star, A., Mechanistic Investigations of horseradish peroxidase-catalyzed degradation of single-walled carbon nanotubes. *J. Am. Chem. Soc.* **2009,** *131*, 17194-17205.
7. Russier, J.; Ménard-Moyon, C.; Venturelli, E.; Gravel, E.; Marcolongo, G.; Meneghetti, M.; Doris, E.; Bianco, A., Oxidative biodegradation of single-and multi-walled carbon nanotubes. *Nanoscale* **2011,** *3*, (3), 893-896.
8. Zhang, L.; Petersen, E. J.; Habteselassie, M. Y.; Mao, L.; Huang, Q., Degradation of multiwall carbon nanotubes by bacteria. *Environ. Pollut. (Oxford, U. K.)* **2013,** *181*, 335-339.
9. Goodwin, D. G.; Marsh, K. M.; Sosa, I. B.; Payne, J. B.; Gorham, J. M.; Bouwer, E. J.; Fairbrother, D. H., Interactions of Microorganisms with Polymer Nanocomposite Surfaces Containing Oxidized Carbon Nanotubes. *Environ. Sci. Technol.* **2015,** *49*, (9), 5484-5492.
10. Ahmed, F.; Santos, C. M.; Vergara, R. A. M. V.; Tria, M. C. R.; Advincula, R.; Rodrigues, D. F., Antimicrobial applications of electroactive PVK-SWNT nanocomposites. *Environ. Sci. Technol.* **2012,** *46*, (3), 1804-1810.
11. Santos, C. M.; Milagros Cui, K.; Ahmed, F.; Tria, M. C. R.; Vergara, R. A. M. V.; de Leon, A. C.; Advincula, R. C.; Rodrigues, D. F., Bactericidal and anticorrosion properties in PVK/MWNT nanocomposite coatings on stainless steel. *Macromol. Mater. Eng.* **2012,** *297*, (8), 807-813.
12. Schiffman, J. D.; Elimelech, M., Antibacterial activity of electrospun polymer mats with incorporated narrow diameter single-walled carbon nanotubes. *ACS Appl. Mater. Interfaces* **2011,** *3*, (2), 462-468.
13. Shimao, M., Biodegradation of plastics. *Curr. Opin. Biotechnol.* **2001,** *12*, (3), 242-247.
14. Gross, R. A.; Kalra, B., Biodegradable Polymers for the Environment. *Science* **2002,** *297*, 803-807.

15. Kim, H.-S.; Chae, Y. S.; Jin, H.-J.; Yoon, J.-S., Preparation and characterization of poly(ε-caprolactone)-grafted-multiwalled carbon nanotubes. *Key Eng. Mater.* **2007,** *334-335*, (Pt. 2, Advances in Composite Materials and Structures), 873-876.
16. Mattioli-Belmonte, M.; Vozzi, G.; Whulanza, Y.; Seggiani, M.; Fantauzzi, V.; Orsini, G.; Ahluwalia, A., Tuning polycaprolactone-carbon nanotube composites for bone tissue engineering scaffolds. *Mater. Sci. Eng., C* **2012,** *32*, (2), 152-159.
17. Chakoli, A. N.; Wan, J.; Feng, J. T.; Amirian, M.; Sui, J. H.; Cai, W., Functionalization of multiwalled carbon nanotubes for reinforcing of poly(-lactide-co-ϵ-caprolactone) biodegradable copolymers. *Appl. Surf. Sci.* **2009,** *256*, (1), 170-177.
18. Pan, L.; Pei, X.; He, R.; Wan, Q.; Wang, J., Multiwall carbon nanotubes/polycaprolactone composites for bone tissue engineering application. *Colloids Surf., B* **2012,** *93*, 226-234.
19. Mitchell, C. A.; Krishnamoorti, R., Dispersion of Single-Walled Carbon Nanotubes in Poly(ε-caprolactone). *Macromolecules* **2007,** *40*, (5), 1538-1545.
20. Wu, D. F.; Zhang, Y. S.; Zhang, M.; Yu, W., Selective localization of multiwalled carbon nanotubes in poly(e-caprolactone)/polylactide blend. *Biomacromolecules* **2009,** *10*, (2), 417-424.
21. Madigan, M. T.; Martinko, J. M.; Dunlap, P. V.; Clark, D. P., *Brock Biology of Microorganisms*. 12th ed.; Pearson: San Francisco, 2009.
22. Khatiwala, V. K.; Shekhar, N.; Aggarwal, S.; Mandal, U. K., Biodegradation of Poly(ε-caprolactone) (PCL) film by Alcaligenes faecalis. *J. Polym. Environ.* **2008,** *16*, (1), 61-67.
23. Lefevre, C.; Tidjani, A.; Vander, W. C.; David, C., The interaction mechanism between microorganisms and substrate in the biodegradation of polycaprolactone. *J. Appl. Polym. Sci.* **2002,** *83*, (6), 1334-1340.
24. Li, S.; Garreau, H.; Pauvert, B.; McGrath, J.; Toniolo, A.; Vert, M., Enzymatic Degradation of Block Copolymers Prepared from ε-Caprolactone and Poly(ethylene glycol). *Biomacromolecules* **2002,** *3*, (3), 525-530.
25. Zeng, H. L.; Gao, C.; Yan, D. Y., Poly(ϵ-caprolactone)-Functionalized Carbon Nanotubes and Their Biodegradation Properties. *Adv. Funct. Mater.* **2006,** *16*, (6), 812-818.
26. Qiu, Z.; Wang, H.; Xu, C., Crystallization, mechanical properties, and controlled enzymatic degradation of biodegradable poly(e-caprolactone)/multi-walled carbon nanotubes nanocomposites. *Nanosci. Nanotechnol.* **2011,** *11*, 7884-7893.
27. Hou, W.-C.; BeigzadehMilani, S.; Jafvert, C. T.; Zepp, R. G., Photoreactivity of Unfunctionalized Single-Wall Carbon Nanotubes Involving Hydroxyl Radical: Chiral Dependency and Surface Coating Effect. *Environ. Sci. Technol.* **2014,** *48*, (7), 3875-3882.
28. Qu, X.; Alvarez, P. J.; Li, Q., Photochemical Transformation of Carboxylated Multiwalled Carbon Nanotubes: Role of Reactive Oxygen Species. *Environ. Sci. Technol.* **2013,** *47*, (24), 14080-14088.
29. De, V. M. F. L.; Tawfick, S. H.; Baughman, R. H.; Hart, A. J., Carbon Nanotubes: Present and Future Commercial Applications. *Science* **2013,** *339*, (6119), 535-539.

30. Moniruzzaman, M.; Winey, K. I., Polymer nanocomposites containing carbon nanotubes. *Macromolecules* **2006,** *39*, (16), 5194-5205.
31. McClory, C.; Chin, S. J.; McNally, T., Polymer/Carbon Nanotube Composites. *Aust. J. Chem.* **2009,** *62*, (8), 762-785.
32. Massardier-Nageotte, V.; Pestre, C.; Cruard-Pradet, T.; Bayard, R., Aerobic and anaerobic biodegradability of polymer films and physico-chemical characterization. *Polym. Degrad. Stab.* **2006,** *91*, (3), 620-627.
33. Shah, A. A.; Hasan, F.; Hameed, A.; Ahmed, S., Biological degradation of plastics: A comprehensive review. *Biotechnol. Adv.* **2008,** *26*, (3), 246-265.
34. International, A., ASTM Standard D6954-04. In *Standard Guide for Exposing and Testing Plastics that Degrade in the Environment by a Combination of Oxidation and Biodegradation*, 2013.
35. International, A., ASTM Standard D7473 − 12. In *Standard Test Method for Weight Attrition of Plastic Materials in the Marine Environment by Open System Aquarium Incubations*, 2012.
36. Wu, C.-S., A comparison of the structure, thermal properties, and biodegradability of polycaprolactone/chitosan and acrylic acid grafted polycaprolactone/chitosan. *Polymer* **2005,** *46*, (1), 147-155.
37. Li, S.; Liu, L.; Garreau, H.; Vert, M., Lipase-Catalyzed Biodegradation of Poly(ε-caprolactone) Blended with Various Polylactide-Based Polymers. *Biomacromolecules* **2003,** *4*, (2), 372-377.
38. Liu, L.; Li, S.; Garreau, H.; Vert, M., Selective Enzymatic Degradations of Poly(L-lactide) and Poly(ε-caprolactone) Blend Films. *Biomacromolecules* **2000,** *1*, (3), 350-359.
39. Reed, R. B.; Goodwin, D. G.; Marsh, K. L.; Capracotta, S. S.; Higgins, C. P.; Fairbrother, D. H.; Ranville, J. F., Detection of single walled carbon nanotubes by monitoring embedded metals. *Environ. Sci.: Processes Impacts* **2013,** *15*, (1), 204-213.
40. Zhang, S.; Li, L.; Kumar, A., *Materials characterization techniques*. CRC press: 2008.
41. Wang, Y.; Rodriguez-Perez, M. A.; Reis, R. L.; Mano, J. F., Thermal and thermomechanical behaviour of polycaprolactone and starch/polycaprolactone blends for biomedical applications. *Macromol. Mater. Eng.* **2005,** *290*, (8), 792-801.
42. Patricio, T.; Bartolo, P., Thermal Stability of PCL/PLA Blends Produced by Physical Blending Process. *Procedia Eng.* **2013,** *59*, 292-297.
43. Sobkowicz, M. J.; Sosa, R.; Dorgan, J. R., Supramolecular bionanocomposites, part 2: Effects of carbon nanoparticle surface functionality on polylactide crystallization. *J. Appl. Polym. Sci.* **2011,** *121*, (4), 2029-2038.
44. Goodwin, D. G.; Xia, Z.; Gordon, T. B.; Gao, C.; Bouwer, E. J.; Fairbrother, D. H., Biofilm development on carbon nanotube/polymer nanocomposites. *Environmental Science: Nano* **2016**.

Chapter 7. Mixed Culture Biodegradation of Carbon Nanotube/Polymer Nanocomposites

7.1. Mixed Cultures

In the environment, most microorganisms live in dynamic consortia with a variety of other species, rather than existing as monocultures.[1] Microbial community members possess unique and often complementary phenotypes, which facilitate survival and adaptation of the entire community to a wide variety of environmental conditions.[2] These communities possess dynamic populations of bacteria, whose total number and relative abundances vary depending on environmental pressure.[3] The movement and transformation of chemical substances throughout the environment is often mediated by microorganisms through cascading metabolic interactions; external chemicals become substrates for microbial growth, subsequent metabolites are cycled between different organisms, and unutilized chemicals accumulate as waste products.[2, 4]

In terms of biodegradation, microbial metabolism can be broadly classified based on the terminal electron acceptor used for growth.[2, 5] Aerobic organisms utilize oxygen as an electron acceptor, and are typically characterized by rapid growth rates due to high energetic reduction potentials.[2] Anaerobic microbes can use less energetically favorable electron accepters such as nitrate, sulfate, and even organic substrates in place of oxygen.[5] Anaerobic microorganisms are typically found in locations with depleted oxygen, such as subsurface sediments, deep waters, digested sludge in wastewater treatment plants, and soils.[5, 6] Anaerobic biodegradation processes are described in more detail in Chapter 8. In mixed cultures, microbial diversity is usually high enough to utilize a variety of electron acceptors, with preferential utilization of the most

energetically favorable available acceptors (oxygen) before the least favorable acceptors (organic substrates).[2] Overall, the electron acceptor in biodegradation processes is involved in driving the metabolic machinery that allows the cell to survive and divide.[5, 6]

The carbon necessary for microorganism growth is obtained from degrading organic molecules (heterotrophy) or fixing inorganic carbon (autotrophy).[5] For most heterotrophic organisms (organotrophs), this organic carbon source also serves as the electron donor providing the energy to drive cell metabolism – other specialized organisms utilize light (photoheterotrophy) and inorganic chemicals (chemoheterotrophs) to produce electrons.[2, 5] Some organic substrates are less energetically favorable to degrade than others, requiring a larger activation energy for bond-breaking due to the type of reaction or steric hindrance limiting access to the substrate by enzymes. Many organic polymers can be used as the carbon source for cell growth; however they can vary in terms of the ease with which they are reduced to smaller components and metabolized by cells.[7] In mixed cultures, microorganisms are able to degrade a wide variety of substrates through adaptation and enrichment of certain microbial species that can metabolize the substrate involved.[8] These robust conditions are ideal for rapidly biodegrading a variety of polymer matrices and are more accurately representative of the diverse population of microorganisms a polymer will encounter when it is disposed of in locales such as landfills, surface waters, soils, sediments, and wastewater treatment plants.[9-13]

Similar to polymer waste, carbon nanotube/polymer nanocomposites (CNT/PNCs), or polymers containing a CNT filler for structural and functional property enhancement, are expected to end up in the same environmental matrices following

consumer use. Since CNTs are known to persist in the environment and their ecotoxicity is of concern, the benefits of using a CNT additive during consumer use may therefore be compromised by the ultimate fate of the CNT/PNC when it biodegrades in landfills, surface waters, and/or wastewater treatment plants.[14-18] Previously, we have investigated biodegradation of CNT/PNCs under model conditions using a single culture (Chapter 6). In this study, CNT/PNCs were exposed to mixed cultures for greater environmental relevance.

In contrast to single cultures, mixed cultures tend to be more robust and able to acclimate to environmental contaminants, even those that are toxic.[6, 19, 20] This is why microorganisms, oftentimes enriched to degrade a substrate, are used in tandem with other microorganisms to bioremediate chemical spill sites.[21] Sediment from contaminated field sites and wastewater from treatment plants are two commonly used mixed culture sources for bioremediation due to the microbes' prolonged exposure and acclimation to a diverse number of contaminants, oftentimes at a high concentration.[22-24] These mixed communities have a high diversity of species and metabolic pathways, which are ideal for assaying the biodegradability of various compounds purposes.[25-27] Although robust, mixed cultures are more complex and challenging to control and characterize in laboratory experiments than single cultures, especially from culture to culture mainly due to varying dilution in the wastewater stream.[28]

Since mixed cultures can acclimate to some toxic substances, the biodegradability of polymers containing CNTs might differ under single and mixed culture conditions. Under single culture conditions, CNTs were shown to have antimicrobial properties when accumulated at the surface of CNT/poly-ε-caprolactone (PCL) nanocomposites and

slower biodegradation rates as a function of CNT mass loading in *Pseudomonas aeruginosa* (*P. aeruginosa*) cultures.[18, 29] Furthermore, CNT/PCL nanocomposites containing a CNT mass loading greater than 2% w/w were fairly persistent under conditions that could fully degrade PCL, with approximately 50% of the polymer matrix remaining after 26 weeks of *P. aeruginosa* exposure (Chapter 6). In this study, the biodegradation rate and persistence of CNT/PNCs was investigated in mixed culture and compared to single culture conditions. Primary effluent, or wastewater that has undergone physical screening and sedimentation, from the Back River Wastewater Treatment Plant (Baltimore, MD) was used as the inoculum since it contains a broad range of microorganisms acclimated to a variety of compounds in the domestic waste stream.[9-12] It was also chosen since a fraction of CNT/PNCs will end up in Wastewater Treatment plants (WWTP) from sewer and rainwater collection systems and from consumer product disposal down drains.[30] In order to examine the effect of CNTs on the biodegradation process, we conducted mass loss measurements of CNT/PNCs. Mass loss is one of several quantitative methods, such as CO_2 detection and oxygen consumption, typically used to assess aerobic biodegradation of pure polymers.[13, 31-36] The decision to use mass loss was also motivated by its ease of use for a large set of samples and previous use of a similar approach by other researchers for in situ biodegradability tests of plastic materials under aerobic composting environments (ASTM D 6003-96).[37, 38]

For comparison, the same solution blended multi-wall CNT (MWCNT)/PCL nanocomposites used under single culture (*Pseudomonas aeruginosa*) conditions (Chapter 6) were exposed to mixed cultures in this study. PCL and MWCNTs were also chosen since 1) they could be blended to produce CNT/PNCs with homogenously

dispersed MWCNTs, 2) MWCNTs are most common in products, and 3) PCL is biodegradable on an experimentally relevant time scale.[15, 39-44] MWCNT/PCL nanocomposites prepared using melt-mixing, a more industrially relevant production method than solution blending, were also exposed to aerobic mixed cultures for mass loss studies.[45] The purpose of using melt-mixed MWCNT/PCL nanocomposites in addition to solution blended MWCNT/PCL nanocomposites was multi-faceted: 1) to biodegrade MWCNT/PCL nanocomposites that did not contain any surfactants such as ethyl cellulose (EC), which is required for CNT dispersion in solution blending techniques and 2) to biodegrade thicker MWCNT/PCL nanocomposites to determine if similar biodegradation trends were observed when more PCL was present in the bulk of the CNT/PCL nanocomposite.

7.2. Experimental

7.2.1. Solution Blended MWCNT/PCL Nanocomposites

PCL (4% w/w EC) and pristine MWCNT/PCL nanocomposites (4% w/w EC) containing MWCNT (NanoLab Inc.) loadings of 0.1, 0.5, 1, 2, and 5% w/w were prepared using the same solution blending methods described in Chapter 6.

7.2.2. Melt-Mixed MWCNT/PCL Nanocomposites

PCL and pristine MWCNT/PCL nanocomposites containing MWCNT (NanoLab Inc.) loadings of 0.1, 0.5, and 2% w/w were prepared using melt-mixing/extrusion as described in Chapter 2. 1 mm thick sheets were cut into 25 mm circles (also called coupons) for biodegradation experiments.

7.2.3. MWCNT/PCL Nanocomposite Characterization

Solution blended and melt-mixed MWCNT/PCL nanocomposites were characterized using scanning electron microscopy (SEM) and differential scanning

calorimetry (DSC) for surface morphology and fraction of crystallinity, respectively, as described in Chapter 6. Specifically, melt mixed, 2% w/w MWCNT/PCL nanocomposites before and after 15 min of acetone soaking as well as melt-mixed PCL were imaged with SEM in this chapter. Furthermore, 2% w/w MWCNT/PCL nanocomposites before and after 56 days of continuous primary effluent biodegradation were imaged with SEM in this chapter. Lastly, DSC analysis of melt-mixed MWCNT/PCL nanocomposites was performed to assess the fraction of crystallinity as a function of MWCNT loading in all melt-mixed MWCNT/PCL nanocomposites. DSC procedures are described in Chapters 5 and 6.

7.2.4. Mixed Culture Inoculum

Primary effluent, or wastewater that had been screened and gone through one stage of settling to remove solids and skimming to remove oil and grease, was the mixed culture inoculum used in this study. Primary effluent was collected from the Back River WWTP in Baltimore, MD and was used within the same day to setup biodegradation studies. If the primary effluent was stored prior to use later in the day, it was kept in the 4 °C refrigerator.

7.2.5. Aerobic Biodegradation of Solution Blended MWCNT/PCL Nanocomposites

Individual MWCNT/PCL nanocomposites with CNT loadings of 0, 0.5, 1, 2, 5, and 10 % (w/w) were placed into 125 mL flasks. 100 mL of BMM, containing 0.200 g/L sodium acetate trihydrate (ReagentPlus®, ≥99.0%, Sigma-Aldrich) (low C BMM) and 10% v/v primary effluent (described in Chapter 5 and 6) was then partitioned into each flask and incubated at 28 °C under static conditions. For microbial population consistency, PCL and MWCNT/PCL nanocomposites in primary effluent were run in sacrifice mode, meaning that all sample sets (seven total) were inoculated at the same

time with one batch of primary effluent and each set was removed at a different time point.[46, 47] A full set of PCL and MWCNT/PCL nanocomposites (0 – 5% w/w) was removed at each sampling time point, with a total of 7 sampling time points ranging from 1 to 55 days. Sacrifice mode was used to 1) minimize changes in the initial inoculum obtained from the WWTP and 2) capture shorter time points more efficiently since preliminary results indicated that mixed culture biodegradation of PCL was much more rapid than single culture biodegradation, which is outlined in Chapter 6. Additionally, for every CNT loading used, triplicate samples were setup for each sampling time point. An abiotic control was setup for PCL and MWCNT/PCL nanocomposites of each loading used. Abiotic controls were sterilized with 70% ethanol for 5 min, placed into 125 mL flasks containing 100 mL sterile BMM, and incubated at 28 °C for 55 days, corresponding to the longest time point used in the biodegradation experiments. At the end of each selected time point, the samples were gently removed from their flasks and dried in a desiccator for at least 24 h to remove all of the adsorbed water. Samples were then weighed (Mettler AT261 DeltaRange, ± 0.03 mg) and photographed.

The sample set that was removed at Day 55 in sacrifice mode was further biodegraded in sampling mode, where samples were re-inoculated with fresh primary effluent bi-weekly after removal, drying, weighing, and photographing. The Day 55 set was run for 10 more weeks in sampling mode, providing a new batch of primary effluent to the samples every two weeks to maximize biodegradation potential. Although the primary effluent cultures varied from time point to time point based on the available nutrients and dilution due to rainwater entering the WWTP, all samples in the Day 55 set experienced the same culture conditions at each time point.

7.2.6. Dissolved Oxygen Measurements

Dissolved oxygen (DO) concentrations (mg/L) were measured in experiments that contained primary effluent in contact with solution-blended PCL and MWCNT/PCL nanocomposites of varied CNT loading to assess the oxygen availability. A Hach IntelliCAL™ standard luminescent/optical DO probe (DO LDO101, 0.2-20 mg/L range, connected to a Hach multi-meter (HQ40D)) was used to make the measurements. The DO probe was sterilized with ethanol prior to use and calibrated with water saturated air according to manufacturer specifications. Triplicate DO measurements were collected at the onset of biodegradation and at every time point used in sacrifice mode (seven time points from 0 – 55 days).

7.2.7. Aerobic Biodegradation of Melt-Mixed MWCNT/PCL Nanocomposites

Melt-mixed PCL and MWCNT/PCL nanocomposites were biodegraded according to a modified version of the procedure used for the solution blended MWCNT/PCL nanocomposites. In contrast to the solution blended PCL and CNT/PCL nanocomposite sampling protocol, one set of melt-mixed PCL and MWCNT/PCL nanocomposites were run in sampling mode the entire length of the experiment, but the primary effluent culture was not refreshed for the first 84 days to minimize changes in the initial inoculum obtained from the WWTP without setting up an enormously large set of samples. Instead, the samples were removed with long, sterile tweezers, desiccated, weighed, and added back to the culture flask they originated from after every two weeks of biodegradation. After 84 days, the melt-mixed PCL and MWCNT/PCL nanocomposites were run in sampling mode with fresh primary cultures added to the flasks bi-weekly. This was done to accelerate biodegradation of the thick MWCNT/PCL nanocomposites and is the same method used for the solution blended samples in sampling mode. These samples were

aerated at 28 °C and 125 rpm to accelerate biodegradation of the thick samples in contrast to the static conditions used for solution blended MWCNT/PCL nanocomposite biodegradation.

7.3. Results and Discussion

Previously, solution blended MWCNT/PCL nanocomposites of varied MWCNT loading were characterized for surface morphology with SEM (Chapter 6). In all MWCNT/PCL nanocomposites, MWCNTs were mostly buried below the MWCNT/PCL nanocomposite surface. However, individual MWCNTs were observed protruding from the MWCNT/PCL nanocomposite surface in random areas, indicating that MWCNTs were homogeneously distributed throughout the PCL matrix. Furthermore, MWCNT/PCL nanocomposites were uniformly dark upon visual inspection, with minimal signs of aggregation (Chapter 6). MWCNT/PCL nanocomposites prepared using melt-mixing, a more industrially relevant CNT/PNC production method, were also characterized with SEM at the highest MWCNT loading prepared (2% w/w) and in the absence of CNTs (pure PCL). SEM images of PCL and 2% w/w MWCNT/PCL nanocomposites prepared from melt-mixing/extrusion are shown in Figure 7.1a. Similar to the solution blended MWCNT/PCL nanocomposites, the MWCNTs were buried below the 2% w/w MWCNT/PCL nanocomposite surface, which looked similar to PCL, and CNT dispersion quality was challenging to assess. Since the melt-mixed MWCNT/PCL nanocomposite were approximately 20x thicker than the solution blended MWCNT/PCL nanocomposites, a melt-mixed 2% w/w MWCNT/PCL nanocomposite was soaked in acetone for 15 min to dissolve away some of the polymer surface (~6% mass loss). As a result of dissolution, the distribution of MWCNTs in the polymer matrix could be imaged

using SEM and a fairly homogeneous distribution of MWCNTs within the polymer matrix was observed (Figure 7.1c-d).

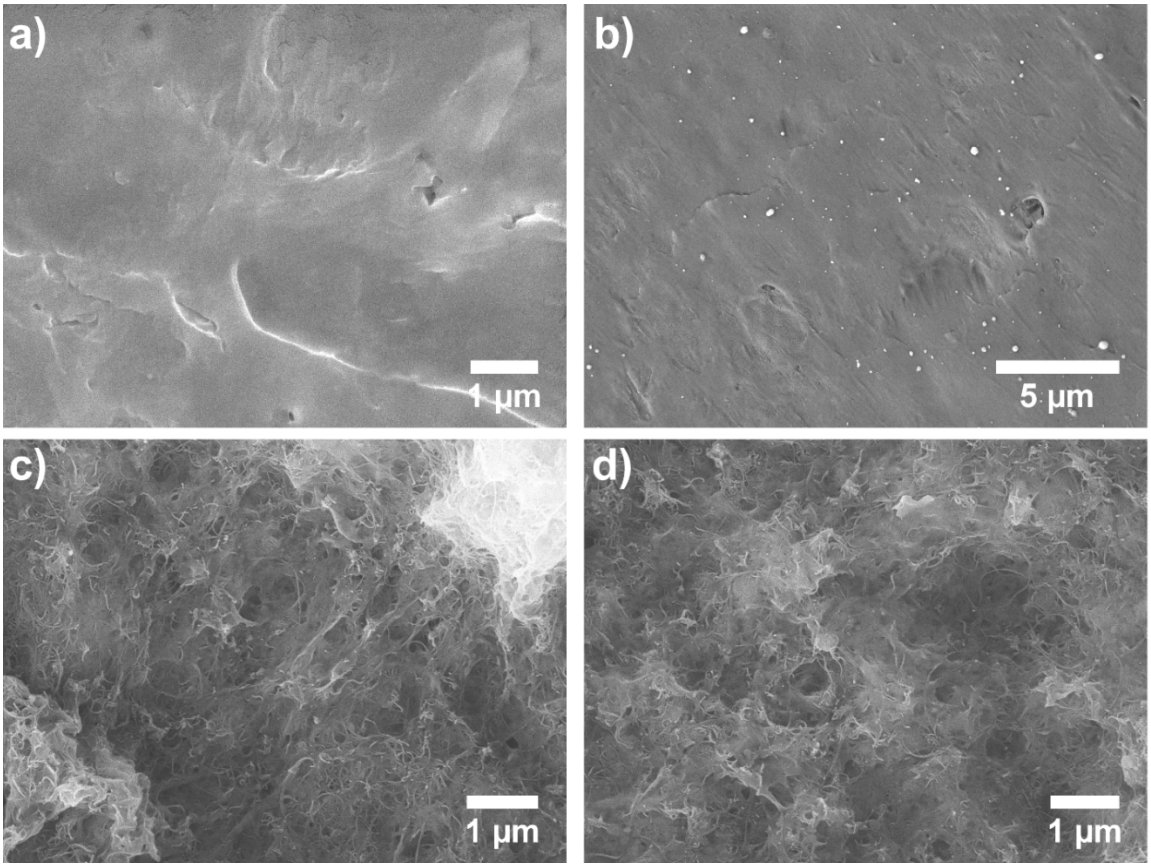

Figure 7.1. SEM images of melt-mixed a) PCL and a 2% w/w MWCNT/PCL nanocomposite b) before and c-d) after a 15 min acetone soak (two separate areas) to show the CNT dispersion quality below the MWCNT/PCL nanocomposite surface.

MWCNT/PCL nanocomposites were also characterized with DSC. The fraction of crystallinity was considered important since a greater fraction of this energetically stable conformation can make the polymer more challenging to enzymatically transform and as a result, can lower the biodegradation rate. Since the incorporation of additives has been shown to alter polymer crystallinity, the effect of CNT incorporation on polymer crystallinity was evaluated to determine whether or not this parameter played a role in CNT/PCL nanocomposite biodegradability as a function of CNT loading.[48] In Chapter 6,

solution blended PCL and LO-MWCNTs were analyzed with DSC from 0.1 – 2% w/w. In this case, the effect of CNT addition on PCL crystallinity was negligible.

Table 7.1. DSC measurements of melt-mixed MWCNT/PCL nanocomposites to assess the fraction of crystallinity as a function of MWCNT loading.

Sample	X_C (%)
PCL	51.7
0.1% w/w	50.7
0.5% w/w	51.5
1% w/w	51.8

As compared to the crystallinity of solution blended LO-MWCNT/PCL nanocomposites, melt-mixed PCL and MWCNT/PCL nanocomposites also did not change in crystallinity with CNT loading (Table 7.1). Although solution blended MWCNT/PCL nanocomposites had not yet been analyzed with DSC at the time this thesis was written, it is most likely that the crystallinity does not vary with CNT loading based on the lack of crystallinity change with CNT loading in the two disparate sets of CNT/PCL nanocomposites already run, each with a different CNT type.

For the melt-mixed samples, the fraction of crystallinity was around 50%. These % crystallinity values are similar to those observed for the solution blended PCL and LO-MWCNT/PCL nanocomposites. However, the solution blended samples contain a small amount of ethyl cellulose (EC) surfactant (4% w/w EC), which has been shown to lower the crystallinity of pure PCL in Chapter 5. In contrast, the melt-mixed samples do not contain EC, and have % crystallinity values slightly lower than pure PCL prepared with solution blending. Thus, the absence of EC in melt-mixed samples has the potential to enhance the rate of MWCNT/PCL nanocomposite biodegradation rate relative to solution blended MWCNT/PCL nanocomposites. However, this potential rate enhancement is not expected to be apparent for melt-mixed samples since their surface area to volume ratio is

much lower than it is for solution blended MWCNT/PCL nanocomposites as a result of a 20x thickness difference. In summary, the crystallinity did not change appreciably with CNT loading for both the solution blended and melt-mixed MWCNT/PCL nanocomposites, indicating that CNTs will not affect the biodegradability of the polymer matrix as a result of crystallinity changes.

In order to determine the biodegradation rate of MWCNT/PCL nanocomposites as a function of CNT loading in an aerobic mixed culture of microorganisms, mass loss measurements were made after MWCNT/PCL nanocomposite exposure to primary effluent. Mass loss of solution blended MWCNT/PCL nanocomposites with varied CNT loadings (0, 0.5, 2, and 5% w/w) are shown for different exposure times in Figure 7.2. In the left-hand portion of the plot (Days 1 – 55), MWCNT/PCL nanocomposites were removed at different time points to measure mass loss due to biodegradation. As a confirmatory measure of MWCNT/PCL nanocomposite biodegradation assessed using mass loss, dissolved oxygen measurements were made between Day 0 and Day 55 to determine the oxygen demand as a result of substrate biodegradation within the sample flasks.

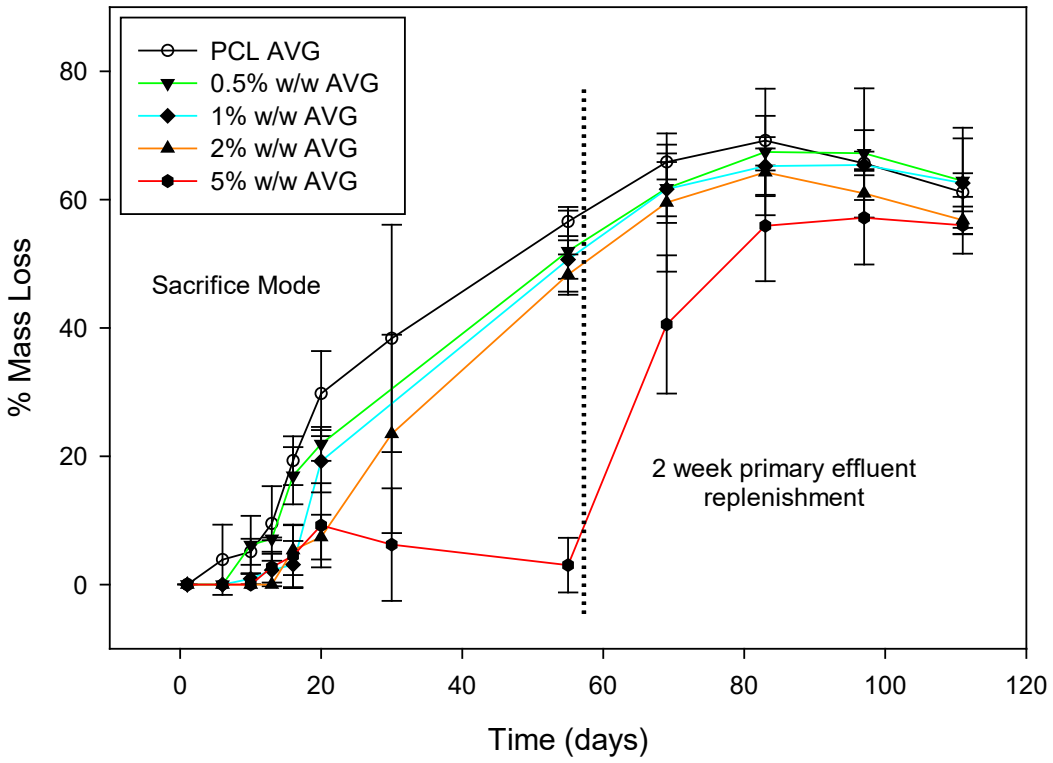

Figure 7.2. A plot of solution blended MWCNT/PCL nanocomposite mass loss for 0, 0.5, 1, 2, and 5% w/w MWCNT/PCL nanocomposites. The samples removed at Day 55 in sacrifice mode were replaced in sampling mode (sampling for mass loss and addition of fresh primary effluent every 14 days) for the remaining time points to the right of the dotted line.

At Day 0, the dissolved oxygen levels were depleted due to metabolism of the supplemental acetate carbon source under static conditions (solution not aerated). It is most likely that this oxygen depletion is a result of the supplemental acetate and not the chemical oxygen demand of the organic material in the wastewater, since the dissolved oxygen levels were saturated (~8 mg/L dissolved O_2) prior to acetate addition. Furthermore, the dissolved oxygen concentrations dropped within an hour of acetate addition and rebounded to a constant O_2 saturated condition for an acclimation period of approximately 5 days, after which oxygen consumption increased again (Figure 7.3).

This is consistent with the time at which mass loss became exponential for all solution blended MWCNT/PCL nanocomposite samples (Figure 7.2). Gradually, the dissolved oxygen concentration returned to oxygen saturated conditions as the rate of MWCNT/PCL nanocomposite mass loss decreased. However, after sampling seven times throughout the course of 55 days, the mass loss plots indicated that PCL and MWCNT/PCL nanocomposites were continuing to lose mass and had not completely degraded (Figure 7.2).

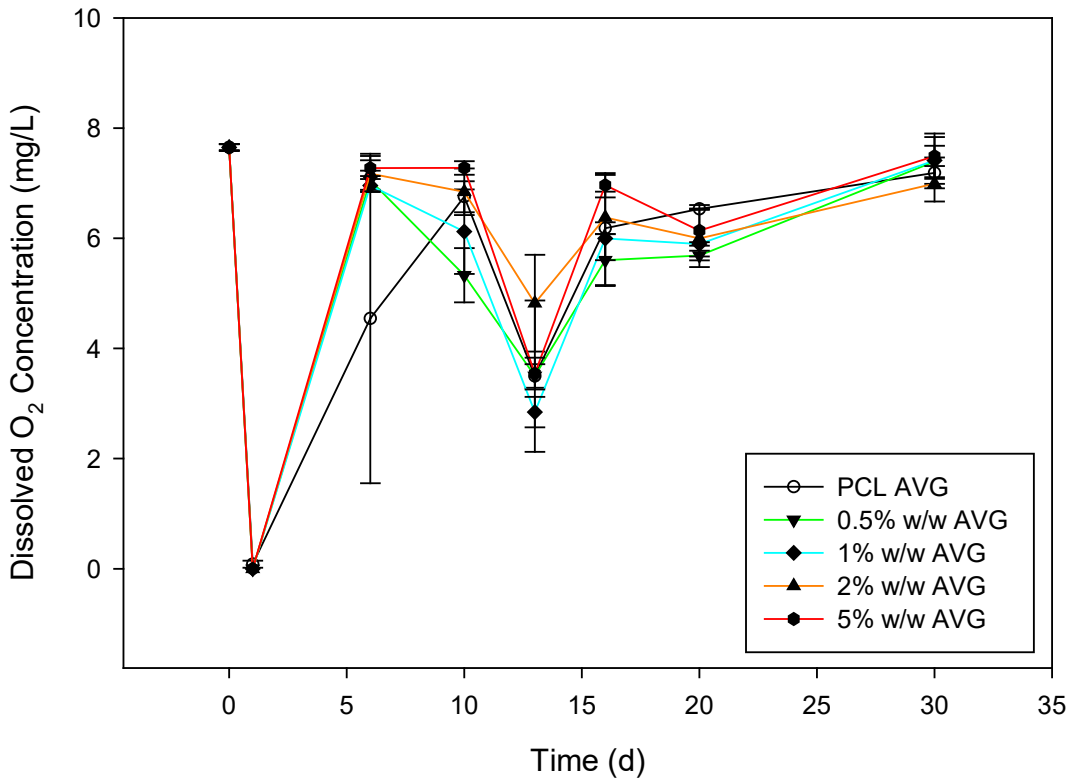

Figure 7.3. Dissolved oxygen consumption as a function of MWCNT/PCL nanocomposite loading for each sacrifice mode time point.

For this reason, the samples removed at Day 55 (Figure 7.2) were submerged in fresh primary effluent for two more weeks. This was repeated every two weeks for several

more time points to maximize biodegradation via mass loss (Figure 7.2). Although the primary effluent could vary in microbial cell density from time point to time point under these conditions, all of the samples were exposed to a consistent culture at each time point. In fact, the dilution of the first primary effluent culture in the wastewater stream is most likely the reason for the fairly slow biodegradation rate observed, as preliminary tests indicated that another batch of primary effluent reached the same mass loss in approximately half the time of this culture (Figure 7.4). From this information, the time scale of PCL biodegradation under mixed culture conditions is on the order of 30-83 days, depending on the primary effluent batch used.

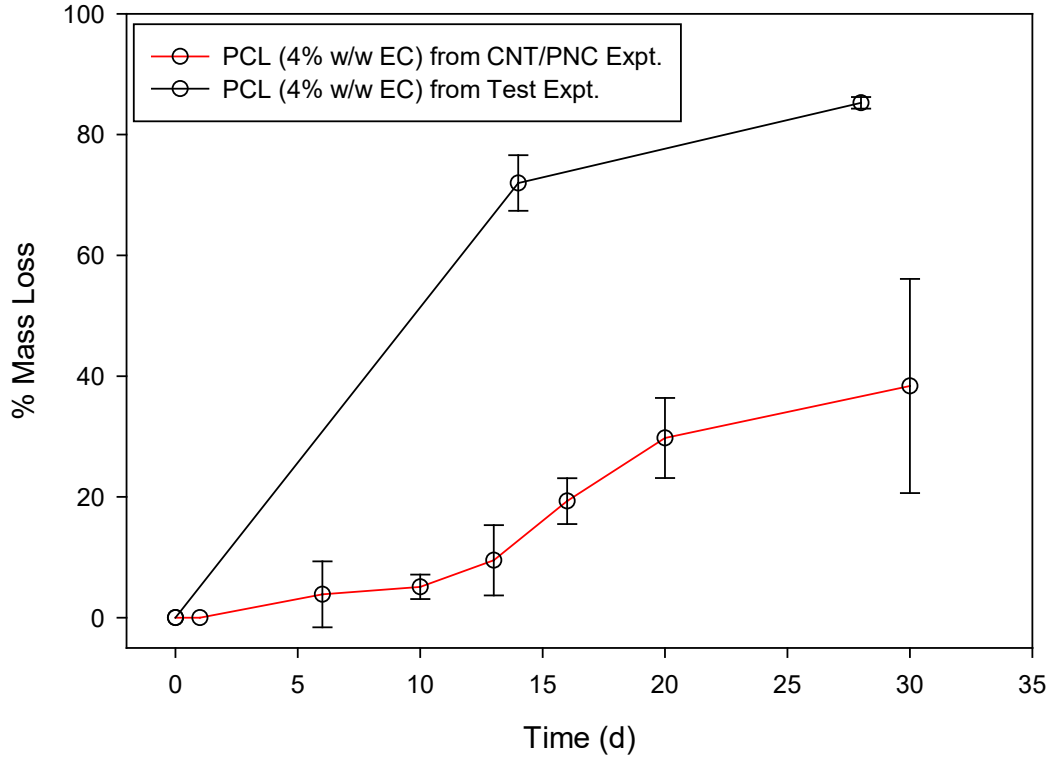

Figure 7.4. A comparison of mass loss for solution blended PCL from **Figure 7.2** to solution blended PCL inoculated with a different batch of primary effluent to show variability in PCL biodegradation rates.

In terms of MWCNT loading, 0.5% w/w biodegraded at a similar rate to that of PCL (Figure 7.2). For 2% w/w, the biodegradation rate is suppressed relative to PCL, mostly at the beginning time points of the experiment (Figure 7.2). At 5% w/w, there is a significant inhibition with less than 10% mass loss over the course of 55 days. However, all MWCNT/PCL nanocomposites reached similar levels of mass loss, even at 5% w/w, at time points longer than 55 days when primary effluent was replenished bi-weekly. The 5% w/w most likely required a replenishment of primary effluent to reach the exponential phase of biodegradation due to the low abundance of microbes in the initial primary effluent culture: with a high mass fraction of CNTs, the initial culture might have required more time to acclimate to the PCL substrate or lost its viability. The mass loss plateau of 5% w/w is probably lower relative to the other CNT loadings due to the larger initial CNT mass that is remaining (Figure 7.2). This phenomenon will be further explored in Chapter 8. Further investigation as to why the mass loss plateaued around 70% is also underway (Figure 7.2). It is possible that byproducts from PCL biodegradation have become recalcitrant under mixed culture conditions. Furthermore, the size of the underlying aluminum foil used to collect the samples was large (~ 6 cm^2) and has been reduced to minimized biomass accumulation in ongoing studies. This biomass accumulation is visually apparent and can reasonably explain the slight decrease in mass loss at the plateau for all of the samples. Overall, the PCL matrix of MWCNT/PCL nanocomposites reached the same level of biodegradation but at a decreased rate relative to the PCL reference as a function of CNT loading, potentially due

to the cytotoxicity and accumulation of CNTs at the PCL surface that can lead to biofouling and decreased enzymatic access to the PCL matrix.

Although the onset of biodegradation might occur at a shorter time point in a more densely populated primary effluent inoculum, the CNTs would still be expected to inhibit this process as a function of CNT loading. This is supported by the melt-mixed MWCNT/PCL nanocomposite data shown in Figure 7.4, which was collected with a different initial primary effluent culture. Relative to solution blended samples, thicker melt-mixed samples could not degrade as rapidly due their lower surface area to volume ratio. These MWCNT/PCL nanocomposites were roughly 20 times larger in mass (24 mm x 1 mm) than the solution blended MWCNT/PCL nanocomposites (30 mm x 20-30 μm). For acceleration of biodegradation, melt-mixed samples were aerated by shaking at 125 rpm. In contrast to the solution blended MWCNT/PCL nanocomposites which were run in sacrifice mode, one melt-mixed sample set was continuously removed, desiccated, weighed, and put back on in the same culture at different time points on the left-hand portion of the plot (< 84 days). To accelerate the experiment further with a slight loss of culture consistency, the samples were exposed to a fresh batch of primary effluent every two weeks after 84 days in one inoculum, as shown on the right-hand side of the plot. Overall, the differences in mass loss rate as a function of CNT loading (0 – 10% w/w) are still most apparent at the beginning of the experiment (< 84 days) despite the replenishment of primary effluent. Although there is no apparent lag time at the beginning of the experiment, the first sampling was at day 14 rather than day 1, which was used in the solution blended MWCNT/PCL nanocomposite sampling scheme.

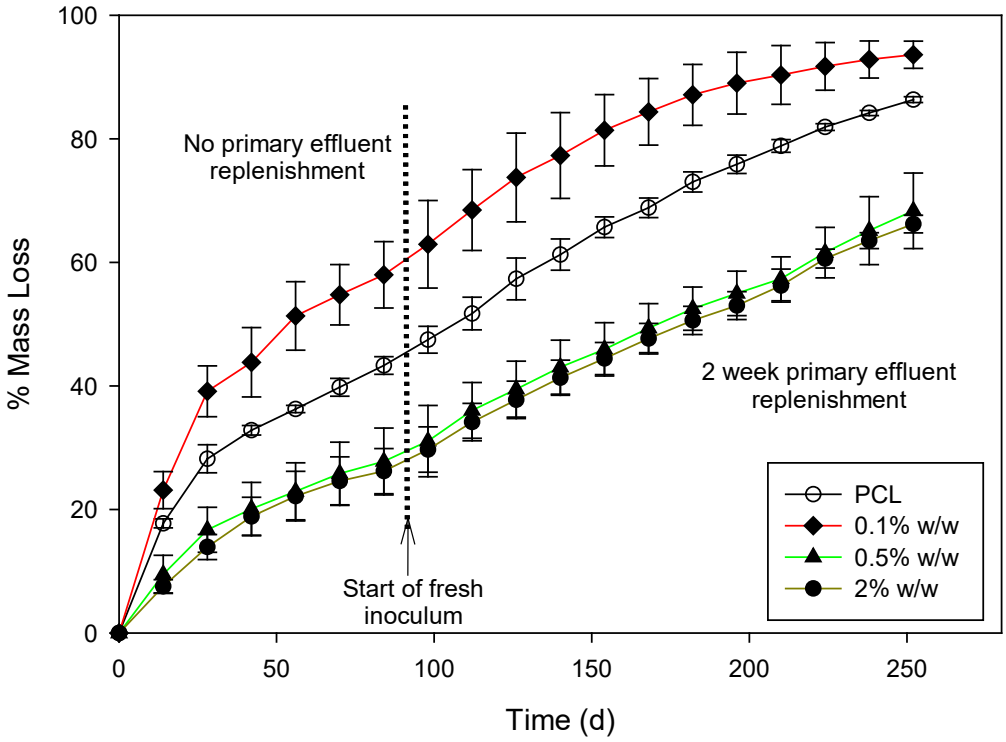

Figure 7.5. A plot of melt-mixed MWCNT/PCL nanocomposite mass loss for 0, 0.1, 0.5, and 2% w/w MWCNT/PCL nanocomposites. The samples removed at day 84 in sacrifice mode were put back on in sampling mode (sampling for mass loss and addition of fresh primary effluent every 2 weeks) for the remaining time points to the right of the dotted line.

As is the case with solution blended MWCNT/PCL nanocomposites, the CNTs retard but do not prevent biodegradation of melt-mixed MWCNT/PCL nanocomposites, even at higher CNT loadings. One further observation is that the 0.1% w/w MWCNT/PCL nanocomposites biodegraded at a faster rate than the PCL samples. This could be a result of poor MWCNT percolation, or connection, within the polymer matrix in the absence of EC at a low MWCNT loading which could enhance enzymatic access to polymer and interfacial regions. This observation was not apparent for low MWCNT loadings in solution blended MWCNT/PCL nanocomposites, but further investigation

into the conditions with which a MWCNT/PCL nanocomposite of low CNT loading will biodegrade faster than the pure polymer are underway. For all melt-mixed MWCNT/PCL nanocomposites, MWCNT/PCL nanocomposites were much thicker and could permit a much greater accumulation of CNTs at the MWCNT/PCL nanocomposite surface relative to solution blended MWCNT/PCL nanocomposites during the biodegradation process. SEM images of MWCNT accumulation at the surface of 2% w/w MWCNT/PCL nanocomposites are shown after approximately 55 days of continuous exposure to primary effluent (Compare Figure 7.6a and b). Despite the significant difference in thickness of melt-mixed samples to solution blended samples, polymer entrapment below the accumulated CNTs and increased cytotoxicity due to the high concentration of surface CNTs did not render the MWCNT/PCL nanocomposites persistent. Instead, the CNTs simply slowed the MWCNT/PCL nanocomposite biodegradation rate as a function of CNT loading. Furthermore, consistent with *P. aeruginosa* studies (Chapter 6), biofilms of microorganisms from primary effluent were prevalent on many areas of the surface despite the accumulation of MWCNTs (Figure 7.6b). Furthermore, the surface morphology became rougher, with many cavities present at the surface following biodegradation (Figure 7.6c). Although MWCNT/PCL nanocomposite biodegradation was not prevented with thicker, melt-mixed CNT/PNCs, the duration of MWCNT/PCL nanocomposite biodegradation was much longer than for the solution blended MWCNT/PCL nanocomposite biodegradation (>252 days versus 83 days).

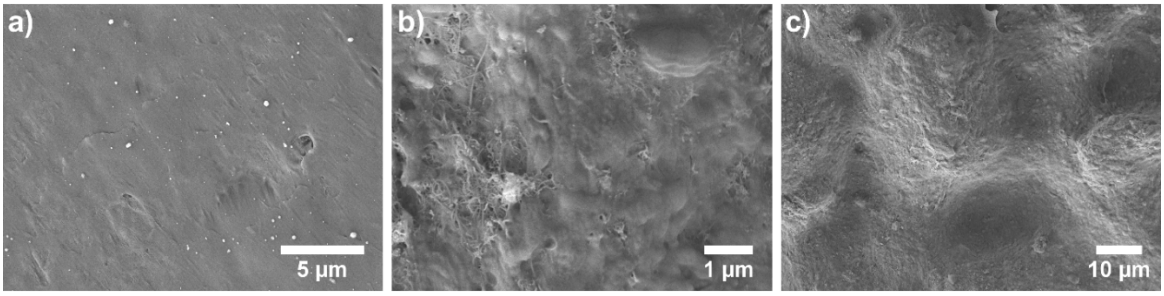

Figure 7.6. SEM images of melt-mixed 2% w/w MWCNT/PCL nanocomposite surfaces a) before and after b-c) 55 days of primary effluent exposure.

In comparison to single culture conditions, MWCNT/PCL nanocomposites biodegraded differently in mixed culture (Figure 7.7). Although not directly comparable in terms of time because of differences in sampling and batch-to-batch inconsistencies in primary effluent, MWCNT/PCL nanocomposites qualitatively degraded at a more rapid time scale in mixed culture than in single culture. Furthermore, the aerobic mixed culture appears to be less sensitive to the presence of CNTs in the PCL matrix than the single culture of *P. aeruginosa*. At lower CNT loadings, the inhibition is much more apparent in single culture than in mixed culture as evidenced by the mostly uninhibited biodegradation rate of 1% w/w MWCNT/PCL nanocomposites under mixed culture conditions and the suppressed rate of 1% w/w MWCNT/PCL nanocomposites in the presence of *P. aeruginosa* (Figure 7.7). Additionally, it is clear from the mass loss plots that a high CNT loading such as 2 and 5% w/w degrades very gradually over time under single culture conditions while it degrades much more rapidly (20-40 d) under mixed culture conditions once the culture has acclimated.

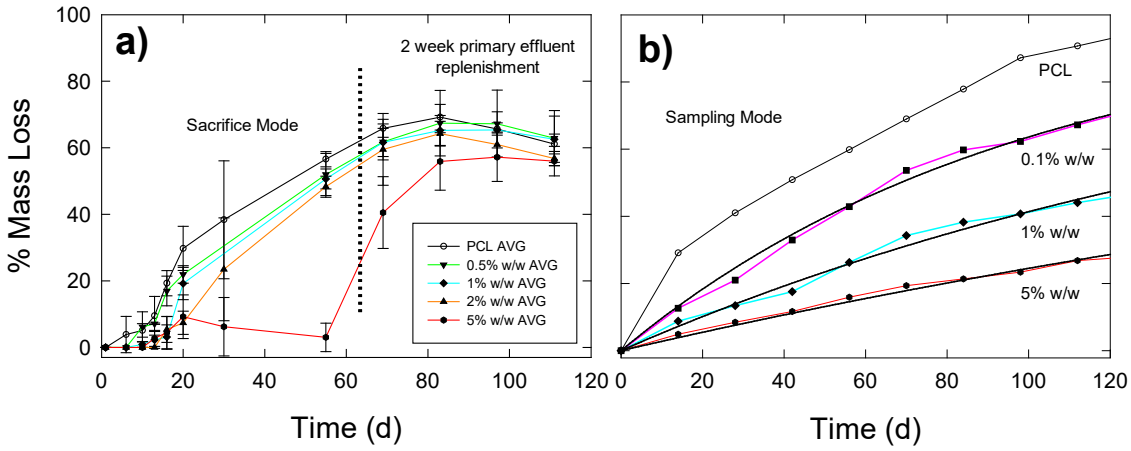

Figure 7.7. A comparison of solution blended MWCNT/PCL nanocomposite mass loss under a) mixed culture b) and single culture conditions. The mass loss of mixed culture/PCL nanocomposites is an average of three replicate samples and the mass loss of the single culture/PCL nanocomposites is one replicate, with the average rate constants and goodness of fits for four replicates shown in Appendix 6.

The difference in sensitivity of the aerobic cultures to the presence of CNTs in the PCL can be attributed to several factors. First, it has been shown that CNTs at the surface of a CNT/PNC are cytotoxic to *P. aeruginosa* in direct contact or proximity.[18] A dead layer of *P. aeruginosa* can coat the surface of the CNT/PNCs, blocking access to the microorganisms that have been shown to actively form a biofilm above the dead layer.[29] Since the dead layer most likely limits the access of the active biofilm to the PCL, the rate of PCL matrix biodegradation is most likely suppressed as a result. In contrast, a subset of the microorganisms in mixed culture are likely more recalcitrant to CNT cytotoxicity than a single culture as a result of physiological diversity. For example, several CNT toxicity studies have suggested that gram negative bacteria are more resistant to toxicity than gram positive bacteria due to the presence of an outer cell membrane.[49, 50] Furthermore, the presence of many diverse metabolic processes in mixed

cultures can lead to more rapid biodegradation of the PCL matrix, lowering the activation energy of the process and as a result, improving the ability of biodegradation processes to overcome the inhibitory effects of CNTs. Overall, MWCNT/PCL biodegradation in aerobic mixed culture shows similar trends as those observed in single culture aerobic biodegradation, but the rate of biodegradation is enhanced and the sensitivity of the culture conditions to CNTs are reduced under aerobic mixed culture conditions. A follow-up to this study should include a survey of the microbial diversity before, during, and after degradation to determine which specific bacteria are responsible for PCL degradation and which are more recalcitrant to the presence of CNTs.

7.4. Appendix 7 Summary

Pictures of primary effluent diluted into BMM (Figure A7.1) for inoculation of replicate PCL and MWCNT/PCL nanocomposites to be biodegraded in sacrifice mode (Figure A7.2); pictures of solution blended (Figure A7.3) and melt-mixed (Figure A7.4) MWCNT/PCL nanocomposites before and after aerobic mixed culture biodegradation.

7.5. References

1. Rosselló-Mora, R.; Amann, R., The species concept for prokaryotes. *FEMS Microbiol. Rev.* **2001,** *25*, (1), 39-67.
2. McCarty, P. L., *Environmental biotechnology: principles and applications*. Tata McGraw-Hill Education: 2012.
3. Fierer, N.; Jackson, R. B., The diversity and biogeography of soil bacterial communities. *Proceedings of the National Academy of Sciences of the United States of America* **2006,** *103*, (3), 626-631.
4. Wagner, M.; Loy, A.; Nogueira, R.; Purkhold, U.; Lee, N.; Daims, H., Microbial community composition and function in wastewater treatment plants. *Antonie Van Leeuwenhoek* **2002,** *81*, (1-4), 665-680.
5. Madigan, M. T.; Martinko, J. M.; Dunlap, P. V.; Clark, D. P., *Brock Biology of Microorganisms*. 12th ed.; Pearson: San Francisco, 2009.
6. Wilson-Durnat, L. P.; D'Adamo, P. C.; Bouwer, E. J., Aromatic Hydrocarbon Biodegradation with Mixtures of Oxygen and Nitrate as Electron Acceptors. *Environmental Engineering Science* **1999,** *16*, 487-500.

7. Mueller, R.-J. In *Biodegradability of polymers: regulations and methods for testing*, 2003; Wiley-VCH Verlag GmbH: 2003; pp 365-391.
8. Shimpi, N.; Borane, M.; Mishra, S.; Kadam, M., Biodegradation of polystyrene (PS)-poly(lactic acid) (PLA) nanocomposites using Pseudomonas aeruginosa. *Macromol. Res.* **2012,** *20*, (2), 181-187.
9. Gilmore, D. F.; Antoun, S.; Lenz, R. W.; Fuller, R. C., Degradation of poly (β-hydroxyalkanoates) and polyolefin blends in a municipal wastewater treatment facility. *J. Environ. Polymer Degradation* **1993,** *1*, (4), 269-274.
10. Massardier-Nageotte, V.; Pestre, C.; Cruard-Pradet, T.; Bayard, R., Aerobic and anaerobic biodegradability of polymer films and physico-chemical characterization. *Polymer Degradation and Stability* **2006,** *91*, (3), 620-627.
11. Leja, K.; Lewandowicz, G., Polymer biodegradation and biodegradable polymers—a review. *Pol. J. Environ. Stud.* **2010,** *19*, (2), 255-266.
12. EPA, 5210B Biochemical Oxygen Demand (BOD) Standard Method. In United States of America, 2001.
13. Mohee, R.; Unmar, G. D.; Mudhoo, A.; Khadoo, P., Biodegradability of biodegradable/degradable plastic materials under aerobic and anaerobic conditions. *Waste Manage. (Amsterdam, Neth.)* **2008,** *28*, (9), 1624-1629.
14. Mittal, V., *Nanocomposites with Biodegradable Polymers: Synthesis, Properties, and Future Perspectives*. Oxford University Press: 2011.
15. De, V. M. F. L.; Tawfick, S. H.; Baughman, R. H.; Hart, A. J., Carbon Nanotubes: Present and Future Commercial Applications. *Science* **2013,** *339*, (6119), 535-539.
16. Gottschalk, F.; Nowack, B., The release of engineered nanomaterials to the environment. *J. Environ. Monit.* **2011,** *13*, (5), 1145-1155.
17. Petersen, E. J.; Zhang, L. W.; Mattison, N. T.; O'Carroll, D. M.; Whelton, A. J.; Uddin, N.; Nguyen, T.; Huang, Q. G.; Henry, T. B.; Holbrook, R. D.; Chen, K. L., Potential release pathways, environmental fate, and ecological risks of carbon nanotubes. *Environ. Sci. Technol.* **2011,** *45*, (23), 9837-9856.
18. Goodwin, D. G.; Marsh, K. M.; Sosa, I. B.; Payne, J. B.; Gorham, J. M.; Bouwer, E. J.; Fairbrother, D. H., Interactions of Microorganisms with Polymer Nanocomposite Surfaces Containing Oxidized Carbon Nanotubes. *Environ. Sci. Technol.* **2015,** *49*, (9), 5484-5492.
19. Bally, D.; Asano, T.; Bhamidimarri, R.; Chin, K. K.; Grabow, W. O. K.; Hall, E. R.; Ohgaki, S.; Orhon, D.; Milburn, A.; Purdon, C. D.; Nagle, P. T.; Buitrón, G.; González, A., Water Quality International '96 Part 3: Modelling of Activated Sludge Processes; Microorganisms in Activated Sludge and Biofilm Processes; Anareobic Biological Treatment; BiofoulingCharacterization of the microorganisms from an acclimated activated sludge degrading phenolic compounds. *Water Sci. Technol.* **1996,** *34*, (5), 289-294.
20. Lallai, A.; Mura, G., Kinetics of growth for mixed cultures of microorganisms growing on phenol. *The Chemical Engineering Journal* **1989,** *41*, (3), B55-B60.
21. Alexander, M., *Biodegradation and bioremediation*. Gulf Professional Publishing: 1999.

22. Bouwer, E. J.; McCarty, P. L., Removal of trace chlorinated organic compounds by activated carbon and fixed-film bacteria. *Environ. Sci. Technol.* **1982,** *16*, (12), 836-843.
23. Leahy, J. G.; Colwell, R. R., Microbial degradation of hydrocarbons in the environment. *Microbiological reviews* **1990,** *54*, (3), 305-315.
24. Shelton, D. R.; Tiedje, J. M., General method for determining anaerobic biodegradation potential. *Appl. Environ. Microbiol.* **1984,** *47*, (4), 850-857.
25. McLellan, S.; Huse, S.; Mueller-Spitz, S.; Andreishcheva, E.; Sogin, M., Diversity and population structure of sewage-derived microorganisms in wastewater treatment plant influent. *Environ. Microbiol.* **2010,** *12*, (2), 378-392.
26. Torsvik, V.; Goksøyr, J.; Daae, F. L., High diversity in DNA of soil bacteria. *Appl. Environ. Microbiol.* **1990,** *56*, (3), 782-787.
27. Torsvik, V.; Sørheim, R.; Goksøyr, J., Total bacterial diversity in soil and sediment communities—a review. *J. Ind. Microbiol.* **1996,** *17*, (3-4), 170-178.
28. Moo-Young, M.; Vezina, C., *Advances in biotechnology:[proceedings of the Sixth International Fermentation Symposium, held in London, Canada, July 20-25, 1980]*. Pergamon Press: 1981.
29. Goodwin, D. G.; Xia, Z.; Gordon, T. B.; Gao, C.; Bouwer, E. J.; Fairbrother, D. H., Biofilm development on carbon nanotube/polymer nanocomposites. *Environmental Science: Nano* **2016**.
30. Bohutskyi, P.; Bouwer, E., Biogas production from algae and cyanobacteria through anaerobic digestion: a review, analysis, and research needs. In *Advanced Biofuels and Bioproducts*, Springer: 2013; pp 873-975.
31. Calmon, A.; Dusserre-Bresson, L.; Bellon-Maurel, V.; Feuilloley, P.; Silvestre, F., An automated test for measuring polymer biodegradation. *Chemosphere* **2000,** *41*, (5), 645-651.
32. Itävaara, M.; Vikman, M., An overview of methods for biodegradability testing of biopolymers and packaging materials. *J. Environ. Polymer Degradation* **1996,** *4*, (1), 29-36.
33. Strotmann, U.; Reuschenbach, P.; Schwarz, H.; Pagga, U., Development and Evaluation of an Online CO(2) Evolution Test and a Multicomponent Biodegradation Test System. *Appl. Environ. Microbiol.* **2004,** *70*, (8), 4621-4628.
34. Khatiwala, V. K.; Shekhar, N.; Aggarwal, S.; Mandal, U. K., Biodegradation of Poly(ε-caprolactone) (PCL) film by Alcaligenes faecalis. *J. Polym. Environ.* **2008,** *16*, (1), 61-67.
35. Pagga, U.; Schäfer, A.; Müller, R.-J.; Pantke, M., Determination of the aerobic biodegradability of polymeric material in aquatic batch tests. *Chemosphere* **2001,** *42*, (3), 319-331.
36. Pelegrini, K.; Donazzolo, I.; Brambilla, V.; Coulon Grisa, A. M.; Piazza, D.; Zattera, A. J.; Brandalise, R. N., Degradation of PLA and PLA in composites with triacetin and buriti fiber after 600 days in a simulated marine environment. *J. Appl. Polym. Sci.* **2016,** *133*, (15), n/a-n/a.
37. ASTM, A. S. f. T. a. M.-. D 6003-96: Standard Test Method for Determining Weight Loss from Plastic Materials Exposed to Simulated Municipal Solid-Wast (MSW) Aerobic Compost Environment. In Annual Book of ASTM Standards: Philadelphia 1996.

38. Krzan, A.; Hemjinda, S.; Miertus, S.; Corti, A.; Chiellini, E., Standardization and certification in the area of environmentally degradable plastics. *Polym. Degrad. Stab.* **2006,** *91*, (12), 2819-2833.
39. Kim, H.-S.; Chae, Y. S.; Jin, H.-J.; Yoon, J.-S., Preparation and characterization of poly(ε-caprolactone)-grafted-multiwalled carbon nanotubes. *Key Eng. Mater.* **2007,** *334-335*, (Pt. 2, Advances in Composite Materials and Structures), 873-876.
40. Mattioli-Belmonte, M.; Vozzi, G.; Whulanza, Y.; Seggiani, M.; Fantauzzi, V.; Orsini, G.; Ahluwalia, A., Tuning polycaprolactone-carbon nanotube composites for bone tissue engineering scaffolds. *Mater. Sci. Eng., C* **2012,** *32*, (2), 152-159.
41. Chakoli, A. N.; Wan, J.; Feng, J. T.; Amirian, M.; Sui, J. H.; Cai, W., Functionalization of multiwalled carbon nanotubes for reinforcing of poly(-lactide-co-ϵ-caprolactone) biodegradable copolymers. *Appl. Surf. Sci.* **2009,** *256*, (1), 170-177.
42. Pan, L.; Pei, X.; He, R.; Wan, Q.; Wang, J., Multiwall carbon nanotubes/polycaprolactone composites for bone tissue engineering application. *Colloids Surf., B* **2012,** *93*, 226-234.
43. Mitchell, C. A.; Krishnamoorti, R., Dispersion of Single-Walled Carbon Nanotubes in Poly(ε-caprolactone). *Macromolecules* **2007,** *40*, (5), 1538-1545.
44. Wu, D. F.; Zhang, Y. S.; Zhang, M.; Yu, W., Selective localization of multiwalled carbon nanotubes in poly(ε-caprolactone)/polylactide blend. *Biomacromolecules* **2009,** *10*, (2), 417-424.
45. Moniruzzaman, M.; Winey, K. I., Polymer nanocomposites containing carbon nanotubes. *Macromolecules* **2006,** *39*, (16), 5194-5205.
46. Madbouly, S. A.; Schrader, J. A.; Srinivasan, G.; Liu, K.; McCabe, K. G.; Grewell, D.; Graves, W. R.; Kessler, M. R., Biodegradation behavior of bacterial-based polyhydroxyalkanoate (PHA) and DDGS composites. *Green Chemistry* **2014,** *16*, (4), 1911-1920.
47. Volova, T. G.; Boyandin, A. N.; Vasil'ev, A. D.; Karpov, V. A.; Kozhevnikov, I. V.; Prudnikova, S. V.; Rudnev, V. P.; Xuån, B. B.; Dũng, V. V.; Gitel'zon, I. I., Biodegradation of polyhydroxyalkanoates (PHAs) in the South China Sea and identification of PHA-degrading bacteria. *Microbiology* **2011,** *80*, (2), 252-260.
48. Schmidt, M. W. I.; Noack, A. G., Black carbon in soils and sediments: Analysis, distribution, implications, and current challenges. *Global Biogeochem. Cycles* **2000,** *14*, (3), 777-793.
49. Liu, S.; Wei, L.; Hao, L.; Fang, N.; Chang, M.-W.; Xu, R.; Yang, Y.; Chen, Y., Sharper and faster "nano darts" kill more bacteria: A study of antibacterial activity of individually dispersed pristine single-walled carbon nanotubes. *ACS Nano* **2009,** *3*, (12), 3891-3902.
50. Akhavan, O.; Ghaderi, E., Toxicity of graphene and graphene oxide nanowalls against bacteria. *ACS Nano* **2010,** *4*, (10), 5731-5736.

Chapter 8. The Effect of Polymer Type on Carbon Nanotube/Polymer Nanocomposite Biodegradation

Parts of this chapter were co-written with the following authors and will be published under the following citations:

David G. Goodwin Jr., Pavlo Bohutskyi, Ben Frank, Duc Phan, Leo Kuwama, Xier Lu, Edward J. Bouwer, D. H. Fairbrother

Environ. Sci. Technol. In preparation.

Duc Phan, David G. Goodwin Jr., Edward J. Bouwer, D. H. Fairbrother

Environ. Sci. Technol. In preparation.

8.1. Introduction

The environmental degradation of carbon nanotube/polymer nanocomposites (CNT/PNCs) warrants investigation since the production and use of CNT/PNCs by consumers will eventually culminate in their disposal. Specifically, the interaction of microorganisms with CNT/PNCs in landfills, surface waters, soils, and wastewater treatment plants can lead to biodegradation of the CNT/PNC polymer matrix, resulting in CNT exposure and release.[1-3] CNTs are of environmental concern as a result of their ecotoxicity, persistence, and ability to facilitate transport of co-contaminants throughout the environment.[1-5] Microbial populations can use polymers as a carbon source, enzymatically breaking down the polymer chains to lower molecular weight, oxidized species that can be used as an energy source to run the metabolic and regulatory machinery of the microorganisms. The energetics of degrading a polymer substrate are

largely dependent on the functional groups, crystallinity, and steric conformation that allow the enzyme to cleave certain covalent bonds of the polymer.[6] In the case of some widely used polymers, such as polyethylene, polystyrene, and epoxy, this process is slow and often requires other environmental conditions to drive the process, such as photo-oxidation and weathering.[7-10] In other polymers such as poly(butylene succinate) (PBS), poly(vinyl alcohol), cellulose, starch, poly-ε-caprolactone (PCL), and polyhydroxyalkanoates (PHA), this process is more kinetically labile and these polymers are considered biodegradable.[4, 7, 10, 11] Many of these biodegradable polymers, with the exception of PBS, have poor properties that prevents or minimizes their use without a CNT filler.[4]

In Chapter 6, the PCL matrices of CNT/PCL nanocomposites were shown to biodegrade despite the presence of CNTs. However, CNTs still had inhibitory effects on the biodegradation process. Specifically, in the presence of a single, primed culture of *Pseudomonas aeruginosa* (*P. aeruginosa*), multi-wall CNT (MWCNT)/PCL and slightly oxidized-MWCNT (LO-MWCNT)/PCL nanocomposites became more resistant to biodegradation as a function of CNT mass loading and as a result, degraded at a slower rate. Under aerobic, mixed culture conditions, the PCL matrices of MWCNT/PCL nanocomposites were also shown to degrade, but on a more rapid time scale and with similar inhibitory effects by CNTs. This is most likely a result of the many diverse metabolic processes in mixed cultures and their ability to acclimate to contaminants and harsh environments.[12-14]

In all of the previous biodegradation studies reported in this thesis, PCL has been the only polymer matrix used; thus, the role of polymer matrix type on the biodegradation

of CNT/PNCs is still unclear. Since polymer types vary widely in terms of their biodegradation rates, the role of CNTs on the biodegradability of PHA, a more rapidly biodegradable polymer than PCL, was investigated under environmentally relevant, mixed culture conditions.[15-28] CNT/PCL biodegradation and CNT/PHA biodegradation were compared in mixed culture because both polymer types could degrade at different rates within a fairly reasonable experimental time frame (days-months). Relative to PHA, PCL can also be considered more representative of synthetically derived polymers such as PE and PS, since these polymers can degrade on an even slower time scale than PCL. The effect of polymer type on CNT/PNC degradability could then be ascertained to determine whether the inhibitory effect of CNTs is present for all or only some polymer types within a particular type of mixed culture.

PHA was also chosen since CNTs can improve its properties for broader use in many applications.[29-34] PHA typically consists of polyhydroxybutyrate (PHB) and polyhydroxybutyrate-hydroxyvalerate (PHB/HV), polyesters that many types of microorganisms, such as *Aeromonas hydrophila* and *Thiococcus pfennigii*, can produce and accumulate for carbon and/or energy storage.[35] PHAs possess some similar properties to synthetic thermoplastics such as polypropylene (PP): for example, the density of PHB and PP are 1250 and 900-910 kg/m^3, respectively and the melting points of PHB and PP are 180 and 176 $^{\circ}$C, respectively. In contrast, PHAs have much poorer mechanical properties then synthetic polymers such as tensile strength, which is 13-40 and 38 MPa for PHB and PP, respectively.[36, 37] With the decreasing production cost of PHA in recent years, PHA is being used as a substitute for traditional plastics in a wide range of applications.[38, 39] Current commercial PHA products include films, pins, and screws

which are produced by some companies in the United States (i.e., Metabolix and TEPHA).[40] Even more applications can be considered if the mechanical properties of PHA can be improved.

In order to further elucidate the effect of CNT fillers on polymer degradation processes in CNT/PNCs, biodegradation under both aerobic and anaerobic mixed cultures was investigated. Both conditions are considered relevant to those that will be experienced by CNT/PNCs in the environment: aerobic conditions will be present in surface waters, the top layer of soils, and effluent in wastewater treatment plants while anaerobic conditions will be present in landfills, soils, sediments, and digested sludge in wastewater treatment plants.[1-3] The mixed cultures of aerobic and anaerobic microorganisms were both obtained from the Back River Wastewater Treatment Plant. The use of wastewater and wastewater sludge was motivated by the fact that polymeric materials and CNT/PNCs might make their way into treatment plants through sewer and rainwater collection systems after consumer product disposal down household drains and from improper disposal in the environment (i.e. littering).[41] Primary wastewater effluent was chosen as the wastewater medium for aerobic cultures since it contains a diverse population of aerobic and facultative anaerobic microorganisms originating from a wide range of sources.[42-45] Similarly, anaerobic digester sludge was chosen because it is commonly used as a source of inoculum for biomethane potential assays under oxygen depleted conditions due to the diverse microbial community it contains.[41, 46, 47] Importantly, microbes from wastewater and anaerobic sludge alike are acclimated to degrade heterogeneous waste and possess multi-faceted types of hydrolytic extracellular enzymes, including enzymes that are capable of PCL and PHA hydrolysis.[41]

The motivation for use of both aerobic and anaerobic microorganisms was to assess the biodegradability of CNT/PNCs by different microbial species and metabolic processes. Specifically, the impact of CNTs might be more pronounced under one mixed culture condition than another for a given polymer type. Overall, the goal was to determine the mixed culture conditions under which CNTs have higher, lower, or similar inhibitory effects. Therefore, data collected for two polymer types under two mixed culture conditions was undertaken to enable greater generalization of biodegradation trends for CNT/PNCs. Thus, solution blended LO-MWCNT/PCL, MWCNT/PCL, and MWCNT/PHA nanocomposites were each exposed to aerobic and/or anaerobic conditions in this study.

The biodegradability of CNT/PNCs was assessed by mass loss under aerobic conditions (which is described in the previous chapter) and by conversion to biogas (CO_2 and CH_4) under anaerobic conditions. In terms of material characterization, CNT/PNCs were characterized using differential scanning calorimetry (DSC) to determine the fraction of crystallinity and scanning electron microscopy (SEM) to evaluate surface structure and morphology. SEM of the CNT/PNC surfaces as well as CNT/PNC thickness changes as a result of polymer biodegradation were also investigated. For anaerobic conditions, biogas production was measured as a function of volume per initial CNT/PNC mass and gas composition using gas chromatography. The protocol for the biogas assay originated from ASTM, 1992 and was further modified by Owen et al.[46, 47]

8.2. Experimental: Aerobic Mixed Culture Biodegradation of CNT/PNCs

8.2.1. MWCNT/PHA Nanocomposite Preparation for Aerobic Mixed Culture Biodegradation

A particular mass loading of pristine multi-wall carbon nanotubes (MWCNTs, NanoLab Inc., PD15L5-20, Lot # 20130820, outer diameter 15 ± 5 nm, length 5-20 μm) and 80 mg ethyl cellulose, hereafter abbreviated as EC (48.0 - 49.5% (w/w) ethoxyl basis, Lot # BCBG4792V, Sigma-Aldrich), were added to 160 mL chloroform ($CHCl_3$, HPLC grade, ≥99.9%, Sigma-Aldrich). A MWCNT suspension stabilized by EC was then produced by sonication using a Branson 1510 ultrasonicator bath operating at 70 watts for 3 h. During this process, the suspension was capped tightly to prevent solvent volatilization. After the MWCNT/EC suspension had been prepared, 1600 mg of PHA (95-100%, Metabolix Inc., Cambridge, MA), a copolymer of poly-3-hydroxybutyrate (P3HB) and poly-4-hydroxybutyrate (P4HB), was added and the mixture was sonicated for an additional 2 h to produce a casting solution. A pre-determined volume of this casting solution was then poured into aluminum dishes (44 mm diameter, 12.5 mm height, Fisherbrand) and allowed to sit overnight for solvent removal by evaporation. The generated MWCNT/PHA nanocomposites were then peeled from the aluminum dishes and consistently trimmed around the edges to obtain flat MWCNT/PHA nanocomposites of similar diameters (~30 mm).

The volume of casting solution needed to produce MWCNT/PHA nanocomposites with the same diameter and mass was found to vary with CNT loading. Initial studies conducted with a constant volume of casting solution (5 mL) revealed that casting solutions containing higher CNT loadings yielded PNCs that were consistently thicker at the bottom of the aluminum dish while casting solutions containing lower CNT loadings produced PNCs that tended to spread out more thinly at the bottom of the dish but spread further up the dish walls. This difference could potentially be a result of the

increased density of CNTs (1.615 g/cm^3 calculated using the method described by Laurent et al.) relative to PHAs (1.240 g/cm^3).[48, 49] This issue could be circumvented by using different volumes of casting solution depending on the CNT loading (10, 9.5, 8, 7.5, 5, and 5 mL of casting solution for 0, 0.5, 1, 2, 5, and 10% w/w MWCNT loading, respectively). Using this approach, it was possible to produce MWCNT/PHA nanocomposites that exhibited similar physical dimensions (28 - 30 μm thickness) and mass (28 - 35 mg).

8.2.2. MWCNT/PCL Nanocomposite Preparation for Aerobic Biodegradation

PCL and MWCNT/PCL nanocomposites containing MWCNT (NanoLab Inc.) loadings of 0.1, 0.5, 1, 2, and 5% w/w were prepared using the same solution blending methods described in Chapter 6 and 7.

8.2.3. MWCNT/PHA Nanocomposite Characterization

8.2.3.1. Differential Scanning Calorimetry (DSC)

DSC measurements were made on PHA and all of the MWCNT/PHA nanocomposites used in this study to characterize the effect of CNT loading on the degree of polymer crystallinity, a property of polymeric materials that can have an effect on biodegradation rates.[50] DSC curves were generated using a TA instrument system operating over a temperature range of 30 to 180 °C with heating and cooling rates of 3 °C/min. DSC measurements were made for duplicate areas of each MWCNT/PHA nanocomposite and for at least two separately prepared coupons for each CNT loading used. The analysis of DSC curves for both the heating and cooling processes was carried out for the first data run using TA Universal Analysis software 2000 (TA instruments, New Castle, Delaware). The enthalpy of fusion was calculated from the area of the

endothermic peak using linear integration from 159 to 179 °C. The crystallinity was determined as the ratio of the experimental MWCNT/PHA nanocomposite enthalpy of fusion to the theoretical enthalpy of fusion (ΔH_0) for 100% crystalline PHA (146.6 J/g).[51]

8.2.3.2. Energy-Dispersive X-ray Analysis (EDS)

EDS was used to measure the chlorine content in samples as a means to ensure that all of the chloroform used to prepare the PHA and MWCNT/PHA coupons had evaporated during the drying process and therefore did not impact the biodegradation results. In these experiments, PHA as well as 5 and 10% (w/w) MWCNT/PHA nanocomposite samples were cut into 1 cm^2 pieces. For a given MWCNT/PHA nanocomposite, four 1 cm^2 pieces were tightly stacked and taped down to the sample stub to eliminate the iron signal from the underlying sample stub. Each PHA and MWCNT/PHA stack was analyzed with EDS (EDAX Genesis 4000 X-ray analysis system, detector resolution of 129 eV) in two areas. Chlorine was not detected in any of the samples analyzed.

8.2.3.3. Scanning Electron Microscopy (SEM)

SEM was used to analyze the surface structure and morphology of MWCNT/PHA nanocomposites before and after biodegradation. For these analyses, samples were cut into 1 cm^2 pieces and sputter-coated with platinum (Quorum Technologies Polaron SC7640 Auto/Manual High Resolution Sputter Coater, 12 mA/800V plasma current, and 5 min at 0.5 nm/min) prior to imaging with SEM (JEOL 6700F, 10 keV, 7.0 nm working distance, LEI & SEI detectors). Prepared MWCNT/PHA samples were imaged prior to biodegradation at either 10,000x, 15,000x, or 30,000x magnification in triplicate areas. The same

approach was used to image MWCNT/PHA nanocomposites at the conclusion of the biodegradation experiments once the samples had been dried. The reproducibility of the data obtained on the biodegraded MWCNT/PHA samples was assessed by imaging two separately prepared 5% w/w MWCNT/PHA nanocomposites after 20 d of biodegradation.

SEM was also used to measure the change in thickness of MWCNT/PHA nanocomposites as a result of biodegradation. In these experiments, duplicate 5% and 10% w/w MWCNT/PHA samples were trimmed into 1 cm^2 pieces and cryosnapped down the middle using liquid nitrogen. Duplicate samples that had been biodegraded for 20 days were collected on top of aluminum foil and cryosnapped. Cryosnapped MWCNT/PHA nanocomposites were then mounted on the side of a sample stub so that the sample cross-section was perpendicular to the direction of the electron beam. Sample cross-sections were imaged at 15,000x and thicknesses were determined in at least six areas per replicate sample using ImageJ software (NIH, Bethesda, MD).

8.2.4. MWCNT/PHA Nanocomposite Characterization

SEM was also used to image PCL and MWCNT/PCL nanocomposites before biodegradation as described in Chapter 7. DSC and EDS measurements were previously made on LO-MWCNT/PCL nanocomposites as described in Chapters 2 and 6. DSC measurements were also made on melt-mixed MWCNT/PCL nanocomposites (Chapter 7). Overall, CNT/PCL nanocomposites did not contain residual chlorine from solvent casting and also did not vary in terms of crystallinity as a function of CNT loading.

8.2.5. Aerobic Biodegradation of MWCNT/PHA Nanocomposites

8.2.5.1. Inoculum and Media Preparation

The inoculum chosen for this biodegradation study was primary effluent provided by the Back River Wastewater Treatment Plant (Baltimore, MD). The inoculum, which is described in Chapter 7, was used the same day it was collected and diluted ten times (v/v) into basal mineral media (BMM, 7.18 mM K_2HPO_4, 2.79 mM KH_2PO_4, 0.757 mM $(NH_4)_2SO_4$, 0.0406 mM $MgSO_4*7H_2O$, 0.5 v/v% Trace Elements Solution: 3.75 mM H_3BO_3, 0.0605 mM $ZnSO_4*7H_2O$, 0.0296 mM $FeSO_4(NH_4)_2SO_4*6H_2O$, 0.034 mM $CoSO_4*7H_2O$, 26 μM $(NH_4)_6Mo_3O_{24}*4H_2O$, 32 μM $CuSO_4*5H_2O$, and 36 μM $MnSO_4*4H_2O$). A 200 mg/L sodium acetate trihydrate (ReagentPlus®, ≥99.0%, Sigma-Aldrich) carbon source, which is equivalent to 35 mg/L carbon, was added to increase the microorganism population for CNT/PNC biodegradation. Abiotic controls were also prepared using BMM without primary effluent to ensure that the mass loss observed in the presence of the primary effluent was exclusively a result of biodegradation and not dissolution.

8.2.5.2. Aerobic Biodegradation Setup

Individual PHA and MWCNT/PHA nanocomposites with CNT loadings of 0, 0.5, 1, 2, 5, and 10 % (w/w) were placed into 125 mL flasks (Fisherbrand). 100 mL of inoculated BMM was then partitioned into each flask and incubated at 28 °C under static conditions. For initial microbial population consistency, PHA and MWCNT/PHA nanocomposites in primary effluent were run in sacrifice mode, meaning that all sample sets were started at the same time with one batch of primary effluent and each set was removed at a different time point.[18, 24] A full

set of PHA and MWCNT/PHA nanocomposites (0 – 10% w/w) was used for each sampling time point, with a total of 12 sampling time points ranging from 1 to 20 days. Samples were incubated at 28 °C under static conditions. Additionally, for every CNT loading used, triplicate samples were setup for removal at each time point. Abiotic controls were setup using four replicate MWCNT/PHA nanocomposites at each CNT loading which were sterilized with 70% ethanol for 5 min, placed into 125 mL flasks containing 100 mL sterile BMM, and incubated at 28 °C for 20 days, corresponding to the longest time point used in the biodegradation experiments. At the end of each selected time point, the PHA and MWCNT/PHA samples were gently removed from their flasks, dried in a desiccator for at least 24 h to remove all of the adsorbed water, and then weighed. The percentage mass loss was calculated with respect to both the total CNT/PNC mass and the PHA matrix mass. The same procedures were used for MWCNT/PCL nanocomposites in Chapter 7.

MWCNT/PCL nanocomposites were setup according to the procedure described in Chapter 7. In brief, samples were run in sacrifice mode for 55 days and the last set of samples removed were weighed and re-inoculated bi-weekly with fresh primary effluent.

8.3. Experimental: Anaerobic Mixed Culture Biodegradation of CNT/PNCs

8.3.1. LO-MWCNT/PCL Nanocomposite Preparation for Anaerobic Biodegradation

PCL and LO-MWCNT/PCL nanocomposites containing a LO-MWCNT (4.1% surface atomic oxygen) loading of 0.1, 0.5, and 2% w/w were prepared using the same solution blending methods described in Chapter 6.

8.3.2. MWCNT/PHA Nanocomposite Preparation for Anaerobic Biodegradation

PHA and PHA/MWCNT nanocomposites were prepared for anaerobic biodegradation according to the same preparation procedure used for aerobic mixed culture experiments.

8.3.3. Biogas and Biomethane Potential Tests (BMP) of CNT/PNCs

The BMP test was utilized to evaluate the amount of biogas and methane production from the polymer matrix in CNT/PNCs of varied CNT loading. The procedure for the BMP test used follows that of Owens et al. and ASTM Standard E1196-92.[46, 47] In 150 mL serum bottles, an estimated 3 g/L COD was used for CNT/PNCs containing PCL and an estimated 1.5 g/L COD was used for CNT/PNCs containing PHA. Specifically, 10-12 LO-MWCNT/PCL nanocomposites were added to each serum bottle to reach a final mass of approximately 300 mg and six MWCNT/PHA nanocomposites were added to each serum bottle to reach a final mass of approximately 150 mg. The inoculum used was anaerobic sludge from the digester that treats sewage sludge at the Back River Wastewater Treatment Plant in Baltimore, MD. The CNT/PNC samples were incubated in a BMP sludge solution at 35 ± 0.5 °C: LO-MWCNT/PCL nanocomposites were incubated for 395 days while MWCNT/PHA nanocomposites were incubated for 60 days. The LO-MWCNT/PCL and MWCNT/PHA nanocomposite sets were analyzed with different batches of digested sludge and for every CNT loading studied, replicate serum bottles were run. Blanks were also run for each CNT/PNC set to subtract off any residual biogas production (< 40 mL, cumulative) from the remaining carbon source within the sludge.

8.3.4. BMP Media/Digested Sludge Preparation

A defined biomethane potential media (BMP) was prepared using concentrated stock solutions (Table 8.1) which were stored at 4 °C. The final assay concentrations of

nitrogen, phosphorus, and alkalinity were, respectively: 122 mg/L N, 19 mg/L P, and 2500 mg/L $CaCO_3$. A 4L BMP solution containing 0.4 L sludge was prepared using the stock solutions (S2-S8) listed in Table 8.1. Fresh digester sludge was obtained from the wastewater treatment plant the day before the experiment, incubated at 35 °C overnight in a slightly crushed container, and only used if the container had expanded by the next day; this ensured that the microorganisms were active within the digester sludge. The protocol used to prepare the BMP media was designed to ensure that substrate degradation is not limited by nutrients, inoculum, pH, oxygen toxicity or substrate overloading.[46, 47] Specifically, a stock solution of resazurin (S2) was used as a redox indicator to confirm the absence of oxygen; this indicator turned the BMP media pink only when oxygen entered into the system. Macronutrients (S3) were also added to ensure that nitrogen, phosphorus and potassium were not limiting. S4 and S5 consisted of trace metals added to prevent the limitation of micronutrients; this was modified from ASTM 1992 to include nickel since Owen et al. found this to be an important micronutrient for methanogen metabolism. Sodium sulfide, a reducing agent, was also added (S5) to remove residual oxygen from the media. Another modification by Owen et al. (1979) included addition of a stock solution containing vitamins and cofactors (S7), which was added to the media used in this study. Finally, sodium bicarbonate was added as a pH buffer to prevent an inhibitory pH drop as a result of acidification during biodegradation.

First, 2 mL of S2 (oxygen indicator), 8 mL of S3 (phosphate buffer), and 40 mL of S4 (macronutrients) were added to 3 L of deionized water while stirring in a 10 L carboy which was marked at 3.6 L. The 3 L solution was then boiled for 30 min for deoxygenation and cooled while purging with N_2 gas at approximately 1 L/min in a water

bath. After the media had cooled to room temperature, 6 mL of S5 (micronutrients), 5.4 mL of S6 (sodium sulfide, a reducing agent to remove oxygen), and 54 mL of S7 (vitamins and co-factors) were added under continuous N_2 purging while stirring. Next, the gas was changed from N_2 to a 20:80 CO_2/N_2 mixture and flushed at 1 L/min to help stabilize the pH. 8.40 g $NaHCO_3$ was added as a powder, the DI water level was adjusted to 3.6 L, and the pH was slowly adjusted to 7.2 by continuous purging with the 20:80 CO_2/N_2 gas mixture.

Next, 0.4 mL of sludge was added into the BMP solution while stirring under continuous 20:80 CO_2/N_2 gas purging. After stirring for 30 min, 100 mL of the sludge/BMP solution was transferred using a syringe and tubing to each serum bottle containing CNT/PNC samples, polymer references, and blanks. The BMP assay was conducted with 150 mL reagent bottles with serum stoppers. Bottles were sparged at a flow rate of approximately 0.5 L/min for 5 min with a mixture of 20:80 CO_2/N_2, then stoppered and equilibrated to room pressure by removal of excess gas from the headspace using a gas tight syringe.

Table 8.1. Stock solutions for preparation of defined BMP media.

Solution	Compound	Concentration, g/L
S1	Sample	<2 g/L degradable COD in assay liquid (estimated)
S2	Resazurin (oxidation-reduction indicator)	1
S3	$(NH_4)_2HPO_4$	26.7
S4	$CaCl_2•2H_2O$	16.7
	NH_4CI	26.6
	$MgCl_2•6H_2O$	120
	KCl	86.7
	$MnCl_2•4H_2O$	1.33
	$CoCl_2•6H_2O$	2
	H_3BO_3	0.38
	$CuCl_2•2H_2O$	0.18
	$Na_2MoO_4•2H_2O$	0.17
	$ZnCl_2$	0.14
S5	$FeCl_2•4H_2O$	370
S6	$Na_2S•9H_2O$	500
S7	Biotin	0.002
	Folic acid	0.002
	Pyridoxine hydrochloride	0.01
	Riboflavin	0.005
	Thiamine	0.005
	Nicotinic acid	0.005
	Pantothenic acid	0.005
	B12	0.0001
	p-aminobenzoic acid	0.005
	Thioctic acid	0.005

8.3.5. Sampling

Volumetric gas-volume sampling during incubation was performed with glass, gastight syringes (5-50 mL depending on gas volume production) which were lubricated with deionized water and equipped with 20-gauge needles. Volumetric readings were made after samples were equilibrated to room temperature. Sampling time points were spaced by 1-3 days during periods of high gas volume production and spaced out by 10-20 days for periods of low gas volume production.[46, 47]

After the volumetric reading was taken, the excess volume of produced gas was removed using the gastight syringe, which as a result, equilibrated the BMP serum bottle headspace to atmospheric pressure. At this point, 250 µL of gas was sampled using a

Hamilton SampleLock syringe and assayed for CH_4 and CO_2 content using gas chromatography, which is described in the next section.[46, 47]

8.3.6. Gas Chromatography (GC)

Gas composition was measured using a Shimadzu GC equipped with a Hayes Q 80/100 column and a thermal conductivity detector (TCD). An injection temperature of 130 °C, a column current of 80 mA, and a He carrier gas pressure of 2 bars were used. Analytical standard N_2, CO_2, and CH_4 gases (>98% purity, Supelco) were each injected into the GC at volumes of 50, 150, and 250 µL to calibrate the GC-TCD prior to sample gas composition measurements.

8.3.7. Activated Sludge for Assessing CNT Toxicity

In place of digested sludge, which has a low level of carbon source, activated sludge was used to assess the effects of CNT powders on anaerobic mixed cultures. Activated sludge was picked up from the wastewater treatment plant a day prior to use. Activated sludge contains a carbon source for microorganisms to degrade since it has not yet been fully digested. CNT powders were added directly to this type of sludge to measure the effect of CNTs on biogas production. The same procedure was used to prepare sludge and BMP media, which were added to replicate serum bottles containing 8 mg of CNT powders. After stoppering, serum bottles were vortexed for approximately 5 min to distribute the CNT powder throughout the sludge and sampled according to the same procedure already outlined, with the sludge carbon source producing the gas instead of a polymer matrix. Total solids and volatile solids were measured to determine the theoretical gas production by the activated sludge.

8.3.8. Measurement of Total Solids and Volatile Solids within Digester Sludge

Activated sludge was analyzed for total solids (TS) and volatile solids (VS) according to standard methods.[41] First, two aluminum dishes were heated in an oven at 550 °C for 60 min and then weighed. Next, 1 mL of sludge (filtered with a large mesh sieve) was transferred into each dish. After sludge transfer, the pipette tip used was washed with Milli-Q water to ensure complete transfer of the sludge to the dish. The dishes were put in an oven for 2 h at 105 °C to remove water and then weighed. The mass of total solids was determined by subtracting the mass after 105 °C treatment from the mass of the dish. The dishes were then put back into the oven at 550 °C for 1 h to burn away all of the organic matter. The mass of volatile solids was then calculated by subtracting the mass of the dish after 105 °C treatment from the mass of the dish after 550 °C treatment. The remaining solids after 550 °C treatment, which are also called fixed solids (e.g. $CaCO_3$), were considered recalcitrant to biodegradation within the sludge.

8.4. Results and Discussion

8.4.1. Aerobic Mixed Culture Biodegradation of MWCNT/PHA and MWCNT/PCL Nanocomposites

In Chapter 7, MWCNT/PCL nanocomposite characterization and biodegradation under aerobic mixed culture conditions are described. In this section, MWCNT/PHA nanocomposite characterization and biodegradation results under mixed culture conditions are discussed.

In terms of MWCNT/PHA characterization, the SEM images in Figure 8.1a show a surface morphology comparison of PHA (0% w/w) and MWCNT/PHA nanocomposites at varied CNT loadings (0.5, 2, and 5% w/w) before exposure to microorganisms. The SEM images indicate that MWCNT/PHA nanocomposites with CNT loadings below 5%

w/w have less than 10 CNTs observable at the surface and a similar surface morphology to that of PHA (Figure 8.1a and Appendix 8). In contrast, CNTs appear at the surface of 5 and 10% w/w MWCNT/PHA nanocomposites with minimal signs of CNT aggregation, indicating that the MWCNTs are well dispersed in the PHA matrix (Figure 8.1a and Appendix 8). The homogenous CNT distribution observed at the MWCNT/PHA nanocomposite surfaces with SEM was further supported by visual observation of a uniformly black color, which systematically increased in darkness with CNT loading for all MWCNT/PHA nanocomposites (Figure 8.1a).

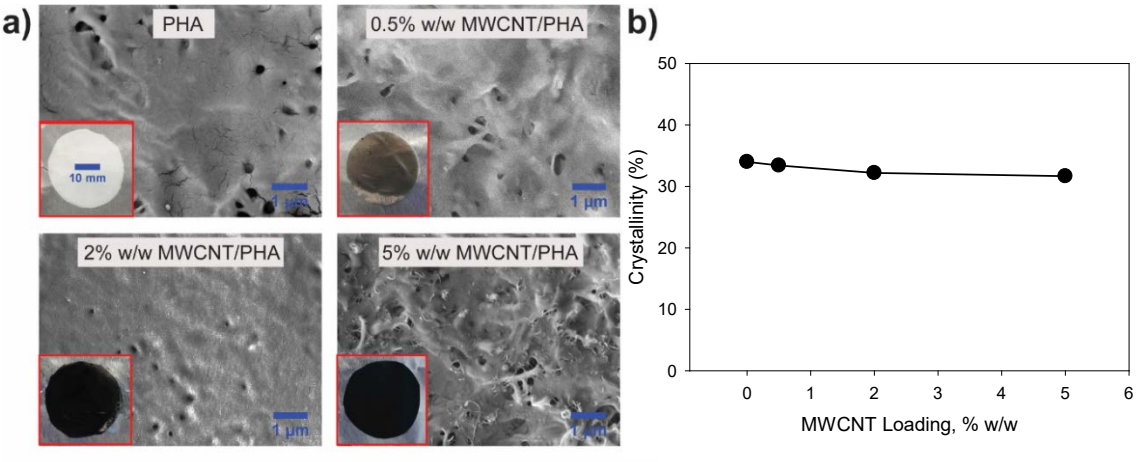

Figure 8.1. a) SEM and b) DSC characterization of MWCNT/PHA nanocomposites at 0, 0.5, 2, and 5% w/w MWCNT/PHA for surface morphology and crystallinity measurements before biodegradation, respectively.

DSC was also used to characterize the degree of crystallinity as a function of CNT loading for all MWCNT/PHA nanocomposites studied (Figure 8.1b). In biodegradation processes, enzymatic degradation of amorphous, or less ordered domains, is more kinetically favorable than degradation of ordered crystalline regions where tightly packed polymer chains are in their most thermodynamically stable configuration and can limit enzymatic access.[52] Since the degree of crystallinity is a factor that affects

biodegradability and the PHA in this study was modified with CNTs, the contribution of CNTs to the crystallinity of PHA was determined when different CNT loadings (0 - 10% w/w) were added to the PHA matrix.[53] Despite the added CNT filler in MWCNT/PHA nanocomposites, the results demonstrate that MWCNT/PHA nanocomposites and PHA have similar degrees of crystallinity (Figure 8.1b). Thus, crystallinity does not play a role in the biodegradability of MWCNT/PHA nanocomposites within the range of CNT loadings used in this study.

Figure 8.2 shows the effect of CNT incorporation at different mass fractions (0.5 - 10% w/w) on the biodegradability of PHA. MWCNT/PHA nanocomposites were degraded in primary effluent and removed in sets at each time point to determine the MWCNT/PHA nanocomposite mass loss (Figure 8.2a) or the percentage of PHA matrix mass loss (Figure 8.2b). Consistent with other studies, PHA readily biodegraded in the presence of an aerobic mixed culture.[16-27] In primary effluent, almost 100% of the PHA degraded (Figure 8.2) after seven days, with some residual PHA not collectible. In contrast, the final mass loss of MWCNT/PHA nanocomposites (Figure 8.2a) after seven days was lower than for that of PHA (0% w/w).

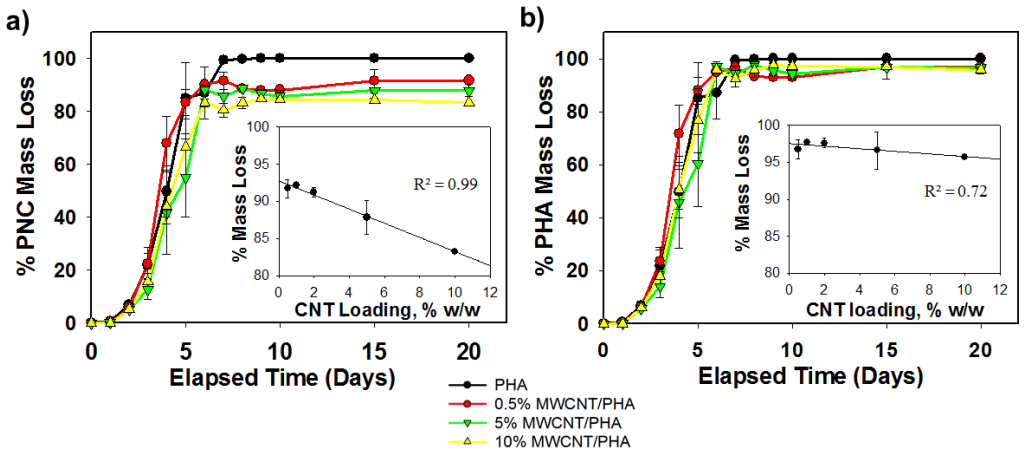

Figure 8.2. a) A plot of MWCNT/PHA nanocomposite mass loss and b) PHA matrix mass loss for 0, 0.5, 5, and 10% w/w MWCNT/PHA nanocomposites. The inset plots show mass loss of a) MWCNT/PHA nanocomposites as function of CNT loading at day 20 and b) mass loss of the PHA matrix as a function of CNT loading at day 20.

Between 0.5 - 10% w/w, the final MWCNT/PHA nanocomposite mass loss decreased with CNT loading (Figure 8.2a inset). However, the primary effluent effectively biodegraded all of the PHA matrix regardless of CNT loading, with at least 92.5% PHA mass loss after seven days of incubation and 95.6% PHA mass loss after 20 days (Figure 8.2b inset). Thus, the mass loss differences observed as function of CNT loading (Figure 8.2a inset) can be attributed to the remaining mass of CNTs. This remaining mass of CNTs reasonably corresponds to the initial mass loading of CNTs plus the fraction of ethyl cellulose per sample (5% w/w) with an average remaining mass fraction of 8.3, 7.8. 8.8, 12.2, and 16.8% for 0.5, 1, 2, 5, and 10% w/w MWCNT/PHA nanocomposites, respectively. Figure 8.2 also demonstrates that the rates of biodegradation for MWCNT/PHA nanocomposites of varied CNT loading are similar to that of PHA (0% w/w). Therefore in aerobic mixed culture, a high concentration of CNT filler does not affect the biodegradation rate of the PHA matrix in MWCNT/PHA nanocomposites. The

ability of the microorganisms to overcome the cytotoxicity of CNTs is most likely a result of the kinetically rapid biodegradation of PHA.

In addition to having similar biodegradation rates, all MWCNT/PHA nanocomposites, including 0.5% w/w, maintained their shape and color despite more than 95% PHA matrix mass loss. Although more brittle, all MWCNT/PHA nanocomposites of varied CNT loading remained intact after 20 days of biodegradation in mixed culture, presumably due to the strong van der Waals forces between individual CNTs. There was also no visual evidence of MWCNT release, potentially due to the fact that all MWCNT/PHA nanocomposites were incubated under static conditions which minimized mechanical agitation (Figure 8.3). The lack of CNT release is also further confirmed by the remaining MWCNT/PHA nanocomposite mass corresponding to the initial CNT loading plus ethyl cellulose.

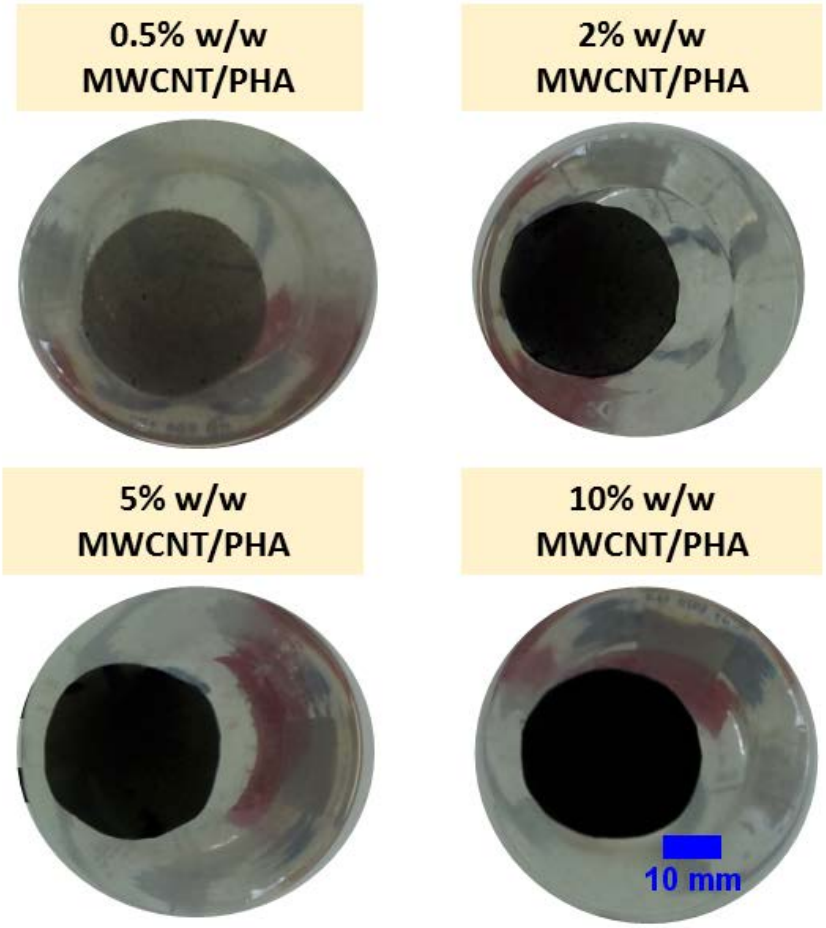

Figure 8.3. MWCNT/PHA nanocomposites in mixed culture remained intact after 20 days of microbial exposure despite significant mass loss (> 95% PHA matrix mass loss).

In order to characterize the change in CNT/PNC surface morphology as a function of CNT/PNC mass loss, 5% w/w MWCNT/PHA nanocomposite surfaces were analyzed with SEM after 1, 3, and 20 days of biodegradation (Figure 8.4). The SEM images indicate that with increasing incubation time and subsequent mass loss, the density of MWCNTs at the surface of 5% w/w MWCNT/PHA clearly increases. This is most evident at Days 3 and 20, where the MWCNTs clearly dominate the surface structure. The SEM images demonstrate that the polymer matrix is consumed by microorganisms

despite their increasing exposure to a high CNT concentration at the surface (Figure 8.4). Previous research has shown that the presence of CNTs at the surface of CNT/PNCs has led to cytotoxic effects on single cultures of microorganisms.[54] In mixed culture, microorganisms are observed consistently across the surface at Day 3 despite the high density of CNTs present in visible patches (Figure 8.4) and biodegradation continues regardless of any cytotoxicity that might be present. The presence of microorganisms at Day 20 is less obvious while CNT accumulation dominates the MWCNT/PHA nanocomposite surface (Figure 8.4). Since biofilm formation is the precursor to biodegradation, the lack of biofilm after 20 days of biodegradation suggests that some of the biofilm sloughed away or collapsed into the CNT network at this level of CNT accumulation.

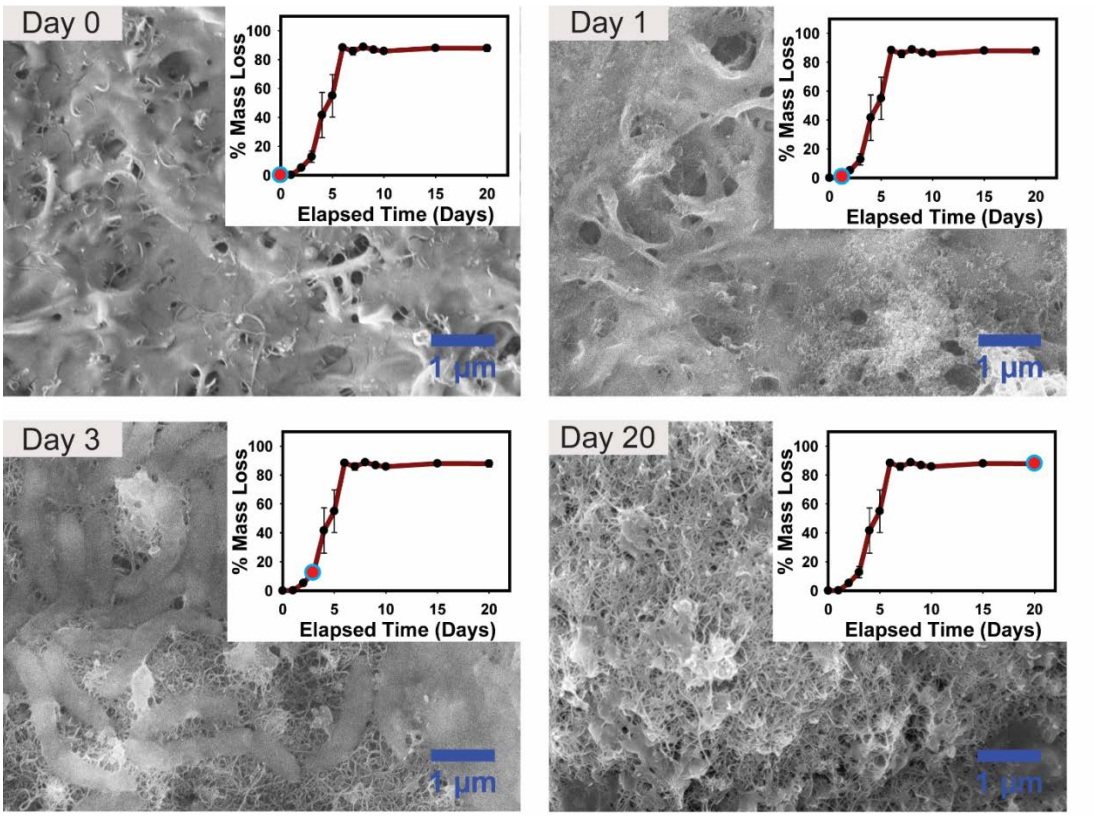

Figure 8.4. Mass loss and SEM characterization of 5% w/w MWCNT/PHA nanocomposites as a function of biodegradation time.

MWCNT/PHA nanocomposites containing other MWCNT loadings were compared to 5% w/w at 20 days of biodegradation since all PNCs maintained their shape at a high mass loss (Figure 8.3). In Figure 8.5, SEM images of 0.5, 2, and 10% w/w MWNCT/PHA nanocomposite surfaces show that in all cases, CNT accumulation dominates the surfaces. Furthermore, the presence of biofilms is minimal after 20 days for all CNT loadings, consistent with the lack of biofilm observed on the 5% w/w after 20 days of biodegradation. The surface structure of the 0.5 and 2% w/w also had a much rougher topography than the 5 and 10% w/w MWCNT/PHA nanocomposite. This is most likely a result of the lower overall density of CNTs in the 0.5 and 2% w/w

MWCNT/PHA nanocomposites which generates a more diffuse, less dense CNT mat after PHA removal (Figure 8.5).

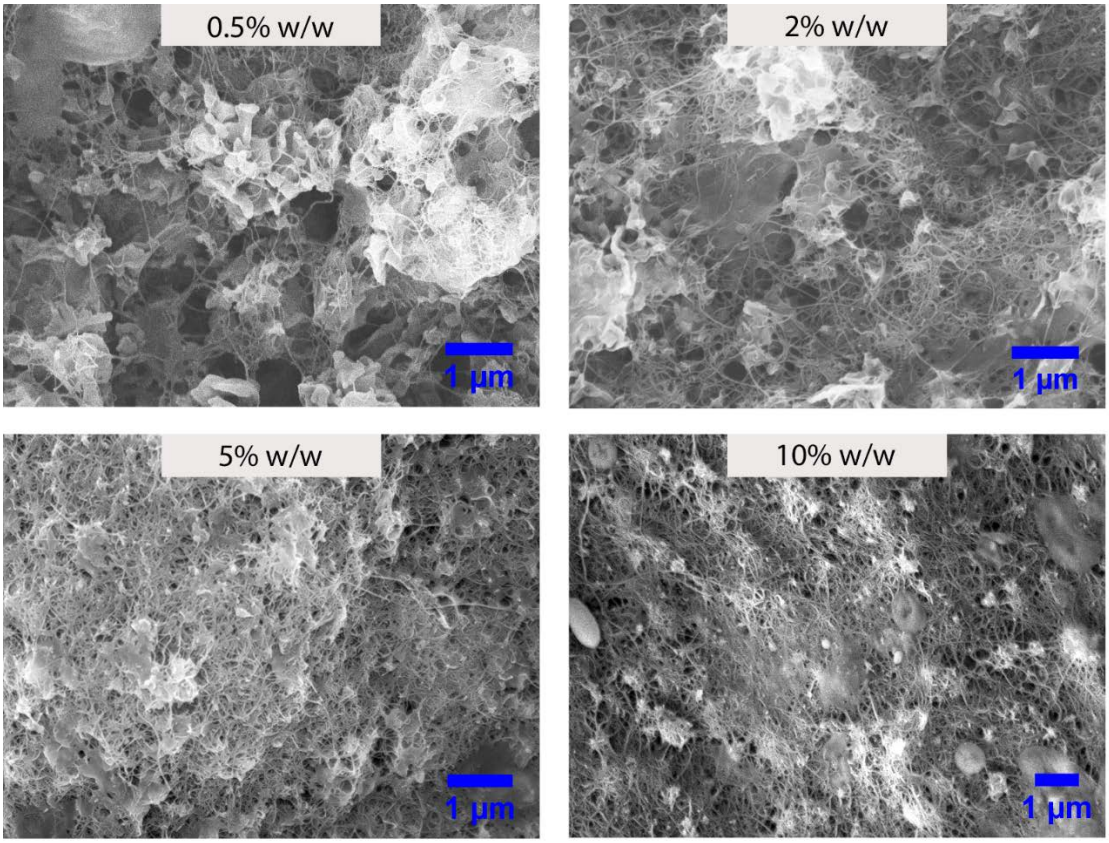

Figure 8.5. SEM images showing MWCNT accumulation at the surfaces of 0.5, 2, 5, and 10% w/w MWCNT/PHA nanocomposites after 20 days of biodegradation.

Thickness measurements of 5 and 10% w/w MWCNT/PHA nanocomposites were made to further quantify MWCNT/PHA biodegradation (Figure 8.6). SEM cross-sections of 5 and 10% w/w were imaged before and after biodegradation; an example image is shown in Figure 8.6a for a 5% w/w MWCNT/PHA nanocomposite. A thickness decrease of 76 and 71%, for 5 and 10% w/w MWCNT/PHA nanocomposites, was observed, respectively (Figure 8.6b). Similar to the mass loss measurements of 5 and 10% w/w MWCNT/PHA nanocomposites (87.8 and 83.2%, respectively), the thickness loss was greater for the 5% w/w than the 10% w/w. This can be attributed to the higher PHA and

lower CNT content in the 5% w/w CNT/PHA nanocomposite. The mass loss and thicknesses, however, do differ by > 10%.

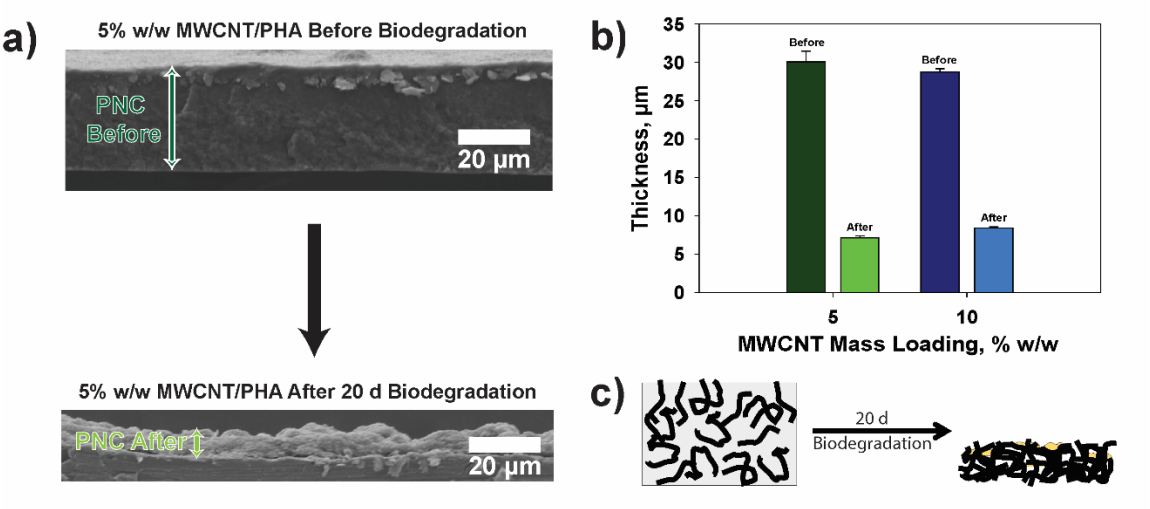

Figure 8.6. a) SEM images showing the cross-section of 5% w/w MWCNT/PHA nanocomposites before and after 20 days of biodegradation. b) The average of six replicate MWCNT/PHA nanocomposite thickness measurements per image were made using ImageJ software to show the decrease in thicknesses of 5 and 10% w/w MWCNT/PHA nanocomposites. The cartoon in c) illustrates the mass loss of PHA and the remaining CNT mat containing ethyl cellulose and biomass.

This suggests that the remaining CNT mat has some expanded structure and is not completely collapsed (Figure 8.6c). This could be a result of the enzymatic degradation process, the CNT structure within the composite maintaining some voids, or the presence of ethyl cellulose, which is inert to biodegradation under a similar time frame and might act as a spacer between MWCNTs.[55] Regardless of the mat thickness, CNTs, ethyl cellulose, and residual biomass are all that remains after 20 days of MWCNT/PHA nanocomposite exposure to mixed culture. This demonstrates that the presence of MWCNTs does not inhibit biodegradation and a persistent CNT mat will remain intact even when all of the polymer matrix is enzymatically removed.

8.4.2. *Comparison of Aerobic Mixed Culture Biodegradation of MWCNT/PHA and MWCNT/PCL Nanocomposites*

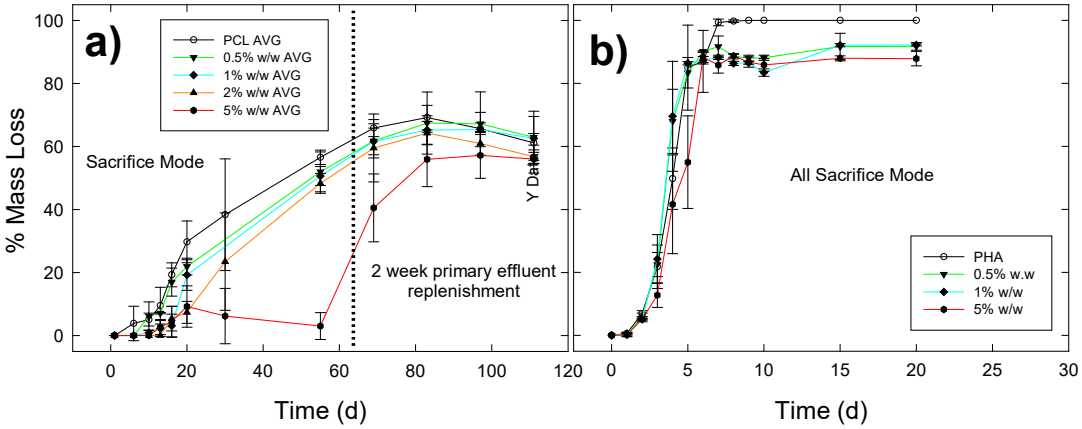

Figure 8.7. A comparison of a) MWCNT/PCL and b) MWCNT/PHA nanocomposite mass loss under aerobic mixed culture conditions. Each data point represents the mass loss of at least three replicate samples. MWCNT/PHA nanocomposites were run in sacrifice mode for the entire length of the experiment while MWCNT/PCL nanocomposites were run in sacrifice mode until day 55; at this point the day 55 samples were further degraded with fresh primary effluent every two weeks in sampling mode.

Figure 8.7 shows a comparison of MWCNT/PCL nanocomposite biodegradation (Figure 8.7a) and MWCNT/PHA nanocomposite biodegradation (Figure 8.7b) under aerobic mixed culture conditions. The results indicate that PHA degrades at a much faster rate than PCL. As a function of CNT loading, the plots show that biodegradation rates of PCL are inhibited by increasing mass fractions of CNTs, especially 5% w/w, while CNT fillers have no effect on the biodegradation rate of a PHA matrix (Figure 8.7). Therefore, a comparison of the mass loss plots (Figure 8.7) demonstrates that the low activation energy of PHA metabolism by microorganisms enables them to overcome the inhibitory effects of CNTs.[15-28] In contrast, PCL metabolism is much slower, allowing the effect of CNTs on biodegradation to become apparent (Figure 8.7a). Other polymer types that are biodegradable, but require greater energy input to biodegrade than PCL, may be even more susceptible to the inhibitory effects of CNTs in aerobic mixed cultures. Therefore,

polymer type plays a significant role in determining how persistent a CNT filler can render a polymer. Despite the increased persistence of polymers containing CNTs, the results of this study show that CNT/PNCs can still eventually biodegrade in the environment when exposed to a mixed population of aerobic microorganisms.

Analogously, biodegradation can occur in anaerobic environments such as landfills, deep water, and digester sludge tanks in wastewater treatment plants.[55] The effect of CNT incorporation on polymer degradation in these systems has not yet been studied. This is considered important since the activation energy to biodegrade PCL and PHA might differ depending on the culture conditions, which can further confirm the role of polymer type on the sensitivity of microorganisms to CNTs during biodegradation and provide some generalization on the biodegradability of CNT/PNCs. For this reason, CNT/PCL and CNT/PHA nanocomposites were biodegraded under anaerobic conditions in the next section.

8.4.3. Comparison of Anaerobic Mixed Culture Biodegradation of MWCNT/PHA and MWCNT/PHA Nanocomposites

The total volumetric biogas production as well as the methane production were used to measure the anaerobic biodegradation rates of LO-MWCNT/PCL nanocomposites (Figure 8.8). All biogas measurements were made over the course of 395 days for 0.1, 0.5, and 2% w/w LO-MWCNT/PCL nanocomposites with PCL used as a reference. In terms of total biogas volume production, 0.1 and 0.5% w/w LO-MWCNT/PCL nanocomposites degraded at a similar rate to that of PCL. In contrast, biogas production for 2% w/w proceeded at a slower rate than PCL and the LO-MWCNT/PCL nanocomposites of lower CNT loading (Figure 8.8a).

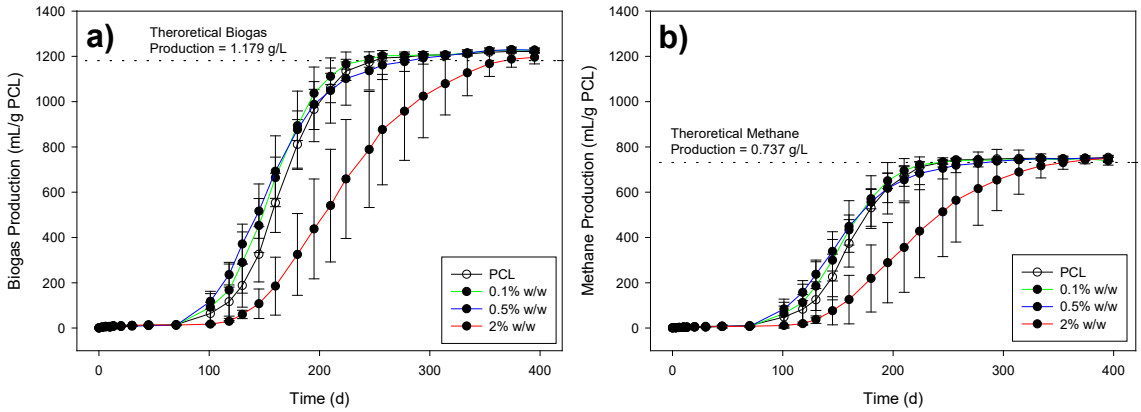

Figure 8.8. a) Biogas and b) methane production from the transformation of PCL and LO-MWCNT/PCL nanocomposites of varied CNT loading during anaerobic biodegradation. The theoretical a) biogas and b) methane production (dotted line) were calculated using the Buswell equation. Each data point represents the average gas volume production from three replicate samples.

This suggests that LO-MWCNTs have an inhibitory effect on the biodegradation of PCL at a CNT loading higher than 2% w/w. This inhibitory effect can potentially result from CNT cytotoxicity, which has been observed under single culture conditions (Chapters 3 and 4). It can also result from a high level of CNT accumulation at the 2% w/w LO-MWCNT/PCL surface, leading to PCL entrapment within the CNTs and minimal access of the enzymes to the PCL substrate. Despite this inhibitory effect at 2% w/w, the LO-MWCNT/PCL nanocomposites degraded to the same extent as the PCL control by 375 days. The 0.1 and 0.5% w/w LO-MWCNT/PCL nanocomposites also reached the same level of CNT/PNC biodegradation after 255 days (Figure 8.8a). This result is similar to the results obtained under aerobic mixed culture conditions in that 2% w/w and 5% w/w MWCNTs had slower biodegradation rates relative to PCL and the MWCNT/PCL nanocomposites containing lower MWCNT loadings (Figure 8.7a). However, despite this similarity, the inhibitory effect of 2% w/w LO-MWCNTs was much more dramatic under

anaerobic conditions, with it taking 120 days longer to reach the same level of biogas production as PCL (Figure 8.8a).

Methane production from PCL and the LO-MWCNT/PCL nanocomposites of each CNT loading was measured using GC headspace analysis (Figure 8.8b). Methane production was investigated since methanogens have been shown to be more sensitive than other anaerobic microbe types to contaminants such as heavy metals, ammonia, and hydrogen sulfide.[41] To our knowledge, the exposure of CNTs to methanogens has not previously been studied. Similar to the total gas volume production rate, Figure 8.8b shows that the rate of methane production for 2% w/w LO-MWCNT/PCL nanocomposites is also inhibited relative to PCL. However, the CNTs do not appear to have a stronger inhibitory effect on the methane production than the total volumetric biogas production (Figure 8.8**)**. If this were the case, lower CNT loadings would most likely have also experienced a decreased methane production rate relative to PCL and the inhibition of methane production rates for the 2% w/w LO-MWCNT/PCL nanocomposites would have been more dramatic than was observed for the total biogas production (Figure 8.8b). Overall, methanogens are similarly affected by the CNTs relative to the other anaerobic microorganisms present.

The theoretical biogas yield of 100% PCL degradation was calculated using the Buswell equation for the PCL matrix.[56] CNTs were not included as part of the biodegradable mass in the theoretical yield calculation since they are bio-persistent, with CNT biodegradation only ever observed in the presence of harsh acellular enzymes.[57] Equations 1-3 show the chemical reaction and stoichiometric yield calculations used to determine total theoretical biogas production as well as theoretical methane and CO_2

production. [56] Methane and CO_2 production can be distinguished within this theoretical yield calculation since CO_2 contains oxygen while methane does not. The oxygen from CO_2 can be stoichiometrically related to the oxygen within the atomic composition of the polymer because external oxygen is not present within the system under anaerobic conditions.[56]

$$\boldsymbol{C_cH_hO_oN_n + yH_2O \rightarrow xCH_4 + nNH_3 + (c - x)CO_2} \quad \text{(Equation 1)}$$

where:

$$\boldsymbol{x = 4c + h - 2o - 3n - 2s/8} \quad \text{(Equation 2)}$$

$$\boldsymbol{y = (4c - h - 2o + 3n + 3s)/4} \quad \text{(Equation 3)}$$

As demonstrated in Figure 8.8, the cumulative biogas yield (g/L) of PCL degradation in all LO-MWCNT/PCL nanocomposites is very similar to the theoretical yield (1.179 g/L). This indicates that despite the presence of CNTs, PCL fully transforms to biogas as a result of biodegradation under anaerobic conditions. Furthermore, the cumulative methane production measured by the end of the experiment was also representative of the theoretical methane yield (0.737 g/L).

The full transformation of PCL to biogas by the end of the experiment was further confirmed by the absence of PCL in Figure 8.9 after 355 days. In contrast, the 2% w/w LO-MWNCT/PCL nanocomposites remained intact (Figure 8.9) despite full degradation of PCL matrix. The ability of the 2% w/w LO-MWCNT/PCL nanocomposite to retain its shape as a CNT mat rather than disperse CNTs into the sludge is most likely a result of the physicochemical properties of CNTs that can lead to CNT entanglement and strong CNT-CNT interactions such as pi-stacking. The implications of this result indicate that CNTs are likely to remain localized, unless mechanical agitation is applied. Further

investigation of the stability of these CNT mats produced from CNT/PNC biodegradation can provide insights into their mechanical properties and CNT release potential.

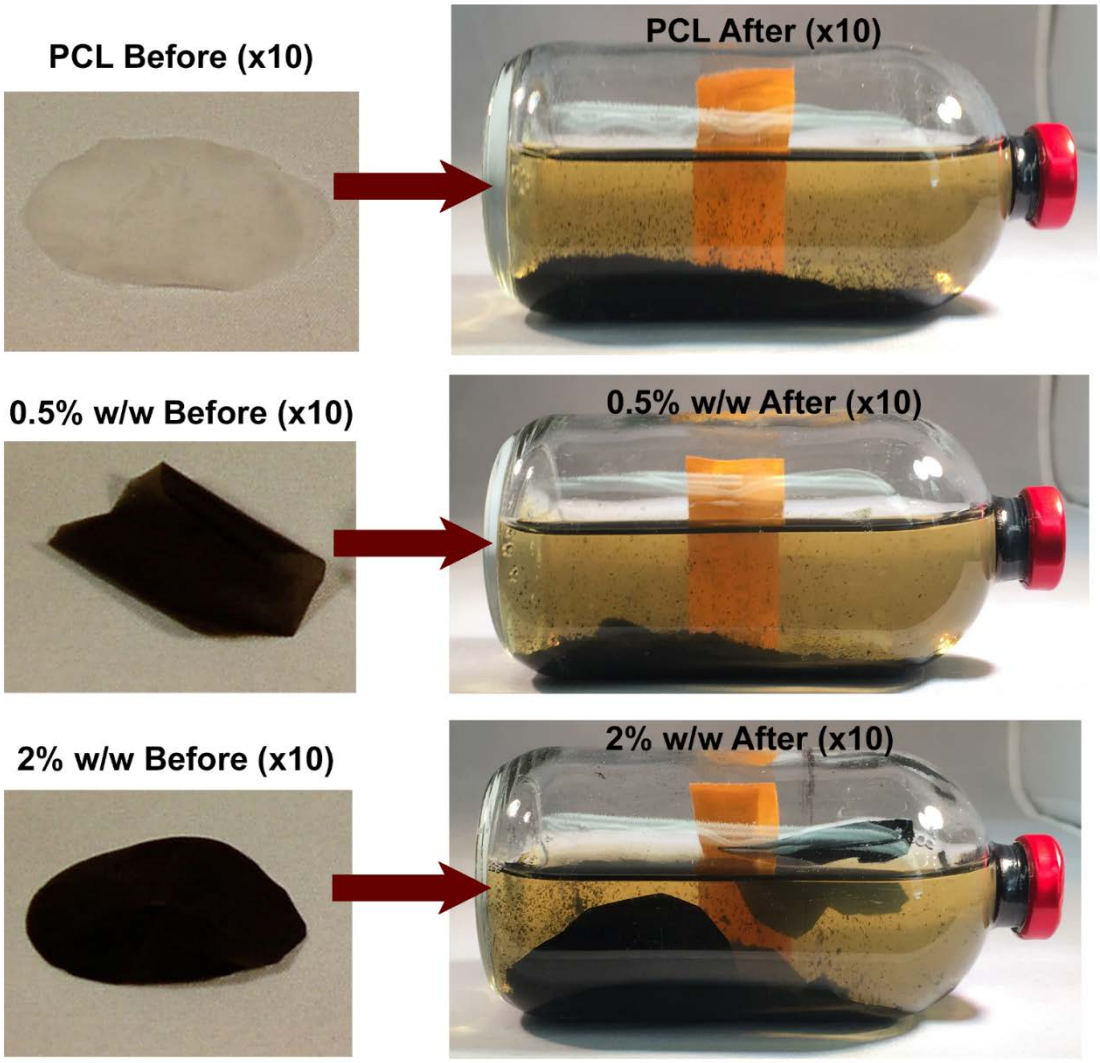

Figure 8.9. LO-MWCNT/PCL nanocomposites of varied CNT loading before and after anaerobic biodegradation. 10-12 LO-MWCNT/PCL nanocomposites were initially added to each serum bottle.

In addition to using PCL as the CNT/PNC matrix, PHA was also used in order to compare the sensitivity of anaerobic microorganisms to CNTs when blended into different polymer types. Under aerobic conditions, the inhibitory effect of CNTs on

polymer biodegradation was more apparent for PCL than PHA, presumably due to differences in polymer crystallinity and chemical structure (Figure 8.7). However, anaerobic microorganisms degrade substrates using different metabolic processes than aerobic microorganisms and as a result, may be affected by CNTs to a greater or lesser extent than under aerobic conditions.

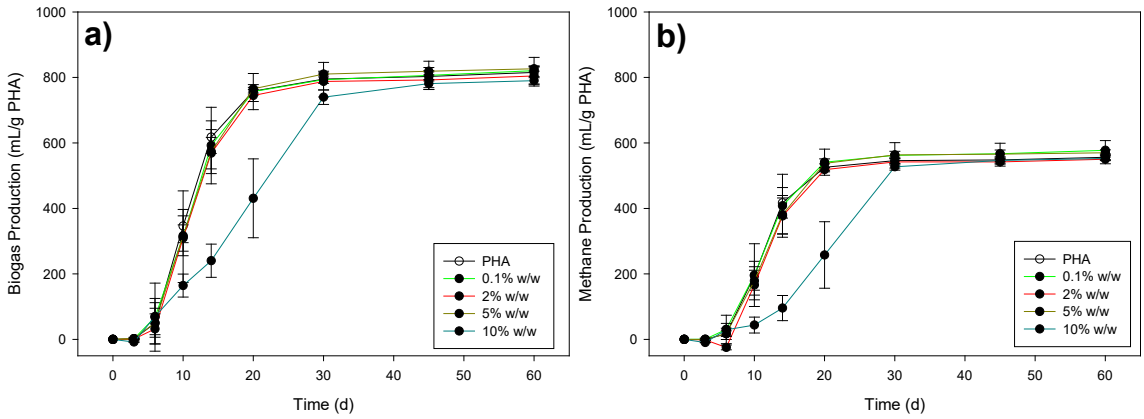

Figure 8.10. a) Biogas and b) methane production from the transformation of PHA and MWCNT/PHA nanocomposites of varied CNT loading during anaerobic biodegradation. The theoretical a) biogas and b) methane production were not calculated since the PHA structure is not well-defined by the manufacturer. Each data point represents the average of gas production from three replicate samples.

Furthermore, the biodegradation rates of PHA and PCL under anaerobic conditions differed from that of aerobic biodegradation rates, providing insight into whether or not CNT inhibitory effects will be generalizable to a wide range of environments and polymer matrices.

In Figure 8.10, biogas production by PHA in MWCNT/PHA nanocomposites containing CNT loadings of 0.1, 0.5, 2, 5, and 10% w/w are shown. In comparison to PHA, all MWCNT/PHA nanocomposites of CNT loadings at and below 5% w/w converted PHA to biogas at a similar rate. However, 10% w/w MWCNT/PHA

nanocomposites produced biogas at a slower rate than PCL and all other MWCNT/PHA nanocomposites. This suggests that the rate of biogas production is affected by the presence of a high CNT loading. This is in contrast to the aerobic mixed culture results, where an inhibitory effect was not evident at 10% w/w and the biodegradation rate was similar to that of PHA (Figure 8.7b). The difference between the biogas production rate under aerobic and anaerobic conditions at 10% w/w is most likely due to the slower rate of PHA biodegradation under anaerobic conditions. This indicates that PHA biodegradation rate can be affected by the presence of a high CNT loading when the kinetics of PHA biodegradation are reduced. This effect was only apparent at CNT loadings of 10% w/w (Figure 8.10).

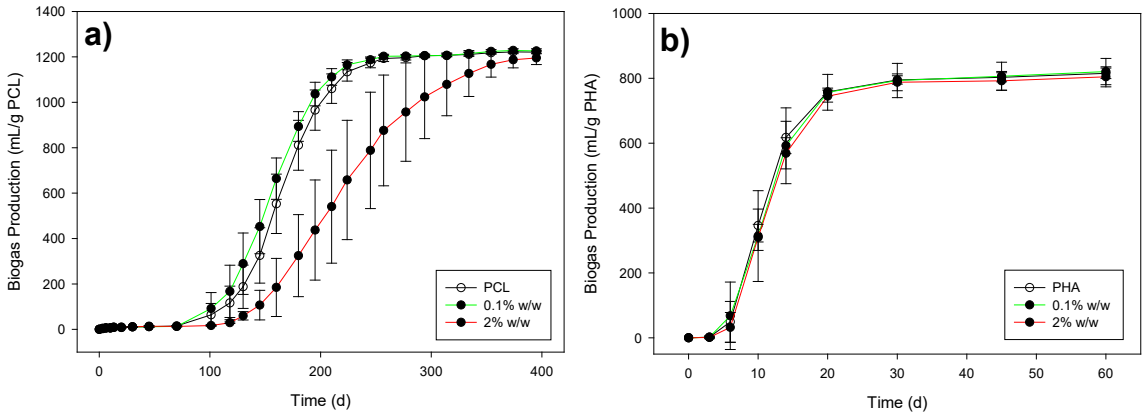

Figure 8.11. A comparison of a) LO-MWCNT/PCL and b) MWCNT/PHA nanocomposite mass loss at common CNT loadings under anaerobic mixed culture conditions. Each data point represents the mass loss of at least three replicate samples.

In Figure 8.11, a comparison of CNT/PCL and CNT/PHA nanocomposite biodegradation under anaerobic conditions is shown for similar CNT loadings. The results indicate that anaerobes are much more sensitive to CNTs in PCL than in PHA. This is evident from the higher CNT loading required to generate an inhibitory effect for

PHA (10% w/w) relative to PCL (2% w/w) (compare Figures 8.10 and 8.8). The difference in anaerobe sensitivity to CNTs as a function of polymer type is similar to that observed for aerobic microorganisms. This suggests that the effect of CNTs on polymer biodegradation is fairly generalizable as a function of polymer type. The slower the rate of pure polymer biodegradation, the more apparent the inhibitory effect of CNTs becomes. For a polymer with a relatively slow biodegradation rate, such as PCL, the activation energy is already high and the addition of increasing CNT mass concentrations can further increase this activation energy to have a much more profound effect on the biodegradation rate. In contrast, the faster rate of PHA degradation indicates that the activation energy is lower. In this case, incrementally increasing this activation energy using a CNT filler does not substantially offset the rate.

It is important to point out that the CNTs used in PCL are different than those used in PHA for anaerobic studies (LO-MWCNT versus pristine MWCNTs, respectively), but are qualitatively comparable since both types of CNT fillers are cytotoxic when embedded in CNT/PNCs and have been shown to have inhibitory effects on PCL biodegradation under both single culture and mixed culture conditions.[5, 55] A direct comparison of CNT type in PCL and PHA is ongoing at the time of this thesis submission (~1 year study).

An evaluation of the cytotoxic effects of both CNT types (LO-MWCNTs and MWCNTs) on anaerobes was conducted by adding CNT powder (8 mg) to serum bottles containing activated sludge. Activated sludge differs from the digested sludge used in the CNT/PNC biogas studies since it contains a carbon source that the anaerobes use to produce gas. In contrast, the polymer matrix was designed to be the sole carbon source in

the digested sludge used for CNT/PNC biogas studies. For the CNT powder experiment, the assay involves biodegradation of the organic matter in the digested sludge and monitoring the inhibition of biogas production as a result of the added contaminant (i.e. CNTs). Both LO-MWCNT and MWCNT powders were analyzed relative to a sludge control, as shown in Figure 8.12.

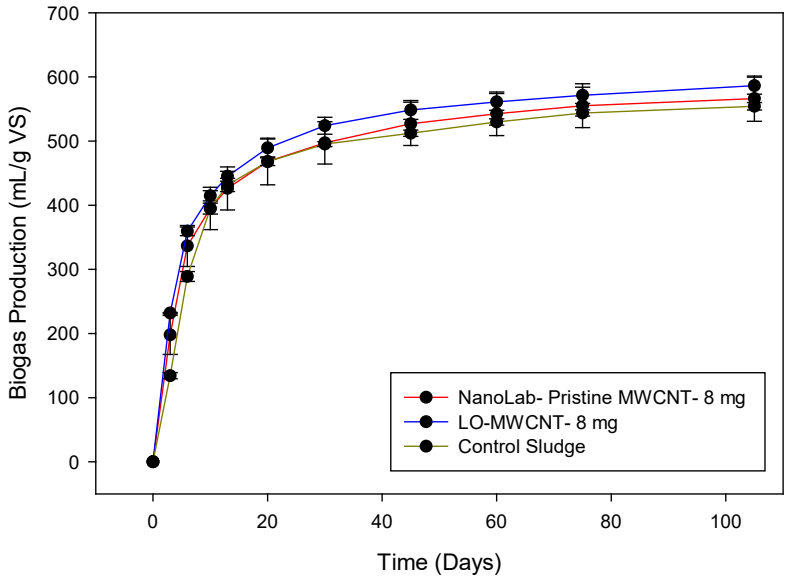

Figure 8.12. Biogas production from the biodegradation of organic matter in activated sludge containing 8 mg of MWCNT and LO-MWCNT powder. The biogas production of activated sludge in the absence of CNTs was used as a control.

For both CNT types, no suppression of biogas volume rate was observed (Figure 8.12). This is most likely a result of CNT aggregation in the media and the requirement that CNTs be in direct contact or very close proximity to microorganisms for a cytotoxic effect to occur (Chapters 3 and 4). In fact, CNT mass concentrations of > 50 mg/L have been required for cytotoxic effects to take place on planktonic cells such as *Salmonella* under single culture conditions.[58] In contrast, CNTs that are uniformly distributed at the surface of a CNT/PNC have had antimicrobial effects at surface concentrations ranging

from 0.1 – 10% w/w.[5] Nonetheless, the cytotoxicity observed was only for microorganisms in contact or close proximity to the CNTs, indicating that CNTs are unlikely to suppress biogas formation of the organic matter from the surrounding activated sludge, especially once CNTs have been coated by organic matter.[5] This is in contrast to the microorganisms that have to make contact or come in close proximity to the CNTs to access the polymer substrate in a CNT/PNC biogas experiment.

8.4.4. The Effect of Polymer Type on Mixed Culture Biodegradation

In conclusion, the results of this study show that polymer type plays an important role during the biodegradation of CNT/PNCs. With the inoculum used, full PCL biodegradation took longer than a year under anaerobic conditions and around 2 months under aerobic conditions. For PHA, full biodegradation took approximately 20 days under anaerobic conditions and less than 10 days under aerobic conditions. Under both conditions, PHA was more rapidly degradable than PCL.

The results of this study imply that CNTs suppress the rate of CNT/PNC mass loss and conversion of polymer to CO_2 and CH_4 when the rate of polymer degradation is slow. In contrast, when the rate of polymer biodegradation is fast, the effect of the CNTs can be overcome, even at CNT loadings as high as 10% w/w. In many cases, the rate of polymer biodegradation will vary between environmental conditions as was observed between aerobic and anaerobic mixed cultures. Under conditions where the rate is reduced, the inhibitory effect of the CNTs becomes more apparent. Despite CNT inhibition under some conditions and with some polymer types, full polymer matrix biodegradation can still occur in the presence of a CNT filler as shown in all aspects of this study. In general, this suggests that CNT/PNCs will become more persistent with an added CNT filler, but will ultimately biodegrade over time.

The generation of an intact CNT mat indicates that the distribution of CNTs throughout the environment will be minimal, but should be investigated further, especially in terms of mechanical agitation. In terms of adding CNTs to polymers with poor properties that are also biodegradable, this strategy is probably not an ideal direction for production since the polymer matrix containing a CNT filler can still be degraded on the order of days to years. This can limit the use of CNT/PNCs prepared with biodegradable polymers in tissue scaffolding applications or consumer products. However, there may be some niche applications where CNT accumulation at the surface of CNT/PNCs after biodegradation could be advantageous, such as in biosensors or membranes to increase flux and contaminant adsorption over time.

8.5. Appendix 8 Summary

Replicate SEM images of PHA, 5, and 10% w/w MWCNT/PHA nanocomposites before biodegradation (Figures A8.1-A8.3) and replicate SEM images of 5% w/w MWCNT/PHA nanocomposites after aerobic mixed culture biodegradation (Figure A8.4).

8.6. References

1. De, V. M. F. L.; Tawfick, S. H.; Baughman, R. H.; Hart, A. J., Carbon Nanotubes: Present and Future Commercial Applications. *Science* **2013,** *339*, (6119), 535-539.
2. Gottschalk, F.; Nowack, B., The release of engineered nanomaterials to the environment. *J. Environ. Monit.* **2011,** *13*, (5), 1145-1155.
3. Petersen, E. J.; Zhang, L. W.; Mattison, N. T.; O'Carroll, D. M.; Whelton, A. J.; Uddin, N.; Nguyen, T.; Huang, Q. G.; Henry, T. B.; Holbrook, R. D.; Chen, K. L., Potential release pathways, environmental fate, and ecological risks of carbon nanotubes. *Environ. Sci. Technol.* **2011,** *45*, (23), 9837-9856.
4. Mittal, V., *Nanocomposites with Biodegradable Polymers: Synthesis, Properties, and Future Perspectives*. Oxford University Press: 2011.
5. Goodwin, D. G.; Marsh, K. M.; Sosa, I. B.; Payne, J. B.; Gorham, J. M.; Bouwer, E. J.; Fairbrother, D. H., Interactions of Microorganisms with Polymer

Nanocomposite Surfaces Containing Oxidized Carbon Nanotubes. *Environ. Sci. Technol.* **2015,** *49*, (9), 5484-5492.
6. Shah, A. A.; Hasan, F.; Hameed, A.; Ahmed, S., Biological degradation of plastics: A comprehensive review. *Biotechnol. Adv.* **2008,** *26*, (3), 246-265.
7. Tokiwa, Y.; Calabia, B. P.; Ugwu, C. U.; Alba, S., Biodegradability of Plastics. *International Journal of Molecular Sciences* **2009,** *10*, (9), 3722-3742.
8. Jones, P. H.; Prasad, D.; Heskins, M.; Morgan, M. H.; Guillet, J. E., Biodegradability of photodegraded polymers. I. Development of experimental procedures. *Environ. Sci. Technol.* **1974,** *8*, (10), 919-923.
9. Gross, R. A.; Kalra, B., Biodegradable Polymers for the Environment. *Science* **2002,** *297*, 803-807.
10. Luckachan, G. E.; Pillai, C. K. S., Biodegradable Polymers-A Review on Recent Trends and Emerging Perspectives. *J. Polym. Environ.* **2011,** *19*, (3), 637-676.
11. R, P.; Doble, M., Biodegradation of polymers. *Indian J. Biotechnol.* **2005,** *4*, 186-193.
12. Wilson-Durnat, L. P.; D'Adamo, P. C.; Bouwer, E. J., Aromatic Hydrocarbon Biodegradation with Mixtures of Oxygen and Nitrate as Electron Acceptors. *Environmental Engineering Science* **1999,** *16*, 487-500.
13. Bally, D.; Asano, T.; Bhamidimarri, R.; Chin, K. K.; Grabow, W. O. K.; Hall, E. R.; Ohgaki, S.; Orhon, D.; Milburn, A.; Purdon, C. D.; Nagle, P. T.; Buitrón, G.; González, A., Water Quality International '96 Part 3: Modelling of Activated Sludge Processes; Microorganisms in Activated Sludge and Biofilm Processes; Anareobic Biological Treatment; BiofoulingCharacterization of the microorganisms from an acclimated activated sludge degrading phenolic compounds. *Water Sci. Technol.* **1996,** *34*, (5), 289-294.
14. Lallai, A.; Mura, G., Kinetics of growth for mixed cultures of microorganisms growing on phenol. *The Chemical Engineering Journal* **1989,** *41*, (3), B55-B60.
15. Bhatt, R.; Shah, D.; Patel, K.; Trivedi, U., PHA–rubber blends: Synthesis, characterization and biodegradation. *Bioresource technology* **2008,** *99*, (11), 4615-4620.
16. Jendrossek, D.; Handrick, R., Microbial degradation of Polyhydroxyalkanoates*. *Annual Review of Microbiology* **2002,** *56*, (1), 403-432.
17. Jendrossek, D.; Knoke, I.; Habibian, R. B.; Steinbüchel, A.; Schlegel, H. G., Degradation of poly(3-hydroxybutyrate), PHB, by bacteria and purification of a novel PHB depolymerase fromComamonas sp. *Journal of environmental polymer degradation 1*, (1), 53-63.
18. Madbouly, S. A.; Schrader, J. A.; Srinivasan, G.; Liu, K.; McCabe, K. G.; Grewell, D.; Graves, W. R.; Kessler, M. R., Biodegradation behavior of bacterial-based polyhydroxyalkanoate (PHA) and DDGS composites. *Green Chemistry* **2014,** *16*, (4), 1911-1920.
19. Mas-Castellà, J.; Urmeneta, J.; Lafuente, R.; Navarrete, A.; Guerrero, R., Biodegradation of Poly-β-hydroxyalkanoates in anaerobic sediments. *International Biodeterioration & Biodegradation* **1995,** *35*, (1–3), 155-174.
20. Numata, K.; Abe, H.; Iwata, T., Biodegradability of poly (hydroxyalkanoate) materials. *Materials* **2009,** *2*, (3), 1104-1126.

21. Ohura, T.; Aoyagi, Y.; Takagi, K.-i.; Yoshida, Y.; Kasuya, K.-i.; Doi, Y., Biodegradation of poly(3-hydroxyalkanoic acids) fibers and isolation of poly(3-hydroxybutyric acid)-degrading microorganisms under aquatic environments. *Polymer Degradation and Stability* **1999,** *63*, (1), 23-29.
22. Shah, A. A.; Hasan, F.; Hameed, A., Degradation of poly(3-hydroxybutyrate-co-3-hydroxyvalerate) by a newly isolated Actinomadura sp. AF-555, from soil. *International Biodeterioration & Biodegradation* **2010,** *64*, (4), 281-285.
23. Shah, A. A.; Hasan, F.; Hameed, A.; Ahmed, S., Biological degradation of plastics: A comprehensive review. *Biotechnology Advances* **2008,** *26*, (3), 246-265.
24. Volova, T. G.; Boyandin, A. N.; Vasil'ev, A. D.; Karpov, V. A.; Kozhevnikov, I. V.; Prudnikova, S. V.; Rudnev, V. P.; Xuån, B. B.; Dũng, V. V.; Gitel'zon, I. I., Biodegradation of polyhydroxyalkanoates (PHAs) in the South China Sea and identification of PHA-degrading bacteria. *Microbiology* **2011,** *80*, (2), 252-260.
25. Volova, T. G.; Boyandin, A. N.; Vasiliev, A. D.; Karpov, V. A.; Prudnikova, S. V.; Mishukova, O. V.; Boyarskikh, U. A.; Filipenko, M. L.; Rudnev, V. P.; Bá Xuân, B.; Việt Dũng, V.; Gitelson, I. I., Biodegradation of polyhydroxyalkanoates (PHAs) in tropical coastal waters and identification of PHA-degrading bacteria. *Polymer Degradation and Stability* **2010,** *95*, (12), 2350-2359.
26. Volova, T. G.; Gladyshev, M. I.; Trusova, M. Y.; Zhila, N. O., Degradation of polyhydroxyalkanoates in eutrophic reservoir. *Polymer Degradation and Stability* **2007,** *92*, (4), 580-586.
27. Weng, Y.-X.; Wang, X.-L.; Wang, Y.-Z., Biodegradation behavior of PHAs with different chemical structures under controlled composting conditions. *Polymer Testing* **2011,** *30*, (4), 372-380.
28. Mergaert, J.; Anderson, C.; Wouters, A.; Swings, J.; Kersters, K., Biodegradation of polyhydroxyalkanoates. *FEMS Microbiol. Lett.* **1992,** *103*, (2-4), 317-321.
29. Armentano, I.; Dottori, M.; Fortunati, E.; Mattioli, S.; Kenny, J. M., Biodegradable polymer matrix nanocomposites for tissue engineering: A review. *Polymer Degradation and Stability* **2010,** *95*, (11), 2126-2146.
30. Huh, M.; Jung, M. H.; Park, Y. S.; Kim, B.-J.; Kang, M. S.; Holden, P. J.; Yun, S. I., Effect of carbon nanotube functionalization on the structure and properties of poly(3-hydroxybutyrate)/MWCNTs biocomposites. *Macromolecular Research* **2014,** *22*, (7), 765-772.
31. Kim, J. Y., Carbon nanotube-reinforced thermotropic liquid crystal polymer nanocomposites. *Materials* **2009,** *2*, (4), 1955-1974.
32. Liao, H.-T.; Wu, C.-S., Poly (3-hydroxybutyrate)/multi-walled carbon nanotubes nanocomposites: Preparation and characterizations. *Designed Monomers and Polymers* **2013,** *16*, (2), 99-107.
33. Velasco-Santos, C.; Martínez-Hernández, A. L.; Fisher, F. T.; Ruoff, R.; Castaño, V. M., Improvement of Thermal and Mechanical Properties of Carbon Nanotube Composites through Chemical Functionalization. *Chemistry of Materials* **2003,** *15*, (23), 4470-4475.
34. Yun, S. I.; Gadd, G. E.; Latella, B. A.; Lo, V.; Russell, R. A.; Holden, P. J., Mechanical Properties of Biodegradable Polyhydroxyalkanoates/Single Wall Carbon Nanotube Nanocomposite Films. *Polymer Bulletin* **2008,** *61*, (2), 267-275.

35. Lee, S. Y.; Choi, J.-i.; Wong, H. H., Recent advances in polyhydroxyalkanoate production by bacterial fermentation: mini-review. *Int. J. Biol. Macromol.* **1999,** *25*, (1–3), 31-36.
36. Harding, K. G.; Dennis, J. S.; von Blottnitz, H.; Harrison, S. T. L., Environmental analysis of plastic production processes: Comparing petroleum-based polypropylene and polyethylene with biologically-based poly-β-hydroxybutyric acid using life cycle analysis. *J. Biotechnol.* **2007,** *130*, (1), 57-66.
37. Roy, I.; Visakh, P., *Polyhydroxyalkanoate (PHA) based blends, composites and nanocomposites*. Royal Society of Chemistry: 2014; Vol. 30.
38. Volova, T. i. a. G. e., *Polyhydroxyalkanoates--plastic materials of the 21st century: production, properties, applications*. Nova publishers: 2004.
39. Sudesh, K., *Polyhydroxyalkanoates from palm oil: biodegradable plastics*. Springer Science & Business Media: 2012.
40. Misra, S. K.; Valappil, S. P.; Roy, I.; Boccaccini, A. R., Polyhydroxyalkanoate (PHA)/Inorganic Phase Composites for Tissue Engineering Applications. *Biomacromolecules* **2006,** *7*, (8), 2249-2258.
41. Bohutskyi, P.; Bouwer, E., Biogas production from algae and cyanobacteria through anaerobic digestion: a review, analysis, and research needs. In *Advanced Biofuels and Bioproducts*, Springer: 2013; pp 873-975.
42. Gilmore, D. F.; Antoun, S.; Lenz, R. W.; Fuller, R. C., Degradation of poly (β-hydroxyalkanoates) and polyolefin blends in a municipal wastewater treatment facility. *J. Environ. Polymer Degradation* **1993,** *1*, (4), 269-274.
43. Massardier-Nageotte, V.; Pestre, C.; Cruard-Pradet, T.; Bayard, R., Aerobic and anaerobic biodegradability of polymer films and physico-chemical characterization. *Polymer Degradation and Stability* **2006,** *91*, (3), 620-627.
44. Leja, K.; Lewandowicz, G., Polymer biodegradation and biodegradable polymers—a review. *Pol. J. Environ. Stud.* **2010,** *19*, (2), 255-266.
45. EPA, 5210B Biochemical Oxygen Demand (BOD) Standard Method. In United States of America, 2001.
46. ASTM, E1196-92 Standard Test Method for Determining the Anaerobic Biodegradation Potential of Organic Chemicals. In American Society for Testing and Materials: West Conshohocken, PA, 1992.
47. Owen, W.; Stuckey, D.; Healy, J.; Young, L.; McCarty, P., Bioassay for monitoring biochemical methane potential and anaerobic toxicity. *Water Res.* **1979,** *13*, (6), 485-492.
48. Laurent, C.; Flahaut, E.; Peigney, A., The weight and density of carbon nanotubes versus the number of walls and diameter. *Carbon* **2010,** *48*, (10), 2994-2996.
49. Metabolix, Material Safety Data Sheet, Polymeric Modifier I6001- Powder. In December 09, 2013.
50. Qiu, Z.; Wang, H.; Xu, C., Crystallization, mechanical properties, and controlled enzymatic degradation of biodegradable poly(ε-caprolactone)/multi-walled carbon nanotubes nanocomposites. *Nanosci. Nanotechnol.* **2011,** *11*, 7884-7893.
51. Barham, P. J.; Keller, A.; Otun, E. L.; Holmes, P. A., Crystallization and morphology of a bacterial thermoplastic: poly-3-hydroxybutyrate. *Journal of Materials Science* **1984,** *19*, (9), 2781-2794.

52. Yildirimer, L.; Buanz, A.; Gaisford, S.; Malins, E. L.; Remzi Becer, C.; Moiemen, N.; Reynolds, G. M.; Seifalian, A. M., Controllable degradation kinetics of POSS nanoparticle-integrated poly(ε-caprolactone urea)urethane elastomers for tissue engineering applications. *Scientific Reports* **2015,** *5*, 15040.
53. Tokiwa, Y.; Calabia, B. P.; Ugwu, C. U.; Aiba, S., Biodegradability of Plastics. *International Journal of Molecular Sciences* **2009,** *10*, (9), 3722-3742.
54. Goodwin Jr, D. G.; Marsh, K.; Sosa, I. B.; Payne, J. B.; Gorham, J. M.; Bouwer, E. J.; Fairbrother, D. H., Interactions of Microorganisms with Polymer Nanocomposite Surfaces Containing Oxidized Carbon Nanotubes. *Environmental science & technology* **2015,** *49*, (9), 5484-5492.
55. Goodwin, D. G.; Xia, Z.; Gordon, T. B.; Gao, C.; Bouwer, E. J.; Fairbrother, D. H., Biofilm development on carbon nanotube/polymer nanocomposites. *Environmental Science: Nano* **2016**.
56. Buswell, A. M.; Mueller, H. F., Mechanism of Methane Fermentation. *Industrial & Engineering Chemistry* **1952,** *44*, (3), 550-552.
57. Zhang, L.; Petersen, E. J.; Habteselassie, M. Y.; Mao, L.; Huang, Q., Degradation of multiwall carbon nanotubes by bacteria. *Environ. Pollut. (Oxford, U. K.)* **2013,** *181*, 335-339.
58. Arias, L. R.; Yang, L., Inactivation of Bacterial Pathogens by Carbon Nanotubes in Suspensions. *Langmuir* **2009,** *25*, (5), 3003-3012.

Appendix 3. Initial Interactions of Microorganisms with Carbon Nanotube/Polymer Nanocomposites

This work was co-written with the following authors and is published under the following citation:

Goodwin Jr, D. G., Marsh, K. M., Sosa, I. B., Payne, J. B., Gorham, J. M., Bouwer, E. J., & Fairbrother, D. H. (2015). Interactions of Microorganisms with Polymer Nanocomposite Surfaces Containing Oxidized Carbon Nanotubes. *Environmental Science & Technology*, *49* (9), 5484-5492.

A3.1. Spray Coating

As shown in Figure A3.1, CNT/PVOH casting solutions were prepared and spray-coated on glass slides to generate well-dispersed O-CNT/PVOH nanocomposites. Although not necessarily representative of nanocomposite surfaces in commercial use, spray-coating can be considered useful for preparing well-defined CNT/PNC surfaces.

A3.2. SEM

To prepare samples specifically for SEM imaging, O-MWCNT and O-SWCNT/PVOH nanocomposites were spray-coated onto 1 cm^2-sized glass pieces and sputter-coated with platinum (Quorum Technologies Polaron SC7640 Auto/Manual High Resolution Sputter Coater, 12 mA/800V plasma current, and ~5 min at 0.5 nm/min) to prevent charging. Samples were imaged using a cold-cathode field emission scanning electron microscope (JEOL 6700F, 10 keV, 7.0 nm working distance, LEI & SEI detectors) with a 1.0 nm resolution at 15 keV equipped with an energy dispersive X-ray analyzer

(EDAX Genesis 4000 X-ray analysis system, detector resolution of 129 eV). Replicate images can be found in Figure A3.2a-i. Samples were imaged at 30,000x magnification in triplicate locations and at a lower magnification of 15,000x; imaged areas were chosen at random to ensure that a uniform CNT dispersion had been obtained across the nanocomposite surface. O-MWCNT/PVOH nanocomposites were also imaged on duplicate glass pieces sprayed at different times to confirm batch-to-batch consistency (Figure A3.2a-i). Additional SEM images were acquired with another microscope as part of the dissolution control studies and to image microbes fixed on nanocomposite surfaces as outlined later in the SI.

A3.3. SEM Broadening

For O-MWCNTs, the diameter of individual CNTs appeared to be on the order of 15-35 nm, which is fairly consistent with the manufacturer's specifications of 15 ± 5 nm plus a sputtered coating of 5-15 nm platinum nanoparticles used to improve sample conductivity. This was also the case for O-SWCNT/PVOH nanocomposites where the CNT diameters appeared to be 10-25 nm due to the platinum coating rather than the reported CNT diameter of 1-2 nm. The more significant broadening of the O-SWCNT diameters relative to the O-MWCNT diameters in the SEM images appeared to be a result of the platinum nanoparticles being raised only slightly above the background by the O-SWCNTs, causing O-SWCNTs to appear wider than expected. In contrast, the platinum nanoparticles appeared to curve around the O-MWCNTs, causing diameter broadening to a lesser degree. Although O-SWCNT bundling was possible, all O-SWCNTs exhibited the same diameter and were well-dispersed in the SEM images, suggesting that they were present as individual particles.

A3.4. XPS

Samples composed of pure PVOH (0% w/w), O-MWCNTs (100% w/w), and O-MWCNT/PVOH nanocomposites with O-MWCNT loadings of 5, 10, 25, 50, 60, and 80% w/w were prepared on 1 cm^2 glass slide pieces and analyzed. Samples composed of pure O-SWCNTs (100% w/w), and O-SWCNT/PVOH nanocomposites with O-SWCNT loadings of 5 and 10% w/w were also prepared and analyzed (Figure A3.3). All %CNT values reported are representative of an average ± one standard deviation from the three unique measurements acquired on different areas of the same CNT/PNC surface. The exception was the pure O-MWCNT sample which represents the average of two measurements.

Samples were mounted onto a sample bar capable of handling multiple samples at one time and were subsequently pumped down in an attached load-lock chamber prior to introduction to the main UHV chamber. The sample bar was then transferred to a stage capable of X, Y, Z, and rotational automated movement for analysis. Spectra were acquired under ultra-high vacuum conditions ($P_{base}<10^{-9}$ torr) on an Axis Ultra DLD Imaging Spectrophotometer from Kratos Analytical, LTD (Chestnut Ridge, NY). Spectra were collected for each sample on three different areas of the surface with care taken to minimize overlap of the points of analysis. Monochromatic Al Kα X-rays (150 W) were used to achieve photo-emission and all O-MWCNT/PVOH nanocomposite samples were analyzed without the charge neutralizer active. However, due to the insulating properties of PVOH, the spectra for these samples were collected with the charge neutralizer on. At each point, the spot size was controlled with a hybrid lens and slot aperture (475 x 1050 μm^2) to maximize the photoelectron count. The C(1s) spectra were analyzed using a hemispherical analyzer at a pass energy of 10 eV at 0.1 eV/step and a dwell time of 1200 s/step. Due to

the variability in conductivity of the O-MWCNT/PVOH nanocomposites, most C (1s) spectra were collected in large energy windows (44-48 eV spectral window for O-MWCNT samples compared to the typical 23 eV spectral window for the PVOH control) to ensure all photoelectron intensity was captured.

Analysis of collected spectra was performed using CasaXPS (Teignmouth, UK). Each C(1s) envelope was fit with a Tougaard background and energy adjusted to the clearly distinguishable O-MWCNT feature taken from the pure O-MWCNT C(1s) spectrum centered at 284.5 eV which is typically associated with CNTs (see Figure 3.2).[1, 2] O-SWCNT/PVOH samples were not fitted with components as the CNT feature was not distinguishable from the PVOH peaks (Figure A3.3).

For pure polyvinyl alcohol, as expected, the C(1s) region showed two peaks of equal intensity separated by 1.4 eV (consistent with (1.6 ± 0.2) eV from Briggs et al.) attributed to the CH_2 and CH(OH) moieties of the polymer (Fig 2a).[3] The C(1s) spectrum of each sample was fitted with 4 components: the O-MWCNT feature from the pure O-MWCNT sample, CH_2 and CH(OH) components of equal value to represent the PVOH present at the surface, and an extra CH_2 component to represent any surface bound hydrocarbon contamination. The pure PVOH spectrum was then energy adjusted using the average fitted CH_2 peak location from the O-MWCNT sample with the lowest O-MWCNT concentration (5% w/w) and fitted using the same components. Based on the component analysis, each C(1s) spectrum could therefore be used to determine the %CNT using the equation:

$$\%CNT = [\text{CNT Component Area}/\text{C(1s) Area}] * 100 \qquad \text{(Equation 1)}$$

The slight deviations in the proportionality fit at low CNT loadings are likely due to the difficulty in obtaining quantitative XPS analysis when one component is present at low concentrations and/or due to a slight degree of CNT enhancement at the surface. XPS (PHI 5600, $P_{base}<10^{-9}$ torr, Mg Kα X-rays (300 W), 187.85 eV pass energy, 0.200 eV/step, 50 ms dwell time, 0.8 x 2 mm area) was also used to estimate the nanocomposite thicknesses at 0% w/w (PVOH) and 10% w/w to obtain an average thickness for the nanocomposites studied (0 – 10% w/w). Since the underlying nanocomposite substrate was glass, we measured the attenuation of the silicon (2p) peak area relative to the silicon (2p) peak area of pure glass. From the equation, $d = \lambda cos\theta \ln\left(\frac{I_0}{I}\right)$,[4] where λ is the inelastic mean free path of the silicon (2p) photoelectron from the literature (2.7 nm),[5] θ is the take-off angle (54.7°), (I/I_0) is the fractional decrease in the Si(2p) signal after the CNT/PNC coating was sprayed, and d is the depth of the CNT/PNC overlayer, we estimate that the average coating thickness is 8 nm for all nanocomposites studied (0 – 10% w/w). Since this analysis was carried out in triplicate on different areas of the sample, it is clear from both XPS and visual observation that the nanocomposite fully coated the glass slides.

A3.5. SEM- Dissolution Controls

In the polymer dissolution control experiments and the microbial fixation procedure, samples were imaged on a lower resolution SEM (3.0 nm resolution at 10 keV) at around 12,000x magnification (FEI Quanta 200 Environmental SEM, 2.5 keV, 9.5 mm working distance, high vacuum mode, Everhart-Thornley detector) to obtain a large number of low magnification images; this was possible with a relatively high concentration of CNTs at the surface of a CNT/PNC (> 5% w/w) despite the low resolution of the FEI Quanta 200 relative to the JEOL 6700F SEM. Prior to imaging, samples were sputter-

coated with platinum (Hummer Sputtering System, Anatech USA, 15 mA plasma current, for 2 min at ~2 nm/min).

5% w/w O-MWCNT/PVOH was chosen to represent the varied CNT/PVOH nanocomposite loadings since changes caused by dissolution at a higher CNT loading would be most obvious with a greater number of CNTs observable at the surface prior to water immersion (Figure A3.4). In addition, a 10% w/w O-MWCNT/PVOH nanocomposite was chosen for 1 and 6 h dissolution control studies since 6 h was the timescale chosen for longer term biofilm studies (Figure A3.5).

In these dissolution control studies, pure PVOH, 5% and 10% w/w O-MWCNT/PVOH nanocomposites were spray-coated onto 1 cm^2 glass slide pieces following the same procedure outlined in the O-CNT/PVOH nanocomposite preparation section. One set of nanocomposite samples (0, 5, and 10% w/w O-MWCNT/PVOH) were placed directly into a dessicator (dry controls) while an identical set was submerged in autoclaved water (dissolution controls) for 1 and/or 6 h. Dissolution control samples were then dried in a dessicator overnight prior to SEM imaging. Multiple large-area images were taken (>25 x 25 μm) under high vacuum mode (P_{base}< $7.5x10^{-5}$ torr) to compare the surface structure of nanocomposites that had been immersed (dissolution controls) to those which had not (dry controls).

A3.6. Microbial Stocks

Pseudomonas aeruginosa (ATC 27853) was originally obtained as a slant culture from the Medical Microbiology Department at the Johns Hopkins School of Medicine. Cells from the slant culture were streaked onto an LB agar plate and grown overnight at 37˚C. A colony was then selected, aseptically added to LB broth and grown at 225 rpm and 37˚C to an optical density (O.D.) within the exponential phase (0.6 - 0.8 O.D. at 540 nm).

To prepare frozen stocks, the cell suspension was distributed into sterile Eppendorf tubes with a final glycerol concentration of 15% v/v and stored at -80˚C. The growth curve of *P. aeruginosa* in LB broth used in the experiments is shown in Figure A3.7 (between 0.6 and 0.8 O.D. at 540 nm). For all growth curves, the exponential growth portion was fit to a first order model to obtain an estimate of k (the specific growth rate) and the R^2 values for the fit in order to compare *P. aeruginosa* growth under different conditions. The specific growth rate of *Pseudomonas aeruginosa* in LB broth at 37˚C was calculated to be 2.74 x 10^{-2} min^{-1} (R^2=0.99) at 540 nm (2.87 x 10^{-2} min^{-1} at 600 nm, R^2=0.99).

A3.7. Basal Mineral Media (BMM) Composition

BMM contained the following: 7.18 mM K_2HPO_4, 2.79 mM KH_2PO_4, 0.757 mM $(NH_4)_2SO_4$, 0.0406 mM $MgSO_4*7H_2O$, 0.5 v/v% Trace Elements Solution: 3.75 mM H_3BO_3, 0.0605 mM $ZnSO_4*7H_2O$, 0.0296 mM $FeSO_4(NH_4)_2SO_4*6H_2O$, 0.034 µM $CoSO_4*7H_2O$, 26 µM $(NH_4)_6Mo_3O_{24}*4H_2O$, 32 µM $CuSO_4*5H_2O$, and 36 µM $MnSO_4*4H_2O$.

A3.8. Microbial Growth

Each experiment involved growing a culture of *P. aeruginosa* from the thawed frozen stock in LB broth at 37˚C and 225 rpm and harvesting the cells in the exponential phase (between 0.6 and 0.8 O.D. at 540 nm, Figure A3.6). The LB broth culture was then diluted 1:1,000 in 100 mL of BMM containing acetate as the carbon source (24 mM sodium acetate); the large dilution was used to minimize the addition of extracellular polymeric substances (EPS) and LB broth. Additionally, cells were harvested at the exponential phase in LB broth to maximize the fraction of living planktonic cells added to BMM since more significant die-off occurred when the culture reached the stationary phase. The *P. aeruginosa* culture in BMM was grown overnight at 25˚C and shaking at 225 rpm to the

exponential phase which is shown in the BMM growth curve in Figure A3.8, (0.04-0.06 O.D. at 540 nm) for addition to the CNT/PVOH samples. The exponential phase was chosen again to maximize the fraction of living planktonic cells in the BMM inoculum used during CNT/PVOH slide immersion. The specific growth rate of *Pseudomonas aeruginosa* in BMM at 25˚C was calculated to be 9.9 x 10^{-3} min^{-1} at 540 nm (average of duplicate cultures, R^2=0.98).

A3.9. BMM Growth Curve, With and Without 90 ppb CNTs

CNT release was also assessed using single-particle ICP-MS, with yttrium nanoparticles used as a proxy for CNT concentration.

A growth curve of *P. aeruginosa* in BMM was carried out with 200 µL of exponential phase LB broth (0.6-0.8 O.D. at 540 nm) diluted into 100 mL of BMM. This dilution was less than that used in the microbe-CNT interaction experiments, but served the purpose of determining the exponential phase of *P. aeruginosa* (Figure A3.8).

Growth curves were also measured in the presence of 90 ppb O-MWCNTs and 90 ppb O-SWCNTs, separately. This CNT concentration was determined to be the upper limit of CNT release that could occur based on ICP-MS experiments outlined later in the SI. No inhibitory effect on microbial growth was observed in the presence of 90 ppb CNTs. The specific growth rates in BMM at 25 °C were 6.7 x 10^{-3} min^{-1} (R^2=0.98) and 9.0 x 10^{-3} min^{-1} (R^2=0.95) at 540 nm for O-MWCNTs and O-SWCNTs, respectively. These specific rate constants were very close to 9.9 x 10^{-3} min^{-1} (R^2=0.99) for the BMM culture without CNTs, further indicating that there was no CNT effect on the *P. aeruginosa* culture. All growth curves, with and without CNTs, were carried out in duplicate and the specific growth rates were calculated from the average of the duplicates (Figure A3.8).

A3.10. LIVE/DEAD Staining Procedure

A LIVE/DEAD biofilm viability kit, purchased from Invitrogen, included two separate stock solutions: (1) 3.34 M SYTO 9 in dimethylsulfoxide (DMSO) to stain living cells, and (2) 20 mM propidium iodide (PI) in DMSO to stain dead cells that were stored at -20˚C. The green fluorescent stain, SYTO 9, can permeate through the membranes of both living and dead cells while the red fluorescent stain, PI, can permeate through the membranes of only dead cells. When they enter a cell, both stains fluoresce as a result of their interactions with DNA. Since only SYTO 9 can enter living cells, these cells fluoresce green during imaging. In contrast, since both PI and SYTO 9 can enter dead cells when used in conjunction, the fluorescence of SYTO 9 is reduced by the presence of PI and as a result, the dead cells appear red during fluorescence imaging.[6]

To stain the *P. aeruginosa* adhered to the nanocomposite slides, an aqueous stock solution containing both SYTO 9 and PI was prepared in a conical tube by adding 3 µL of SYTO 9 stock (1) and 3 µL of PI stock (2) for every 1 mL of autoclaved Milli-Q water. This stock solution was then shaken and wrapped in aluminum foil to minimize its exposure to light due to the photosensitivity of both stains.[6]

Following *P. aeruginosa* inoculation (described in the experimental section) and washing in depleted media, slides were transferred to sterile petri dishes where the stock solution was gently added to the surface of the wet nanocomposites. Enough stock solution (0.5 mL) was prepared so that each slide could be completely covered. To keep the nanocomposite surfaces wet at all times and thereby prevent changes in cell death upon drying, staining was carried out in a staggered fashion; one slide was transferred to a petri dish, 0.5 mL of the stain solution was aseptically added to the slide, and then the next slide

was transferred to repeat the process. Each slide was stained for 20 min and protected from light by covering the petri dishes with aluminum foil.[6]

After staining, each nanocomposite slide was removed from its petri dish and placed gently into depleted media (DM, basal mineral media with no acetate food source) for 30 s to remove excess stain and then transferred to a second DM dish for temporary storage until imaging. To ensure that all samples were exposed to the LIVE/DEAD stains for equal amounts of time, the order in which the slides were rinsed and stored was the same as the order in which they were stained. At this stage, nanocomposite slides were transported in DM to the Johns Hopkins Integrated Imaging Center (IIC) and analyzed. The following procedures were carried out to obtain consistent and reliable staining information:

1) Each time microbes on CNT/PNCs were imaged, living and dead controls were included to ensure that the laser gains were set appropriately on the CLSM. The living control was generated by performing LIVE/DEAD staining on *P. aeruginosa* which had been in contact with a pure PVOH surface for 1 or 6 h. A PVOH living control exposed to *P. aeruginosa* for 6 h is shown in Figure A3.9, which was run concurrently with the 6 h-exposed, 10% w/w O-MWCNT/PVOH sample shown in Figure 3.3 of the main text. The same procedure was used for the dead control but the cells were first immersed in 70% v/v ethanol for 5 min prior to staining to cause intentional cell death (Figure A3.10).
2) Three nanocomposites of a particular CNT loading (at least two of which were spray-coated on separate occasions) were run at different times with three

separately grown cultures to ensure cell attachment consistency and multiple areas (225 x 225) μm were imaged for each run (Figure A3.6).

3) Polymer and nanocomposite surfaces were always kept wet to prevent artificial cell death. This is because drying can potentially increase membrane permeability and lead to increased PI uptake and/or loss of uptaken SYTO 9, as over-counting of red fluorescent cells was observed in trial experiments where samples were dried out.[6] Thus, samples were kept wet at all times by running no more than four to five nanocomposite slides at a time and staggering the staining process. Imaging of the wet slides was also performed using a 40x water immersion objective without a cover slip to prevent drying or pressure gradients.
4) The frozen stock solutions of each fluorescent stain had to be fully thawed before use or stain concentrations varied. This possibly occurred as a result of the stains thawing at different rates than the solvent (DMSO).
5) The stock solution containing the stains that was added directly to the samples was prepared in autoclaved water to minimize reaction with phosphates in media. Phosphates are known to interact with the stains over time, reducing the concentration of SYTO 9 and PI.
6) The underlying glass slides were frosted on one end, which is where they were picked up with forceps. This part of the slide was selected because it could easily be distinguished from the rest of the slide. The stain was added carefully at the frosted end. Imaging was never performed on the frosted end where the stain was added to prevent disruption of attached cells.

7) Stained slides were rinsed and stored in DM. This helped to remove excess stains and prevent drying prior to imaging. DM was used instead of autoclaved Milli-Q water to prevent an increase in membrane permeability that could lead to a corresponding increase in the number of dead cells due to a loss of ionic strength. The use of DM in place of BMM also helped to minimize further cell division on nanocomposite surfaces prior to imaging by minimizing the presence of an acetate food source.

A3.11. Confocal Laser Scanning Microscope (CLSM)

Using the eye piece, the objective was manually brought into focus on the sample for a minimal amount of time to limit light exposure from the mercury vapor short-arc lamp (HBO 100 Microscope Illuminator, HBO 103W/2 bulb 100W, 23V) equipped with a 488 nm FITC filter or a 543 nm red filter. Following the initial focus, the objective was moved to another area on the slide where light exposure had not occurred and the sample thickness was manually set using the fine focus and the image read-out from the scanning lasers. The lasers used were a 488 nm Argon laser (30 mW at 5% output) to excite the green fluorescence of the SYTO 9 stain and a 543 nm HeNe laser (1.2 mW) to excite the red fluorescence of the PI stain. A composite green- and red-fluorescent image with a 225 x 225 μm area was subsequently collected. Several images were taken on different areas of each nanocomposite surface. Image analysis software was used to count the living and dead cells at each CNT loading.

A3.12. LIVE/DEAD Cell Counting using Image Analysis Software

Confocal images of LIVE/DEAD stained *P. aeruginosa* on O-CNT/PVOH nanocomposites were analyzed to determine the percentage of living microbes based on

the red and green stains. CLSM files generated during image capture were opened in ImageJ (NIH, Bethesda, MD), converted into a composite image (Color: Channel Tools), converted to RGB, and saved as an image sequence.

The most focused image plane of the image sequence was then opened in MATLAB R2011b (The MathWorks Inc., Natick, MA) and particle-counting and live/dead thresholding code was run (written by Alice Sanchez, Integrated Imaging Center, JHU). The code works by particle-counting, finding the average pixel area and standard deviation of counted cells, and breaking up aggregates and larger "particles" into one or more cells if their size exceeds one standard deviation of the average pixel area. For a counted cell, the sum of the green intensity of each pixel in the cell area to the sum of the red intensity of each pixel in the cell area was ratioed. Cells were counted as alive if the ratio was greater than one and dead if the ratio was less than one.

A3.13. Background Fluorescence Controls

Pure PVOH, 10% w/w O-MWCNT/PVOH, and 10% O-SWCNT/PVOH samples were stained without bacteria and imaged using CLSM to determine if there were any fluorescence contributions from polymer and/or CNT-stain interactions. The image plane was located using either the bright field objective (for PVOH) or by finding a piece of dust or contaminant that weakly fluoresced on the O-CNT/PVOH nanocomposites (bright field imaging is not possible with opaque nanocomposite slides). These images clearly showed no background fluorescence (Figure A3.11).

A3.14. Cell Attachment Controls

To confirm that the majority of cells stained came from the 1 h microbial exposure process and not from cell attachment during transfer through the air-liquid interface, PVOH, 10% w/w O-MWCNT/PVOH, and 10% w/w O-SWCNT/PVOH samples were

fully immersed into and then immediately (< 5 s) removed from the inoculum and stained. These control studies showed that minimal cell attachment (1-5 cells) occurred relative to the >1500 cells attached after one immersion in the inoculum (Figure A3.12).

A3.15. Fluorescence Photobleaching and Quenching Controls

To ensure the integrity of the LIVE/DEAD fluorophores was maintained during the time frame of image acquisition, controls were prepared with the highest CNT loading nanocomposites as well as pure PVOH. A pure PVOH, a 10% w/w O-MWCNT/PVOH and a 10% w/w O-SWCNT/PVOH nanocomposite were inoculated for 1 h and stained according to the procedure outlined in the LIVE/DEAD staining section. Each sample was imaged with CLSM and then re-imaged in the same location after 5 min. The same procedure was followed with staining solutions containing only SYTO 9 and only PI to assess the effect of using 488 nm and 543 nm laser excitations on each of the fluorophores separately (Figures A3.13-A3.15). Results from these studies indicate that loss of fluorescence intensity from each fluorophore, together and separately, did not occur within the timeframe of this study. Thus, any issues or experimental artifacts that could occur as a result of photobleaching, decomposition of a fluorophore by light, or fluorescence quenching caused by energy or electron transfer to CNTs did not influence the results presented in this investigation.

A3.16. EPS Staining

PVOH, 10% w/w O-MWCNT/PVOH and 10% w/w O-SWCNT/PVOH samples were exposed to *P. aeruginosa* for 1 h. The FilmTracer SYPRO Ruby Red Biofilm Viability Kit (Invitrogen, Life Technologies) was then used to stain the EPS with the same washing procedures used for the LIVE/DEAD stains and in accordance with the SYPRO Ruby Red Biofilm Matrix Stain manual.[7] Minimal EPS was observed on all sample

surfaces (Figure A3.16). Background fluorescent controls were also run for this stain (Figure A3.17). The SYPRO stain was excited in CLSM with the Argon laser (excitation around 450 nm) and fluoresced at 610 nm.

A3.17. SEM Imaging of Fixed *P. aeruginosa* on O-CNT/PVOH Nanocomposites

Pure PVOH and 10% w/w O-MWCNT/PVOH nanocomposites were spray-coated onto thin, circular, 1-cm diameter glass cover slips and inoculated for 1 h with *P. aeruginosa*. Samples were stored in DM and then fixed to preserve cell membrane structure during dehydration and to help dissipate charge at the cell membrane surface during SEM imaging. Fixation of the microbes was carried out using 3.0% v/v formaldehyde and 1.5% v/v glutaraldehyde in 0.1 M sodium cacodylate solution containing 5 M $CaCl_2$ and 2.5% v/v sucrose at pH 7.4 and room temperature for 1 h. The samples were washed three times for 15 min each in 0.1 M sodium cacodylate containing 2.5% v/v sucrose at pH 7.4. Samples were then post-fixed with 10 mL of Palade's OsO_4 solution (1% v/v OsO_4, 0.1 M sodium cacodylate containing 2.5% v/v sucrose at pH 7.4) for 30 min at room temperature to preserve lipid and polysaccharide structure. Each sample was rinsed for 30 s in deionized water and then rinsed for 30 s in cold (4˚C), 50% v/v ethanol. At this time, samples were gradually dehydrated with a graded series of cold (4˚C) ethanol (70, 95, and 100% v/v) followed by three 15 min washes in 100% ethanol.[8] This removed all water within the cells while maintaining their membrane structure so that they could be imaged under high vacuum mode ($P_{base} < 7.5x10^{-5}$ torr).

Ethanol was then removed from the samples by exchange with CO_2 in a CO_2 critical point drier (Samdri®-795, Tousimis Research Corporation, Rockville, MD 20852). At this stage, the samples were sputter-coated with platinum (Hummer Sputtering System, Anatech USA, 15 mA plasma current, for 2 min at 2 nm/min) to prevent charging and then

imaged at 6,500x and 2.5 eV using the FEI Quanta 200 Environmental; in some cases microorganisms were artificially cropped and then moved around on an SEM image to assess the relative size of the microorganisms to the CNTs (Figures A3.18, A3.19, A3.20, and A3.22). The dimensional relationship of the SEM images to the CLSM images is also shown in Figures A3.18 and A3.19 with "live on top of dead" structures circled in the CLSM images. The SEM images of the fixed microbes, without alteration, are shown in Figure A3.20.

A3.18. Antimicrobial Trends of O-MWCNTs versus O-SWCNTs in PVOH

Two-parameter exponential decay profiles were fit to the % living cells as a function of CNT loading for both O-MWCNT and O-SWCNT/PVOH nanocomposites (Figure A3.21). From comparison of the b parameters (0.37 vs. 1.14), it can be roughly estimated that the O-SWCNT nanocomposites are roughly three times more cytotoxic than O-MWCNT nanocomposites at a given CNT loading due to a number density effect. A graphic depicting the difference in CNT number density and available CNT-microbe contact area is shown for O-MWCNTs and O-SWCNTs at the same CNT loading (1% w/w) in Figure A3.22.

A3.19. Metal Ion Release Studies

The residual metal content (from CNT synthesis) of each CNT type used is shown in Table A3.1. This metal content was determined via energy dispersive X-ray analysis (EDS, EDAX Genesis 4000 X-ray analysis system, detector resolution of 129 eV).

Metal ion release controls for 10% w/w O-MWCNT and O-SWCNT/PVOH nanocomposites were run to determine the concentration of yttrium that leached from the surfaces over the course of the experiment. Samples were placed in sterilized Milli-Q water for 1 h in duplicate according to the procedure outlined in the microbial growth section.

Each supernatant was collected in a polypropylene tube and filtered with a 0.02 µm glass fiber membrane to remove any released CNTs prior to analysis for detection of only metal ions. Dissolved yttrium was detected with ICP-MS (Perkin Elmer NexION 300q with S10 autosampler) to determine if it had an effect on cytotoxicity. Dissolved Y calibration standards were prepared using Claritas PPT (SPEX Certiprep) ICP-MS standard grade stock solutions. A calibration curve (sum of counts) of dissolved Y standards was generated; the data was collected with a 0.1 ms dwell time, 0.975 mL/min flow rate, and a 3% transport efficiency. For the metal release control supernatants, data was collected with a 0.1 ms dwell time, 0.300 mL/min flow rate, with a 9.5% transport efficiency in duplicate (A&B) and the yttrium concentration was calculated from the dissolved yttrium calibration curve (Figure A3.23).

ICP-MS in single particle mode was also used (sp-ICPMS) to indirectly detect O-SWCNTs by using yttrium nanoparticles as a proxy for released CNTs from nanocomposites during 1 h of aqueous submersion. Released CNT concentrations were obtained from the pre-filtered supernatants on the same samples described in the previous paragraph, in duplicate. The CNT concentrations from release were calculated from a calibration curve of yttrium particle number as a function of O-SWCNT mass concentration prepared with controlled loadings of O-SWCNTs in suspension. The CNT concentration was estimated to be 90 ppb or less. A growth curve in BMM containing 90 ppb of O-SWCNTs and another containing 90 ppb O-MWCNTs were carried out, as described earlier in the SI, to ensure that cell death was not occurring more readily in CNT-containing solutions at a 90 ppb CNT concentration relative to CNT-free solutions. The growth curve was unaffected, indicating that the low concentration of released CNTs had

little effect on the microbes in the exponential phase, the point at which the cells were attaching to the nanocomposite surfaces (Figure A3.8).

A3.20. LIVE/DEAD Staining of *P. aeruginosa* Exposed to a Hydrophobic Surface for 1 h

A hydrophobic polymer, poly-ε-caprolactone (PCL), was dissolved at 2 mg/mL in chloroform and spray-coated onto octadecyltrichlorosilane-modified glass slides at 60 °C. It was then exposed to *P. aeruginosa* for 1 h and stained according to the experimental protocol used for O-CNT/PVOH nanocomposites. Relative to any of the O-CNT/PVOH nanocomposites used in the study, PCL samples could dry-out rather quickly so were kept wet using VectaShield mounting media. This hydrophobic PCL surface appeared to be benign to *P. aeruginosa*, indicating that hydrophobicity is not leading to cell death in this study (Figure A3.24).

A3.21. References

1. Petersen, E. J.; Lam, T.; Gorham, J. M.; Scott, K. C.; Long, C. J.; Stanley, D.; Sharma, R.; Alexander Liddle, J.; Pellegrin, B.; Nguyen, T., Methods to assess the impact of UV irradiation on the surface chemistry and structure of multiwall carbon nanotube epoxy nanocomposites. *Carbon* **2014,** *69*, (0), 194-205.
2. Wepasnick, K. A.; Smith, B. A.; Bitter, J. L.; Fairbrother, D. H., Chemical and structural characterization of carbon nanotube surfaces. *Anal. Bioanal. Chem.* **2010,** *396*, (3), 1003-1014.
3. Briggs, D.; Beamson, G., Primary and secondary oxygen-induced C1s binding energy shifts in x-ray photoelectron spectroscopy of polymers. *Anal. Chem.* **1992,** *64*, (15), 1729-36.
4. Vickerman, J. C.; Gilmore, I. S., *Surface analysis: the principal techniques*. Wiley Online Library: 2009; Vol. 2.
5. Tanuma, S.; Powell, C. J.; Penn, D. R., Calculations of electorn inelastic mean free paths. II. Data for 27 elements over the 50–2000 eV range. *Surface and Interface Analysis* **1991,** *17*, (13), 911-926.
6. Invitrogen, FilmTracer LIVE/DEAD Biofilm Viability Kit. In Probes, M., Ed. 2009.
7. Invitrogen, FilmTracer SYPRO Ruby Biofilm Matrix Stain. In Probes, M., Ed. 2009.

8. Perkins, E. M.; McCaffery, J. M., Conventional and immunoelectron microscopy of mitochondria. In *Mitochondria*, Springer: 2007; pp 467-483.

A3.22. Figures

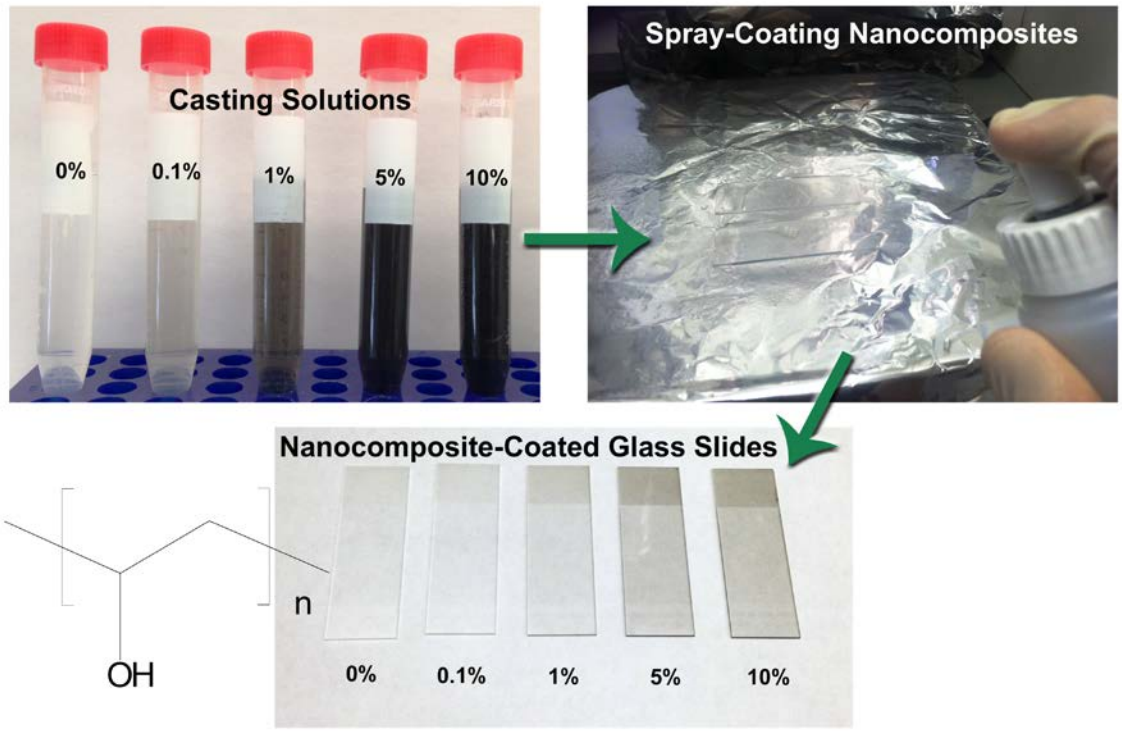

Figure A3.1. Preparation of well-dispersed O-CNT/PVOH nanocomposites using spray-coating.

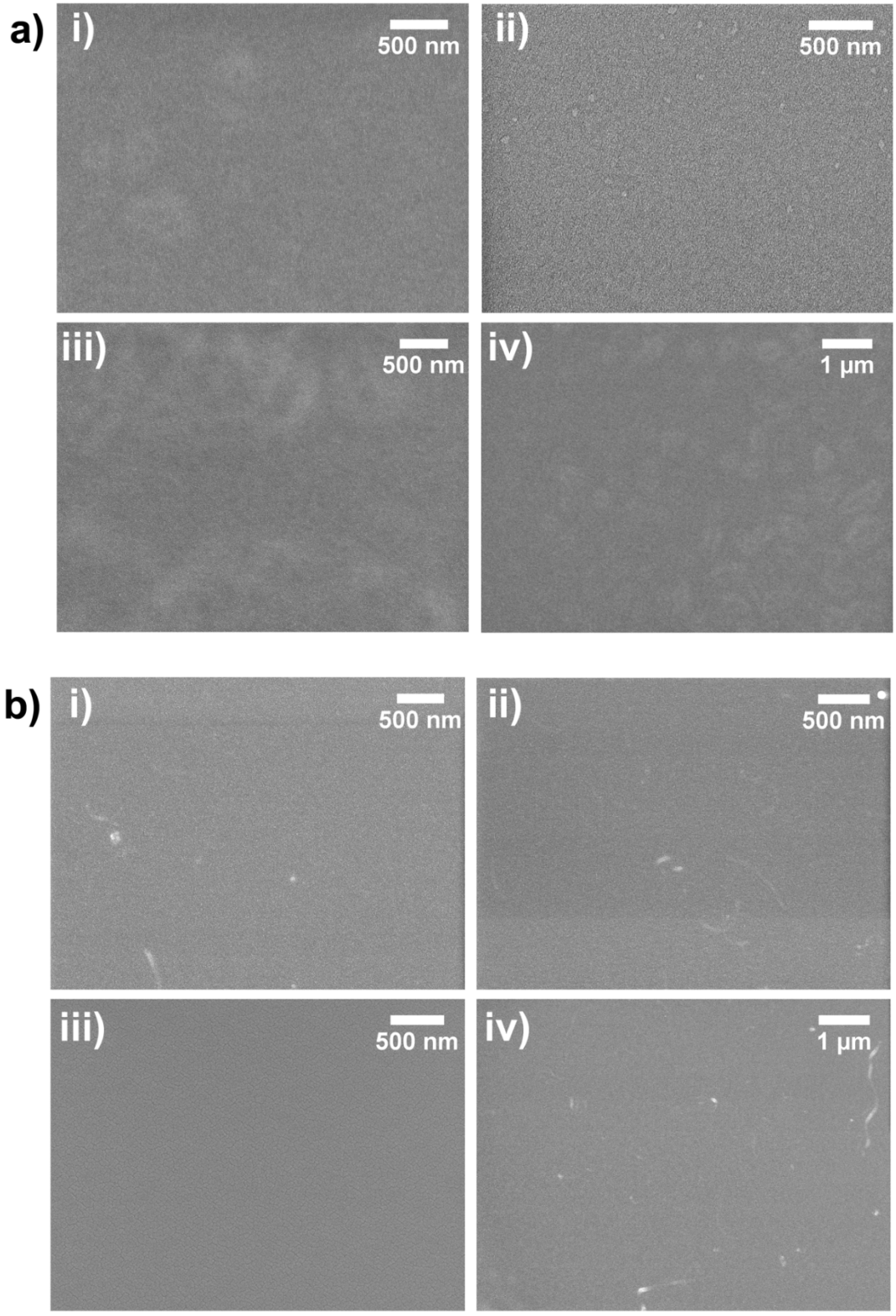
a)
i)
500 nm
ii)
500 nm
iii)
500 nm
iv)
1 µm
b)
i)
500 nm
ii)
500 nm
iii)
500 nm
iv)
1 µm

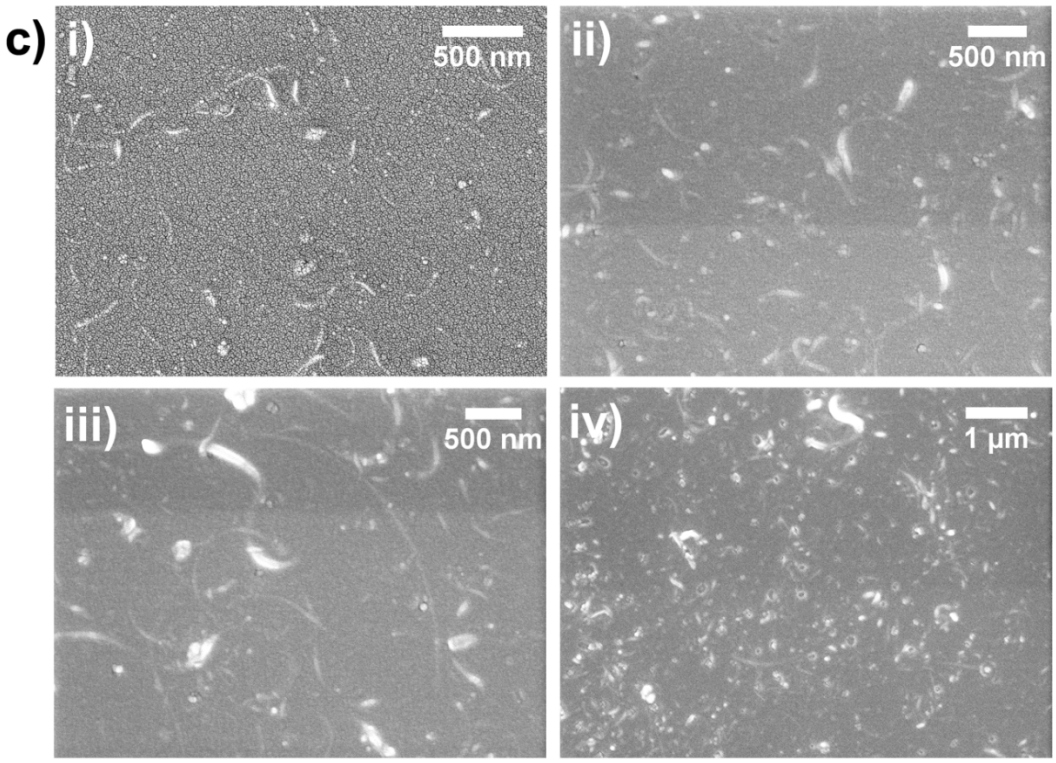
c)
i)
500 nm
ii)
500 nm
iii)
500 nm
iv)
1 µm

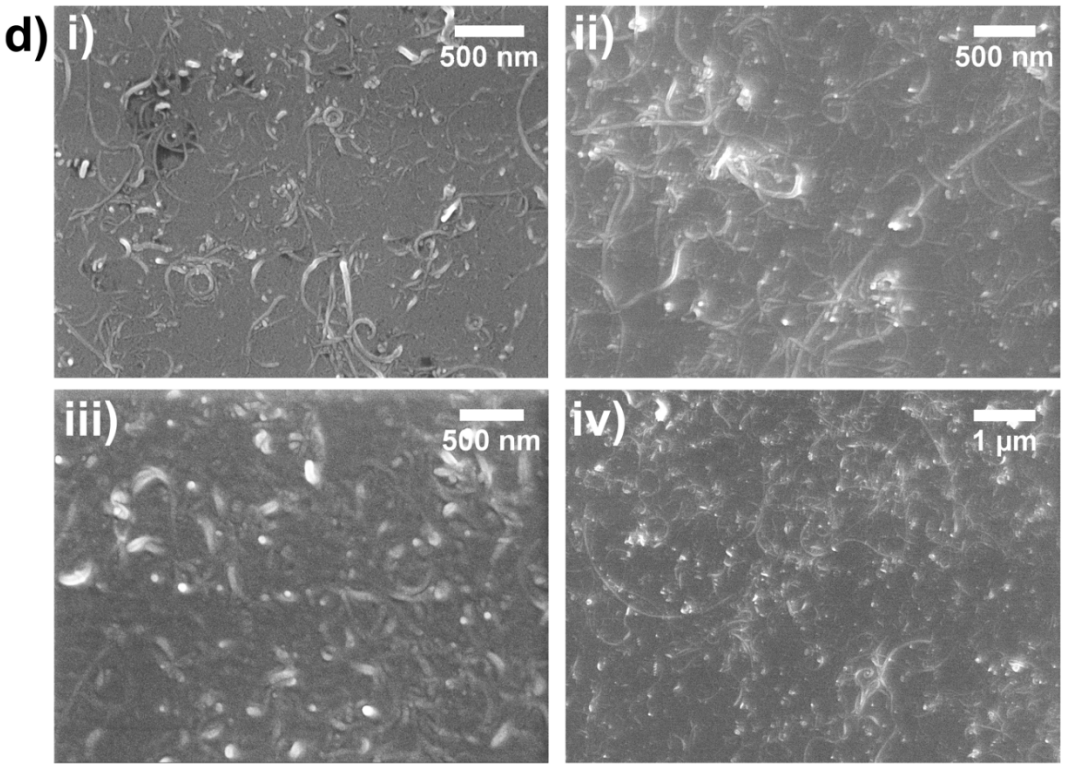
d)
i)
500 nm
ii)
500 nm
iii)
500 nm
iv)
1 µm

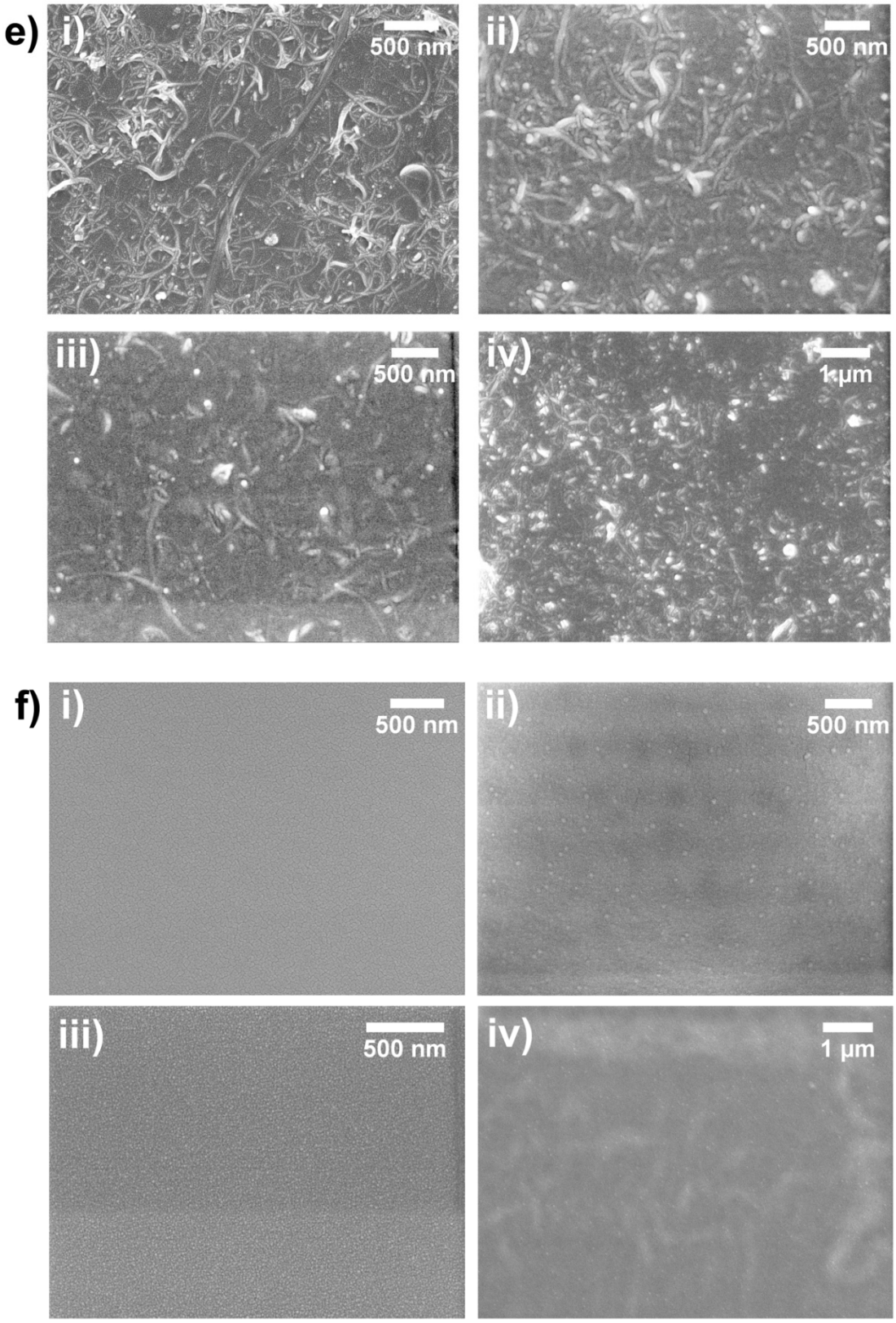
e)
i)
500 nm
ii)
500 nm
iii)
500 nm
iv)
1 µm
f)
i)
500 nm
ii)
500 nm
iii)
500 nm
iv)
1 µm

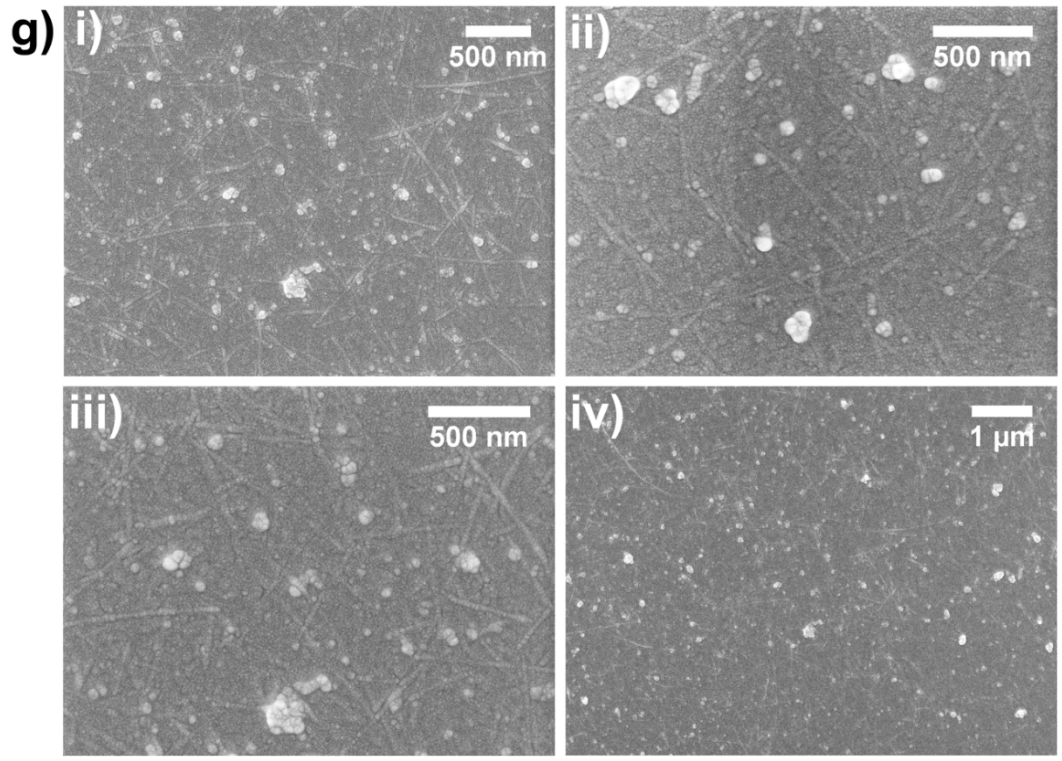
g)
i)
500 nm
ii)
500 nm
iii)
500 nm
iv)
1 µm

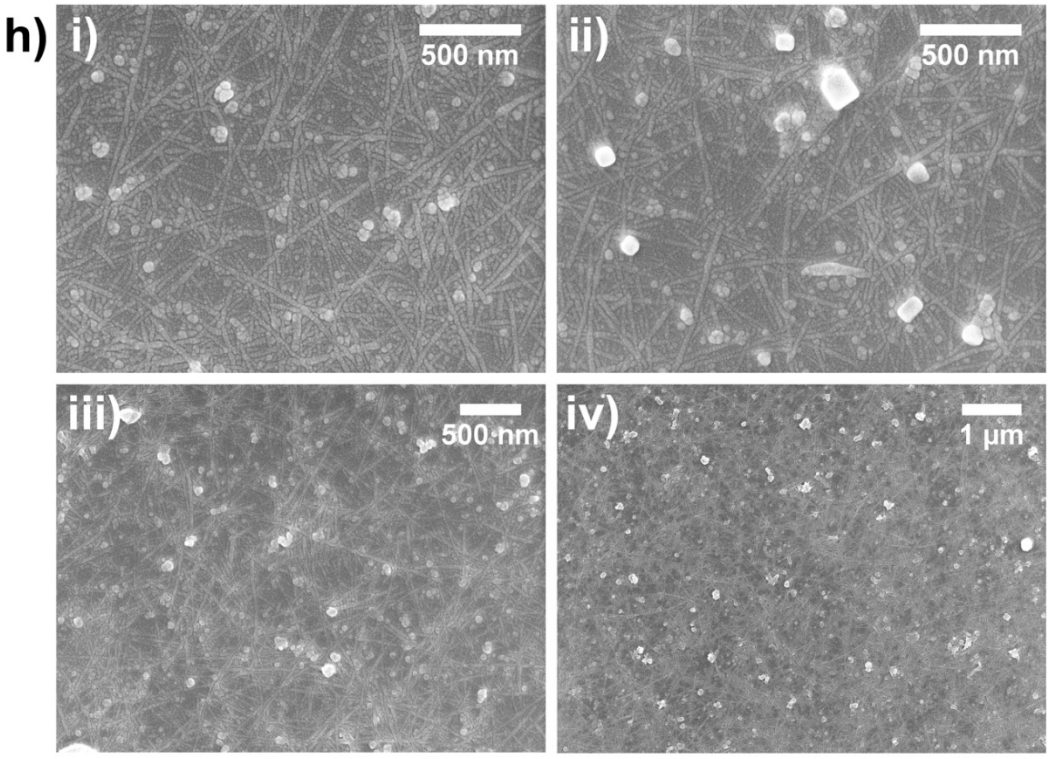
h)
i)
500 nm
ii)
500 nm
iii)
500 nm
iv)
1 µm

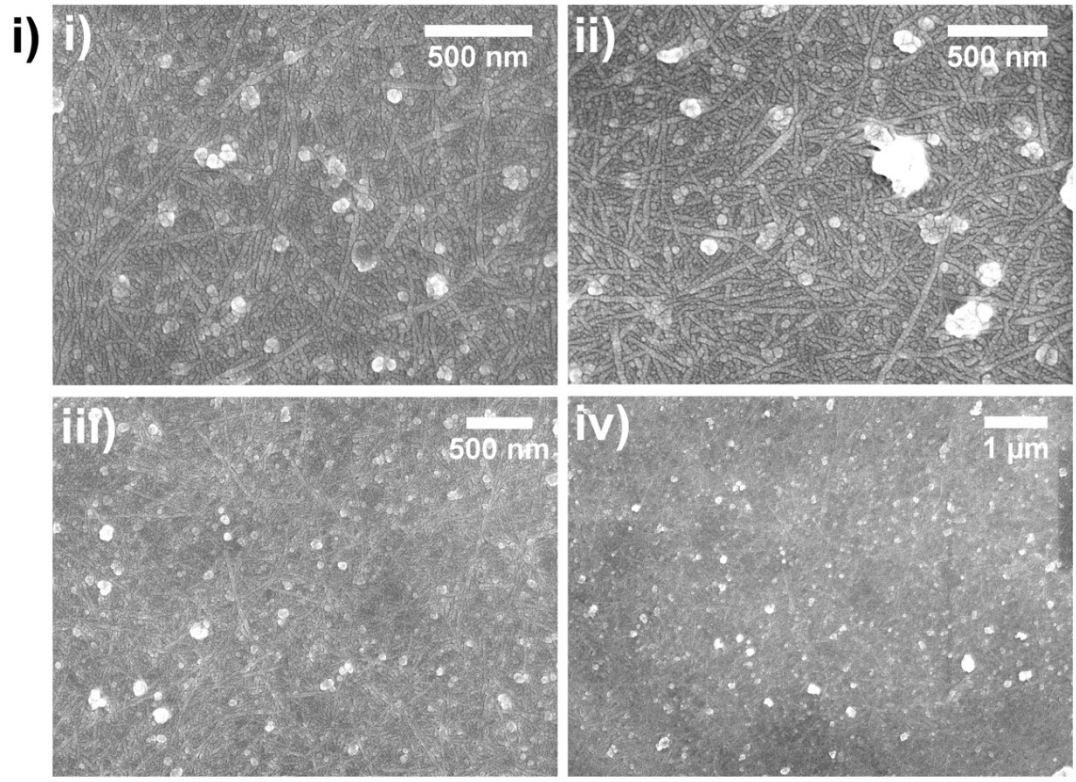

Figure A3.2. SEM images of 0, 0.1, 1, 5, and 10% w/w O-MWCNT/PVOH nanocomposites (a-e), and 0, 0.1, 1, 5, and 10% w/w O-SWCNT/PVOH nanocomposites (f-i). Each sample was imaged in replicate areas (i-iv). For the O-MWCNT/PVOH nanocomposites, at least one of the images is from a second sample.

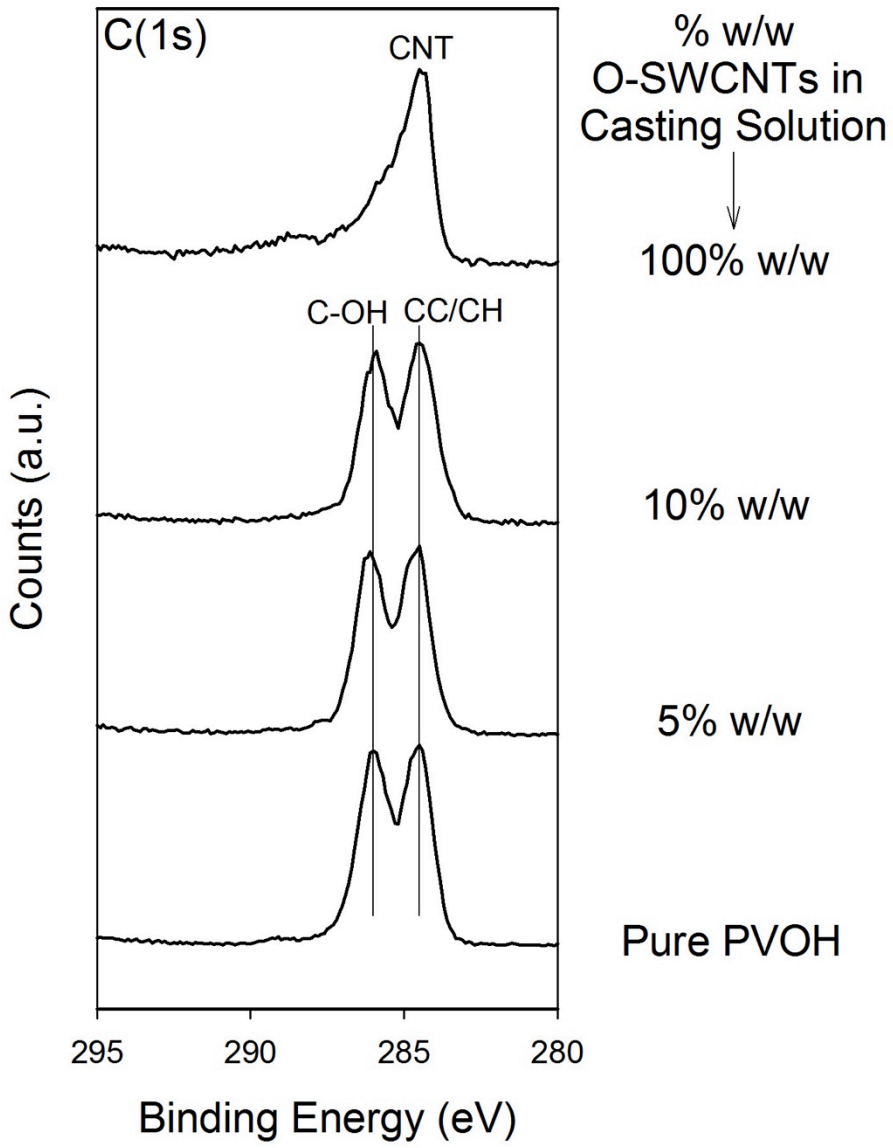

Figure A3.3: X-ray photoelectron spectroscopy (XPS) characterization of O-SWCNT/PVOH nanocomposites; C(1s) region of O-SWCNT/PVOH nanocomposites with increasing O-SWCNT loading. The O-SWCNT component did not separate in binding energy from the PVOH components (CC/CH and C-OH) so quantitative analysis was not possible. The 100% w/w O-SWCNT peak and the CC/CH components of the PVOH-containing PNCs were aligned at 284.5 eV.

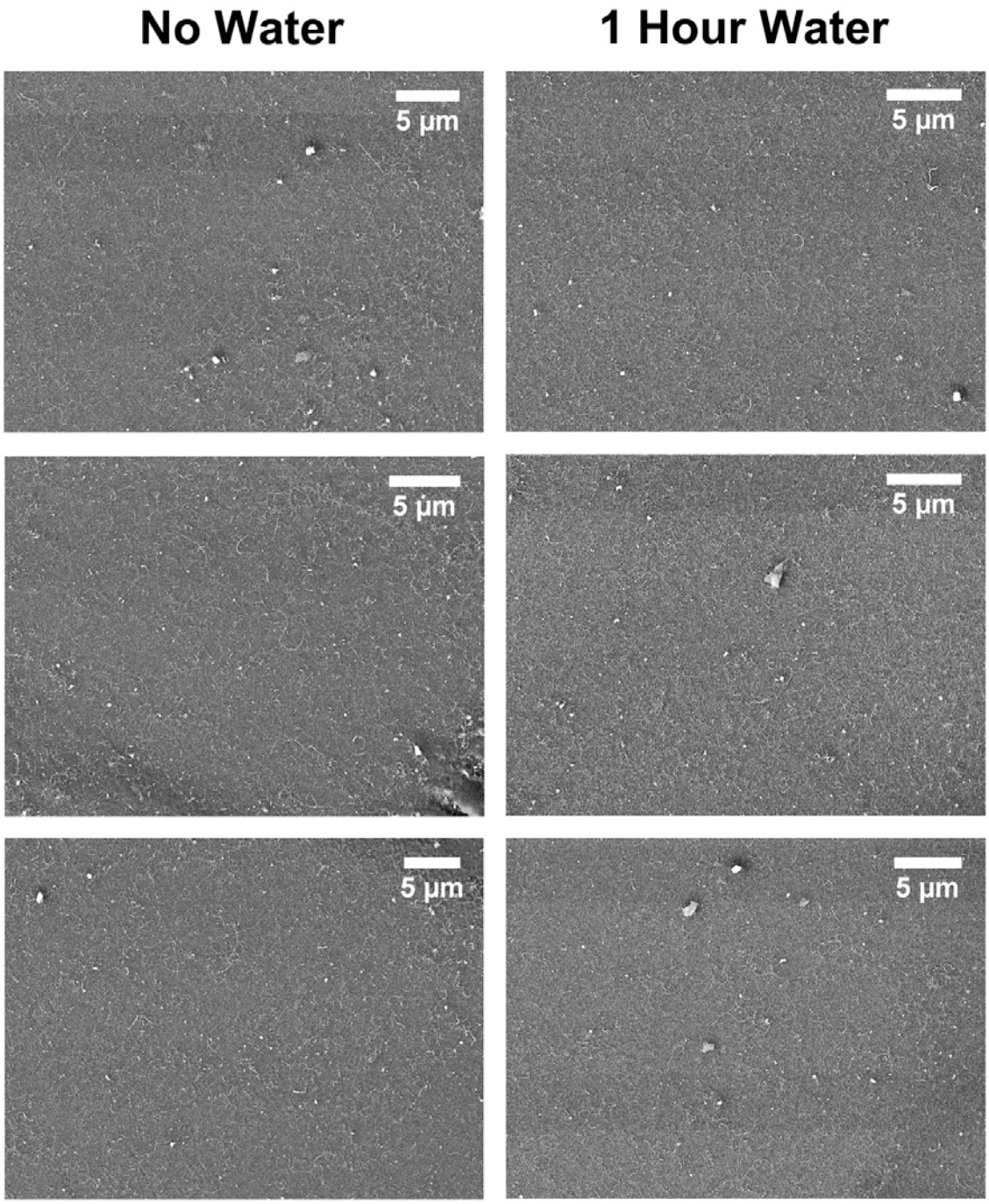

Figure A3.4. Dissolution controls of 5% w/w O-MWCNT/PVOH nanocomposites with no water submersion and 1 h of water submersion.

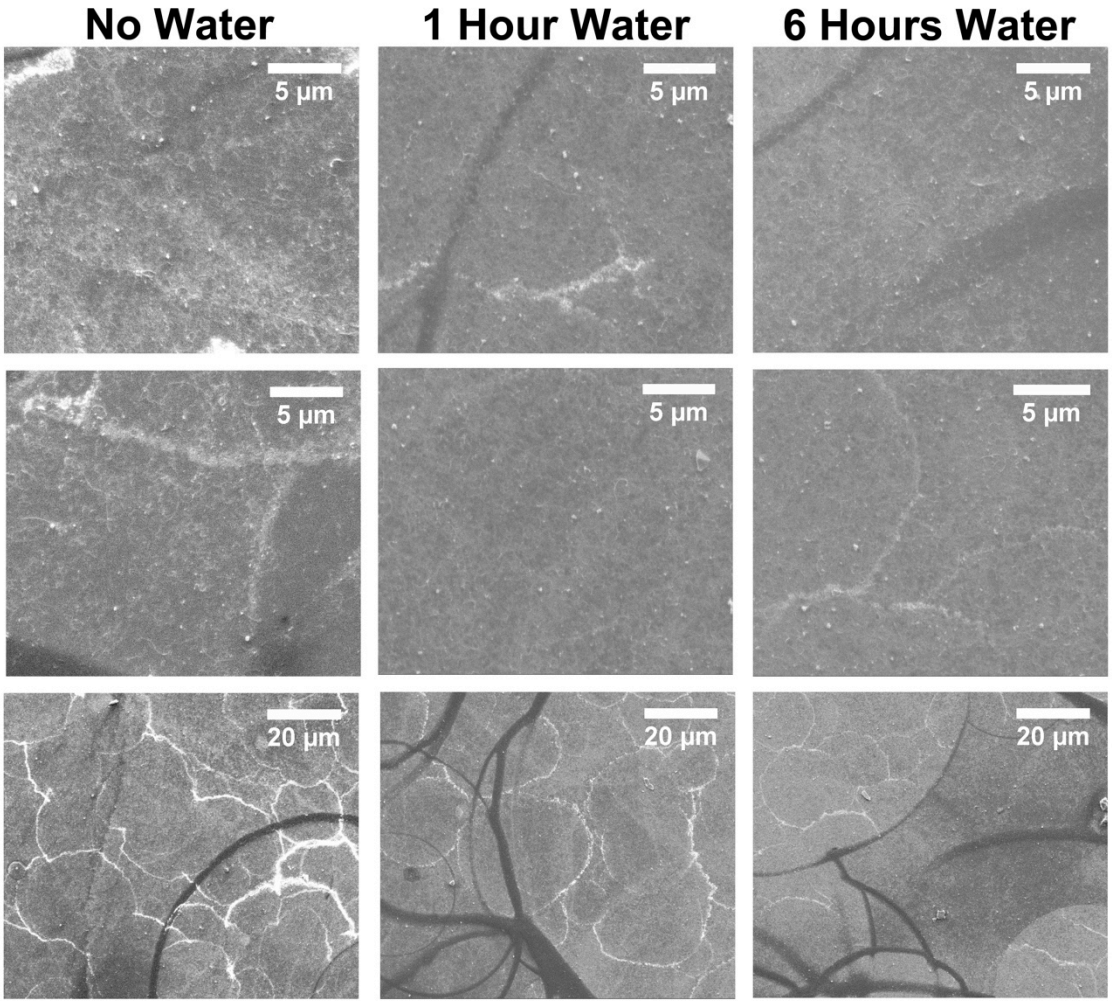

Figure A3.5. Macroscopic-scale dissolution controls of 10% w/w O-MWCNT/PVOH nanocomposites with no water submersion, 1 h water submersion, and 6 h water submersion.

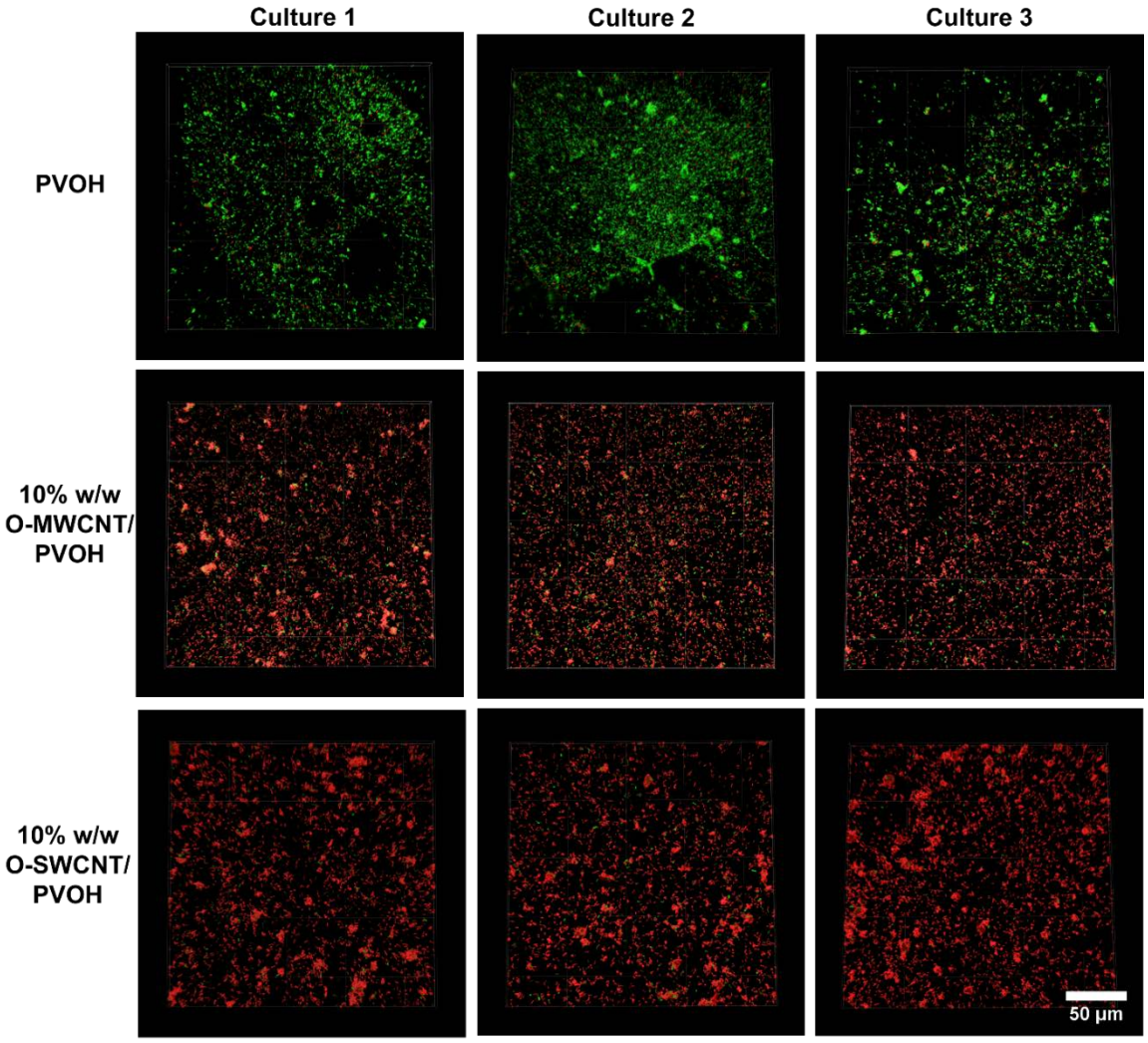

Figure A3.6. Replicate CLSM images of *P. aeruginosa* LIVE/DEAD stained on PVOH, 10% w/w O-MWCNT/PVOH, and 10% O-SWCNT/PVOH nanocomposite surfaces. Each column represents images from separately grown cultures.

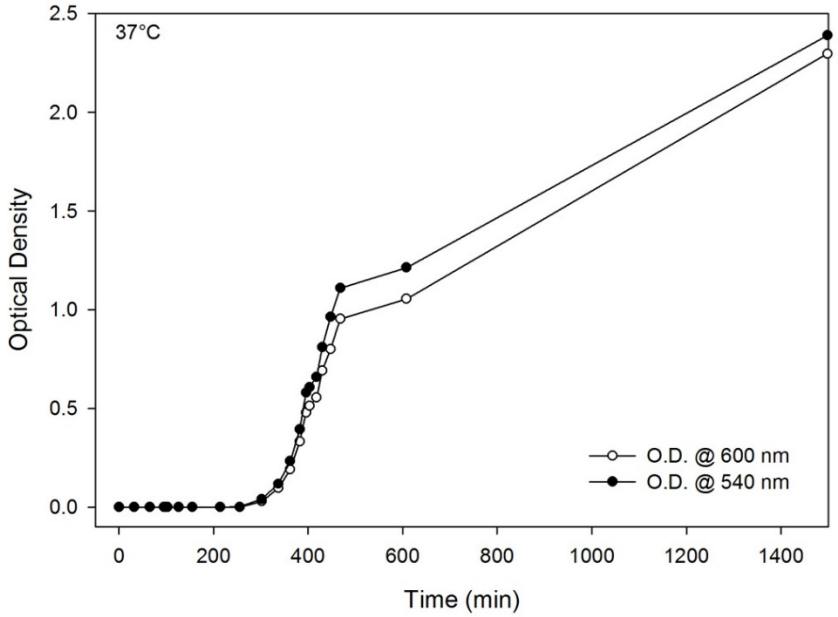

Figure A3.7. Growth curve of *P. aeruginosa* in LB broth at 540 and 600 nm.

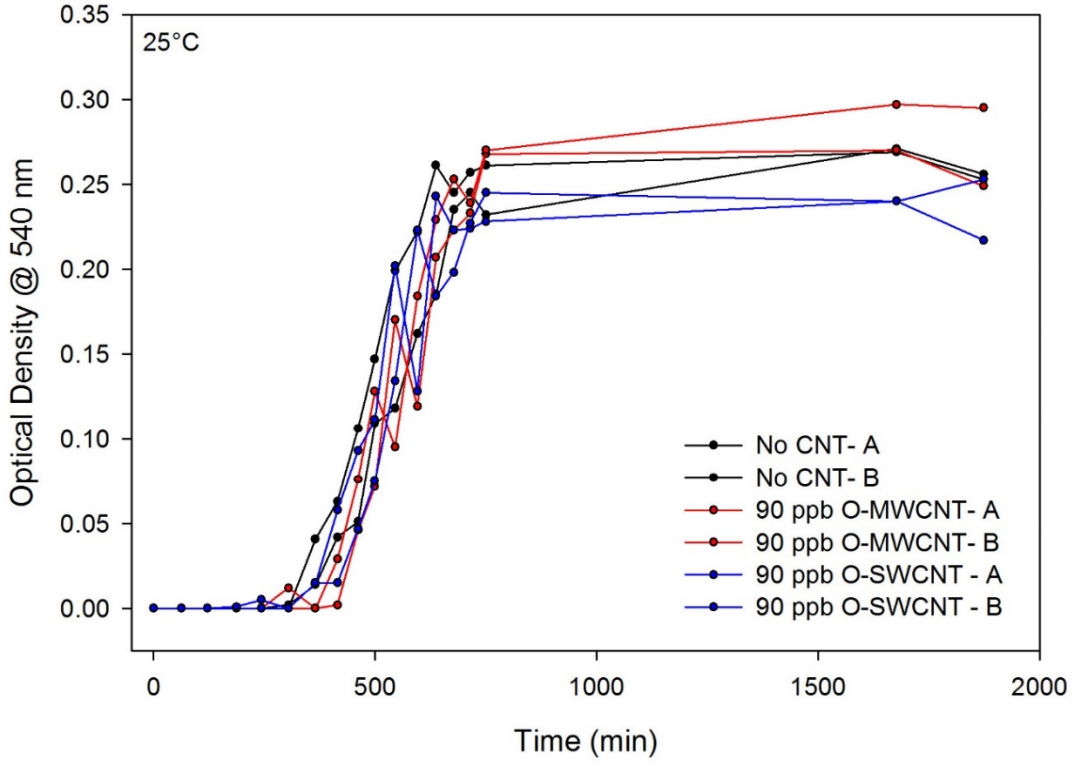

Figure A3.8. Growth curve of *P. aeruginosa* in basal mineral media (BMM) at 540 nm. The growth curve was also carried out in 90 ppb O-MWCNT and O-SWCNT/BMM suspensions.

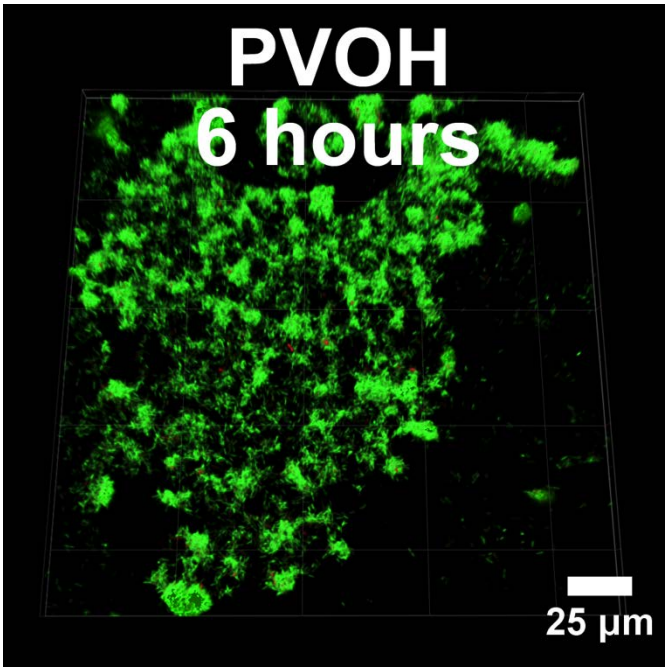

Figure A3.9. CLSM image of LIVE/DEAD stained *P. aeruginosa* grown statically for 6 h on pure PVOH.

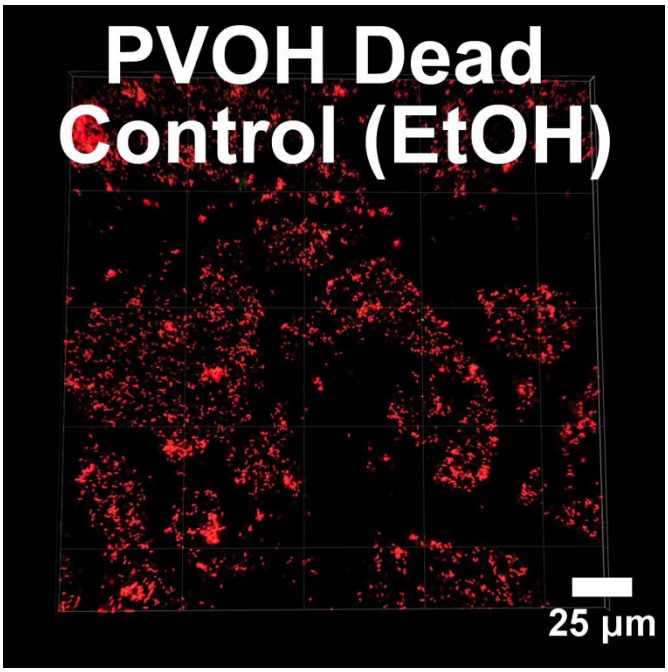

Figure A3.10. LIVE/DEAD staining and CLSM of *P. aeruginosa* grown statically for 1 h on PVOH followed by immersion in ethanol to intentionally cause cell death.

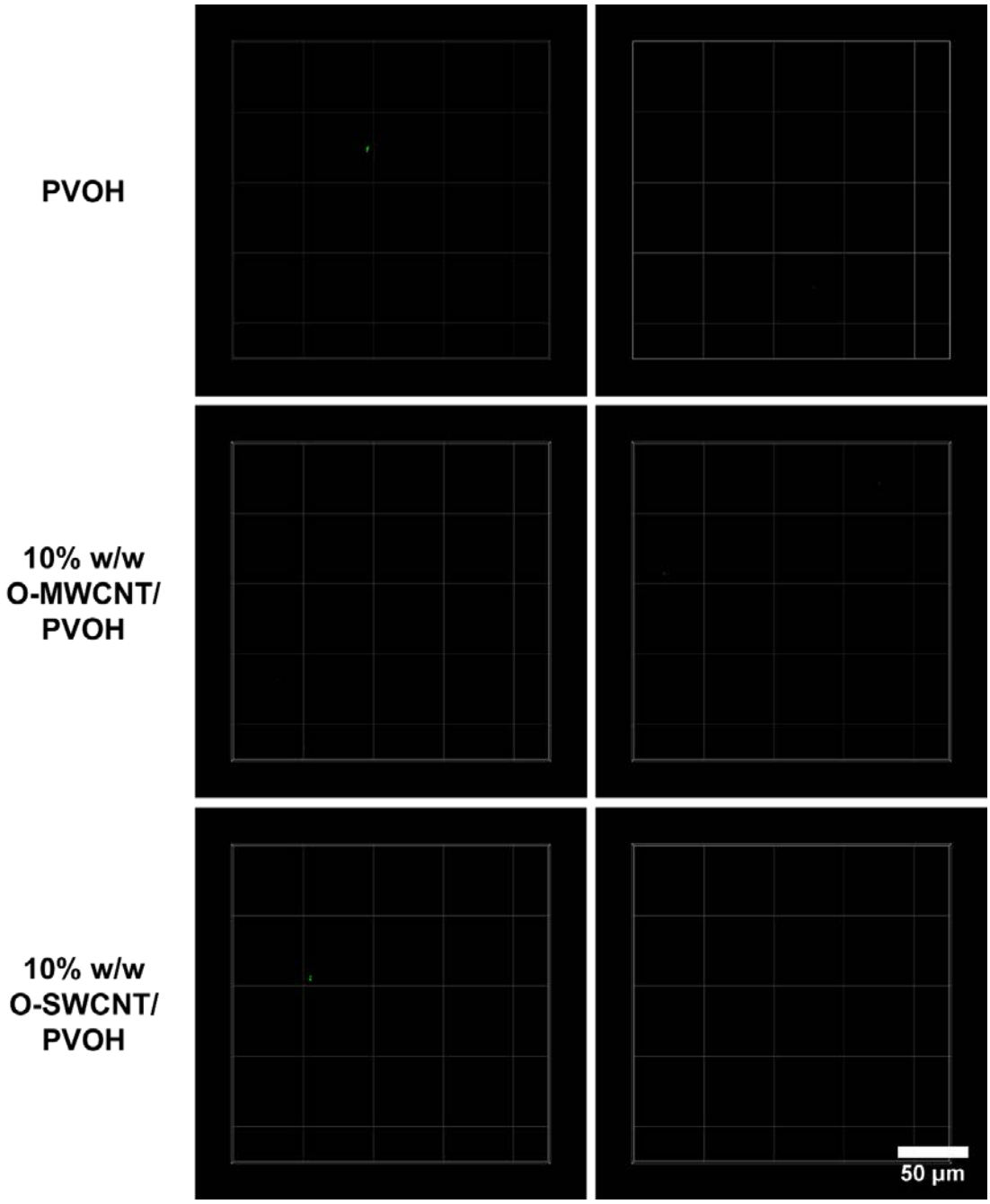

Figure A3.11. Abiotic background fluorescence controls of LIVE/DEAD stained surfaces of PVOH, 10% w/w O-MWCNT/PVOH, and 10% w/w O-SWCNT/PVOH nanocomposites.

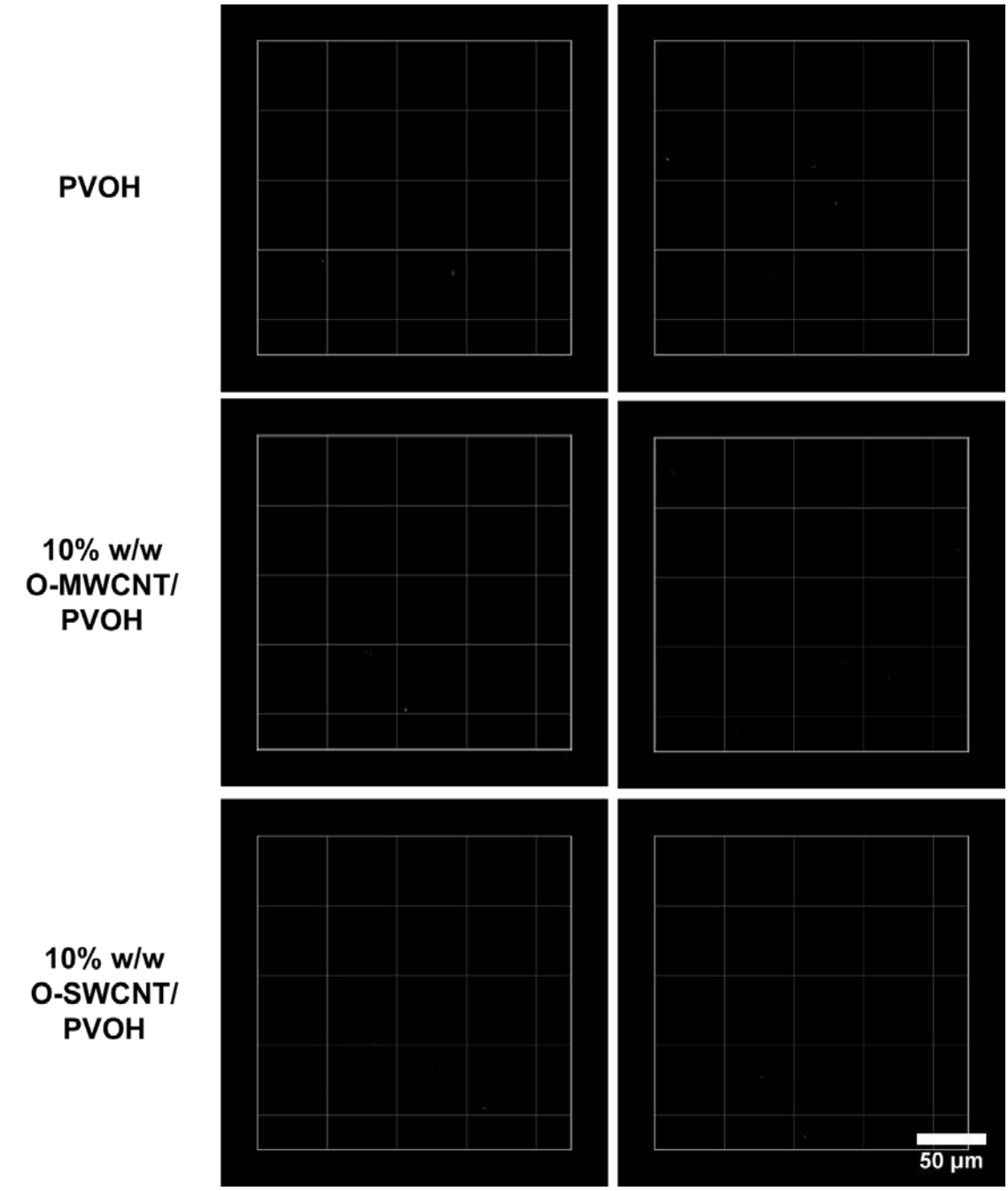

Figure A3.12. PVOH, 10% w/w O-MWCNT/PVOH, and 10% w/w O-SWCNT/PVOH samples dipped into and out of inoculum and stained according to the LIVE/DEAD staining procedure to determine the degree of cell attachment during transfer of samples through the air-liquid interface.

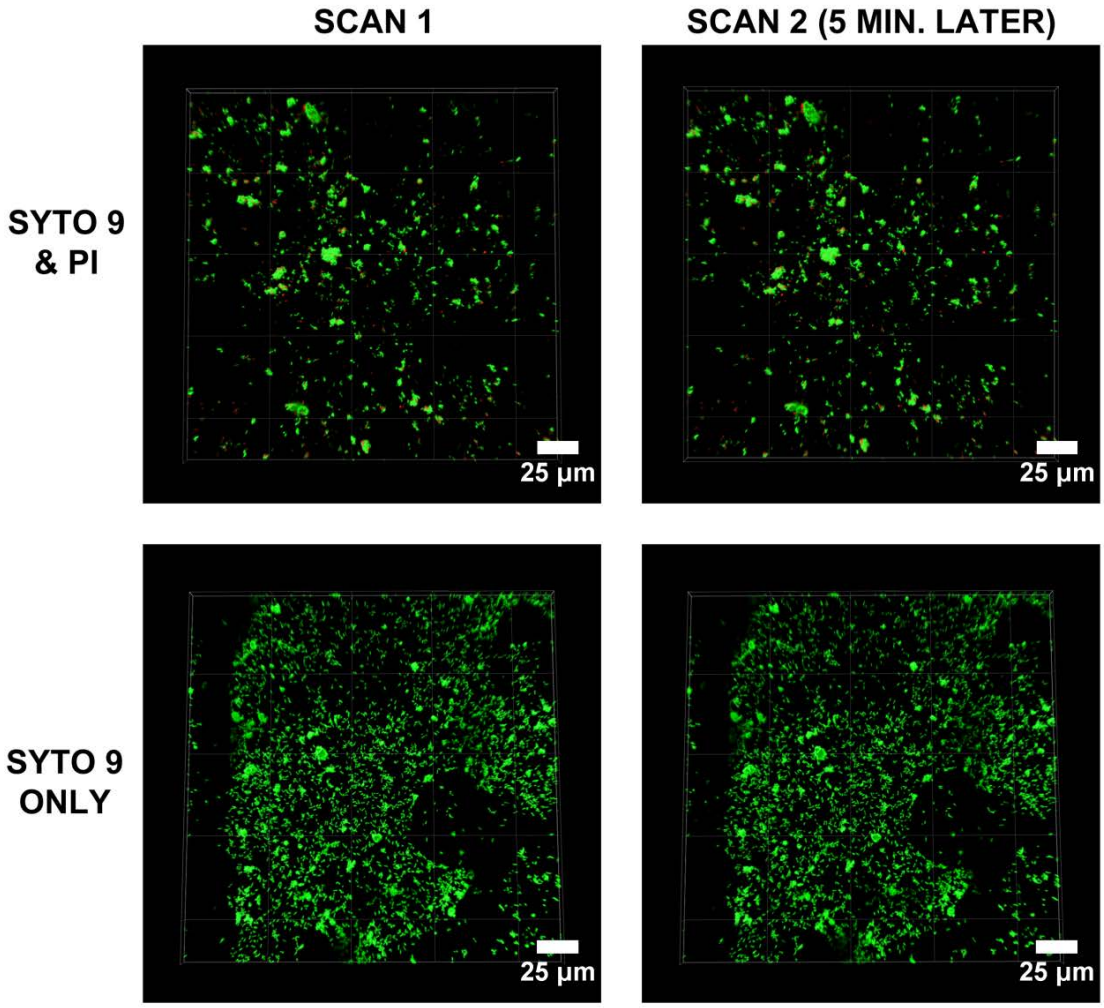

Figure A3.13. CLSM images of LIVE/DEAD stained *P. aeruginosa* grown statically for 1 h on PVOH slides for photobleaching controls. Slides were stained with both SYTO 9 and PI (top row) and SYTO 9 only (bottom row) and imaged once and then again after 5 min to check for changes in fluorescence intensity during the image acquisition time.

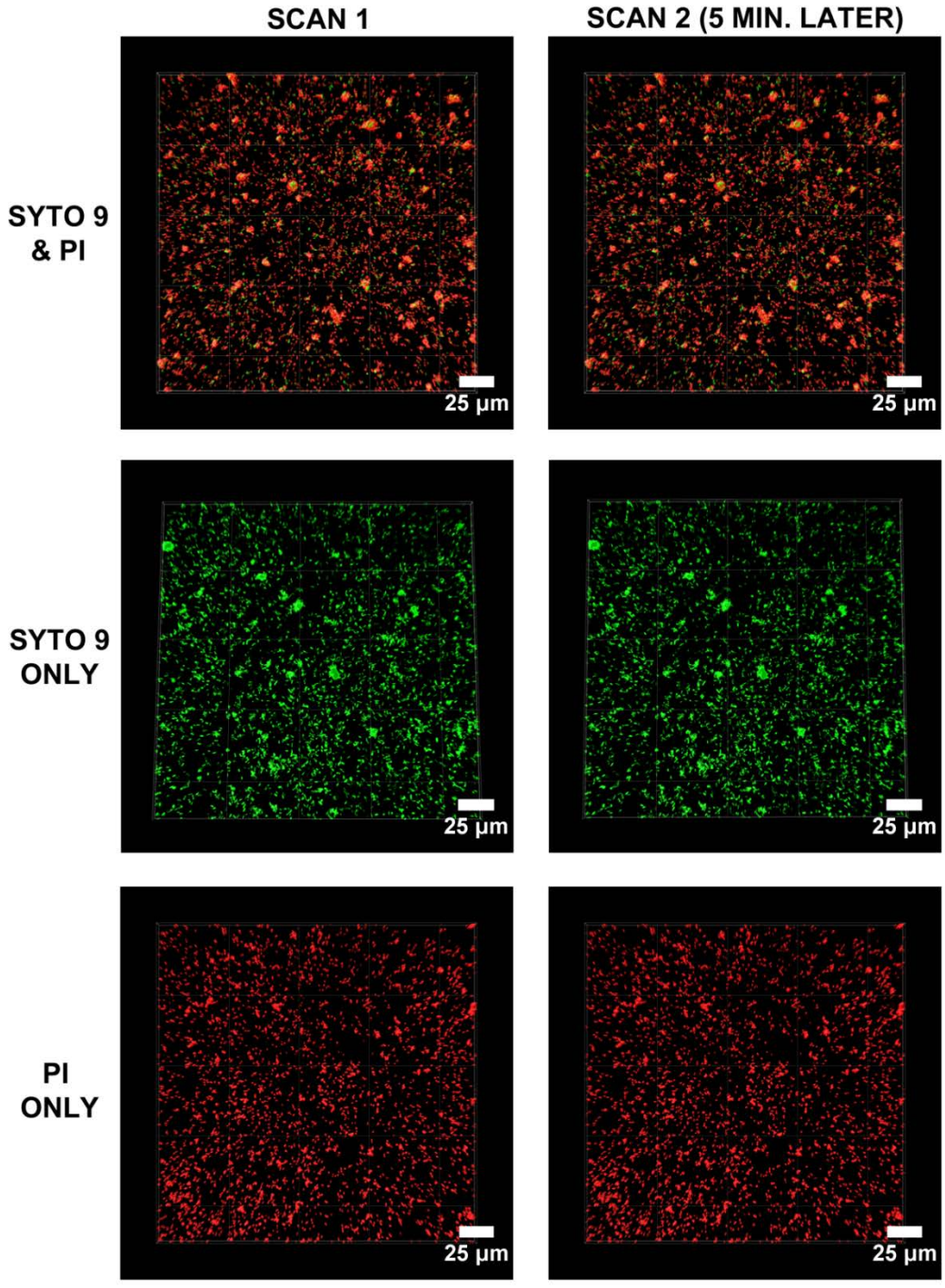

Figure A3.14. CLSM images of LIVE/DEAD stained *P. aeruginosa* grown statically for 1 h on 10% w/w O-MWCNT/PVOH slides for photobleaching controls. Slides were stained with both SYTO 9 and PI (top row), SYTO 9 only (middle row) and PI only (bottom row) Slides were imaged once and then again after 1 min to check for changes in fluorescence intensity during the image acquisition time.

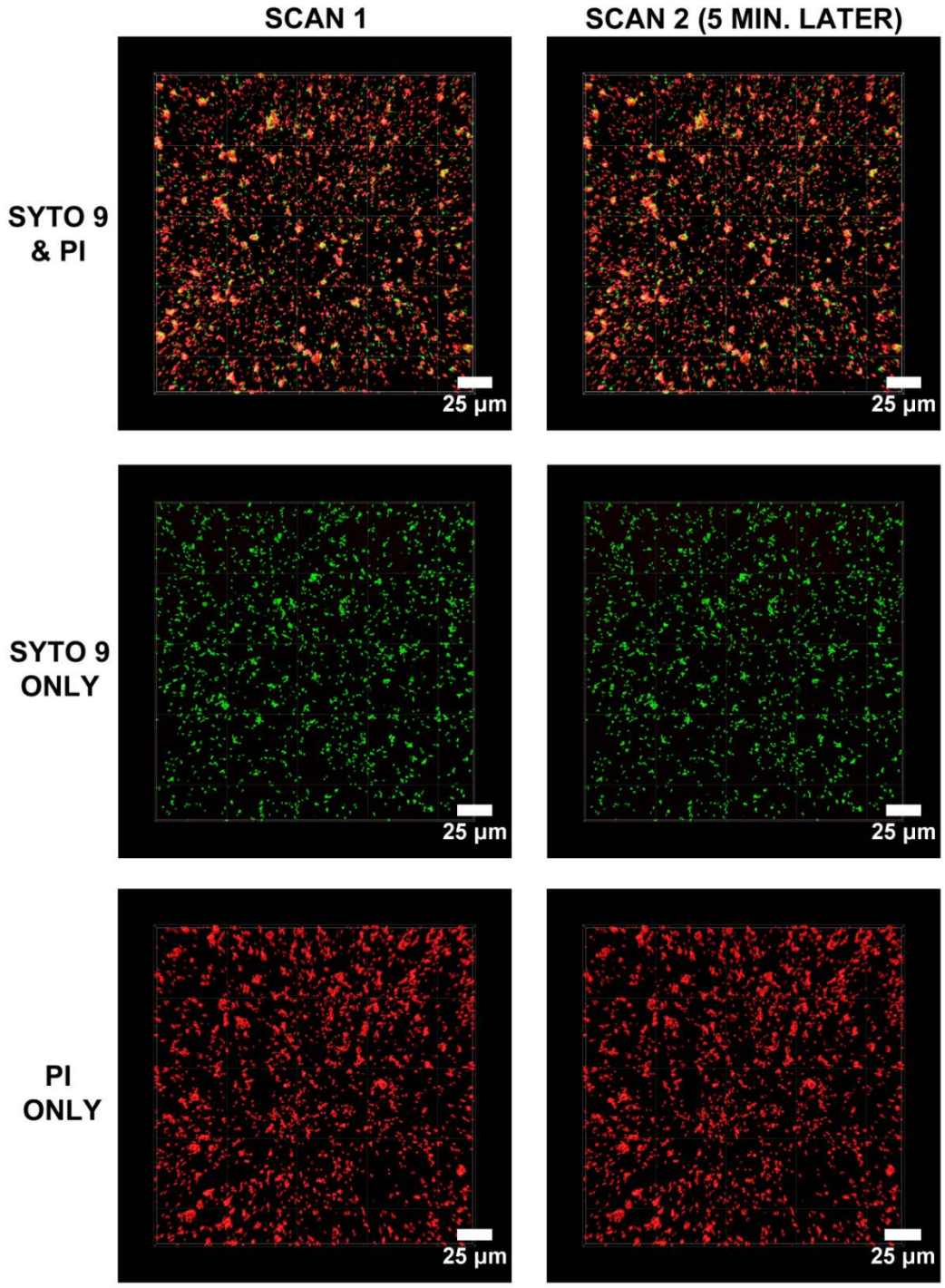

Figure A3.15. CLSM images of LIVE/DEAD stained *P. aeruginosa* grown statically for 1 h on 10% w/w O-SWCNT/PVOH slides for photobleaching controls. Slides were stained with both SYTO 9 and PI (top row), SYTO 9 only (middle row) and PI only (bottom row) Slides were imaged once and then again after 1 min to check for changes in fluorescence intensity during the image acquisition time period.

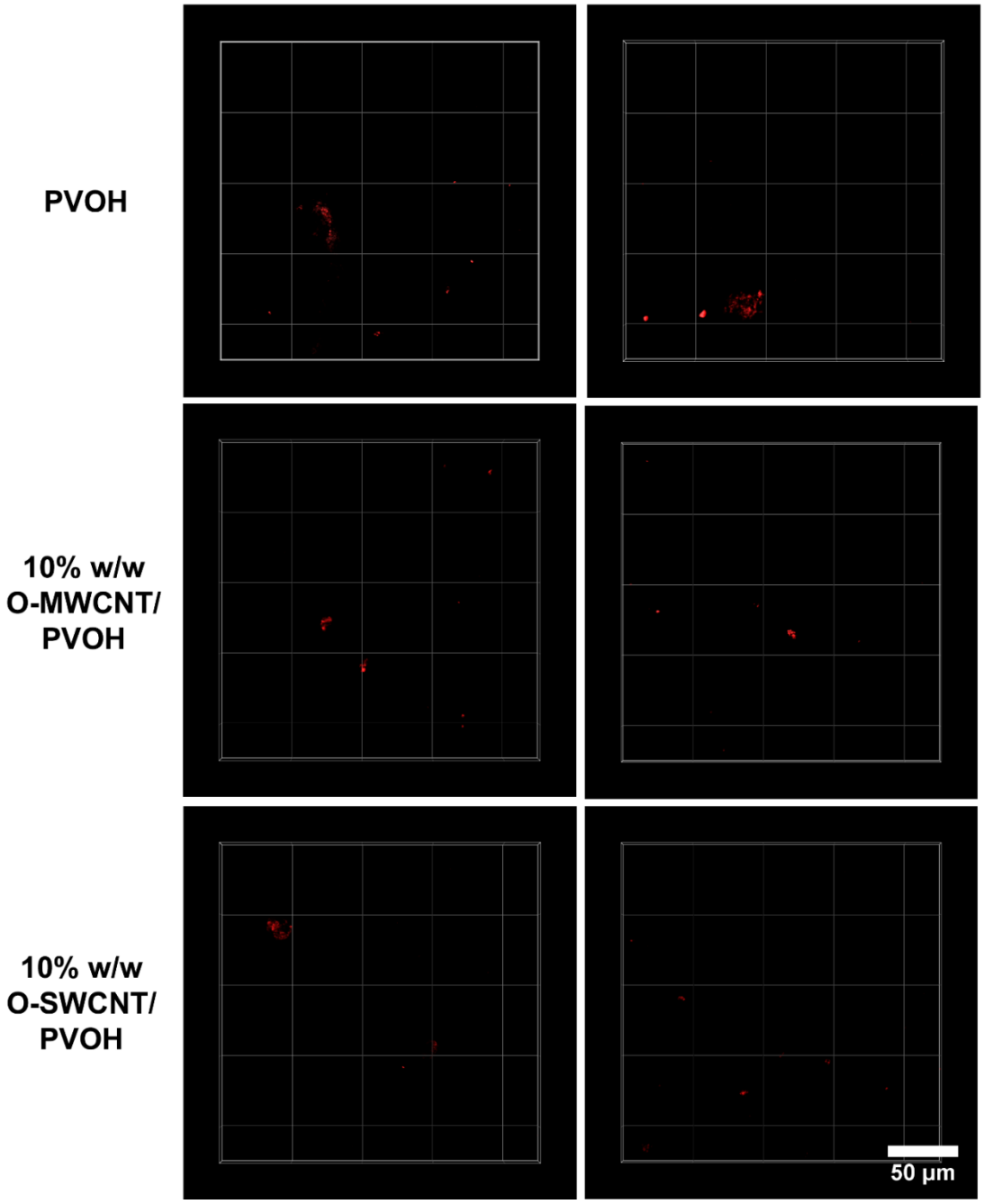

Figure A3.16. SYPRO Ruby Biofilm Matrix stained EPS from *P. aeruginosa* exposed to PVOH, 10% w/w O-MWCNT/PVOH, and 10% w/w O-SWCNT/PVOH nanocomposites for 1 h.

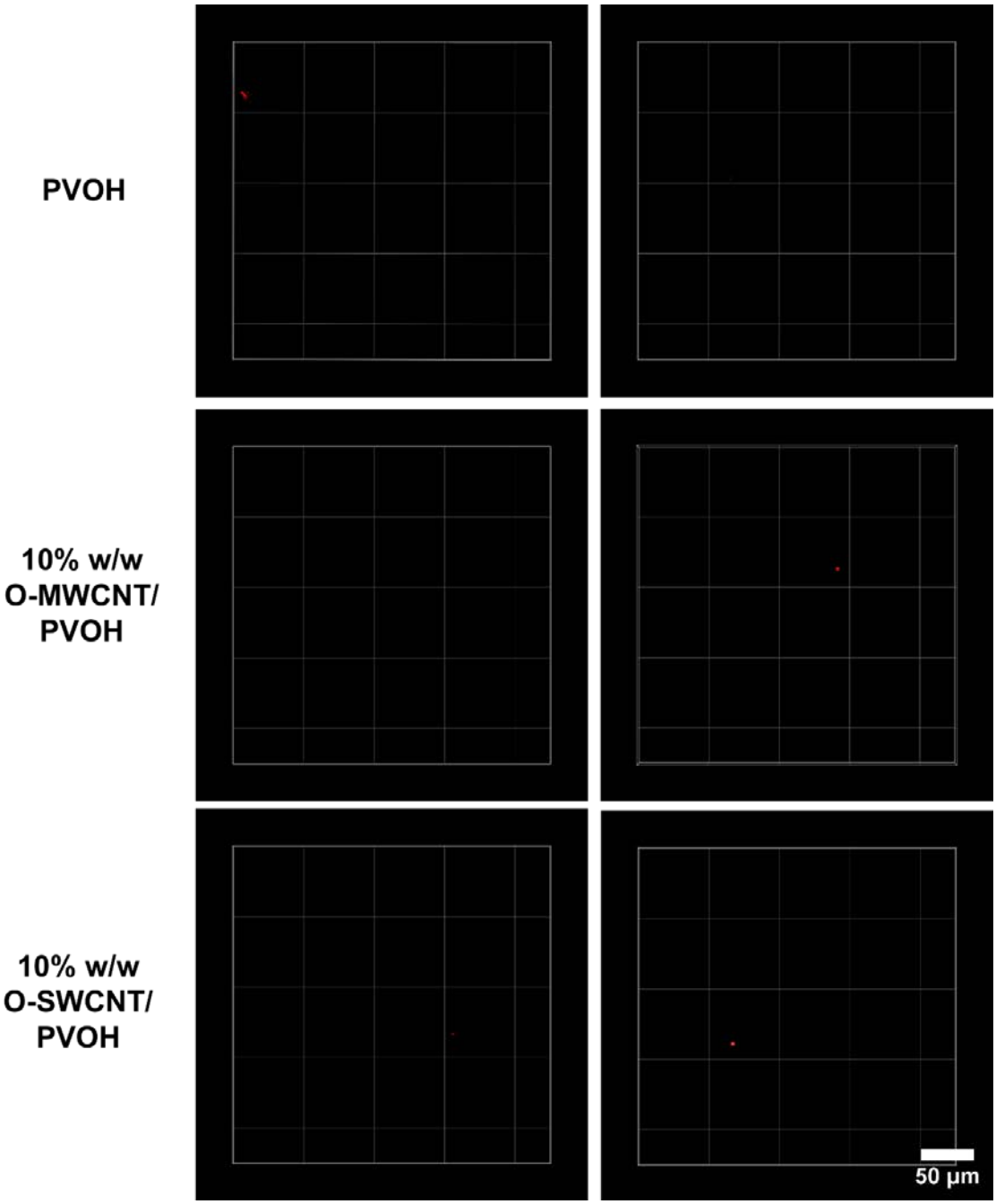

Figure A3.17. Abiotic background fluorescence controls of PVOH, 10% w/w O-MWCNT/PVOH, and 10% w/w O-SWCNT/PVOH nanocomposites stained with SYPRO Ruby Biofilm Matrix Stain.

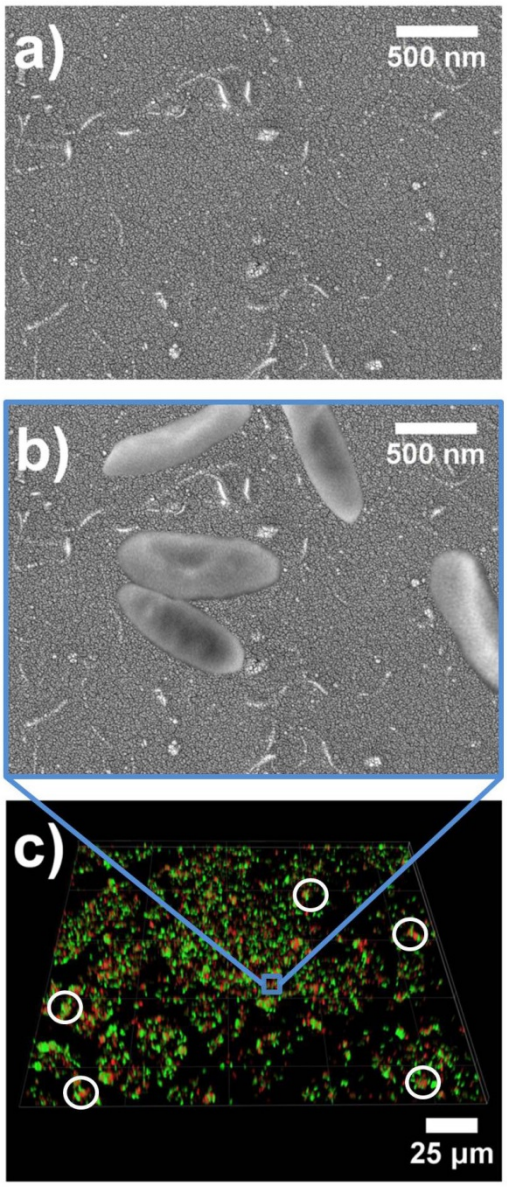

Figure A3.18. A 1% w/w O-MWCNT/PVOH (a) nanocomposite surface in relation to the microorganism size (b) and CLSM image (c). The *P. aeruginosa* in (b) are to scale and are oriented to show positions in which CNT contact does not occur. In (c), examples of living (green) cells atop of dead cells are shown at a 1 h time point.

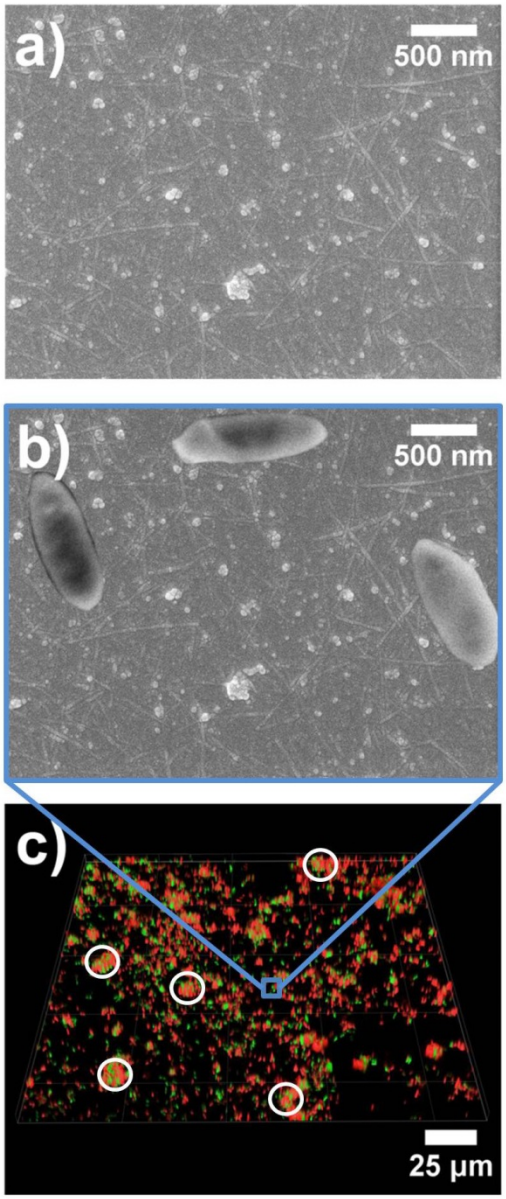

Figure A3.19. A 1% w/w O-SWCNT/PVOH (a) nanocomposite surface in relation to the microorganism size (b) and CLSM image (c). The *P. aeruginosa* in (b) are to scale and are oriented to show positions in which CNT contact is minimized, but in this case almost always occurs. In (c), examples of living (green) cells atop of dead cells are shown at a 1 h time point.

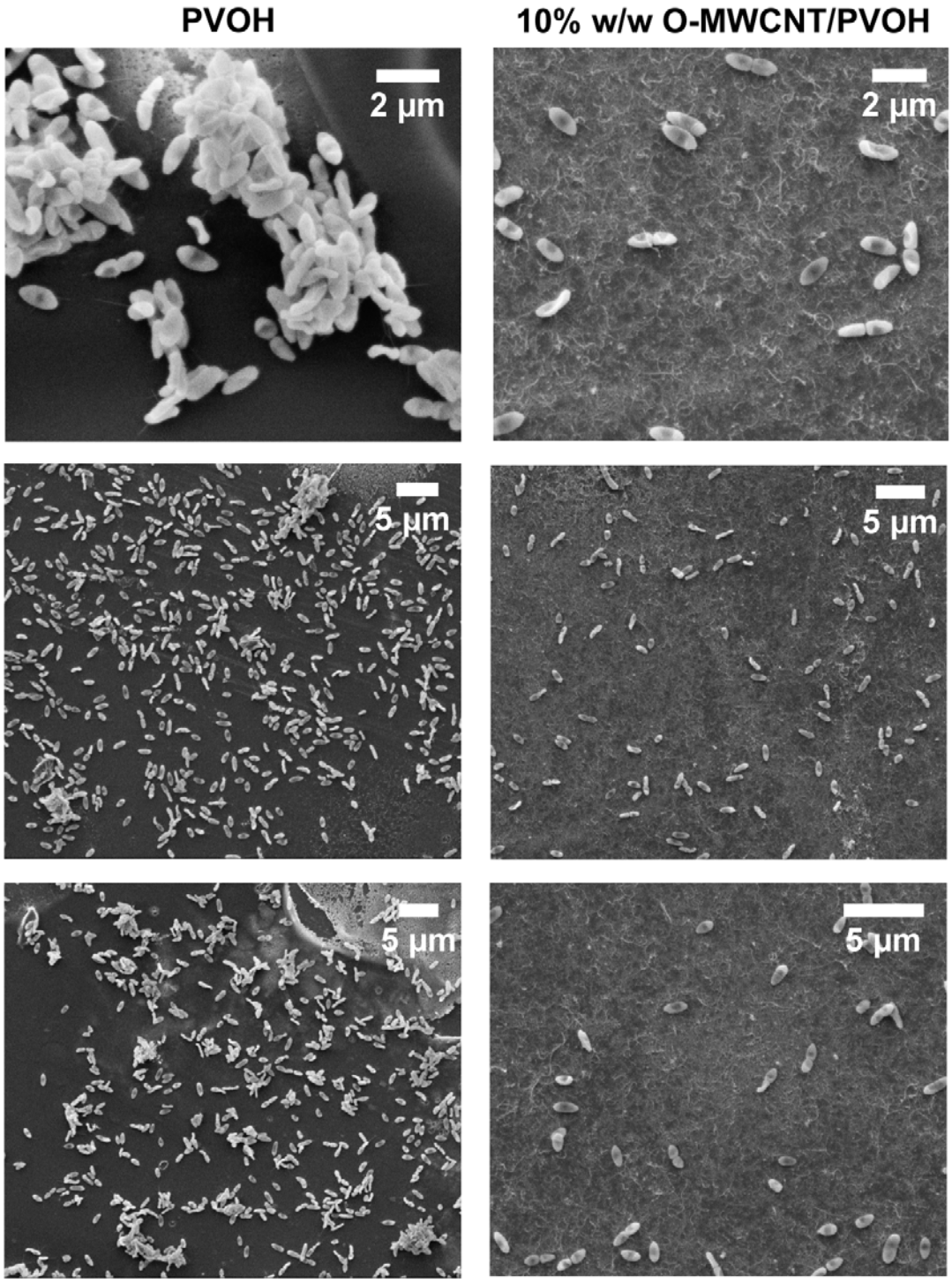

Figure A3.20. SEM images of fixed *P. aeruginosa* on PVOH and 10% w/w O-MWCNT/PVOH nanocomposites.

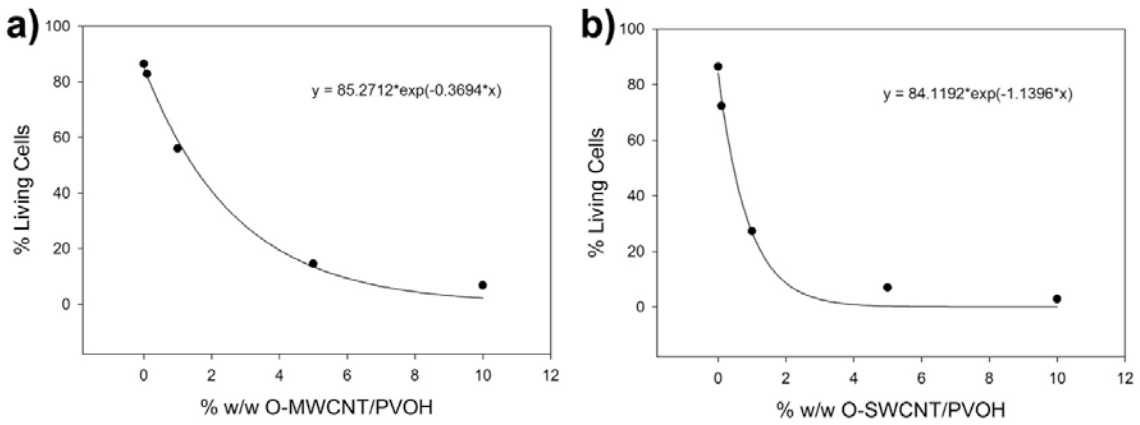

Figure A3.21. Percentage of living cells as a function of CNT loading in PVOH nanocomposites. O-MWCNT and O-SWCNT/PVOH plots were both fit to a two parameter exponential decay, where the b parameter is roughly 3 times greater for the O-SWCNT/PVOH samples, indicating a faster rate of cell death at increasing CNT loadings.

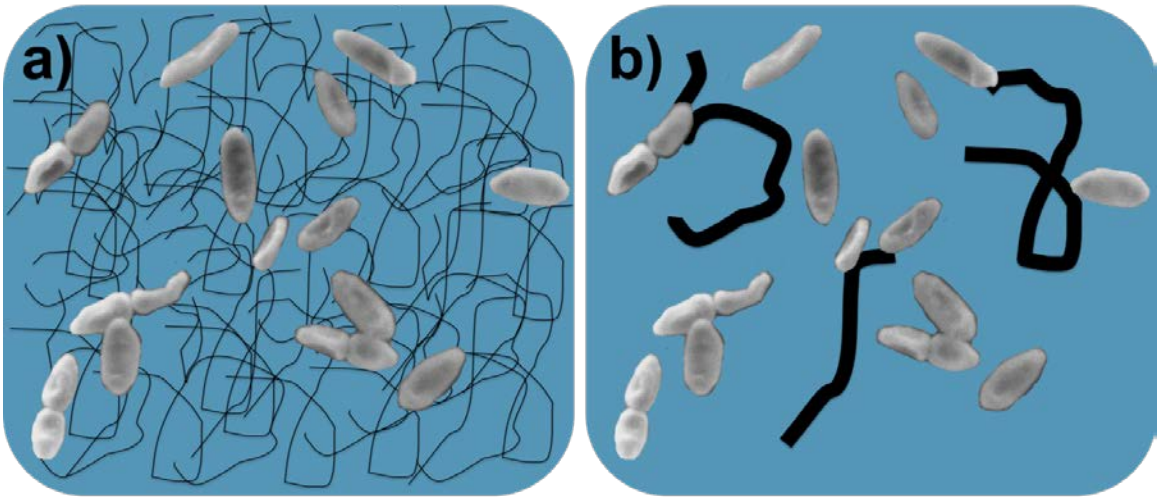

Figure A3.22. Comparison of CNT surface coverage of 1% w/w O-MWCNT (a) to 1% w/w O-SWCNT in PVOH (b). Since the O-MWCNTs are roughly 15 times larger in diameter, there are approximately 15 times more O-SWCNTs than O-MWCNTs in a given nanocomposite area, assuming ideal length and dispersion quality, meaning greater CNT-microbe contact on an O-SWCNT/PVOH nanocomposite.

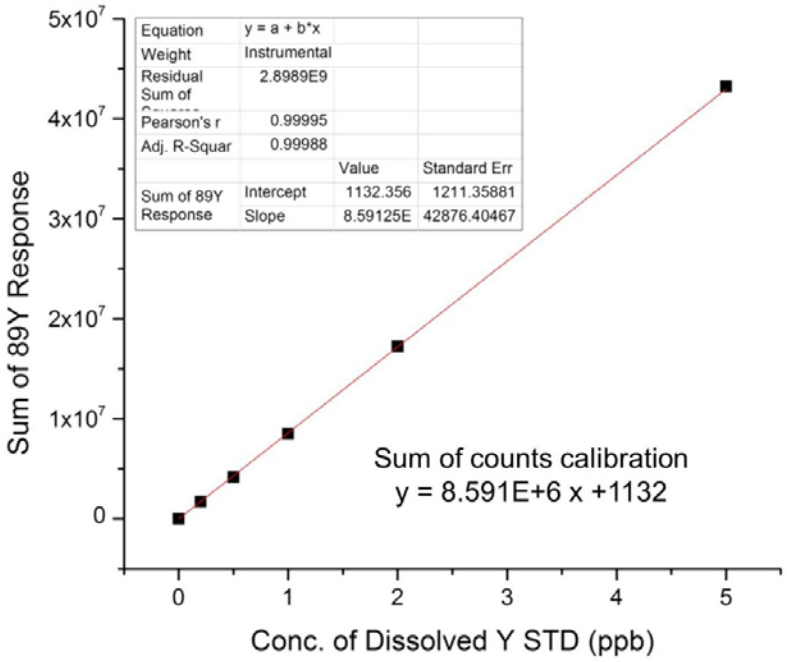

Y Concentration of:	A (Sum of Counts)	A (ppt)	B (Sum of Counts)	#B (ppt)
Supernatant 1	4146	0.2	5781	0.4
Supernatant 2	3435	0.1	4339	0.2

Figure A3.23. ICP-MS Y calibration curve (sum of counts) of dissolved Y standards used to determine the concentration of released yttrium ions from autoclaved milli-Q water used to submerge duplicate 10% w/w O-SWCNT/PVOH (1&2) for 1 h. Concentrations shown in the table were extremely low, at the detection limit of the instrument and each supernatant was sampled twice (A&B).

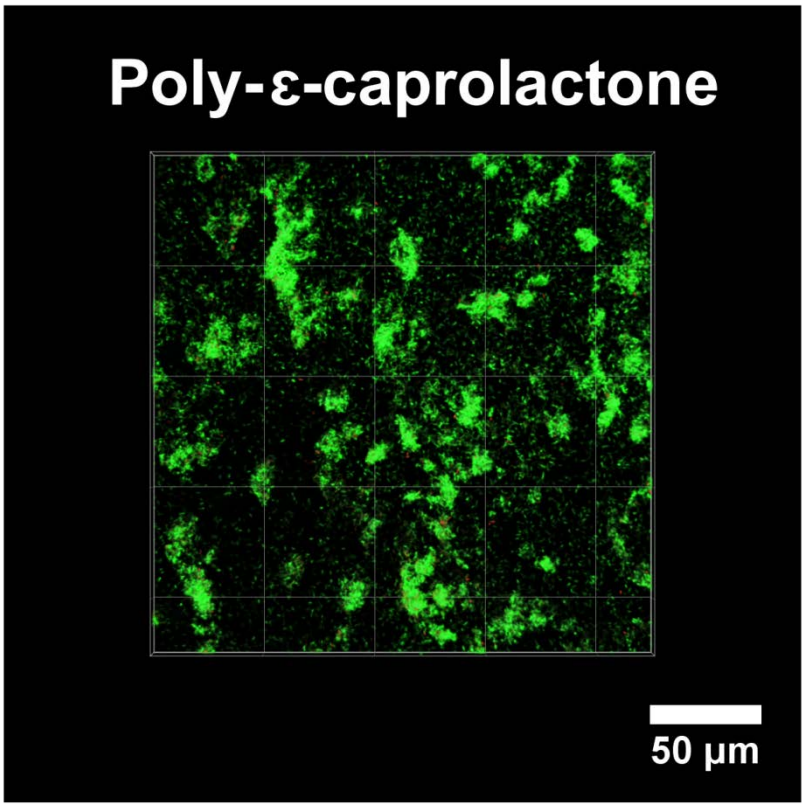

Figure A3.24. CLSM images of LIVE/DEAD stained *P. aeruginosa* grown statically for 1 h on a hydrophobic poly-ε-caprolactone surface.

Table A3.1. EDS to determine metal content of O-SWCNTs and O-MWCNTs used in this study.

O-SWCNTs, Carbon Solutions			O-MWCNTs, NanoLab Inc.		
	At%	Wt%		At%	Wt%
C K	82.0	69.9	*C K*	89.7	83.9
O K	14.5	16.5	*O K*	8.5	10.5
Ni L	2.1	8.7	*Fe L*	0.8	3.3
Y L	0.4	2.3	*Na K*	0.5	0.9
S K	0.5	1.1	*S K*	0.6	1.4
Cl K	0.6	1.5			

Appendix 4. Biofilm Development on Carbon Nanotube/Polymer Nanocomposites

This work was co-written with the following authors and is adapted from following the published work:

Goodwin, D. G., Xia, Z., Gordon, T. B., Gao, C., Bouwer, E. J., & Fairbrother, D. H. (2016). Biofilm Development on Carbon Nanotube/Polymer Nanocomposites. *Environmental Science: Nano*.

A4.1. MWCNT Oxidation

Pristine MWCNTs were oxidized by adding 1 gram of MWCNTs (Nanocyl NC7000, outer diameter 9.5 nm, 1.5 μm length, 90% purity) to 0.3 M HNO_3 and refluxing for 5 h at 110 °C. The resulting O-MWCNTs were washed with deionized water continuously until the pH of the filtrate reached 7 and then dried in an oven (Forced Convection Oven, Felisa Ovens, Zapopan, Jalisco, Mexico) overnight at 80 °C.[1] The O-MWCNTs had an oxygen content of 4.1% as determined by X-ray photoelectron spectroscopy (XPS) (PHI 5600 XPS, 58.7 eV pass energy, 0.125 eV/step, Mg Kα X-rays) and CasaXPS software (Teignmouth, UK).

A4.2. Octadecyltrichlorosilane (OTS) Modification of Glass Slides

A4.2.1. Reaction of OTS with Glass Slide Surfaces

Glass slides (1 x 25 x 75 mm, FisherBrand Frosted Microscope Slides, Cat #12-550-13) were first soaked in detergent solution (Alconox, Cat #1004) for 30 min and then rinsed with Milli-Q water. Slides were next etched with 4.0 M NaOH for 30 min, rinsed with Milli-Q water, and dried in a uniform stream of nitrogen gas. Subsequently, the

clean glass slides were placed in a gravity convection oven (Model 16 GCA, cat.# 31477, Precision) at 85 °C and dried overnight. The next day, slides were immersed in a 0.2% v/v OTS/hexane (95% GR ACS, Cat #HX0302-3, EMD) solution for 30 min and then ultra-sonicated in hexanes followed by ethanol to remove excess OTS and hexanes, respectively. Slides were then dried with a uniform stream of nitrogen, put in the oven at 85 °C for 30 min, and autoclaved.[2-5]

A4.2.2. Characterization of OTS Modification

XPS analysis of OTS-modified slides revealed a decrease in the Si(2p) signal and an increase in the C(1s) signal compared to a native glass microscope slide, consistent with the expectations of OTS modification. Specifically, we used the equation, $\boldsymbol{d = \lambda cos\theta \ln\left(\frac{I_0}{I}\right)}$,[6] where λ is the inelastic mean free path of the silicon (2p) photoelectron from the literature (2.7 nm),[7] θ is the take-off angle (54.7°), (I_0/I) represents the fractional change in the Si(2p) signal after OTS modification, and d is the depth of the OTS overlayer. The decrease in Si(2p) signal was indicative of a film approximately 1 nm thick over a large sample area (0.8 x 2 mm). These results indicate that the glass slide was sufficiently coated by an OTS layer to allow the CNT/PCL samples to attach to the underlying support. A lack of CNT/PCL detachment in aqueous media in all aspects of this study provided further evidence that the OTS layer firmly adhered the CNT/PCL to the OTS-modified glass surface.

A4.3. Preparation of PCL and CNT/PCL Samples

A4.3.1. Spray-Coating PCL and O-CNT/PCL Nanocomposites on OTS-modified Glass Slides for Biofilm Studies

To prepare CNT/PNC samples, OTS-modified glass slides were placed onto a hot plate (Fisher Scientific™ Isotemp™ Basic Stirring Hotplates) at 85 ˚C and sprayed with

approximately 4 mL (200 sprays) of CNT/PNC casting solution at a pressure of 30 PSI using a Badger 200 Single Action, Internal Mix Series Air-brush (Badger Air-Brush Co. Franklin Park, IL). Two slides were placed in a row and sprayed together from a distance of approximately 15 cm. After spray-coating, samples were immediately put into separate sterile containers. Spray-coating was performed inside a sterile biosafety cabinet (Labconco Purifier Class II Biosafety Cabinet) as shown in Figure A4.2.

A4.3.2. Slow-drying Thicker CNT/PCL Nanocomposites for Photolysis

To prepare thicker CNT/PCL nanocomposites suitable for photolysis, the 2% w/w O-MWCNT/PCL casting solution was added in 5 mL aliquots to aluminum dishes (44 mm diameter, 12.5 mm height, Fisherbrand) and the CNT/PCL samples were subsequently generated by solvent evaporation overnight. Once the CNT/PCL nanocomposites had dried, they were peeled from the aluminum dishes.

A4.3.3. Spray-Coating CNT/PVOH Nanocomposites for SEM

As a comparison to O-MWCNT/PCL nanocomposites, the surface structure of an O-MWCNT/PVOH nanocomposite with the same O-MWCNT loading was imaged using SEM. To prepare these O-MWCNT/PVOH nanocomposites, a 2 mg/mL stock PVOH solution (Sigma Aldrich, M_w=31,000-50,000, 98%-99% hydrolyzed) and a 0.05 mg/mL O-MWCNT stock suspension (NanoLab Inc., PD15L5-20-COOH, Lot. # 06-16-10, outer diameter 15 ± 5 nm, length 5-20 μm from the manufacturer) were combined aseptically to prepare a casting solution containing 2% w/w O-MWCNT/PVOH. A pure PVOH solution was also prepared as a reference. These casting solutions were then shaken vigorously, sonicated for 5 min, and added to spray bottles. Autoclaved glass slide pieces (1 cm^2) were placed onto a hot plate at 150 ˚C and sprayed 30 times (1.07 mL/spray ± 0.05 mL/spray) from a consistent distance (approximately 25 cm) in 10 s intervals to

flash dry the casting solution upon contact. All spray-coating was carried out inside a sterile biosafety cabinet (Labconco Purifier Class II Biosafety Cabinet).

A4.4. SEM Analysis

For SEM analysis, PCL, CNT/PCL, PVOH, and CNT/PVOH nanocomposites were spray-coated onto 1-cm^2-sized OTS-modified glass pieces according to the procedures described in Section I of the experimental section and sputter-coated with platinum (Quorum Technologies Polaron SC7640 Auto/Manual High Resolution Sputter Coater, 12 mA/800V plasma current, and ~3 min at 0.5 nm/min) to prevent charging under the electron beam. A cold-cathode field emission scanning electron microscope (JEOL 6700F, 10 keV, 8.0 nm working distance, LEI & SEI detectors) with a 1.0 nm resolution at 15 keV was used to image samples. For each sample, replicate images (≥ 5 images) of random areas across the surface were taken. To demonstrate sample-to-sample consistency, 2% w/w O-MWCNT/PCL nanocomposites were spray-coated on different occasions and imaged.

A4.5. Microbial Frozen Stocks

To prepare the frozen stocks, cells were grown in LB broth (Lennox, Fisher Scientific) overnight at 37 °C to the exponential phase. The cell suspensions were distributed into 1 mL Eppendorf tubes with sterile glycerol (10% v/v final concentration) and stored at -80 °C.

A4.6. Basal Mineral Media (BMM) Composition

BMM contained 7.18 mM K_2HPO_4, 2.79 mM KH_2PO_4, 0.757 mM $(NH_4)_2SO_4$, 0.0406 mM $MgSO_4*7H_2O$, and 0.5 v/v% trace elements solution (3.75 mM H_3BO_3,

0.0605 mM $ZnSO_4*7H_2O$, 0.0296 mM $FeSO_4(NH_4)_2SO_4*6H_2O$, 0.034 μM$CoSO_4*7H_2O$, 26 μM $(NH_4)_6Mo_3O_{24}*4H_2O$, 32 μM $CuSO_4*5H_2O$, and 36 μM $MnSO_4*4H_2O$).

A4.7. LIVE/DEAD Staining and Biofilm Imaging

A4.7.1. LIVE/DEAD Staining Procedure

The LIVE/DEAD biofilm viability kit consists of two nucleic acid molecular probes: green-fluorescent SYTO 9 to stain living cells and red-fluorescent propidium iodide (PI) to stain dead cells. An aqueous stain stock solution was prepared containing 3 μL of 3.34 mol/L SYTO 9 in dimethylsulfoxide (DMSO) and 3 μL of 20 mmol/L propidium iodide (PI) in DMSO for every 1 mL of autoclaved Milli-Q water.[8] This stock solution was shaken and covered with aluminum foil to minimize light exposure to the photosensitive stains. After an experiment, samples were transferred to a 20 mL depleted media (DM) bath to remove loosely adhered cells by holding the frosted end of the underlying glass slides with forceps since this was an area of the sample that was never imaged. Immediately after removal from DM, 0.5 mL of the aqueous stain stock solution was added gently to the samples and left to sit for 20 min in the dark. Samples were then washed, stained, washed, and coated in VectaShield in a staggered fashion and immediately brought to the Integrated Imaging Center at JHU for imaging.

Several staining procedures were followed that were utilized in our previous study. These included prevention of sample dry-out during the staining process, washing samples with depleted media to maintain ionic strength and prevent lysis, and complete

thawing of the frozen LIVE/DEAD stain stocks to ensure the proper concentrations of stains were used.

A4.7.2. Confocal Laser Scanning Microscopy (CLSM) Imaging

CLSM imaging was performed using a Zeiss LSM 510 Multiphoton Confocor 3 laser scanning microscope (Carl Zeiss, Germany) in the Integrated Imaging Center at JHU. Images were obtained using a 40x water immersion objective with a 1.2 numerical aperture (N.A.). A 488 nm Argon laser (30 mW at 5% output) to excite the SYTO 9-stained cells and a 543 nm He/Ne laser (1.2 mW) to excite PI-stained cells were used in dual channel mode. The gains were adjusted using the brightest red and green cells in the range indicator mode: this was possible since the biofilms always contained a small number of living and dead cells. Images were obtained using ZEN software (Carl Zeiss, 2009, Thornwood, NY).

A4.8. LIVE/DEAD Staining Controls

A4.8.1. Background Staining Controls

PCL, 2% w/w O-MWCNT/PCL, and photodegraded 2% w/w O-MWCNT/PCL samples were LIVE/DEAD stained in the absence of *P. aeruginosa*. This allowed the CNT/PNC contribution to the fluorescence background to be assessed. A small amount of background fluorescence was present for all three PCL-containing samples, although the laser gains had to be increased by approximately 10% on these confocal image to obtain a visibly fluorescent image.[9] Additionally, the background fluorescence faded during imaging which was not the case for the biofilms imaged in this study. Nevertheless, care was taken to eliminate any contribution from PCL or CNT fluorescence by choosing the

lower boundary of the confocal stack based on a strong fluorescent signal and clear evidence of microbial shapes.

A4.8.2. OTS Staining Control

OTS-modification of glass slides is often used in studies involving microorganisms and has not been shown to cause cell death.[10, 11] Nevertheless, to ensure OTS had no cytotoxic effect on *P. aeruginosa*, OTS slides were inoculated under static conditions for 6 h, a sufficient length of time to coat the OTS slides with microorganisms. Samples were LIVE/DEAD stained and imaged in replicate areas according to the protocol used in this study (Figure A4.16). In line with expectations, results from these studies revealed that minimal cell death occurred on OTS-modified glass surfaces.

A4.9. Confocal Image Analysis

A4.9.1. COMSTAT 2 Analysis of Biofilm Images

Since SYTO 9 stains all biofilm cells while PI only stains dead cells, the green fluorescent (SYTO 9) channel was chosen to determine biomass and biofilm thickness. Since SYTO 9 only weakly fluoresces in dead cells, the green fluorescent signal threshold was increased to 150 for COMSTAT 2 analysis to ensure all biofilm cells were counted. Connected volume filtering was used to exclude planktonic cells in the biofilm analysis.[12-14]

A4.9.2. Manual Thickness Measurements of Confocal Images for Comparison to COMSTAT 2 Analysis

To validate the COMSTAT 2 results, the COMSTAT 2 thickness analysis was compared to manual thickness measurements using ImageJ software (NIH, Bethesda, MD) for PCL and 2% w/w O-MWCNT/PCL samples under both DFR and static conditions. Manual thickness measurements were made in five areas of each biofilm

using the side view of each reconstructed XYZ projection. At least 6 replicate side views were measured and averaged for each biofilm regime. The dead layer thicknesses were also measured manually for the red fluorescent microbial layer that formed under drip flow reactor conditions (Figure 4.2) and for the red-fluorescent microbial layer that formed on the photodegraded CNT/PCL nanocomposites (Figure 4.5). Only manual thickness measurements were made for the photodegraded CNT/PCL nanocomposites because COMSTAT 2 analysis of the biofilm coating was not possible with the curved configuration of the underlying CNT/PNC (wrapped around a glass slide for photodegradation).

A4.10. References

1. H. Y. Zhao, H. M. Zhou, J. X. Zhang, W. Zheng and Y. F. Zheng, *Biosens. Bioelectron.*, 2009, 25, 463-468.
2. M. E. McGovern, K. M. R. Kallury and M. Thompson, *Langmuir*, 1994, 10, 3607-3614.
3. P. H. Mutin, G. Guerrero and A. Vioux, *J. Mater. Chem.*, 2005, 15, 3761-3768.
4. M. Sodagari, H. Wang, B.-m. Z. Newby and L.-K. Ju, *Colloids Surf. B. Biointerfaces*, 2013, 103, 121-128.
5. H. Wang, M. Sodagari, Y. Chen, X. He, B.-m. Z. Newby and L.-K. Ju, *Colloids Surf. B. Biointerfaces*, 2011, 87, 415-422.
6. J. C. Vickerman and I. S. Gilmore, *Surface analysis: the principal techniques*, Wiley Online Library, 2009.
7. S. Tanuma, C. J. Powell and D. R. Penn, *Surf. Interface Anal.*, 1991, 17, 911-926.
8. Invitrogen, *Journal*, 2009.
9. D. G. Goodwin, K. M. Marsh, I. B. Sosa, J. B. Payne, J. M. Gorham, E. J. Bouwer and D. H. Fairbrother, *Environ. Sci. Technol.*, 2015, 49, 5484-5492.
10. M. Sodagari, H. Wang, B.-m. Z. Newby and L.-K. Ju, *Colloids Surf., B*, 2013, 103, 121-128.
11. A. Razatos, Y.-L. Ong, F. Boulay, D. L. Elbert, J. A. Hubbell, M. M. Sharma and G. Georgiou, *Langmuir*, 2000, 16, 9155-9158.
12. A. Heydorn, A. T. Nielsen, M. Hentzer, C. Sternberg, M. Givskov, B. K. Ersbøll and S. Molin, *Microbiology*, 2000, 146, 2395-2407.
13. M. Vorregaard, Technical University of Denmark, DTU, DK-2800 Kgs. Lyngby, Denmark, 2008.
14. Comstat 2 Homepage, www.comstat.dk

A4.11. Figures

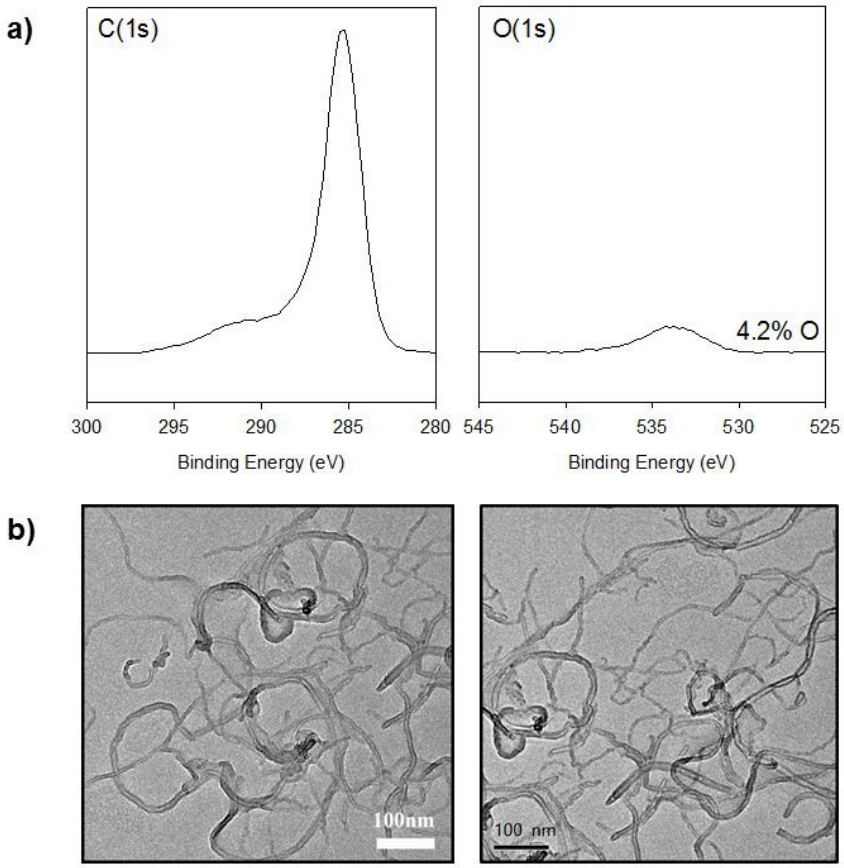

Figure A4.1. Characterization of O-MWCNTs by a) XPS and b) TEM. Using the TEM images, an O-MWCNT diameter distribution of 9.4 ± 1.2 nm was calculated as the average of 15-20 measurements using DigitalMicrograph software.

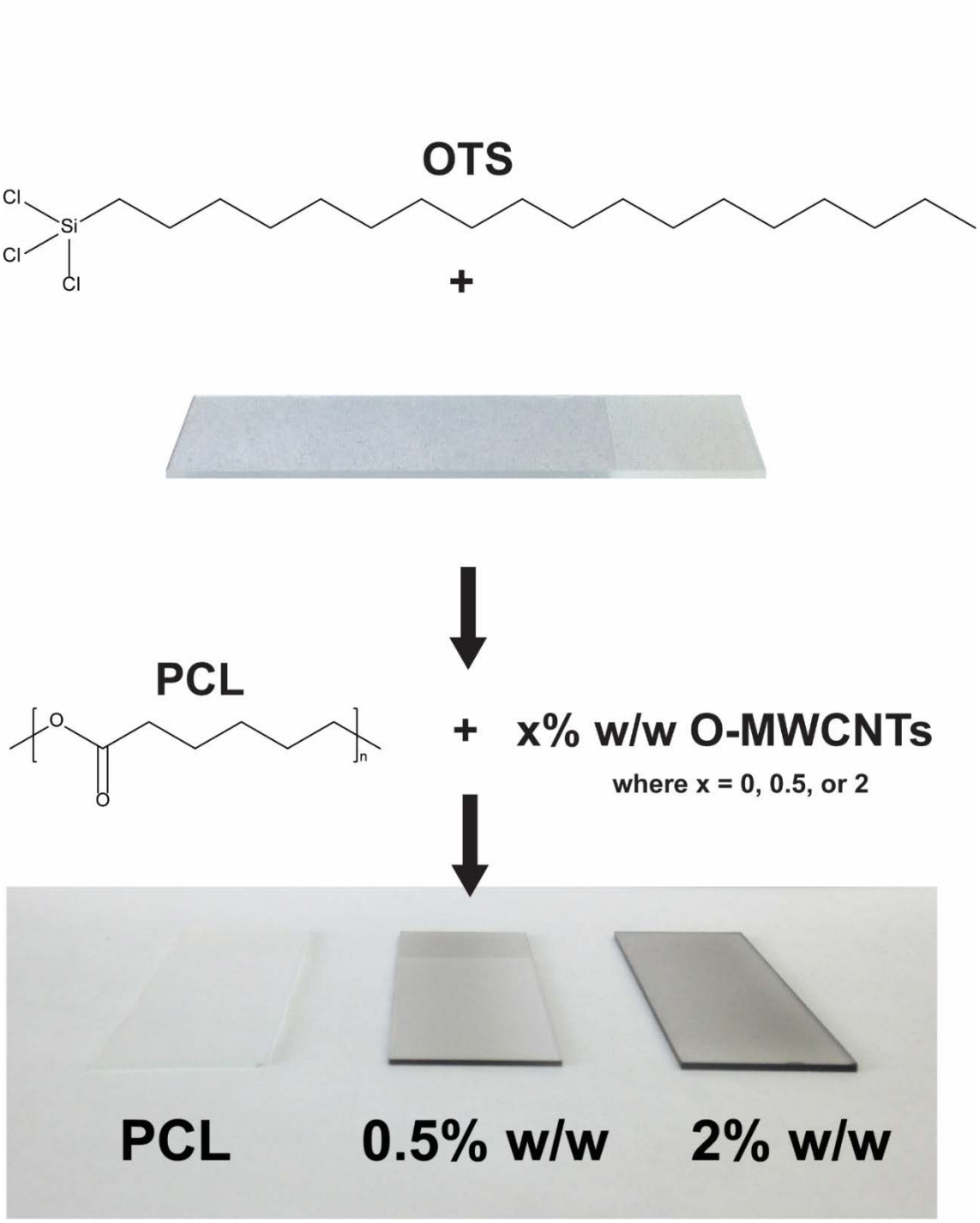

Figure A4.2. Octadecyltrichlorosilane-modified glass slides spray-coated with PCL, 0.5% w/w O-MWCNT/PCL, and 2% w/w O-MWCNT/PCL casting solutions.

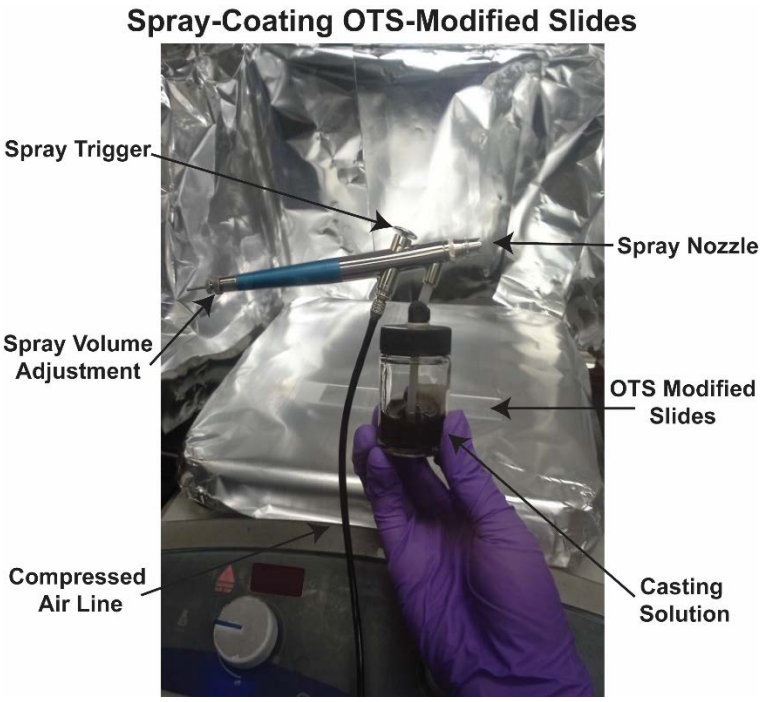

Figure A4.3. The setup used to spray-coat the CNT/PNC casting solutions onto OTS-modified glass slides.

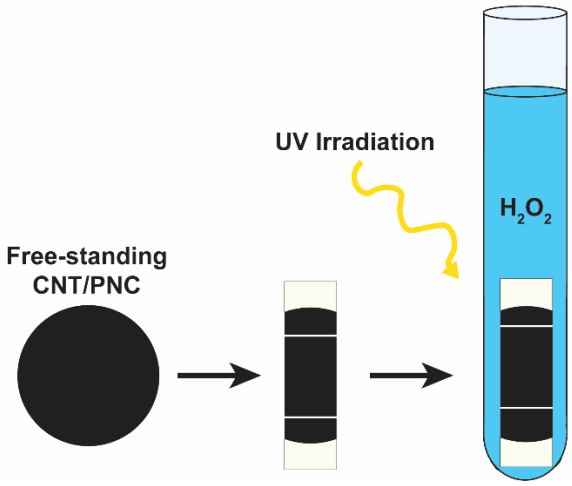

Figure A4.4. An illustration depicting the simulated weathering of CNT/PNCs. 2% w/w O-MWCNT/PCL nanocomposites were photolyzed in the presence of H_2O_2 to accumulate CNTs at the surface of the nanocomposite prior to microbial exposure.

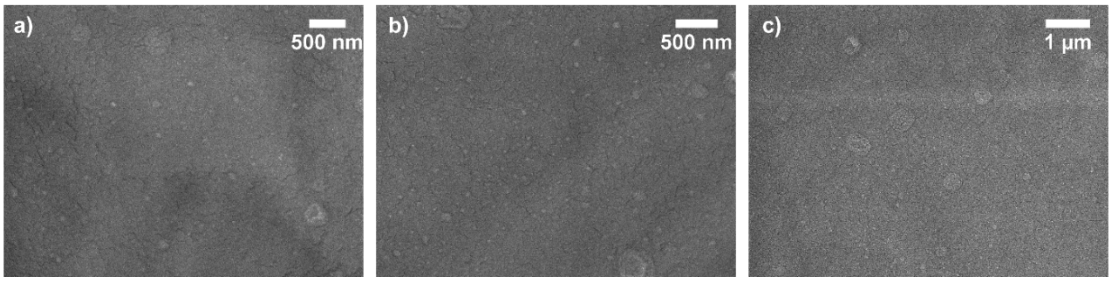

Figure A4.5. SEM images of PCL samples in replicate areas.

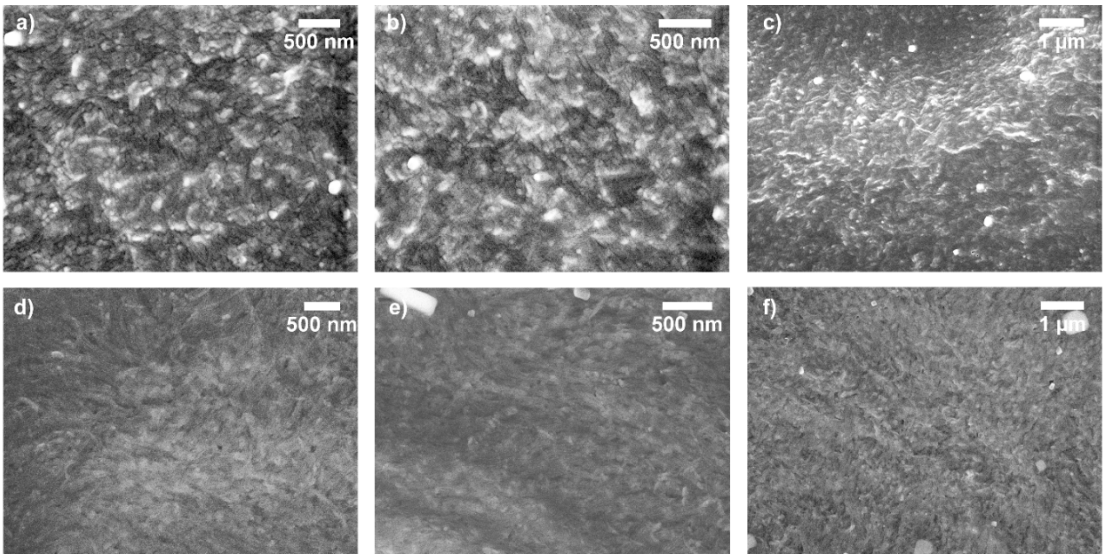

Figure A4.6. SEM images of 2% w/w O-MWCNT/PCL samples. The top row and second row are SEM images from two separately prepared samples. Each row contains replicate areas from that particular sample.

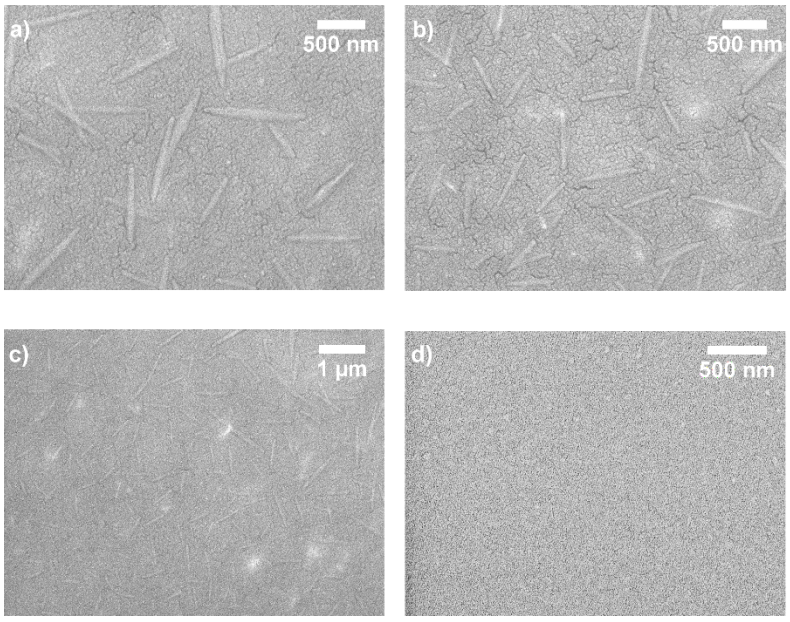

Figure A4.7. SEM images of 2% w/w O-MWCNT/PVOH (a-c) samples in replicate areas as well as pure PVOH (d) for reference.

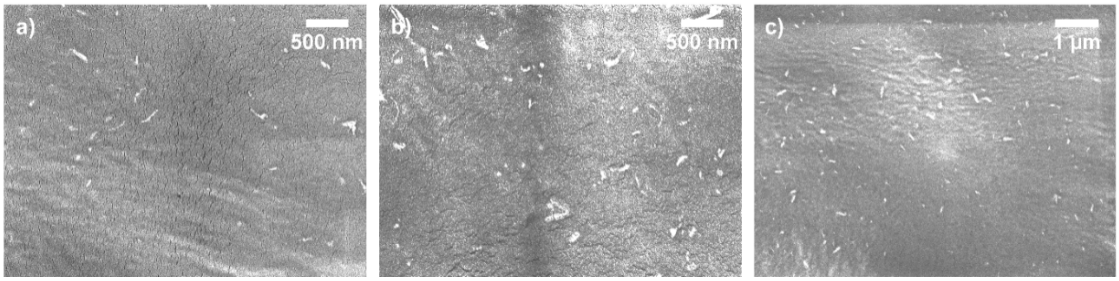

Figure A4.8. SEM images of 0.5% w/w O-MWCNT/PCL samples in replicate areas.

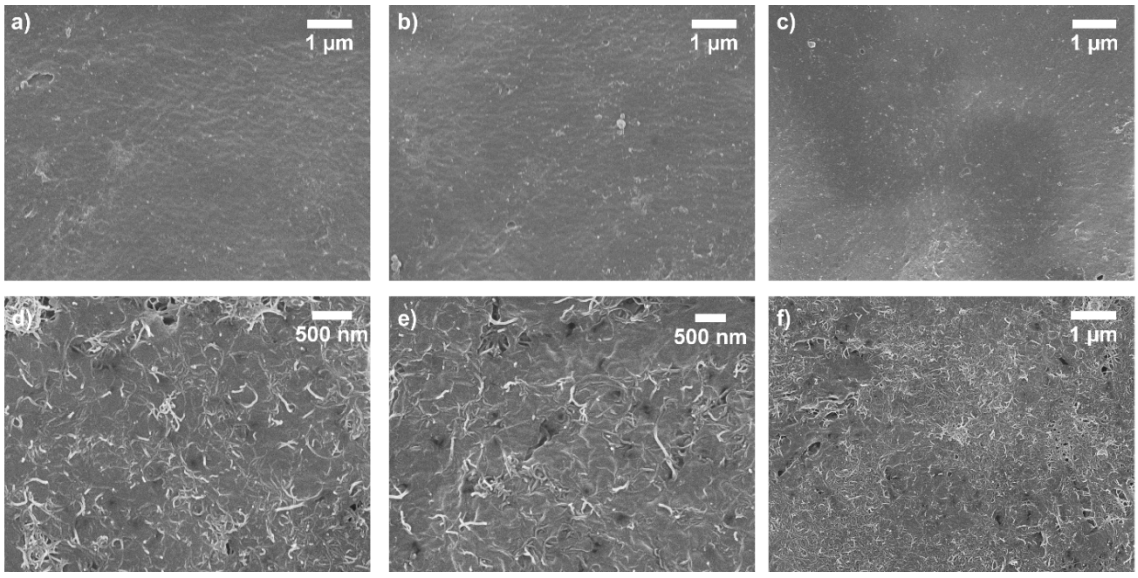

Figure A4.9. SEM of thick 2% w/w O-MWCNT/PCL nanocomposites (replicate areas) with no underlying support before (a-c) and after (d-f) irradiation in the presence of 0.5 M H_2O_2.

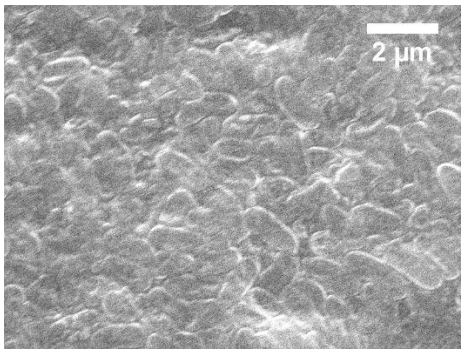

Figure A4.10. SEM image of a 2% w/w O-MWCNT/PCL nanocomposite surface after an attempt to remove attached biofilms with sodium polyphosphate. Despite treatment, biofilms still covered the underlying material.

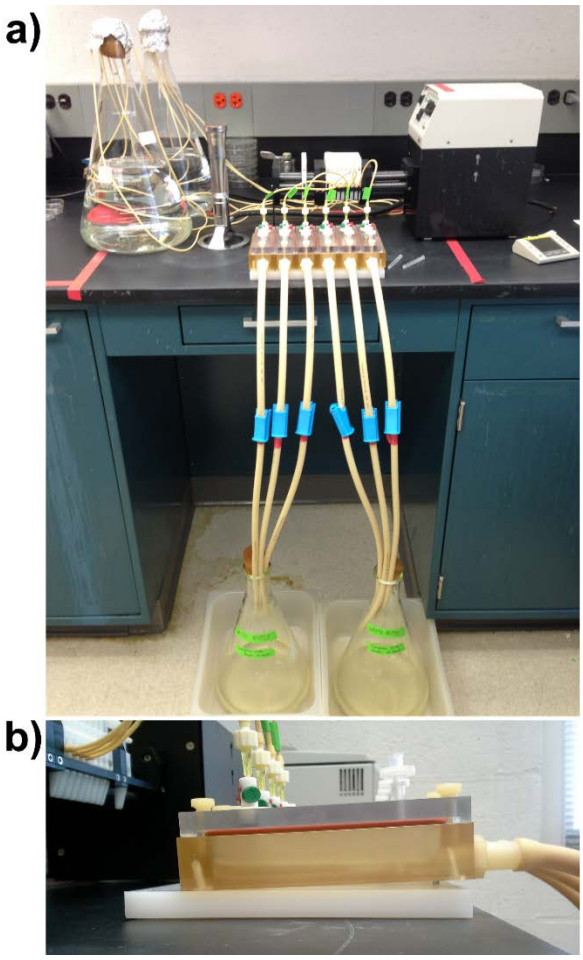

Figure A4.11. Drip flow reactor setup (a) with a side view of the negative angle used to fully cover the hydrophobic slides (b).

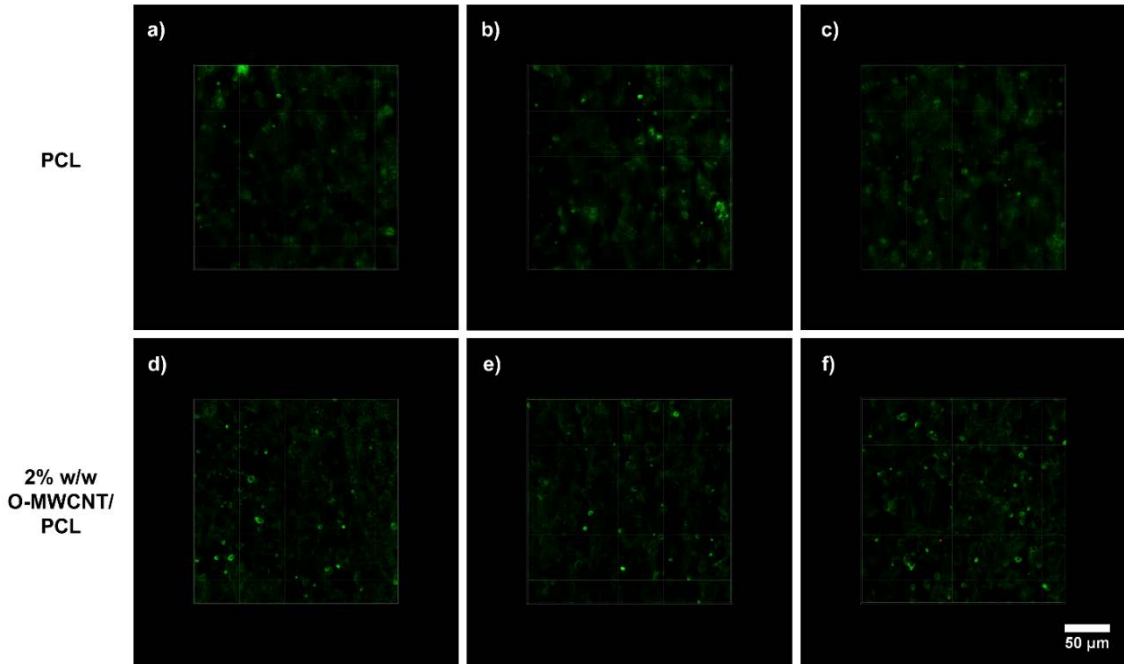

Figure A4.12. Abiotic background fluorescence controls of LIVE/DEAD stained PCL and 2% w/w O-MWCNT/PCL nanocomposite surfaces. Gains were adjusted approximately 10% higher than those used for biofilm-containing samples to make the background staining slightly more visible in the images.

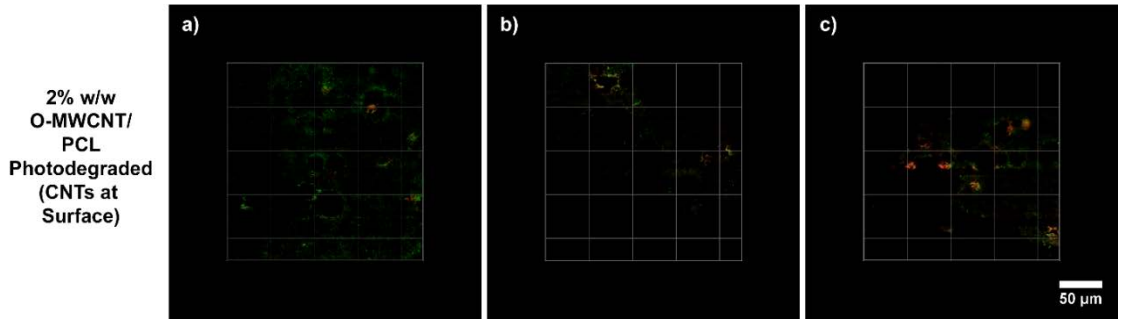

Figure A4.13. Abiotic background fluorescence controls of LIVE/DEAD stained 2% w/w O-MWCNT/PCL nanocomposite surfaces that had been photodegraded. Gains were adjusted approximately 10% higher than those used for biofilm-containing samples to make the background staining slightly more visible in the images.

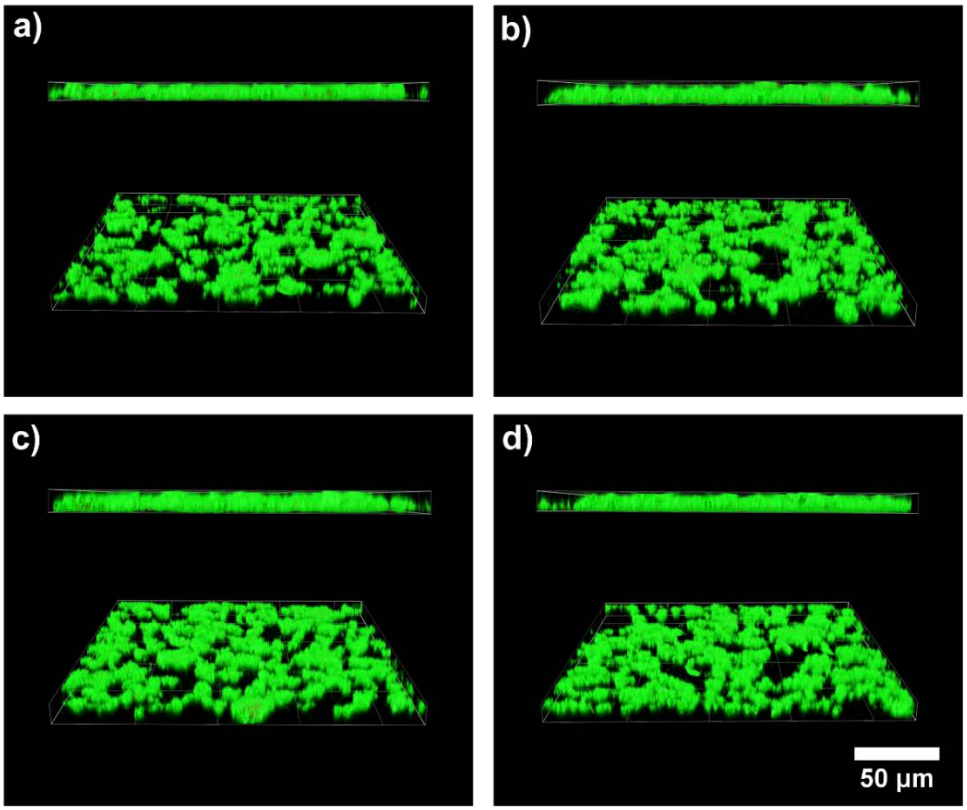

Figure A4.14. CLSM images of LIVE/DEAD stained biofilms on glass slides grown under static conditions for 2 weeks (similar to Regime 3 in Figure 4). Replicate areas of the same sample are shown.

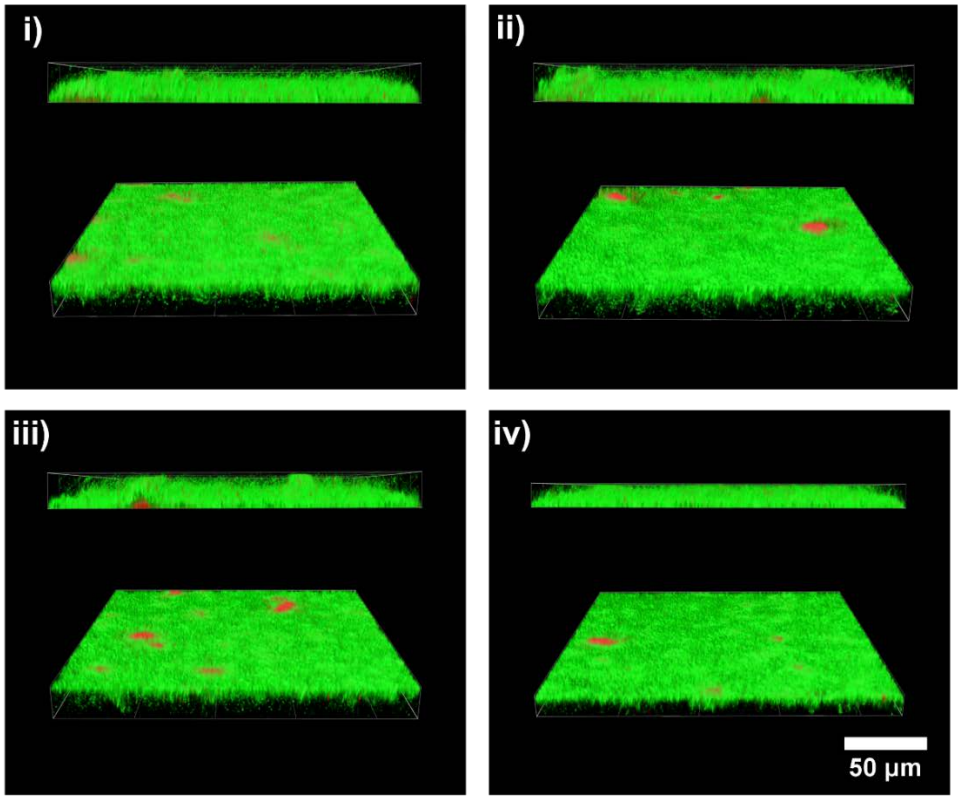

Figure A4.15. CLSM images of LIVE/DEAD stained biofilms on glass slides grown under DFR conditions for 72-96 h (similar to regime 4 in Figure 2). Replicate areas of the same sample are shown.

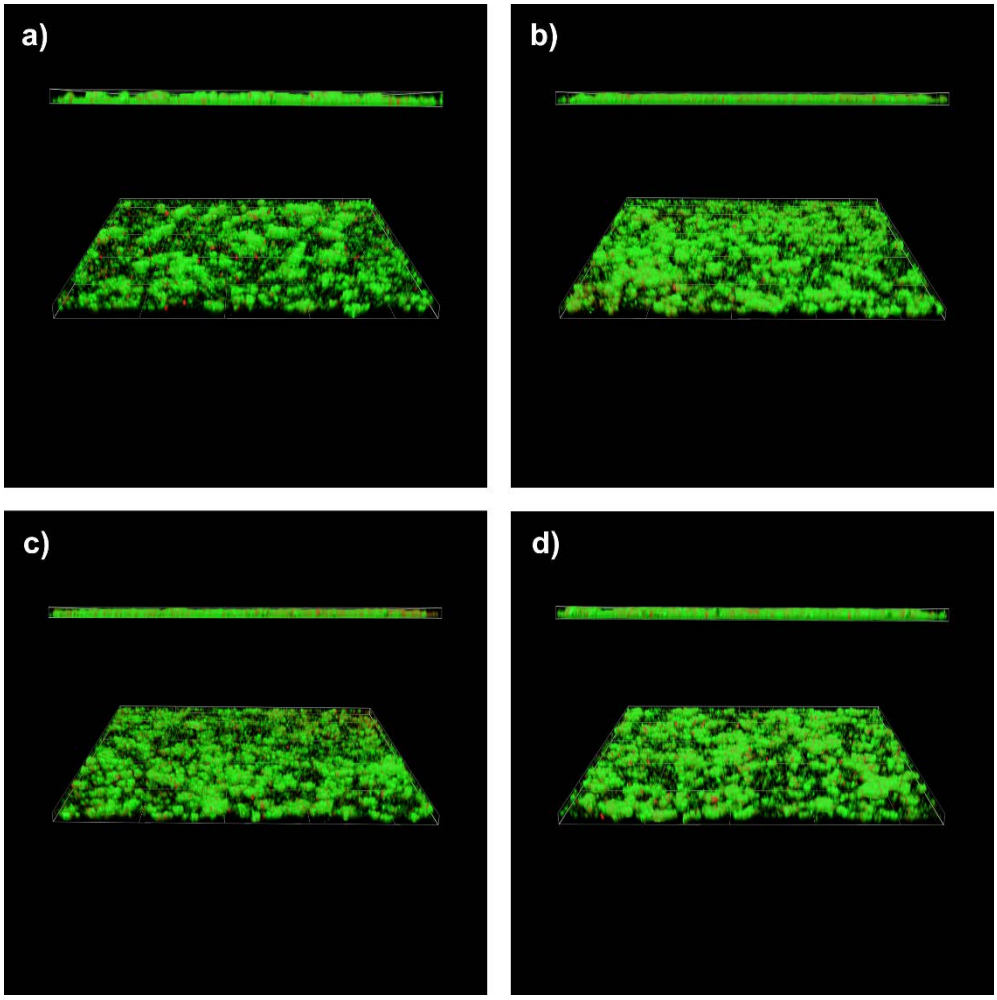

Figure A4.16. CLSM images of LIVE/DEAD stained biofilms grown on OTS-modified glass slides under static conditions for 6 h. Minimal cell death occurred as indicated by the large number of green-fluorescent cells. Replicate areas of the same sample are shown.

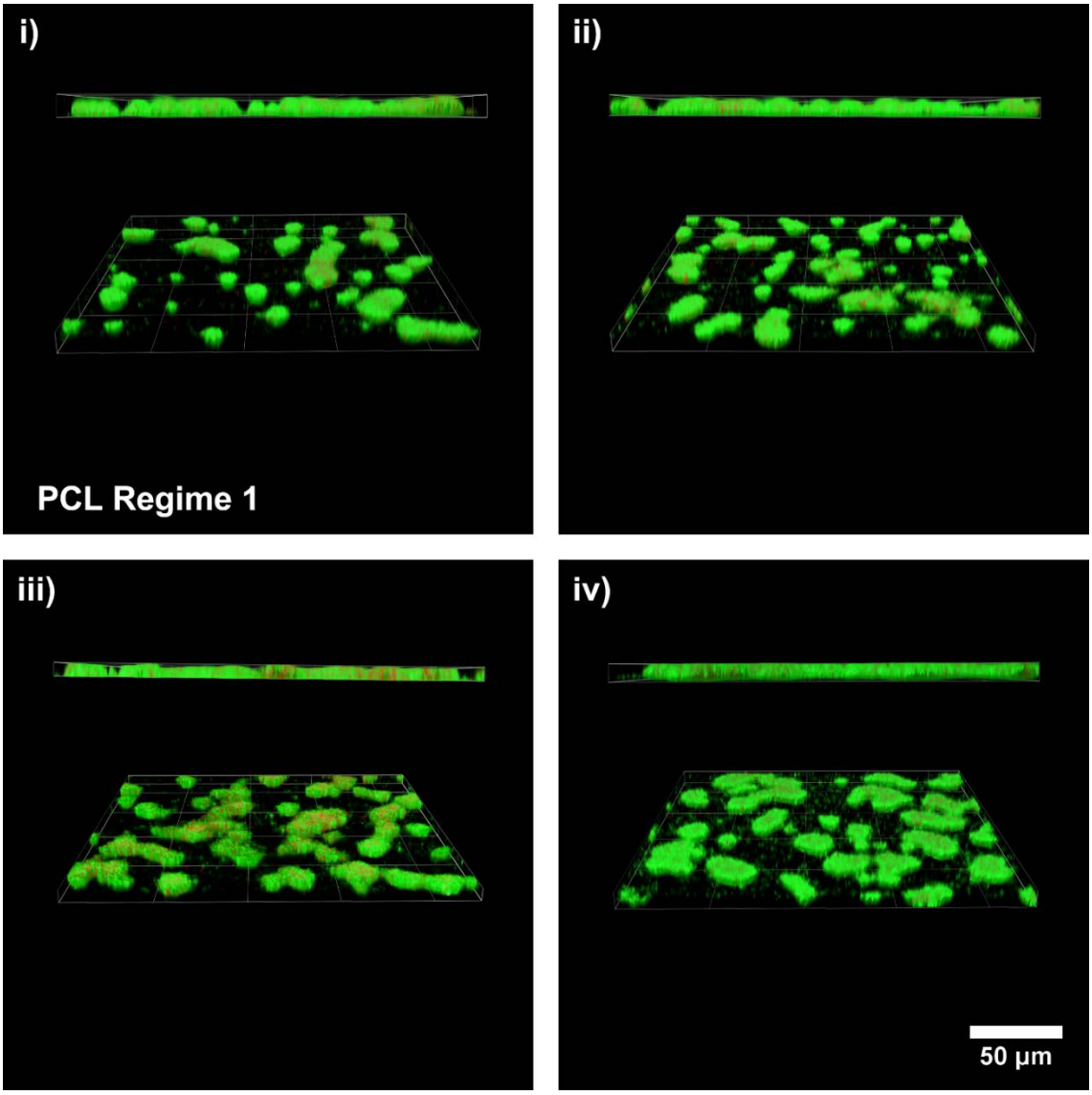
i)
ii)
PCL Regime 1
iii)
iv)
50 µm

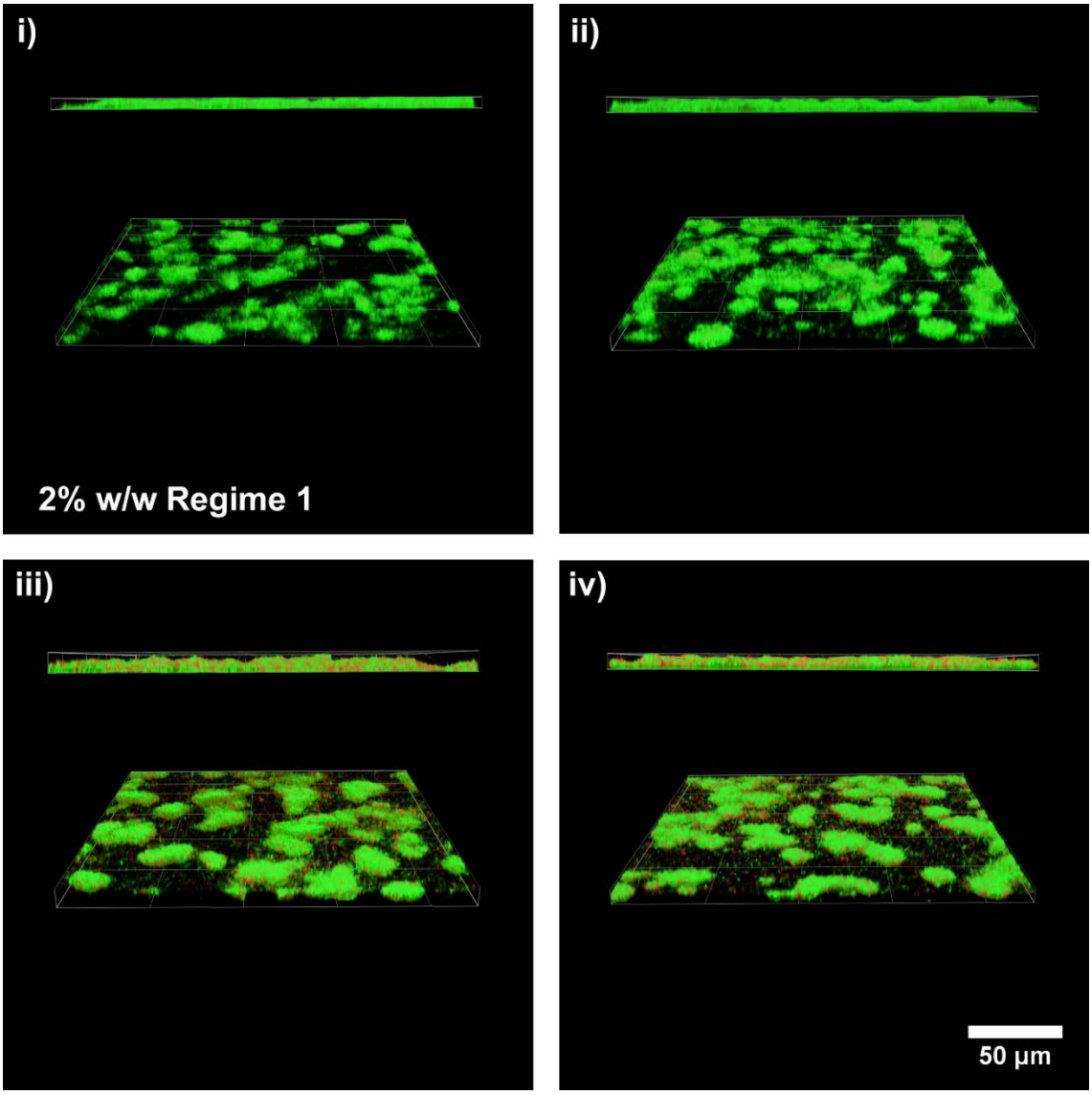
i)
2% w/w Regime 1
ii)
iii)
iv)
50 µm

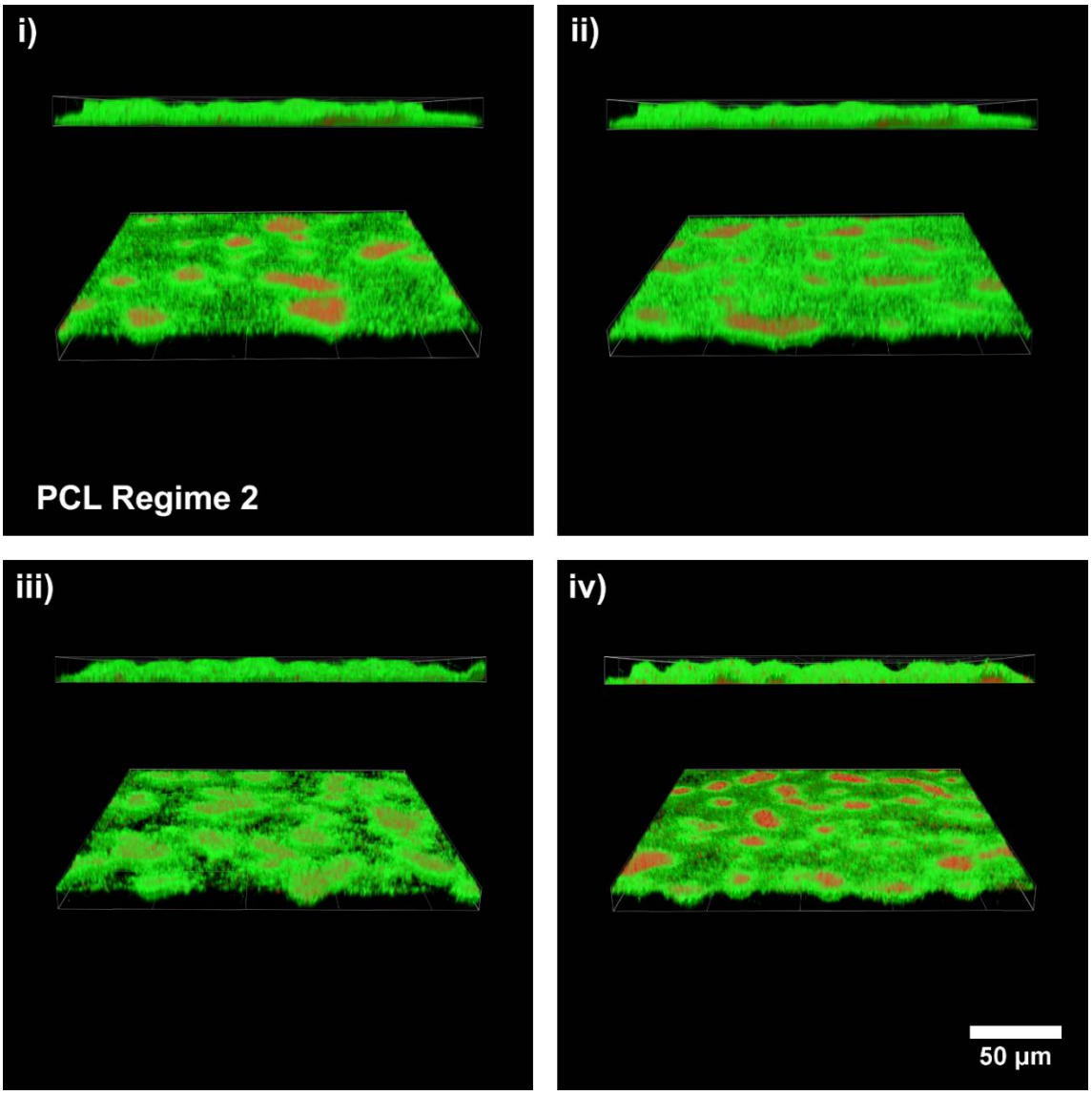
i)
ii)
PCL Regime 2
iii)
iv)
50 µm

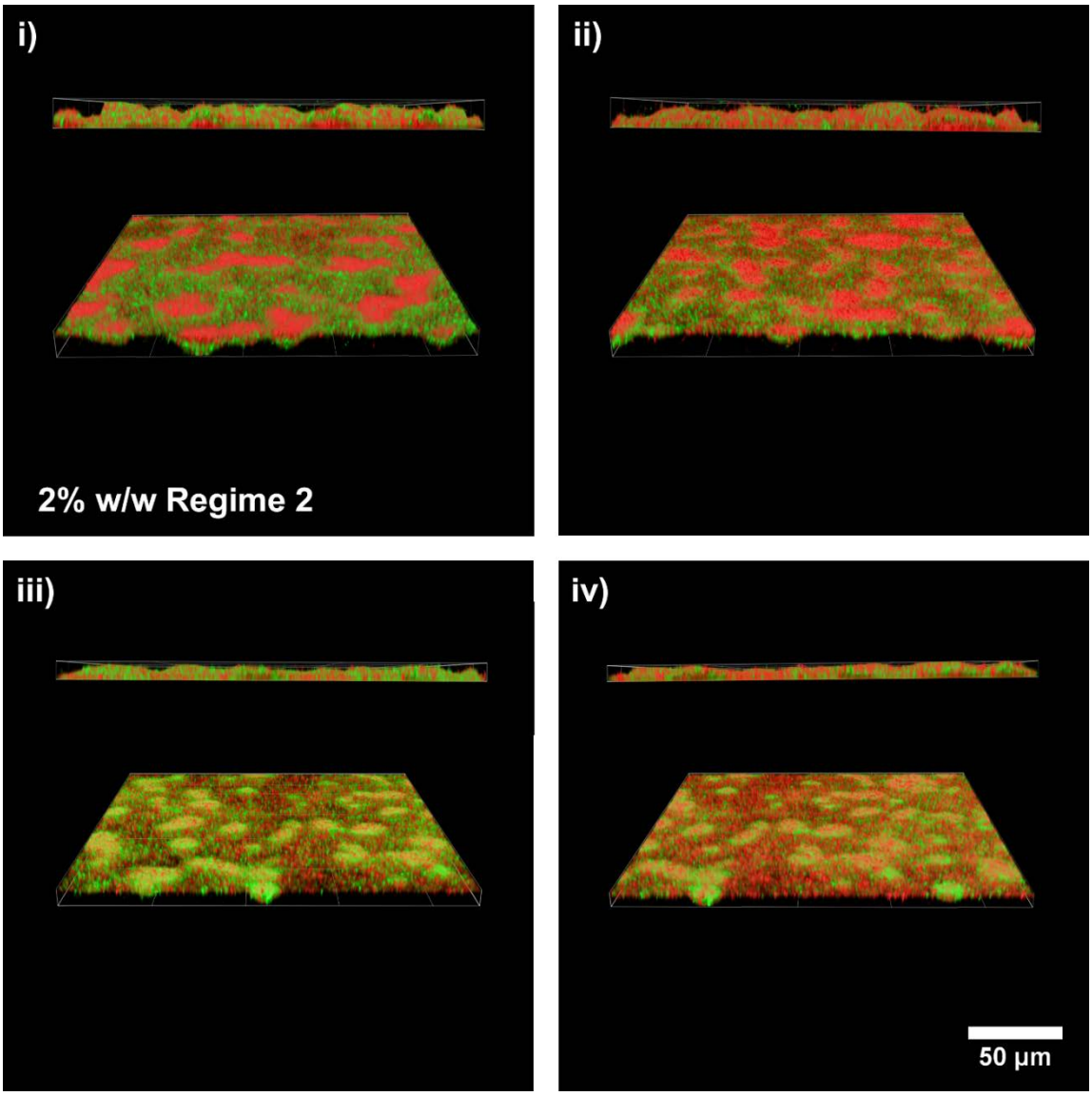
i)
ii)
2% w/w Regime 2
iii)
iv)
50 µm

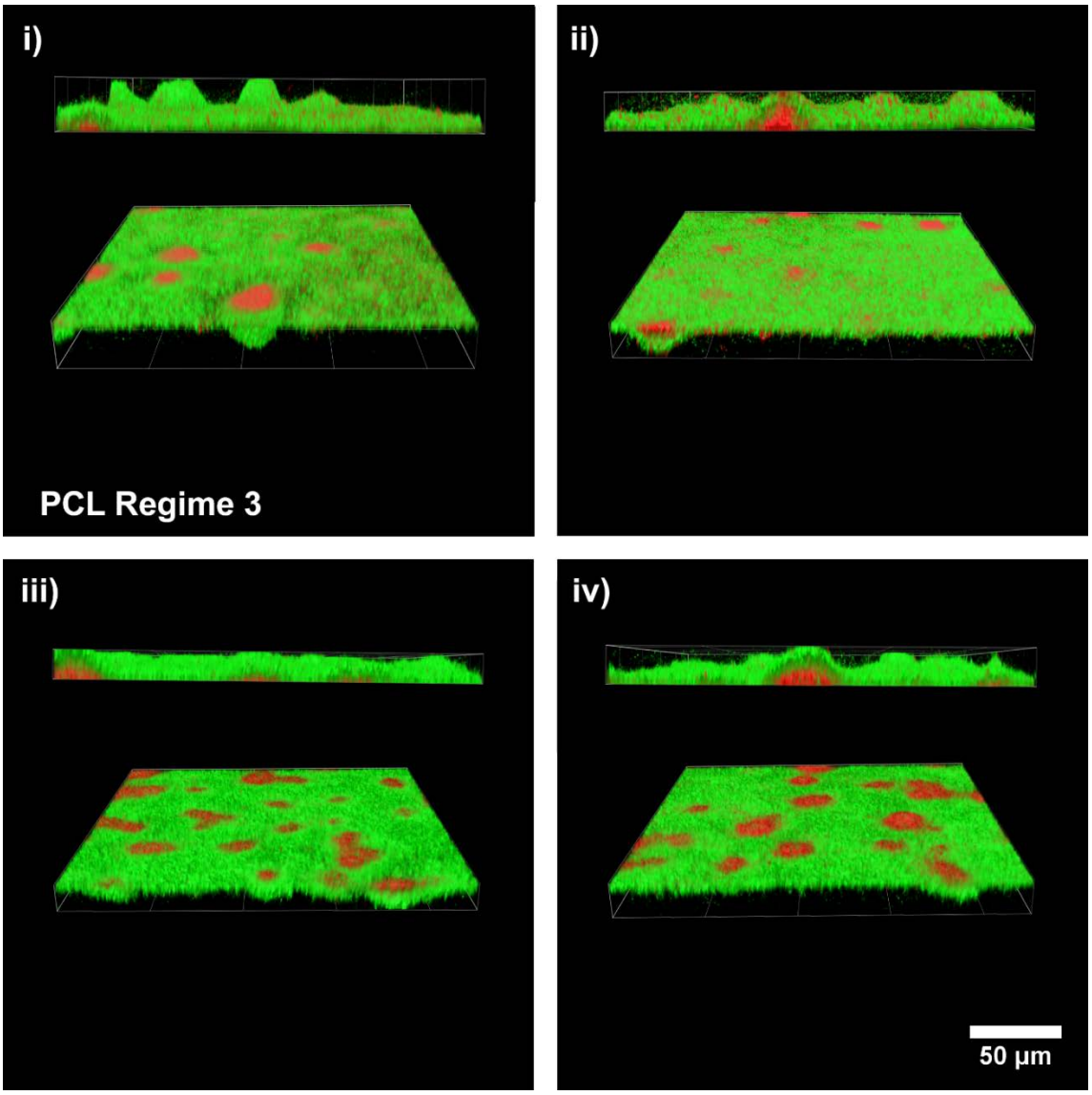
i)
ii)
PCL Regime 3
iii)
iv)
50 µm

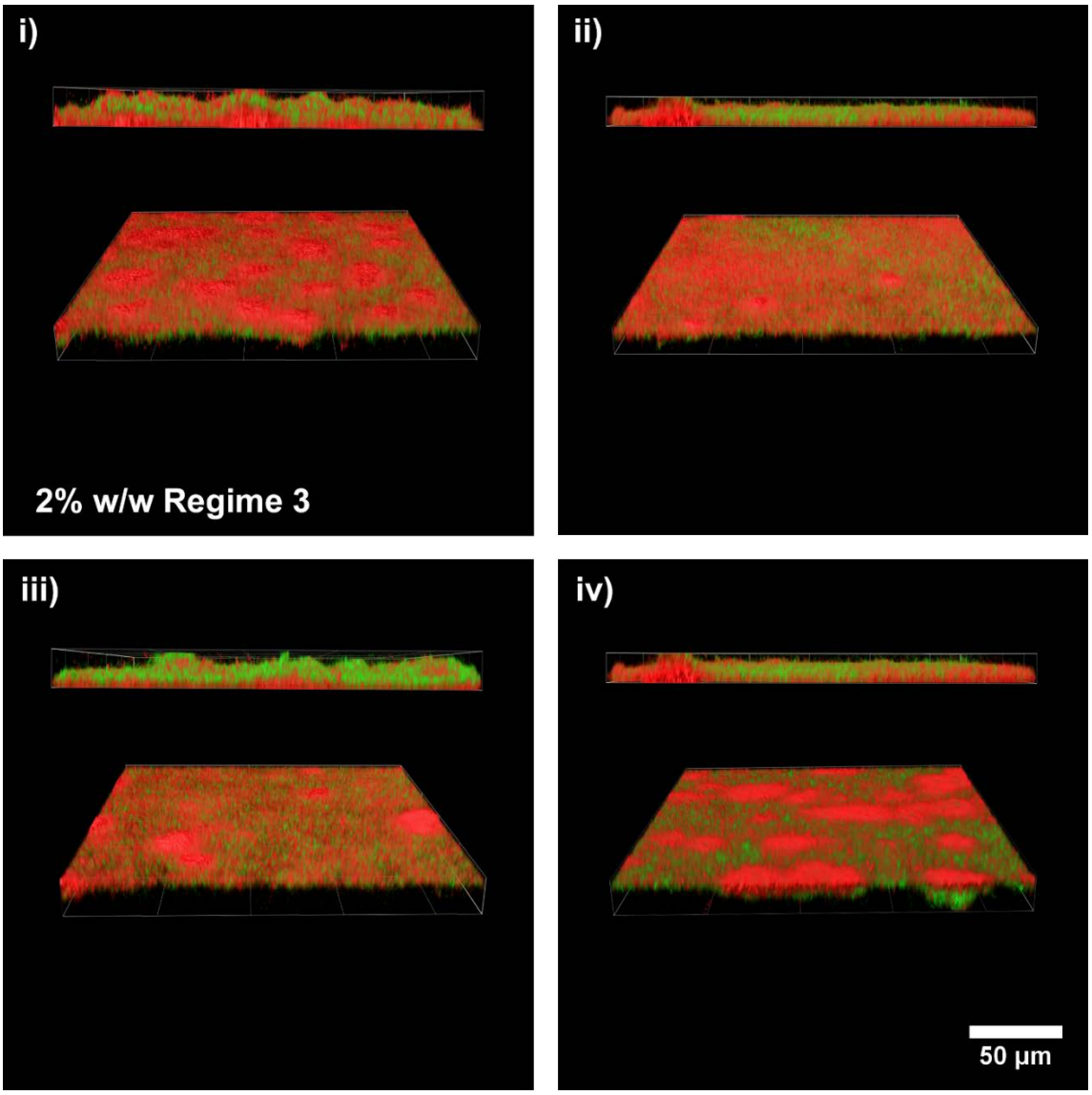
i)
2% w/w Regime 3
ii)
iii)
iv)
50 µm

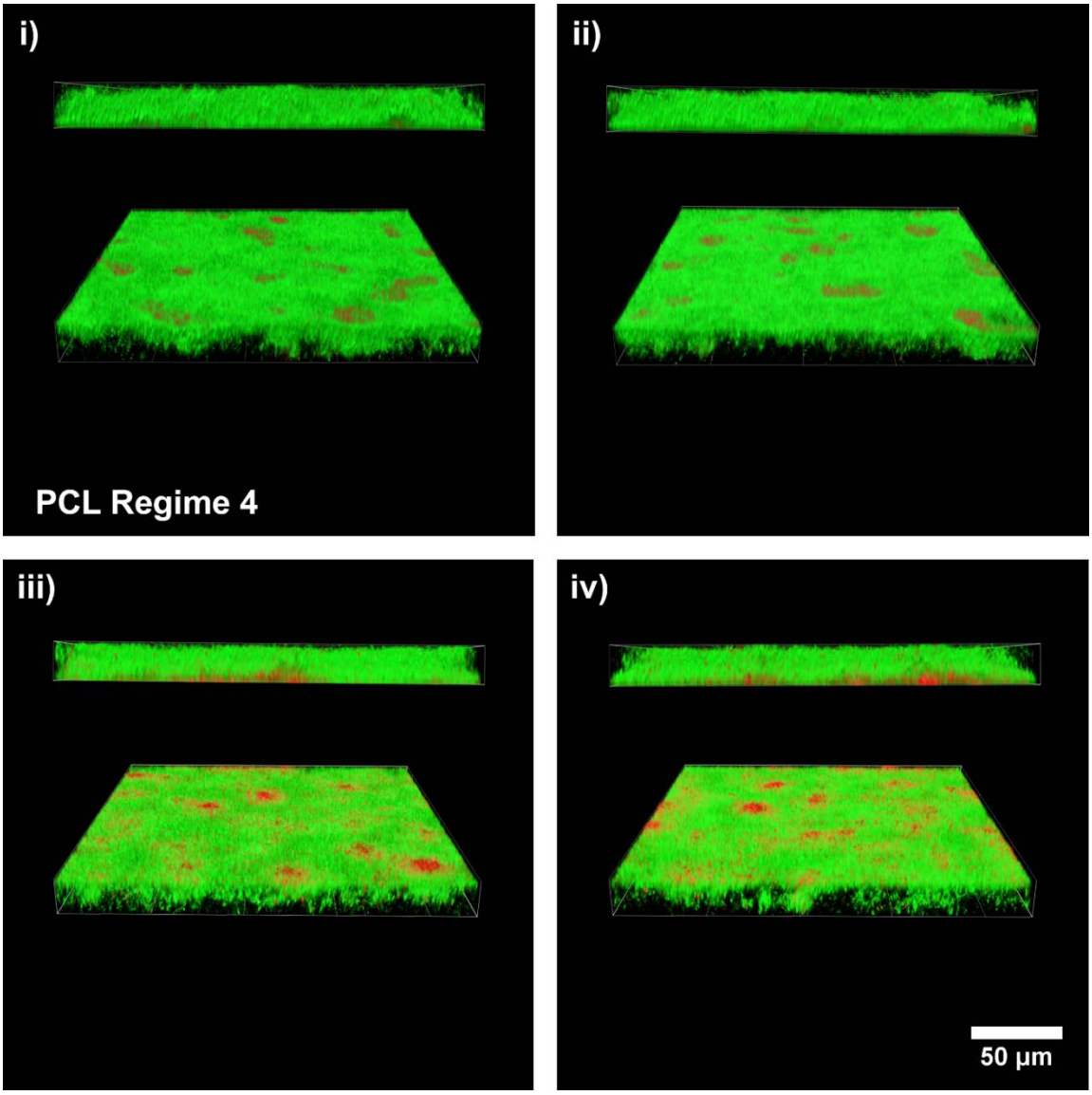
i)
ii)
PCL Regime 4
iii)
iv)
50 µm

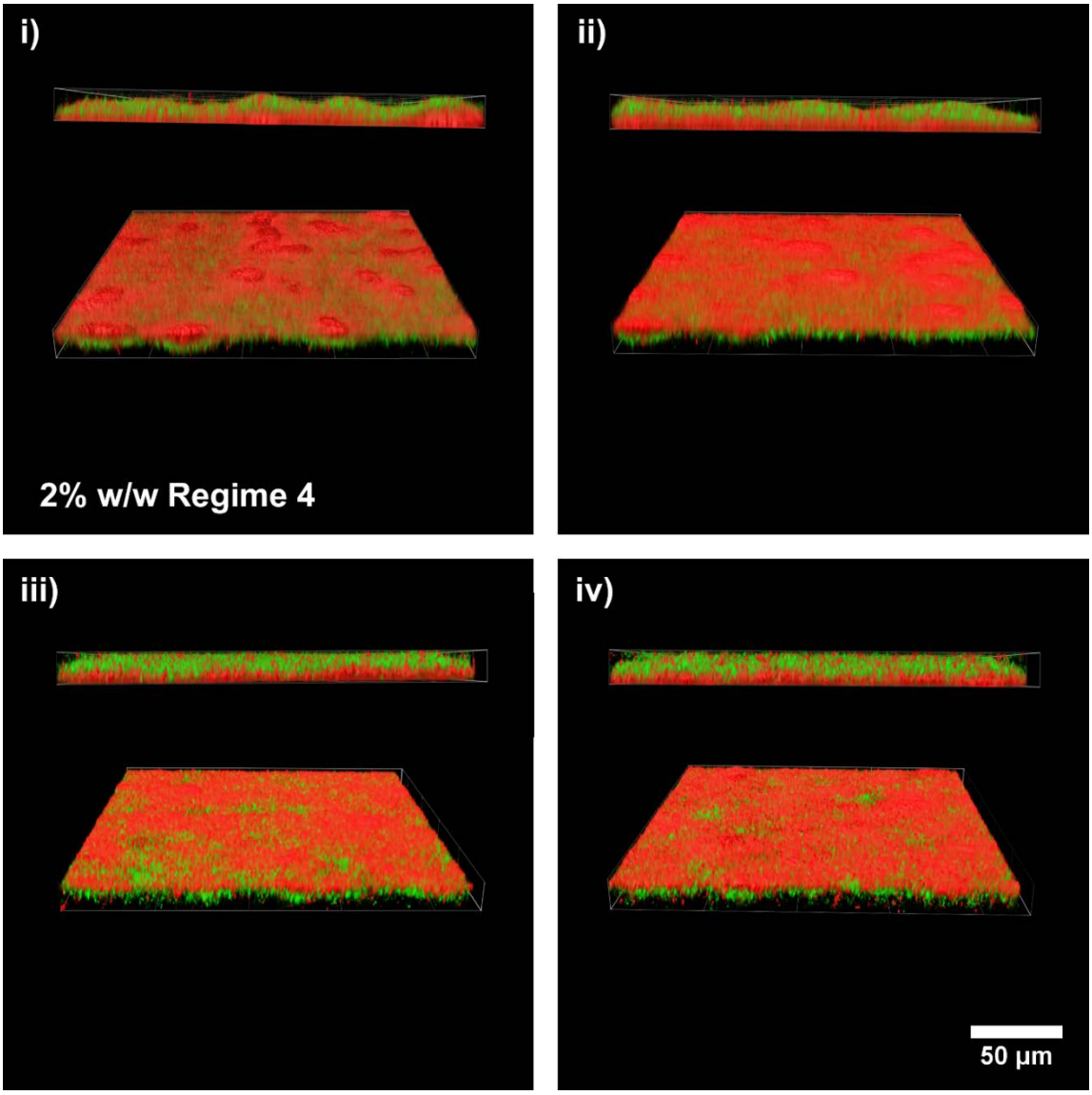

Figure A4.17. CLSM images of biofilms on PCL and 2% w/w O-MWCNT/PCL at Regimes 1-4 grown in the drip flow reactor. The top row of each 4-panel set represents replicate images from one sample while the bottom row represents replicate images from a second sample inoculated on a different occasion. The biofilms grown on PCL in each regime correspond to the 2% w/w biofilms by row; these biofilms on PCL were grown at the same time and under the exact same conditions as those on the 2% w/w.

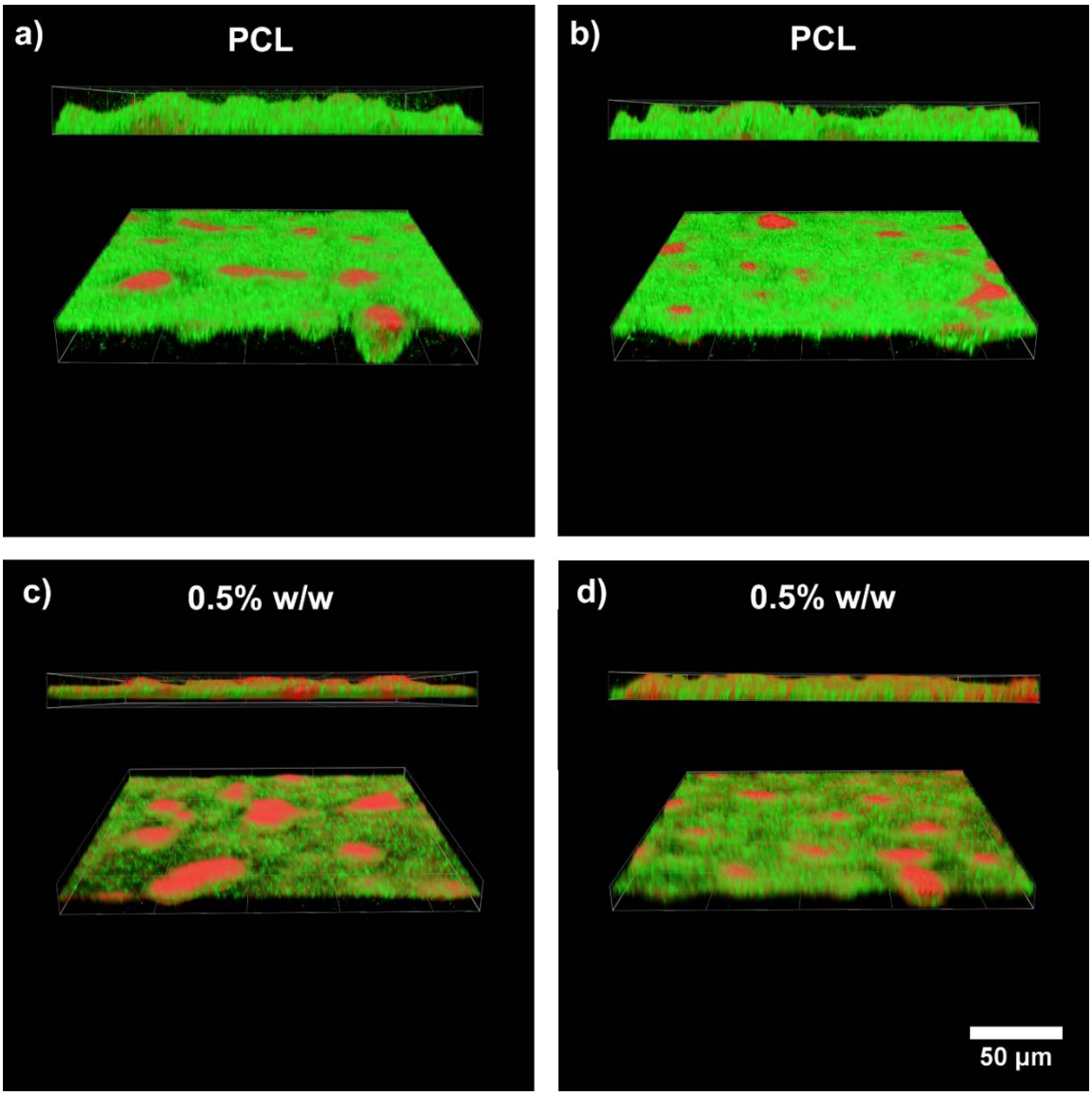

Figure A4.18. CLSM images of biofilms on PCL and 0.5% w/w O-MWCNT/PCL grown in the drip flow reactor to Regime 4 (22 ± 3 µm thickness for PCL). The top row represents duplicate images (different sample areas) of biofilms grown on PCL (a and b) at the same time and under the same conditions as the duplicate images (different sample areas) of biofilms grown on 0.5% w/w in the bottom row (c and d).

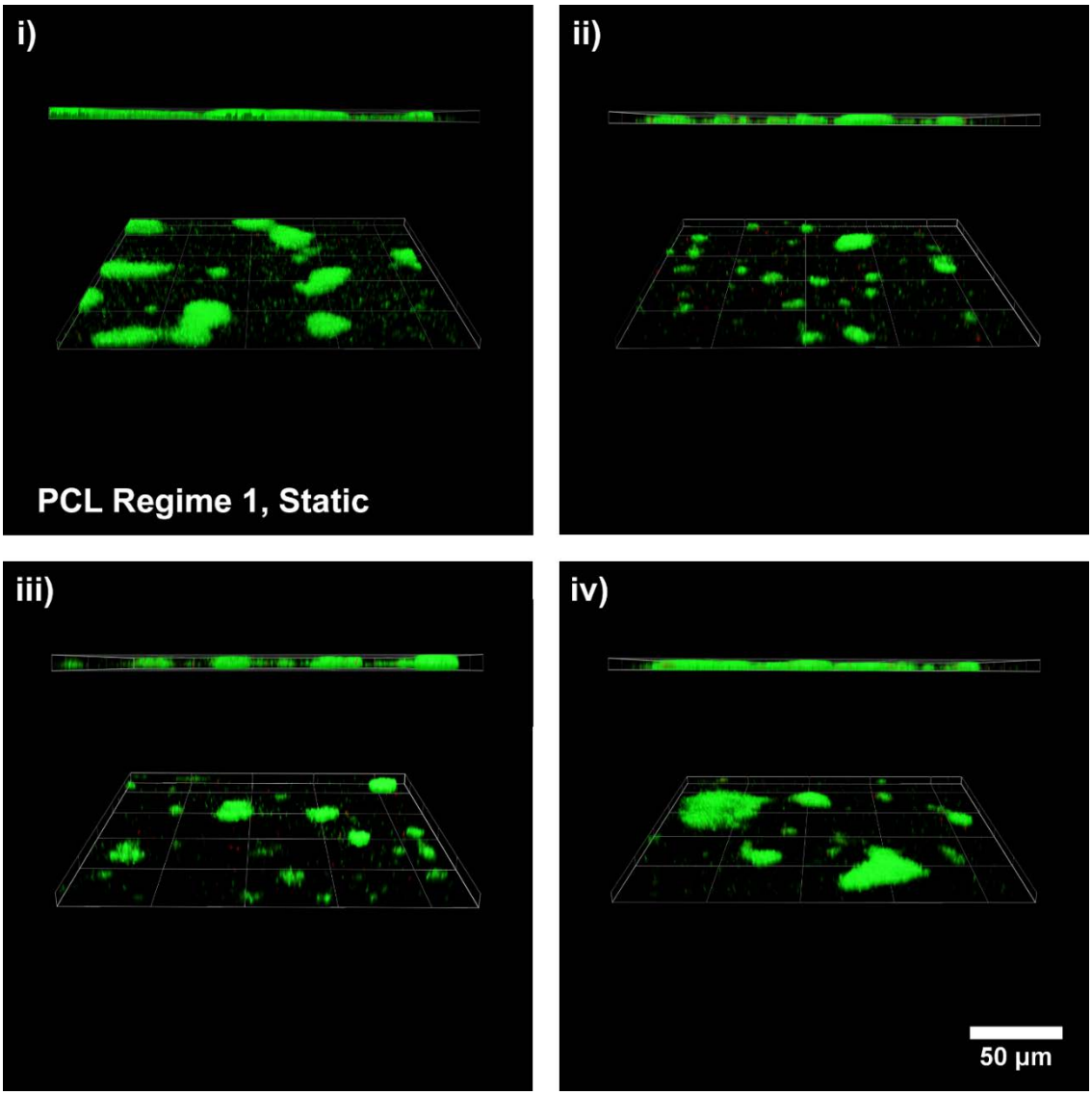
i)
ii)
PCL Regime 1, Static
iii)
iv)
50 µm

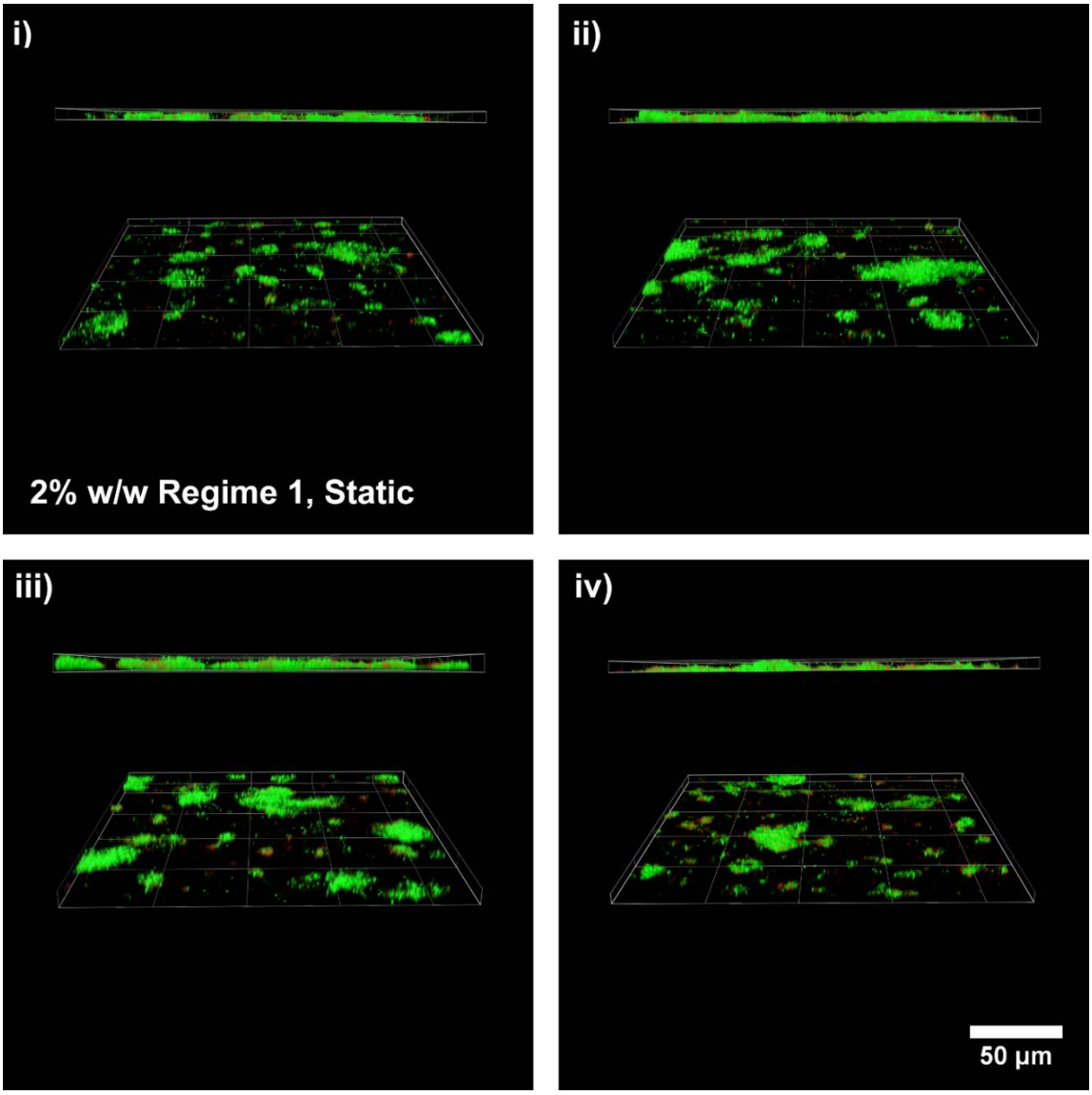
i)
ii)
2% w/w Regime 1, Static
iii)
iv)
50 µm

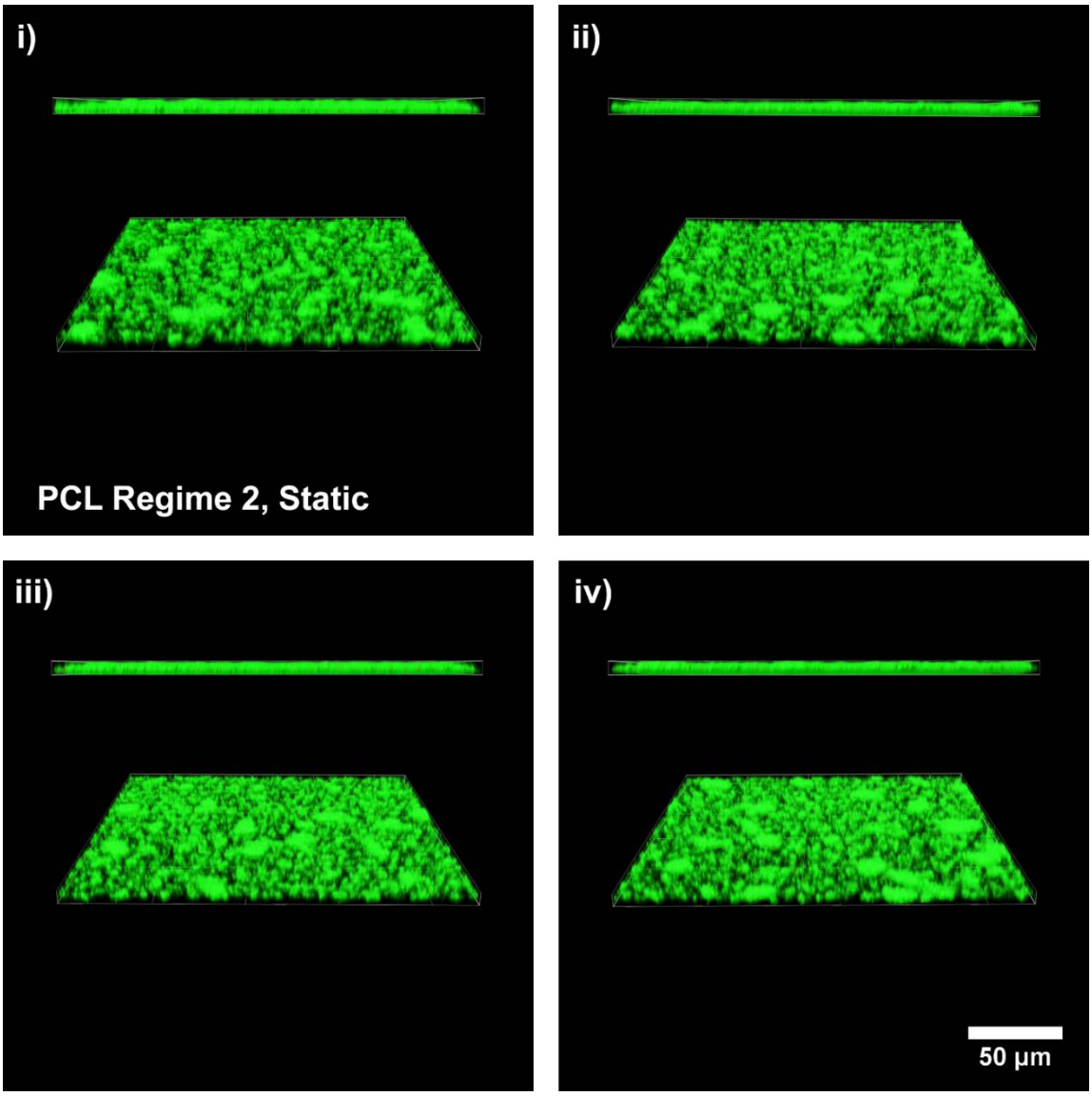
i)
ii)
PCL Regime 2, Static
iii)
iv)
50 µm

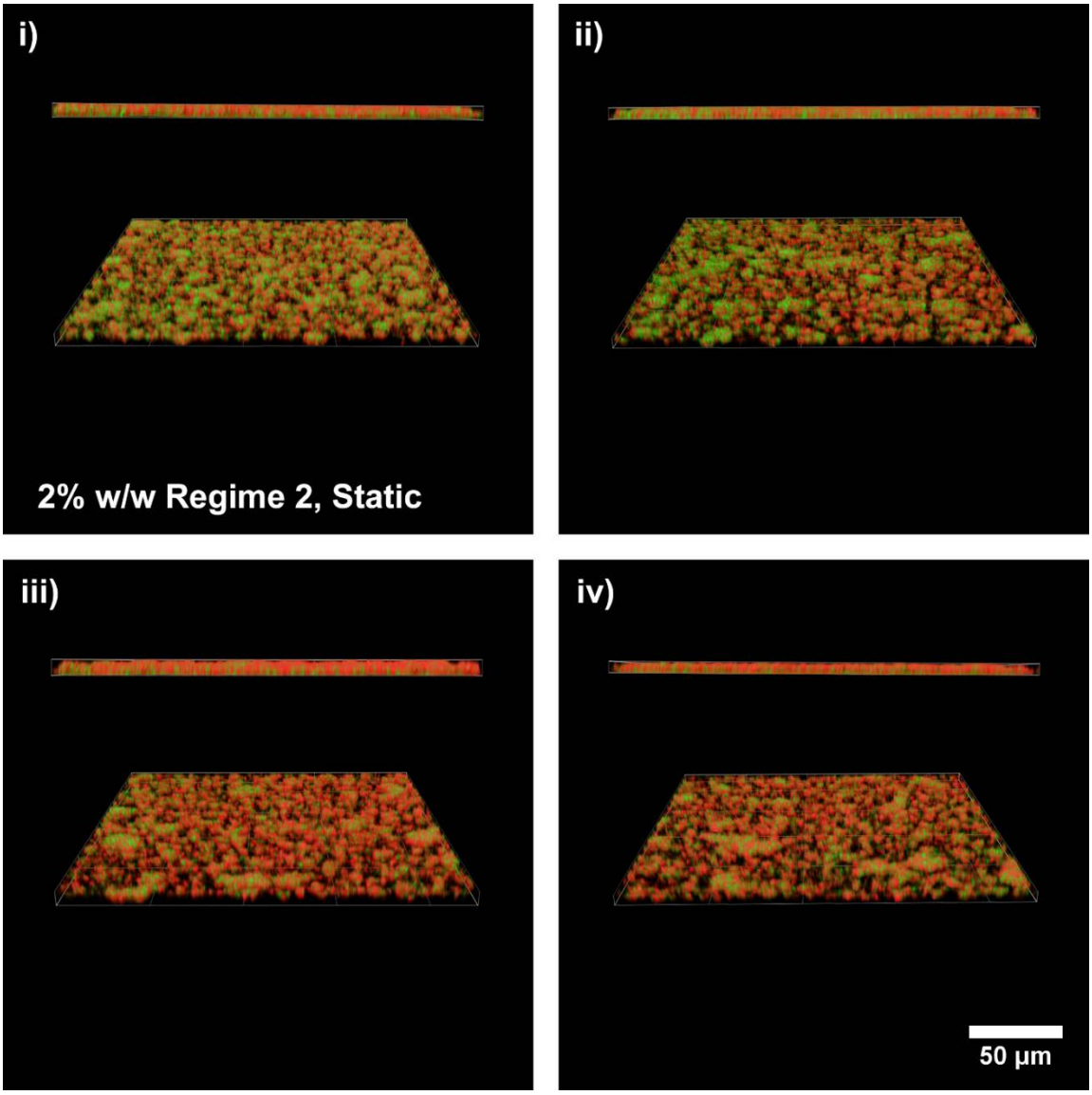
i)
ii)
2% w/w Regime 2, Static
iii)
iv)
50 µm

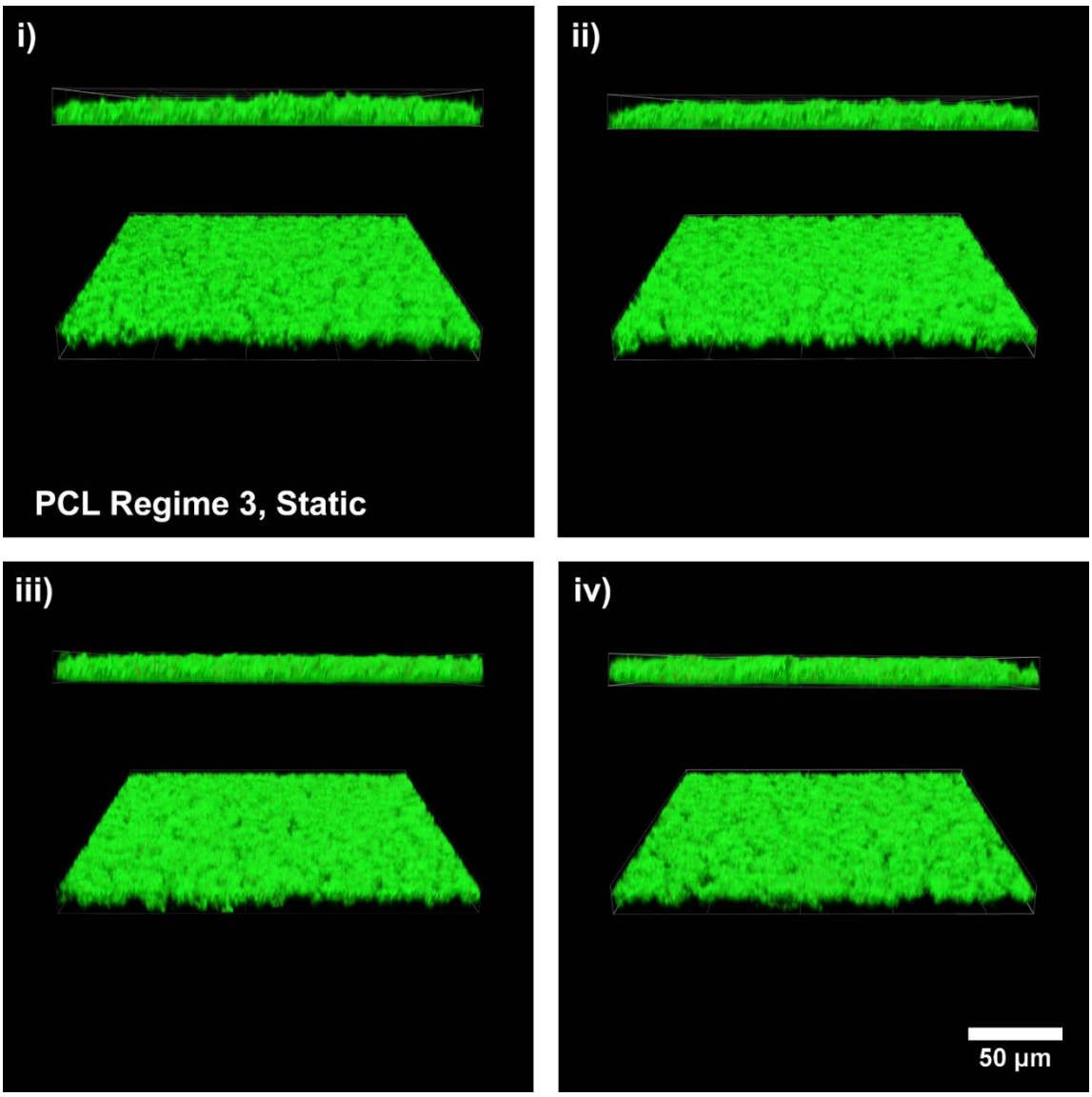
i)
ii)
PCL Regime 3, Static
iii)
iv)
50 µm

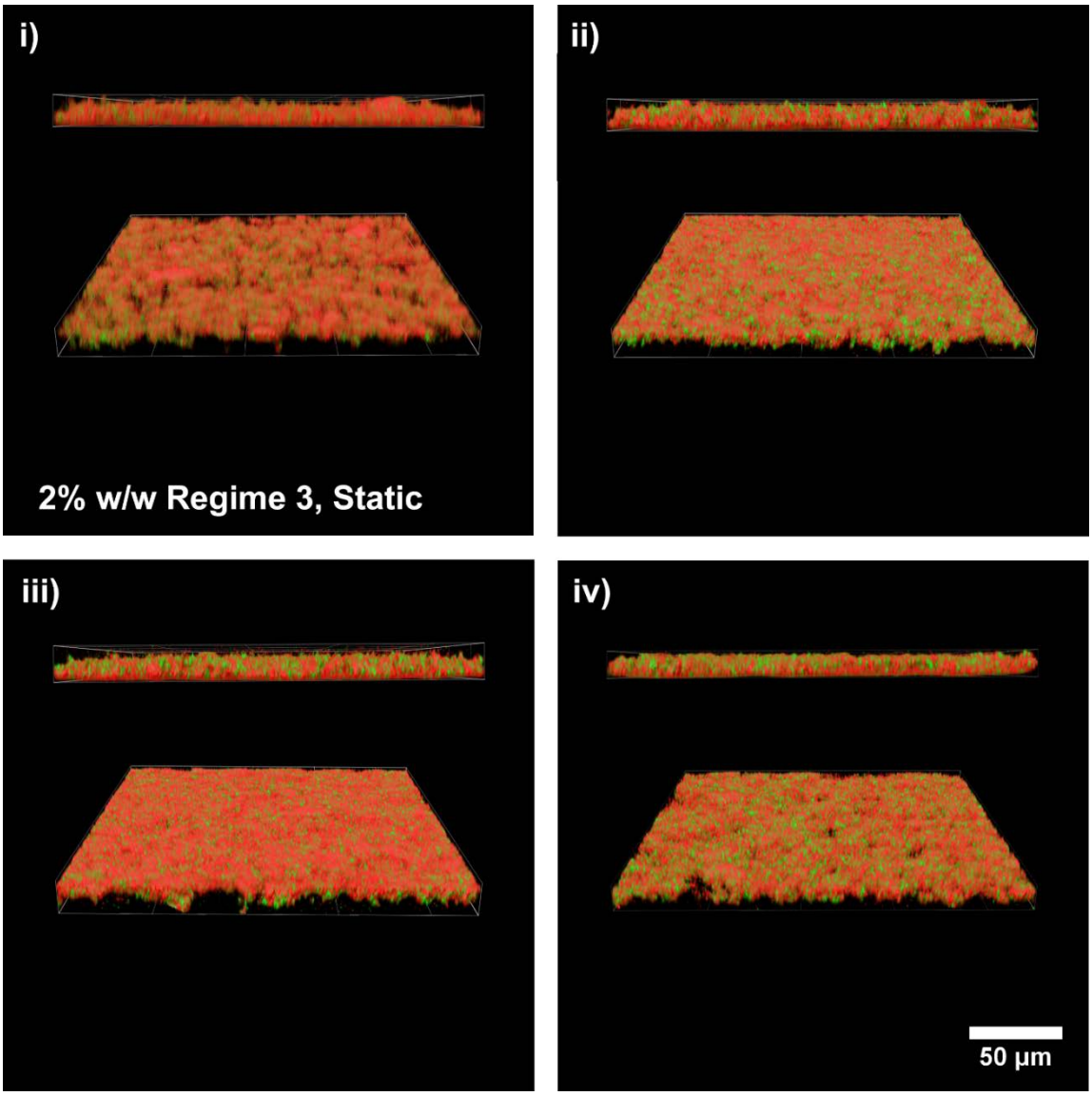

Figure A4.19. CLSM images of LIVE/DEAD stained biofilms on PCL and 2% w/w O-MWCNT/PCL at Regimes 1-3 grown under static conditions. The biofilms grown on PCL in each regime correspond to the 2% w/w biofilms below for each 4-panel set; these biofilms on PCL were grown at the same time and under the exact same conditions as those on the 2% w/w. Each 4-panel set contains images from different areas of one sample.

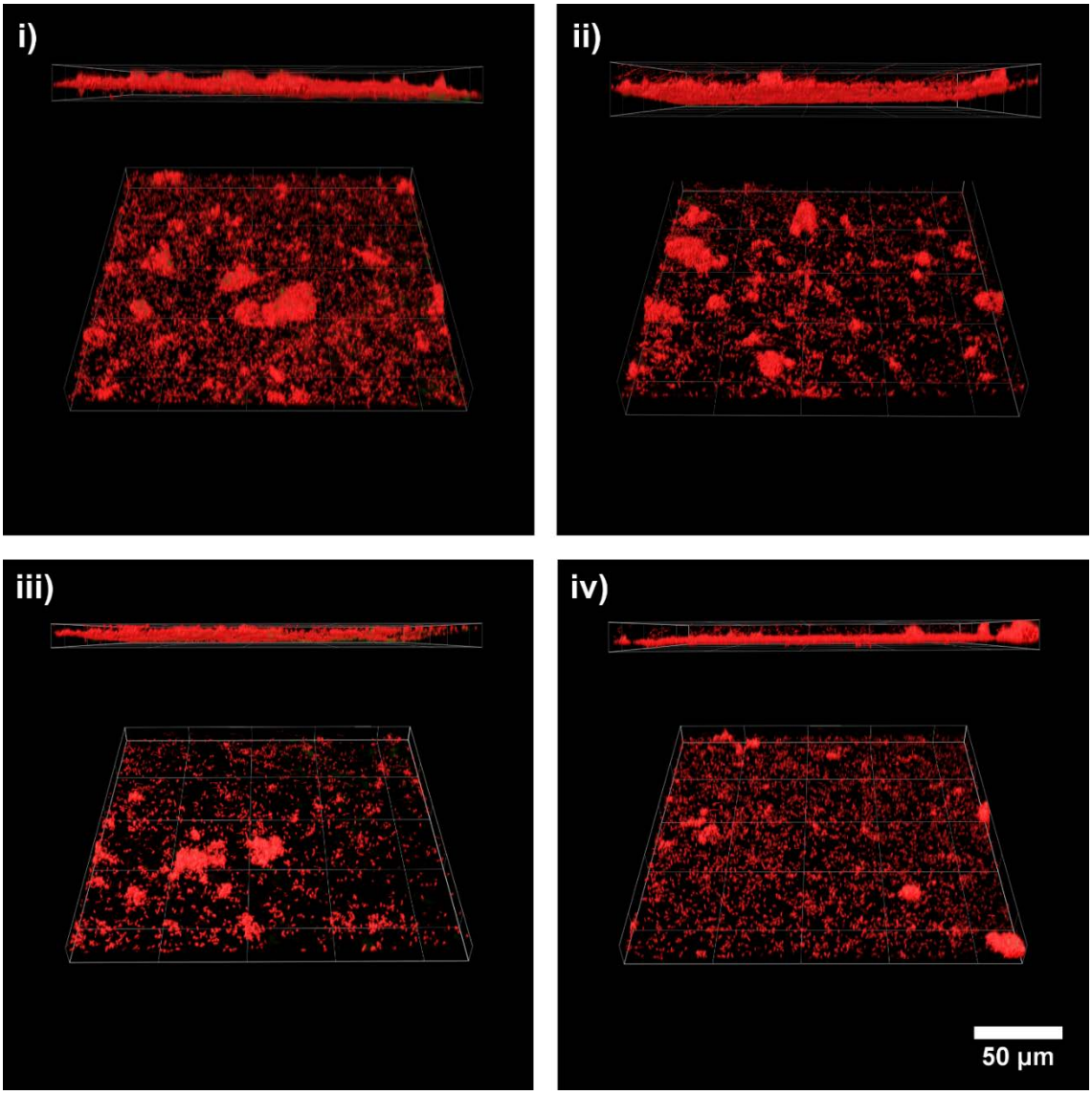

Figure A4.20. Replicate CLSM images of LIVE/DEAD stained *P. aeruginosa* exposed for 1 h to photodegraded 2% w/w O-MWCNT/PCL nanocomposites. Replicates are from different areas of the same sample.

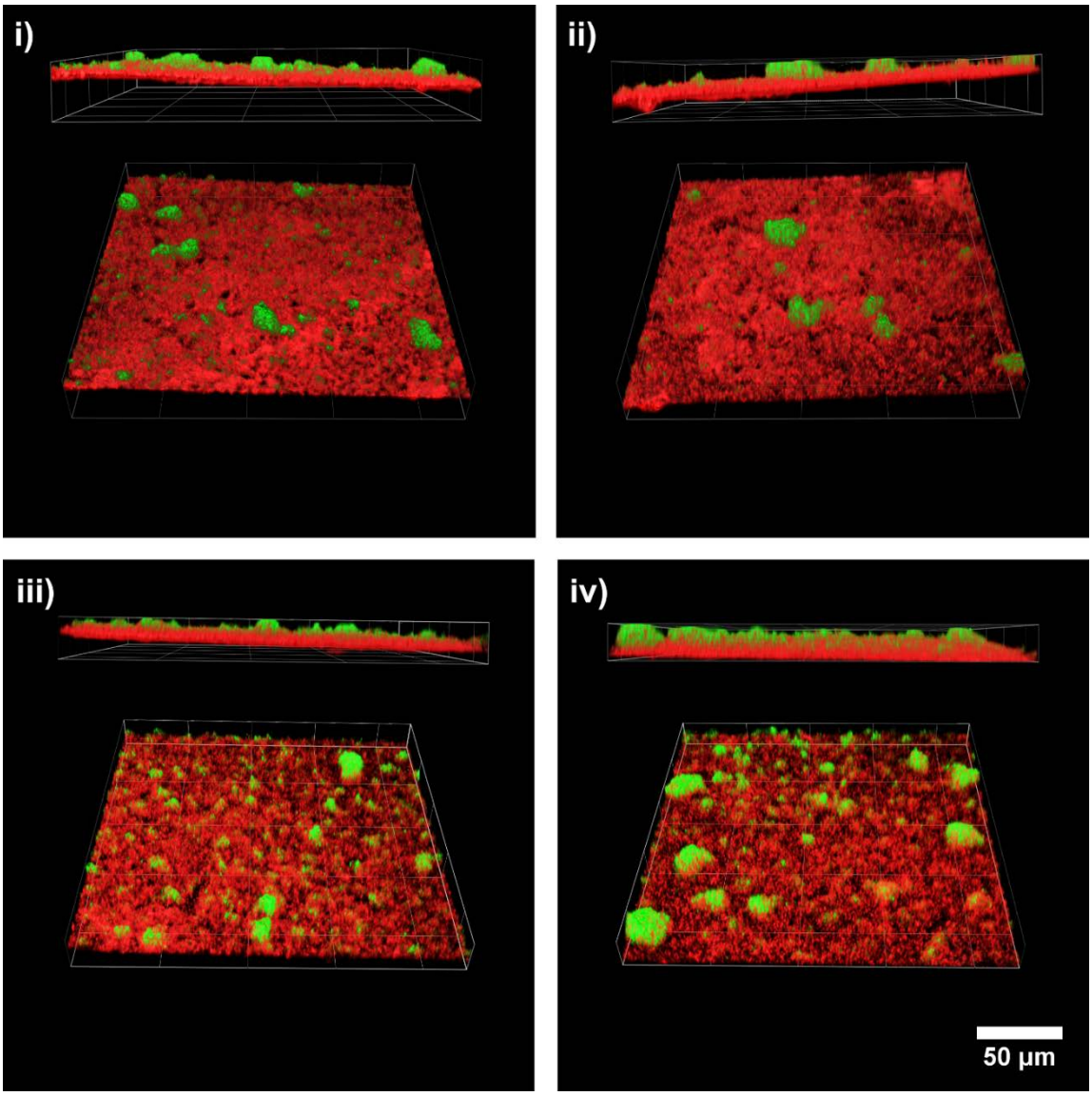

Figure A4.21. CLSM images of LIVE/DEAD stained *P. aeruginosa* exposed for 2 weeks to photodegraded 2% w/w O-MWCNT/PCL nanocomposites with the acetate food source replenished twice. Replicate images are from different areas of the same sample.

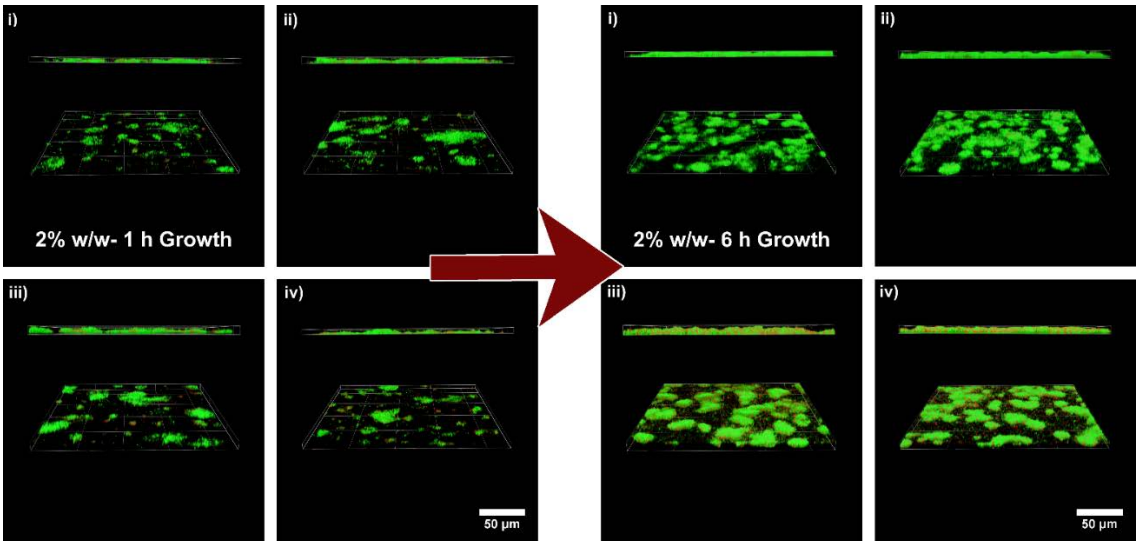

Figure A4.22. Replicate CLSM images of LIVE/DEAD stained *P. aeruginosa* after 1 h of initial attachment (left) and 6 h of static growth on different areas of 2% w/w O-MWCNT/PCL nanocomposite samples. The progression from 1 to 6 h shows the initially benign nature of the CNT/PCL nanocomposite containing a buried CNT network.

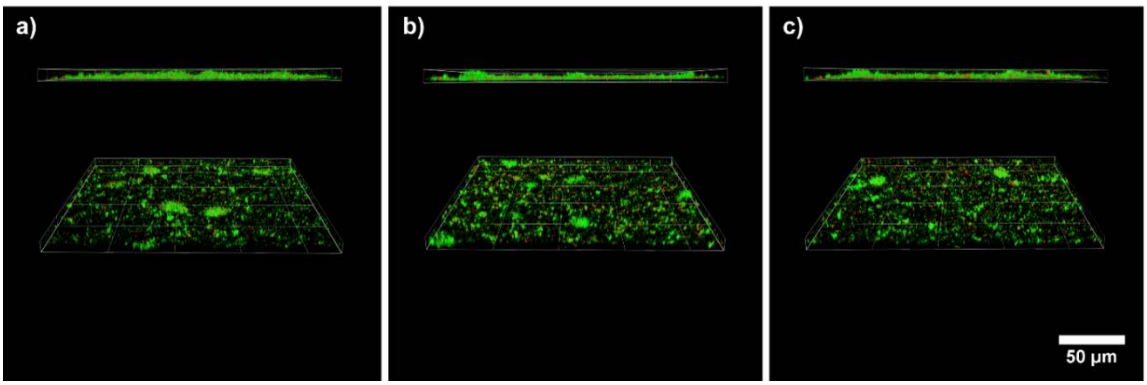

Figure A4.23. Replicate CLSM images of LIVE/DEAD stained *P. aeruginosa* after 1 h of initial attachment on different areas of a 0.5% w/w O-MWCNT/PCL nanocomposite sample.

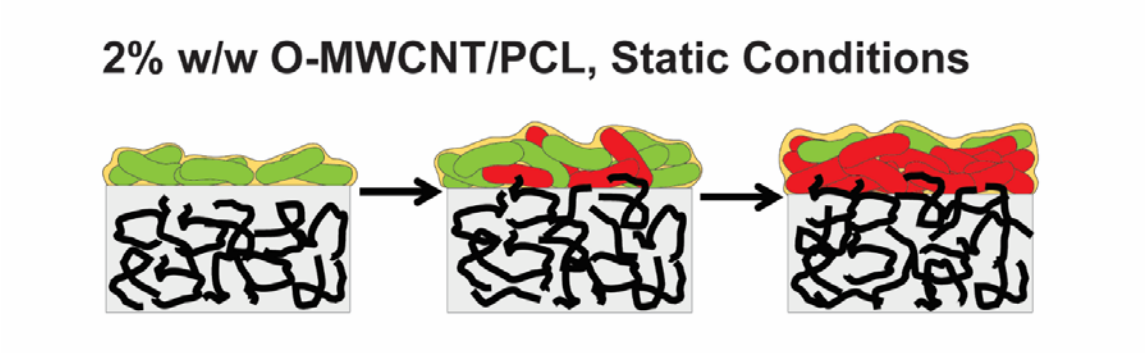

Figure A4.24. Illustration of biofilm development on 2% w/w O-MWCNT/PCL transformed as a result of polymer biodegradation under static conditions.

Table A4.1. Comparison of manual and COMSTAT 2 biofilm thickness measurements as well as biomass volume measurements on PCL and 2% w/w O-MWCNT/PCL under DFR (a) and static conditions (b). COMSTAT 2 biofilm thickness and biomass volume measurements on 0.5% w/w O-MWCNT/PCL under DFR conditions (c) and dead layer analysis of biofilms grown on 2% w/w O-MWCNT/PCL nanocomposites in regime 3 and 4 (DFR) as well as on 2% w/w photodegraded O-MWCNT/PCL (static). Each measurement represents the average and standard deviation of at least six samples.

a)

Drip Flow Reactor Conditions (2% w/w vs PCL)

	Manual **Thickness** Measurement				COMSTAT **Thickness** Measurement				COMSTAT **Biomass** Measurement			
Regime	PCL Thickness	Std. Dev	2% w/w Thickness	Std. Dev.	PCL Thickness	Std. Dev	2% w/w Thickness	Std. Dev.	PCL Biomass	Std. Dev	2% w/w Biomass	Std. Dev.
1	8.5	0.6	7.0	0.6	8.2	1.3	6.5	1.5	3.7	1.0	3.3	1.0
2	12.2	1.9	9.6	1.2	13.2	2.2	10.3	2.3	8.7	1.7	5.6	1.2
3	17.2	2.5	15.9	1.5	19.4	5.0	18.5	3.6	9.9	1.3	9.1	1.1
4	20.4	1.8	14.9	1.1	21.8	4.6	15.3	3.1	15.5	4.6	11.2	1.2

b)

Static Conditions (2% w/w vs PCL)

	Manual **Thickness** Measurement				COMSTAT **Thickness** Measurement				COMSTAT **Biomass** Measurement			
Regime	PCL Thickness	Std. Dev	2% w/w Thickness	Std. Dev.	PCL Thickness	Std. Dev	2% w/w Thickness	Std. Dev.	PCL Biomass	Std. Dev	2% w/w Biomass	Std. Dev.
1	7.1	0.6	4.7	0.7	4.8	0.6	5.0	1.4	0.9	0.4	0.8	0.3
2	7.5	0.3	7.1	0.5	6.2	0.6	5.9	1.0	6.8	0.5	4.6	0.7
3	15.0	0.6	13.0	1.1	16.2	1.3	12.5	1.9	13.8	0.5	8.4	0.9

c)

Drip Flow Reactor Conditions (0.5% w/w vs PCL)

	COMSTAT **Thickness** Measurement				COMSTAT **Biomass** Measurement			
Regime	PCL Thickness	Std. Dev	0.5% w/w Thickness	Std. Dev.	PCL Biomass	Std. Dev	0.5% w/w Biomass	Std. Dev.
4	21.8	3.5	14.7	1.3	12.1	1.7	8.5	1.7

d)

Dead Layer Thickness (Drip Flow Reactor- 2% w/w)

	Manual **Thickness Measurement**	
Regime	Thickness	Std. Dev
3	7.1	0.8
4	6.7	0.6

Dead Layer Thickness (2% w/w Photodegraded)

	Manual **Thickness Measurement**	
	Thickness	Std. Dev
1 hour	5.4	1.2
2 weeks	4.8	0.9

Appendix 6. Aerobic Single Culture Biodegradation of Carbon Nanotube/Polymer Nanocomposites

A6.1. Experimental

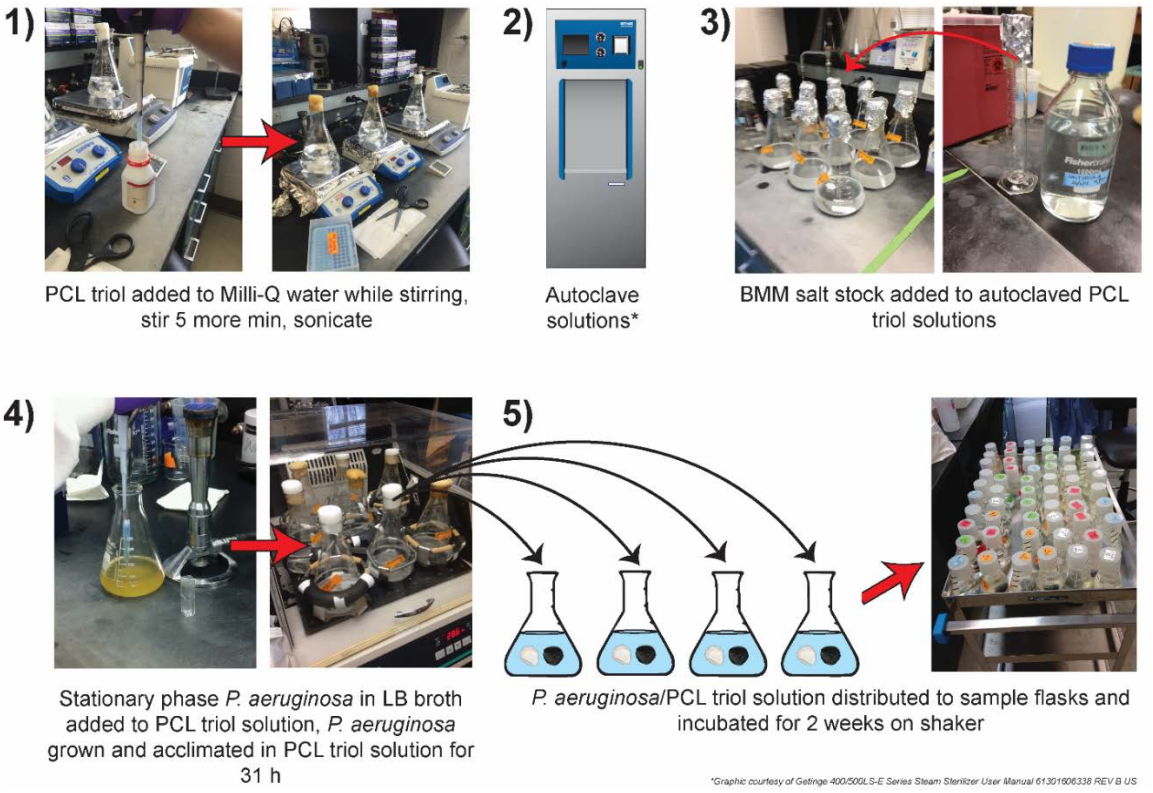

Scheme A6.1. Preparation, inoculation, and distribution of PCL triol/basal mineral media solutions to flasks containing carbon nanotube (CNT)/poly-ε-caprolactone (PCL) nanocomposites paired with internal PCL references.

A6.2. Replicate Scanning Electron Microscopy (SEM) images of PCL and CNT/PCL Nanocomposites

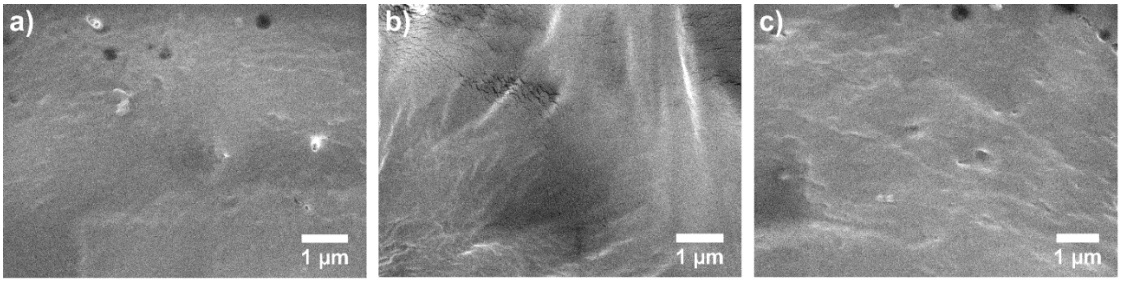

Figure A6.1. SEM images of replicate PCL (4% w/w ethyl cellulose (EC)) samples before biodegradation.

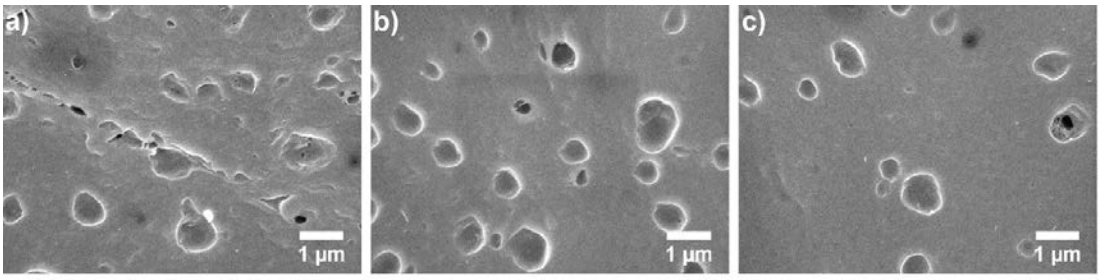

Figure A6.2. SEM images of replicate 0.5% w/w slightly oxidized multi-wall CNT (LO-MWCNT)/PCL nanocomposites before biodegradation.

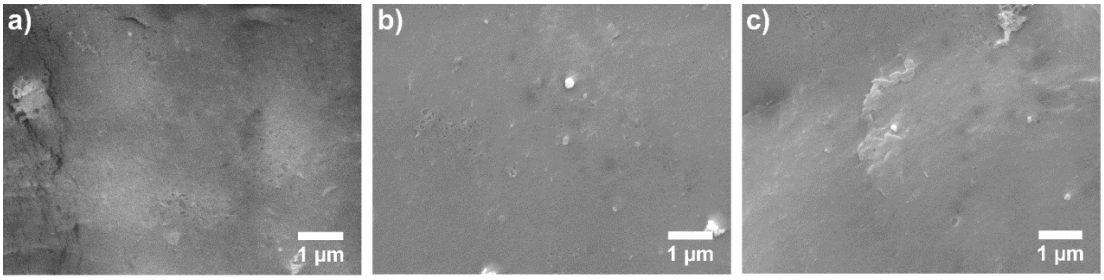

Figure A6.3. SEM images of replicate 2% w/w LO-MWCNT/PCL nanocomposites before biodegradation.

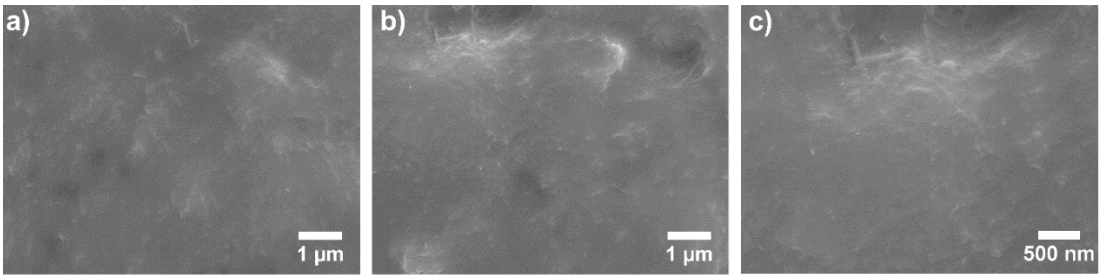

Figure A6.4. SEM images of replicate 5% w/w LO-MWCNT/PCL nanocomposites before biodegradation.

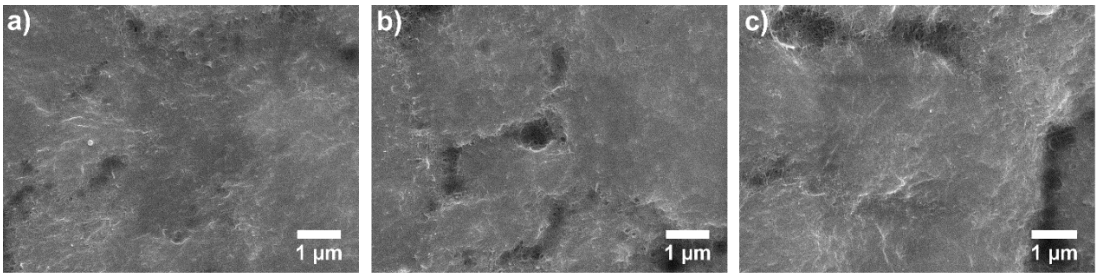

Figure A6.5. SEM images of replicate 10% w/w LO-MWCNT/PCL nanocomposites before biodegradation.

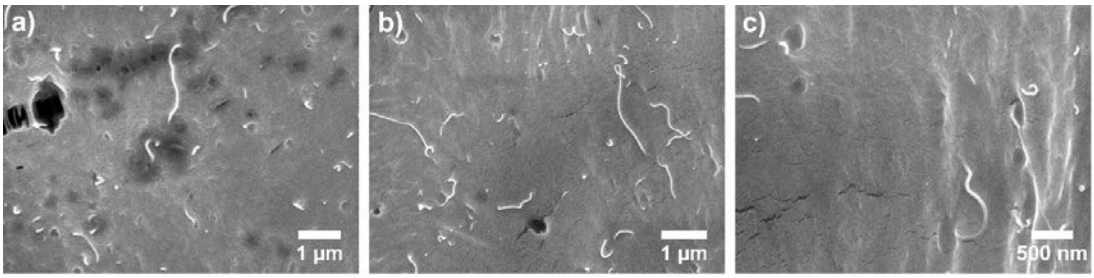

Figure A6.6. SEM images of replicate 0.5% w/w multi-wall (MWCNT)/PCL nanocomposites before biodegradation.

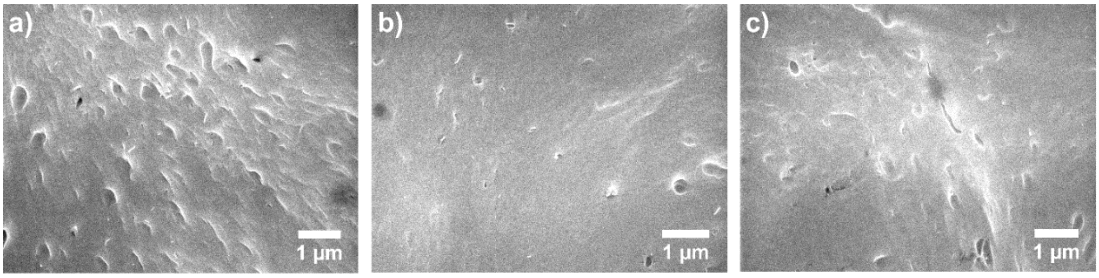

Figure A6.7. SEM images of replicate 2% w/w MWCNT/PCL nanocomposites before biodegradation.

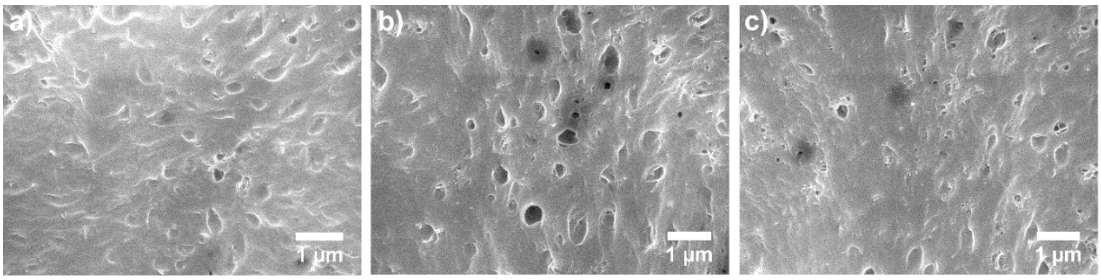

Figure A6.8. SEM images of replicate 5% w/w MWCNT/PCL nanocomposites before biodegradation.

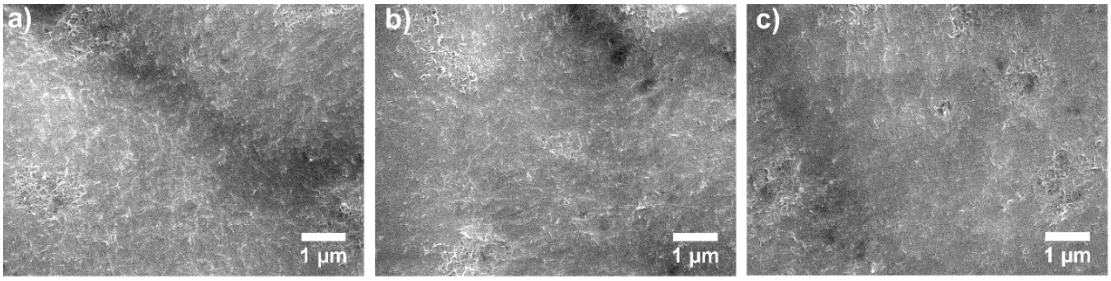

Figure A6.9. SEM images of replicate 5% w/w MWCNT/PCL nanocomposites used for release studies (before biodegradation).

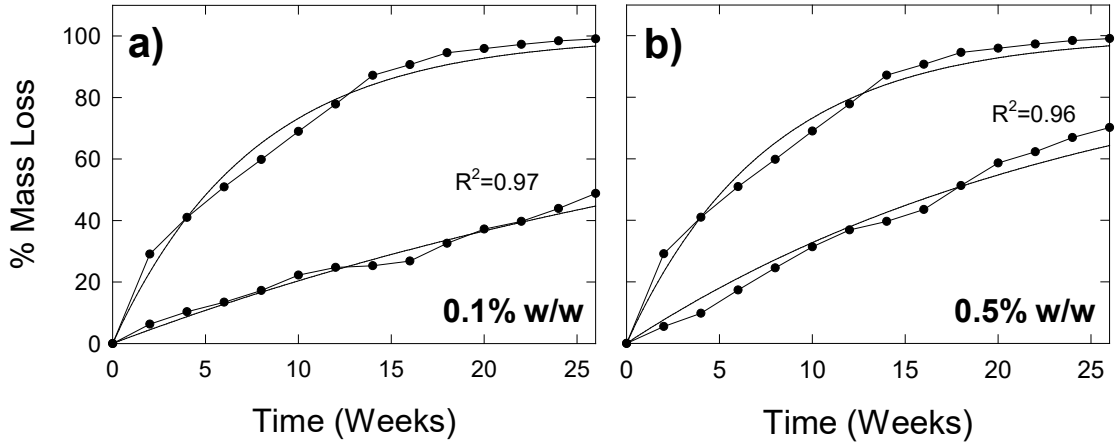

Figure A6.10. Mass loss of 0.1 and 0.5% LO-MWCNT/PCL nanocomposites relative to mass loss of an external PCL reference as a result of *P. aeruginosa* biodegradation in 3 g/L PCL triol/BMM solution. The R^2 for each CNT loading is an average of fits (one fit shown) for at least three replicates.

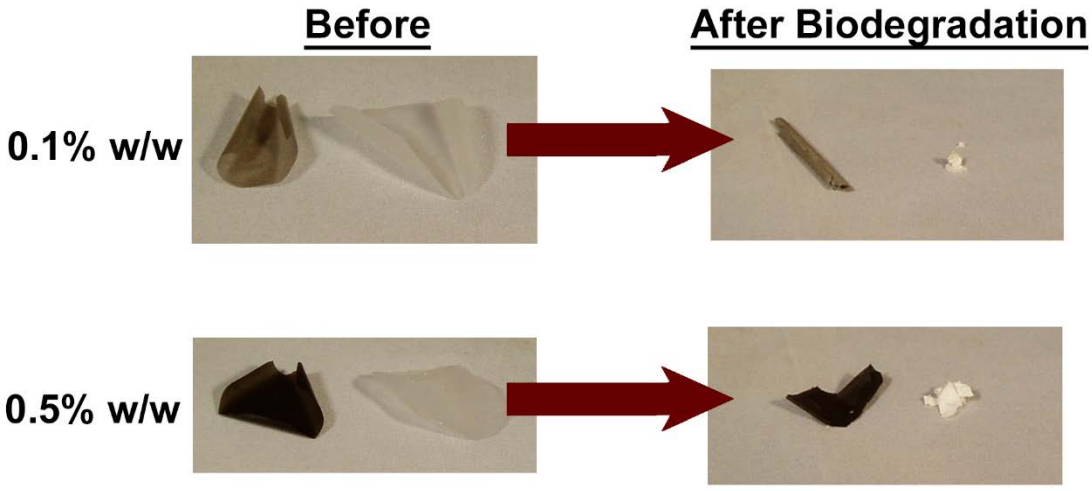

Figure A6.11. 0.1 and 0.5% w/w LO-MWCNT/PCL nanocomposites and their paired, internal PCL reference before and after 26 weeks of *P. aeruginosa* biodegradation.

Table A6.1. The effect of CNT loading on the rate of mass loss for replicate internal PCL references (paired with LO-MWCNT/PCL nanocomposites) during *P. aeruginosa* biodegradation. Rate constants were extracted from exponential rise fits of the PCL mass loss profiles.

	k_{PCL} (weeks^{-1})	Std. Dev.	R^2	Std. Dev.
PCL-1	0.1422		0.98	
PCL-2	0.1845		0.99	
PCL-3	0.0927		0.97	
PCL-AVG	**0.1398**	0.0375	**0.99**	0.00
0.1% w/w-1	0.1108		0.90	
0.1% w/w-3	0.0962		0.98	
0.1% w/w-4	0.0389		0.95	
0.1% w/w-AVG	**0.1035**	0.0073	**0.94**	0.03
0.5% w/w-2	0.0743		0.98	
0.5% w/w-4	0.1722		0.98	
0.5% w/w-AVG	**0.1233**	0.0490	**0.98**	0.00
1% w/w-1	0.2061		0.90	
1% w/w-2	0.0768		0.84	
1% w/w-3	0.4347		0.94	
1% w/w-4	0.1385		0.91	
1% w/w-AVG	**0.2140**	0.1354	**0.90**	0.04
2% w/w-1	0.0651		0.99	
2% w/w-2	0.0828		0.97	
2% w/w-3	0.0809		0.95	
2% w/w-4	0.0777		0.95	
2% w/w-AVG	**0.0766**	0.0069	**0.96**	0.02
5% w/w-1	0.0336		0.95	
5% w/w-2	0.0386		0.75	
5% w/w-3	0.0649		0.95	
5% w/w-4	0.0467		0.99	
5% w/w-AVG	**0.0460**	0.0119	**0.91**	0.09
10% w/w-1	0.0467		0.98	
10% w/w-2	0.038		0.93	
10% w/w-3	0.0434		0.97	
10% w/w-4	0.0373		0.83	
10% w/w-AVG	**0.0414**	0.0039	**0.93**	0.06

Table A6.2. The effect of CNT loading on the rate of mass loss for replicate LO-MWCNT/PCL nanocomposites during *P. aeruginosa* biodegradation. Rate constants were extracted from exponential rise fits of the CNT/PCL nanocomposite mass loss profiles.

	$k_{CNT/PNC}$ (weeks^{-1})	Std. Dev.	R^2	Std. Dev.
0.1% w/w-1	0.0228		0.98	
0.1% w/w-3	0.0326		0.99	
0.1% w/w-4	0.0206		0.93	
0.1% w/w-AVG	**0.0277**	0.0049	**0.97**	0.03
0.5% w/w-2	0.0397		0.98	
0.5% w/w-4	0.0562		0.95	
0.5% w/w-AVG	**0.0480**	0.0083	**0.96**	0.01
1% w/w-1	0.0556		0.98	
1% w/w-2	0.0282		0.94	
1% w/w-3	0.0435		0.99	
1% w/w-4	0.0435		0.99	
1% w/w-AVG	**0.0427**	0.0097	**0.98**	0.02
2% w/w-1	0.0265		0.99	
2% w/w-2	0.0292		0.99	
2% w/w-3	0.0256		0.99	
2% w/w-4	0.0246		0.94	
2% w/w-AVG	**0.0265**	0.0017	**0.98**	0.02
5% w/w-1	0.0156		0.92	
5% w/w-2	0.0165		0.58	
5% w/w-3	0.0194		0.94	
5% w/w-4	0.0226		0.91	
5% w/w-AVG	**0.0185**	0.0027	**0.84**	0.15
10% w/w-1	0.0127		0.99	
10% w/w-2	0.0141		0.91	
10% w/w-3	0.0137		0.96	
10% w/w-4	0.0138		0.89	
10% w/w-AVG	**0.0136**	0.0005	**0.94**	0.04

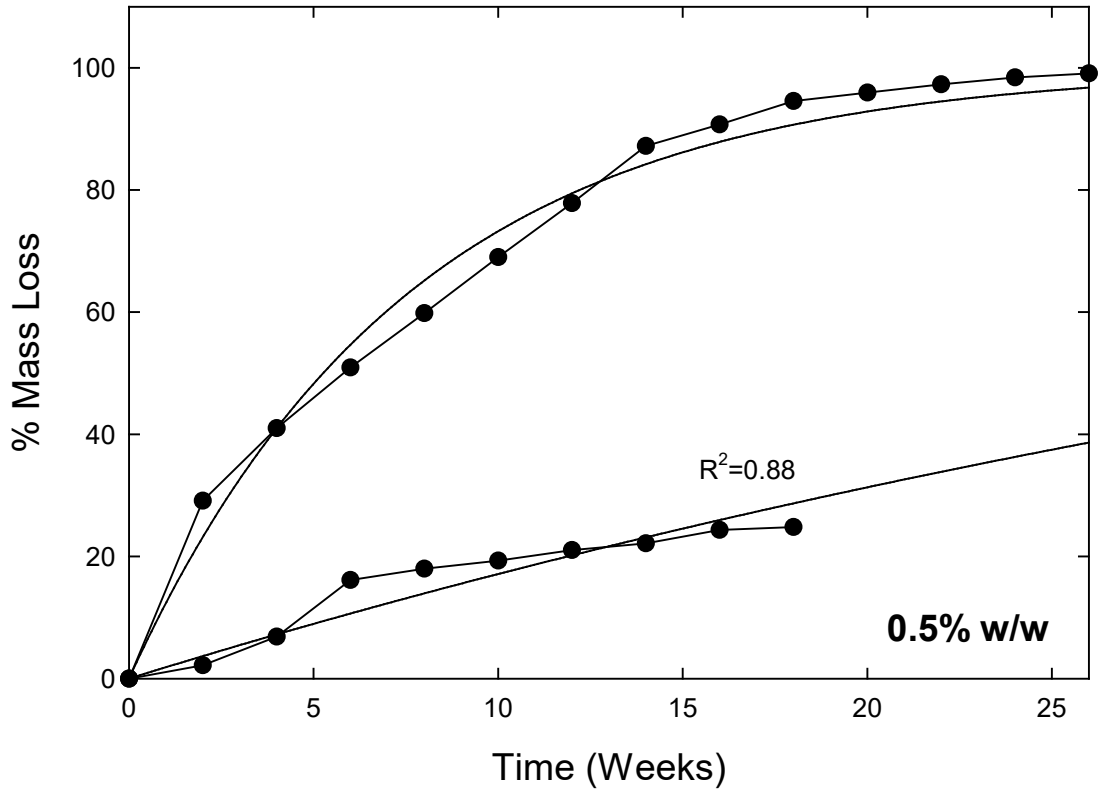

Figure A6.12. Mass loss of a 0.5% MWCNT/PCL nanocomposite relative to mass loss of an external PCL reference as a result of *P. aeruginosa* biodegradation in 3 g/L PCL triol/BMM solution. The R^2 for each CNT loading is an average of fits (one fit shown) for at least three replicates.

Table A6.3. The effect of CNT loading on the rate of mass loss for replicate internal PCL references (paired with MWCNT/PCL nanocomposites) during *P. aeruginosa* biodegradation. Rate constants were extracted from exponential rise fits of the PCL mass loss profiles.

	k_{PCL} (weeks^{-1})	Std. Dev.	R^2	Std. Dev.
PCL-1	0.1422		0.98	
PCL-2	0.1845		0.99	
PCL-3	0.0927		0.97	
PCL-AVG	**0.1398**	0.0375	**0.99**	0.00
0.1% w/w-1	0.0696		0.95	
0.1% w/w-2	0.0562		0.98	
0.1% w/w-3	0.1131		0.77	
0.1% w/w-4	0.0473		0.91	
0.1% w/w-AVG	**0.0716**	0.0218	**0.90**	0.08
0.5% w/w-1	0.0559		0.97	
0.5% w/w-2	0.0272		0.81	
0.5% w/w-3	0.0293		0.93	
0.5% w/w-4	0.0448		0.94	
0.5% w/w-AVG	**0.0504**	0.0056	**0.91**	0.06
1% w/w-1	0.0506		0.68	
1% w/w-2	0.0901		0.88	
1% w/w-3	0.0525		0.92	
1% w/w-4	0.0633		0.46	
1% w/w-AVG	**0.0641**	0.0158	**0.74**	0.18
2% w/w-1	0.0360		0.99	
2% w/w-2	0.0210		0.85	
2% w/w-3	0.0465		0.83	
2% w/w-4	0.0735		0.88	
2% w/w-AVG	**0.0443**	0.0192	**0.88**	0.06
5% w/w-1	0.0600		0.97	
5% w/w-2	0.0640		0.79	
5% w/w-3	0.0390		0.96	
5% w/w-4	0.0841		0.81	
5% w/w-AVG	**0.0618**	0.0160	**0.88**	0.08

Table A6.4. The effect of CNT loading on the rate of mass loss for replicate MWCNT/PCL nanocomposites during *P. aeruginosa* biodegradation. Rate constants were extracted from exponential rise fits of the CNT/PCL nanocomposite mass loss profiles.

	$k_{CNT/PNC}$ (weeks^{-1})	Std. Dev.	R^2	Std. Dev.
0.1% w/w-1	0.0610		0.92	
0.1% w/w-2	0.0334		0.99	
0.1% w/w-3	0.0708		0.99	
0.1% w/w-4	0.0662		0.98	
0.1% w/w-AVG	**0.0579**	0.0049	**0.97**	0.03
0.5% w/w-1	0.0232		0.94	
0.5% w/w-2	0.0190		0.80	
0.5% w/w-3	0.0188		0.90	
0.5% w/w-4	0.0143		0.89	
0.5% w/w-AVG	**0.0188**	0.0045	**0.88**	0.05
1% w/w-1	0.0332		0.58	
1% w/w-2	0.0288		0.99	
1% w/w-3	0.0267		1.00	
1% w/w-4	0.0374		0.99	
1% w/w-AVG	**0.0315**	0.0041	**0.89**	0.18
2% w/w-1	0.0157		0.97	
2% w/w-2	0.0199		0.85	
2% w/w-3	0.0318		0.55	
2% w/w-4	0.0301		0.71	
2% w/w-AVG	**0.0244**	0.0068	**0.77**	0.15
5% w/w-1	0.0316		0.78	
5% w/w-2	0.0185		0.61	
5% w/w-3	0.0197		0.99	
5% w/w-4	0.0223		0.97	
5% w/w-AVG	**0.0230**	0.0051	**0.84**	0.15

Appendix 7. Mixed Culture Biodegradation of Carbon Nanotube/Polymer Nanocomposites

A7.1. Aerobic Mixed Culture Setup Using Primary Effluent

Figure A7.1. Primary effluent (10% v/v) added to basal mineral media (BMM) (right) for distribution (middle) to flasks containing carbon nanotube/polymer nanocomposites (CNT/PNCs) (left).

Figure A7.2. Replicate solution blended PCL and multi-wall CNT (MWCNT)/poly-ε-caprolactone (PCL) nanocomposite samples containing primary effluent/BMM (10% v/v primary effluent) run in sacrifice mode.

A7.2. Pictures of Solution Blended MWCNT/PCL Nanocomposites Before and After Aerobic Mixed Culture Biodegradation

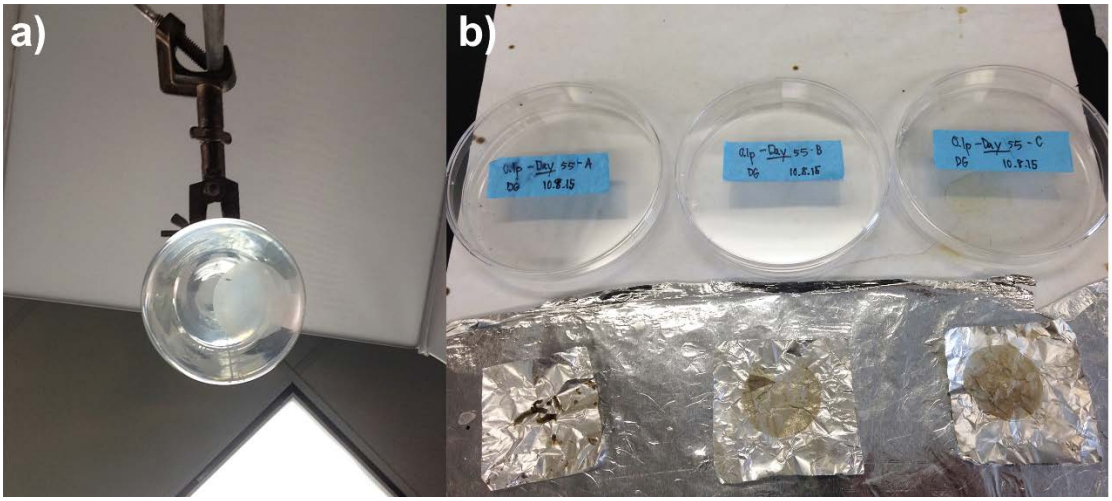
a)
b)

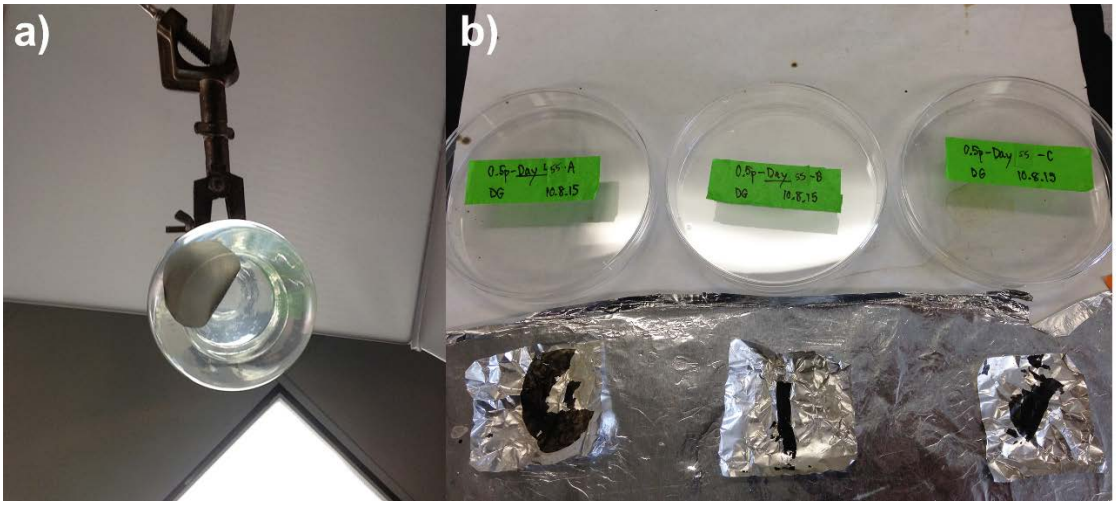
a)
b)

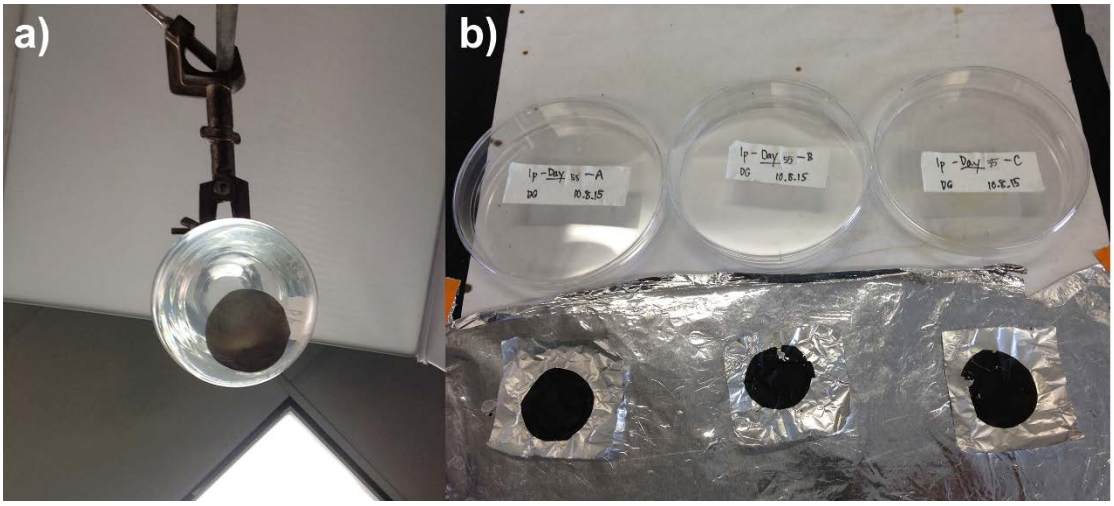
a)
b)

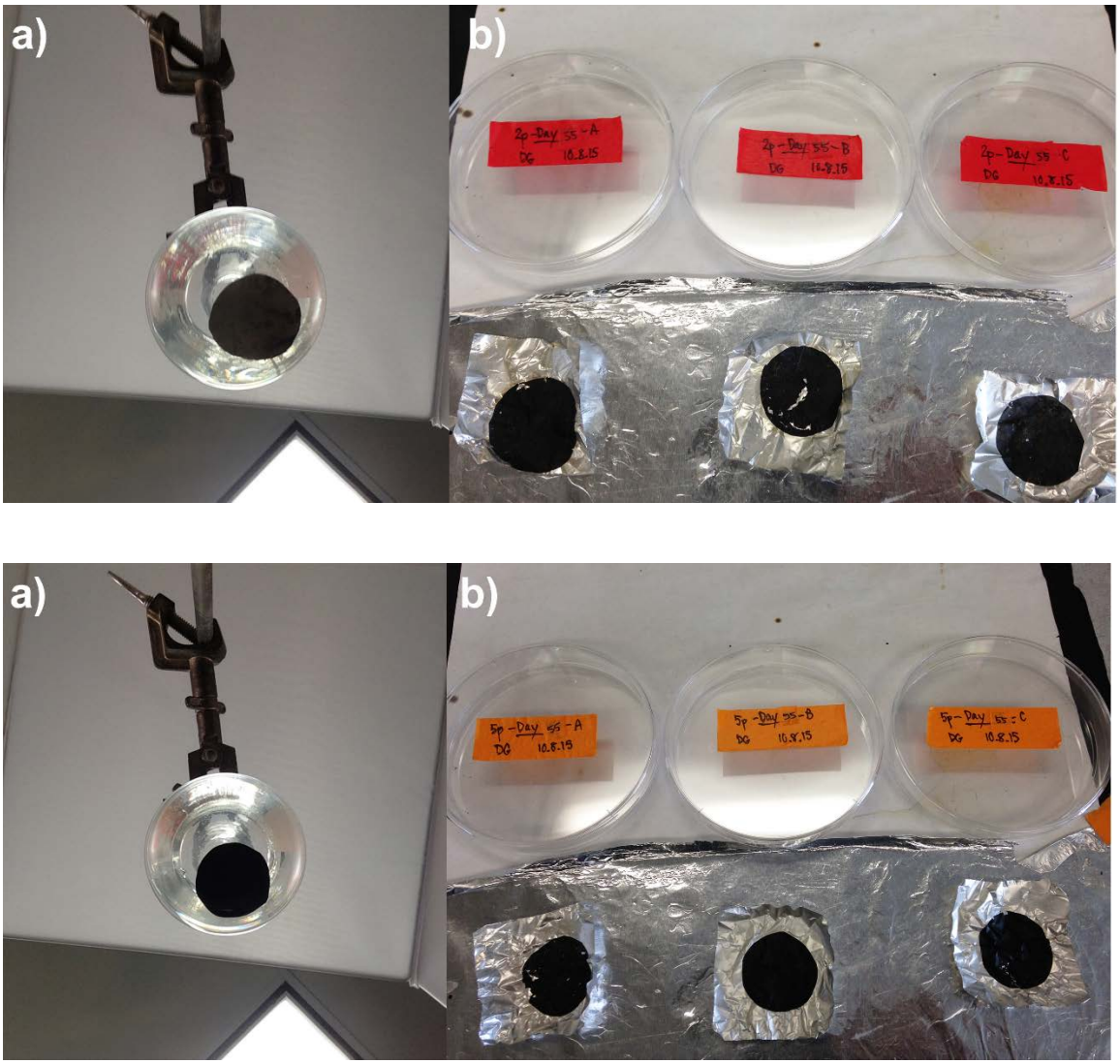

Figure A7.3. Solution blended PCL and MWCNT/PCL nanocomposites a) before and b) after >100 d aerobic mixed culture (primary effluent) biodegradation. Triplicate PCL, 0.1, 0.5, 1, 2, and 5% w/w MWCNT/PCL nanocomposites are shown, respectively.

A7.3. Pictures of Melt-Mixed MWCNT/PCL Nanocomposites Before and After Aerobic Mixed Culture Biodegradation

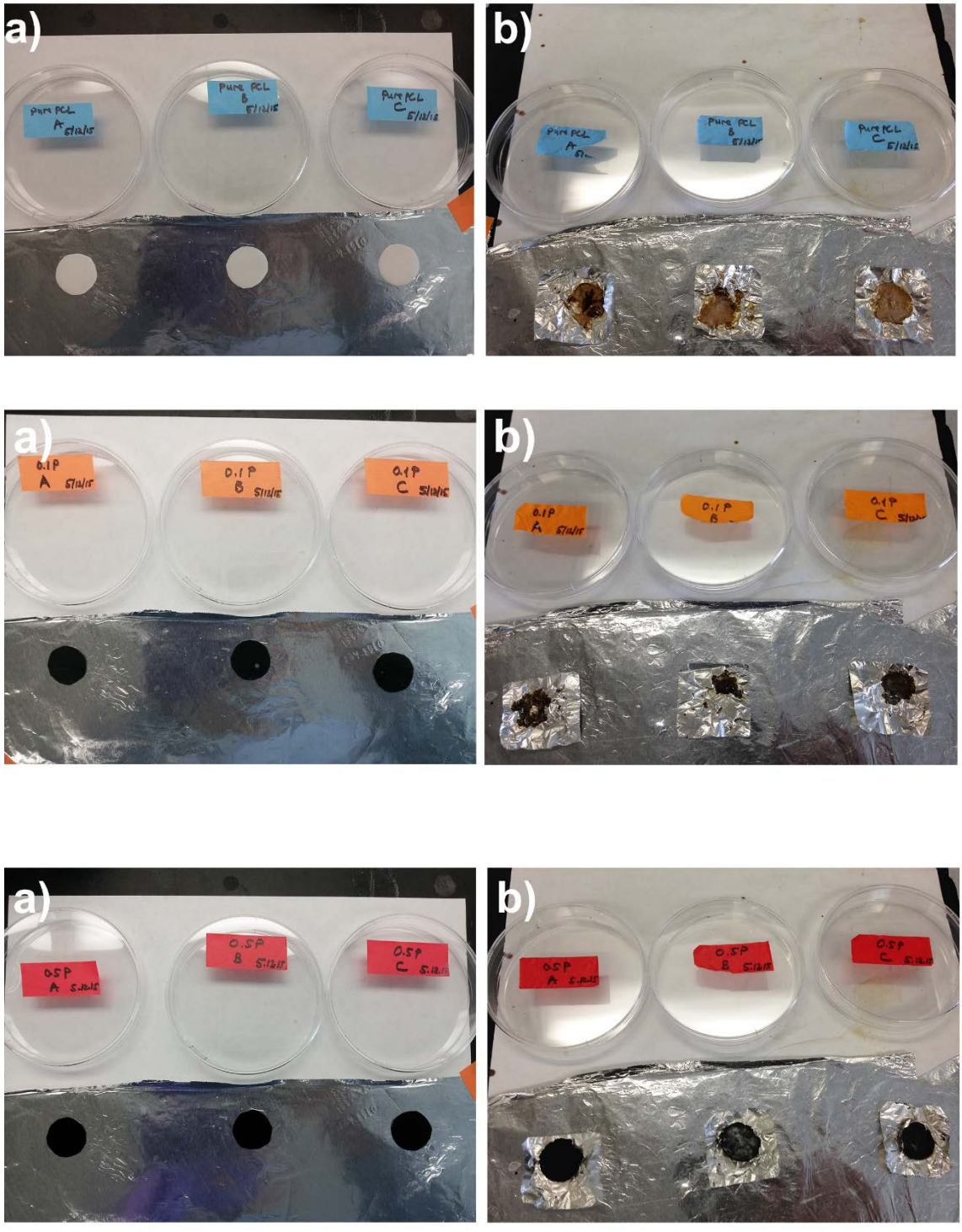
a)
b)
a)
b)
a)
b)

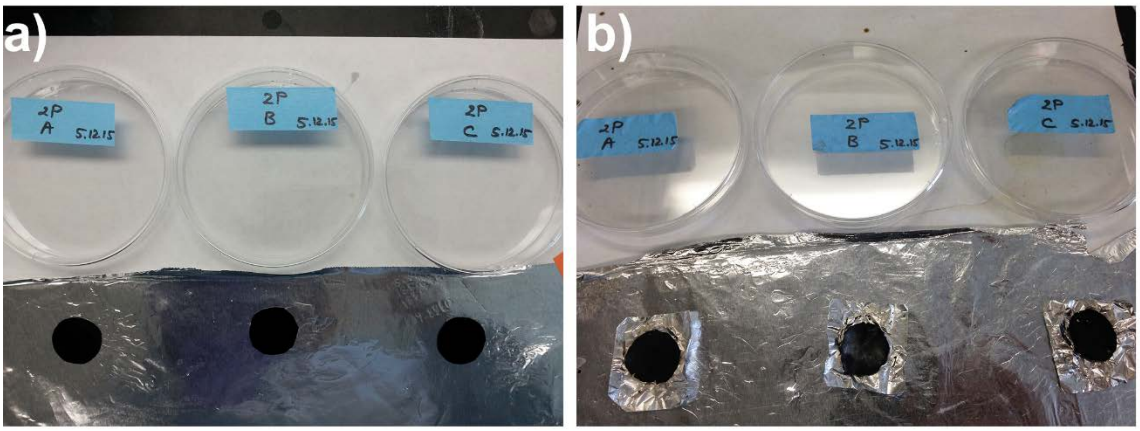

Figure A7.4. Melt-mixed PCL and MWCNT/PCL nanocomposites a) before and b) after >230 d aerobic mixed culture (primary effluent) biodegradation. Triplicate PCL, 0.1, 0.5, and 2% w/w MWCNT/PCL nanocomposites are shown, respectively.

Appendix 8. The Effect of Polymer Type on Carbon Nanotube/Polymer Nanocomposite Biodegradation

A8.1. Scanning Electron Microscopy (SEM) Replicates

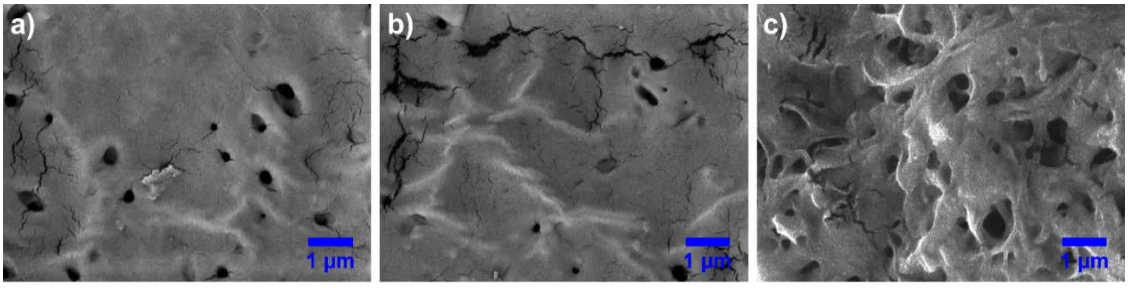

Figure A8.1. The structure and surface morphology of polyhydroxyalkanoates (PHA) (5% w/w ethyl cellulose (EC)) taken in a-b) replicate areas and on a c) separately prepared PHA sample before biodegradation using SEM.

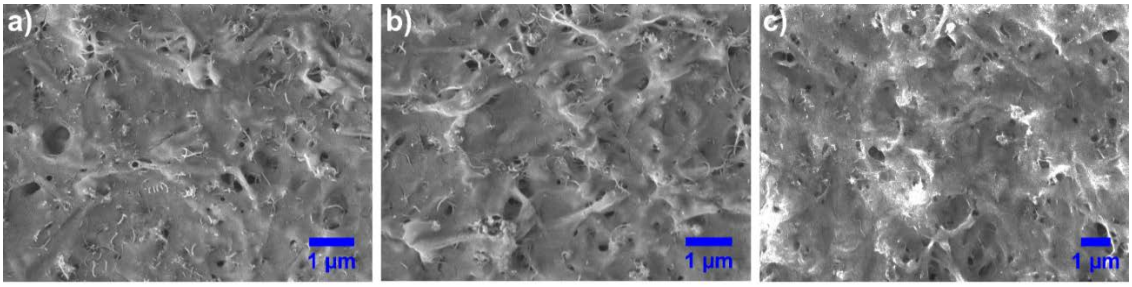

Figure A8.2. The structure and surface morphology of 5% w/w multi-wall (MWCNT)/PHA nanocomposites taken in a-b) replicate areas and on a c) separately prepared MWCNT/PHA nanocomposite sample before biodegradation using SEM.

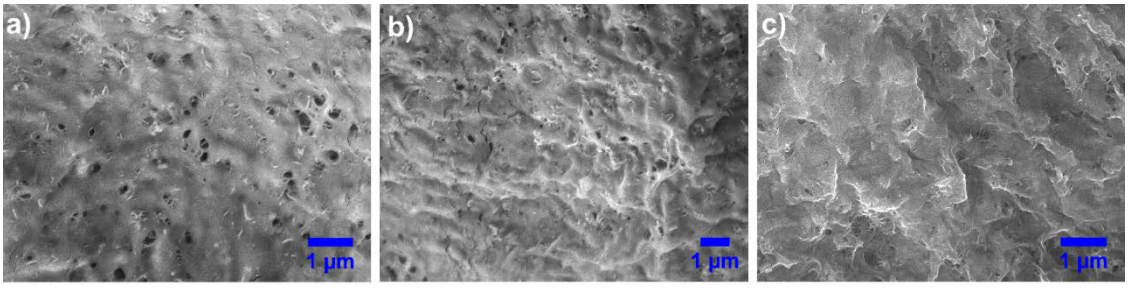

Figure A8.3. The structure and surface morphology of 10% w/w MWCNT/PHA nanocomposites taken in a-b) replicate areas and on a c) separately prepared MWCNT/PHA nanocomposite sample before biodegradation using SEM.

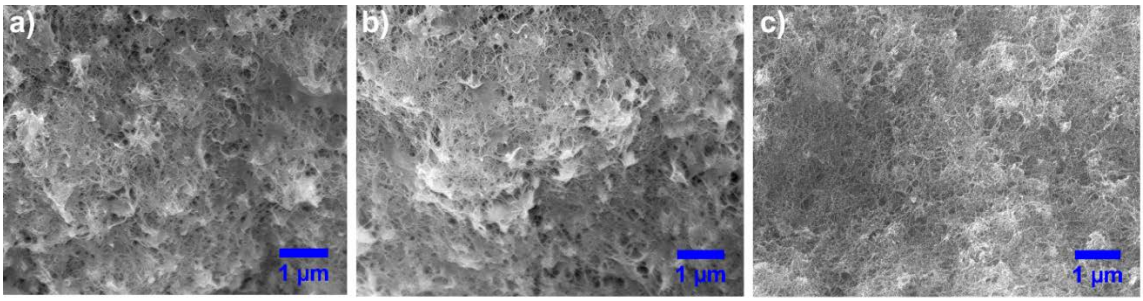

Figure A8.4. The structure and surface morphology of 5% w/w MWCNT/PHA nanocomposites after aerobic mixed culture biodegradation in primary effluent taken in a-b) replicate areas and on a c) separately prepared MWCNT/PHA nanocomposite sample using SEM.

DAVID G. GOODWIN JR.

3121 N. CALVERT ST, APT 3 • BALTIMORE, MD 21218
PHONE (215) 498-0374 • E-MAIL DGOODWI8@JHU.EDU

EDUCATION

Ph.D. Candidate in Chemistry, Present — **The Johns Hopkins University**, 3400 N. Charles St, Baltimore, MD

Masters of Arts in Chemistry, May 2012
Department of Chemistry, Cumulative GPA: 3.64/4.00

Coursework: Surface Chemistry, Aquatic Chemistry, Advanced Mechanistic Organic Chemistry, Spectroscopic Methods, Environmental Colloidal Phenomena, Polymer Chemistry, Electron Transfer Processes, Advanced Physical Chemistry

Bachelor's of Science in Chemistry — **Lafayette College**, Easton, PA, May 2010
Cumulative GPA: 3.64/4.00, Dean's List (4 semesters)

Select Relevant Coursework (*w/laboratory): Organic Chemistry I & II(*), Advanced Organic Chemistry, Environmental Chemistry, Thermodynamics, Mechanics, Calculus I-III, Linear Algebra, Analytical Chemistry I and II(*), Physical Chemistry I and II(*), Biochemistry, Inorganic Chemistry(*), Advanced Topics in Forensic Chemistry (Independent Study) (*), Spectroscopic Methods, , Advanced Inorganic Chemistry(*), Thesis(*)

RESEARCH EXPERIENCE

Graduate Research Assistant, Baltimore, MD — Summer 2010 - Present
Supervisor: Dr. D. Howard Fairbrother, Professor, Department of Chemistry at the Johns Hopkins University

1) **Thesis project- Environmental degradation of carbon nanotube/polymer nanocomposites:** Researching the environmental fate and transformations of carbon nanotube/polymer nanocomposites (CNT/PNCs), materials that are projected for use in consumer products, by means of microbial interactions, fungal interactions, weathering, and photolysis (microbial interactions in collaboration with Dr. Ed Bouwer, Professor and Department Chair of Geography and Environmental Engineering).
   - Development of CNT/PNC preparation protocols involving spray-coating and casting techniques.
   - Materials characterization of CNT/PNCs before and after environmental transformations using surface and bulk analytical techniques (see instrument skills section).
   - Evaluating the initial interactions of CNT/PNCs with microorganisms as a function of CNT loading using microbial staining and confocal laser scanning microscopy.
   - Assessing biofilm growth characteristics on CNT/PNCs under static and flow cell conditions.
   - Using mass loss and biogas evolution to determine the effect of CNT loading on CNT/PNC biodegradation in both single and mixed culture. Biogas composition measured with gas chromatography.
2) **Phototransformations of graphene oxide in sunlight:** Surface characterization of the photochemical transformation products of graphene oxide in the presence of air, N_2, and hydrogen peroxide under simulated sunlight conditions using X-ray Photoelectron Spectroscopy (XPS) and ATR-IR spectroscopy (in collaboration with the Environmental Protection Agency, Athens, GA) resulting in two peer reviewed publications.
3) **Carbon nanomaterial (CNM) characterization:**

DAVID G. GOODWIN JR.

3121 N. CALVERT ST, APT 3 • BALTIMORE, MD 21218
PHONE (215) 498-0374 • E-MAIL DGOODWI8@JHU.EDU

- Effectively working in a multi-tasking, cross-functional environment that balances CNT/PNC degradation research with multiple collaborative projects involving Yale, EPA Athens, Colorado School of Mines, Purdue University, and multiple departments at Johns Hopkins University. These projects investigate various environmental or synthetic transformations of CNMs and their resulting properties.
- Oxidation of carbon nanotubes and preparation of CNT suspensions in various solvents.
- Improvement and application of an in-house technique used to tag oxygen functional groups (hydroxyl, carbonyl, and carboxyl) on CNMs with fluorine-containing reagents for quantification with XPS.
- Developing CNT detection techniques for CNT release from degraded CNT/PNCs using single particle ICP-MS with Colorado School of Mines.

4) **Teamwork and management experience:**
   - Coordinating and supervising the research activities of one research technologist, one master's student, twelve undergraduates, and three visiting international graduate students. Training several Ph.D. level graduate students.
   - Working on team projects to develop preliminary data for grant proposals or project ideas.
   - Addressing strategic and technical issues with advisor on an array of projects.
   - Organizing interdisciplinary meetings between two advisors and other graduate students.
   - Maintaining well-organized data and records while working between several departments.
   - Performing literature searches, maintaining laboratory and coordinating efforts with facilities manager, attending departmental meetings and seminars, budgeting, prospective graduate student recruitment, editing documents for co-workers and the principal investigator, and preparing group presentations.
5) **Communication and writing experience:**
   - Presented research findings at eight different national conferences.
   - Extensively edited eight manuscripts (two first-author to date) through all stages of the peer review process.
   - Played a key role in gathering content and obtaining results for several successfully funded grant proposals, one of which supported main Ph.D. project.
   - Preparing annual reports for funding agencies.

Undergraduate Researcher, Easton, PA and Ewing, NJ Fall 2008 – Summer 2010
Supervisors: Dr. John Allison, Director and Professor of Forensic Chemistry at the College of New Jersey and Dr. Chip Nataro, Professor of Inorganic Chemistry at Lafayette College

Analyzed the mechanism by which $Co(SCN)_2$ reacts with cocaine to produce a color change in the Scott Test, indicating the presence of the illegal drug to help further validate this presumptive field test for law enforcement.

Lafayette College Excel Scholar Undergraduate Researcher, Easton, PA
Summer 2008 – Fall 2008
Supervisor: Dr. Tina Huang, Assistant Professor of Analytical Chemistry, Lafayette College

Researched the use of polymer-coated single-walled carbon nanotubes as semi-conductors in electronic devices.

TEACHING EXPERIENCE

Teacher's Assistant, Baltimore, MD Fall 2010 – Spring 2012

DAVID G. GOODWIN JR.

3121 N. CALVERT ST, APT 3 • BALTIMORE, MD 21218
PHONE (215) 498-0374 • E-MAIL DGOODWI8@JHU.EDU

Head TA for Introductory Chemistry I Lecture. Taught one section of Physical Chemistry Laboratory and two sections of Organic Chemistry II Lecture.

Teacher's Assistant, Easton, PA Fall 2008 – Spring 2010

Taught three sections of General Chemistry II Laboratory. Gave lectures, graded lab reports and handled issues as they arose. Experienced in troubleshooting, explaining techniques and maintaining laboratory function and organization.

PRESENTATIONS (MOST RECENT)

1) Goodwin, D.G, D. Phan, Z. Xia, T. Gordon, K.L. Marsh, I.B. Sosa, T. Devahif, C. Gao, E.J. Bouwer, and D.H. Fairbrother. Carbon Nanotube (CNT) Loading Impact on Polymer Biodegradability in CNT/Polymer Nanocomposites. Gordon Research Conference, Environmental Nanotechnology. West Dover, VT, June 21-26, **2015**. Poster.
2) Goodwin, D.G., I.B. Boyer, T. Devahif, Z. Xia, J.B. Payne, R.S. Go, D.H. Fairbrother, and E.J. Bouwer.
   Influence of Carbon Nanotube Loading on the Biodegradation of Polymer Nanocomposites. 248th American Chemical Society Meeting, Environmental Division. San Francisco, CA. August 10-14, 2014.
3) Goodwin, D.G, I.B. Boyer, T. Devahif, J.B Payne, R.S. Go, E.J. Bouwer, and D.H. Fairbrother. Fate of Carbon Nanotube Polymer Nanocomposites in the Presence of Microorganisms. 88th American Chemical Society Colloid and Surface Science Symposium. Philadelphia, PA, June 22-25, 2014.

JOURNAL PUBLICATIONS

1) Goodwin Jr., D. G.; Xia, Z.; Gordon, T.; Gao, C; Bouwer, E. J.; Fairbrother, D. H., Biofilm Development on Carbon Nanotube/Polymer Nanocomposites. *Environmental Science: Nano.* **2016.**
2) Chowdhury, I.; Hou, W. C. .; Goodwin Jr., D. G.; Henderson, M.; Zepp, R.G.; Bouchard, D. Sunlight Affects Aggregation and Deposition of Graphene Oxide in Aquatic Systems. *Water Res*. **2015.** *78*, 37-46.
3) Goodwin Jr., D. G.; Marsh, K. M.; Sosa, I.B.; Payne, J. B.; Gorham, J. M.; Bouwer, E. J.; Fairbrother, D. H., Interactions of Microorganisms with Polymer Nanocomposite Surfaces Containing Oxidized Carbon Nanotubes. *Environmental Science and Technology*. **2015.** *49*, (9), 5484-5492.
4) Hou, W. C.; Chowdhury, I.; Goodwin Jr., D. G.; Henderson, M.; Fairbrother, D. H.; Bouchard, D.; Zepp, R.G., Photochemical Transformation of Graphene Oxide in Sunlight. *Environmental Science and Technology*, **2015,** *49*, (6), 3435-3443.
5) Wu, Jiewei; Goodwin, D.; Peter, K.; Benoit, D.; Li, W.; Fairbrother, D. H.; Fortner, J., Photo-Oxidation of Hydrogenated Fullerene (Fullerane) in Water. *Environmental Science and Technology Letters.* **2014,** *1*, (12)**,** 490-494.
6) Gilbertson, L. M.; Goodwin Jr., D. G.; Taylor, A. D.; Pfefferle, L., Zimmerman, J. B., Towards Tailored Functional Design of Multi-Walled Carbon Nanotubes (MWNTs): Electrochemical and Antimicrobial Activity Enhancement via Oxidation and Selective Reduction. *Environmental Science and Technology*. **2014,** *48*, (10), 5938-5945.
7) Reed, R. B.; Goodwin, D. G.; Marsh, K. L.; Capracotta, S. S.; Higgins, C. P.; Fairbrother, D. H.; Ranville, J. F., Detection of single walled carbon nanotubes by monitoring embedded metals. *Environmental Science: Processes and Impacts* **2013,** *15*, (1), 204-213.

DAVID G. GOODWIN JR.

3121 N. CALVERT ST, APT 3 • BALTIMORE, MD 21218
PHONE (215) 498-0374 • E-MAIL DGOODWI8@JHU.EDU

8) Ajmani, G. S.; Goodwin, D.; Marsh, K.; Fairbrother, D. H.; Schwab, K. J.; Jacangelo, J. G.; Huang, H., Modification of low pressure membranes with carbon nanotube layers for fouling control. *Water Res.* **2012,** *46*, (17), 5645-5654.

ACTIVITIES

Member of the American Chemical Society
Member of the Student Liaison Committee, Department of Chemistry, Johns Hopkins University September 2011 – Present

AWARDS

Owens Graduate Fellowship, Department of Chemistry, Johns Hopkins University
June 2014 – June 2015

Funded by NSF CBET Grant #1236493
November 2012 – June 2014, June 2015- November 2015

SKILLS

Qualitative: Excellent coordinator and team member. Well organized and proficient at oral and written communication; objective in examinations; thorough and meticulous in the laboratory; strong work ethic; able to adapt quickly to changing priorities.

Technical:

1) **Instrument skills:** Can independently run scanning electron (SEM) and confocal laser scanning microscopy (CLSM), transmission IR, attenuated total reflectance infrared (ATR-IR), X-ray photoelectron (XPS), energy dispersive X-ray (EDS) and UV-Vis spectroscopy, differential scanning calorimetry (DSC), and bomb calorimetry. Workable knowledge in atomic force, transmission electron, and NMR spectroscopy. Utilized 1H, 13C, COSY, and HETCOR NMR techniques in undergraduate research. Performed GC-MS and collaborated on an ICP-MS project. Familiar with dynamic light scattering (DLS), DLVO theory, and Raman spectroscopy.
2) **Laboratory Techniques:** Skilled in microbial cultivation, sterile technique, wet chemistry (acid/base, sonication, centrifugation, gas tank usage, serial dilutions, extractions, distillation, use of analytical balance, waste disposal, etc.), spin-coating polymers, preparing nanocomposites, preparing colloidal suspensions, oxidation of carbon nanotubes, chemical derivatization of oxygen functional groups on CNT surfaces for quantification using vapor phase reactions, and ball-milling powders.
3) **Software:** Proficient in Microsoft Office, Sigma Plot, CasaXPS, AugerScan, ChemDraw and EndNote software. Experienced in XPS peak-fitting and data analysis. Experienced in molecular structure determination using NMR, IR, and MS data.